

Patrick C. Hallenbeck *Editor*

Modern Topics in the Phototrophic Prokaryotes

Metabolism, Bioenergetics, and Omics



Springer

Modern Topics in the Phototrophic Prokaryotes

Patrick C. Hallenbeck

Editor

Modern Topics in the Phototrophic Prokaryotes

Metabolism, Bioenergetics, and Omics

 Springer

Editor

Patrick C. Hallenbeck
Department of Biology
Life Sciences Research Center
United States Air Force Academy, USA

Département de microbiologie, infectiologie et immunologie
Université de Montréal
Montréal, Québec, Canada

ISBN 978-3-319-51363-8 ISBN 978-3-319-51365-2 (eBook)
DOI 10.1007/978-3-319-51365-2

Library of Congress Control Number: 2017933463

© Springer International Publishing AG 2017

This work is subject to copyright. All rights are reserved by the Publisher, whether the whole or part of the material is concerned, specifically the rights of translation, reprinting, reuse of illustrations, recitation, broadcasting, reproduction on microfilms or in any other physical way, and transmission or information storage and retrieval, electronic adaptation, computer software, or by similar or dissimilar methodology now known or hereafter developed.

The use of general descriptive names, registered names, trademarks, service marks, etc. in this publication does not imply, even in the absence of a specific statement, that such names are exempt from the relevant protective laws and regulations and therefore free for general use.

The publisher, the authors and the editors are safe to assume that the advice and information in this book are believed to be true and accurate at the date of publication. Neither the publisher nor the authors or the editors give a warranty, express or implied, with respect to the material contained herein or for any errors or omissions that may have been made. The publisher remains neutral with regard to jurisdictional claims in published maps and institutional affiliations.

Printed on acid-free paper

This Springer imprint is published by Springer Nature
The registered company is Springer International Publishing AG
The registered company address is: Gewerbestrasse 11, 6330 Cham, Switzerland

Contents

Regulation of Nitrogen Fixation in Photosynthetic Purple Nonsulfur Bacteria	1
Bernd Masepohl	
Sulfur Metabolism in Phototrophic Bacteria	27
Christiane Dahl	
Biochemistry of Chlorophyll Biosynthesis in Photosynthetic Prokaryotes	67
Yuichi Fujita and Hisanori Yamakawa	
The Maintenance of Iron Homeostasis Among Prokaryotic Phototrophs	123
Sébastien Zappa and Carl E. Bauer	
Cyanobacterial Photosynthesis: The Light Reactions	163
Sascha Rexroth, Marc M. Nowaczyk, and Matthias Rögner	
Photosynthesis in the Purple Bacteria	193
Robert A. Niederman	
Proteome Analysis of Phototrophic Adaptation	225
Frédéric Deschoenmaecker, Baptiste Leroy, and Ruddy Wattiez	
Photosynthetic Carbon Metabolism and CO₂-Concentrating Mechanism of Cyanobacteria	271
Natalia A. Pronina, Elena V. Kupriyanova, and Abir U. Igamberdiev	
Biosynthesis of Cyanobacterial Light-Harvesting Pigments and Their Assembly into Phycobiliproteins	305
Benjamin Ledermann, Marco Aras, and Nicole Frankenberg-Dinkel	
Index	341

Regulation of Nitrogen Fixation in Photosynthetic Purple Nonsulfur Bacteria

Bernd Masepohl

Abstract Biological nitrogen fixation (BNF) is the nitrogenase-catalyzed process in which dinitrogen (N_2) is reduced to ammonia (NH_3), the preferred nitrogen source in bacteria. All N_2 -fixing or diazotrophic bacteria have molybdenum-nitrogenases. In addition, some diazotrophs possess one or two alternative Mo-free nitrogenases, namely a vanadium and/or an iron-only nitrogenase, which are less efficient than Mo-nitrogenase in terms of ATP-consumption per N_2 reduced. BNF is widespread in photosynthetic purple nonsulfur bacteria, which are capable of using light energy to generate ATP for nitrogenase activity. This review focusses on BNF regulation in the purple nonsulfur bacteria *Rhodobacter capsulatus*, *Rhodospseudomonas palustris*, and *Rhodospirillum rubrum*. *Rp. palustris* is one of few diazotrophs having both alternative nitrogenases, whereas *Rb. capsulatus* and *Rs. rubrum* have Fe-nitrogenases but no V-nitrogenase. Purple nonsulfur bacteria regulate BNF in response to ammonium, molybdenum, iron, oxygen, and light. BNF regulation involves common regulatory proteins including the two-component nitrogen regulatory system NtrB-NtrC, the transcriptional activator NifA, the nitrogen-specific sigma factor RpoN, the DraT-DraG system for posttranslational nitrogenase regulation, and at least two PII signal transduction proteins. When ammonium is limiting, NtrB phosphorylates NtrC, which in turn activates expression of *nifA* and other BNF-related genes. NifA and its homologs VnfA and AnfA activate expression of Mo, V, and Fe-nitrogenase genes, respectively, in concert with RpoN. DraT mediates nitrogenase switch-off by ADP-ribosylation upon ammonium addition or light deprivation, the latter condition causing energy depletion. DraG reactivates nitrogenase upon ammonium consumption or reillumination. PII-like proteins integrate the cellular nitrogen, carbon, and energy levels, and control activity of NtrB, NifA, DraT, and DraG. Beside these similarities in BNF regulation, there are species-specific differences. NifA is active as synthesized in *Rb. capsulatus*, but requires activation by PII in *Rp. palustris* and *Rs. rubrum*. Reversible ADP-ribosylation is the only mechanism regulating nitrogenase in *Rs. rubrum*, whereas *Rb. capsulatus* and *Rp. palustris* have additional ADP-ribosylation-independent mechanisms. Last but not least, molybdate directly

B. Masepohl (✉)

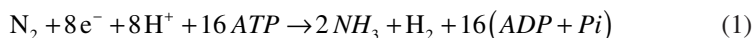
Lehrstuhl für Biologie der Mikroorganismen, Fakultät für Biologie und Biotechnologie,
Ruhr-Universität Bochum, 44780 Bochum, Germany
e-mail: bernd.masepohl@rub.de

represses *anfA* transcription and hence, Fe-nitrogenase expression in *Rb. capsulatus*, whereas expression of the alternative nitrogenases in *Rp. palustris* and *Rs. rubrum* respond to Mo-nitrogenase activity rather than to molybdate directly.

Keywords Nitrogen fixation • Nitrogenase • Rhodobacter • Rhodospseudomonas • Rhodospirillum • Regulation

Introduction to Biological Nitrogen Fixation

Growth of all eukaryotes and most prokaryotes requires a fixed nitrogen source like ammonium, nitrate, or amino acids. Quite a few prokaryotes, however, can reduce the chemically inert molecular dinitrogen (N_2) to ammonia (NH_3) by a process called biological nitrogen fixation (BNF). No eukaryote is capable of directly fixing N_2 but several eukaryotes like legumes and termites make indirectly use of N_2 by forming symbiotic associations with nitrogen-fixing bacteria or archaea (Hongoh 2010; Oldroyd 2013). BNF depends on complex metalloenzymes called nitrogenases, which catalyze the overall reaction shown in Eq. (1), and require a theoretical minimum of 16 ATP per N_2 reduced (Igarashi and Seefeldt 2003). In addition to N_2 reduction, nitrogenases produce hydrogen gas (H_2) in an obligate side reaction and, in the absence of N_2 , nitrogenases exclusively reduce protons to H_2 . Nitrogenase-catalyzed production of H_2 as a biofuel has extensively been studied in photosynthetic bacteria (Adessi et al. 2016; Heiniger et al. 2012; Huang et al. 2010; McKinlay and Harwood 2010; Rey et al. 2007) and is discussed in more detail elsewhere in this book series.



All N_2 -fixing (diazotrophic) bacteria and archaea possess a molybdenum-dependent nitrogenase containing the catalytic iron-molybdenum cofactor, FeMoco (Zhang and Gladyshev 2008). In addition to Mo-nitrogenase, some diazotrophs synthesize alternative Mo-free nitrogenases containing the iron-vanadium cofactor, FeVco, or the iron-only cofactor, FeFeco (Dos Santos et al. 2012; McGlynn et al. 2013). The three nitrogenases are encoded by distinct gene sets, namely *nifHDK* (Mo-nitrogenase), *vnfHDGK* (V-nitrogenase), and *anfH-DGK* (Fe-nitrogenase). Beside the structural nitrogenase genes, diazotrophs have numerous genes involved in cofactor biosynthesis, electron supply, and regulation (see below).

In addition to N_2 and protons, nitrogenases reduce the artificial substrate acetylene (C_2H_2). Mo-nitrogenases reduce acetylene to ethylene (C_2H_4), whereas alternative nitrogenases reduce acetylene to ethylene and in part, to ethane (C_2H_6). In the laboratory, gas chromatography-based acetylene reduction assays have been established to quantify nitrogenase activity and to detect activity of alternative nitrogenases (Dilworth et al. 1988).

Mo, V, and Fe-nitrogenases consist of two components each, the catalytic dinitrogenases and the dinitrogenase reductases, the latter serving as the ultimate electron donors to their respective dinitrogenases (Curatti and Rubio 2014; Hu and Ribbe 2016). The three dinitrogenase reductases are collectively called Fe-proteins (homodimers of NifH, VnfH, and AnfH), all of which coordinate one [4Fe-4S] cluster involved in electron transfer. The Mo, V, and Fe-dinitrogenases are called MoFe-protein (heterotetramer of NifDK containing two FeMoco), VFe-protein (heterohexamer of VnfDGK containing two FeVco), and FeFe-protein (heterohexamer of AnfDGK containing two FeFeco), respectively. In addition to the catalytic cofactors, the dinitrogenases contain two P-clusters (see below) involved in electron transfer from the Fe-proteins to the catalytic cofactors.

Biosynthesis of the Mo-nitrogenase cofactors ([4Fe-4S] cluster, P-cluster, and FeMoco) is complex and requires several *nif* gene products including NifU, NifS, NifB, NifV, NifE, NifN, NifH, NifD, and NifK as shown for *Klebsiella pneumoniae* and *Azotobacter vinelandii* (Curatti and Rubio 2014; Hu and Ribbe 2016; and the references therein). Briefly, NifU and NifS function as the scaffold protein and sulfur donor, respectively, for biosynthesis of [4Fe-4S] clusters, which are either inserted into apo-NifH or serve as building blocks for P-cluster and FeMoco formation. The P-cluster is formed in situ on the apo-NifDK protein, whereas the FeMoco is synthesized ex situ prior to insertion into the apo-NifDK protein. P-cluster biosynthesis starts with the transfer of two [4Fe-4S] clusters to the apo-NifDK protein followed by NifH-mediated reductive coupling to form the [8Fe-7S] or P-cluster. FeMoco biosynthesis starts with the coupling of two [4Fe-4S] clusters on NifB involving S-adenosylmethionine-dependent carbon (C) insertion to form an [8Fe-9S-C] cluster. This cluster is further processed on the NifEN scaffold by insertion of Mo and homocitrate (the product of homocitrate synthase, NifV) resulting in the [Mo-7Fe-9S-C-homocitrate] cluster or FeMoco, which is finally inserted into the apo-NifDK protein.

NifU, NifS, NifB, and NifV are required for activity of Mo, V, and Fe-nitrogenases in *A. vinelandii* indicating that the biosynthetic pathways of FeMoco, FeVco, and FeFeco overlap to a certain extent (Drummond et al. 1996; Kennedy and Dean 1992). Formation of FeVco involves the Vnf-specific NifEN homolog, VnfEN, instead of NifEN (Hu and Ribbe 2016; and the references therein). Possibly, the last steps of FeFeco biosynthesis occur in situ on the AnfDGK protein, since no NifEN homolog is required for Fe-nitrogenase activity (Schüddekopf et al. 1993).

Diazotrophs regulate BNF in response to several environmental factors including ammonium, molybdenum, iron, oxygen, and in case of photosynthetic bacteria, light. Since BNF is a highly energy-demanding process, diazotrophs typically induce nitrogenase expression only when ammonium, the product of BNF, is limiting. Mo-nitrogenase is more efficient than the alternative nitrogenases in terms of consumption of ATP and reductant per N₂ reduced (Hu et al. 2012; Schneider et al. 1997) and hence, expression of alternative nitrogenases is typically repressed as long as Mo-nitrogenase is active. Most bacteria possess *modABC* genes encoding

high-affinity ABC transporters, which support uptake of molybdate, the only bio-available form of molybdenum, under Mo-limiting conditions (Zhang and Gladyshev 2008; Zhang and Gladyshev 2010). All three nitrogenases are irreversibly damaged by oxygen (Blanchard and Hales 1996; Chisnell et al. 1988; Gollan et al. 1993) and diazotrophs have evolved different strategies to cope with this problem.

Diazotrophic and non-diazotrophic bacteria utilize similar proteins to sense the cellular nitrogen status and to control nitrogen assimilation. Among these proteins are the bifunctional uridylyltransferase/uridylyl-removing enzyme GlnD, the PII signal transduction proteins GlnB and GlnK, the two-component regulatory system NtrB-NtrC, and the ammonium transporter AmtB, which are best characterized in the non-diazotrophic enterobacterium *Escherichia coli* (van Heeswijk et al. 2013; and the references therein).

Briefly, GlnD senses the cellular nitrogen status through the glutamine level (Jiang et al. 1998a). Under low glutamine levels (N-limiting conditions), GlnD modifies GlnB and GlnK by uridylylation of conserved tyrosine residues within their T-loops. Under high glutamine levels (N-replete conditions), GlnD catalyzes the reverse reaction by hydrolyzing GlnB-UMP and GlnK-UMP. Trimeric PII proteins can be fully uridylylated (PII-UMP₃), partially uridylylated (PII-UMP₂ or PII-UMP₁), or completely unmodified (PII). PII proteins directly sense the cellular carbon and energy status by binding 2-oxoglutarate (2OG) and ATP/ADP, respectively (Radchenko et al. 2013). 2OG joins nitrogen and carbon metabolism as it serves as the carbon skeleton for ammonium assimilation by the GS-GOGAT (glutamine synthetase–glutamate synthase) pathway. Taken together, PII proteins integrate the cellular nitrogen (glutamine), carbon (2OG), and energy (ATP/ADP) levels, and transduce these signals to target proteins by physical interaction.

Under N-limiting conditions, the response regulator NtrC is phosphorylated by its cognate sensor kinase NtrB (Jiang et al. 1998b). In turn, NtrC-P activates transcription of *glnA* encoding glutamine synthetase, the *glnK-amtB* operon, and genes required for generation of ammonia from “poor” nitrogen sources like amino acids. Under N-replete conditions, unmodified GlnB forms a complex with NtrB to stimulate dephosphorylation and hence, inactivation of NtrC. In parallel, unmodified GlnK forms a complex with AmtB thereby inhibiting ammonium uptake under N-replete conditions.

This review deals with the regulation of nitrogen fixation in photosynthetic purple nonsulfur bacteria, which are capable of using light energy to generate the ATP required for nitrogenase activity. Purple nonsulfur bacteria are known for their extreme metabolic versatility enabling growth under photoautotrophic, photoheterotrophic, chemoautotrophic, and chemoheterotrophic conditions (Madigan et al. 1984). BNF is widespread in purple nonsulfur bacteria and has been extensively studied in *Rhodobacter capsulatus*, *Rhodospseudomonas palustris*, and *Rhodospirillum rubrum*, whose complete genome sequences have been determined (Larimer et al. 2004; Madigan et al. 1984; Munk et al. 2011; Strnad et al. 2010). In addition to Mo-nitrogenase, *Rb. capsulatus* and *Rs. rubrum* synthesize Fe-nitrogenases (Davis et al. 1996; Lehman and Roberts 1991; Schneider et al. 1991; Schneider et al. 1997),

whereas *Rp. palustris* is one of the few diazotrophs synthesizing Mo, V, and Fe-nitrogenases (Oda et al., 2005).

Organization of Nitrogen Fixation Genes in Purple Nonsulfur Bacteria

All diazotrophs including *Rb. capsulatus*, *Rp. palustris*, and *Rs. rubrum* contain a common set of nitrogen fixation genes, namely the structural genes of Mo-nitrogenase (*nifH*, *nifD*, and *nifK*) and genes involved in [4Fe-4S] cluster, P-cluster, and FeMoco biosynthesis (*nifU*, *nifS*, *nifB*, *nifV*, *nifE*, and *nifN*) (Curatti and Rubio 2014; Hu and Ribbe 2016; Larimer et al. 2004; MacKellar et al. 2016; Masepohl and Klipp 1996; Munk et al. 2011; Oda et al. 2005; Strnad et al. 2010; Wang et al. 2013). These common *nif* genes cluster with species-specific *nif* genes involved in regulation, electron transport to nitrogenase, and genes of unknown function (Fig. 1). Expression of common and species-specific *nif* genes requires the central transcriptional activator NifA, which enhances transcription by RNA polymerase containing the nitrogen-specific sigma factor RpoN (also called NtrA or σ^{54}) as is the case in other proteobacterial diazotrophs (see below). NifA proteins consist of an N-terminal GAF domain involved in the response to the cellular nitrogen status, a central AAA domain involved in the interaction with RNA polymerase and ATP hydrolysis, and a C-terminal HTH (helix-turn-helix) domain involved in binding to promoter DNA (Fischer 1994). Noteworthy, *Rb. capsulatus* synthesizes two structurally and functionally highly similar NifA proteins: NifA1 and NifA2 (Masepohl et al. 1988; Paschen et al. 2001).

Electron transport to nitrogenase in *Rb. capsulatus* involves the *mfABCDEFGH* genes (Jeong and Jouanneau 2000; Jouanneau et al. 1998; Kumagai et al. 1997; Schmehl et al. 1993), which are lacking in *Rs. rubrum* and *Rp. palustris*. Instead, the latter two strains contain the *fixABCD* genes, whose products form the major electron transport pathway in *Rs. rubrum* (Edgren and Nordlund 2004) and possibly also in *Rp. palustris* (Huang et al. 2010).

Many diazotrophs including *Rb. capsulatus* and *Rp. palustris* have *iscN-nifUSVW* operons, whereas *Rs. rubrum* lacks an *nifS* gene at the corresponding position between *nifU* and *nifV*. However, *Rs. rubrum* contains three *nifS*-like genes elsewhere in the chromosome, one of which possibly serves as a sulfur donor for biosynthesis of iron-sulfur clusters under N_2 -fixing conditions.

The structural genes of Fe-nitrogenase *anfHDGK* and the Fe-nitrogenase-associated genes *anfOR* form conserved operons in *Rh. capsulatus*, *Rp. palustris*, and *Rs. rubrum* (Fig. 2) (Larimer et al. 2004; Munk et al. 2011; Oda et al. 2005; Schüddekopf et al. 1993; Strnad et al. 2010). Expression of these *anf* operons is activated by AnfA, an NifA-like regulator (Kutsche et al. 1996; Schüddekopf et al. 1993). Activation of the V-nitrogenase-related genes *vnfH*, *vnfDGK*, and *vnfENX* in *Rp. palustris* depends on VnfA, another NifA-like activator. Like NifA, AnfA and VnfA act in concert with the sigma factor RpoN.

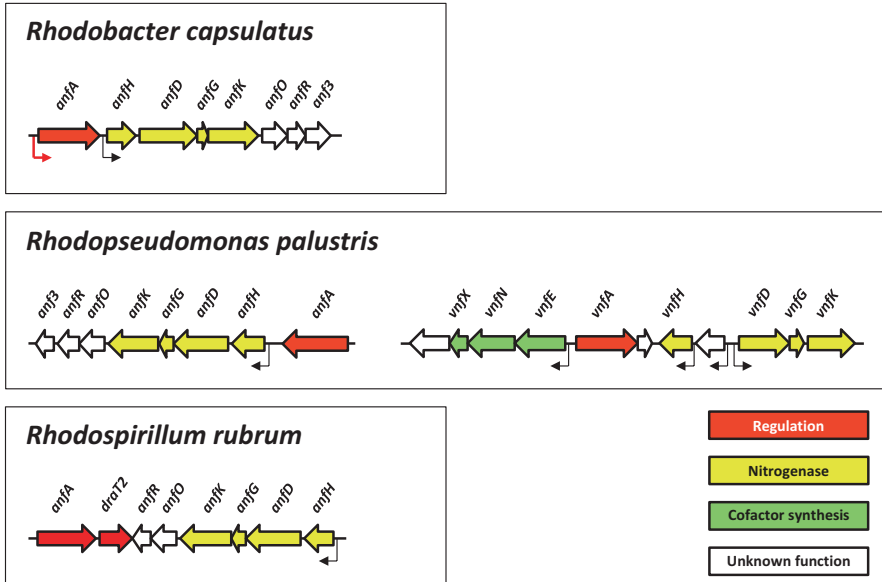


Fig. 2 Organization of Fe and V-nitrogenase-related genes. Genetic maps are based on the genome sequences of *Rh. capsulatus* SB 1003 (Strnad et al. 2010), *Rp. palustris* CGA009 (Larimer et al. 2004), and *Rs. rubrum* S1 (Munk et al. 2011). Bent arrows in red or black mark possible NtrC and RpoN recognition sequences, respectively

Cascade Activation of Nitrogen Fixation in *Rhodobacter capsulatus*

Rb. capsulatus is capable of growing with many different nitrogen sources including ammonium, urea, most amino acids, and N_2 (Hillmer and Gest 1977; Masepohl et al. 2001). Expression of urease and N_2 fixation genes strictly depends on NtrC (Hübner et al. 1991; Kranz and Haselkorn 1985; Kutsche et al. 1996; Masepohl et al. 2001). As described above for *E. coli*, *Rb. capsulatus* NtrC is phosphorylated, and thus activated, by NtrB under ammonium-limiting conditions (Cullen et al. 1996). In contrast to NtrC from *E. coli* and other bacteria, which require the nitrogen-specific sigma factor RpoN to activate transcription of their target genes, *Rb. capsulatus* NtrC activates gene expression in concert with the housekeeping sigma factor RpoD (Bowman and Kranz 1998; Foster-Hartnett et al. 1994).

Upon phosphorylation, *Rb. capsulatus* NtrC activates transcription of *nifA1*, *nifA2*, *mopA-modABC*, and *anfA* (Fig. 3). Activation involves binding of NtrC to sequences similar to the *Rb. capsulatus* NtrC binding site consensus CGCC- N_9 -GGC- N_{4-14} -CGCC- N_9 -GGC (Foster-Hartnett and Kranz 1994; Kutsche et al. 1996). NifA1 and NifA2 differ only in their very N-terminal amino acid residues, and consequently, can functionally substitute for each other in transcriptional activation of Mo-nitrogenase genes (Masepohl et al. 1988; Paschen et al. 2001). Expression of Fe-nitrogenase genes is activated by AnfA (Kutsche et al., 1996). Transcriptional activation by NifA1, NifA2, and AnfA depends on RpoN as is the

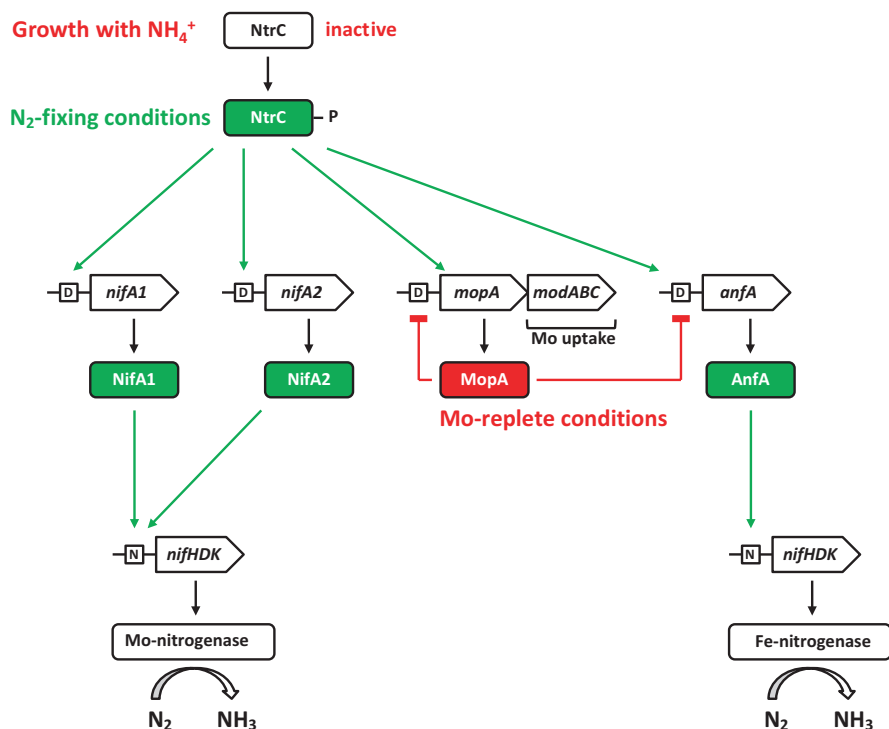


Fig. 3 Cascade regulation of nitrogen fixation in *Rh. capsulatus*. During growth with ammonium, NtrC is inactive, but is activated by phosphorylation upon ammonium consumption. NtrC-P activates RpoD-dependent promoters (boxed D), whereas NifA1, NifA2, and AnfA activate RpoN-dependent promoters (boxed N). MopA represses transcription of the *mopA-modABC* and *anfA* genes under Mo-replete conditions. For clarity, the second Mo-responsive regulator, MopB, is not shown

case in other proteobacterial diazotrophs (Hübner et al. 1991; Schüddekopf et al. 1993). The *Rb. capsulatus rpoN* gene forms part of the *nifU2-rpoN* operon, whose expression is activated by NifA1, NifA2, and presumably also by AnfA (Cullen et al. 1994; Preker et al. 1992). A weak primary NtrC-independent promoter located in the *nifU2-rpoN* intergenic region drives initial expression of *rpoN*, while a secondary promoter upstream of *nifU2* is required to increase *rpoN* expression under N₂-fixing conditions (Cullen et al. 1994).

All *Rb. capsulatus nif* promoters including the *nifU2* promoter as well as the *anfH* promoter contain sequences highly similar to the RpoN binding site consensus CTGC-N₈-TTGC typically located at position -24/-12 relative to the transcription start site (Fig. 1) (Morett and Buck 1989; Schmehl et al. 1993). The *nif* promoters are preceded by sequences similar to the NifA binding site consensus TGT-N₁₀-ACA (Morett and Buck 1988). As expected for an AnfA-dependent promoter, the *anfH* promoter lacks an NifA binding site; however, the AnfA binding site has not yet been identified.

Ammonium Inhibition of Nitrogen Fixation in *Rhodobacter capsulatus*

The levels of *Rb. capsulatus* NtrC remain constant under N-limiting and N-replete conditions, but NtrC activity clearly responds to the cellular nitrogen status (Cullen et al. 1998). Ammonium keeps NtrC in its dephosphorylated inactive state, thus preventing expression of the *nifA1*, *nifA2*, and *anfA* genes, and consequently, all the other nitrogen fixation genes (Foster-Hartnett and Kranz 1992; Preker et al. 1992).

Ammonium addition to an N₂-fixing *Rb. capsulatus* culture causes three effects, namely (1) inactivation of NtrC-P by dephosphorylation, (2) inhibition of NifA1, NifA2, and AnfA activity, and (3) “switch-off” of Mo and Fe-nitrogenases (Drepper et al. 2003; Hallenbeck 1992; Hallenbeck et al. 1982; Jouanneau et al. 1983; Masepohl et al. 1993; Paschen et al. 2001; Pierrard et al. 1993a, b; Schüddekopf et al. 1993).

Ammonium-induced inactivation of NtrC prevents further expression of *nifA1*, *nifA2*, and *anfA*. A strain lacking GlnB expresses *nifA1* (and probably also *nifA2* and *anfA*) even in the presence of ammonium (Drepper et al. 2003). NtrB specifically interacts with GlnB but not with GlnK (Pawlowski et al. 2003) suggesting that inactivation of *Rb. capsulatus* NtrC is catalyzed by an NtrB-GlnB complex exhibiting phosphatase activity as described above for *E. coli*.

Ammonium inhibition of NifA1, NifA2, and AnfA activity prevents further expression of all the other nitrogen fixation genes (Paschen et al. 2001; Schüddekopf et al. 1993). Either GlnB or GlnK is sufficient to inhibit NifA1 and NifA2, whereas a strain lacking both PII signal transduction proteins no longer inhibits activity of the NifA regulators (Drepper et al. 2003). Both NifA proteins interact with GlnB and GlnK (Pawlowski et al. 2003) suggesting that NifA inhibition is mediated by physical contact with the PII proteins. The strain lacking both PII proteins still expresses Mo-nitrogenase (Drepper et al. 2003) indicating that the *Rb. capsulatus* NifA proteins are active as synthesized and do not require activation by PII as is the case in *Rp. palustris* and *Rs. rubrum* (Heiniger et al. 2012; Rey et al. 2007; Zhang et al. 2000, 2004; Zhou et al. 2008; Zhu et al. 2006). In contrast to PII-mediated NifA inhibition in *Rb. capsulatus*, AnfA inhibition is not relieved in the strain lacking both PII proteins indicating that ammonium inhibition of NifA and AnfA involves different mechanisms (Drepper et al. 2003).

Ammonium addition to an N₂-grown culture rapidly represses activity of Mo and Fe-nitrogenases, an effect immediately reversed upon ammonium consumption (Hallenbeck 1992; Hallenbeck et al. 1982; Jouanneau et al. 1983; Masepohl et al. 1993; Pierrard et al. 1993a). In *Rb. capsulatus*, nitrogenase “switch-off” is caused by at least two mechanisms, one blocking activity of the Fe-proteins, NifH and AnfH, by ADP-ribosylation, and another possibly blocking the ATP or the electron supply to nitrogenase (Förster et al. 1999; Pierrard et al. 1993a, b). Evidence for the second mechanism comes from the observation that *Rb. capsulatus* strains expressing mutant NifH proteins, which are no longer ADP-ribosylated, as well as a *draTG* mutant strain still exhibit ammonium-induced nitrogenase switch-off (Förster et al. 1999;

Pierrard et al. 1993a; Yakunin and Hallenbeck 1998b). Ammonium-induced nitrogenase switch-off independent of ADP-ribosylation has been reported in many other diazotrophs, but the underlying mechanisms are unknown (Huergo et al. 2012; and the references therein). In *Rb. capsulatus*, a further nitrogenase switch-off mechanism called “magnitude response” reflects the amount of added ammonium (Yakunin and Hallenbeck 1998b; Yakunin et al. 1999).

ADP-ribosylation is catalyzed by DraT (dinitrogenase reductase ADP-ribosyl transferase), whereas DraG (dinitrogenase reductase-activating glycohydrolase) mediates the reverse reaction (Huergo et al. 2012; Nordlund and Högbom 2013; and the references therein). ADP-ribosylation at arginine residue 101 of one subunit of the *Rb. capsulatus* NifH homodimer is sufficient to prevent electron transfer to the MoFe protein and consequently, N₂ reduction by Mo-nitrogenase (Jouanneau et al. 1989). Proper regulation of nitrogenase modification and switch-off requires GlnB, GlnK, and AmtB, and disruption of the *amtB* gene abolishes ADP-ribosylation and switch-off (Drepper et al. 2003; Tremblay et al. 2007; Tremblay and Hallenbeck 2008; Yakunin and Hallenbeck 2002). The *amtB* strain exhibits wild-type growth properties with ammonium as sole nitrogen source indicating that AmtB is dispensable for ammonium uptake, but primarily serves as an ammonium sensor for ammonium-induced switch-off of nitrogenase (Tremblay and Hallenbeck 2009).

Figure 4 shows a model of DraTG-mediated ammonium regulation of Mo-nitrogenase and possibly also of Fe-nitrogenase in *Rb. capsulatus*. The mechanisms of DraT activation and DraG inactivation can be summarized as follows: (1) Under N₂-fixing conditions, both PII proteins are uridylylated, but upon ammonium addition, GlnK-UMP and GlnB-UMP are deuridylylated. (2) Next, DraG is inactivated by membrane sequestration as a ternary DraG-GlnK-AmtB complex and DraT is activated by complex formation with GlnB. In turn, the GlnB-DraT complex mediates ADP-ribosylation of the Fe-protein. (3) Upon ammonium consumption, DraG is released from the membrane and reactivates the Fe-protein by removing the ADP-ribose moiety.

Ammonium Regulation of Nitrogen Fixation in *Rhodopseudomonas palustris*

Expression and activity of Mo-nitrogenase in *Rp. palustris* is regulated at three levels, namely (1) control of *nifA* transcription, (2) control of NifA activity, and (3) switch-off control of Mo-nitrogenase as is the case for *Rb. capsulatus* (Heiniger et al. 2012; Rey et al. 2007). Ammonium regulation at all three levels involves PII proteins in both diazotrophs. In contrast to *Rb. capsulatus*, which has two PII genes, *glnB* and *glnK*, *Rp. palustris* has three PII genes forming part of the *glnB-glnA* and the *glnK1-amtB1-glnK2-amtB2* clusters (Connelly et al. 2006). GlnB, GlnK1, and GlnK2 undergo uridylylation under ammonium-starved (N₂-fixing) conditions, but are deuridylylated under ammonium-replete conditions. Under N₂-fixing conditions, NtrC activates transcription of the *nifA* gene (level 1). Only after binding to GlnB,

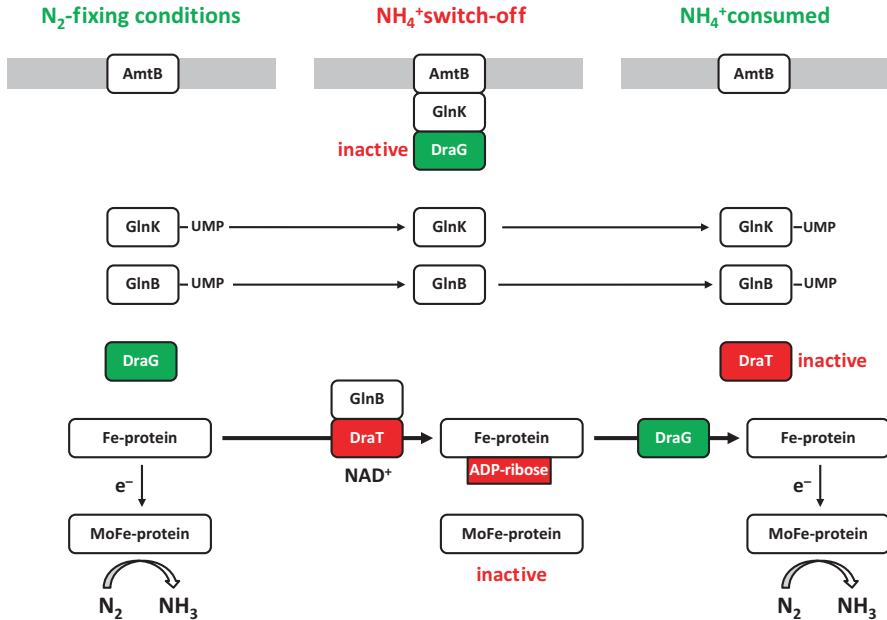


Fig. 4 Model of ammonium-responsive nitrogenase regulation in *Rb. capsulatus*. Upon ammonium addition to a nitrogen-fixing culture, GlnK-UMP and GlnB-UMP are deuridylylated. In turn, DraT is activated by GlnB, while DraG is inactivated by GlnK-mediated membrane sequestration. DraT-mediated ADP-ribosylation of the Fe-protein prevents electron (e^-) transfer to the MoFe-protein. Upon ammonium consumption, DraG is released from the membrane and reactivates the Fe-protein by removing the ADP-ribose moiety

Rp. palustris NifA is capable of activating Mo-nitrogenase gene expression (level 2). Upon ammonium addition to an N_2 -grown culture, GlnK2 and DraT2 form a complex to inactivate Mo-nitrogenase by ADP-ribosylation. In addition, *Rp. palustris* DraT2 possibly regulates electron transfer to nitrogenase as discussed for *Rb. capsulatus* DraT (Förster et al. 1999; Heiniger et al. 2012; Pierrard et al. 1993a, b). Like Mo-nitrogenase, the V and Fe-nitrogenases in *Rp. palustris* are modified upon ammonium addition (Heiniger and Harwood 2015).

Rp. palustris strains synthesizing mutant NifA* proteins with single amino acid substitutions or small deletions in the Q-linker constitutively express nitrogenase and produce H_2 even in the presence of ammonium (Heiniger et al. 2012; Rey et al. 2007). The Q-linker is located between the nitrogen-responsive GAF domain and the RNA polymerase-binding AAA domain (Fischer 1994). Three observations explain, how the *nifA** mutants bypass the elaborated regulatory cascade otherwise limiting N_2 fixation to ammonium-starved conditions in the wild-type. First, *Rp. palustris* synthesizes low amounts of NifA independent of NtrC activation. Second, mutant NifA* proteins do not require activation by GlnB and thus, appear to be more active than wild-type NifA proteins. Consequently, NifA* strains overexpress Mo-nitrogenase explaining at least in part resistance against DraT2-mediated nitrogenase switch-off. Third, DraT2

activity requires GlnK2, whose expression depends on NtrC, which is synthesized only at low levels in the presence of ammonium (Conlan et al. 2005). NtrC activates transcription of the *ntrC* gene in *Rp. palustris* (Conlan et al. 2005), whereas NtrC is constitutively synthesized in *Rb. capsulatus* (Cullen et al. 1998).

Ammonium Regulation of Nitrogen Fixation in *Rhodospirillum rubrum*

Transcription of *nifA* completely or for the most part depends on NtrC in *Rb. capsulatus* and *Rp. palustris*, respectively (Foster-Hartnett and Kranz 1992; Heiniger et al. 2012; Hübner et al. 1993; Preker et al. 1992; Rey et al. 2007), whereas NtrC appears to be dispensable for *nifA* expression in *Rs. rubrum* (Zhang et al. 1995). However, the *Rs. rubrum nifA* gene is preceded by a possible NtrC binding site (Fig. 1) suggesting that NtrC contributes to *nifA* expression. Disruption of *ntrC* impairs nitrogenase switch-off in *Rs. rubrum*, likely because NtrC is required for maximal *glnBA* expression, and GlnB is essential for DraT activation (Cheng et al. 1999; Zhang et al. 1995).

Rs. rubrum NifA is synthesized in an inactive form, which requires activation by GlnB as is the case in *Rp. palustris* (Zhang et al. 2000, 2001, 2004). Neither of the other two PII proteins synthesized by *Rs. rubrum*, GlnK and GlnJ, can substitute for GlnB in NifA activation. GlnD is essential for NifA activation indicating that only GlnB-UMP but not its unmodified form, GlnB, is capable of activating NifA (Zhang et al. 2005). GlnB* variants mediating NifA activity in a strain lacking GlnD contain single amino acid substitutions in the T-loop apparently mimicking the uridylylated form of GlnB (Zhang et al. 2004; Zhu et al. 2006). NifA* variants no longer requiring activation by GlnB-UMP contain amino acid substitutions in the N-terminal GAF domain, which is involved in interaction between wild-type NifA and GlnB-UMP (Fischer 1994; Zhou et al. 2008). Nitrogenase activity is still switched-off by ammonium in *Rs. rubrum nifA** strains, whereas ammonium switch-off is mostly relieved in *Rp. palustris nifA** strains as described above (Heiniger et al. 2012; Rey et al. 2007; Zhou et al. 2008). *Rs. rubrum nifA** strains lacking DraT, however, exhibit high nitrogenase activity in the presence of ammonium.

DraT-mediated ADP-ribosylation appears to be the only mechanism controlling nitrogenase activity in *Rs. rubrum* (Zhang et al. 1996). In contrast, nitrogenase activity is controlled by two mechanisms, one DraT-dependent and another DraT-independent mechanism, in many other diazotrophs including *Azoarcus* sp. strain BH72, *Azospirillum brasilense*, *Herbaspirillum seropedicae*, and *Rb. capsulatus* (Förster et al. 1999; Fu and Burris 1989; Huergo et al. 2012; Oetjen and Reinhold-Hurek 2009; Pierrard et al. 1993a, b; Yakunin and Hallenbeck 1998b; Zhang et al. 1996).

Rs. rubrum has three PII genes forming part of the *glnB-glnA*, *glnJ-amtB1*, and *glnK-amtB2* operons (Munk et al. 2011). Upon ammonium addition to an N₂-grown culture, DraT is activated by interaction with unmodified GlnB, and DraG is inacti-

vated by membrane sequestration involving AmtB1, unmodified GlnJ, and possibly an unknown membrane protein (Nordlund and Högbom 2013; Teixeira et al. 2008; Wang et al. 2005; Wolfe et al. 2007; Zhang et al. 2006).

Darkness Regulation of Nitrogenase

Like ammonium addition, light deprivation causes nitrogenase switch-off in photosynthetic bacteria (Huerger et al. 2012; Nordlund and Högbom 2013; Pierrard et al. 1993b; Selao et al. 2011; Yakunin and Hallenbeck 2002; Zhang et al. 1995, 2001, 2006). In *Rs. rubrum*, ammonium and darkness-induced nitrogenase regulation by reversible ADP-ribosylation involve the same proteins, namely DraT, DraG, GlnB, GlnJ, and AmtB1, but the signaling mechanisms transducing the cellular nitrogen and energy levels differ (Teixeira et al. 2010; Zhang et al. 2001, 2006). While ammonium addition to an N₂-grown culture causes a big increase in the cellular glutamine concentration leading to GlnD-mediated deuridylylation of GlnB-UMP and GlnJ-UMP, light deprivation does not affect the glutamine pool or induce PII demodification on a big scale (Li et al. 1987; Teixeira et al. 2010). Full uridylylation of trimeric PII prevents “plug-in” interaction with AmtB, whereas partially uridylylated PII proteins form a complex with AmtB in *A. brasilense* (Rodrigues et al. 2011). Hence, DraG inactivation in *Rs. rubrum* may either be achieved by GlnJ-independent membrane sequestration or involve complex formation between partially deuridylylated GlnJ and AmtB1 (Huerger et al. 2012; Nordlund and Högbom 2013).

Iron Regulation of Electron Transport to Nitrogenase

Rb. capsulatus utilizes two parallel acting electron transport pathways to nitrogenase, the RnfABCDGEH-FdxN and the NifJ-NifF pathway, in which the ferredoxin FdxN and the flavodoxin NifF act as the ultimate electron donors to NifH and possibly also to AnfH (Gennaro et al. 1996; Hallenbeck and Gennaro 1998; Jeong and Jouanneau 2000; Jouanneau et al. 1998; Kumagai et al. 1997; Schmehl et al. 1993; Yakunin et al. 1993; Yakunin and Hallenbeck 1998a). The Rnf proteins form an energy-coupling NADH oxidoreductase complex that catalyzes the reduction of FdxN. The NifJ protein is a pyruvate-flavodoxin oxidoreductase mediating electron transfer from pyruvate to NifF. In contrast to the situation in *Rb. capsulatus*, the NifJ-NifF pathway constitutes the sole electron transport pathway to nitrogenase in *K. pneumoniae* (Hill and Kavanagh 1980; Shah et al. 1983).

Unlike the *rnf* and *fdxN* genes, the *Rb. capsulatus nifF* and *nifJ* genes are not contained in the major *nif* clusters (Fig. 1). However, the *nifF* gene belongs to the NifA regulon and accordingly, *nifF* is specifically expressed under N₂-fixing conditions as is the case for the *rnf* and *fdxN* genes (Gennaro et al. 1996; Schmehl et al. 1993). In contrast to *nifF*, the *nifJ* gene is expressed under ammonium-replete conditions and its

expression increases only slightly under N_2 -fixing conditions indicating that NifJ function is not restricted to N_2 fixation (Yakunin and Hallenbeck 1998a). The NifJ-NifF pathway contributes significantly to electron transfer to nitrogenase under iron-replete conditions, but is essential under iron-limiting conditions (Gennaro et al. 1996; Yakunin et al. 1993; Yakunin and Hallenbeck 1998a). Accordingly, *nifF* expression and NifF accumulation is higher under iron-deficient than under iron-sufficient conditions, while *rmf* transcription and Rnf accumulation decreases upon iron limitation (Jouanneau et al. 1998). Apparently, *Rb. capsulatus* copes with iron limitation by replacing the iron-containing ferredoxin FdxN by the Fe-free flavodoxin NifF, but the iron-responsive mechanisms controlling *nifF* and *rmf* expression remain unknown to date.

Rs. rubrum lacks *rmfABCDGEH* genes but instead has *fixABCX* genes (Fig. 1), whose products form the major electron transport pathway to nitrogenase in this diazotroph (Edgren and Nordlund 2004). In addition, *Rs. rubrum* has an *nifJ*-like gene encoding a pyruvate-ferredoxin oxidoreductase (Edgren and Nordlund 2006). In both the FixABCX and the NifJ pathways ferredoxin N (encoded by the *fdxN* gene located downstream of *nifB*; Fig. 1) is the ultimate electron donor to nitrogenase (Edgren and Nordlund 2005, 2006). Like *Rs. rubrum*, *Rp. palustris* lacks *rmfABCDGEH* genes but has *fixABCX* genes (Fig. 1), which are essential for diazotrophic growth (Huang et al. 2010) suggesting that electron transport to nitrogenase in *Rp. palustris* involves a similar mechanism as in *Rs. rubrum*.

Regulation of Molybdate Uptake and Alternative Nitrogenases

Most bacteria synthesize high-affinity molybdate transporters (*modABC*-encoded) suggesting that they have to cope at least temporarily with Mo limitation (Zhang and Gladyshev 2008). Under Mo-replete conditions, *E. coli* represses *modABC* transcription by the molybdate-responsive one-component regulator ModE, thus limiting expression of the Mo uptake system to Mo-limiting conditions. ModE binds a palindromic sequence called Mo-box overlapping the *modA* transcription start site thereby preventing binding of RNA polymerase (Studholme and Pau 2003).

Rb. capsulatus has two *modE* homologs, *mopA* and *mopB*, belonging to divergently transcribed operons, *mopA-modABCD* and *mopB* (Fig. 1). Upon molybdate-binding MopA and MopB repress transcription of the *mopA-modABCD* and *anfA* genes by binding the Mo-boxes overlapping the transcription start sites of *mopA* and *anfA* (Fig. 5) (Kutsche et al. 1996; Müller et al. 2010; Wiethaus et al. 2006). Either MopA or MopB is sufficient to repress transcription from the *mopA* and *anfA* promoters. Beside its role as a repressor, MopA acts as a transcriptional activator of the *mop* gene encoding a molybdate-binding hexameric protein (Wiethaus et al. 2009). In contrast to the *mopA* and *anfA* Mo-boxes, which overlap the transcription start sites, the *mop* Mo-box is located at some distance upstream of the transcription start site as expected for an enhancer binding site. In line with the proposed role of the Mop protein in Mo storage, Mop accumulates to high levels with increasing Mo concentrations (Hoffmann et al. 2016).

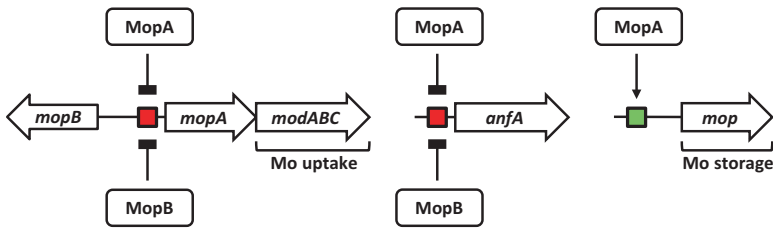
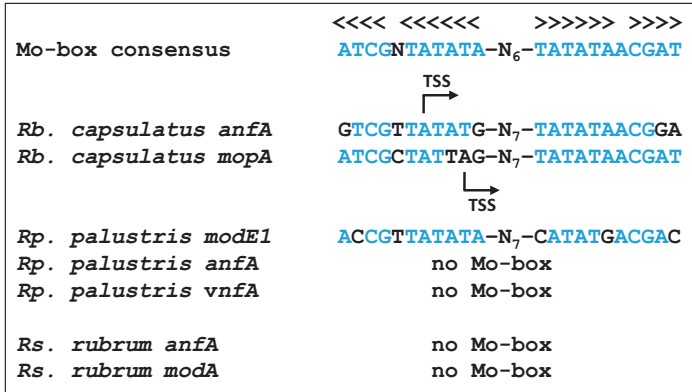


Fig. 5 Nitrogen fixation and molybdate transport-related Mo-boxes. Mo-boxes are highly conserved palindromic sequences (marked by *arrow heads*) serving as binding sites for ModE-type regulators (Studholme and Pau 2003). Conserved Mo-box nucleotides in the promoters of *Rb. capsulatus anfA* and *mopA*, and *Rp. palustris modE1* are highlighted in blue. *Rb. capsulatus* synthesizes two ModE-like regulators, MopA and MopB, which repress transcription of the *mopA-modABC* and *anfA* genes by binding Mo-boxes (*red squares*) overlapping the transcription start sites (TSS) of *mopA* and *anfA* (Kutsche et al. 1996). In addition, MopA activates *mop* transcription by binding the Mo-box (*green square*) preceding the *mop* TSS (Wiethaus et al. 2006)

While Mo represses *mopA*, the *mopB* gene is constitutively transcribed and accordingly, the MopA/MopB ratio varies in response to Mo availability (Hoffmann et al. 2016; Wiethaus et al. 2006, 2009). Under Mo-limiting conditions, MopA is more abundant than MopB, whereas only MopB is left under Mo-replete conditions. MopA and MopB form homodimers as well as heteromers (Wiethaus et al. 2009). Disruption of *mopB* enhances *mop* expression suggesting that MopA-MopB heteromer formation counteracts *mop* activation by MopA homodimers.

Since AnfA is essential for Fe-nitrogenase expression, *anfA* repression by MopA and MopB prevents Fe-nitrogenase expression at high Mo concentrations (Fig. 3). In contrast, Mo-nitrogenase levels increase with increasing Mo concentrations involving a yet unknown post-transcriptional control mechanism (Hoffmann et al. 2014a, 2016).

In addition to ModABC, which imports molybdate at nanomolar concentrations in the environment, *Rb. capsulatus* synthesizes the oxyanion transporter PerO, which imports molybdate in micromolar ranges (Gisin et al. 2010). Besides molybdate,

PerO transports tungstate, vanadate, and sulfate. In contrast to the *modABC* genes, transcription of *perO* is not repressed by molybdate.

Like *Rb. capsulatus*, *Rp. palustris* has two *modE* genes, one of which, *modE1*, clusters with *modABC* genes, while the other is located at a distant position in the chromosome (Larimer et al. 2004). The *modE1* promoter contains a likely Mo-box (Fig. 5) indicating that ModE1 autoregulates its own expression in response to molybdate availability as is the case for *Rb. capsulatus* MopA. In contrast to the *Rb. capsulatus* *anfA* promoter, the *Rp. palustris* *anfA* and *vnfA* promoters do not encompass an obvious Mo-box suggesting that *anfA* and *vnfA* do not belong to the ModE1 regulon (see below). Unlike *Anabaena variabilis* ATCC 29413, which synthesizes a high-affinity vanadate transporter, VupABC, sustaining V-nitrogenase activity under vanadate-limiting conditions, *Rp. palustris* lacks *vupABC* homologs (Pratte and Thiel 2006).

Disruption of the Mo-nitrogenase genes induces expression of V and Fe-nitrogenases in *Rp. palustris* even at high molybdate concentrations otherwise sufficient to repress Fe-nitrogenase in *Rb. capsulatus* (Oda et al. 2005; Wang et al. 1993). Similar to the situation in *Rp. palustris*, *Rs. rubrum* strains lacking active Mo-nitrogenase express Fe-nitrogenase irrespective of Mo availability (Lehman and Roberts 1991). Hence, the mechanisms controlling expression of the alternative nitrogenases in *Rp. palustris* and *Rs. rubrum* differ from that in *Rb. capsulatus*.

Nitrogenase Protection Against Oxygen Damage

Mo, V, and Fe-nitrogenases are irreversibly damaged by oxygen (Blanchard and Hales 1996; Chisnell et al. 1988; Gollan et al. 1993), and thus, many diazotrophs synthesize nitrogenase only under anaerobic or microaerobic conditions. Other diazotrophs have evolved different strategies to protect nitrogenase at high ambient oxygen concentrations. Some filamentous cyanobacteria develop specialized N₂-fixing cells called heterocysts, which have thick cell walls limiting oxygen entry and lack the oxygen-evolving photosystem PSII. Most rhizobia express nitrogenase exclusively within special plant organs called nodules, in which oxygen partial pressure is sufficiently low. Other strategies involve cytochrome *bd* oxidase (*cydAB*-encoded) or the Shetna's protein II (*fesII*-encoded) mediating "respiratory" and "conformational" protection of nitrogenase, respectively, in *A. vinelandii*, *Gluconacetobacter diazotrophicus*, and *Rb. capsulatus* (Hoffmann et al., 2014a; Kelly et al. 1990; Moshiri et al. 1994; Schlesier et al. 2016; Ureta and Nordlund 2002). Conformational protection depends on a ternary complex formed by FeSII, the Fe-protein, and the MoFe-protein (Schlesier et al. 2016).

The *Rb. capsulatus* FeSII homolog, FdxD, supports diazotrophic growth via Mo-nitrogenase (but not via Fe-nitrogenase) under semiaerobic conditions (Hoffmann et al. 2014a). Expression of the *fdxD* gene, which is located immediately upstream of the *nifHDK* genes, is activated by NifA1 and NifA2 but not by AnfA. Hence, the *fdxD* gene belongs to the Mo-nitrogenase regulon, and its product specifically protects Mo-nitrogenase against oxygen damage.

NifA-dependent *fdxD* expression decreases with increasing oxygen concentrations (Hoffmann et al. 2014a). This regulation is possibly explained by oxygen sensitivity of NifA1 and NifA2, which belong to the class of oxygen-sensitive NifA regulators (Fischer 1994; Paschen et al. 2001). Members of this class contain an additional domain absent in oxygen-tolerant NifA proteins, the interdomain linker domain, which is located between the central AAA and the C-terminal HTH domain. The interdomain linker domain is implicated in metal (possibly Fe) binding and oxygen or redox sensing in *Bradyrhizobium japonicum* and *Herbaspirillum seropedicae* (Fischer et al. 1988, 1989; Oliveira et al. 2009).

Maximal *fdxD* expression requires both NifA1 and NifA2 (Hoffmann et al. 2014a), and maximal *nifA2* expression depends on the two-component regulatory system RegB-RegA (Elsen et al. 2000). In contradiction to the original assumption that oxygen directly inhibits RegB kinase activity (Mosley et al. 1994; Sganga and Bauer. 1992), the RegB-RegA system apparently responds to the cellular redox state (Elsen et al. 2000). Besides controlling nitrogen fixation (via *nifA2*), the RegB-RegA system regulates photosynthesis, carbon dioxide assimilation, and hydrogen oxidation, thus acting as a master regulator of important energy-generating and energy-consuming processes.

Nitrogenase Protection Against Carbon Monoxide Inhibition

Carbon monoxide (CO) inhibits all nitrogenase-catalyzed substrate reductions except for proton reduction by blocking intramolecular electron flow and hence, CO hampers N₂ fixation and diazotrophic growth (Hwang et al. 1973; Lee et al. 2009; Lockshin and Burris 1965; Rivera-Ortiz and Burris 1975; Shen et al. 1997; Yan et al. 2012). A small protein, CowN, sustains N₂-dependent growth of *Rb. capsulatus* and *Rs. rubrum* in the presence of CO (Hoffmann et al. 2014b; Kerby and Roberts 2011). CowN has been suggested to form a complex with nitrogenase like the Shetna protein but experimental evidence supporting this assumption is lacking (Kerby and Roberts 2011). In both *Rb. capsulatus* and *Rs. rubrum*, *cowN* expression is induced by CO, but *cowN* activation depends on different transcription activators in these species.

CO induction of *Rb. capsulatus cowN* expression is mediated by the CO-responsive regulator CooA (Hoffmann et al. 2014b), which belongs to the family of heme-containing transcription factors (Roberts et al. 2005). Expression of *cooA* is activated by NifA1 and NifA2, whereas AnfA represses *cooA* and consequently, *cowN*. Accordingly, CowN specifically sustains diazotrophic growth via Mo-nitrogenase but not Fe-nitrogenase-dependent growth in the presence of CO.

The *Rs. rubrum* CooA homolog activates expression of CO dehydrogenase genes, but is dispensable for *cowN* expression (Fox et al. 1996; Kerby and Roberts 2011; Shelper et al. 1995). Instead, *cowN* expression in *Rs. rubrum* requires another CO-responsive regulator, RcoM (Kerby et al. 2008; Kerby and Roberts 2011), which is lacking in *Rb. capsulatus*.

Genes similar to *cowN* are widespread in bacteria (Kerby and Roberts 2011). Apparently, all bacteria harboring a *cowN* homolog also possess *nifHDK* genes implying that CowN-mediated Mo-nitrogenase protection is a common mechanism. In contrast to strict ammonium repression of the *nifHDK* genes, however, *cowN* is only partially repressed by ammonium in *Rb. capsulatus* and *Rs. rubrum* suggesting that CowN function is not restricted to nitrogenase protection (Hoffmann et al. 2014b; Kerby and Roberts 2011).

References

- Adessi A, Concato M, Sanchini A, Rossi F, De Philippis R (2016) Hydrogen production under salt stress conditions by a freshwater *Rhodopseudomonas* strain. *Appl Microbiol Biotechnol* 100:2917–2926
- Blanchard CZ, Hales BJ (1996) Isolation of two forms of the nitrogenase VFe protein from *Azotobacter vinelandii*. *Biochemistry* 35:472–478
- Bowman WC, Kranz RG (1998) A bacterial ATP-dependent, enhancer binding protein that activates the housekeeping RNA polymerase. *Genes Dev* 12:1884–1893
- Cheng J, Johansson M, Nordlund S (1999) Expression of P_{II} and glutamine synthetase is regulated by P_{II}, the *ntfBC* products, and processing of the *glnBA* mRNA in *Rhodospirillum rubrum*. *J Bacteriol* 181:6530–6534
- Chisnell JR, Premakumar R, Bishop PE (1988) Purification of a second alternative nitrogenase from a *nifHDK* deletion strain of *Azotobacter vinelandii*. *J Bacteriol* 170:27–33
- Conlan S, Lawrence C, McCue LA (2005) *Rhodopseudomonas palustris* regulons detected by cross-species analysis of alphaproteobacterial genomes. *Appl Environ Microbiol* 71:7442–7452
- Connelly HM, Pelletier DA, Lu TY, Lankford PK, Hettich RL (2006) Characterization of PII family (GlnK1, GlnK2, and GlnB) protein uridylylation in response to nitrogen availability for *Rhodopseudomonas palustris*. *Anal Biochem* 357:93–104
- Cullen PJ, Bowman WC, Foster-Hartnett D, Reilly SC, Kranz RG (1998) Translational activation by an NtrC enhancer-binding protein. *J Mol Biol* 278:903–914
- Cullen PJ, Bowman WC, Kranz RG (1996) In vitro reconstitution and characterization of the *Rhodobacter capsulatus* NtrB and NtrC two-component system. *J Biol Chem* 271:6530–6536
- Cullen PJ, Foster-Hartnett D, Gabbert KK, Kranz RG (1994) Structure and expression of the alternative sigma factor, RpoN, in *Rhodobacter capsulatus*; physiological relevance of an autoactivated *nifU2-rpoN* superoperon. *Mol Microbiol* 11:51–65
- Curatti L, Rubio LM (2014) Challenges to develop nitrogen-fixing cereals by direct *nif*-gene transfer. *Plant Sci* 225:130–137
- Davis R, Lehman L, Petrovich R, Shah VK, Roberts GP, Ludden PW (1996) Purification and characterization of the alternative nitrogenase from the photosynthetic bacterium *Rhodospirillum rubrum*. *J Bacteriol* 178:1445–1450
- Dilworth MJ, Eady RR, Eldridge ME (1988) The vanadium nitrogenase of *Azotobacter chroococcum*. Reduction of acetylene and ethylene to ethane. *Biochem J* 249:745–751
- Dos Santos PC, Fang Z, Mason SW, Setubal JC, Dixon R (2012) Distribution of nitrogen fixation and nitrogenase-like sequences amongst microbial genomes. *BMC Genomics* 13:162
- Drepper T, Groß S, Yakunin AF, Hallenbeck PC, Masepohl B, Klipp W (2003) Role of GlnB and GlnK in ammonium control of both nitrogenase systems in the phototrophic bacterium *Rhodobacter capsulatus*. *Microbiology* 149:2203–2212
- Drummond M, Walmsley J, Kennedy C (1996) Expression from the *nifB* promoter of *Azotobacter vinelandii* can be activated by NifA, VnfA, or AnfA transcriptional activators. *J Bacteriol* 178:788–792

- Edgren T, Nordlund S (2004) The *fixABCX* genes in *Rhodospirillum rubrum* encode a putative membrane complex participating in electron transfer to nitrogenase. *J Bacteriol* 186:2052–2060
- Edgren T, Nordlund S (2005) Electron transport to nitrogenase in *Rhodospirillum rubrum*: identification of a new *fdxN* gene encoding the primary electron donor to nitrogenase. *FEMS Microbiol Lett* 245:345–351
- Edgren T, Nordlund S (2006) Two pathways of electron transport to nitrogenase in *Rhodospirillum rubrum*: the major pathway is dependent on the *fix* gene products. *FEMS Microbiol Lett* 260:30–35
- Elsen S, Dischert W, Colbeau A, Bauer CE (2000) Expression of uptake hydrogenase and molybdenum nitrogenase in *Rhodobacter capsulatus* is coregulated by the RegB-RegA two-component regulatory system. *J Bacteriol* 182:2831–2837
- Fischer H-M (1994) Genetic regulation of nitrogen fixation in Rhizobia. *Microbiol Rev* 58:352–386
- Fischer H-M, Bruderer T, Hennecke H (1988) Essential and non-essential domains in the *Bradyrhizobium japonicum* NifA protein: identification of indispensable cysteine residues potentially involved in redox reactivity and/or metal binding. *Nucleic Acids Res* 16:2207–2224
- Fischer H-M, Fritsche S, Herzog B, Hennecke H (1989) Critical spacing between two essential cysteine residues in the interdomain linker of the *Bradyrhizobium japonicum* NifA protein. *FEBS Lett* 255:167–171
- Förster B, Maner K, Fassbinder F, Oelze J (1999) Reversible inactivation of nitrogenase in *Rhodobacter capsulatus* strain W107I deleted in the *draTG* gene region. *FEMS Microbiol Lett* 170:167–171
- Foster-Hartnett D, Kranz RG (1992) Analysis of the promoters and upstream sequences of *nifA1* and *nifA2* in *Rhodobacter capsulatus*; activation requires *ntnC* but not *rpoN*. *Mol Microbiol* 6:1049–1060
- Foster-Hartnett D, Kranz RG (1994) The *Rhodobacter capsulatus glnB* gene is regulated by NtrC at tandem *rpoN*-independent promoters. *J Bacteriol* 176:5171–5176
- Foster-Hartnett D, Cullen PJ, Monika EM, Kranz RG (1994) A new type of NtrC transcriptional activator. *J Bacteriol* 176:6175–6187
- Fox JD, He Y, Shelver D, Roberts GP, Ludden PW (1996) Characterization of the region encoding the CO-induced hydrogenase of *Rhodospirillum rubrum*. *J Bacteriol* 178:6200–6208
- Fu H, Burris RH (1989) Ammonium inhibition of nitrogenase activity in *Herbaspirillum seropedicae*. *J Bacteriol* 171:3168–3175
- Gennaro G, Hübner P, Sandmeier U, Yakunin AF, Hallenbeck PC (1996) Cloning, characterization, and regulation of *nifF* from *Rhodobacter capsulatus*. *J Bacteriol* 178:3949–3952
- Gisin J, Müller A, Pfänder Y, Leimkühler S, Narberhaus F, Masepohl B (2010) A *Rhodobacter capsulatus* member of a universal permease family imports molybdate and other oxyanions. *J Bacteriol* 192:5943–5952
- Gollan U, Schneider K, Müller A, Schüdekopf K, Klipp W (1993) Detection of the in vivo incorporation of a metal cluster into a protein. The FeMo cofactor is inserted into the FeFe protein of the alternative nitrogenase of *Rhodobacter capsulatus*. *Eur J Biochem* 215:25–35
- Hallenbeck PC (1992) Mutations affecting nitrogenase switch-off in *Rhodobacter capsulatus*. *Biochim Biophys Acta* 1118:161–168
- Hallenbeck PC, Gennaro G (1998) Stopped-flow kinetic studies of low potential electron carriers of the photosynthetic bacterium, *Rhodobacter capsulatus*: ferredoxin I and NifF. *Biochim Biophys Acta* 1365:435–442
- Hallenbeck PC, Meyer CM, Vignais PM (1982) Nitrogenase from the photosynthetic bacterium *Rhodopseudomonas capsulata*: purification and molecular properties. *J Bacteriol* 149:708–717
- Heiniger EK, Harwood CS (2015) Posttranslational modification of a vanadium nitrogenase. *MicrobiologyOpen* 4:597–603
- Heiniger EK, Oda Y, Samanta SK, Harwood CS (2012) How posttranslational modification of nitrogenase is circumvented in *Rhodopseudomonas palustris* strains that produce hydrogen gas constitutively. *Appl Environ Microbiol* 78:1023–1032
- Hill S, Kavanagh EP (1980) Roles of *nifF* and *nifJ* gene products in electron transport to nitrogenase in *Klebsiella pneumoniae*. *J Bacteriol* 141:470–475

- Hillmer P, Gest H (1977) H₂ metabolism in the photosynthetic bacterium *Rhodospseudomonas capsulata*: H₂ production by growing cultures. *J Bacteriol* 129:724–731
- Hoffmann M-C, Müller A, Fehringer M, Pfänder Y, Narberhaus F, Masepohl B (2014a) Coordinated expression of *fdxD* and molybdenum nitrogenase genes promotes nitrogen fixation by *Rhodobacter capsulatus* in the presence of oxygen. *J Bacteriol* 196:633–640
- Hoffmann M-C, Pfänder Y, Fehringer M, Narberhaus F, Masepohl B (2014b) NifA- and CooA-coordinated *cowN* expression sustains nitrogen fixation by *Rhodobacter capsulatus* in the presence of carbon monoxide. *J Bacteriol* 196:3494–3502
- Hoffmann M-C, Wagner E, Langklotz S, Pfänder Y, Hött S, Bandow JE, Masepohl B (2016) Proteome profiling of the *Rhodobacter capsulatus* molybdenum response reveals a role of IscN in nitrogen fixation by Fe-nitrogenase. *J Bacteriol* 198:633–643
- Hongoh Y (2010) Diversity and genomes of uncultured microbial symbionts in the termite gut. *Biosci Biotechnol Biochem* 74:1145–1151
- Hu Y, Ribbe MW (2016) Biosynthesis of the metalloclusters of nitrogenases. *Annu Rev Biochem* 85:3.1–3.29
- Hu Y, Lee CC, Ribbe MW (2012) Vanadium nitrogenase: a two-hit wonder? *Dalton Trans* 41:1118–1127
- Huang JJ, Heiniger EK, McKinlay JB, Harwood CS (2010) Production of hydrogen gas from light and the inorganic electron donor thiosulfate by *Rhodospseudomonas palustris*. *Appl Environ Microbiol* 76:7717–7722
- Hübner P, Masepohl B, Klipp W, Bickle TA (1993) *nif* gene expression studies in *Rhodobacter capsulatus*: *ntrC*-independent repression by high ammonium concentrations. *Mol Microbiol* 10:123–132
- Hübner P, Willison JC, Vignais PM, Bickle TA (1991) Expression of regulatory *nif* genes in *Rhodobacter capsulatus*. *J Bacteriol* 173:2993–2999
- Huergo LF, Pedrosa FO, Muller-Santos M, Chubatsu LS, Monteiro RA, Merrick M, Souza EM (2012) P_{II} signal transduction proteins: pivotal players in post-translational control of nitrogenase activity. *Microbiology* 158:176–190
- Hwang JC, Chen CH, Burris RH (1973) Inhibition of nitrogenase-catalyzed reductions. *Biochim Biophys Acta* 292:256–270
- Igarashi RY, Seefeldt LC (2003) Nitrogen fixation: the mechanism of the Mo-dependent nitrogenase. *Crit Rev Biochem Mol Biol* 38:351–384
- Jeong H-S, Jouanneau Y (2000) Enhanced nitrogenase activity in strains of *Rhodobacter capsulatus* that overexpress the *rnf* genes. *J Bacteriol* 182:1208–1214
- Jiang P, Peliska JA, Ninfa AJ (1998a) Enzymological characterization of the signal-transducing uridylyltransferase/uridylyl-removing enzyme (EC 2.7.7.59) of *Escherichia coli* and its interaction with the PII protein. *Biochemistry* 37:12782–12794
- Jiang P, Peliska JA, Ninfa AJ (1998b) Reconstitution of the signal-transduction bicyclic cascade responsible for the regulation of Ntr gene transcription in *Escherichia coli*. *Biochemistry* 37:12795–12801
- Jouanneau Y, Jeong H-S, Hugo N, Meyer C, Willison JC (1998) Overexpression in *Escherichia coli* of the *rnf* genes from *Rhodobacter capsulatus*. Characterization of two membrane-bound iron-sulfur proteins. *Eur J Biochem* 251:54–64
- Jouanneau Y, Meyer CM, Vignais PM (1983) Regulation of nitrogenase activity through iron protein interconversion into an active and an inactive form in *Rhodospseudomonas capsulata*. *Biochim Biophys Acta* 749:318–328
- Jouanneau Y, Roby C, Meyer CM, Vignais PM (1989) ADP-ribosylation of dinitrogenase reductase in *Rhodobacter capsulatus*. *Biochemistry* 28:6524–6530
- Kelly MJ, Poole RK, Yates MG, Kennedy C (1990) Cloning and mutagenesis of genes encoding the cytochrome *bd* terminal oxidase complex in *Azotobacter vinelandii*: mutants deficient in the cytochrome *d* complex are unable to fix nitrogen in air. *J Bacteriol* 172:6010–6019
- Kennedy C, Dean D (1992) The *nifU*, *nifS* and *nifV* gene products are required for activity of all three nitrogenases of *Azotobacter vinelandii*. *Mol Gen Genet* 231:494–498

- Kerby RL, Roberts GP (2011) Sustaining N₂-dependent growth in the presence of CO. *J Bacteriol* 193:774–777
- Kerby RL, Youn H, Roberts GP (2008) RcoM: a new single-component transcriptional regulator of CO metabolism in bacteria. *J Bacteriol* 190:3336–3343
- Kranz RG, Haselkorn R (1985) Characterization of *nif* regulatory genes in *Rhodospseudomonas capsulata* using *lac* gene fusions. *Gene* 40:203–215
- Kumagai H, Fujiwara T, Matsubara H, Saeki K (1997) Membrane localization, topology, and mutual stabilization of the *rmfABC* gene products in *Rhodobacter capsulatus* and implications for a new family of energy-coupling NADH oxidoreductases. *Biochemistry* 36:5509–5521
- Kutsche M, Leimkühler S, Angermüller S, Klipp W (1996) Promoters controlling expression of the alternative nitrogenase and the molybdenum uptake system in *Rhodobacter capsulatus* are activated by NtrC, independent of σ^{54} , and repressed by molybdenum. *J Bacteriol* 178:2010–2017
- Larimer FW, Chain P, Hauser L, Lamerdin J, Malfatti S, Do L, Land ML, Pelletier DA, Beatty JT, Lang AS, Tabita FR, Gibson JL, Hanson TE, Bobst C, Torres Y, Torres JL, Peres C, Harrison FH, Gibson J, Harwood CS (2004) Complete genome sequence of the metabolically versatile photosynthetic bacterium *Rhodospseudomonas palustris*. *Nat Biotechnol* 22:55–61
- Lee CC, Hu Y, Ribbe MW (2009) Unique features of the nitrogenase VFe protein from *Azotobacter vinelandii*. *Proc Natl Acad Sci U S A* 106:9209–9214
- Lehman LJ, Roberts GP (1991) Identification of an alternative nitrogenase system in *Rhodospirillum rubrum*. *J Bacteriol* 173:5705–5711
- Li JD, Hu CZ, Yoch DC (1987) Changes in amino acid and nucleotide pools of *Rhodospirillum rubrum* during switch-off of nitrogenase activity initiated by NH₄⁺ or darkness. *J Bacteriol* 169:231–237
- Lockshin A, Burris RH (1965) Inhibitors of nitrogen fixation in extracts from *Clostridium pasteurianum*. *Biochim Biophys Acta* 111:1–10
- MacKellar D, Lieber L, Norman JS, Bolger A, Tobin C, Murray JW, Oksaksin M, Chang RL, Ford TJ, Nguyen PQ, Woodward J, Permingeat HR, Joshi NS, Silver PA, Usadel B, Rutherford AW, Friesen ML, Prell J (2016) *Streptomyces thermoautotrophicus* does not fix nitrogen. *Sci Rep* 6:20086
- Madigan MT, Cox SS, Stegeman RA (1984) Nitrogen fixation and nitrogenase activities in members of the family *Rhodospirillaceae*. *J Bacteriol* 157:73–78
- Masepohl B, Klipp W (1996) Organization and regulation of genes encoding the molybdenum nitrogenase and the alternative nitrogenase in *Rhodobacter capsulatus*. *Arch Microbiol* 165:80–90
- Masepohl B, Kaiser B, Isakovic N, Richard CL, Kranz RG, Klipp W (2001) Urea utilization in the phototrophic bacterium *Rhodobacter capsulatus* is regulated by the transcriptional activator NtrC. *J Bacteriol* 183:637–643
- Masepohl B, Klipp W, Pühler A (1988) Genetic characterization and sequence analysis of the duplicated *nifA/nifB* gene region of *Rhodobacter capsulatus*. *Mol Gen Genet* 212:27–37
- Masepohl B, Krey R, Klipp W (1993) The *draTG* gene region of *Rhodobacter capsulatus* is required for post-translational regulation of both the molybdenum and the alternative nitrogenase. *J Gen Microbiol* 139:2667–2675
- McGlynn SE, Boyd ES, Peters JW, Orphan VJ (2013) Classifying the metal dependence of uncharacterized nitrogenases. *Front Microbiol* 3:419
- McKinlay JB, Harwood CS (2010) Photobiological production of hydrogen gas as a biofuel. *Curr Opin Biotechnol* 21:244–251
- Morett E, Buck M (1988) NifA-dependent in vivo protection demonstrates that the upstream activator sequence of *nif* promoters is a protein binding site. *Proc Natl Acad Sci U S A* 85:9401–9405
- Morett E, Buck M (1989) In vivo studies on the interaction of RNA polymerase- σ^{54} with *Klebsiella pneumoniae* and *Rhizobium meliloti nifH* promoters: The role of NifA in the formation of an open promoter complex. *J Mol Biol* 210:65–77
- Moshiri F, Kim JW, Fu C, Maier RJ (1994) The FeSII protein of *Azotobacter vinelandii* is not essential for aerobic nitrogen fixation, but confers significant protection to oxygen-mediated inactivation of nitrogenase in vitro and in vivo. *Mol Microbiol* 14:101–114

- Mosley CS, Suzuki JY, Bauer CE (1994) Identification and molecular genetic characterization of a sensor kinase responsible for coordinately regulating light harvesting and reaction center gene expression in response to anaerobiosis. *J Bacteriol* 176:7566–7573
- Müller A, Püttmann L, Barthel R, Schön M, Lackmann J-W, Narberhaus F, Masepohl B (2010) Relevance of individual Mo-box nucleotides to DNA binding by the related molybdenum-responsive regulators MopA and MopB in *Rhodobacter capsulatus*. *FEMS Microbiol Lett* 307:191–200
- Munk AC, Copeland A, Lucas S, Lapidus A, Del Rio TG, Barry K, Detter JC, Hammon N, Israni S, Pitluck S, Brettin T, Bruce D, Han C, Tapia R, Gilna P, Schmutz J, Larimer F, Land M, Kyrpidis NC, Mavromatis K, Richardson P, Rohde M, Göker M, Klenk H-P, Zhang Y, Roberts GP, Reslewic S, Schwartz DC (2011) Complete genome sequence of *Rhodospirillum rubrum* type strain (S1^T). *Stand Genomic Sci* 4:293–302
- Nordlund S, Högbom M (2013) ADP-ribosylation, a mechanism regulating nitrogenase activity. *FEBS J* 280:3484–3490
- Oda Y, Samanta SK, Rey FE, Wu L, Liu X, Yan T, Zhou J, Harwood CS (2005) Functional genomic analysis of three nitrogenase isozymes in the photosynthetic bacterium *Rhodospseudomonas palustris*. *J Bacteriol* 187:7784–7794
- Oetjen J, Reinhold-Hurek B (2009) Characterization of the DraT/DraG system for posttranslational regulation of nitrogenase in the endophytic betaproteobacterium *Azoarcus* sp. strain BH72. *J Bacteriol* 191:3726–3735
- Oldroyd GED (2013) Speak, friend, and enter: signaling systems that promote beneficial symbiotic associations in plants. *Nat Rev Microbiol* 11:252–263
- Oliveira MAS, Baura VA, Aquino B, Huergo LF, Kadowaki MAS, Chubatsu LS, Souza EM, Dixon R, Pedrosa FO, Wasseem R, Monteiro RA (2009) Role of conserved cysteine residues in *Herbaspirillum seropedicae* NifA activity. *Res Microbiol* 160:389–395
- Paschen A, Drepper T, Masepohl B, Klipp W (2001) *Rhodobacter capsulatus* nifA mutants mediating nif gene expression in the presence of ammonium. *FEMS Microbiol Lett* 200:207–213
- Pawlowski A, Riedel K-U, Klipp W, Dreiskemper P, Groß S, Bierhoff H, Drepper T, Masepohl B (2003) Yeast two-hybrid studies on interaction of proteins involved in regulation of nitrogen fixation in the phototrophic bacterium *Rhodobacter capsulatus*. *J Bacteriol* 185:5240–5247
- Pierrard J, Ludden PW, Roberts GP (1993a) Posttranslational regulation of nitrogenase in *Rhodobacter capsulatus*: existence of two independent regulatory effects of ammonium. *J Bacteriol* 175:1358–1366
- Pierrard J, Willison JC, Vignais PM, Gaspar JL, Ludden PW, Roberts GP (1993b) Site-directed mutagenesis of the target arginine for ADP-ribosylation of nitrogenase component II in *Rhodobacter capsulatus*. *Biochem Biophys Res Commun* 192:1223–1229
- Pratte BS, Thiel T (2006) High-affinity vanadate transport system in the cyanobacterium *Anabaena variabilis* ATCC 29413. *J Bacteriol* 188:464–468
- Preker P, Hübner P, Schmehl M, Klipp W, Bickle TA (1992) Mapping and characterization of the promoter elements of the regulatory nif genes rpoN, nifA1 and nifA2 in *Rhodobacter capsulatus*. *Mol Microbiol* 6:1035–1047
- Radchenko MV, Thornton J, Merrick M (2013) P_{II} signal transduction proteins are ATPases whose activity is regulated by 2-oxoglutarate. *Proc Natl Acad Sci U S A* 110:12948–12953
- Rey FE, Heiniger EK, Harwood CS (2007) Redirection of metabolism for biological hydrogen production. *Appl Environ Microbiol* 73:1665–1671
- Rivera-Ortiz JM, Burris RH (1975) Interactions among substrates and inhibitors of nitrogenase. *J Bacteriol* 123:537–545
- Roberts GP, Kerby RL, Youn H, Conrad M (2005) CooA, a paradigm for gas sensing regulatory proteins. *J Inorg Biochem* 99:280–292
- Rodrigues TE, Souza VE, Monteiro RA, Gerhardt EC, Araújo LM, Chubatsu LS, Souza EM, Pedrosa FO, Huergo LF (2011) In vitro interaction between the ammonium transport protein AmtB and partially uridylylated forms of the P_{II} protein GlnZ. *Biochim Biophys Acta* 1814:1203–1209
- Schlesier J, Rohde M, Gerhardt S, Einsle O (2016) A conformational switch triggers nitrogenase protection from oxygen damage by Shetna protein II (FeSII). *J Am Chem Soc* 138:239–247

- Schmehl M, Jahn A, zu Vilsendorf AM, Hennecke S, Masepohl B, Schuppler M, Marxer M, Oelze J, Klipp W (1993) Identification of a new class of nitrogen fixation genes in *Rhodobacter capsulatus*: a putative membrane complex involved in electron transport to nitrogenase. *Mol Gen Genet* 241:602–515
- Schneider K, Gollan U, Dröttboom M, Selsemeier-Voigt S, Müller A (1997) Comparative biochemical characterization of the iron-only nitrogenase and the molybdenum nitrogenase from *Rhodobacter capsulatus*. *Eur J Biochem* 244:789–800
- Schneider K, Müller A, Schramm U, Klipp W (1991) Demonstration of a molybdenum- and vanadium-independent nitrogenase in a *nifHDK*-deletion strain of *Rhodobacter capsulatus*. *Eur J Biochem* 195:653–661
- Schüddekopf K, Hennecke S, Liese U, Kutsche M, Klipp W (1993) Characterization of *anf* genes specific for the alternative nitrogenase and identification of *nif* genes required for both nitrogenases in *Rhodobacter capsulatus*. *Mol Microbiol* 8:673–684
- Selao TT, Edgren T, Wang H, Norén A, Nordlund S (2011) Effect of pyruvate on the metabolic regulation of nitrogenase activity in *Rhodospirillum rubrum* in darkness. *Microbiology* 157:1834–1840
- Sganga MW, Bauer CE (1992) Regulatory factors controlling photosynthetic reaction center and light-harvesting gene expression in *Rhodobacter capsulatus*. *Cell* 68:945–954
- Shah VK, Stacey G, Brill WJ (1983) Electron transport to nitrogenase. Purification and characterization of pyruvate:flavodoxin oxidoreductase, the *nifJ* gene product. *J Biol Chem* 258:12064–12068
- Shelver D, Kerby RL, He Y, Roberts GP (1995) Carbon monoxide-induced activation of gene expression in *Rhodospirillum rubrum* requires the product of *coaA*, a member of the cyclic AMP receptor protein family of transcriptional regulators. *J Bacteriol* 177:2157–2163
- Shen J, Dean DR, Newton WE (1997) Evidence for multiple substrate-reduction sites and distinct inhibitor-binding sites from an altered *Azotobacter vinelandii* nitrogenase MoFe protein. *Biochemistry* 36:4884–4894
- Strnad H, Lapidus A, Paces J, Ulbrich P, Vlcek C, Paces V, Haselkorn R (2010) Complete genome sequence of the photosynthetic purple nonsulfur bacterium *Rhodobacter capsulatus* SB1003. *J Bacteriol* 192:3545–3546
- Studholme DJ, Pau RN (2003) A DNA element recognized by the molybdenum-responsive transcription factor ModE is conserved in proteobacteria, green sulphur bacteria and archaea. *BMC Microbiol* 3:24
- Teixeira PF, Jonsson A, Frank M, Wang H, Nordlund S (2008) Interaction of the signal transduction protein GlnJ with the cellular targets AmtB1, GlnE and GlnD in *Rhodospirillum rubrum*: dependence on manganese, 2-oxoglutarate and the ADP/ATP ratio. *Microbiology* 154:2336–2347
- Teixeira PF, Wang H, Nordlund S (2010) Nitrogenase switch-off and regulation of ammonium assimilation in response to light deprivation in *Rhodospirillum rubrum* are influenced by the nitrogen source used during growth. *J Bacteriol* 192:1463–1466
- Tremblay P-L, Hallenbeck PC (2008) Ammonia-induced formation of an AmtB-GlnK complex is not sufficient for nitrogenase regulation in the photosynthetic bacterium *Rhodobacter capsulatus*. *J Bacteriol* 190:1588–1594
- Tremblay P-L, Hallenbeck PC (2009) Of blood, brains and bacteria, the Amt/Rh transporter family: emerging role of Amt as a unique microbial sensor. *Mol Microbiol* 71:12–22
- Tremblay P-L, Drepper T, Masepohl B, Hallenbeck PC (2007) Membrane sequestration of PII proteins and nitrogenase regulation in the photosynthetic bacterium *Rhodobacter capsulatus*. *J Bacteriol* 189:5850–5859
- Ureta A, Nordlund S (2002) Evidence for conformational protection of nitrogenase against oxygen in *Gluconacetobacter diazotrophicus* by a putative FeSII protein. *J Bacteriol* 184:5805–5809
- Van Heeswijk WC, Westerhoff HV, Booger FC (2013) Nitrogen assimilation in *Escherichia coli*: putting molecular data into a systems perspective. *Microbiol Mol Biol Rev* 77:628–695
- Wang G, Angermüller S, Klipp W (1993) Characterization of *Rhodobacter capsulatus* genes encoding a molybdenum transport system and putative molybdenum-pterin-binding proteins. *J Bacteriol* 175:3031–3042

- Wang H, Franke CC, Nordlund S, Norén A (2005) Reversible membrane association of dinitrogenase reductase activating glycohydrolase in the regulation of nitrogenase activity in *Rhodospirillum rubrum*; dependence on GlnJ and AmtB1. *FEMS Microbiol Lett* 253:273–279
- Wang L, Zhang L, Liu Z, Zhao D, Liu X, Zhang B, Xie J, Hong Y, Li P, Chen S, Dixon R, Li J (2013) A minimal nitrogen fixation gene cluster from *Paenibacillus* sp. WLY78 enables expression of active nitrogenase in *Escherichia coli*. *PLoS Genet* 9:e1003865
- Wiethaus J, Müller A, Neumann M, Neumann S, Leimkübler S, Narberhaus F, Masepohl B (2009) Specific interactions between four molybdenum-binding proteins contribute to Mo-dependent gene regulation in *Rhodobacter capsulatus*. *J Bacteriol* 191:5205–5215
- Wiethaus J, Wirsing A, Narberhaus F, Masepohl B (2006) Overlapping and specialized functions of the molybdenum-dependent regulators MopA and MopB in *Rhodobacter capsulatus*. *J Bacteriol* 188:8441–8451
- Wolfe DM, Zhang Y, Roberts GP (2007) Specificity and regulation of interaction between the PII and AmtB1 proteins in *Rhodospirillum rubrum*. *J Bacteriol* 189:6861–6869
- Yakunin AF, Hallenbeck PC (1998a) Purification and characterization of pyruvate oxidoreductase from the photosynthetic bacterium *Rhodobacter capsulatus*. *Biochim Biophys Acta* 1409:39–49
- Yakunin AF, Hallenbeck PC (1998b) Short-term regulation of nitrogenase activity by NH_4^+ in *Rhodobacter capsulatus*: multiple in vivo nitrogenase responses to NH_4^+ addition. *J Bacteriol* 180:6392–6395
- Yakunin AF, Hallenbeck PC (2002) AmtB is necessary for NH_4^+ -induced nitrogenase switch-off and ADP-ribosylation in *Rhodobacter capsulatus*. *J Bacteriol* 184:4081–4088
- Yakunin AF, Gennaro G, Hallenbeck PC (1993) Purification and properties of a *nif*-specific flavodoxin from the photosynthetic bacterium *Rhodobacter capsulatus*. *J Bacteriol* 175:6775–6780
- Yakunin AF, Laurinavichene TV, Tsygankov AA, Hallenbeck PC (1999) The presence of ADP-ribosylated Fe protein of nitrogenase in *Rhodobacter capsulatus* is correlated with cellular nitrogen status. *J Bacteriol* 181:1994–2000
- Yan L, Pelmentschikow V, Dapper CH, Scott AD, Newton WE, Cramer SP (2012) IR-monitored photolysis of CO-inhibited nitrogenase: a major EPR-silent species with coupled terminal CO ligands. *Chemistry* 18:16349–16357
- Zhang Y, Gladyshev VN (2008) Molybdoproteomes and evolution of molybdenum utilization. *J Mol Biol* 379:881–899
- Zhang Y, Gladyshev VN (2010) General trends in trace element utilization revealed by comparative genomic analysis of Co, Cu, Mo, Ni, and Se. *J Biol Chem* 285:3393–3405
- Zhang Y, Burris RH, Ludden PW, Roberts GP (1996) Presence of a second mechanism for the post-translational regulation of nitrogenase activity in *Azospirillum brasilense* in response to ammonium. *J Bacteriol* 178:2948–2993
- Zhang Y, Cummings AD, Burris RH, Ludden PW, Roberts GP (1995) Effect of an *ntrBC* mutation on the posttranslational regulation of nitrogenase activity in *Rhodospirillum rubrum*. *J Bacteriol* 177:5322–5326
- Zhang Y, Pohlmann EL, Ludden PW, Roberts GP (2000) Mutagenesis and functional characterization of the *glnB*, *glnA*, and *nifA* genes from the photosynthetic bacterium *Rhodospirillum rubrum*. *J Bacteriol* 182:983–992
- Zhang Y, Pohlmann EL, Ludden PW, Roberts GP (2001) Functional characterization of three GlnB homologs in the photosynthetic bacterium *Rhodospirillum rubrum*: roles in sensing ammonium and energy status. *J Bacteriol* 183:6159–6168
- Zhang Y, Pohlmann EL, Roberts GP (2004) Identification of critical residues in GlnB for its activation of NifA activity in the photosynthetic bacterium *Rhodospirillum rubrum*. *Proc Natl Acad Sci U S A* 101:2782–2787
- Zhang Y, Pohlmann EL, Roberts GP (2005) GlnD is essential for NifA activation, NtrB/NtrC-regulated gene expression, and posttranslational regulation of nitrogenase activity in the photosynthetic, nitrogen-fixing bacterium *Rhodospirillum rubrum*. *J Bacteriol* 187:1254–1265
- Zhang Y, Wolfe DM, Pohlmann EL, Conrad MC, Roberts GP (2006) Effect of AmtB homologues on the post-translational regulation of nitrogenase activity in response to ammonium and energy signals in *Rhodospirillum rubrum*. *Microbiology* 152:2075–2089

Zhou X, Zhu Y, Pohlmann EL, Li J, Zhang Y, Roberts GP (2008) Identification and functional characterization of NifA variants that are independent of GlnB activation in the photosynthetic bacterium *Rhodospirillum rubrum*. *Microbiology* 154:2689–2699

Zhu Y, Conrad MC, Zhang Y, Roberts GP (2006) Identification of *Rhodospirillum rubrum* GlnB variants that are altered in their ability to interact with different targets in response to nitrogen status signals. *J Bacteriol* 188:1866–1874

Sulfur Metabolism in Phototrophic Bacteria

Christiane Dahl

Abstract Sulfur is one of the most versatile elements in life due to its reactivity in different oxidation and reduction states. In contrast to the assimilatory provision of sulfur-containing cell constituents that is found in most taxonomic groups, dissimilation is restricted to prokaryotes and serves energy-yielding processes where sulfur compounds are donors or acceptors of electrons. In many anoxygenic phototrophic bacteria, reduced sulfur compounds play a prominent role as electron donors for photosynthetic carbon dioxide fixation. This process is especially characteristic for the green sulfur bacteria (GSB) and the purple sulfur bacteria (PSB). *Allochromatium vinosum* and *Chlorobaculum tepidum*, representatives of the PSB and GSB, respectively, are the workhorses for detailed elucidation of sulfur oxidation pathways. Genes identified in these organisms served as the basis of a genome-based survey of the distribution of genes involved in the oxidation of sulfur compounds in other genome-sequenced anoxygenic phototrophs. These analyses show that dissimilatory sulfur metabolism is very complex and built together from various modules encoding different enzymes in the different organisms. Comparative genomics in combination with biochemical data also provide a clear picture of sulfate assimilation in anoxygenic phototrophs.

Keywords Sulfur metabolism • Purple sulfur bacteria • Sulfur globules • Sulfide • Thiosulfate • Tetrathionate • Sulfate • *Allochromatium vinosum* • Green sulfur bacteria • Sulfur oxidation • Assimilatory sulfate reduction

Introduction

Sulfur exhibits high reactivity in reduced forms and occurs in several stable oxidation states. Sulfate or sulfide in water and soil and sulfur dioxide in the atmosphere constitute the majority of sulfur in nature (Middelburg 2000). Smaller but significant roles are played by polysulfide, polythionates, thiosulfate, sulfoxides, as well

C. Dahl (✉)

Institut für Mikrobiologie & Biotechnologie, Rheinische Friedrich-Wilhelms-Universität
Bonn, Meckenheimer Allee 168, 53115 Bonn, Germany
e-mail: ChDahl@uni-bonn.de

as elemental sulfur. Sulfur is the element with the highest number of allotropes but only a few occur in biological systems. Sulfur appears in all organisms in many different organic compounds such as amino acids, enzyme cofactors, (poly)peptides, sulfolipids, vitamins, or carbohydrates. The biological roles of inorganic sulfur compounds are comparatively restricted: (1) They can serve as sources for sulfur assimilation and incorporation into the abovementioned organic compounds. (2) They can be employed as donors or acceptors of electrons for energy-generating electron transport. Dissimilatory sulfur-based energy generation goes along with mass transformations and occurs almost exclusively among prokaryotes, while assimilatory sulfur metabolism is not only very common in prokaryotes but also occurs in plants, algae, and fungi.

In oxygenic phototrophic organisms, the redox properties of sulfur-containing metabolites and of sulfur in proteins are very important for the interplay between the reductive assimilative processes of photosynthesis and reactive oxygen species that are formed as side products of photosynthetic electron transport (Dahl et al. 2008b). In anoxygenic phototrophic bacteria, reduced sulfur compounds can play a particularly important role as electron donors for photosynthetic carbon dioxide fixation. In fact, the utilization of sulfur compounds is common to almost all groups of phototrophic prokaryotes: certain species of the cyanobacteria can perform anoxygenic photosynthesis at the expense of sulfide as an electron donor (Arieli et al. 1991, 1994; Shahak and Hauska 2008). A few representatives of the strictly anaerobic Gram-positive heliobacteria as well as members of the filamentous anoxygenic phototrophic (FAP) bacteria of the phylum *Chloroflexi* are able to oxidize reduced sulfur compounds, thiosulfate oxidation is widespread among the photoheterotrophic aerobic anoxygenic phototrophic bacteria, and many of the classical purple non-sulfur bacteria can use thiosulfate and/or sulfide as electron donors. Utilization of reduced sulfur compounds is best known and studied for the purple (families *Chromatiaceae* and *Ectothiorhodospiraceae*) and green sulfur bacteria (phylum *Chlorobi*).

In this chapter the sulfur-oxidizing capabilities of the various groups of phototrophic bacteria will be only briefly described. The reader is referred to a number of previous reviews that still provide valuable sources of information on sulfur compounds used by the various groups as well as on sulfur oxidation patterns (Brune 1989; Brune 1995b; Dahl 2008; Frigaard and Bryant 2008a, b; Frigaard and Dahl 2009; Gregersen et al. 2011; Sander and Dahl 2009). Here, I will focus on new developments arising from studies performed during the past 8–10 years that substantially broadened our knowledge of the biochemical details of the different sulfur oxidation pathways. In addition, a substantial number of additional genome sequences for purple sulfur bacteria became available that allows to draw additional information from comparative analyses of gene arrangements and occurrence. Transcriptomic profiling and comparative proteome analyses for phototrophic model organisms provide further crucial information resources (Eddie and Hanson 2013; Falkenby et al. 2011; Weissgerber et al. 2013, 2014a). A brief overview of assimilatory sulfate reduction metabolism will also be given. Organosulfur compound metabolism will not be dealt with here, and the reader is referred to information provided by others (Baldock et al. 2007; Denger et al. 2004, 2006; Kappler and Schäfer 2014; Visscher and Taylor 1993).

Sulfur Oxidation Capabilities of Phototrophic Bacteria

In the following section, the sulfur oxidation capabilities of the various groups of anoxygenic phototrophic bacteria are very briefly summarized.

Purple Sulfur Bacteria

Purple sulfur bacteria of the families *Chromatiaceae* and *Ectothiorhodospiraceae* preferentially use reduced sulfur compounds as electron donors during photolithoautotrophic growth. The most important difference between the two families is that *Chromatiaceae* produce intracellular sulfur globules when growing on sulfide, thiosulfate, polysulfides, or elemental sulfur, while the *Ectothiorhodospiraceae* accumulate extracellular sulfur. For one member of the *Ectothiorhodospiraceae*, *Thiorhodospira sibirica*, extra- as well as intracellular sulfur deposition has been reported (Bryantseva et al. 1999). All phototrophic members of the *Chromatiaceae* use sulfide and sulfur of the oxidation state zero as photosynthetic electron donors. Several species are limited to these compounds while a range of more versatile species uses several reduced sulfur compounds including thiosulfate and sulfite. Polysulfide oxidation is probably ubiquitous. This does not appear astonishing because polysulfides are formed as intermediates of the oxidation of sulfide en route to sulfur globules (Prange et al. 2004). Polysulfides are especially stable intermediates of sulfide oxidation by members of the *Ectothiorhodospiraceae* because these thrive under alkaline growth conditions which are essential for longer-term stability of polysulfides. Utilization of sulfide, elemental sulfur, and thiosulfate is common to the species of the genus *Ectothiorhodospira*, while species of the genera *Halorhodospira* and *Thiorhodospira* oxidize sulfide to sulfur which is further oxidized to sulfate by some species. Thiosulfate is used only by *Halorhodospira halophila* (Raymond and Sistrom 1969).

Green Sulfur Bacteria

GSB exhibit very little variation in their ability to oxidize sulfur compounds. Almost all members of this group oxidize sulfide and elemental sulfur to sulfate. The only exception is *Chlorobium ferrooxidans* for which only Fe^{2+} and hydrogen are suitable photosynthetic electron donors. In general, GSB have a very high affinity for sulfide, and it is the preferred sulfur substrate even in the presence of other reduced sulfur compounds. Typically, sulfide is first transformed into zero-valent sulfur which is deposited as extracellular sulfur globules. Some strains of the genera *Chlorobaculum* and *Chlorobium* can oxidize thiosulfate (Imhoff 2003), and one strain has been reported to be capable of tetrathionate utilization (Khanna and Nicholas 1982).

Purple Non-sulfur Bacteria

Purple non-sulfur bacteria are to a much lesser extent capable of tolerating and using toxic sulfur compounds such as sulfide than the PSB. The phototrophic *Betaproteobacteria* of the orders *Rhodocyclales* and *Burkholderiales* have not been reported to use reduced sulfur compounds as electron donors. Sulfide inhibits growth at low concentrations (Imhoff et al. 2005). In the genome of *Rubrivivax gelatinosus*, *sox* genes are present indicating the potential for thiosulfate oxidation (Sander and Dahl 2009). Sulfate can be reductively assimilated. Within the alphaproteobacterial purple non-sulfur bacteria, the ability to use reduced sulfur compounds is widespread. Intermediates and final products formed vary considerably between species. Complete oxidation of sulfide to sulfate has been described for several species (Frigaard and Dahl 2009; Imhoff et al. 2005; Sander and Dahl 2009). Thiosulfate is used by many species and either completely oxidized to sulfate or transformed into tetrathionate. Sulfur is also used as a substrate by some species (Sander and Dahl 2009).

Aerobic Bacteriochlorophyll-Containing Bacteria

Aside from cyanobacteria and proteorhodopsin-containing bacteria, aerobic anoxygenic phototrophic (AAP) bacteria are the third most numerous group of phototrophic prokaryotes in the ocean. This functional group represents a diverse assembly of species which taxonomically belong to various subgroups of *Alpha-*, *Beta-*, and *Gammaproteobacteria*. AAP bacteria are facultative photoheterotrophs which use bacteriochlorophyll-containing reaction centers to harvest light energy under fully oxic in situ conditions (Koblizek 2015). Almost 60 strains of AAP are currently fully genome sequenced (tabulated in Koblizek 2015).

In general AAP bacteria cannot grow photolithoautotrophically on reduced sulfur compounds. However, many representatives of this physiological group can oxidize sulfur compounds as additional sources of electrons and grow as sulfur-oxidizing lithoheterotrophs. The ability for thiosulfate oxidation appears to be especially widespread (Sorokin et al. 2000; Yurkov et al. 1994). The genomes of many AAP bacteria contain the genes *soxB*, *soxAX*, *soxYZ*, and *soxCD* encoding a periplasmic thiosulfate-oxidizing multienzyme complex (Friedrich et al. 2005; Sander and Dahl 2009). A recent study furthermore revealed that *sox* genes are present mainly in those members of the widespread and ecologically very important OM60/NOR5 clade that also encode genes enabling aerobic anoxygenic photoheterotrophy, like *Congregibacter litoralis* (*C. litoralis*) DSM 17192^T, *Congregibacter* sp. strain NOR5-3, or *Luminiphilus syltensis* DSM 22749^T (Spring 2014). However, a stringent correlation of genes encoding Sox proteins and subunits of the photosynthetic apparatus was not apparent, because some bacteriochlorophyll *a*-containing strains do not encode Sox proteins.

Acidobacteria

The phylum *Acidobacteria*, a sister clade to the δ -*Proteobacteria* in the domain *Bacteria*, encompasses a large and physiologically diverse group of microorganisms (Ciccarelli et al. 2006). Recently, a phototrophic member of this group was described, *Chloracidobacterium thermophilum* (Bryant et al. 2007; Tank and Bryant 2015a, 2015b), the first aerobic chlorophototroph that has a type I, homodimeric reaction center (RC). Key genes for all known carbon fixation pathways are absent as are genes for assimilatory sulfate reduction. *Cab. thermophilum* is unable to use sulfate as a sulfur source and instead relies on reduced sulfur sources such as thio-glycolate, cysteine, methionine, or thiosulfate. Cultures containing sodium sulfide did not show sustained growth, but microscopic analyses revealed that sulfur globules were produced. Similar to green sulfur bacteria, these globules remained associated with the outer surfaces of cells and suggested that sulfide oxidation occurred. The genome lacks any known enzymes for the oxidation of sulfide, so how sulfide oxidation occurs is not clear (Tank and Bryant 2015b).

Phototrophic Gemmatimonadetes

Very recently a BChl *a*-producing, semiaerobic anoxygenic photoheterotroph from the phylum *Gemmatimonadetes*, *Gemmatimonas phototrophica*, has been described (Zeng et al. 2014, 2015). Sulfur oxidation capabilities have not been reported. None of the genome-sequenced members of the *Gemmatimonadetes* contain *sox* genes.

Sulfur Oxidation Pathways

With regard to their sulfur metabolism, phototrophic bacteria are characterized by a great variability of sulfur substrates used and pathways employed. On a molecular genetic and biochemical level, sulfur oxidation is best described in the purple sulfur bacterium *Allochromatium vinosum* and in the green sulfur bacterium *Chlorobaculum tepidum*. An overview of the currently proposed model of sulfur oxidation in *A. vinosum* is shown in Fig. 1. The figure is based on a combination of biochemical evidence, genome sequence information, as well as whole genome transcriptomic profiling and comparative quantitative proteomics (Weissgerber et al. 2011, 2013, 2014a).

Many enzymes involved in sulfur metabolism can readily be identified in genome sequences by sequence homology with known enzymes. The genome sequences of 15 strains of GSB have already been available for several years, and the occurrence of genes related to sulfur oxidation in these organisms has already been extensively tabulated and discussed (Frigaard and Bryant 2008b; Frigaard and Dahl 2009; Gregersen et al. 2011; Venceslau et al. 2014). A greater number of genome sequences

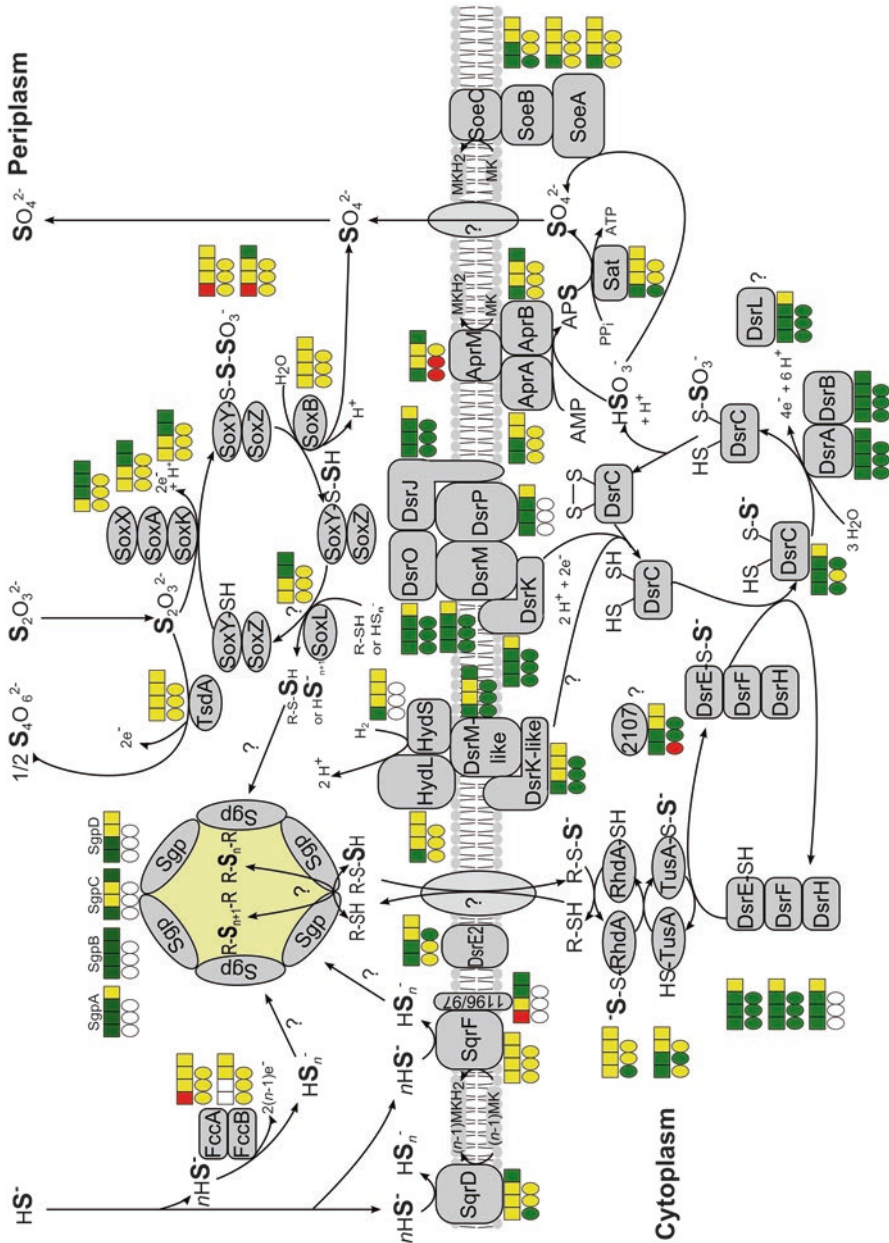


Fig. 1 Current model of sulfur oxidation in *Allochromatium vinosum* (Figure taken from Weissgerber et al. 2014a) (Copyright © American Society for Microbiology, Applied and Environmental Microbiology 80, 2014, 2279–92, doi: [10.1128/AEM.04182-13](https://doi.org/10.1128/AEM.04182-13)). The proteomic profiles (circles) and transcriptomic profiles (boxes) are depicted next to the respective proteins. Relative fold changes in mRNA levels above 2 (green) were considered significant enhancement. Relative changes smaller than 0.5 (red) were considered to indicate significant decreases in mRNA levels. Relative fold changes between 0.5 and 2 (yellow) indicated unchanged mRNA levels.

for purple sulfur bacteria only became available over the last few years (Table 1). This chapter will therefore focus on analyzing this comparatively new set of sequence information.

Oxidation of Thiosulfate

Thiosulfate ($S_2O_3^{2-}$) oxidation is conducted by a large number of photo- and chemotrophic sulfur-oxidizing bacteria. In general, two completely different pathways can be differentiated. In the first, two thiosulfate anions are oxidized to tetrathionate. In the second, catalyzed by the periplasmic Sox multienzyme system (Dahl et al. 2008a; Friedrich et al. 2001), multiple steps lead to complete oxidation to sulfate. In some bacteria including *A. vinosum* both pathways coexist (Hensen et al. 2006; Smith and Lascelles 1966). The occurrence of genes related with the two pathways in purple sulfur bacteria is summarized in Table 2.

Oxidation of Thiosulfate to Tetrathionate

The ability to perform the very simple oxidation of two molecules of thiosulfate to tetrathionate according to the equation $2 S_2O_3^{2-} \rightarrow S_4O_6^{2-} + 2e^-$ is widespread among prokaryotes. The reaction is not only well-established intermediate step in the oxidation of reduced sulfur compounds to sulfate in many obligately chemolithoautotrophic bacteria (Lu and Kelly 1988; Müller et al. 2004; Wentzien et al. 1994) but also known for some purple non-sulfur bacteria like *Rhodomicrobium vannielii* and *Rhodospila globiformis* and purple sulfur bacteria including *A. vinosum* (Frigaard and Dahl 2009; Hensen et al. 2006; Then and Trüper 1981).

Despite the well-documented significance of tetrathionate formation in aquatic and terrestrial habitats (Barbosa-Jefferson et al. 1998; Podgorsek and Imhoff 1999; Sorokin 2003), the membrane-bound *doxDA* encoding thiosulfate/quinone oxidoreductase from the thermoacidophilic archaeon *Acidianus ambivalens* was the only tetrathionate-forming enzyme characterized on a molecular level for a long time (Müller et al. 2004). Genes homologous to *doxDA* do not occur in phototrophic prokaryotes. Instead, a gene (*tsdA*) encoding a novel periplasmic 27.2 kDa diheme cytochrome *c* thiosulfate dehydrogenase was identified in *A. vinosum* (Denkman et al. 2012). The crystal structure of the enzyme revealed two typical class I *c*-type

←
Fig. 1 (continued) The same color coding is applied to changes on the protein level. Here, values above 1.5 (*green*) and below 0.67 (*red*) were considered significant. Those cases where transcriptomic data were not available or the respective protein was not detected in the proteomic approach are indicated by *white squares or circles*. Changes are depicted that occurred upon a switch from photoorganoheterotrophic growth on malate to photolithoautotrophic growth on, from left to right, sulfide, thiosulfate, elemental sulfur, and sulfite. Changes on sulfite were not determined on the proteome level

Table 1 Genome-sequenced purple sulfur bacteria

Organism	Accession number	S ²⁻	S ⁰	S ₂ O ₃ ²⁻	Reference (genome or organism)
<i>Chromatiaceae</i>					
<i>Allochromatium vinosum</i> DSM 180 ^T	NC_013851, NC_013852, NC_013851	+	+	+	Weissgerber et al. (2011)
<i>Thiorhodovibrio</i> sp. 970	NZ_AFW02000000	+	+	-	Unpublished
<i>Lamprocystis purpurea</i> DSM 4197	NZ_ARBC00000000	+	+	+	Imhoff (2001)
<i>Thiocapsa marina</i> 5811 DSM 5653 ^T	NZ_AFWV00000000	+	+	+	Caumette et al. (2004)
<i>Thiocapsa</i> sp. KS1	CVPF01000000	+	+	+	Unpublished
<i>Thiohalocapsa</i> ML1	GCA_001469165	+	+	+	Hamilton et al. (2014)
<i>Thiorhodococcus</i> sp. AK35	NZ_AONC01000000	+	+	+	Unpublished
<i>Thiorhodococcus drewsii</i> AZ1 DSM 15006 ^T	NZ_AFWT00000000	+	+	+	Zaar et al. (2003)
<i>Thiocystis violascens</i> DSM 198 ^T	NC_018012	+	+	+	Imhoff et al. (1998)
<i>Marichromatium purpuratum</i> 984 DSM 1591 ^T	NZ_CP007031	+	+	+	Imhoff et al. (1998)
<i>Thioflaviococcus mobilis</i> DSM 8321 ^T	NC_019940, NC_019941	+	+	-	Imhoff and Pfennig (2001)
<i>Ectothiorhodospiraceae</i>					
<i>Halorhodospira halophila</i> SL1 DSM 244 ^T	NC_008789	+	+	+	(Challacombe et al. 2013)
<i>Halorhodospira halochloris</i> str. A DSM 1059 ^T	CP007268	+	-	+	Singh et al. (2014)
<i>Thiorhodospira sibirica</i> ATCC 700588 ^T	NZ_AGFD00000000	+	+	-	Bryantseva et al. (1999)
<i>Ectothiorhodospira haloalkaliphila</i> ATCC 51935 ^T	NZ_AJUE00000000	+	+	+	(Imhoff and Siling 1996)
<i>Ectothiorhodospira</i> sp. PHS-1	AGBG00000000	nd	nd	nd	Kulp et al. (2008)

cytochrome domains wrapped around two hemes. Heme 1 exhibits His/Cys iron coordination and constitutes the active site of the enzyme (Brito et al. 2015). His/Cys heme iron ligation is rare among prokaryotes, usually leads to a low redox potential of the corresponding heme (Bradley et al. 2012; Kappler et al. 2008; Pires et al. 2006; Reijerse et al. 2007), and appears to be of special importance in sulfur-based energy metabolism. In the oxidized state, Heme 2 iron is axially ligated by a histidine and a lysine residue (Fig. 2). Upon reduction, a switch occurs at this heme

Table 2 Genes related to thiosulfate oxidation in genome-sequenced purple sulfur bacteria^a

Organism	<i>soxBXAKL</i>	<i>soxYZ</i>	<i>tsdBA</i>
<i>Chromatiaceae</i>			
<i>Allochromatium vinosum</i> DSM 180 ^T	Alvin_2167–2171	Alvin_2111/12	Alvin_0091 (only <i>tsdA</i>)
<i>Thiorhodovibrio</i> sp. 970	–	Thi970DRAFT_01660	Thi970DRAFT_02035/36
<i>Lamprocystis purpurea</i> DSM 4197	WP_026199596, WP_020506632–36	WP_020506368/67	–
<i>Thiocapsa marina</i> 5811 DSM 5653 ^T	ThimaDRAFT_4579–75	ThimaDRAFT_0728/29, 3536–37	–
<i>Thiocapsa</i> sp. KS1	THIOKS1620009–14	THIOKS11770013/12	–
<i>Thiohalocapsa</i> ML1	WP_058554073–79	WP_058556710/09	–
<i>Thiorhodococcus</i> sp. AK35	D779_4156–52	D779_3946–47	D779_1816 (<i>tsdBA</i> fusion)
<i>Thiorhodococcus drewsii</i> AZ1 DSM 15006 ^T	ThidrDRAFT_2415–19	ThidrDRAFT_2534/35	ThidrDRAFT_3922 (<i>tsdBA</i> fusion)
<i>Thiocystis violascens</i> DSM 198 ^T	Thivi_2200, Thivi_3804–01	Thivi_3138/39	Thivi_3993 (<i>tsdBA</i> fusion)
<i>Marichromatium purpuratum</i> 984 DSM 1591 ^T	MARPU_05475–55	MARPU_13720/15	MARPU_02550 (<i>tsdBA</i> fusion)
<i>Thioflavococcus mobilis</i> DSM 8321 ^T	–	–	Thimo_0460 (<i>tsdBA</i> fusion)
<i>Ectothiorhodospiraceae</i>			
<i>Haloerhodospira halophila</i> SL1 DSM 244 ^T	Hhal_1939, Hhal_1948 (<i>soxXA</i> fusion), no <i>soxKL</i>	Hhal_1941/42	–
<i>Haloerhodospira halochloris</i> str. A DSM 1059 ^T	M911_11275 (<i>soxB</i>), no <i>soxBXAKL</i>	M911_11265/70	–
<i>Thiorhodospira sibirica</i> ATCC 700588 ^T	–	ThisDRAFT_0337/36	–
<i>Ectothiorhodospira haloalkaliphila</i> ATCC 51935 ^T	WP_025282121 (<i>soxB</i>), no <i>soxBXAKL</i>	No <i>soxY</i> , WP_025282120 (<i>soxZ</i>)	–
<i>Ectothiorhodospira</i> sp. PHS1	ECTPHS_10791, (<i>soxB</i>), no <i>soxBXAKL</i>	ECTPHS_10801/796	–

^aGenomes were analyzed by BLAST searches using the resources provided by Integrated Microbial Genomes (DOE Joint Genomes Institute, <http://img.jgi.doe.gov>) and GenBank (<http://www.ncbi.nlm.nih.gov>). Bait: *soxBXAKL* (ADC63088–ADC63092), *soxYZ* (*soxY*, ADC63033; *soxZ*, ADC63034), and *TsdA* (ADC61061) from *A. vinosum*, *TsdB* from *Thiomonas intermedia* (D5WYQ6)

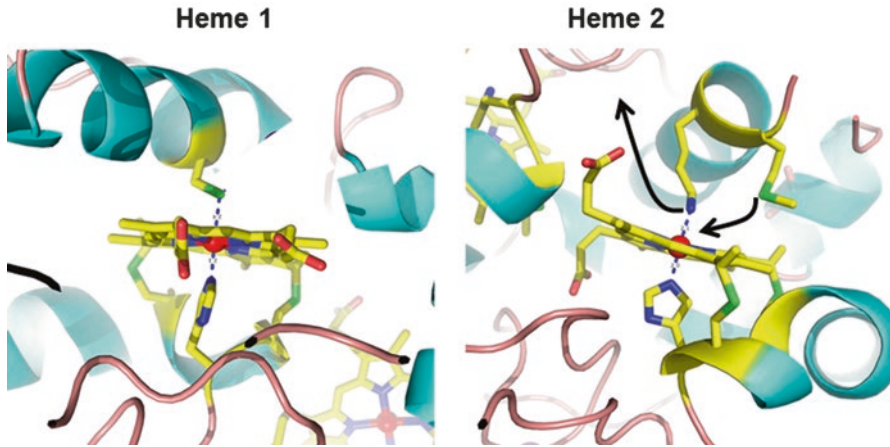


Fig. 2 Heme coordination of *A. vinosum* TsdA (Brito et al. 2015). *Left*: Heme 1 is coordinated by His⁵³ and Cys⁹⁶. *Right*: Heme 2 is coordinated by His^{His165} and Lys²⁰⁸. Upon reduction, a ligand switch from Lys²⁰⁸ to Met²⁰⁹ occurs. Sulfur atoms are shown in green

from Lys to Met axial ligation. This change probably affects the redox potential of Heme 2 and may be an important step during the reaction cycle (Brito et al. 2015).

TsdA enzymes of various source organisms exhibit different catalytic bias (Kurth et al. 2015). While the enzyme from the sulfur oxidizer *A. vinosum* is strongly biased toward catalyzing thiosulfate oxidation (Brito et al. 2015), TsdA from *Campylobacter jejuni* acts primarily as a tetrathionate reductase and enables the organism to use tetrathionate as alternative electron acceptor for anaerobic respiration (Liu et al. 2013).

Currently it is largely unclear which redox carriers mediate the flow of electrons arising from thiosulfate oxidation into respiratory or photosynthetic electrons chains. In several organisms including *Thiomonas intermedia*, *Sideroxydans lithotrophicus*, and *Pseudomonas stutzeri*, *tsdA* is immediately preceded by a gene encoding another diheme cytochrome, TsdB (Denkmann et al. 2012). TsdB is not itself reactive with thiosulfate but accepts electrons from TsdA even when TsdA and TsdB do not originate from the same source organism (Denkmann et al. 2012). In the anoxygenic phototrophic purple sulfur bacterium *Marichromatium purpuratum*, TsdA and TsdB form a fusion protein with TsdB constituting the amino-terminal domain. TsdBA fusion proteins are also encoded in other members of the *Chromatiaceae*, e.g., *Thiorhodococcus* sp. AK35, *Thiocystis violascens*, *Thiorhodococcus drewsii*, and *Thioflaviococcus mobilis* (Table 2). However, TsdBA fusions are not a common trait in purple sulfur bacteria. In *A. vinosum*, a *tsdB* gene is not present (Denkmann et al. 2012). In *A. vinosum*, the protein with the closest relationship to *T. intermedia* or *P. stutzeri* TsdB is Alvin_2879. This cytochrome *c*₄ (previously cytochrome *c*⁻⁵⁵³⁽⁵⁵⁰⁾) is membrane bound possibly via the hydrophobic protein Alvin_2880 and has a positive redox potential of +330 mV (Cusanovich and Bartsch 1969).

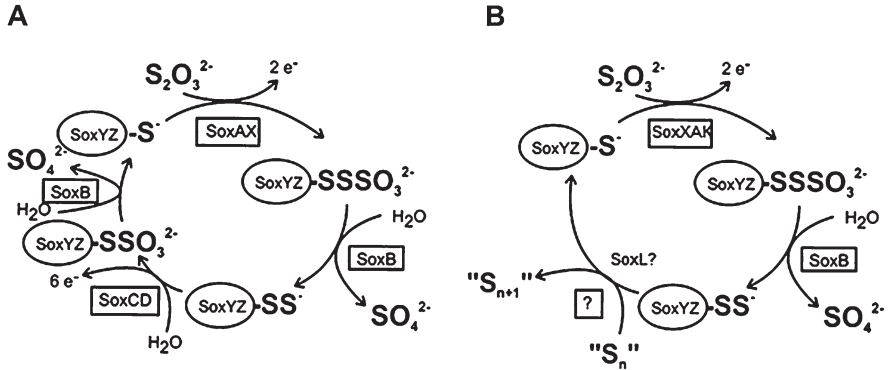


Fig. 3 Model of Sox-mediated thiosulfate oxidation in *Paracoccus pantotrophus* (left) and (a) *A. vinosum* (right). Adapted from (Sander and Dahl 2009). All reactions take place in the periplasm

Another candidate for accepting electrons from TsdA in purple anoxygenic phototrophic bacteria is the high potential iron-sulfur protein (HiPIP). *A. vinosum* and *M. purpuratum* produce HiPIP, and as this protein has a quite positive reduction potential (+350 mV) (Bartsch 1978), it would be well suitable as an electron acceptor for TsdA.

Oxidation of Thiosulfate to Sulfate

The Sox pathway of thiosulfate oxidation is a prime example for the oxidation of protein-bound sulfur atoms in the bacterial periplasm (Friedrich et al. 2001; Zander et al. 2010). Among the many organisms pursuing this pathway, some store sulfur globules as intermediates (e.g., *A. vinosum*), whereas others do not form sulfur deposits (e.g., *Paracoccus pantotrophus*). The Sox pathway in these two physiological groups appears to have one fundamental difference, and this is the involvement of the hemomolybdoprotein SoxCD (Fig. 3).

In non-sulfur-storing organisms, the proposed mechanism for sulfur oxidation requires four different proteins: SoxB, SoxXA, SoxYZ, and SoxCD (Friedrich et al. 2001). The heterodimeric SoxYZ protein acts as the central player and carries pathway intermediates covalently bound to a cysteine residue located near the carboxy-terminus of the SoxY subunit (Appia-Ayme et al. 2001; Quentmeier and Friedrich 2001; Sauvé et al. 2007). The *c*-type cytochrome SoxXA(K) catalyzes the oxidative formation of a disulfide linkage between the sulfane sulfur of thiosulfate and the cysteine of SoxY (Bamford et al. 2002; Ogawa et al. 2008). The sulfone group is then hydrolytically released as sulfate in a reaction catalyzed by SoxB (Sauvé et al. 2009). The next step is oxidation of the SoxY-bound sulfane sulfur to a sulfone by the hemomolybdoprotein SoxCD and again hydrolytic release of sulfate (Zander et al. 2010).

In those organisms forming sulfur as an intermediate, SoxCD is not present and the SoxY-bound sulfane sulfur is transferred to zero-valent sulfur stored in sulfur globules residing in the periplasm by an unknown mechanism, possibly involving the rhodanese-like protein SoxL (Welte et al. 2009). In *A. vinosum*, *sox* genes are present in two clusters (*soxBXAKL*, Alvin_2167 to 2171, and *soxYZ*, Alvin_2111 and 2112) with *soxBXA* and *soxYZ* being indispensable for thiosulfate oxidation (Hensen et al. 2006). The protein encoded by *soxK* has been identified as a subunit of a SoxXAK complex in the green sulfur bacterium *Chlorobaculum tepidum* (Ogawa et al. 2008) and probably fulfills the same function in purple sulfur bacteria.

Oxidation of Sulfide

Different enzymes are candidates for sulfide oxidation: sulfide/quinone oxidoreductases (SQR) (Schütz et al. 1997) and a flavocytochrome *c* sulfide dehydrogenase (FccAB) (Chen et al. 1994; Meyer and Cusanovich 2003) (Table 3). In *Rhodovulum sulfidophilum*, a member of the *Rhodobacteraceae*, the Sox system is not only essential for thiosulfate oxidation but also indispensable for the oxidation of sulfide in vivo (Appia-Ayme et al. 2001). The same might well be the case for other non-sulfur bacteria containing *sox* genes. In *A. vinosum* mutants deficient in either flavocytochrome *c* (Reinartz et al. 1998), *sox* genes (Hensen et al. 2006), or both (D. Hensen, B. Franz, C. Dahl, unpublished), sulfide oxidation proceeds with wild-type rates indicating that SQR plays the major role.

All characterized SQRs are single-subunit flavoproteins associated with the cytoplasmic membrane (Marcia et al. 2009, 2010b; Shahak and Hauska 2008). Based on the protein structure, six distinct SQR types were identified (Marcia et al. 2010a). Here, the nomenclature suggested by Frigaard and coworkers is followed (Gregersen et al. 2011) to clearly identify the multiple types of *sqr* genes often found in the same organism (Table 3). Members of types SqrA, SqrB, SqrC, SqrE, and SqrF have been biochemically characterized (Arieli et al. 1994; Brito et al. 2009; Cherney et al. 2010; Griesbeck et al. 2002; Marcia et al. 2009; Shuman and Hanson 2016; Zhang and Weiner 2014). The SqrA type exemplified by the functionally well-characterized enzyme from the cyanobacterium *Oscillatoria limnetica* (Bronstein et al. 2000) and the purple non-sulfur bacterium *Rhodobacter capsulatus* (Schütz et al. 1999) does neither occur in green (Gregersen et al. 2011) nor in purple sulfur bacteria (Table 3). The same holds true for SqrE. The SqrD and SqrF types appear to be especially widespread in the family *Chromatiaceae*, while members of the *Ectothiorhodospiraceae* all contain a gene encoding SqrB. The SqrF-type enzyme from *C. tepidum* has recently been shown to have a low affinity for sulfide and a high enzymatic turnover rate consistent with a function as a high sulfide adapted SQR (Chan et al. 2009; Eddie and Hanson 2013). The primary reaction product of the SQR reaction is soluble polysulfide (Griesbeck et al. 2002).

In a variety of sulfide-oxidizing species, flavocytochrome *c* is present as a soluble protein in the periplasm or as a membrane-bound enzyme (Kostanjevecki et al. 2000). The protein consists of a larger flavoprotein (FccB) and a smaller hemoprotein

Table 3 Genes related to sulfide oxidation in genome-sequenced purple sulfur bacteria^a

Organism	<i>sqrB</i>	<i>sqrC</i>	<i>sqrD</i>	<i>sqrF</i>	Alvin_1196/97	<i>fccBA</i>
<i>Chromatiaceae</i>						
<i>Allochromatium vinosum</i> DSM 180 ^T	-	-	Alvin_2145	Alvin_1195	Alvin_1196/97	Alvin_1092/93
<i>Thiorhodovibrio</i> sp. 970	-	-	Thi970DRAFT_02097	Thi970DRAFT_01366	Thi970DRAFT_01366	Thi970DRAFT_02375/76
<i>Lamprocystis purpurea</i> DSM 4197	-	-	WP_020502950	WP_020508508	-	WP_020504674/73
<i>Thiocapsa marina</i> 5811 DSM 5653 ^T	-	-	ThimaDRAFT_0111	ThimaDRAFT_0710	-	ThimaDRAFT_3288/87 ThimaDRAFT_4140/39
<i>Thiocapsa</i> sp. KS1	-	THIOKS1270020	THIOKS12830013	THIOKS11770025	-	THIOKS11060009/07, THIOKS12860008/09
<i>Thiohalocapsa</i> ML1	-	-	WP_058557406	WP_058558070	-	WP_058554707/06
<i>Thiorhodococcus</i> sp. AK35	-	-	D779_2797	D779_4227	D779_0811/12	D779_2091/90
<i>Thiorhodococcus drewsii</i> AZ1 DSM 15006 ^T	-	-	ThidrDRAFT_1076	ThidrDRAFT_2526	ThidrDRAFT_3416/17	-
<i>Thiocystis violascens</i> DSM 198 ^T	-	-	Thivi_0965	Thivi_3129	-	Thivi_4480/81, Thivi_1815/16
<i>Marichromatium purpuratum</i> 984 DSM 1591 ^T	-	MARPU_16030	MARPU_12080	MARPU_13750	-	MARPU_11175/70
<i>Thioflavococcus mobilis</i> DSM 8321 ^T	-	-	Thimo_0569	Thimo_1567	-	Thimo_2236/35

(continued)

Table 3 (continued)

Organism	<i>sqrB</i>	<i>sqrC</i>	<i>sqrD</i>	<i>sqrF</i>	Alvin_1196/97	<i>fccBA</i>
<i>Ectothiorhodospiraceae</i>						
<i>Halorhodospira halophila</i> SL1 DSM 244 ^T	Hhal_1665	–	–	–	–	Hhal_1331, Hhal_1163, no <i>fccA</i>
<i>Halorhodospira halochloris</i> str. A DSM 1059 ^T	M911_12365	–	–	–	–	M911_16440, no <i>fccA</i>
<i>Thiorhodospira sibirica</i> ATCC 700588 ^r	ThisiDRAFT_1596	–	ThisiDRAFT_0159	–	–	ThisiDRAFT_0473, no <i>fccA</i>
<i>Ectothiorhodospira haloalkaliphila</i> ATCC 51935 ^T	WP_025282304	–	–	–	–	WP_025283024, no <i>fccA</i>
<i>Ectothiorhodospira</i> sp. PHS1	ECTPHS_10089	–	–	–	–	ECTPHS_01469, no <i>fccA</i>

^aGenomes were analyzed by BLAST searches using the resources provided by Integrated Microbial Genomes (DOE Joint Genomes Institute, <http://img.jgi.doe.gov>) and GenBank (<http://www.ncbi.nlm.nih.gov>). Baits: *FccAB* from *A. vinosum* (AAA23316 and AAB86576), *SqrA* from *Aquifex aeolicus* (NP_214500), *SqrB* from *Halorhodospira halophila* (WP_011814451), *SqrC* from *Chlorobaculum tepidum* (NP_661917), *SqrD* from *Chlorobaculum tepidum* (NP_661023), *SqrE* from *Chlorobaculum tepidum* (NP_661769), *SqrF* from *Aquifex aeolicus* (NP_213539)

(FccA) subunit. The proteins show sulfide/cytochrome *c* activity in vitro (Bosshard et al. 1986). FccAB occurs in many purple and green sulfur bacteria but there are also species that lack it (Frigaard and Dahl 2009; Sander and Dahl 2009). It is possible that FccAB is advantageous under certain growth conditions, and it has been speculated that it might represent a high-affinity system for sulfide oxidation especially suited at very low sulfide concentrations (Brune 1995b).

Oxidation of Polysulfides

Polysulfides occur as the primary reaction product of the oxidation of sulfide in purple (Franz et al. 2009; Prange et al. 2004) and green (Marnocha et al. 2016) sulfur bacteria. It is still unclear how polysulfides are converted into sulfur globules (Fig. 1). Theoretically this could be purely chemical spontaneous process as longer polysulfides are in equilibrium with elemental sulfur (Stuedel et al. 1990).

Oxidation of External Sulfur

Many green and purple sulfur bacteria are able to oxidize externally supplied elemental sulfur. Sulfur of oxidation state zero mainly consists of S₈ rings and chain-like polymeric sulfur. Traces of S₇ rings are also present. Elemental sulfur is virtually insoluble in water, and it is still unclear how exactly phototrophs are able to bind, activate, and take up this substrate. *A. vinosum* uses only the polymeric sulfur fraction of commercially available sulfur (Franz et al. 2007). Soluble intermediates like sulfide, polysulfides, or polythionates do not appear to be formed. It therefore seems unlikely that mobilization of elemental sulfur by purple sulfur bacteria involves excretion of soluble sulfur-containing substances that would be able to act on substrate distant from the cells (Franz et al. 2009). Instead, direct cell-sulfur contact appears to be necessary for uptake of elemental sulfur by *A. vinosum* (Franz et al. 2007).

Properties of Sulfur Globules

In anoxygenic phototrophic sulfur bacteria, sulfur formed as an intermediate is never deposited in the cytoplasm. Green sulfur bacteria and members of the *Ectothiorhodospiraceae* form extracellular sulfur globules, and the globules of the members of the family *Chromatiaceae* are located in the periplasmic space (Pattaragulwanit et al. 1998). Independent of the site of deposition, the sulfur appears to be of similar speciation, i.e., long sulfur chains that might be terminated by organic residues in purple sulfur bacteria (Prange et al. 2002). While proteinaceous envelopes have never been reported for extracellular sulfur globules, the

sulfur globules in the *Chromatiaceae* are enclosed by a protein envelope (Brune 1995a). In *A. vinosum* this envelope is a monolayer of 2–5 nm consisting of four different hydrophobic sulfur globule proteins, SgpABCD (Brune 1995a; Pattaragulwanit et al. 1998; Weissgerber et al. 2014a). All of these proteins are synthesized with cleavable N-terminal peptides mediating Sec-dependent transport to the periplasm and share a highly repetitive amino acid sequence rich in regularly spaced proline residues. They are predicted to act purely as structural proteins. A covalent attachment of sulfur chains to the proteins is unlikely as none of the Sgps contains any cysteine residues. The envelope is indispensable for formation and deposition of intracellular sulfur in *A. vinosum*. The 10.5 kDa SgpA and SgpB proteins resemble each other and are in part able to replace each other. SgpC is important for expansion of the globules (Prange et al. 2004). SgpD was only recently detected by investigating the sulfur globule proteome and proved to be the most abundant of the four sulfur globule proteins (Weissgerber et al. 2014a). The relative mRNA levels for the corresponding gene increased drastically with addition of sulfide or thiosulfate to the growth medium (Weissgerber et al. 2013). Genes encoding sulfur globule proteins occur in all genome-sequenced purple sulfur bacteria of the family *Chromatiaceae* but are absent in *Ectothiorhodospiraceae*. The combination of sulfur globule proteins appears to be variable (Table 4).

Oxidation of Stored Sulfur to Sulfite

The oxidative degradation of sulfur deposits in phototrophic sulfur bacteria is still a major subject of research. Besides the comparatively well-characterized Dsr (dissimilatory sulfite reductase) system, a completely new pathway of sulfur oxidation involving a heterodisulfide reductase-like enzyme system is currently emerging (Dahl 2015; Venceslau et al. 2014) and appears to be implemented in several phototrophic members of the family *Ectothiorhodospiraceae* (Table 5).

The Dsr System of Sulfur Oxidation

Currently, the best studied of the sulfur oxidation pathways operating in the cytoplasm is the so-called Dsr pathway (Fig. 4) involving the enzyme reverse dissimilatory sulfite reductase (DsrAB) (Dahl et al. 2005; Pott and Dahl 1998). Low-molecular-weight organic persulfides such as glutathione amide persulfide have been proposed as carrier molecules transferring sulfur from the periplasmic or extracellular sulfur deposits into the cytoplasm (Frigaard and Dahl 2009). It is not yet known how exactly the proposed persulfidic carrier molecules are generated and whether specific enzymes are involved in this process nor have transporters for such molecules be characterized from any sulfur-oxidizing prokaryote. An extensive Cys-SSH-based sulfur relay system exists in *A. vinosum* (Figs. 1 and 4) that traffics sulfur atoms stemming ultimately from sulfur stored in sulfur globules, through a

Table 4 Genes for sulfur globule proteins in genome-sequenced purple sulfur bacteria^a

Organism	<i>sgpA</i>	<i>sgpB</i>	<i>sgpC</i>	<i>sgpD</i>
<i>Chromatiaceae</i>				
<i>Allochromatium vinosum</i> DSM 180 ^T	Alvin_1905	Alvin_0358	Alvin_1325	Alvin_2515
<i>Thiorhodovibrio</i> sp. 970	Thi970DRAFT_01708	Thi970DRAFT_04390	–	–
<i>Lamprocystis purpurea</i> DSM 4197	WP_020505111	–	–	WP_020502765
<i>Thiocapsa marina</i> 5811 DSM 5653 ^T	ThimaDRAFT_1252	ThimaDRAFT_2318	ThimaDRAFT_0183	ThimaDRAFT_1208
<i>Thiocapsa</i> sp. KS1	THIOKS11660013	THIOKS12350047, THIOKS11380015, THIOKS11380003	THIOKS12740024	THIOKS11710009
<i>Thiohalocapsa</i> ML1	WP_058555283	WP_058553807	–	WP_058558285
<i>Thiorhodococcus</i> sp. AK35	D779_0250	D779_1210	D779_3526	D779_1498
<i>Thiorhodococcus drewsii</i> AZ1 DSM 15006 ^T	THIOKS11660013	THIOKS12350047, THIOKS11380015, THIOKS11380003	THIOKS12740024	THIOKS11710009
<i>Thiocystis violascens</i> DSM 198 ^T	Thivi_3565	Thivi_3773	Thivi_4580	Thivi_3369
<i>Marichromatium purpuratum</i> 984 DSM 1591 ^T	–	MARPU_02625	MARPU_02425	MARPU_10340

(continued)

Table 4 (continued)

Organism	<i>sgpA</i>	<i>sgpB</i>	<i>sgpC</i>	<i>sgpD</i>
<i>Thioflaviococcus mobilis</i> DSM 8321 ^T	–	Thimo_3285	Thimo_1531	–
<i>Ectothiorhodospiraceae</i>				
<i>Halorhodospira halophila</i> SL1 DSM 244 ^T	–	–	–	–
<i>Halorhodospira halochloris</i> str. A DSM 1059 ^T	–	–	–	–
<i>Thiorhodospira sibirica</i> ATCC 700588 ^T	–	–	–	–
<i>Ectothiorhodospira haloalkaliphila</i> ATCC 51935	–	–	–	–
<i>Ectothiorhodospira</i> sp. PHS1	–	–	–	–

^aGenomes were analyzed by BLAST searches using the resources provided by Integrated Microbial Genomes (DOE Joint Genomes Institute, <http://img.jgi.doe.gov>) and GenBank (<http://www.ncbi.nlm.nih.gov>). Baits: *SgpA* (Alvin_1905), *SgpB* (Alvin_0358), *SgpC* (Alvin_1325), and *SgpD* (Alvin_2515) from *A. vinosum*

Table 5 Genes related to stored sulfur oxidation in genome-sequenced purple sulfur bacteria^a

Organism	<i>rhd-tusA-dsrE2</i>	<i>dsr</i>	<i>hdr</i> -like	<i>lbpA</i> and biosynthesis
<i>Chromatiaceae</i>				
<i>Allochrochromatium vinosum</i> DSM 180 ^T	Alvin_2599–2601	Alvin_1251–1265	–	–
<i>Thiorhodovibrio</i> sp. 970	Thi970DRAFT_01020–22	Thi970DRAFT_01389–75	–	–
<i>Lamprocystis purpurea</i> DSM 4197	WP_040527681 (rhd), WP_02050658081	WP_020504936–22	–	–
<i>Thiocapsa marina</i> 5811 DSM 5653 ^T	ThimaDRAFT_2004–2002	ThimaDRAFT_2915–2901	–	–
<i>Thiocapsa</i> sp. KS1	THIOKS1130019–17	THIOKS12910007–23	–	–
<i>Thiohalocapsa</i> ML1	WP_058553476–74	WP_058553439–426	–	–
<i>Thiorhodococcus</i> sp. AK35	D779_3058–56	D779_2143–2157	–	–
<i>Thiorhodococcus drevsiii</i> AZ1 DSM 15006 ^T	ThidrDRAFT_0819–817	ThidrDRAFT_2036–2022	–	–
<i>Thiocystis violascens</i> DSM 198 ^T	Thivi_2161–2159	Thivi_0544--0556, 0030/29 (<i>dsrRS</i>)	–	–
<i>Marichromatium purpuratum</i> 984 DSM 1591 ^T	MARPU_12295–12,285	MARPU_10915–10,850, no <i>dsrS</i>	–	–
<i>Thioflavococcus mobilis</i> DSM 8321 ^T	Thimo_2639–2637	Thimo_0143–0156, 1749 (<i>dsrS</i>)	–	–

(continued)

Table 5 (continued)

Organism	<i>rhd-tusA-dsrE2</i>	<i>dsr</i>	<i>hdr</i> -like	<i>lbpA</i> and biosynthesis
<i>Ectothiorhodospiraceae</i>				
<i>Halorhodospira halophila</i> SL1 DSM 244 ^T	no <i>rhd</i> , Hhal_1937 (<i>tusA</i>) no <i>dsrE2</i>	Hhal_1951–1963, no <i>dsrRS</i>		
<i>Halorhodospira halochloris</i> str. A DSM 1059 ^T	M911_16670 (<i>rhd</i>) M911_11250–11,245	–	M911_11240–11,215	M911_11210– M911_11180
<i>Thiorhodospira sibirica</i> ATCC 700588 ^T	ThisiDRAFT_1542–1540	–	ThisiDRAFT_1539–1534	ThisiDRAFT_1533 (<i>lbpA1</i>), 2311–12 (<i>dsrE2-lbpA2</i>), 0082 (<i>radSAM1</i>), 0513 (<i>lplA</i>), 1283 (<i>ger</i>), 1859 (<i>radSAM2</i>)
<i>Ectothiorhodospira haloalkaliphila</i> ATCC 51935 ^T	no <i>rhd</i> , WP_025282116/15	–	WP_025282114–111 (<i>hdrCI-hyp</i>), WP_025280421 (<i>hdrC2</i>) WP_025282109 (<i>hdrB2</i>)	WP_025282108–105 (<i>lbpA1</i> - <i>rad SAM1</i>), WP_026623531 (<i>lplA</i>), WP_025282103/02 (<i>ger-radSAM2</i>)
<i>Ectothiorhodospira</i> sp. PHS1	ECTPHS_01344 (<i>rhd</i>), 10,821,10,826	–	ECTPHS_10831–10,856	EctPHS_10861–10,891

The following abbreviations designate occurrence of a core set of several genes: *dsr*, *dsrABCFEHHMKLJOPNRS*; *hdr*-like, *hdrC1B1A1hypC2B2*; *lbpA* and biosynthesis, *lbpA1-dsrE3-lpA2-radSAM1-lplA-ger-radSAM2*

^aGenomes were analyzed by BLAST searches using the resources provided by Integrated Microbial Genomes (DOE Joint Genomes Institute, <http://img.jgi.doe.gov>) and GenBank (<http://www.ncbi.nlm.nih.gov>). Baits: *Rhd* (Alvin_2599), *TusA* (Alvin_2600), *DsrE2* (Alvin_2601), and *Dsr* proteins (U84760) from *A. vinosum*. *Hdr*-like proteins from *Acidithiobacillus caldus* SM-1: *HdrC1*, *Atc_2352*; *HdrB1*, *Atc_2351*; *HdrA*, *Atc_2350*; *Hyp*, *Atc_2349*; *HdrC2*, *Atc_2348*; *HdrB2*, *Atc_2347*; lipooate-binding protein *LbpA* and its biosynthesis, *LbpA1* (*Atc_2346*), *DsrE3* (*Atc_2345*), and *LbpA2* (*Atc_2344*); radical SAM protein 1 (*Atc_2343*); single-domain *LplA* (*Atc_2342*); geranyl geranyl reductase-like (*Atc_2341*); and radical SAM protein 2 (*Atc_2340*) from *Acidithiobacillus caldus* SM-1

cascade of protein persulfide intermediates hosted on a rhodanese, TusA, possibly DsrE2A, DsrE, and DsrC (Stockdreher et al. 2012) to the active site of the enzyme sulfite reductase (Cort et al. 2008; Dahl et al. 2008c; Dahl 2015), the enzyme that catalyzes formation of sulfite.

A *rhd-tusA-dsrE2* or at least a *tusA-dsrE2* arrangement occurs in all currently genome-sequenced sulfur oxidizers harboring the Dsr system (Venceslau et al. 2014) (Table 5). In *A. vinosum* the *tusA* and the *rhd* and the *dsrE2* gene follow the same pattern of transcription as observed for the established cytoplasmic sulfane sulfur-oxidizing proteins (i.e., the Dsr system) (Stockdreher et al. 2014; Weissgerber et al. 2013). A *rhd-tusA-dsrE2*-deficient *A. vinosum* mutant strain, although not viable in liquid culture, was clearly sulfur oxidation negative upon growth on solid media containing sulfide (Stockdreher et al. 2014). TusA is one of the major proteins in *A. vinosum*, and the *rhd* and possibly also the *dsrE2A* encoded protein were identified as entry points for sulfur delivery to this protein (Stockdreher et al. 2014). The rhodanese-like Rhd protein (Alvin_2599) catalyzes sulfur transfer from thio-sulfate or glutathione persulfide (GSSH) to cyanide in vitro, and the TusA protein was clearly established as a protein accepting sulfane sulfur from the *A. vinosum* rhodanese (Stockdreher et al. 2014). The DsrE2A protein is less well characterized and its role remains elusive at present (Stockdreher et al. 2014). It is firmly established that *A. vinosum* TusA is an interaction partner of DsrEFH, a hexameric protein arranged in a $\alpha_2\beta_2\gamma_2$ structure (Dahl et al. 2008c). Sulfur transfer between TusA and DsrEFH is reversible in vitro (Stockdreher et al. 2014). From DsrEFH sulfur is transferred to DsrC (Stockdreher et al. 2012).

The eminently important DsrC protein works as the physiological partner of the DsrAB sulfite reductase not only in sulfur-oxidizing but also in sulfate-reducing prokaryotes (Venceslau et al. 2014). DsrC is a member of the DsrC/TusE/RpsA superfamily and contains two strictly conserved redox active cysteines in a flexible carboxy-terminal arm (Cort et al. 2008): Cys_A is the penultimate residue at the C-terminus and Cys_B is located ten residues upstream (Venceslau et al. 2014). When combined in solution in their native, non-persulfurated state, DsrEFH and DsrC form a tight complex (Stockdreher et al. 2012), and each DsrE₂F₂H₂ heterohexamer associates with either one or two DsrC molecules. Interaction of DsrEFH with DsrC is strictly dependent on the presence of DsrE-Cys₇₈ and DsrC-Cys_A (Cort et al. 2008; Stockdreher et al. 2012).

In Fig. 1 the concept is implemented that persulfurated DsrC serves as the substrate for DsrAB and oxidation of DsrC-Cys_A-S⁻ by this enzyme is thought to result in persulfonated DsrC (DsrC-Cys_A-SO₃⁻) from which sulfite is possibly released by the formation of a disulfide bridge between Cys_A and Cys_B (Stockdreher et al. 2014; Venceslau et al. 2014). However, this proposal is challenged by the very recent finding that a DsrC trisulfide, in which a sulfur atom is bridging the two conserved cysteine residues, is released as the product of the reverse reaction, i.e., sulfite reduction, upon catalysis by DsrAB from a sulfate reducer (Santos et al. 2015). An alternative model is represented in Fig. 4 integrating formation of a DsrC trisulfide possibly by the action of the membrane-bound DsrMKJOP electron-transporting complex that contains the heterodisulfide reductase-like subunit DsrK which could

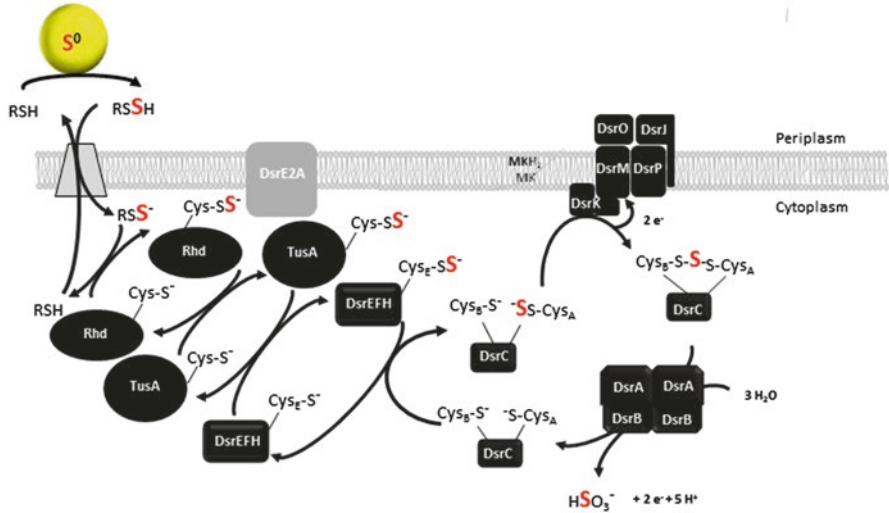


Fig. 4 Model of Dsr-mediated sulfane sulfur oxidation in *A. vinosum* integrating a sulfur-mobilizing function for Rhd, sulfur transfer functions for TusA and DsrEFH, and a substrate-donating function for DsrC. As detailed in the text, the model is based on biochemical as well as on molecular genetic evidence

well characterize the suggested reaction (Grein et al. 2010a, 2010b, 2013; Sander et al. 2006). Electrons released during oxidation of the DsrC trisulfide to DsrC and sulfite may be transferred to the protein DsrL. This iron-sulfur flavoprotein is essential for sulfur oxidation in *A. vinosum* (Dahl et al. 2005; Lübke et al. 2006). It bears striking sequence similarity to the electron-bifurcating subunit of the NfnAB complex from *Thermotoga maritima* (Demmer et al. 2015) and would have the theoretical capacity for reduction of NAD^+ ; however, experimental evidence substantiating this idea is currently completely lacking. Understanding the exact mechanistic details of the interaction of DsrC, DsrAB, and the other Dsr proteins is, in fact, one of the most challenging points in research on sulfur-oxidizing prokaryotes.

The Hdr-Like System of Sulfur Oxidation

The *rhd-tusA-dsrE2* arrangement does not only occur in all currently genome-sequenced sulfur oxidizers harboring the Dsr system but also in a wide array of chemo- and also phototrophic sulfur oxidizers that do not contain the Dsr pathway (Venceslau et al. 2014) (Table 5). In these sulfur oxidizers, a gene cluster *hdrC1B1A-hyphdrC2B2* encoding an array of proteins resembling different subunits of archaeal heterodisulfide reductases is inevitably present (Venceslau et al. 2014). As shown in Table 5, genes encoding a putative *hdr*-like complex occur in several phototrophic representatives of the family *Ectothiorhodospiraceae*. The typical arrangement of the *hdr*-like gene cluster is shown in Fig. 5 for a chemotrophic sulfur oxidizer

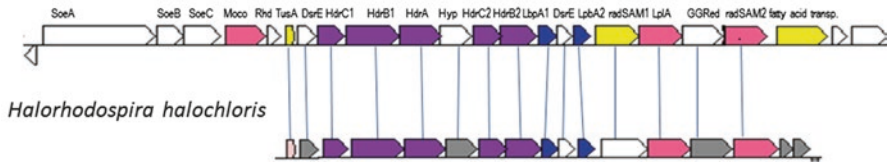
Acidithiobacillus caldus SM-1

Fig. 5 Comparison of the *hdr*-like gene cluster in *Acidithiobacillus caldus* and *Halorhodospira halophila*. The *soeABC* genes encode a membrane-bound cytoplasmically oriented sulfite-oxidizing enzyme. Rhd, TusA, and DsrE are sulfur-mobilizing and sulfur-transferring proteins, respectively. HdrB1, HdrB2, HdrC1, HdrC2, and HdrA bear similarity to the HdrABC subunits of soluble heterodisulfide reductases from methanogens. Hyp indicates a gene for a hypothetical protein. LbpA1 and LbpA2, lipoate-binding proteins, and LplA, single-domain protein lipoate ligase or more probably octanoylate transferase (Christensen et al. 2011; Christensen and Cronan 2010). radSAM1 and radSAM2 are annotated as radical SAM proteins and could insert sulfur into octanoylated LbpA. Several of the *hdr*-like gene clusters in sulfur oxidizers encode a protein putatively involved in fatty acid transport which could play a role in import of lipoate precursors GGred, similarity to geranyl geranyl reductase, and could be involved in modification of imported fatty acids before they are channeled into the specific lipoylation pathway

(*Acidithiobacillus caldus*) and the phototroph *Halorhodospira halochloris*. In almost all cases, the *hdr*-like gene set is immediately linked with *rhd-tusA-dsrE2* or *rhd-dsrE2* arrangements promoting the notion that an Hdr-like protein complex is involved in the generation of sulfite from disulfide or even more likely protein-bound persulfide intermediates formed during sulfur oxidation. Heterodisulfide reductases (Hdr) are enzymes present in methanogenic archaea and catalyze the reduction of the heterodisulfide, CoM-S-S-CoB, formed in the last step of methanogenesis (Hedderich et al. 2005; Thauer et al. 2008). The general idea of an involvement of a Hdr-like complex and probably also specialized sulfurtransferases (Rhd, DsrE, TusA) in sulfite formation was first put forward by Quatrini and coworkers on the basis of microarray transcriptome profiling and quantitative RT-PCR analyses performed with *A. ferrooxidans* ATCC 23270 (Quatrini et al. 2006, 2009). The suggestion found support in further transcriptional regulation studies not only on several *Acidithiobacillus* species (Chen et al. 2012; Ehrenfeld et al. 2013; Latorre et al. 2016) and the Gram-positive *Sulfobacillus thermosulfidooxidans* (Guo et al. 2014) but also on the thermoacidophilic archaeon *Metallosphaera sedula* (Auernik and Kelly 2010). In addition, proteomic studies showed high levels of Hdr-like proteins in the presence of reduced sulfur compounds (Mangold et al. 2011; Osorio et al. 2013; Ouyang et al. 2013). In several of the cited studies, upregulation in the presence of reduced inorganic sulfur compounds affected the *hdr*-like genes as well as the sulfur transferase genes. Tight functional interaction of the encoded proteins is further indicated by the observation that genes *dsrE* to *hdrB2* constitute a single, distinct transcriptional unit in *A. ferrooxidans* ATCC 16786 (Ehrenfeld et al. 2013). The whole concept is further substantiated by the recent purification of a Hdr-like complex from membranes of *Aquifex aeolicus* (Boughanemi et al. 2016).

Ehrenfeld et al. 2013 were the first to point out the presence of a *gvcH*-like gene encoding a lipoate-binding protein (Ehrenfeld et al. 2013). On the basis of striking sequence similarity and the presence of a strictly conserved lysine residue known to be required for lipoate attachment (Spalding and Prigge 2010), the name LbpA (lipoate-binding protein A) is suggested for this single lipoyl domain protein. Many sulfur oxidizers carry two copies of the gene indicating a functional dimer. Furthermore, genes encoding another DsrE-like sulfurtransferase and proteins with the potential to act in biosynthesis of protein-bound lipoic acid (two radical SAM proteins, a lipoate-protein ligase, and geranyl geranyl reductase-like protein) are inevitably found in organisms containing *hdr*-like genes but not in sulfur oxidizers pursuing the Dsr pathway (Fig. 5, Table 5). In most cases these genes are immediately linked with the *hdr* genes as shown in Fig. 5, and in some cases they are located at other places in the genome (e.g., in the purple sulfur bacterium *Thiorhodospira sibirica*, Table 5).

Overall, the present circumstantial evidence is quite overwhelming in the argument that a Hdr-like enzyme system including dedicated sulfur transferases (Rhd, DsrE, TusA) and also a dedicated lipoate-binding protein is a central and key element in the bioenergetics of sulfur-oxidizing prokaryotes devoid of the Dsr system (Bobadilla Fazzini et al. 2013; Chen et al. 2012; Dahl 2015; Guo et al. 2014; Mangold et al. 2011; Quatrini et al. 2009; Venceslau et al. 2014). However, genetic experiments that would finally prove this omics-derived concept have so far not been published for any organism, and biochemical studies that would shed light on the underlying reaction mechanism(s) are completely lacking.

Currently, it appears premature to suggest a more detailed model of the Hdr-like mechanism. The LbpA protein is a prime candidate as a sulfur substrate-binding entity that presents the sulfur substrate to different catalytic entities. However, further functions can at present not be assigned.

Oxidation of Sulfite to Sulfate

The last step in the oxidation of reduced sulfur compounds is the oxidation of sulfite yielding sulfate as the final product. Sulfate formation from sulfite is energetically favorable and carried out by a wide range of organisms (Simon and Kroneck 2013). In addition, many purple sulfur bacteria can even use externally available sulfite as photosynthetic electron donor. Two fundamentally different pathways for sulfite oxidation have been well characterized in chemotrophic and phototrophic sulfur-oxidizing bacteria: (1) direct oxidation and (2) indirect, AMP-dependent oxidation via the intermediate adenylylsulfate (adenosine-5'-phosphosulfate).

Oxidation of Sulfite in the Periplasm

Many sulfite-oxidizing enzymes catalyzing direct oxidation of sulfite are located outside the cytoplasmic membrane (in the periplasm in Gram-negative bacteria). The best characterized enzyme belonging to this group, SorAB, stems from the

chemotroph *Starkeya novella* and consists of a molybdopyranopterin (Mo-PPT) cofactor-carrying subunit (SorA) and a monoheme cytochrome *c* (SorB) (Kappler et al. 2000; Kappler and Bailey 2005). SorA-type molybdoproteins without a SorB subunit have been termed SorT (D'Errico et al. 2006; Wilson and Kappler 2009), but recently this discrimination has been questioned (Simon and Kroneck 2013). Neither genes closely related to *sorAB* nor those encoding SorT sulfite dehydrogenases occur in the currently available genomes of anoxygenic phototrophic bacteria.

A second option for oxidation of sulfite in the periplasm is the Sox system. It has been shown that sulfite is accepted *in vitro* as a substrate of the reconstituted Sox system from the chemotroph *Paracoccus denitrificans* (Friedrich et al. 2001; Frigaard and Dahl 2009; Sander and Dahl 2009). Notably, Friedrich and coworkers proved this reaction to be independent on the presence of SoxCD, a molybdohemoprotein catalyzing the six-electron oxidation of SoxY-cysteine-bound persulfide to sulfone sulfur. Purple bacteria that form sulfur globules during thiosulfate oxidation contain the Sox system albeit without the SoxCD proteins (Frigaard and Dahl 2009; Hensen et al. 2006; Meyer et al. 2007). Notably, the presence of SoxB and SoxXA is not essential for sulfite oxidation in *A. vinosum* (Hensen et al. 2006).

However, the periplasmic sulfur substrate-binding protein SoxYZ is needed in parallel to cytoplasmic enzymes for effective sulfite oxidation in *A. vinosum* (Dahl et al. 2013). Genes for this protein are present in purple sulfur bacteria irrespective of the organisms' substrate range with only one exception (*Thioflaviococcus mobilis*), while the presence of SoxXA(K) and SoxB appears to be strictly linked to the ability of the cells to utilize thiosulfate (Table 2).

Oxidation in the Cytoplasm

Indirect Pathway via Adenosine 5'-Phosphosulfate

It is firmly established that a number of purple as well as green anoxygenic phototrophic sulfur bacteria oxidize sulfite in the cytoplasm using an indirect pathway via adenosine-5'-phosphosulfate (APS) catalyzed by APS reductase (AprBA) and ATP sulfurylase (Sat) (Dahl 1996; Frigaard and Dahl 2009; Parey et al. 2013; Rodriguez et al. 2011; Sanchez et al. 2001) (Fig. 1).

In *A. vinosum*, the *sat* gene encoding ATP sulfurylase (Alvin_1118) is located immediately upstream of the *aprMBA* genes encoding membrane-bound APS reductase (Alvin_1119–1121) (Hipp et al. 1997; Weissgerber et al. 2011). AprM is predicted to contain five transmembrane helices with no sequence similarity to any currently known conserved domain or cofactor binding site in the databases. An essential function of AprM as a membrane anchor that allows spatial and functional association of this type of oxidative APS reductase with the membrane has been postulated, and it has been suggested that AprM serves as an entry point into the membrane for the electrons released during formation of APS from sulfite and AMP (Meyer and Kuever 2007). In the currently available complete genome sequences of phototrophic members of the family *Chromatiaceae*, the same gene arrangement

is present in *Thiorhodovibrio* sp. 970 (Table 6). In *Thiocapsa marina* 5811, *Thiorhodococcus drewsii* AZ1, *Thiocystis violascens* DSM 198^T, and *Thioflaviooccus mobilis* DSM 8321^T, *sat* and *aprMBA* are not linked on the chromosome (Table 6). The occurrence of *aprMBA* has also been reported for *Thiococcus pfenigii* 4520 (Gregersen et al. 2011).

The QmoABC complex was first identified in the dissimilatory sulfate-reducing bacterium *Desulfovibrio desulfuricans* (Pires et al. 2003). The complex consists of one membrane (QmoC) and two cytoplasmic subunits (QmoAB). The two QmoC hemes *b* are reduced by quinols, and experimental evidence strongly indicates that the Qmo complex participates in electron flow between the quinone pool and the cytoplasm, i.e., that it acts as the electron-donating unit for APS reductase in sulfate reducers (Frigaard and Dahl 2009; Ramos et al. 2012). The *qmoABC* genes are not only present in sulfate-reducing prokaryotes (Ramos et al. 2012) but occur also in many chemotrophic sulfur-oxidizing bacteria as well as in green sulfur bacteria (Frigaard and Dahl 2009; Rodriguez et al. 2011) and in one further purple sulfur bacterium (*Thiodictyon* sp. Cad16 (Gregersen et al. 2011)). In sulfur oxidizers, QmoABC is thought to act as electron acceptor for the electrons released during formation of APS and would thus have a function analogous to that of AprM. It is thus conceivable to state that the electrons generated by the oxidative formation of APS from sulfite and AMP are fed into the photosynthetic electron transport chain on the level of menaquinone either by AprM or by the much better characterized QmoABC complex (Grein et al. 2013; Meyer and Kuever 2007; Ramos et al. 2012; Rodriguez et al. 2011). It may be especially advantageous to be equipped with the Qmo-related electron-accepting unit for APS reductase. The presence of the HdrA-like QmoA in the Qmo complex opens the possibility that—in reverse to the mechanism suggested for sulfate reducers (Grein et al. 2013; Ramos et al. 2012)—an electron bifurcation occurs that could result in simultaneous reduction of low potential electron acceptors like ferredoxin or NAD⁺. Such a process would be of significant energetic advantage especially for chemolithoautotrophic growth because it would result in a lower energy demand for reverse electron flow.

Direct Pathway via SoeABC

Notably the APS reductase pathway is neither generally present in purple sulfur bacteria (Table 6) nor is it essential in *A. vinosum* (Dahl 1996; Sanchez et al. 2001). The *sat* and *aprBA* genes are not present in some members of the *Chromatiaceae* (Meyer and Kuever 2007) and generally absent in *Ectothiorhodospiraceae* (Table 6). Recently the membrane-bound iron-sulfur molybdoprotein SoeABC was identified as a major enzyme catalyzing direct oxidation of sulfite to sulfate in the cytoplasm of *A. vinosum* (Dahl et al. 2013). The function of SoeABC was proven by strongly reduced specific oxidation rates for externally supplied sulfite and by massive excretion of sulfite into the medium during oxidation of sulfide in *A. vinosum* SoeABC-deficient strains. Crude extract of a SoeABC-deficient *A. vinosum* lacked

Table 6 Genes related to sulfite oxidation in genome-sequenced purple sulfur bacteria^a

Organism	<i>sat</i>	<i>aprBA</i>	<i>aprM</i>	<i>qmoABC</i>	<i>soeABC</i>
<i>Chromatiaceae</i>					
<i>Allochromatium vinosum</i> DSM 180 ^T	Alvin_1118	Alvin_1120/21	Alvin_1119	–	Alvin_2491/90/89
<i>Thiorhodovibrio</i> sp. 970	Thi970DRAFT_00961	Thi970DRAFT_00963/64	Thi970DRAFT_00962	–	Thi970DRAFT_00955/56/57
<i>Lamprocystis purpurea</i> DSM 4197	WP_026199081	WP_020504060/59	–	WP_020504182/83/84	WP_020508252/50/49
<i>Thiocapsa marina</i> 5811 DSM 5653 ^T	ThimaDRAFT_0331	ThimaDRAFT_4551/52	ThimaDRAFT_4550	–	ThimaDRAFT_0331/30/29
<i>Thiocapsa</i> sp. KS1	THIOKS1630011	–	–	THIOKS11840023/24/26	THIOKS12550011/12/13
<i>Thiohalocapsa</i> ML1	WP_058556167	WP_058557029/30	WP_058557048	–	WP_058553485/83/82
<i>Thiorhodococcus</i> sp. AK35	D779_2633	D779_0177/78	D779_0176	–	D779_1687/86/85
<i>Thiorhodococcus drewsii</i> AZ1 DSM 15006 ^T	ThidrDRAFT_3161	ThidrDRAFT_1495/96	ThidrDRAFT_1494	–	ThidrDRAFT_2883/82/81
<i>Thiocystis violascens</i> DSM 198 ^T	Thivi_0893	Thivi_3300/299	–	Thivi_3114/13/12	Thivi_4531/32/33
<i>Marichromatium purpuratum</i> 984 DSM 1591 ^T	–	–	–	–	MARPU_14905/00/14895

(continued)

Table 6 (continued)

Organism	<i>sat</i>	<i>aprBA</i>	<i>aprM</i>	<i>qmoABC</i>	<i>soeABC</i>
<i>Thioflavivococcus mobilis</i> DSM 8321 ^T	Thimo_1948	Thimo_1220/19	Thimo_1221	–	Thimo_1580/81/82
<i>Ectothiorhodospiraceae</i>					
<i>Halorhodospira halophila</i> SL1 DSM 244 ^T	–	–	–	–	Hhal_1934/35/36
<i>Halorhodospira halochloris</i> str. A DSM 1059 ^T	–	–	–	–	M911_11365/01475/01495
<i>Thiorhodospira sibirica</i> ATCC 700588 ^T	–	–	–	–	ThisIDRAFT_1377/0834/2148
<i>Ectothiorhodospira haloalkaliphila</i> ATCC 51935 ^T	–	–	–	–	WP_025282138, WP_025281124, WP_025280412
<i>Ectothiorhodospira</i> sp. PHS1	–	–	–	–	ECTPHS_02816/02811/02806

^aGenomes were analyzed by BLAST searches using the resources provided by Integrated Microbial Genomes (DOE Joint Genomes Institute, <http://img.jgi.doe.gov>) and GenBank (<http://www.ncbi.nlm.nih.gov>). Baitis: APS reductase (AprMBA) from *A. vinosum* (U84759), Qmo proteins from *C. tepidum* (QmoA, CT0866; QmoB, CT0867; QmoC, CT0868), SoeABC from *A. vinosum* (SoeA, ADC63403; SoeB, ADC63402; SoeC, ADC63401)

AMP-independent sulfite-oxidizing activity. Further indication for an involvement of SoeABC in dissimilatory sulfur oxidation in *A. vinosum* was gathered during recent genome-wide transcriptional profiling (Weissgerber et al. 2013). Relative transcription of all three *A. vinosum* *soe* genes was found to be increased about threefold during photolithoautotrophic growth on sulfide or thiosulfate than during photoorganoheterotrophic growth on malate (2.99-, 2.77-, and 2.93-fold increase on sulfide and 1.96-, 1.98-, and 3.00-fold increase on thiosulfate, for *soeA*, *soeB*, and *soeC*, respectively). Changes in the same range were observed for the genes encoding the enzymes of the APS reductase pathway when thiosulfate replaced malate, while relative transcript levels for the *sat-aprMBA* genes were 7.6–9.7-fold higher in the presence of sulfide compared to the presence of malate

In *A. vinosum*, SoeABC is encoded by genes Alvin_2491 (*soeA*), Alvin_2490 (*soeB*), and Alvin_2489 (*soeC*). The protein consists of the 108.95 kDa molybdo-protein SoeA carrying one [Fe₄S₄] cluster at the N-terminus; the 26.995 kDa iron-sulfur protein SoeB, which upon comparison with related structurally characterized proteins (Jormakka et al. 2008) is predicted to bind four [Fe₄S₄] clusters; and a 35.715 kDa NrfD-/PsrC-like membrane protein (Simon and Kern 2008) with eight transmembrane helices. Neither AvSoeA and AvSoeB nor any of the other purple sulfur bacterial SoeA or SoeB proteins listed in Table 6 are synthesized with cleavable TAT signal peptides that are usually present on the active site subunits of the biochemically well-characterized periplasmic sulfur-metabolizing complex iron-sulfur molybdoproteins, i.e., polysulfide and sulfur reductase (PsrABC, SreABC), thiosulfate reductase (PhsABC), or tetrathionate reductase (TrABC) (Heinzinger et al. 1995; Hensel et al. 1999; Krafft et al. 1992; Laska et al. 2003). SoeA and SoeB are thus located in the cytoplasm and attached to the cytoplasmic membrane by interaction with SoeC. The holoprotein is therefore well suited for oxidation of sulfite generated in the cytoplasm. It should be noted that SoeABC and the periplasmic Sor-type sulfite dehydrogenases belong to completely different families of molybdoenzymes.

Genes encoding proteins related to SoeABC are present in purple as well as green sulfur bacteria and have in the past years repeatedly been speculated to be involved in the oxidation of sulfite generated by the Dsr system in the cytoplasm (Frigaard and Bryant 2008b; Frigaard and Dahl 2009) (Table 6). Notably, *soeABC*-like genes co-localize with *dsr* genes in several green sulfur bacteria and in *Halorhodospira halophila* (Dahl 2008; Frigaard and Dahl 2009).

The possession of the APS reductase pathway in addition to or instead of SoeABC may be advantageous because additional energy is gained by substrate phosphorylation in the ATP sulfurylase catalyzed step by transferring the AMP moiety of APS onto pyrophosphate (Parey et al. 2013).

Sulfate Assimilation

Sulfate assimilation by in anoxygenic phototrophic bacteria has been extensively covered in previous reviews (Frigaard and Dahl 2009; Sander and Dahl 2009). Some anoxygenic phototrophic bacteria are very much specialized for living in

habitats with reduced sulfur compounds and such bacteria usually completely lack a sulfate reduction pathway. On the other hand, very many versatile purple sulfur and non-sulfur bacteria and even a few green bacteria are able to assimilate and reduced sulfate in the absence of a reduced source of sulfur. Among the filamentous anoxygenic bacteria, the ability to assimilate sulfate may or may not be present.

Here, the assimilatory sulfate reduction pathway in *A. vinosum* is presented as an example (Fig. 6). The pathway commences with the uptake of sulfate via the membrane-bound components of a periplasmic substrate-binding transport system similar to the situation in *E. coli* (Kredich 1996). Once inside the cell, sulfate is activated to adenosine-5'-phosphosulfate by the enzyme ATP sulfurylase (Leustek and Saito 1999). Assimilatory ATP sulfurylases occur in two different forms: a heterodimeric CysDN type as in *E. coli* (Leyh 1993) and a homo-oligomeric Sat-related type as found in other bacteria, plants, and fungi (Foster et al. 1994; MacRae et al. 2001). Both types occur in anoxygenic phototrophic bacteria (Frigaard and Dahl 2009; Sander and Dahl 2009). The sulfate reduction pathway in *A. vinosum* does not involve formation of phosphoadenosine-5'-phosphosulfate (Neumann et al. 2000). Instead, a CysH-type iron-sulfur cluster binding APS reductase catalyzes reductive cleavage of APS yielding sulfite and AMP. Sulfite is finally reduced to sulfide by an assimilatory sulfite reductase. In the case of *A. vinosum*, this enzyme is a ferredoxin-dependent CysI-type siroheme-[4Fe-4S] cluster-containing protein as it also occurs in cyanobacteria, algae, and higher plants (Dhillon et al. 2005). This enzyme type is common in anoxygenic phototrophic bacteria (Frigaard and Dahl 2009). Biosynthesis of cysteine requires the formation of *O*-acetyl-L-serine, which is then further transformed to cysteine catalyzed by cysteine synthase B (CysM) in a reaction that is dependent on the availability of sulfide (Fig. 6) (Hensel and Trüper 1976). It is well established that the CysTWA ABC-type transporter in conjunction with the periplasmic binding protein CysP transports not only sulfate but also thiosulfate into the cytoplasm (Sirko et al. 1995). In *Salmonella typhimurium* and *E. coli*, cysteine synthase B (CysM) also accepts thiosulfate as a substrate and hooks it up to *O*-acetylserine resulting in the formation of *S*-sulfocysteine (Kredich 1992). *S*-sulfocysteine is then reduced to cysteine resulting in the release of sulfite (Nakatani et al. 2012; Sekowska et al. 2000). Glutathione, thioredoxins, or glutaredoxins have been discussed as possible reductants in this reaction (Funane et al. 1987; Nakatani et al. 2012; Woodin and Segel 1968). A similar reaction sequence is also probable for the assimilation of thiosulfate in *A. vinosum* (Fig. 6). In fact, thiosulfate was previously detected intracellularly in *A. vinosum* (Franz et al. 2009).

During photoorganoheterotrophic growth of *A. vinosum* on organic acids like malate, sulfide for biosynthesis of sulfur-containing cell constituents is provided by the assimilatory sulfate reduction pathway in an energy-consuming process (Fig. 6) (Neumann et al. 2000), while sulfide is readily available without any input of energy under sulfur-oxidizing conditions. Accordingly, the presence of reduced sulfur compounds results in elevated relative mRNA and protein levels for genes/proteins of central enzymes of oxidative sulfur metabolism, while transcript and protein levels for genes/proteins involved in assimilatory sulfate reduction are negatively affected (Weissgerber et al. 2013, 2014a). These responses are positively correlated to the

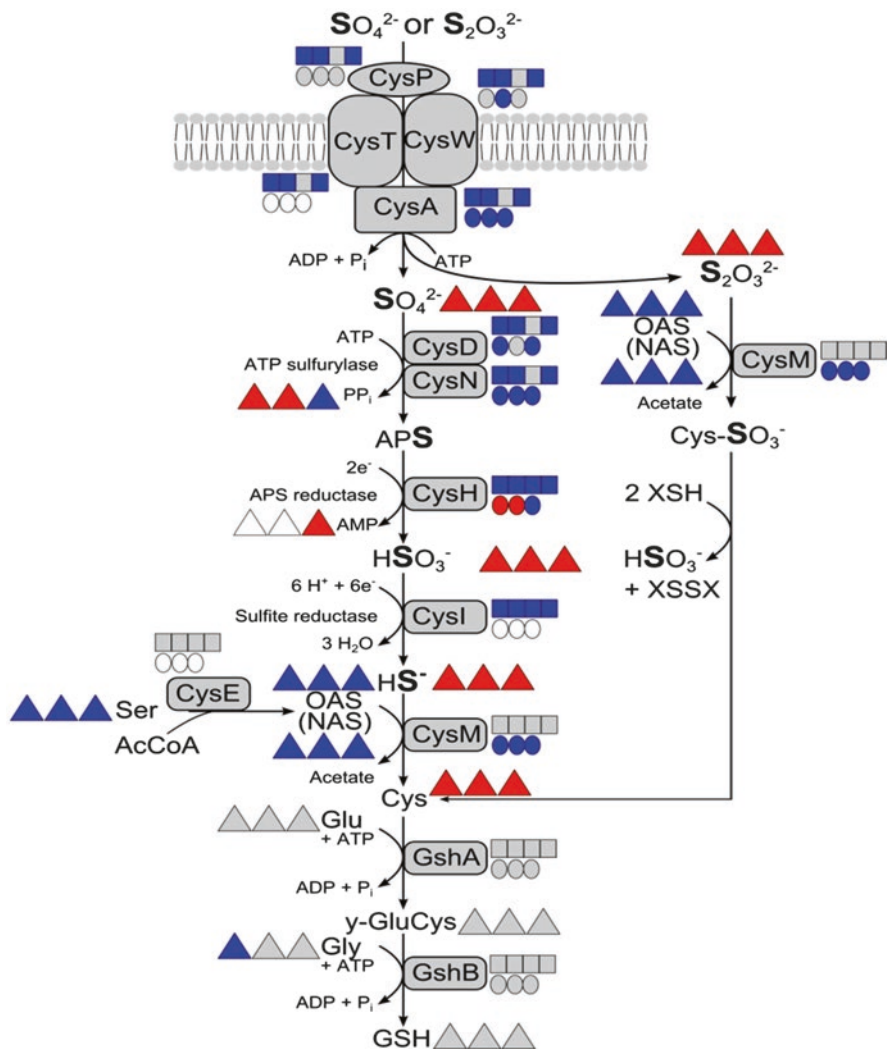


Fig. 6 Current model of assimilatory sulfate reduction in *A. vinosum*. *CysE* serine *O*-acetyltransferase (Alvin_0683), *CysM* cysteine synthase B (Alvin_2228), *GshA* glutamate/cysteine ligase (Alvin_0863), *CysM* cysteine synthase B (Alvin_2228); *GshA* glutamate/cysteine ligase (Alvin_800), *GshB* glutathione synthetase (Alvin_0197), γ -*GluCys* γ -glutamylcysteine, *GSH* glutathione, *XSH* glutathione, reduced thioredoxin or glutaredoxin, *XSSX* oxidized glutathione, thioredoxin or glutaredoxin (see text for further explanation). The transcriptomic (boxes) (Weissgerber et al. 2013), proteomic (circles) (Weissgerber et al. 2014a), and metabolomic profiles (triangles) (all relative to growth on malate) are depicted next to the respective protein/metabolite. Relative fold changes in mRNA levels above 2 (red) were considered significantly enhanced. Relative changes smaller than 0.5 (blue) were considered as indicating significant decreases in mRNA levels. Relative fold changes between 0.5 and 2 (gray) indicated unchanged mRNA levels. The same color coding is applied to changes on the protein and metabolome levels. Here, values above 1.5 (red) and below 0.67 (blue) were considered significant. Those cases, where transcriptomic data was not available or the respective protein or metabolite was not detected in the proteomic or metabolomic approach, respectively, are indicated by white squares, circles, or triangles. Sulfur compounds added, from left to right, sulfide, thiosulfate, elemental sulfur, and sulfite. Changes on sulfite were not determined on the proteome and metabolome levels. Figure reproduced from (Weissgerber et al. 2014b)

concentration changes of the metabolites of the affected metabolic pathways (Weissgerber et al. 2014b) (Fig. 6). It is conceivable to assume that the interplay between the processes of dissimilatory sulfur oxidation and assimilatory sulfate reduction is regulated in a similar manner in other anoxygenic phototrophic bacteria capable of pursuing both pathways.

Acknowledgments Support by the Deutsche Forschungsgemeinschaft (Grant Da 351/6-2) is gratefully acknowledged.

References

- Appia-Ayme C, Little PJ, Matsumoto Y et al (2001) Cytochrome complex essential for photosynthetic oxidation of both thiosulfate and sulfide in *Rhodovulum sulfidophilum*. *J Bacteriol* 183:6107–6118
- Arieli B, Padan E, Shahak Y (1991) Sulfide-induced sulfide—quinone reductase activity in thylakoids of *Oscillatoria limnetica*. *J Biol Chem* 266:104–111
- Arieli B, Shahak Y, Taglicht D et al (1994) Purification and characterization of sulfide-quinone reductase, a novel enzyme driving anoxygenic photosynthesis in *Oscillatoria limnetica*. *J Biol Chem* 269:5705–5711
- Auernik KS, Kelly RM (2010) Physiological versatility of the extremely thermoacidophilic archaeon *Metallosphaera sedula* supported by transcriptomic analysis of heterotrophic, autotrophic, and mixotrophic growth. *Appl Environ Microbiol* 76:931–935
- Baldock MI, Denger K, Smits THM et al (2007) *Roseovarius* sp. strain 217: aerobic taurine dissimilation via acetate kinase and acetate-CoA ligase. *FEMS Microbiol Lett* 271:202–206
- Bamford VA, Bruno S, Rasmussen T et al (2002) Structural basis for the oxidation of thiosulfate by a sulfur cycle enzyme. *EMBO J* 21:5599–5610
- Barbosa-Jefferson VL, Zhao FJ, Mcgrath SP et al (1998) Thiosulphate and tetrathionate oxidation in arable soils. *Soil Biol Biochem* 30:553–559
- Bartsch RG (1978) Cytochromes. In: Clayton RK, Sistrom WR (eds) *The photosynthetic bacteria*. Plenum Press, New York, pp 249–279
- Bobadilla Fazzini RA, Cortes MP, Padilla L et al (2013) Stoichiometric modeling of oxidation of reduced inorganic sulfur compounds (Riscs) in *Acidithiobacillus thiooxidans*. *Biotechnol Bioeng* 110:2242–2251
- Bosshard HR, Davidson MW, Knaff DB et al (1986) Complex formation and electron transfer between mitochondrial cytochrome c and flavocytochrome c552 from *Chromatium vinosum*. *J Biol Chem* 261:190–193
- Boughanemi S, Lyonnet J, Infossi P et al (2016) Microbial oxidative sulfur metabolism: biochemical evidence of the membrane-bound heterodisulfide reductase-like complex of the bacterium *Aquifex aeolicus*. *FEMS Microbiol Lett* 363
- Bradley JM, Marritt SJ, Kihlken MA et al (2012) Redox and chemical activities of the hemes in the sulfur oxidation pathway enzyme SoxAX. *J Biol Chem* 287:40350–40359
- Brito JA, Denkmann K, Pereira IAC et al (2015) Thiosulfate dehydrogenase (TsdA) from *Allochromatium vinosum*: Structural and functional insights into thiosulfate oxidation. *J Biol Chem* 290:9222–9238
- Brito JA, Sousa FL, Stelter M et al (2009) Structural and functional insights into sulfide:quinone oxidoreductase. *Biochemistry* 48:5613–5622
- Bronstein M, Schütz M, Hauska G et al (2000) Cyanobacterial sulfide-quinone reductase: cloning and heterologous expression. *J Bacteriol* 182:3336–3344
- Brune DC (1989) Sulfur oxidation by phototrophic bacteria. *Biochim Biophys Acta* 975:189–221

- Brune DC (1995a) Isolation and characterization of sulfur globule proteins from *Chromatium vinosum* and *Thiocapsa roseopersicina*. Arch Microbiol 163:391–399
- Brune DC (1995b) Sulfur compounds as photosynthetic electron donors. In: Blankenship RE, Madigan MT, Bauer CE (eds) Anoxygenic photosynthetic bacteria. Kluwer Academic Publishers, Dordrecht, pp 847–870
- Bryant DA, Costas AMG, Maresca JA et al (2007) *Candidatus Chloracidobacterium thermophilum*: an aerobic phototrophic Acidobacterium. Science 317:523–526
- Bryantseva IA, Gorlenko VM, Kompantseva EI et al (1999) *Thiorhodospira sibirica* gen. nov., sp. nov., a new alkaliphilic purple sulfur bacterium from a Siberian Soda lake. Int J Syst Bacteriol 49:697–703
- Caumette P, Guyoneaud R, Imhoff JF et al (2004) *Thiocapsa marina* sp. nov., a novel, okenone-containing, purple sulfur bacterium isolated from brackish coastal and marine environments. Int J Syst Evol Microbiol 54:1031–1036
- Challacombe JF, Majid S, Deole R et al (2013) Complete genome sequence of Halorhodospira halophila SL1. Stand Genomic Sci 8:206–214
- Chan L-K, Morgan-Kiss R, Hanson TE (2009) Functional analysis of three sulfide:quinone oxidoreductase homologs in *Chlorobaculum tepidum*. J Bacteriol 191:1026–1034
- Chen ZW, Koh M, van Driessche G et al (1994) The structure of flavocytochrome c sulfide dehydrogenase from a purple phototrophic bacterium. Science 266:430–432
- Chen L, Ren Y, Lin J et al (2012) *Acidithiobacillus caldus* sulfur oxidation model based on transcriptome analysis between the wild type and sulfur oxygenase reductase defective mutant. PLoS One 7:e39470
- Cherney MM, Zhang Y, Solomonson M et al (2010) Crystal structure of sulfide:quinone oxidoreductase from *Acidithiobacillus ferrooxidans*: insights into sulfidrotrophic respiration and detoxification. J Mol Biol 398:292–305
- Christensen QH, Cronan JE (2010) Lipoic acid synthesis: a new family of octanoyltransferases generally annotated as lipoate protein ligases. Biochemistry 49:10024–10036
- Christensen QH, Martin N, Mansilla MC et al (2011) A novel amidotransferase required for lipoic acid cofactor assembly in *Bacillus subtilis*. Mol Microbiol 80:350–363
- Ciccarelli FD, Doerks T, von Mering C et al (2006) Toward automatic reconstruction of a highly resolved tree of life. Science 311:1283–1287
- Cort JR, Selan UM, Schulte A et al (2008) *Allochromatium vinosum* DsrC: solution-state NMR structure, redox properties and interaction with DsrEFH, a protein essential for purple sulfur bacterial sulfur oxidation. J Mol Biol 382:692–707
- Cusanovich MA, Bartsch RG (1969) A high potential cytochrome c from *Chromatium vinosum* chromatophores. Biochim Biophys Acta 189:245–255
- D’Errico G, Di Salle A, La Cara F et al (2006) Identification and characterization of a novel bacterial sulfite oxidase with no heme binding domain from *Deinococcus radiodurans*. J Bacteriol 188:694–701
- Dahl C (1996) Insertional gene inactivation in a phototrophic sulphur bacterium: APS-reductase-deficient mutants of *Chromatium vinosum*. Microbiology 142:3363–3372
- Dahl C (2008) Inorganic sulfur compounds as electron donors in purple sulfur bacteria. In: Hell R, Dahl C, Knaff DB, Leustek T (eds) Sulfur in phototrophic organisms. Springer, Dordrecht, pp 289–317
- Dahl C (2015) Cytoplasmic sulfur trafficking in sulfur-oxidizing prokaryotes. Iubmb Life 67:268–274
- Dahl C, Friedrich CG, Kletzin A (2008a) Sulfur oxidation in prokaryotes. In: Encyclopedia of Life Sciences (ELS), John Wiley & Sons, Ltd., Chichester, p <http://www.els.net/> [DOI: 10.1002/9780470015902.a0021155]
- Dahl C, Hell R, Leustek T, Knaff DB (2008b) Introduction to sulfur metabolism in phototrophic organisms. In: Hell R, Dahl C, Knaff DB, Leustek T (eds) Sulfur metabolism in phototrophic organisms. Springer, Dordrecht, pp 1–14
- Dahl C, Schulte A, Stockdreher Y et al (2008c) Structural and molecular genetic insight into a wide-spread bacterial sulfur oxidation pathway. J Mol Biol 384:1287–1300

- Dahl C, Engels S, Pott-Sperling AS et al (2005) Novel genes of the *dsr* gene cluster and evidence for close interaction of Dsr proteins during sulfur oxidation in the phototrophic sulfur bacterium *Allochromatium vinosum*. *J Bacteriol* 187:1392–1404
- Dahl C, Franz B, Hensen D et al (2013) Sulfite oxidation in the purple sulfur bacterium *Allochromatium vinosum*: identification of SoeABC as a major player and relevance of SoxYZ in the process. *Microbiology* 159:2626–2638
- Demmer JK, Huang H, Wang S et al (2015) Insights into flavin-based electron bifurcation via the NADH-dependent reduced ferredoxin:NADP oxidoreductase structure. *J Biol Chem* 290:21985–21995
- Denger K, Smits THM, Cook AM (2006) Genome-enabled analysis of the utilization of taurine as sole source of carbon or of nitrogen by *Rhodobacter sphaeroides* 2.4.1. *Microbiology* 152: 3197–3206
- Denger K, Weinitschke S, Hollemeyer K et al (2004) Sulfoacetate generated by *Rhodopseudomonas palustris* from taurine. *Arch Microbiol* 182:154–158
- Denkmann K, Grein F, Zigann R et al (2012) Thiosulfate dehydrogenase: a wide-spread unusual acidophilic c-type cytochrome. *Environ Microbiol* 14:2673–2688
- Dhillon A, Goswami S, Riley M et al (2005) Domain evolution and functional diversification of sulfite reductases. *Astrobiology* 5:18–29
- Eddie BJ, Hanson TE (2013) *Chlorobaculum tepidum* TLS displays a complex transcriptional response to sulfide addition. *J Bacteriol* 195:399–408
- Ehrenfeld N, Levicán G, Parada P (2013) Heterodisulfide reductase from *Acidithiobacilli* is a key component involved in metabolism of reduced inorganic sulfur compounds. *Adv Mater Res* 825:194–197
- Falkenby LG, Szymanska M, Holkenbrink C et al (2011) Quantitative proteomics of *Chlorobaculum tepidum*: insights into the sulfur metabolism of a phototrophic green sulfur bacterium. *FEMS Microbiol Lett* 323:142–150
- Foster BA, Thomas SM, Mahr JA et al (1994) Cloning and sequencing of ATP sulfurylase from *Penicillium chrysogenum*: identification of a likely allosteric domain. *J Biol Chem* 269: 19777–19786
- Franz B, Gehrke T, Lichtenberg H et al (2009) Unexpected extracellular and intracellular sulfur species during growth of *Allochromatium vinosum* with reduced sulfur compounds. *Microbiology* 155:2766–2774
- Franz B, Lichtenberg H, Hormes J et al (2007) Utilization of solid “elemental” sulfur by the phototrophic purple sulfur bacterium *Allochromatium vinosum*: a sulfur K-edge XANES spectroscopy study. *Microbiology* 153:1268–1274
- Friedrich CG, Bardischewsky F, Rother D et al (2005) Prokaryotic sulfur oxidation. *Curr Opin Microbiol* 8:253–259
- Friedrich CG, Rother D, Bardischewsky F et al (2001) Oxidation of reduced inorganic sulfur compounds by bacteria: emergence of a common mechanism? *Appl Environ Microbiol* 67: 2873–2882
- Frigaard N-U, Bryant DA (2008a) Genomic and evolutionary perspectives on sulfur metabolism in green sulfur bacteria. In: Dahl C, Friedrich CG (eds) *Microbial sulfur metabolism*. Springer, Heidelberg, Heidelberg, pp 60–76
- Frigaard N-U, Bryant DA (2008b) Genomic insights into the sulfur metabolism of phototrophic green sulfur bacteria. In: Hell R, Dahl C, Knaff DB, Leustek T (eds) *Sulfur metabolism in phototrophic organisms*. Springer, Dordrecht, pp 337–355
- Frigaard N-U, Dahl C (2009) Sulfur metabolism in phototrophic sulfur bacteria. *Adv Microb Physiol* 54:103–200
- Funane K, Iwahashi H, Nakamura T (1987) Metabolism of S-sulfocysteine in *Salmonella typhimurium*. Role of thioredoxin in the reduction of S-sulfocysteine. *Agric Biol Chem* 51: 1247–1256
- Gregersen LH, Bryant DA, Frigaard N-U (2011) Mechanisms and evolution of oxidative sulfur metabolism in green sulfur bacteria. *Front Microbiol* 2:116. doi:10.3389/fmicb.2011.00116

- Grein F, Pereira IAC, Dahl C (2010a) The *Allochromatium vinosum* DsrMKJOP transmembrane complex: biochemical characterization of individual components aids understanding of complex function in vivo. *J Bacteriol* 192:6369–6377
- Grein F, Ramos AR, Venceslau SS et al (2013) Unifying concepts in anaerobic respiration: Insights from dissimilatory sulfur metabolism. *Biochim Biophys Acta* 1827:145–160
- Grein F, Venceslau SS, Schneider L et al (2010b) DsrJ, an essential part of the DsrMKJOP complex in the purple sulfur bacterium *Allochromatium vinosum*, is an unusual triheme cytochrome c. *Biochemistry* 49:8290–8299
- Griesbeck C, Schütz M, Schödl T et al (2002) Mechanism of sulfide-quinone oxidoreductase investigated using site-directed mutagenesis and sulfur analysis. *Biochemistry* 41:11552–11565
- Guo X, Yin H, Liang Y et al (2014) Comparative genome analysis reveals metabolic versatility and environmental adaptations of *Sulfobacillus thermosulfidooxidans* strain ST. *PLoS One* 9:e99417
- Hamilton TL, Bovee RJ, Thiel V et al (2014) Coupled reductive and oxidative sulfur cycling in the phototrophic plate of a meromictic lake. *Geobiology* 12:451–468
- Hedderich R, Hamann N, Bennati M (2005) Heterodisulfide reductase from methanogenic archaea: a new catalytic role for an iron-sulfur cluster. *Biol Chem* 386:961–970
- Heinzinger NK, Fujimoto SY, Clark MA et al (1995) Sequence analysis of the *phs* operon in *Salmonella typhimurium* and the contribution of thiosulfate reduction to anaerobic energy metabolism. *J Bacteriol* 177:2813–2820
- Hensel G, Trüper HG (1976) Cysteine and S-sulfocysteine biosynthesis in phototrophic bacteria. *Arch Microbiol* 109:101–103
- Hensel M, Hinsley AP, Nikolaus T et al (1999) The genetic basis of tetrathionate respiration in *Salmonella typhimurium*. *Mol Microbiol* 32:275–287
- Hensen D, Sperling D, Trüper HG et al (2006) Thiosulphate oxidation in the phototrophic sulphur bacterium *Allochromatium vinosum*. *Mol Microbiol* 62:794–810
- Hipp WM, Pott AS, Thum-Schmitz N et al (1997) Towards the phylogeny of APS reductases and sirohaem sulfite reductases in sulfate-reducing and sulfur-oxidizing prokaryotes. *Microbiology* 143:2891–2902
- Imhoff JF (2001) Transfer of *Pfennigia purpurea* Tindall 1999 (*Amoebobacter purpureus* Eichler and Pfennig 1988) to the genus *Lamprocystis* as *Lamprocystis purpurea* comb. nov. *Int J Syst Evol Microbiol* 51:1699–1701
- Imhoff JF (2003) Phylogenetic taxonomy of the family *Chlorobiaceae* on the basis of 16S rRNA and *fmo* (Fenna-Matthews-Olson protein) gene sequences. *Int J Syst Evol Microbiol* 53:941–951
- Imhoff JF, Pfennig N (2001) *Thioflaviccoccus mobilis* gen. nov., sp. nov., a novel purple sulfur bacterium with bacteriochlorophyll *b*. *Int J Syst Evol Microbiol* 51:105–110
- Imhoff JF, Süling J (1996) The phylogenetic relationship among Ectothiorhodospiraceae: a reevaluation of their taxonomy on the basis of 16S rDNA analyses. *Arch Microbiol* 165:106–113
- Imhoff JF, Hiraishi A, Süling J (2005) Anoxygenic phototrophic purple bacteria. In: Brenner DJ, Krieg NR, Staley JT, Garrity GM (eds) *Bergey's manual of systematic bacteriology*. Springer, New York, pp 119–132
- Imhoff JF, Süling J, Petri R (1998) Phylogenetic relationships among the *Chromatiaceae*, their taxonomic reclassification and description of the new genera *Allochromatium*, *Halochromatium*, *Isochromatium*, *Marichromatium*, *Thiococcus*, *Thiohalocapsa*, and *Thermochromatium*. *Int J Syst Bacteriol* 48:1129–1143
- Jormakka M, Yokoyama K, Yano T et al (2008) Molecular mechanism of energy conservation in polysulfide respiration. *Nat Struct Mol Biol* 15:730–737
- Kappler U, Bailey S (2005) Molecular basis of intramolecular electron transfer in sulfite-oxidizing enzymes is revealed by high resolution structure of a heterodimeric complex of the catalytic molybdopterin subunit and a c-type cytochrome subunit. *J Biol Chem* 280:24999–25007
- Kappler U, Schäfer H (2014) Transformations of dimethylsulfide. *Met Ions Life Sci* 14: 279–313

- Kappler U, Bennett B, Rethmeier J et al (2000) Sulfite: cytochrome *c* oxidoreductase from *Thiobacillus novellus*—Purification, characterization, and molecular biology of a heterodimeric member of the sulfite oxidase family. *J Biol Chem* 275:13202–13212
- Kappler U, Bernhardt PV, Kilmartin J et al (2008) SoxAX cytochromes, a new type of heme copper protein involved in bacterial energy generation from sulfur compounds. *J Biol Chem* 283:22206–22214
- Khanna S, Nicholas DJD (1982) Utilization of tetrathionate and ³⁵S-labelled thiosulphate by washed cells of *Chlorobium vibrioforme* f. sp. *thiosulfatophilum*. *J Gen Microbiol* 128:1027–1034
- Koblizek M (2015) Ecology of aerobic anoxygenic phototrophs in aquatic environments. *FEMS Microbiol Rev* 39:854–870
- Kostanjevecki V, Brige A, Meyer TE et al (2000) A membrane-bound flavocytochrome *c*-sulfide dehydrogenase from the purple phototrophic sulfur bacterium *Ectothiorhodospira vacuolata*. *J Bacteriol* 182:3097–3103
- Krafft T, Bokranz M, Klimmek O et al (1992) Cloning and nucleotide sequence of the *psrA* gene of *Wolinella succinogenes* polysulphide reductase. *Eur J Biochem* 206:503–510
- Kredich NM (1992) The molecular basis for positive regulation of *cys* promoters in *Salmonella typhimurium* and *Escherichia coli*. *Mol Microbiol* 6:2747–2753
- Kredich NM (1996) Biosynthesis of cysteine. In: Neidhardt FC (ed) *Escherichia coli* and *Salmonella typhimurium*. Cellular and molecular biology. American Society for Microbiology, Washington, pp 514–527
- Kulp TR, Hoft SE, Asao M et al (2008) Arsenic(III) fuels anoxygenic photosynthesis in hot spring biofilms from Mono Lake, California. *Science* 321:967–970
- Kurth J, Dahl C, Butt JN (2015) Catalytic protein film electrochemistry provides a direct measure of the tetrathionate/thiosulfate reduction potential. *J Am Chem Soc* 137:13232–13235
- Laska S, Lottspeich F, Kletzin A (2003) Membrane-bound hydrogenase and sulfur reductase of the hyperthermophilic and acidophilic archaeon *Acidianus ambivalens*. *Microbiology* 149:2357–2371
- Latorre M, Ehrenfeld N, Cortes MP et al (2016) Global transcriptional responses of *Acidithiobacillus ferrooxidans* Wenelen under different sulfide minerals. *Bioresour Technol* 200:29–34
- Leustek T, Saito K (1999) Sulfate transport and assimilation in plants. *Plant Physiol* 120:637–643
- Leyh TS (1993) The physical biochemistry and molecular genetics of sulfate activation. *Crit Rev Biochem Mol Biol* 28:515–542
- Liu Y-W, Denkmann K, Kosciow K et al (2013) Tetrathionate stimulated growth of *Campylobacter jejuni* identifies TsdA as a new type of bi-functional tetrathionate reductase that is widely distributed in bacteria. *Mol Microbiol* 88:188
- Lu W-P, Kelly DP (1988) Respiration-driven proton translocation in *Thiobacillus versutus* and the role of the periplasmic thiosulphate-oxidizing enzyme system. *Arch Microbiol* 149:297–302
- Lübbe YJ, Youn H-S, Timkovich R et al (2006) Siro(haem)amide in *Allochromatium vinosum* and relevance of DsrL and DsrN, a homolog of cobyrinic acid *a,c* diamide synthase for sulphur oxidation. *FEMS Microbiol Lett* 261:194–202
- MacRae IJ, Segel IH, Fisher AJ (2001) Crystal structure of ATP sulfurylase from *Penicillium chrysogenum*: insights into the allosteric regulation of sulfate assimilation. *Biochemistry* 40:6795–6804
- Mangold S, Valdés J, Holmes DS et al (2011) Sulfur metabolism in the extreme acidophile *Acidithiobacillus caldus*. *Front Microbiol*. doi:10.3389/fmicb.2011.00017
- Marcia M, Ermler U, Peng GH et al (2010a) A new structure-based classification of sulfide:quinone oxidoreductases. *Proteins: Struct, Funct, Bioinf* 78:1073–1083
- Marcia M, Langer JD, Parcej D et al (2010b) Characterizing a monotopic membrane enzyme. Biochemical, enzymatic and crystallization studies on Aquifex aeolicus sulfide:quinone oxidoreductase. *Biochim Biophys Acta, Biomembr* 1798:2114–2123
- Marcia M, Ermler U, Peng GH et al (2009) The structure of *Aquifex aeolicus* sulfide:quinone oxidoreductase, a basis to understand sulfide detoxification and respiration. *Proc Natl Acad Sci U S A* 106:9625–9630

- Marnocha CL, Levy AT, Powell DH et al (2016) Mechanisms of extracellular S(0) globule production and degradation in *Chlorobaculum tepidum* via dynamic cell-globule interactions. *Microbiology* 162(7):1125–1134
- Meyer TE, Cusanovich MA (2003) Discovery and characterization of electron transfer proteins in the photosynthetic bacteria. *Photosynth Res* 76:111–126
- Meyer B, Kuever J (2007) Molecular analysis of the distribution and phylogeny of dissimilatory adenosine-5'-phosphosulfate reductase-encoding genes (*aprBA*) among sulfur-oxidizing prokaryotes. *Microbiology* 153:3478–3498
- Meyer B, Imhoff JF, Kuever J (2007) Molecular analysis of the distribution and phylogeny of the *soxB* gene among sulfur-oxidizing bacteria—evolution of the Sox sulfur oxidation enzyme system. *Environ Microbiol* 9:2957–2977
- Middelburg J (2000) The geochemical sulfur cycle. In: Lens P, Hulshoff Pol W (eds) *Environmental technologies to treat sulfur pollution*. IWA Publishing, London, pp 33–46
- Müller FH, Bandejas TM, Urich T et al (2004) Coupling of the pathway of sulphur oxidation to dioxygen reduction: characterization of a novel membrane-bound thiosulphate:quinone oxidoreductase. *Mol Microbiol* 53:1147–1160
- Nakatani T, Ohtsu I, Nonaka G et al (2012) Enhancement of thioredoxin/glutaredoxin-mediated L-cysteine synthesis from S-sulfocysteine increases L-cysteine production in *Escherichia coli*. *Microb Cell Fact* 11:62
- Neumann S, Wynen A, Trüper HG et al (2000) Characterization of the *cys* gene locus from *Allochromatium vinosum* indicates an unusual sulfate assimilation pathway. *Mol Biol Rep* 27:27–33
- Ogawa T, Furusawa T, Nomura R et al (2008) SoxAX binding protein, a novel component of the thiosulfate-oxidizing multienzyme system in the green sulfur bacterium *Chlorobium tepidum*. *J Bacteriol* 190:6097–6110
- Osorio H, Mangold S, Denis Y et al (2013) Anaerobic sulfur metabolism coupled to dissimilatory iron reduction in the extremophile *Acidithiobacillus ferrooxidans*. *Appl Environ Microbiol* 79:2172–2181
- Ouyang J, Liu Q, Li B et al (2013) Proteomic analysis of differential protein expression in *Acidithiobacillus ferrooxidans* grown on ferrous iron or elemental sulfur. *Indian J Microbiol* 53:56–62
- Parey K, Demmer U, Warkentin E et al (2013) Structural, biochemical and genetic characterization of ATP sulfurylase from *Allochromatium vinosum*. *PLoS One* 8:e74707
- Pattaragulwanit K, Brune DC, Trüper HG et al (1998) Molecular genetic evidence for extracytoplasmic localization of sulfur globules in *Chromatium vinosum*. *Arch Microbiol* 169:434–444
- Pires RH, Lourenco AI, Morais F et al (2003) A novel membrane-bound respiratory complex from *Desulfovibrio desulfuricans* ATCC 27774. *Biochim Biophys Acta* 1605:67–82
- Pires RH, Venceslau SS, Morais F et al (2006) Characterization of the *Desulfovibrio desulfuricans* ATCC 27774 DsrMKJOP complex—a membrane-bound redox complex involved in the sulfate respiratory pathway. *Biochemistry* 45:249–262
- Podgorssek L, Imhoff JF (1999) Tetrathionate production by sulfur oxidizing bacteria and the role of tetrathionate in the sulfur cycle of Baltic Sea sediments. *Aquat Microb Ecol* 17:255–265
- Pott AS, Dahl C (1998) Sirohaem-sulfite reductase and other proteins encoded in the *dsr* locus of *Chromatium vinosum* are involved in the oxidation of intracellular sulfur. *Microbiology* 144:1881–1894
- Prange A, Chauvistré R, Modrow H et al (2002) Quantitative speciation of sulfur in bacterial sulfur globules: X-ray absorption spectroscopy reveals at least three different speciations of sulfur. *Microbiology* 148:267–276
- Prange A, Engelhardt H, Trüper HG et al (2004) The role of the sulfur globule proteins of *Allochromatium vinosum*: mutagenesis of the sulfur globule protein genes and expression studies by real-time RT PCR. *Arch Microbiol* 182:165–174
- Quatrini R, Appia-Ayme C, Denis Y et al (2006) Insights into the iron and sulfur energetic metabolism of *Acidithiobacillus ferrooxidans* by microarray transcriptome profiling. *Hydrometallurgy* 83:263–272

- Quatrini R, Appia-Ayme C, Denis Y et al (2009) Extending the models for iron and sulfur oxidation in the extreme acidophile *Acidithiobacillus ferrooxidans*. *BMC Genomics* 10:394
- Quentmeier A, Friedrich CG (2001) The cysteine residue of the SoxY protein as the active site of protein-bound sulfur oxidation of *Paracoccus pantotrophus* GB17. *FEBS Lett* 503:168–172
- Ramos AR, Keller KL, Wall JD et al (2012) The membrane QmoABC complex interacts directly with the dissimilatory adenosine 5'-phosphosulfate reductase in sulfate reducing bacteria. *Front Microbiol* 3:137
- Raymond JC, Sistrom WR (1969) *Ectothiorhodospira halophila*—a new species of the genus *Ectothiorhodospira*. *Arch Mikrobiol* 69:121–126
- Reijerse EJ, Sommerhalter M, Hellwig P et al (2007) The unusual redox centers of SoxXA, a novel c-type heme-enzyme essential for chemotrophic sulfur-oxidation of *Paracoccus pantotrophus*. *Biochemistry* 46:7804–7810
- Reinartz M, Tschäpe J, Brüser T et al (1998) Sulfide oxidation in the phototrophic sulfur bacterium *Chromatium vinosum*. *Arch Microbiol* 170:59–68
- Rodríguez J, Hiras J, Hanson TE (2011) Sulfite oxidation in *Chlorobaculum tepidum*. *Front Microbiol* 2:112. doi:10.3389/fmicb.2011.00112
- Sanchez O, Ferrera I, Dahl C et al (2001) In vivo role of APS reductase in the purple sulfur bacterium *Allochromatium vinosum*. *Arch Microbiol* 176:301–305
- Sander J, Dahl C (2009) Metabolism of inorganic sulfur compounds in purple bacteria. In: Hunter CN, Daldal F, Thurnauer MC, Beatty JT (eds) *Purple bacteria*. Springer, Dordrecht, pp 595–622
- Sander J, Engels-Schwarzlose S, Dahl C (2006) Importance of the DsrMKJOP complex for sulfur oxidation in *Allochromatium vinosum* and phylogenetic analysis of related complexes in other prokaryotes. *Arch Microbiol* 186:357–366
- Santos AA, Venceslau SS, Grein F et al (2015) A protein trisulfide couples dissimilatory sulfate reduction to energy conservation. *Science* 350:1541–1545
- Sauvé V, Bruno S, Berks BC et al (2007) The SoxYZ complex carries sulfur cycle intermediates on a peptide swinging arm. *J Biol Chem* 282:23194–23204
- Sauvé V, Roversi P, Leath KJ et al (2009) Mechanism for the hydrolysis of a sulfur-sulfur bond based on the crystal structure of the thiosulfohydrolase SoxB. *J Biol Chem* 284:21707–21718
- Schütz M, Maldener I, Griesbeck C et al (1999) Sulfide-quinone reductase from *Rhodobacter capsulatus*: requirement for growth, periplasmic localization, and extension of gene sequence analysis. *J Bacteriol* 181:6516–6523
- Schütz M, Shahak Y, Padan E et al (1997) Sulfide-quinone reductase from *Rhodobacter capsulatus*. *J Biol Chem* 272:9890–9894
- Sekowska A, Kung HF, Danchin A (2000) Sulfur metabolism in *Escherichia coli* and related bacteria: facts and fiction. *J Mol Microbiol Biotechnol* 2:145–177
- Shahak Y, Hauska G (2008) Sulfide oxidation from cyanobacteria to humans: sulfide-quinone oxidoreductase (SQR). In: Hell R, Dahl C, Knaff DB, Leustek T (eds) *Sulfur metabolism in phototrophic organisms*. Springer, Dordrecht, pp 319–335
- Shuman KE, Hanson TE (2016) A sulfide:quinone oxidoreductase from *Chlorobaculum tepidum* displays unusual kinetic properties. *FEMS Microbiol Lett* 363
- Simon J, Kern M (2008) Quinone-reactive proteins devoid of haem b form widespread membrane-bound electron transport modules in bacterial respiration. *Biochem Soc Trans* 36:1011–1016
- Simon J, Kroneck PM (2013) Microbial sulfite respiration. *Adv Microb Physiol* 62:45–117
- Singh KS, Kirksey J, Hoff WD et al (2014) Draft genome sequence of the extremely halophilic phototrophic purple sulfur bacterium *Halorhodospira halochloris*. *J Genet* 2:118–120
- Sirko A, Zatyka M, Sadowy E et al (1995) Sulfate and thiosulfate transport in *Escherichia coli* K-12: evidence for a functional overlapping of sulfate- and thiosulfate-binding proteins. *J Bacteriol* 177:4134–4136
- Smith AJ, Lascelles J (1966) Thiosulphate metabolism and rhodanese in *Chromatium* sp. strain D. *J Gen Microbiol* 42:357–370

- Sorokin DY (2003) Oxidation of inorganic sulfur compounds by obligately organotrophic bacteria. *Microbiology* 72:641–653
- Sorokin DY, Tourova TP, Kuznetsov BB et al (2000) *Roseinatronobacter thiooxidans* gen. nov., sp. nov., a new alkaliphilic aerobic bacteriochlorophyll a—containing bacterium isolated from a soda lake. *Microbiology* 69:75–82
- Spalding MD, Prigge ST (2010) Lipoic acid metabolism in microbial pathogens. *Microbiol Mol Biol Rev* 74:200–228
- Spring S (2014) Function and evolution of the Sox multienzyme complex in the marine Gamma-proteobacterium *Congregibacter litoralis*. ISRN Microbiol 2014:597418
- Studel R, Holdt G, Visscher PT et al (1990) Search for polythionates in cultures of *Chromatium vinosum* after sulfide incubation. *Arch Microbiol* 155:432–437
- Stockdreher Y, Sturm M, Josten M et al (2014) New proteins involved in sulfur trafficking in the cytoplasm of *Allochromatium vinosum*. *J Biol Chem* 289:12390–12403
- Stockdreher Y, Venceslau SS, Josten M et al (2012) Cytoplasmic sulfurtransferases in the purple sulfur bacterium *Allochromatium vinosum*: evidence for sulfur transfer from DsrEFH to DsrC. *PLoS One* 7:e40785
- Tank M, Bryant DA (2015a) *Chloracidobacterium thermophilum* gen. nov., sp. nov.: an anoxygenic microaerophilic chlorophotoheterotrophic acidobacterium. *Int J Syst Evol Microbiol* 65:1426–1430
- Tank M, Bryant DA (2015b) Nutrient requirements and growth physiology of the photoheterotrophic Acidobacterium, *Chloracidobacterium thermophilum*. *Front Microbiol* 6:226
- Thauer RK, Kaster AK, Seedorf H et al (2008) Methanogenic archaea: ecologically relevant differences in energy conservation. *Nat Rev Microbiol* 6:579–591
- Then J, Trüper HG (1981) The role of thiosulfate in sulfur metabolism of *Rhodospseudomonas globiformis*. *Arch Microbiol* 130:143–146
- Venceslau SS, Stockdreher Y, Dahl C et al (2014) The “bacterial heterodisulfide” DsrC is a key protein in dissimilatory sulfur metabolism. *Biochim Biophys Acta* 1837:1148–1164
- Visscher PT, Taylor BF (1993) Organic thiols as organolithotrophic substrates for growth of phototrophic bacteria. *Appl Environ Microbiol* 59:93–96
- Weissgerber T, Sylvester M, Kröninger L et al (2014a) A comparative quantitative proteome study identifies new proteins relevant for sulfur oxidation in the purple sulfur bacterium *Allochromatium vinosum*. *Appl Environ Microbiol* 80:2279–2292
- Weissgerber T, Watanabe M, Hoefgen R et al (2014b) Metabolomic profiling of the purple sulfur bacterium *Allochromatium vinosum* during growth on different reduced sulfur compounds and malate. *Metabolomics* 10:1094–1112
- Weissgerber T, Dobler N, Polen T et al (2013) Genome-wide transcriptional profiling of the purple sulfur bacterium *Allochromatium vinosum* DSM 180^T during growth on different reduced sulfur compounds. *J Bacteriol* 195:4231–4245
- Weissgerber T, Zigann R, Bruce D et al (2011) Complete genome sequence of *Allochromatium vinosum* DSM 180^T. *Stand Genomic Sci* 5:311–330. doi:10.4056/sigs.2335270
- Welte C, Hafner S, Krätzer C et al (2009) Interaction between Sox proteins of two physiologically distinct bacteria and a new protein involved in thiosulfate oxidation. *FEBS Lett* 583:1281–1286
- Wentzien S, Sand W, Albertsen A et al (1994) Thiosulfate and tetrathionate degradation as well as biofilm generation by *Thiobacillus intermedius* and *Thiobacillus versutus* studied by microcalorimetry, HPLC, and ion-pair chromatography. *Arch Microbiol* 161:116–125
- Wilson JJ, Kappler U (2009) Sulfite oxidation in *Sinorhizobium meliloti*. *Biochim Biophys Acta* 1787:1516–1525
- Woodin TS, Segel IH (1968) Glutathione reductase-dependent metabolism of cysteine-S-sulfate by *Penicillium chrysogenum*. *Biochim Biophys Acta* 167:78–88
- Yurkov VV, Krasil'nikova EN, Gorlenko VM (1994) Thiosulfate metabolism in the aerobic bacteriochlorophyll-a-containing bacteria *Erythromicrobium hydrolyticum* and *Roseococcus thiosulfatophilus*. *Microbiology* 63:91–94

- Zaar A, Fuchs G, Golecki JR et al (2003) A new purple sulfur bacterium isolated from a littoral microbial mat, *Thiorhodococcus drewsii* sp. nov. Arch Microbiol 179:174–183
- Zander U, Faust A, Klink BU et al (2010) Structural basis for the oxidation of protein-bound sulfur by the sulfur cycle molybdohemo-enzyme sulfane dehydrogenase SoxCD. J Biol Chem 286:8349–8360
- Zeng Y, Feng F, Medova H et al (2014) Functional type 2 photosynthetic reaction centers found in the rare bacterial phylum Gemmatimonadetes. Proc Natl Acad Sci U S A 111:7795–7800
- Zeng Y, Selyanin V, Lukes M et al (2015) Characterization of the microaerophilic, bacteriochlorophyll a-containing bacterium *Gemmatimonas phototrophica* sp. nov., and emended descriptions of the genus *Gemmatimonas* and *Gemmatimonas aurantiaca*. Int J Syst Evol Microbiol 65:2410–2419
- Zhang Y, Weiner JH (2014) Characterization of the kinetics and electron paramagnetic resonance spectroscopic properties of *Acidithiobacillus ferrooxidans* sulfide:quinone oxidoreductase (SQR). Arch Biochem Biophys 564:110–119

Biochemistry of Chlorophyll Biosynthesis in Photosynthetic Prokaryotes

Yuichi Fujita and Hisanori Yamakawa

Abstract Chlorophylls (Chls) are tetrapyrrole pigments that are essential for photosynthesis, which supports almost all organisms on the planet. Thus, elucidation of the molecular mechanisms of Chl biosynthesis is a major biological challenge. Nearly 100 different Chls with differing ring structures and substituents are represented by Chls *a*, *b*, *c*, *d*, and *f* and bacteriochlorophylls *a*, *b*, *c*, *d*, *e*, and *g*. Phototrophic prokaryotes perform photosynthesis using specific sets of Chls that capture available light under the conditions of their natural habitats. For example, cyanobacteria grow photosynthetically in the top layers of water columns using Chl *a*, whereas purple bacteria perform anoxygenic photosynthesis using bacteriochlorophyll *a* in the deeper layers of the water columns. Extensive gene searches have been performed in photosynthetic prokaryotes since the 1990s, and the largely complete scheme of Chl biosynthetic pathways includes a core pathway that is conserved among all photosynthetic organisms and comprises diverse reactions for the production of a variety of Chls. With this framework of biosynthetic pathways, further studies of Chl biosynthesis are directed at understanding the physiological and biochemical aspects. The physiological aspects include elucidation of regulatory networks that are integrated with other cellular processes, and the biochemical aspects include elucidation of three-dimensional structures of Chl biosynthetic enzymes to understand molecular mechanisms. In this chapter, we describe the current investigations of molecular mechanisms of enzymes in the Mg branch focusing on the latter aspects.

Keywords Bacteriochlorophyll • Chlorophyll • Crystal structures • Cyanobacteria • Photosynthetic bacteria • Mg branch

Introduction

Chlorophylls (Chls) are tetrapyrrole pigments that are essential for photosynthesis. Chls harvest light and transfer the energy to neighboring Chl molecules, and only select Chls participate in the first electron transfer event. Chls comprise multiple

Y. Fujita (✉) • H. Yamakawa
Graduate School of Bioagricultural Sciences, Nagoya University, Nagoya, Japan
e-mail: fujita@agr.nagoya-u.ac.jp

combinations of ring structures and pyrrole ring substituents, and nearly 100 different Chls have been identified in photosynthetic organisms (Scheer 2006). However, phototrophic organisms utilize light energy using specific sets of Chls with chemical structures that efficiently harvest light under unique environmental habitats.

Chls are classified into porphyrin, chlorin, and bacteriochlorin according to the oxidation states of the cyclic tetrapyrrole ring (Fig. 1; Rüdiger 2003; Scheer 2006). Ring structures profoundly affect the spectroscopic properties of the Chl pigments in addition to pyrrole rings substituents. However, bacteriochlorophylls (BChls) do not necessarily have bacteriochlorin rings, and BChls *c*, *d*, and *e* are chlorins that are similar to Chl *a* rather than bacteriochlorins.

Substituents of Chl variants predominantly occur at C3, C7, C8, and C12 positions (Fig. 1). However, the recently identified Chl *f* carries a formyl group at the C2 position. Novel Chls with different combinations of substituents will likely be discovered in future studies. In addition, novel Chls can be produced by the introduction of novel combinations of substituents using gene manipulation. Accordingly, BChl *f* was artificially produced by inactivation of the *bchU* gene in the green bacterium *Chlorobaculum limnaeum* (Harada et al. 2012; Vogl et al. 2012).

Only a specific set of Chls (Chl *a*, Chl *a*₂, BChl *a*, BChl *b*, Zn-BChl *a*, Chl *d*, and BChl *g* and their epimers) can operate as a special pair Chl to initiate charge separation events and function as antenna Chls. Other Chls function as antenna pigments that are engaged in harvesting light and transferring exciton energy to the neighboring Chls (Blankenship 2014; Fujita 2015). Photosynthetic prokaryotes produce all types of Chl except for Chl *c* and are used as model organisms for the molecular studies of Chl biosynthesis, which is a major challenge in biology.

Early searches for genes encoding Chl biosynthetic enzymes were performed using genetic analyses of the purple bacterium *Rhodobacter capsulatus* (Yen and Marrs 1976; Yang and Bauer 1990; Bollivar et al. 1994). These investigations were largely completed upon identification of the *chlF* gene, which encodes a Chl *f* synthase that catalyzes the formation of C2-formyl groups to convert Chl(ide) *a* to Chl(ide) *f* in cyanobacteria (Ho et al. 2016). Given the full gene list (Table 1) and corresponding “road map” (Fig. 2) of Chl biosynthesis, further studies of Chl biosynthesis are focused on detailed biochemical analyses of structure-based molecular mechanisms in diverse enzymes. These new research goals include elucidation of molecular mechanisms for efficient assembly of Chl-binding proteins into photosystems, light-harvesting complexes, and chlorosomes.

During the biogenesis of photosystems, Chl supply is coordinated with the production of apoproteins that avoids photooxidative damage by free Chl molecules (Nickelsen and Rengstl 2013; Yang et al. 2015; Heinz et al. 2016; Komenda and Sobotka 2016). In contrast with cyanobacteria and purple bacteria that have relatively simple Chl compositions, green bacteria produce at least three different types of Chl, including BChl *c*, *d*, or *e*, BChl *a*, and the Chl *a* derivative Chl *a*_{PD}, which has a *phytadienol* instead of a *phytol*. BChls *c*, *d*, or *e* work exclu-

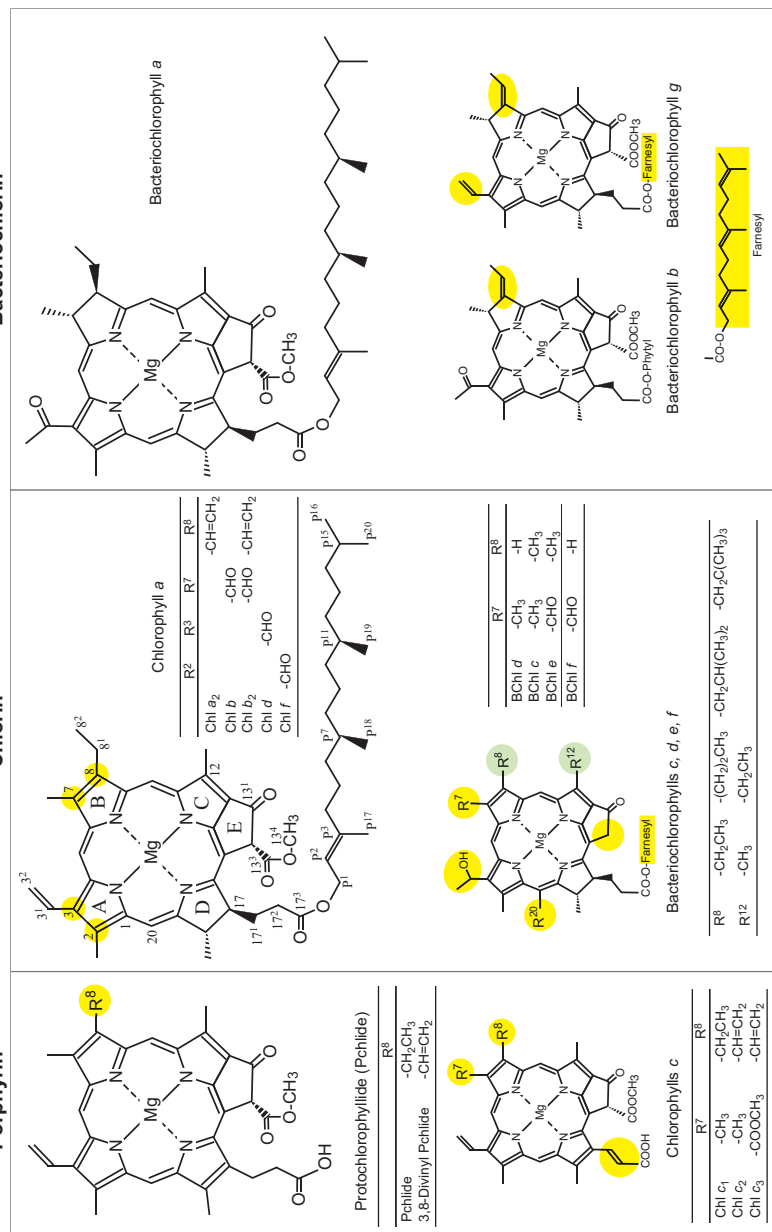


Fig. 1 Structures of various Chls. All Chls are classified as porphyrin, chlorin, or bacteriochlorin. As representatives of the three Chls, protochlorophyllide, Chl *a*, and BChl *a* are shown at the tops. In addition, Chl *c*; BChls *b* and *g* are shown below. Substituent groups are shown in *yellow* and are given in the accompanying small tables. Chls *a*₂ and *b*₂ are 3,8-divinyl Chls *a* and *b*, respectively, in the upper table in chlorin. BChls *c*, *d*, *e*, and *f* with R⁸- and R¹²-substituents are shown in *light green* to indicate that these Chls exist as mixtures of methylated homologs in chlorosomes. *S* and *R* configurations at C3' hydroxylated carbons of BChls *c*, *d*, *e*, and *f* are present as epimers in chlorosomes. In bacteriochlorin, structures of BChls *b* and *g* that differ from those of BChl *a* are highlighted in *yellow*

Table 1 List of genes involved in Chl and BChl biosynthetic pathways

No.	Enzyme	E.C. number	Gene (BChl <i>a</i>)	Gene (Chl <i>a</i>)	Comments
1	5-Aminolevulinate synthase	2.3.1.37	<i>hemA</i>	–	
2	Glutamyl-tRNA synthetase	6.1.1.17		<i>glTX</i>	Shared with protein synthesis
3	Glutamyl-tRNA reductase	1.2.1.70		<i>hemA</i>	First regulatory target of tetrapyrrole biosynthesis
4	Glutamate-1-semialdehyde 2,1-aminomutase	5.4.3.8		<i>hemL</i>	
5	5-Aminolevulinate dehydratase	4.2.1.24		<i>hemB</i>	
6	Porphobilinogen deaminase	2.5.1.61		<i>hemC</i>	
7	Uroporphyrinogen III synthase	4.2.1.75		<i>hemD</i>	
8	Uroporphyrinogen III decarboxylase	4.1.1.37		<i>hemE</i>	
9	Coproporphyrinogen III oxidase (oxygen independent)	1.3.99.22		<i>hemN</i>	Radical SAM family
10	Coproporphyrinogen III oxidase (oxygen dependent)	1.3.3.3		<i>hemF</i>	
11	Protoporphyrinogen IX oxidase	1.3.5.3		<i>hemY</i>	
12	Protoporphyrinogen IX oxidase	1.3.5.3		<i>hemG</i>	
13	Protoporphyrinogen IX oxidase	–		<i>hemJ</i>	
14	Protoporphyrin IX: Mg chelatase	6.6.1.1	<i>bchI</i> <i>bchD</i> <i>bchH</i>	<i>chlI</i> <i>chlD</i> <i>chlH</i>	Class I chelatase, AAA ⁺ family, I ₆ D ₆ hexamer, H ₂ dimer Stimulated by Gun4
15	Mg-protoporphyrin IX methyltransferase	2.1.1.11	<i>bchM</i>	<i>chlM</i>	Class I methyltransferase
16	Mg-protoporphyrin IX monomethyl ester cyclase (oxygen independent)	4.–.–.–	<i>bchE</i>	<i>chlE</i>	Radical SAM family, vitamin B ₁₂
17	Mg-protoporphyrin IX monomethyl ester cyclase (oxygen dependent)	1.14.13.81	<i>acsF</i>	<i>acsF</i> (<i>chlA</i> , <i>cyclI</i>)	Monooxygenase, binuclear irons
18	3,8-Divinyl chlorophyllide <i>a</i> 8-vinyl reductase	1.3.1.75	<i>bciA</i>	<i>bciA</i> (<i>dvr</i>)	NADPH dependent (N-DVR)
19	3,8-Divinyl protochlorophyllide 8-vinyl reductase	1.3.7.–	<i>bciB</i>	<i>bciB</i> (<i>cvrA</i>)	Ferredoxin dependent (F-DVR), FrhB-like, 2x[4Fe-4S] clusters, FAD

(continued)

Table 1 (continued)

No.	Enzyme	E.C. number	Gene (BChl <i>a</i>)	Gene (Chl <i>a</i>)	Comments
20	Protochlorophyllide oxidoreductase (light independent)	1.3.7.7	<i>bchL</i> <i>bchN</i> <i>bchB</i>	<i>chlL</i> <i>chlN</i> <i>chlB</i>	Nitrogenase-like, ferredoxin dependent, ATP-dependent reductase component as L ₂ dimer, catalytic component as N ₂ B ₂ heterotetramer, NB cluster
21	Protochlorophyllide oxidoreductase (light dependent)	1.3.3.33	<i>por</i>	<i>por</i>	SDR family, Light and NADPH dependent
22	(Bacterio)chlorophyll <i>a</i> synthase	2.5.1.62	<i>bchG</i>	<i>chlG</i>	
23	Geranylgeranyl reductase	1.3.1.83	<i>bchP</i>	<i>chlP</i>	
24	Chlorophyll(ide) <i>a</i> oxygenase	1.4.13.122		<i>cao</i>	Rieske Fe-S cluster, mononuclear iron
25	Chlorophyllide <i>a</i> oxidoreductase (3,8-divinyl chlorophyllide <i>a</i> 8-vinyl reductase)	1.3.7.35	<i>bchX</i> <i>bchY</i> <i>bchZ</i>		Nitrogenase-like, ferredoxin dependent, ATP-dependent reductase component as X ₂ dimer, catalytic component as Y ₂ Z ₂ heterotetramer, [4Fe-4S] cluster a-COR
26	C8-Ethylidene synthase	–			b-COR
27	(Bacterio)chlorophyllide <i>a</i> 3-vinyl hydroxylase	4.2.1.–	<i>bchF</i>		
28	3-Hydroxy (bacterio) chlorophyllide <i>a</i> dehydrogenase	1.–.–.–	<i>bchC</i>		
29	Chlorophyllide <i>a</i> demethoxycarbonylase	–	<i>bciC</i>		
30	3-Vinyl bacteriochlorophyllide <i>d</i> C8 ² -methyltransferase	2.1.1.–	<i>bchQ</i>		Radical SAM family
31	3-Vinyl bacteriochlorophyllide <i>d</i> C12 ² -methyltransferase	2.1.1.–	<i>bchR</i>		Radical SAM family
32	3-Vinyl bacteriochlorophyllide <i>d</i> 3 ¹ -hydroxylase	–	<i>bchV</i>		BchF-like
33	Bacteriochlorophyllide <i>d</i> C20-methyltransferase	2.1.1.–	<i>bchU</i>		Class I methyltransferase

(continued)

Table 1 (continued)

No.	Enzyme	E.C. number	Gene (BChl <i>a</i>)	Gene (Chl <i>a</i>)	Comments
34	Bacteriochlorophyllide <i>c</i> hydratase	–	<i>bciD</i>		Radical SAM family
35	Bacteriochlorophyll <i>d/c/e</i> synthase	2.5.1.–	<i>bchK</i>		ChlG/BchG-like
36	Chlorophyll(ide) <i>f</i> synthase	–		<i>chlF</i>	PsbA paralog

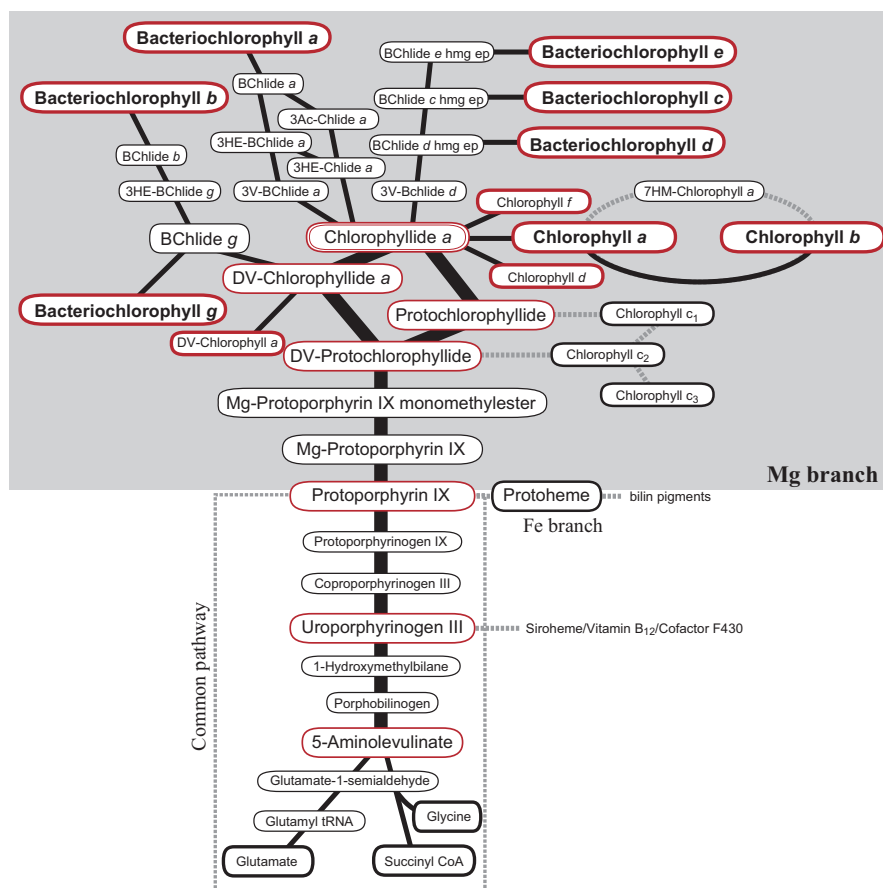


Fig. 2 A complete picture of Chl biosynthesis. All Chls diverge from protoporphyrin IX, which is produced by the common pathway. The Mg branch is shown with a *gray background*. *Thick black lines* indicate the core pathway from 5-aminolevulinate to Chlide *a*. Important intermediates that are shared by pathways are shown as *red circles* with thin lines. Final Chls are shown as *red circles* with thick lines. Chlide *a* is a hub intermediate and is shown in *red double circles* with thin lines. Pathways with *dotted lines* are eukaryotic photosynthetic organisms that are beyond the scope of this chapter. Abbreviations: *Chlide*, chlorophyllide; *BChlide*, bacteriochlorophyllide; *DV*, 3,8-divinyl; *3HE*, 3-hydroxyethyl; *3Ac*, 3-acetyl; *7HM*, 7-hydroxymethyl; *hmg*, homologs; and *ep*, epimers

sively as antenna Chls and are localized in chlorosomes (Pedersen et al. 2010). In contrast, BChl *a* is incorporated into reaction centers and FMO proteins, and Chl *a*_{PD} is incorporated in the reaction center as primary electron acceptor. These Chls appear to share biosynthetic pathways and unique biosynthetic branches, suggesting the presence of mechanisms that control localization of these Chls into various cellular compartments.

In this chapter, we briefly introduce the first nine Chl biosynthetic reactions, which are shared with heme biosynthesis, and then describe recent advances in the understanding of the Mg branch and specific pathways of Chl and BChl biosynthesis. Other aspects of Chl biosynthesis have been reviewed previously (Chew and Bryant 2007a, b; Tanaka and Tanaka 2007, 2011; Masuda and Fujita 2008; Stenbaek and Jensen 2010; Czarnecki and Grimm 2012; Chen 2014; Brzezowski et al. 2015).

Common Pathway

The first nine Chl biosynthetic reactions are common to the heme biosynthesis pathway and can be divided into three parts with three reactions each as follows: (1) 5-aminolevulinic acid (ALA) formation (Fig. 3), (2) formation of uroporphyrinogen III (Urogen) (Fig. 4), and (3) conversion to protoporphyrin IX (Proto) (Fig. 5).

Common Pathway 1: 5-Aminolevulinic Acid Formation

ALA is the common first precursor for all tetrapyrrole pigments, including Chls, hemes, bilins, and vitamin B₁₂ (Beale 2006; Jahn and Heinz 2009), and is produced (Fig. 3) from succinyl-CoA and glycine in condensation reaction of ALA synthase (1). This pathway is known as the C4 pathway or Shemin pathway and is distributed among α -proteobacteria, which are the most common type of photosynthetic bacteria.

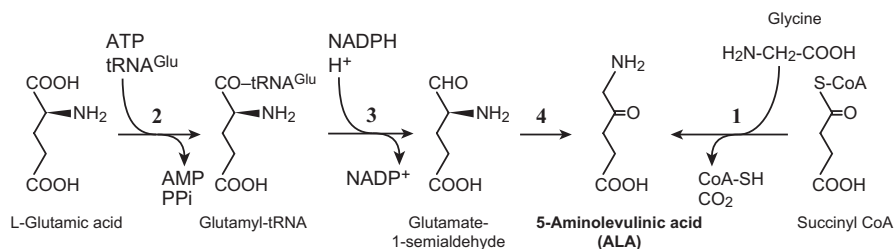


Fig. 3 First stage of the common pathway; ALA formation. The C4 (1) and C5 (2, 3 and 4) pathways are shown at the *right and left*, respectively. Numbers in **bold** (in Figs. 3 to 23) indicate the enzyme that catalyzes the reactions shown in Table 1

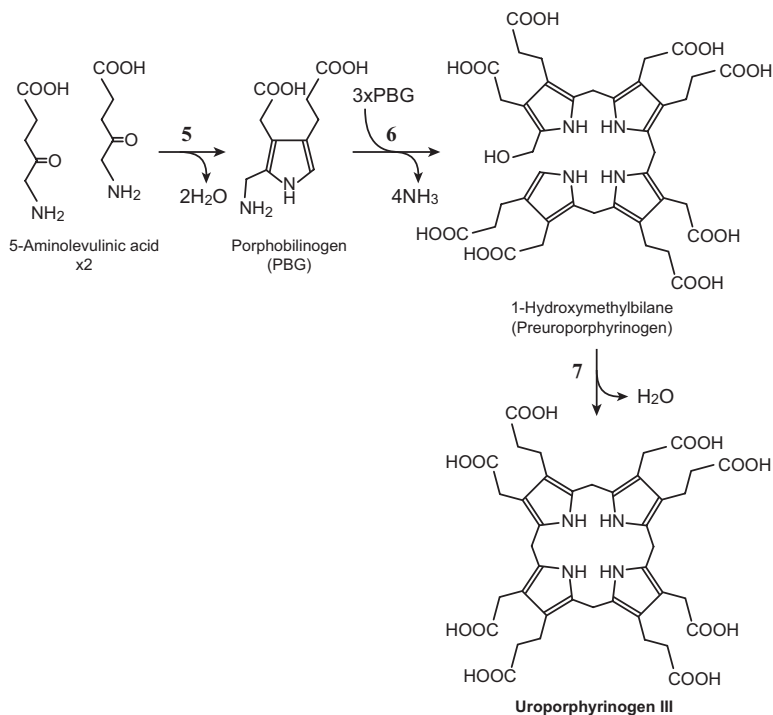


Fig. 4 Second stage of the common pathway. Three reactions (5, 6 and 7) from ALA to Urogen

Alternatively, ALA is synthesized in the C5 pathway, which comprises glutamyl-tRNA synthetase (2), glutamyl-tRNA reductase, (3) and glutamate-1-semialdehyde 2,1-aminomutase (4). The C5 pathway is more broadly distributed than the C4 pathway, and with the exception of purple bacteria (α -proteobacteria), most phototrophic prokaryotes produce ALA by the C5 pathway. Glutamyl-tRNA reductase is the target enzyme for feedback regulation of Chl and heme biosynthesis.

Common Pathway 2: From 5-Aminolevulinatate to Uroporphyrin III

Eight ALA molecules are sequentially condensed to form uroporphyrinogen III (Urogen) (Fig. 4; Schubert et al. 2009). Urogen is the precursor for vitamin B₁₂ and F430 and is the first branching point for these tetrapyrrole pigments. Initially, two ALA molecules are condensed to form the pyrrole unit porphobilinogen (PBG) by ALA dehydratase (5). PBG deaminase (6) then condenses four PBG molecules to form 1-hydroxymethylbilane (preuroporphyrinogen), the first tetrapyrrole pigment. Subsequently, Urogen synthase (7) cyclizes the linear tetrapyrrole to form Urogen with inversion of the D ring, leading to the asymmetry of porphyrin.

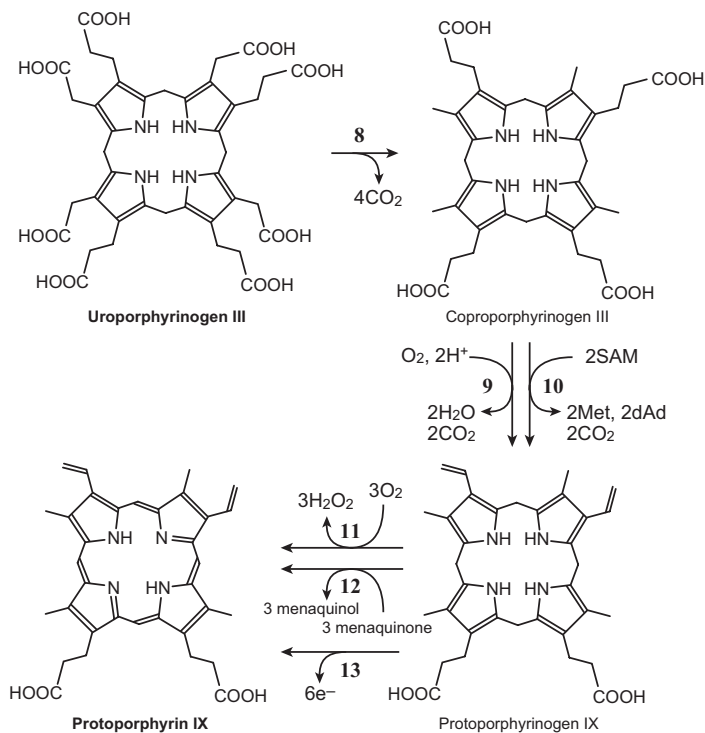


Fig. 5 Third stage of the common pathway involving three reactions from Urogen to Proto. After the first reaction by Urogen decarboxylase (8), two (9 and 10) and three (11, 12 and 13) analogous enzymes are present in Cpgen oxidase and PPgen oxidase reactions, respectively

Common Pathway 3: From Uroporphyrinogen III to Protoporphyrin

Urogen is converted to protoporphyrin (Proto) by three reactions (Fig. 5; Cornah and Smith 2009), and Proto is the final common intermediate for Chls and heme. Initially, four carboxy groups of Urogen are shortened to methyl groups by Urogen decarboxylase to form coproporphyrinogen III (CPgen) (8). Subsequently, two of the four propionate groups are shortened to vinyl groups by CPgen oxidase (CPO) to form protoporphyrinogen IX (PPgen) (9, 10). Two evolutionarily unrelated CPOs have been identified, including HemF, which requires oxygen for the reaction (9), and the oxygen-independent CPO HemN (10). Most purple bacteria and cyanobacteria use these enzymes differentially in response to environmental oxygen levels. Accordingly, HemF is a constitutive CPO, whereas HemN is induced when cells are exposed to hypoxic environments. PPgen is finally converted to Proto by PPgen oxidase (PPO) (11, 12, 13). Three evolutionarily unrelated PPOs (HemY, HemG, and HemJ) were previously identified (Kobayashi et al. 2014). Among these, HemY is most ubiquitously distributed among green bacteria and among some cyanobacteria, plants, animals, and fungi (11). PPO supplies Proto for Mg chelatase and ferrochelatase that

produce Chls and heme, respectively. Direct interactions between PPO (HemY) and ferrochelatase have been proposed to be associated with efficient transfer of the strong photosensitizer Proto in tobacco plants (Koch et al. 2004), and a probable complex of PPO (HemY) and the H subunit of Mg chelatase was recently proposed (see below; Chen et al. 2015a). HemG is only found in γ -proteobacteria and green bacteria (12), and HemJ was identified in the cyanobacterium *Synechocystis* sp. PCC 6803 (*Synechocystis* 6803) (Kato et al. 2010) (13) and is distributed among purple bacteria and cyanobacteria.

Due to close relationship with the production of erythrocytes in humans, all heme biosynthetic enzymes have been extensively studied in medical research fields. Moreover, with exception of HemG and HemJ, crystal structures of these enzymes are available (Masuda and Fujita 2008). In contrast, little is known of Mg branch enzymes, despite recent structural studies (Fig. 6).

A Core Pathway of the Mg Branch: Protoporphyrin IX to Chlorophyllide *a*

The Mg branch comprises more than 20 distinct enzymes that are involved in the biosynthesis of Chls *a* and *b* and BChls *a*, *b*, *c*, *d*, and *e*. However, three-dimensional structures are only available for four of these enzymes including Mg chelatase (MgCh), ChlM, dark-operative protochlorophyllide (Pchlde) oxidoreductase (DPOR), and BchU and for the accessory protein GUN4 (Fig. 6). Although whole structures and reaction mechanisms were proposed in DPOR, structures for Mg Ch remain incomplete and only include the catalytic component ChlH and a low-resolution structure of the ID complex. As indicated in Fig. 6, Mg Ch and DPOR are especially large complexes in the Chl *a* biosynthesis. In the following sections, we describe properties of individual Mg branch enzymes in detail.

Mg Chelatase

MgCh is a key enzyme at the branch point between heme and Chl biosynthesis pathways (Fig. 7, 14; Willows and Hansson 2003) and catalyzes ATP-dependent insertion of Mg^{2+} into Proto to form Mg-protoporphyrin IX (Mg-Proto) as the first committed enzyme of the Mg branch. This reaction is complicated by the involvement of three-subunit proteins and the three substrates, Proto, Mg^{2+} , and ATP. In addition, Mg^{2+} is incorporated into Proto and is separately required for ATP hydrolysis.

Class I chelatases include MgCh, cobalt chelatase in vitamin B₁₂ biosynthesis, and nickel chelatase in F430 biosynthesis (Bollivar 2010), whereas Class II chelatases include ferrochelatase and sirohydrochlorin ferrochelatase, which incorporate iron but do not require ATP (Romão et al. 2011). In contrast with the

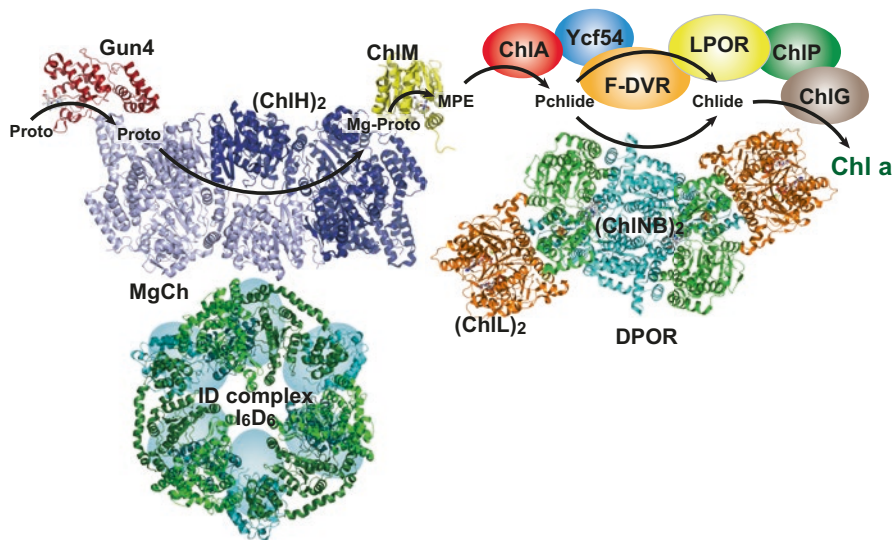


Fig. 6 A graphical summary of Chl *a* biosynthesis in cyanobacteria. Four crystallographic structures of MgCh, Gun4, ChlM, and DPOR are shown in the same scale. The other enzymes are included schematically. Note that MgCh (the ChlH dimer and the ID complex) and DPOR [a stabilized complex of the L protein (ChlL)₂ and the NB protein (ChlNB)₂] complexes are very large compared with ChlM and Gun4 proteins of about 30 kD. In the ID complex, the integrin I domain of ChlD (C-terminal domain) is shown in *cyan ellipses*. Spatial arrangements of Gun4 and ChlM on ChlH are hypothetical, although experiments suggest that both proteins are physically associated with ChlH. Accession codes in the Protein Data Bank of ChlH, ID complex, Gun4, ChlM, and DPOR complex are 4ZHD, 2X31, 4XKB, and 2YNM, respectively

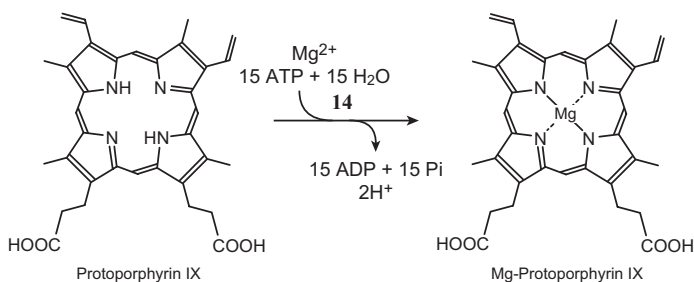


Fig. 7 Reaction of Mg chelatase. About 15 ATP molecules are hydrolyzed by the I subunit, and Mg²⁺ is incorporated into the center of Proto on the catalytic subunit H through formation of a transient holoenzyme with the ID complex (see Figs. 8 and 9)

single polypeptide enzyme ferrochelatase (HemH), MgCh comprises I (ChlI/BchlI, ca. 40 kD), D (ChlD/BchlD, ca. 70 kD), and H (ChlH/BchlH, ca. 140 kD) subunits, and the transient holoenzyme complex, the IDH complex, appears to dissociate after the reaction.

The I Subunit (BchI/ChII)

The I subunit is a member of the ATPases associated with diverse cellular activities (AAA⁺) superfamily and plays roles as the ATPase subunit and the Mg²⁺ donor. Walker A and B motifs are conserved in the N-terminal region of the I subunit, and the X-ray crystallographic structure was determined in BchI from *R. capsulatus* as a monomeric form at a resolution of 2.1 Å (Fodje et al. 2001). Moreover, BchI forms a hexameric structure in the presence of ATP (Hansson et al. 2002), and electron microscopy analyses identified this structure as a ring with a diameter of 120 Å (Fodje et al. 2001). Although the crystal structure was only solved as a monomeric form, the hexameric structure was simulated based on the homologous hexameric protein HslU.

The D Subunit (BchD/ChID)

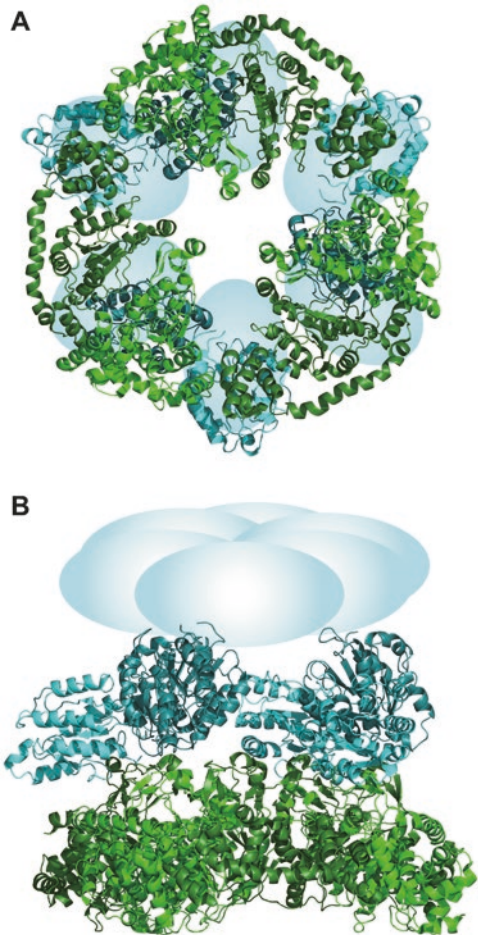
The D subunit also has an N-terminal AAA⁺ domain with relatively high similarity to that of the I subunit. Because the Walker motif is incomplete, the D subunit does not have ATPase activity. Moreover, the N-terminal domain is connected to the unique C-terminal region via Pro-rich and acidic linker regions. A unique C-terminal domain of about 200 amino acid residues is referred to as the integrin I domain and is present as a component of integral membrane receptor proteins that are involved in cell–cell and cell–matrix interactions in animal cells. The integrin I domain contains the unique short metal iron-dependent adhesion site (MIDAS) motif (DxSxS) as a specific metal-binding site, and the MIDAS motif is associated with other conserved motifs of the other subunits (LDV in H subunit and RGE/D in I subunit), suggesting interactions of the D subunit with H and I subunits (Fodje et al. 2001).

D subunits form a hexamer in the absence of ATP and may serve as a scaffold for assembly of the I hexamer into the ID complex, which is dependent on ATP. Three structures of the ID complex (ID–ADP, ID–AMPPNP, and ID–ATP) from *R. capsulatus* were reconstructed at 7.5, 14, and 13 Å, respectively, using single-particle cryo-electron microscopy and confirmed the two-tiered hexameric ring structure (Figs. 6 and 8; Lundqvist et al. 2010). Structural differences between these three ID complexes suggest that conformational changes in integrin I domains of the D subunits modulate interaction modes with protomer interfaces of the I hexamer. This conformational change may be coupled with the insertion of Mg²⁺ into Proto on the H subunit, which binds the ID complex transiently to complete chelation.

The H Subunit (BchH/ChIH)

When the largest subunit H is overexpressed in *Escherichia coli*, it was purified as a Proto-bound form, suggesting involvement as the catalytic component of MgCh (Gibson et al. 1995). In accordance with a current hypothesis, the Proto-bound H subunit interacts with the ID complex to form a transient holoenzyme. Subsequently,

Fig. 8 Crystal structures of *top* (A) and *side* (B) views of the ID complex. Contiguous protomers of the ChII hexamer are shown in *green* and *dark green*. Contiguous protomers of the ChID hexamer are shown in *cyan* and *dark cyan*. C-terminal domains (integrin I domain) are shown schematically as *light cyan* ellipses



Mg-Proto is produced on the H subunit following ATP hydrolysis by the I subunit, and the holoenzyme complex dissociates immediately (Axelsson et al. 2006; Lundqvist et al. 2010). The released Mg-Proto is then delivered to the enzyme ChlM, either directly or via GUN4, and is not released into the solution (Shepherd et al. 2005).

Initially, three-dimensional structures of the H subunit were determined using electron microscopy and single-particle reconstruction techniques in BchH from *R. capsulatus* (Sirijovski et al. 2008). The low-resolution structure at a 25 Å resolution showed that the apo form of ChlH comprises three lobe-shaped domains (lobes I, II, and III). Whereas lobes I and III are characteristic protruding “thumb” and “finger” structures, respectively, these unique structures are fused in another structure of the substrate-bound form (BchH-Proto, at about 28 Å resolution), indicating a substrate-induced conformational change. In concomitant proteolytic analyses, Apo-BchH (130 kDa) was digested by a protease into a 45-kDa C-terminal domain, whereas the

substrate-bound form (BchH-Proto) was resistant to proteolysis. This observation suggests that substrate-induced conformational changes increase structural rigidity.

Recently, an X-ray crystallographic structure of ChlH from *Synechocystis* 6803 was determined at 2.5 Å (Chen et al. 2015a, Figs. 6 and 9), and domains I–VI (numbered from the N-terminal) were identified. In these analyses, domains III and IV formed a cage-like structure, and domains I and II formed head and neck structures, respectively. The Proto substrate-binding pocket was proposed to be a hydrophobic cleft between domains III and V, mediating Proto interactions with six residues in domain III and thirteen residues in domain V. This scattered distribution of associated amino acid residues may be consistent with previous proteolytic digestion and Proto-binding analyses of BchH (Sirijovski et al. 2008).

Substrate binding of a full-length apo-BchH protein was lost upon truncation of N-terminal and C-terminal domain proteins. However, further structural analyses are required to elucidate mechanisms of Mg chelation. In addition, structural insights into the interaction between the H subunit and the ID complex remain uncharacterized, reflecting poor understanding of how the dimeric H subunit interacts with the three-fold symmetric structure of the ID complex.

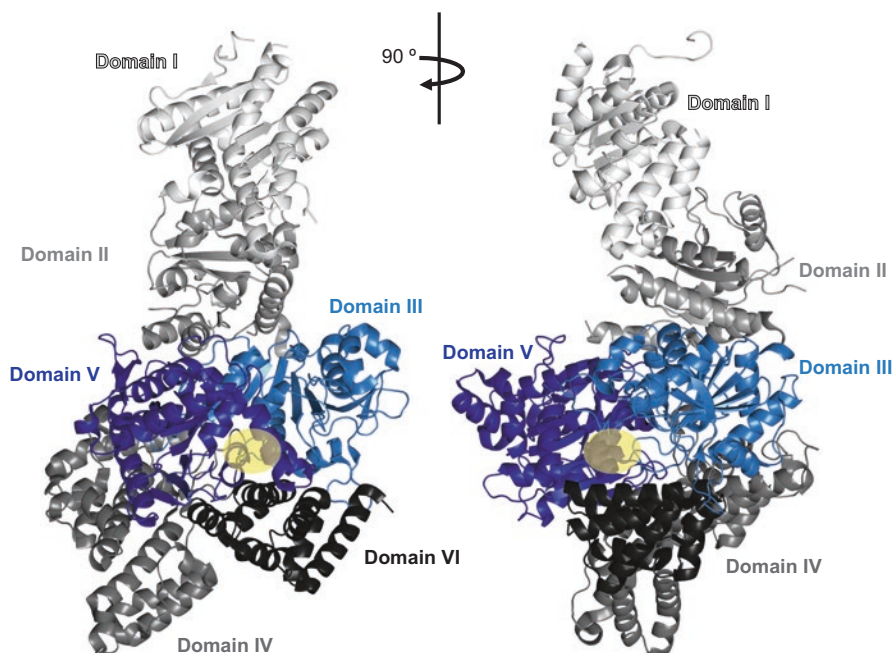


Fig. 9 Crystal structures of the ChlH monomer from *Synechocystis* 6803. Although the crystal structure of ChlH is a homodimer (Fig. 6), the monomer structure is shown here. ChlH comprises domains I–VI. A probable Proto-binding site (shown by a yellow circle) was proposed as an internal pocket between domains III (blue) and V (dark blue)

Interactions of the H Subunit with Other Enzymes for Substrate/Product Channeling

The MgCh substrate Proto is provided by PPO (see above), and because Proto is a potent photosensitizer, it should not be present as a free form in the cytosol. The crystal structure of ChlH was used to model a complex with tobacco PPO1 and to investigate efficient channeling of Proto (Chen et al. 2015a). In this model, a PPO1 dimer interacts with a ChlH dimer, and the distance between probable substrate-binding sites of PPO1 and ChlH was reportedly about 49 Å in the supercomplex PPO1–ChlH. However, dynamic conformational changes of both enzymes are required for direct channeling of Proto. In addition, the PPO types, HemY, HemG, and HemJ, are widely distributed among photosynthetic prokaryotes (Kobayashi et al. 2014), but are evolutionarily unrelated. Specifically, tobacco PPO1 corresponds with HemY, whereas PPO corresponds with HemJ in most cyanobacteria, such as *Synechocystis* 6803 (Kato et al. 2010). Thus, the crystal structure of HemJ is required to investigate channeling between PPO and MgChl in cyanobacteria.

GUN4

Gun4 is a porphyrin-binding protein (22–27 kD) that is involved in the regulation of tetrapyrrole biosynthesis. The *gun4* gene was identified in *Arabidopsis thaliana* as a genome locus and mutation caused a genome uncoupling phenotype, in which nuclear and plastid genes were decoupled (Larkin et al. 2003). In wild-type *A. thaliana*, functional decreases in plastid suppress nuclear genes encoding plastid-localized proteins, such as light-harvesting Chl *alb*-binding proteins (LHCB), implying the presence of a retrograde signal from plastids to nuclei. Moreover, lesions on genes for H subunits (*gun5*) and Gun4 commonly caused the “*gun*” phenotype, suggesting retrograde signaling by Mg-Proto (Mochizuki et al. 2001). However, this model was later questioned due to the lack of correlations between Mg-Proto contents and *Lhcb* gene expression (Mochizuki et al. 2008; Moulin et al. 2008). As an alternative, singlet oxygen generated by photosensitization of Mg-Proto may mediate complex feedback regulation of ALA synthesis (Schlicke et al. 2014).

Gun4 from *Synechocystis* 6803 stimulates MgCh activity by binding and transferring the porphyrin substrate to the H subunit via direct interactions, resulting in stimulation of MgCh activity (Larkin et al. 2003). Interestingly, Gun4 alleviates impairments of MgCh activity caused by ChlH variants with point substitutions (Ala942 in *gun5* and Pro595 in *cch*) (Davison and Hunter 2011), confirming that Gun4 and ChlH interact directly.

The X-ray crystal structure of Gun4 from *Synechocystis* 6803 was revealed at 2.3 Å, and a probable Proto-binding site was proposed (Verdecia et al. 2005). Moreover, crystal structures of Gun4 complexes with deuteroporphyrin IX (1.5 Å) and Mg-deuteroporphyrin IX (2.0 Å) were recently determined (Chen et al. 2015b, Figs. 6 and 10), and the proposed binding mode was confirmed. Deuteroporphyrin IX is a comparatively stable Proto analogue, and both of these porphyrins bound

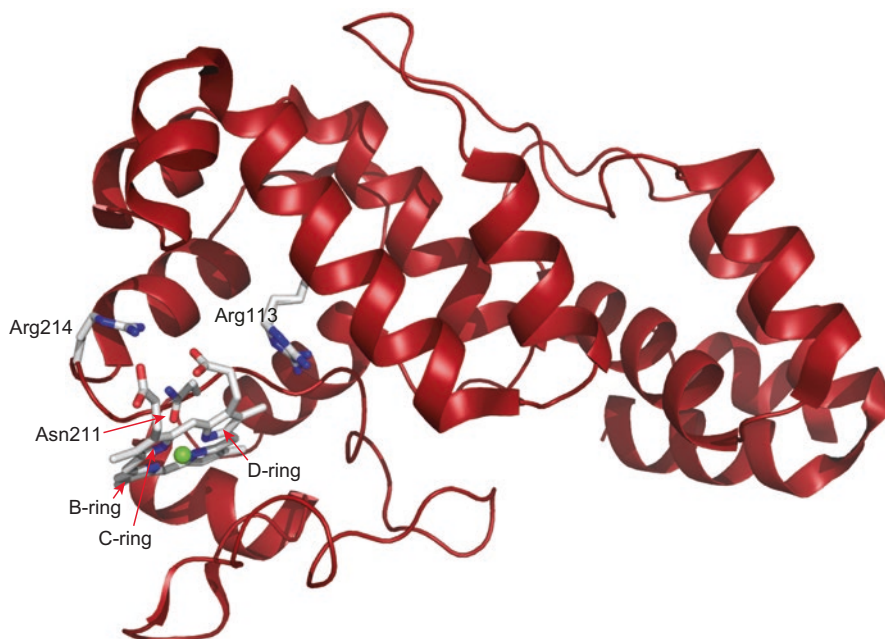


Fig. 10 Crystal structure of Mg-deuteroporphyrin IX-bound Gun4 from *Synechocystis* 6803. Note that Mg-deuteroporphyrin IX is arranged as B- and C-rings exposed to the solvent. Two positive charges from Arg113 and Arg214 interact with the negatively charged C17 and C13 propionates, respectively, which may facilitate the binding of Mg-Proto or Proto. In addition, Asn211 serves as an axial ligand to the central Mg^{2+} ion of Mg-deuteroporphyrin IX

Gun4 through extensive hydrophobic interactions in the binding pocket, leading to exposure of their B- and C-rings to the solvent, thus facilitating direct transfer of Proto and Mg-Proto to the H subunit and ChlM, respectively.

The *gun4* gene is ubiquitously distributed among oxygenic phototrophic organisms including cyanobacteria, but was not found in *Gloeobacter violaceus* PCC 7421. Moreover, no *gun4* homologs were identified in anoxygenic photosynthetic bacteria. However, *gun4* gene is conserved in chloroplast DNA of some eukaryotic photosynthetic organisms, such as the red algae *Cyanidium caldarium* and *Porphyra purpurea* (De Las Rivas et al. 2002), and this gene is denoted *yef53* as a conserved open reading frame in the chloroplast genome (Peter et al. 2011).

To assess physiological roles of Gun4 in cyanobacteria, mutant *Synechocystis* 6803 cells lacking a *gun4* ortholog (*sll0558*) were isolated (Wilde et al. 2004; Sobotka et al. 2008). The *gun4*-mutant lost photoautotrophic growth ability but grew in the presence of glucose, reflecting decreased MgCh activity and Chl contents (8% of WT) and accumulation of Proto under medium light intensity ($50 \mu\text{mol m}^{-2} \text{s}^{-1}$). In addition, ferrochelatase activity was greatly decreased suggesting that Gun4 modulates metabolic flow between Mg and Fe branches of tetrapyrrole biosynthesis in cyanobacteria.

Mg-Protoporphyrin IX Methyltransferase

The C13 propionate of Mg-Proto is methylated by Mg-Proto methyltransferase (ChlM/BchM, Fig. 11A, 15). Mg-Proto has two propionate groups in symmetric positions at C13 and C17, and methylation of these is nearly random in chemical modification. In contrast, ChlM strictly methylates the C13 propionate group giving rise to Mg-Proto monomethyl ester (MPE). Similar to other methyltransferases, ChlM requires the methyl donor *S*-adenosyl methionine (SAM), which is converted to *S*-adenosyl homocysteine (SAH) after the transfer of methyl group to Mg-Proto.

ChlM is a member of the Class I methyltransferase family, which includes various methyltransferases with various substrates (Schubert et al. 2003). A unique feature of ChlM is that it methylates carboxyl groups. His-tagged ChlM protein was a monomer (26 kD) in gel filtration chromatography analyses. The enzyme activity was observed with purified ChlM proteins from *R. sphaeroides* (Gibson and Hunter 1994) and *Synechocystis* 6803 (Shepherd et al. 2003). Steady kinetics analyses of cyanobacterial ChlM revealed a random-order mechanism, in which SAM and Mg-Proto bind to free ChlM in either order and form the ternary complex ChlM–Mg-Proto–SAM and then the products SAH and MPE are released from the enzyme in either order (Shepherd et al. 2003). In a subsequent study, a reaction intermediate was detected using a stopped-flow technique, and the initial phase of the reaction was analyzed for the first time in enzymes of Chl biosynthesis (Shepherd et al. 2005).

The H subunit of MgCh (ChlH) stimulates ChlM activity, and quenched-flow analysis suggested that this follows accelerated formation and decay of a reaction intermediate in the catalytic cycle (Shepherd et al. 2005). As mentioned above, MgCh is the first committed enzyme of the Mg branch. Hence, tight coupling between the sequential reactions of MgCh and ChlM methyltransferase may contribute to a regulatory mechanism that controls the metabolic flow of Proto.

Recently X-ray crystal structures of cyanobacterial ChlM complexes with SAM and SAH were determined at a resolution of 1.6 and 1.7 Å, respectively (Figs. 6 and 11B, Chen et al. 2014). As expected from other methyltransferases, ChlM carries the core fold of seven-stranded β -sheets that interact with five α -helices. Moreover, in these crystal structures, SAM and SAH are bound by the conserved motifs DXGCGXG and DI in the same orientation. However, attempts to crystallize ChlM in complex with Mg-Proto were unsuccessful, and binding of Mg-Proto was simulated based on structures of SAM/SAH-bound ChlM. These simulations indicated a deep hydrophobic cleft in the vicinity of the SAM-binding site, suggesting that the carboxylate at the C13 propionate of Mg-Proto forms hydrogen bonds with the conserved Tyr28 and His139 residues. His139 may also deprotonate the C13-propionate group, potentially facilitating direct methyl transfer from SAM to the negatively charged carboxylate. In addition, Tyr28 may contribute to the proper orientation of donor and acceptor groups during catalysis (Fig. 11B).

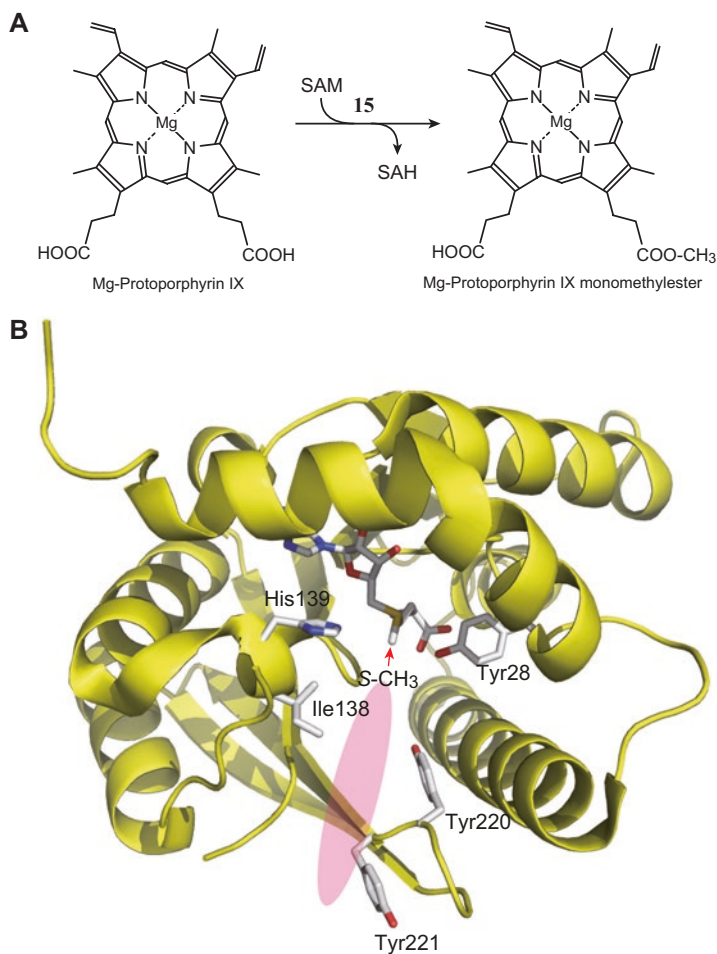


Fig. 11 (A) Reaction of Mg-Proto methyltransferase (**15**). The methyl group of SAM is specifically transferred to the C13 propionate by the methyltransferase ChlM. This reaction appears to be tightly coupled with the MgCh reaction. (B) Crystal structure of the ChlM-SAM complex from *Synechocystis* 6803. The spatial arrangement of the substrate Mg-Proto has not yet been determined. However, a cleft (shown by a pink ellipse) close to the S-methyl group (indicated by arrow) is proposed to be the Mg-Proto-binding pocket. Ile138, Tyr220, and Tyr221 in the cleft may have hydrophobic interactions with the Mg-Proto. Two conserved amino acid residues Tyr28 and His139 may be involved in methyl transfer

Mg-Protoporphyrin IX Monomethyl Ester Oxidative Cyclase

The fifth ring (E-ring) is a unique structure of Chl-related tetrapyrrole pigments. This complex structure is formed by an oxidative cyclization reaction of Mg-Proto monomethyl ester (MPE) that is catalyzed by MPE cyclase (Fig. 12). Two evolutionarily unrelated enzyme systems have been identified, involving the

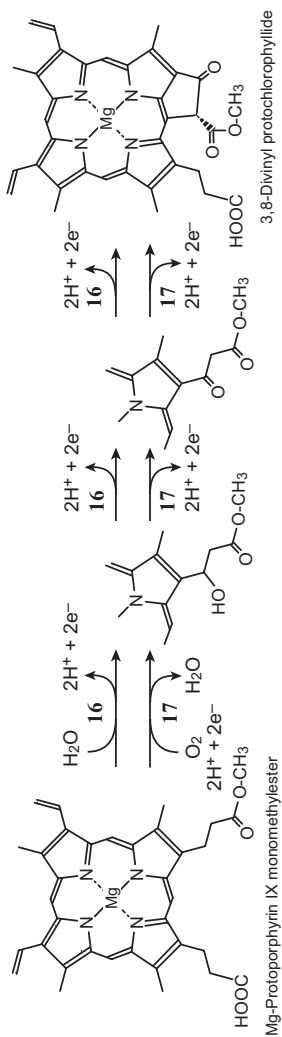


Fig. 12 Reactions of MPE cyclase involving two enzymes. Oxygen-independent MPE cyclase BchE (16) uses water as the oxygen donor for the C13¹ oxo group. Oxygen-dependent MPE cyclase AscF/ChIA (17) is a monooxygenase that uses oxygen (O₂) to form the C13¹ oxo group. Two common intermediates are assumed for both enzymes

oxygen-independent and oxygen-dependent enzymes, BchE (Fig. 12, 16) and AcsF/ChlA (Fig. 12, 17), respectively. However, both reactions remain undefined due to the absence of established reconstitution systems with purified enzymes.

Oxygen-Independent MPE Cyclase BchE

bchE was identified as the responsible gene for the accumulation of MPE in the photosynthetic gene cluster of *R. capsulatus* (Bollivar et al. 1994). This gene is distributed among most photosynthetic bacteria, but is not found in eukaryotic photosynthetic organisms. Three genes were assumed to be *bchE* orthologs in the genome of the cyanobacterium *Synechocystis* 6803. However, phenotype and pigment analyses of knockout mutants of these genes failed to show BchE-type MPE cyclase activities of the gene products (Minamizaki et al. 2008). Instead, we demonstrated that two homologous genes for AcsF-type MPE cyclase (named ChlA_I and ChlA_{II}) operate differentially in *Synechocystis* 6803. Subsequently, however, using abundant genome sequence data for many cyanobacteria, Bandyopadhyay et al. pointed out the more plausible *bchE*-like genes in the *Cyanothece* species PCC 7425 and 7822 (Bandyopadhyay et al. 2011). Accordingly, we introduced these *bchE*-like genes into a *bchE*-lacking mutant of *R. capsulatus* and showed that both transconjugants grew photosynthetically with restored production of BChl. Thus, we concluded that these *bchE*-like genes are *bchE* orthologs that should be called *chlE* (Yamanashi et al. 2015). However, the distribution of *bchE* in cyanobacteria is sporadic, suggesting that *bchE* was lost during evolution in many cyanobacterial lineages.

The amino acid sequence of BchE indicates that BchE belongs to the radical SAM superfamily. In particular, the central domain of BchE carries a typical Cys motif (CxxxCxxC) that binds a [4Fe-4S] cluster, which is a common feature of radical SAM family enzymes. The [4Fe-4S] cluster is bound by three conserved Cys, and the fourth ligand is the amide group of SAM in HemN, a representative of radical SAM enzymes (Layer et al. 2003). The presence of an Fe-S cluster in BchE was indicated by characteristic absorption spectra of an insoluble fraction from *E. coli* overexpressing BchE (Ouchane et al. 2004). Moreover, an N-terminal motif for binding of vitamin B₁₂ was identified in BchE. Finally, vitamin B₁₂-requiring mutants of *R. capsulatus* accumulate MPE, suggesting probable vitamin B₁₂-dependency of BchE (Gough et al. 2000).

The origin of the 13¹-oxo group of the product 3,8-divinyl Pchl_{id} is an oxygen atom from a water molecule in BchE, and a radical-mediated reaction mechanism was proposed (Gough et al. 2000). In this model, the first hydroxylation to form 13¹-hydroxy MPE is an oxidation reaction that removes two electrons and two protons. Subsequently, the 13¹-hydroxy group is converted to a 13¹-oxo group in a second oxidation step, also involving removal of two electrons and two protons. The product 3,8-divinyl Pchl_{id} is then formed by a final oxidation process that forms a C–C bond between C13² and C15 with the removal of two electrons and two protons. Initial break of the C–H bond of the C13¹ methylene group may be accomplished by the attack from an adenosyl radical, similar to other radical SAM enzymes (Fig. 12, 16). However, cofactors that accept electrons and protons in these sequential reactions remain unidentified.

Oxygen-Dependent MPE Cyclase AcsF/ChlA

An alternative MPE cyclase was identified in the purple bacterium *Rubrivivax gelatinosus* using a targeted mutagenesis of an unidentified open reading frame (Pinta et al. 2002). This mutant only accumulated MPE only under high oxygenation conditions, in which the wild type still produces small amounts of BChl, whereas under photosynthetic (anoxic) conditions, BChl production is similar in mutant and wild-type cells. Pinta et al. named this gene *acsF* (aerobic Chl synthesis with Fe), because the amino acid sequence of the gene has two putative iron-binding motifs (Pinta et al. 2002), and the mutant phenotype was interpreted according to BchE activity under anoxic conditions. Subsequently, differential regulation of AcsF and BchE by a transcriptional regulator Fur was demonstrated in *R. galatinosus* (Ouchane et al. 2007). Moreover, *acsF* orthologous genes were identified in plants (*CHL27* in *A. thaliana*, Tottey et al. 2003; *xanthan-1* in barley, Rzeznicka et al. 2005) and in the green algae (*crd1* and *chl1* in the green alga *Chlamydomonas reinhardtii*, Moseley et al. 2000; Moseley et al. 2002).

Two cyanobacterial *acsF* homologs (*chlA_I* and *chlA_{II}*, Minamizaki et al. 2008, or *cyclI* and *cyclII*, Peter et al. 2009) were identified in *Synechocystis* 6803, and whereas ChlA_I is constitutively expressed, ChlA_{II} is only induced under micro-oxic conditions. Accordingly, phenotypic and pigment analyses revealed that ChlA_I is essential for photosynthetic growth under aerobic conditions and that ChlA_{II} plays an important role under micro-oxic conditions. However, no *bchE* orthologs are present in *Synechocystis* 6803, and under low oxygen conditions, the transcriptional regulator ChlR activates the transcription of the *chlA_{II}* gene with the contiguous genes *ho2* and *hemN* (Aoki et al. 2012).

Because molecular oxygen is the origin of the 13¹-oxo group of 3,8-divinyl Pchl_{id}, AcsF/ChlA is a monooxygenase with similar activities to HemF and NrdB, which require oxygen and may have common binuclear iron centers (Ouchane et al. 2004). The reaction catalyzed by AcsF/ChlA (Fig. 12, 17) likely involves initial formation of a C13² hydroxy group. In this reaction, the proton donor to form the hydroxy group and H₂O is assumed to be NADPH, and following oxidation, two successive removals of two electrons and two protons lead to formation of 3,8-divinyl Pchl_{id}. Recently, Jensen et al. suggested that the plastoquinone pool in the thylakoid membrane accepts electrons from MPE (Steccanella et al. 2015). In addition, reduced quinone may reduce probable iron centers (Fe³⁺ to Fe²⁺) of the AcsF protein of the MPE cyclase. These investigations also demonstrated that octyl gallate inhibits the MPE cyclase reaction, potentially in a manner that is similar to those of the plastid terminal oxidase and the alternative oxidase that interact with quinone.

Although oxygen-dependent MPE cyclase reactions can be assayed in crude extracts, no reconstitution system with purified AcsF/ChlA proteins has been established. Moreover, additional subunits are probably required for this reaction, as suggested by the requirement of membrane fractions in crude assay systems. Genetic analyses of barley also support this hypothesis (Rzeznicka et al. 2005).

AcsF/ChlA is affected by NADPH-dependent thioredoxin isoform C (NTRC) and 2-Cys peroxiredoxin, which stimulates AcsF/ChlA activity in barley etioplasts (Stenbaek et al. 2008). In *Synechocystis* 6803, Slr1780 interacts with CycI (ChlA_I), and its gene was named *ycf54* as an ortholog from the conserved open reading frame in the chloroplast genome of algae (Hollingshead et al. 2012). Fully

segregated mutants lacking *ycf54* ($\Delta ycf54$) show severe Chl-deficient phenotypes, with accumulating MPE and 3-formyl MPE (Hollingshead et al. 2016). However, a small amount of Chl (about 13%) is still detected in $\Delta ycf54$ cells, suggesting that Ycf54 is not essential for CycI activity, but may participate in the assembly of CycI with unknown subunits. In agreement, CycI levels markedly decreased in $\Delta ycf54$ cells.

Accumulations of AcsF were unexpectedly found in chlorosome fraction from *Chloroflexus aurantiacus* (Tang et al. 2009), implying that AcsF has additional unknown roles, potentially in iron transport accumulation of iron in chlorosome.

3,8-Divinyl (Proto)chlorophyllide a 8-Vinyl Reductase

Most Chls possess an ethyl group at the C8 position, although a vinyl group originally occupies this position at the stage of protoporphyrin IX, except in *Prochlorococcus* species, which have 3,8-divinyl Chl pigments. Thus, the 8-vinyl group should be reduced during any steps from Proto to chlorophyllide (Chlide) *a*, and three evolutionarily unrelated enzymes, BciA (N-DVR), BciB (F-DVR), and Chlide *a* oxidoreductase (COR), are known to catalyze reduction of 8-vinyl group of Chl intermediates.

(NADPH-Dependent 8-Vinyl Reductase) BciA

In 2004, a gene (At5G18660; *dvr*) encoding an 8-vinyl reductase (DVR) was identified in *A. thaliana* following extensive screening of mutants producing 3,8-divinyl Chl *a* (Nagata et al. 2005). Independently, an identical gene was identified as responsible for the *pcb2* (pale-green and chlorophyll *b* reduced 2) locus (Nakanishi et al. 2005). This *dvr* gene was the last identified Chl *a* biosynthesis gene, at least in angiosperm plants (Beale 2005), but was the first identified gene for DVR in photosynthetic organisms. Nagata et al. (2005) showed that marine cyanobacteria that produce 3,8-divinyl Chl *a* exclusively, such as *Prochlorococcus*, lack the *dvr* gene, whereas other groups of marine cyanobacteria that produce Chl *a*, such as *Synechococcus*, have the *dvr* gene. Subsequently, *dvr* orthologs were identified in other angiosperms and photosynthetic bacteria and were named *bciA* accordingly to involvement in BChl biosynthesis (Chew and Bryant, 2007). BciA is NADPH dependent and was therefore named N-DVR, and the preferred substrate of N-DVR in *A. thaliana* is 3,8-divinyl Chlide *a* rather than 3,8-divinyl Pchlde (Fig. 13, 18) (Ito and Tanaka 2014).

During early searches for genes of BChl biosynthesis, a *bchJ*-lacking mutant of *R. capsulatus* accumulated 3,8-divinyl Pchlde, suggesting that the *bchJ* gene encodes a 3,8-divinyl Pchlde DVR (Suzuki and Bauer 1995a, b). Subsequently, BchJ was shown to have no activity of DVR, and BchJ may play roles as substrate channeling or regulation of BChl biosynthesis in *C. tepidum* (Chew and Bryant 2007a, b). Recently Willows et al. reported that BchJ forms a 1:1 complex with ChlH and ChlM, suggesting roles as a porphyrin carrier in *R. capsulatus*, similar to that of Gun4 (Sawicki and Willows 2010).

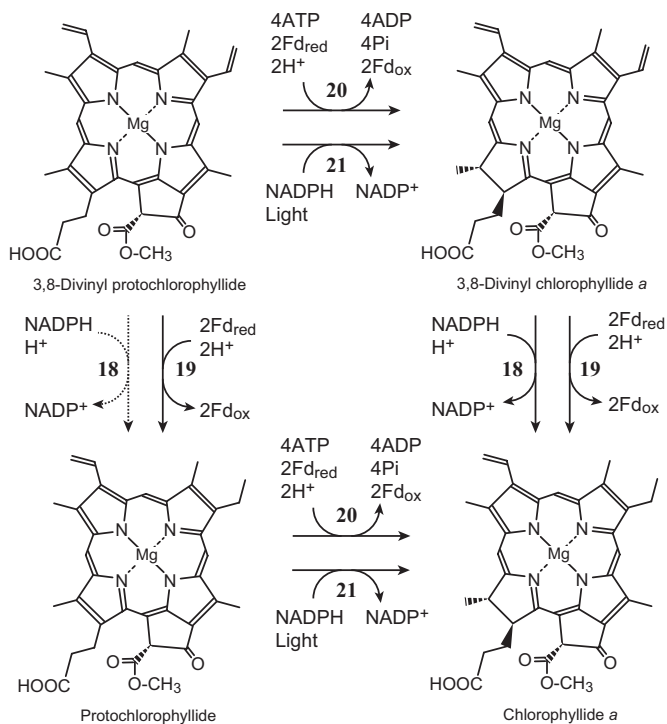


Fig. 13 Two reactions from 3,8-divinyl Pchl_{id}e to Chl_{id}e *a*. Both DPOR (20) and LPOR (21) accept either 3,8-divinyl Pchl_{id}e or Pchl_{id}e as substrates. Two of the three DVRs, BciA (N-DVR, 18) and BciB (F-DVR, 19), are shown. BciA has substrate preference for 3,8-divinyl Chl_{id}e *a*. In contrast, BciB shows broader substrate specificity and reduces either 3,8-divinyl Pchl_{id}e or 3,8-divinyl Chl_{id}e *a*. Thus, in most cyanobacteria harboring BciB, there are two routes from 3,8-divinyl Pchl_{id}e to Chl_{id}e *a*

N-DVR is distributed among eukaryotic photosynthetic organisms, some minor cyanobacterial strains, such as *Leptolyngbya* and marine *Synechococcus*, and among photosynthetic bacteria, such as *C. tepidum* and *R. sphaeroides* (Chen et al. 2016). *Acaryochloris marina* is a unique cyanobacterium that produces Chl *d* and harbors both *bciA* and *bciB* genes. In addition, corresponding enzyme activities were confirmed by heterologous expression in *bciB*-lacking mutant of *Synechocystis* 6803 (Chen et al. 2016).

Ferredoxin-Dependent 8-Vinyl Reductase BciB

Although the gene encoding DVR was identified in *A. thaliana*, no *bciA* homologous genes were found in the cyanobacterium *Synechocystis* 6803, suggesting that this cyanobacterial strain expresses another DVR that may be unrelated to BciA. Subsequently, two research groups independently identified a novel gene (*slr1923*) encoding a second DVR in *Synechocystis* 6803 using distinct techniques

(Islam et al. 2008; Ito et al. 2008). This gene (*cvrA*) encodes a ferredoxin-dependent DVR (F-DVR), with no amino acid sequence similarity to that of N-DVR, indicating different evolutionary origins. However, F-DVR is closely related to the F420-dependent [NiFe]-hydrogenase subunit FrhB in methanogenic archaea.

The amino acid sequence of F-DVR includes two Cys motifs (CxxCxxC and CxxC) that may be involved in chelation of [4Fe-4S] clusters. Moreover, UV-visible spectra of *Chloroherpeton thalassium* BciB purified from *E. coli* suggested the presence of Fe-S clusters and FAD, and subsequent EPR spectroscopy and determinations of iron and sulfur suggested that BciB binds two [4Fe-4S] clusters, of which one may be essential for activity. Reduction of the 8-vinyl group of 3,8-divinyl Pchl_{id}e is dependent on reduced ferredoxin or dithionite, and a structural model of BciB was proposed based on the crystal structure of FrhB (Saunders et al. 2013).

F-DVR shows broader substrate specificity than N-DVR. In particular, F-DVR from *Synechocystis* 6803 reduces 3,8-divinyl forms of both Chl_{id}e *a* and Pchl_{id}e (Fig. 13, 19). Moreover, in the reconstitution assays with BciB from *C. thalassium*, 3,8-divinyl Pchl_{id}e was used as the substrate (Saunders et al. 2013). This substrate specificity is supported by exclusive accumulation of Pchl_{id}e, not 3,8-divinyl Pchl_{id}e, in DPOR-lacking cyanobacterial mutants of *L. boryana* in the dark (Yamamoto, Esaka and Fujita, unpublished result).

COR: A Third 8-Vinyl Reductase

Tamiaki et al. found that a *bciA*-lacking mutant of *C. tepidum* produced normal BChl *a* with the 8-ethyl group, despite the absence of a *bciB* homologs. These observations strongly suggested the presence of a third type of DVR in *C. tepidum* (Mizoguchi et al. 2012), as proposed in *R. sphaeroides* (Canniffe et al. 2013). This third DVR was identified as a latent activity of COR, which normally reduces C7=C8 double bond of chlorin ring to form bacteriochlorin ring (Nomata et al. 2006a, b). Tsukatani et al. found that purified *R. capsulatus* COR converts 3,8-divinyl Chl_{id}e *a* to Chl_{id}e *a* by reducing the C8¹=C8² double bond (Tsukatani et al. 2013a, b; Yamamoto et al. 2014). The in vivo activity of COR was also confirmed in *C. tepidum* (Harada et al. 2014), and the probable mechanism is discussed in the section of *Chlorophyllide a oxidoreductase*.

Protochlorophyllide Oxidoreductase

The C17=C18 double bond of Pchl_{id}e is stereospecifically reduced by Pchl_{id}e reductase to form Chl_{id}e *a*, which is the direct precursor of Chl *a* (Fig. 13, 20, 21). Given that biosynthetic pathways toward various BChls diverge from Chl_{id}e *a*, Pchl_{id}e reduction can be regarded as the final step of the core pathway of Chl biosynthesis. Two evolutionarily unrelated Pchl_{id}e reductases have been identified, including a light-independent (dark-operative) Pchl_{id}e oxidoreductase (DPOR; Fig. 13, 20) and a light-dependent Pchl_{id}e oxidoreductase (LPOR; Fig. 13, 21).

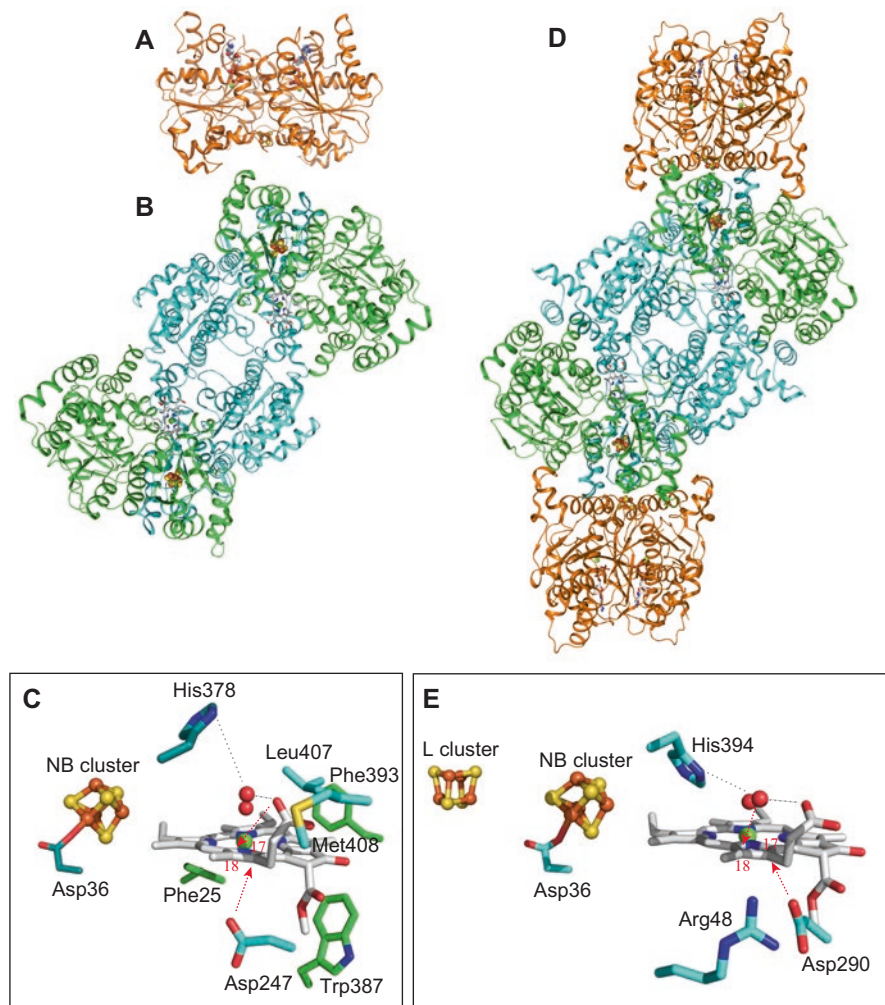


Fig. 14 Crystal structures of the L protein from *R. sphaeroides* (A). The NB protein (a Pchlde-bound form) from *R. capsulatus* (B) and a stabilized complex of L protein and NB protein complex from *Prochlorococcus marinus* (D). The L protein is shown in orange, and the BchN/ChlN and BchB/ChlB subunits of the NB protein are shown in green and blue, respectively. Pchlde is shown in white stick, and iron and sulfur atoms of the NB cluster are shown as orange and yellow balls, respectively. Close-up views of the Pchlde-binding sites of the NB proteins of *R. capsulatus* (C) and *P. marinus* (E). Probable stereospecific hydrogenations of the C17=C18 double bond of Pchlde are shown as red dotted arrows. The hydrogen bonds that appear to be important for proton transfer to C18 are shown as gray dotted lines. Two water molecules are shown as red spheres; one is an axial ligand of the central Mg^{2+} of Pchlde, and the other is a water molecule that may mediate proton transfer from the His residue to C18. In the close-up view of *R. capsulatus*, additional residues (Phe25, Phe393, Trp387, Leu407, and Met408) for binding Pchlde are shown

Interestingly, there is no significant sequence similarity between them, suggesting that they were derived from different ancestral genes. Their unique properties, the light requirement of LPOR and the oxygen sensitivity of DPOR (see below), closely reflect ecological niches of respective photosynthetic organisms.

Light-Independent (Dark-Operative) Pchlide Oxidoreductase DPOR

DPOR is a nitrogenase-like enzyme comprising an ATP-dependent reductase component (L protein) and a catalytic component (NB protein), which are cognates of Fe protein and MoFe protein of nitrogenase, respectively (Fujita and Bauer 2003; Reinbothe et al. 2010). Moreover, the L protein is a homodimer of BchL in anoxygenic photosynthetic bacteria and of ChlL in oxygenic phototrophs (Nomata et al. 2005; Bröcker et al. 2008a, b). A [4Fe-4S] cluster is bound between the protomers (Nomata et al. 2006a, b; Bröcker et al. 2008a, b) by two conserved Cys residues of BchL (ChlL) (Bröcker et al. 2008a, b). This [4Fe-4S] cluster is extremely vulnerable to oxygen, similar to that of nitrogenase Fe protein, and upon exposure to air the purified L protein from *R. capsulatus* is quickly inactivated, with a half-life of only 20 s (Nomata et al. 2006a, b).

The NB protein is a heterotetramer of BchN (ChlN) and BchB (ChlB) and provides the catalytic site of Pchlide (Bröcker et al. 2008a, b; Nomata et al. 2008a, b). Another iron–sulfur cluster (NB cluster) is bound in the interface between BchN and BchB (Muraki et al. 2010) and uniquely held by three Cys from BchN and one Asp from BchB. Similar clusters are found in ferredoxin of *Pyrococcus furiosus* (Calzolari et al. 1995), Fnr (Gruner et al. 2011) and IspG (three Cys and one Glu coordination, Lee et al. 2010). Following reducing by the L protein, the NB cluster mediates electron transfer to the substrate Pchlide and is less sensitive to oxygen than Fe-S cluster of the L protein (Nomata et al. 2008a, b).

Pchlide reduction by DPOR requires ATP hydrolysis and the presence of electron donors such as ferredoxin or dithionite (Fujita and Bauer 2000). Although at least four ATP molecules are required for each Pchlide, this value linearly increases up to ten with increasing ratios of L protein to NB protein from one to eight (Nomata et al. 2016).

DPOR genes are ubiquitously distributed among photosynthetic prokaryotes, including cyanobacteria, and among eukaryotic photosynthetic organisms, and all three genes are encoded by chloroplast DNA in some algae, moss, and gymnosperms. However, DPOR genes are absent in angiosperms and in many classes of algae (Fujita and Bauer 2003). The mosaic distribution of DPOR in eukaryotic algae suggests extensive evolutionary loss, which might be linked to the presence of LPOR (Hunsperger et al. 2015).

The X-ray crystal structure of DPOR has been solved for the L protein (Sarma et al. 2008) and the NB protein (Bröcker et al. 2010; Muraki et al. 2010) and for a stabilized complex of the two components (Moser et al. 2013). The crystal structure of the L protein from *R. sphaeroides* is very similar to that of the Fe protein of nitrogenase, including the overall structure and geometry of the [4Fe-4S] cluster (Fig. 14A; Sarma et al. 2008). A unique charge distribution around the [4Fe-4S] cluster may be involved in specific electron transfer to the NB protein.

The NB protein from *R. capsulatus* has been solved as substrate Pchl_{ide}-bound and Pchl_{ide}-free forms (Fig. 14B; Muraki et al. 2010), indicating an overall structure of a pseudosymmetric dimer of the heterodimer BchN–BchB, in which the two catalytic units are assembled via interactions only between the BchB protomers, as described for the MoFe protein of nitrogenase. The substrate Pchl_{ide} is held in a cavity surrounded by largely hydrophobic residues from BchN and BchB, including some hydrophobic residues from the other symmetric protomer BchB', such as BchB'-Met408 (Fig. 14C). Interestingly, no axial ligand for the central Mg²⁺ ion of Pchl_{ide} is present, except for one water molecule. Moreover, the distance between the NB cluster and Pchl_{ide} is about 10 Å, which is short enough for direct electron transfer (Fig. 14C; Muraki et al. 2010).

The crystal structure of the NB protein with its substrate enabled a proposal about the structural basis of the stereospecificity of C17=C18 double-bond reduction. Specifically, the uniquely distorted C17-propionate residue of Pchl_{ide} is very close to C18 (4.8 Å), and BchB-Asp274 is also close to C17 (4.9 Å). Hence, the spatial arrangement of the propionate and Asp274 suggests that two protons are transferred stereospecifically to C18 and C17, respectively, to form Chl_{ide} *a* (Fig. 14C). Accordingly, this proton transfer is abolished in experiments with a substrate analogue Chl *c* and a site-directed variant BchB-D274A (Muraki et al. 2010). However, the crystal structure of the stabilized complex from *P. marinus* (Fig. 14d) suggested notable differences in the proton donor for C18, in which a water molecule may directly mediate proton transfer from His394 or C17-propionate to C18 (Fig. 14E; Moser et al. 2013).

Pchl_{ide} reduction requires two electrons and two protons, which are coordinated with each other during the reaction. Subsequently, electron paramagnetic resonance (EPR) analyses of the DPOR reaction with the BchB-D274A variant suggested that Pchl_{ide} reduction proceeds via Pchl_{ide} radicals that are formed following transfer of one electron and one proton (Nomata et al. 2014). Thus, DPOR is a very unique Fe-S enzyme that generates substrate radicals by direct electron transfer from the NB cluster.

A crystal structure of the L-protein–NB-protein complex stabilized by ADP-AIF₃ was determined (Figs. 6 and 14D; Moser et al. 2013). The L protein and the NB protein interact specifically to form a transient complex for electron transfer from the [4Fe-4S] cluster of the L protein to the NB cluster, which is coupled with ATP hydrolysis by the L protein. This transient complex was stabilized by an ATP analogue ADP-AIF₃ that was also used to stabilize a complex of Fe protein and MoFe protein of nitrogenase (Schindelin et al. 1997). In structural comparisons of the free form of L protein and the complex, the [4Fe-4S] cluster of the L protein moved 3.2 Å toward the NB cluster to facilitate electron transfer. In the stabilized complex, the [4Fe-4S] cluster of the L protein, the NB cluster, and Pchl_{ide} are arranged on a straight line (Fig. 14D, E).

Nicotinamide reportedly inhibits the production of BChl, leading to accumulation of Pchl_{ide} in *R. sphaeroides* (Shioi et al. 1988). In agreement, the DPOR assay system revealed that nicotinamide inhibits electron transfer from the L protein to the NB protein (Nomata et al. 2013), and this specific inhibitor was then used to investigate the reaction cycle of DPOR.

Light-Dependent Protochlorophyllide Oxidoreductase

LPOR is a unique enzyme that requires light for catalysis. In nature, the only other enzyme with such light requirement is DNA photolyase (Suzuki and Bauer 1995a, b), although a recently discovered Chl *f* synthase may have similar properties (Ho et al. 2016). Because LPOR is the sole Pchlde reductase in plants, Chl biosynthesis is arrested at the Pchlde reduction stage in angiosperm seedlings in the dark. Thus, LPOR is the key enzyme for light-dependent greening in plants. Although LPOR had been considered specific to photosynthetic eukaryotes, a cyanobacterial *chlL*-lacking mutant retained the ability to produce Chl under light conditions, clearly indicating the presence of a LPOR in cyanobacteria (Fujita et al. 1992). Subsequently, a cyanobacterial gene encoding LPOR (*por*) was successfully cloned as a recombinant cosmid that complemented the photosynthetic growth of DPOR-lacking mutants of *R. capsulatus* (Suzuki and Bauer 1995a, b), indicating that LPOR is ubiquitous among cyanobacteria. Recently, a photosynthetic bacterium harboring the *por* gene was identified (Kaschner et al. 2014), and sequence homology analyses suggested that this gene was transmitted from cyanobacteria by lateral gene transfer. Moreover, in photosynthetic eukaryotes, *por* is a nuclear gene and is often present in multiple copies (Skinner and Timko 1998; Hunsperger et al. 2015).

LPOR is a single polypeptide enzyme with a molecular mass of 30–35 kD and belongs to the short-chain dehydrogenase/reductase (SDR) family, which commonly utilizes the pyridine nucleotides NAD(P)H or NAD(P)⁺ as cofactors (Fig. 13, 21; Labesse et al. 1994).

Proteins of the SDR family commonly comprise 250–300 amino acid residues, and in the N-terminal domain, GxxxGxxG serves as the NAD(P)H- or NAD(P)⁺-binding site, and a common motif KxxxY in the central part provides the catalytic center (Kavanagh et al. 2008). In addition to these residues, the active site contains of an Asn-Ser-Tyr-Lys tetrad. Enzymes of the SDR family show widely varying activities and encompass oxidoreductases (EC 1), lyases (EC 2) and epimerases (EC 5). Although sequence homology among these enzymes is relatively low (10–30%), X-ray crystallography data indicates high conservation of three-dimensional structures comprising a twisted parallel β -sheet flanked by two to three α -helices and a Rossmann fold. These features may be also conserved in LPOR, and critical roles of Lys and Tyr residues of the active site were confirmed in pea LPOR using site-directed mutagenesis (Wilks and Timko 1995). According to the ensuing catalytic model, the Lys residue lowers the p*K* value of the Tyr residue, which serves as a proton donor for the substrate. Subsequently, hydride is transferred from the *pro-S* phase of NADPH nicotinamide that is induced by light absorption of the bound Pchlde molecule. In agreement, transfer of a hydride and a proton is a common feature of SDR enzyme activities. Moreover, the unique light requirement of LPOR may be derived from a 33-amino acid extension that is not found in other SDR family enzymes. Hence, the structure of LPOR was simulated according to reported structures of SDR family enzymes, and spatial arrangement of the active site that enable unique light-dependent reactions was simulated (Menon et al. 2016).

The light-triggering property of LPOR provides a unique system to investigate initial stages of the ensuing enzyme reaction in ultrafast timescale (Heyes et al. 2002). Thus, using a recombinant cyanobacterial LPOR protein, a series of detailed spectroscopic analyses were performed under low temperature, and a catalytic cycle was proposed (Heyes et al. 2003) as follows: initially, photon absorption by the bound Pchl_{id} molecule activates its conformation, and absorption of a second photon triggers a series of light-driven hydride and proton transfers that lead to the formation of Chl_{id} (Sytnina et al. 2008).

Recently a chaperone-like protein CPP1 was identified as a protein that is critical for normal LPOR accumulation in *Nicotiana benthamiana* and *A. thaliana* (Lee et al. 2013). This gene was also found in cyanobacteria, and a mutant lacking the CPP1 gene (*slr1918*) in *Synechocystis* 6803 showed a high light-sensitive phenotype. This phenotype may reflect significantly decreased LPOR under a high-light condition ($100 \mu\text{mol m}^{-2} \text{s}^{-1}$), as observed in a *por*-lacking mutant of *L. boryana* (Fujita et al. 1998, see below).

Functional Differentiation of DPOR and LPOR and Evolutionary Implications

Although Pchl_{id} reduction is catalyzed exclusively by DPOR in photosynthetic bacteria (Bollivar et al. 1994), LPOR and DPOR coexist in cyanobacteria. As mentioned above, DPOR catalyzes radical-mediated Pchl_{id} reduction using oxygen-sensitive Fe-S clusters, but remains active in the dark. In contrast, LPOR is an oxygen-tolerant enzyme that requires light. These enzymatic properties of DPOR and LPOR suggest functional differentiation in cyanobacterial cells (Fujita et al. 1998), as confirmed in detailed phenotype analyses of cyanobacterial mutants lacking either enzyme. Specifically, an LPOR-lacking mutant of the cyanobacterium *Leptolyngbya boryana* (*Plectonema boryanum*) showed retardation of photosynthetic growth under light intensities higher than $25 \mu\text{E m}^{-2} \text{s}^{-1}$ and a lethal phenotype under higher light intensities ($>130 \mu\text{E m}^{-2} \text{s}^{-1}$). These observations were interpreted as partial inactivation of DPOR by oxygen from photosystem II under medium light intensity, increased oxygen generation under higher light intensity, and then complete inactivation of DPOR under light intensity $>130 \mu\text{E m}^{-2} \text{s}^{-1}$.

Under anaerobic conditions, in which cultures were bubbled with N₂ gas containing 0% O₂, the LPOR-lacking mutant grew photosynthetically under high light intensity. In these experiments, the maximal oxygen level for growth of the LPOR-lacking mutant was 3%, which was referred to as the “Chlorophyll Pasteur Point” because LPOR becomes essential for photosynthetic growth of cyanobacteria at higher oxygen concentrations than this critical oxygen concentration (Yamazaki et al. 2006). Interestingly, this oxygen concentration coincides with that of the atmosphere following the Great Oxidation Event (GOE) about 2.45 billion years ago (Sessions et al. 2009). During early evolution of photosynthesis (>3.7 billion years ago), Pchl_{id} reduction in Chl or BChl biosynthesis was catalyzed by the older enzyme DPOR, which had evolved from a lineage common to nitrogenase.

Subsequently, extensive oxygen production by ancient cyanobacteria that have only DPOR caused the GOE. The resulting oxygen level often inactivates DPOR, and this environment may have acted as a main selective pressure for the evolution of an alternative oxygen-tolerant Pchl_{id} reductase LPOR from the SDR family (Yamazaki et al. 2006).

In contrast with LPOR-lacking mutants, DPOR-lacking mutants have no detectable phenotype under most tested conditions. However, mild growth retardation may occur under long-term low-light or green-light conditions. In agreement, a liverwort (*Marchantia polymorpha*) mutant, in which the *chlB* gene in chloroplast DNA was inactivated, showed poor growth under short-day conditions (Ueda et al. 2014).

The expression of *chlLNB* genes is upregulated in the cyanobacterium *Fremyella diplosiphon* under green-light conditions. Because the action spectra of LPOR indicate that green light is ineffective for the photoreaction (Shui et al. 2009), these data suggest that DPOR compensates for low LPOR activity. In addition, the transcriptional regulator PedR senses cellular redox status and represses the expression of DPOR genes in response to oxidative stress in *Synechocystis* 6803 (Nakamura and Hihara 2006). These regulatory systems may provide molecular basis for differential use of these enzymes according to their intrinsic enzyme properties under fluctuating environments.

Final Two Steps from Chlorophyllide *a* to Chlorophyll *a*

Chlorophyll Synthase ChlG and Bacteriochlorophyll Synthase BchG

The final step in Chl *a* biosynthesis is the esterification of Chlide *a* by phytol (Fig. 15, 22). This reaction is catalyzed by Chl *a* synthase ChlG. Heterologous expression of the *chlG* gene from *Synechocystis* 6803 (*slr0056*) in *E. coli* leads to detectable Chl *a* synthase activities in crude lysates of the recombinant *E. coli* cells. This activity was dependent on the presence of Chlide *a* and phytol diphosphate. Geranylgeranyl diphosphate was accepted as the substrate, yielding geranylgeranylated Chl *a* (Oster et al. 1997; see “*Geranylgeranyl reductase ChlP/BchP*”).

The final step of BChl *a* biosynthesis also involves esterification of bacteriochlorophyllide (BChlide) *a* with phytol by the BChl *a* synthase BchG. BchG activity was also confirmed in crude lysate of *E. coli* expressing *bchG* from *R. capsulatus*, and geranylgeranyl diphosphate was the substrate. ChlG and BchG enzymes discriminate between Chlide *a* and BChlide *a*, and ChlG does not accept BChlide *a* as a substrate and *vice versa* (Oster et al. 1997). This property of Chl/BChl synthases suggests that photosynthetic bacteria that produce multiple Chls, such as BChl *a*, Chl *a*_{PD}, and BChls *c/d/e* in green bacteria, have Chl synthase isoforms that are specific for respective Chls. In addition, because BChls *c*, *d*, and *e* have farnesyl

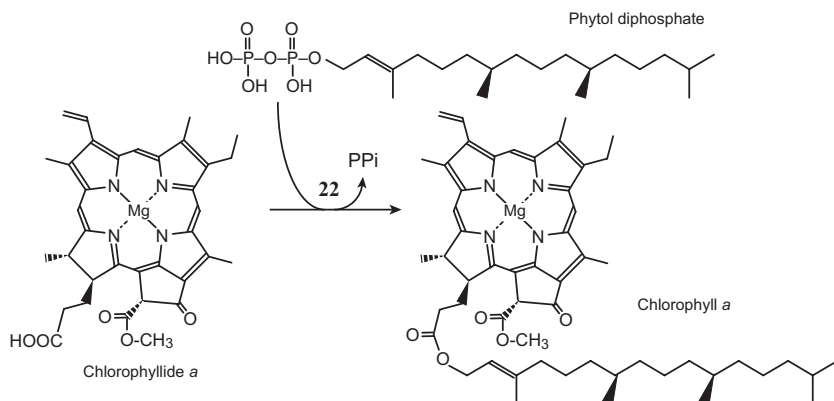


Fig. 15 Reaction of Chl synthase ChlG. Chlide *a* is converted to Chl *a* by the attachment of a phytol tail by Chl synthase (22), which is the final reaction of Chl *a* biosynthesis. In BChl *a* biosynthesis, the attachment of phytol to BChlide *a* is catalyzed by the homologous enzyme BchG

groups instead of phytol groups, the corresponding BChl synthase must accept farnesyl diphosphate as substrate.

Recently, one-amino acid substitutions in ChlG (I44F) and BchG (F28I) reciprocally altered the specificity of Chlide *a* and BChlide *a*. Hence, residues Ile44 in ChlG and F28 in BchG may be involved in the recognition of Chlide *a* and BChlide *a*, respectively (Kim et al. 2016), warranting future crystallographic analysis of Chl/BChl synthases.

Geranylgeranyl Reductase ChlP/BchP

Following esterification of Chlide *a* with geranylgeranyl diphosphate instead of phytol diphosphate, the successive reduction steps of the geranylgeranyl group to phytol is regarded as an alternative final step of Chl *a* biosynthesis (Fig. 16, 23). Geranylgeranyl reductase (GGR) is encoded by the *chlP* gene in cyanobacteria and the *bchP* gene in photosynthetic bacteria. Geranylgeranyl diphosphate produced by isoprenoid biosynthesis carries the four double bonds, C2=C3, C6=C7, C10=C11, and C14=C15, and three of these (C6=C7, C10=C11, and C14=C15) are successively reduced to produce phytol diphosphate. GGR accepts both geranylgeranyl diphosphate and geranylgeranylated Chl *a* as the substrate.

Photosynthetic growth was arrested in a *chlP*-lacking mutant ($\Delta chlP$) of *Synechocystis* 6803, whereas photomixotrophic growth was accompanied with high light sensitivity. Similarly, tocopherol biosynthesis was altered in the $\Delta chlP$ mutant, leading to reduced α -tocotrienol concentrations instead of α -tocopherol in the wild-type strain, suggesting an additional role of ChlP in vitamin E biosynthesis (Shpilyov et al. 2005).

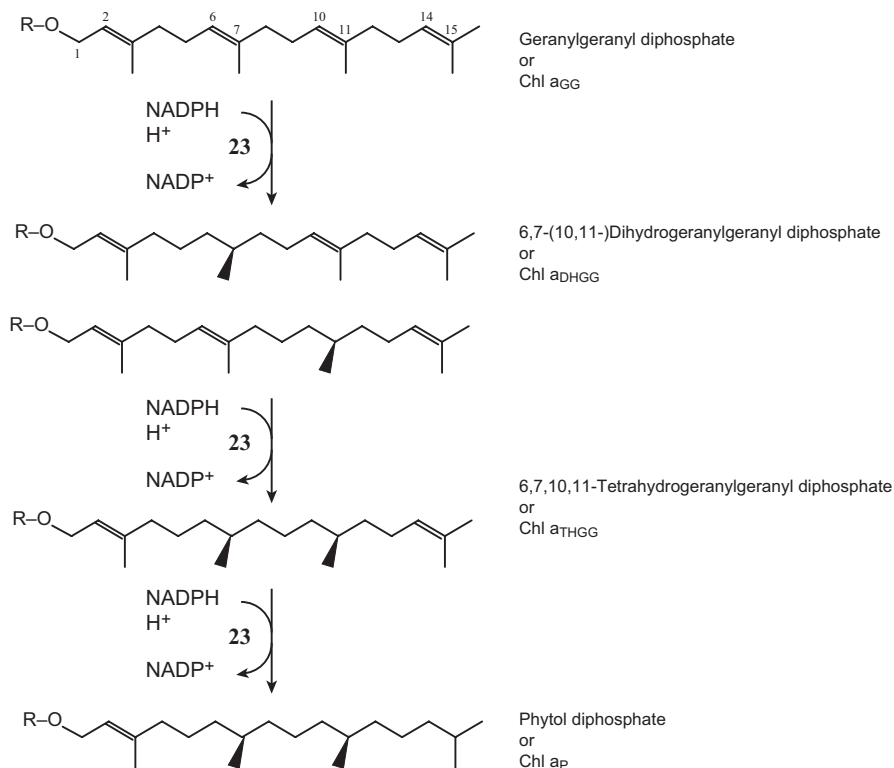


Fig. 16 Sequential hydrogenation reactions of geranylgeranyl diphosphate by geranylgeranyl reductase ChlP. Three double bonds of geranylgeranyl diphosphate are reduced with NADPH by ChlP (23). The first targets of the sequential reductions are either C6=C7 or C10=C11, giving stereospecific hydrogenations, and the last target is C14=C15

HPLC and NMR spectroscopy analyses of BChls from *Rhodospseudomonas palustris* indicated that geranylgeranyl diphosphate double bonds are reduced in the order C6=C7, C10=C11, and C14=C15 (Mizoguchi et al. 2006). However, Tamiaki et al. identified a BChl *a* species with a single C10–C11 bond, suggesting that the first two reduction reactions fluctuate, whereas the third is fixed at C14=C15 (Tamiaki et al. 2016). It is noteworthy that the first two reductions are stereospecific 7*S* and 11*S* configurations, warranting further interpretation according to GGR structure.

Specific Pathways for Various Chlorophylls

Biosynthetic pathways of Chl *a* and other (B)Chls diverge following formation of Chlide *a* (Fig. 2), and although most substituents formation and modification reactions are unique for individual (B)Chls, some are biochemically and evolutionarily related.

Chlorophyll(ide) a Oxygenase for Production of Chlorophyll b

Prochloron and *Prochlorothrix* are marine cyanobacterial genera that are characterized by the presence of accessory Chl *b* (Lewin 1976). Moreover, the marine cyanobacterial genus *Prochlorococcus* is unique in its exclusive use of divinyl Chls, such as 3,8-divinyl Chl *a* and 3,8-divinyl Chl *b* (Chisholm et al. 1988). Chl(ide) *a* oxygenase (CAO; Fig. 17, 24) is responsible for the formation of Chl *b* from Chl *a* and was identified in the green alga *C. reinhardtii* (Tanaka et al. 1998) and subsequently in *Prochlorothrix* and *Prochloron*, which carry divinyl Chl *b* (Tomitani et al. 1999). CAO has a motif (CxH—CxxH) for a Rieske-type iron–sulfur cluster and another for mononuclear iron binding. Interestingly, *Prochlorococcus* CAO diverged from plant and *Prochlorothrix/Prochloron* CAOs, and despite the evolutionary distance, the two sequence motifs are completely conserved (Tomitani et al. 1999). This divergence may reflect the different *Prochlorococcus* substrate 3,8-divinyl Chl *a*. Based on similarities with other monooxygenases with Rieske iron–sulfur clusters and mononuclear iron, such as 2-oxoquinoline 8-monooxygenase (Martins et al. 2005), Tanaka et al. suggested that CAO operates as trimer and larger complexes (Kunugi et al. 2013).

In vitro experiments indicate that Chlide *a* is the substrate of CAO (Oster et al. 2000). However, Chl *a* to Chl *b* conversion is observed in cucumber cotyledons in the dark (Tanaka and Tsuji 1981, 1982). Thus, CAO may accept Chl *a* as a substrate *in vivo*, although the insolubility of Chl *a* precludes in vitro experiments that may confirm its acceptability as a substrate.

Tanaka et al. suggested that Chl(ide) *a* is converted to dihydroxymethyl Chl(ide) *a* by two sequential monooxygenation reactions, followed by spontaneous dehydration to produce Chl(ide) *b*. This reaction mechanism likely requires NADPH as the electron donor (Fig. 17; Tanaka and Tanaka 2011).

Bacteriochlorophylls a, b, and g

Chlorophyllide a Oxidoreductase

To convert chlorin ring structures of Chlide *a* to the bacteriochlorin rings for biosynthesis of BChl *a*, the second nitrogenase-like enzyme, COR, catalyzes alternative stereospecific reduction of C7=C8 double bond in B-ring of Chlide *a* (Fig. 18, 25). COR comprises the three subunits BchX, BchY, and BchZ (Burke et al. 1993a, b; Nomata et al. 2006a, b), which have similar amino acid sequences to the DPOR subunits BchL, BchN, and BchB, respectively (Burke et al. 1993a, b). Moreover, similar to the subunits of DPOR, BchX forms a homodimer (the X protein) and functions as the ATP-dependent reductase component, and BchY and BchZ form a heterotetramer (the YZ protein) that functions as the catalytic component. The requirement of dithionite and ATP for the COR reaction was experimentally confirmed in a reconstitution system with purified X protein and YZ protein from *R. capsulatus* (Nomata et al. 2006a, b). Similarly, sequential reactions of DPOR and

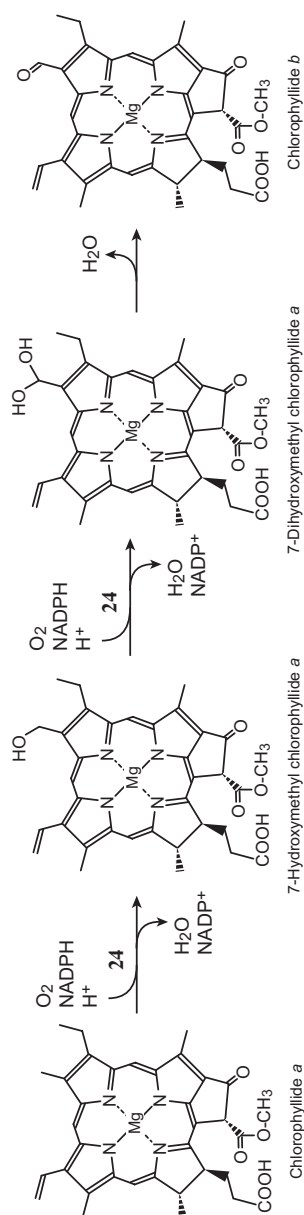
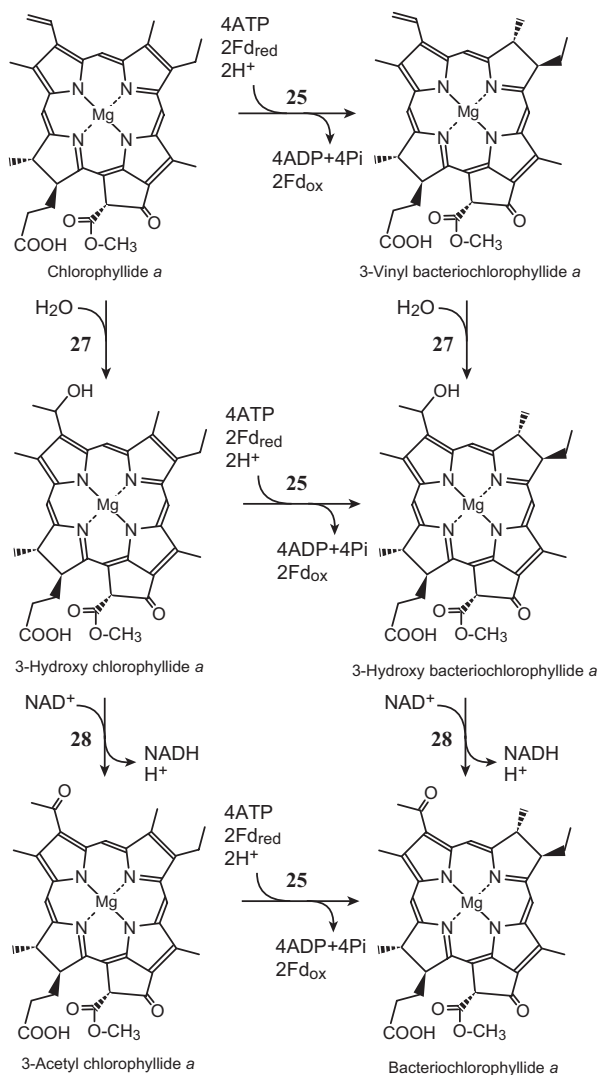


Fig. 17 Reaction of CAO to convert Chloride *a* to Chloride *b*; CAO appears to catalyze two sequential hydroxylation reactions to form 7-dihydroxymethyl Chloride *a*, followed by the formation of Chloride *b* by a spontaneous dehydration (24). Chl *b* is formed by phytylation, which may be catalyzed by ChIG (Fig. 15, 22)

Fig. 18 A reaction lattice from Chlide *a* to BChlide *a* comprising the three enzymes: COR (25), BchF (27), and BchC (28). Stoichiometry of COR is temporarily estimated to be the same as that of DPOR (4ATP/2e⁻). COR catalyzes the reduction of C7=C8 double bond in Chlide *a*, 3-hydroxy Chlide *a*, or 3-acetyl Chlide *a* to form respective BChlide homologs. BchF and BchC accept either chlorin or bacteriochlorin structures as substrates. Thus, there are three routes from Chlide *a* to BChlide *a*



COR were reconstituted with purified proteins using Pchl_{id}e as the substrate (Yamamoto et al. 2014).

Similar to the L protein in DPOR, EPR spectral and site-directed mutagenesis analyses showed that the X protein carries a [4Fe-4S] cluster that is bound by two Cys residues, as in BchL (Kiesel et al. 2015). The YZ protein also carries two [4Fe-4S] clusters per heterotetramer, as in the NB protein (Kiesel et al. 2015). However, in contrast with the NB cluster, four Cys residues chelate the cluster in the YZ protein, as indicated by typical EPR spectra for [4Fe-4S] clusters (Nomata et al. 2008a, b). Finally, site-directed mutagenesis analyses of BchY and BchZ from *Roseobacter denitrificans* indicate that three conserved Cys in BchY (Cys62, Cys87, and Cys145) and one Cys in BchZ (Cys35) are essential for the activity (Kiesel et al. 2015).

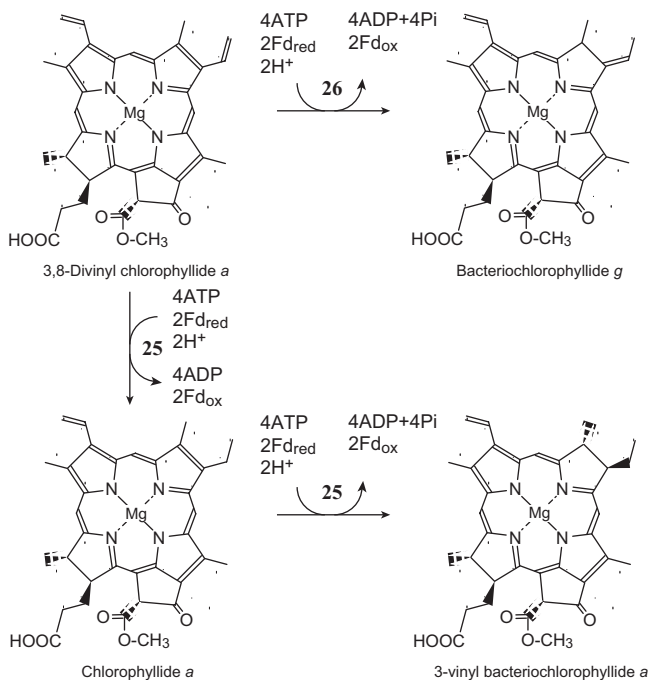


Fig. 19 Reactions of a-COR and b-COR. b-COR works as the C8-ethylidene synthase that converts 3,8-divinyl Chlide *a* to BChlide *g* (26), which is converted to BChlide *b* by BchF and BchC. a-COR has DVR activity in addition to C7=C8 reduction activity (25). The stoichiometry of these reactions may be the same as that of DPOR

Although X proteins from *C. tepidum* and *R. denitrificans* partially reduce the NB protein from *C. tepidum*, no reduction of the NB protein from cyanobacteria (*T. elongatus* and *P. marinus*) was observed (Wätzlich et al. 2009). In addition, the L protein from *R. capsulatus* failed to transfer electrons to the YZ protein from *R. capsulatus* (Nomata and Fujita, unpublished). These varying compatibilities of chimeric components of COR and DPOR may reflect fitness between docking surfaces of reductase and catalytic components.

As mentioned above, COR from *R. capsulatus* reduces 8-vinyl group of Chlide *a* to form Chlide *a* (Tsukatani et al. 2013a, b; Yamamoto et al. 2014; Fig. 19, 25). However, the DVR activity of COR is obscured in wild-type *R. capsulatus* cells because BciA is the main DVR.

COR from the BChl *b* producing photosynthetic bacterium *Blastochloris viridis* that catalyzes the formation of 8-ethylidene from 8-vinyl groups but has no C7=C8 reduction activity (Tsukatani et al. 2013a, b; Fig. 19, 26). The gene encoding ethylidene synthase remained elusive for many years (Xiong et al. 1998), and no corresponding genes were identified in photosynthetic bacteria that produce BChl *b* or BChl *g*. Thus, the discovery of ethylidene synthase activity of the known enzyme COR was unexpected (Tsukatani et al. 2013a, b), but was confirmed in COR from BChl *g*-producing *Heliobacterium modesticaldum* (Tsukatani et al. 2013a, b). The absence of genes for

DVR (*bciA* or *bciB*) is a common trait of BChl *b* and BChl *g* producing bacteria, in which the substrate for COR is exclusively 3,8-divinyl Chlide *a*. Finally, heliobacterial BChlide *g* is farnesylated by BChl *g* synthase, giving rise to BChl *g*.

Tamiaki *et al.* classified COR enzymes as a- and b-COR types (Tamiaki *et al.* 2016). Specifically, a-COR (1,2-type COR) reduces sequentially C7=C8 and C8¹=C8² double bonds (Fig. 19, 25) and is distributed among normal BChl *a* producing photosynthetic bacteria. In contrast, b-COR (1,4-type COR) catalyzes the formation of C8-ethylidene group from 3,8-divinyl Chlide *a* (Fig. 19, 26) and is distributed only among BChl *b* producing purple bacteria, such as *B. viridis*, and among BChl *g*-producing heliobacteria. However, molecular phylogenetic analyses of BchX, BchY, and BchZ amino acid sequences failed to discriminate between a-COR and b-COR, because b-COR occurs in a mosaic manner and does not form subclades (Tsukatani *et al.* 2013a, b). Moreover, reduction reactions of a-COR and b-COR are commonly hydrogenations of two carbons. In a-COR, the target two carbons (C7 and C8) are contiguous (a 1,2 hydrogenation) and the distance is 1.37 Å. In contrast, the two terminal carbons in the butadiene structure (C=C–C=C) are hydrogenated in b-COR (a 1,4 hydrogenation), and the distance between C7 and C8² carbons is 3.13 Å. Thus, a slight spatial shift in the distance between amino acid proton donors may alter catalytic activities of 1,2 and 1,4 hydrogenations. Because these subtle structural changes may be caused by substitutions of few amino acid residues, simple comparison of their amino acid sequences offers little explanatory value. Hence, X-ray crystallographic analyses of COR, especially the YZ protein with its substrate, are awaited to further define the catalytic mechanisms of CORs and the structural basis for catalytic differences between a-COR and b-COR.

Due to high oxygen vulnerability, COR enzymes are only functional under anaerobic conditions. Moreover, exposure of COR to low oxygen conditions leads to the production of superoxide radicals (Kim *et al.* 2008), potentially contributing selective pressures against retention of CORs in ancient oxygenic photosynthetic bacteria (ancient cyanobacteria) that produce both Chl *a* and BChl *a* (Phase I', Masuda and Fujita 2008). This hypothesis is supported by lethal phenotype of *Synechocystis* 6803 expressing COR in the presence of oxygen (Kim *et al.* 2009).

Formation of C3-Acetyl Group by BchF and BchC

Following formation of the bacteriochlorin ring, the final stage of BChls *a* and *b* biosynthesis pathway is the conversion of vinyl group to acetyl group at the C3 position. Genetic analyses of *R. capsulatus* indicated that *bchF* and *bchC* genes are involved in this conversion (Bollivar *et al.* 1994). In particular, the *bchF* gene encodes 3-vinyl BChlide *a* hydroxylase, which hydroxylates the vinyl group at the C3 position (Fig. 18, 27). The ensuing hydroxymethyl group at the C3 position is then converted to acetyl group by 3-hydroxyethyl BChlide *a* dehydrogenase (BchC), giving rise to BChlide *a* (Fig. 18, 28).

The first enzymatic analyses of BchF and BchC from *C. tepidum* have recently been reported (Kiesel *et al.* 2015), about 20 years after the identification of the *bchF* and *bchC* genes in *R. capsulatus* (Bollivar *et al.* 1994). In these analyses, *bchF*

(CT1421) from *C. tepidum* was overexpressed in *E. coli*, and BchF was solubilized with Triton X-100. Then, the activity was confirmed in mixed reactions with DPOR, in which Pchlide was converted to 3-hydroxyethyl Chlide *a* via Chlide *a* by sequential activities of DPOR and BchF.

The *bchC* (CT1422) gene of *C. tepidum* was also overexpressed in *E. coli*, and BchC protein was purified. Following addition of BchC to reaction mixtures containing DPOR and BchF, the substrate Pchlide was converted to 3-acetyl Chlide *a*. These analyses indicated that BchC accepts chlorin (3-hydroxyethyl Chlide *a*) as the substrate, and the ensuing specificity suggested three pathways from Chlide *a* to BChlide *a*, including COR→BchF→BchC, BchF→COR→BchC, and BchF→BchC→COR (Fig. 18; Kiesel et al. 2015).

Another *bchF*-like gene, *bchV* (CT1776), was identified in the *C. tepidum* genome, with about 50% amino acid sequence identity with BchF. This *bchF*-like gene may be specifically involved in hydroxylation at C3¹ during biosynthesis of BChls *c*, *d*, and *e* (see Fig. 22, 32), but not in BChl *a* biosynthesis. Recently, Harada *et al.* demonstrated that BchF and BchV are partially differentiated to BChl *a* and BChl *c*, respectively, and that these genes are partially compatible with each other (Harada et al. 2015).

BchF and BchV bear the stereospecificity of the configuration (*S/R*) of the hydroxyl group at the C3¹ position. Accordingly, *in vitro* assays of BchF and BchV indicated dominant *R*-epimer formation over *S*-epimer by both enzymes. However, these biochemical data were not necessarily consistent with the compositions of BChl *c* homologs in $\Delta bchF$ and $\Delta bchV$ mutants, suggesting the presence of unknown factors that influence *R*- and *S*-epimer ratios in *C. tepidum* chlorosomes (Harada et al. 2015).

Bacteriochlorophylls *c*, *d*, and *e*

Despite the nomenclature, BChls *c*, *d*, and *e* are chlorins that uniquely possess the 3¹-hydroxyethyl group and lack the C13²-methoxycarbonyl group. In addition, these molecules are present in mixtures of homologs that have varying alkyl groups at C8 and C12 positions and varying *S*- and *R*-epimeric configurations of the C3¹-hydroxyethyl group (Fig. 1). These unique structures may provide the molecular basis for formation of high BChl aggregation states in chlorosomes that function as unique protein-independent antenna systems in green sulfur bacteria, filamentous anoxygenic phototrophs, and phototrophic acidobacteria. To generate these unique features, biosynthetic pathways of BChls *c*, *d*, and *e* share four common enzymes, including C13¹-demethoxycarbonylase (BciC), C3-methyl hydroxylase (BchF and BchV), C8-methyl transferase (BchQ), and C12-methyl transferase (BchR).

Chlide *a* C13²-Demethoxycarbonylase BciC

The first committed enzyme BciC catalyzes demethoxycarbonylation at the C13² position (Fig. 20, 29). The *bciC* gene has been identified in *C. tepidum* (CT1077) and *Candidatus Chloracidobacterium thermophilum* (Cabther_B0031; Liu and Bryant

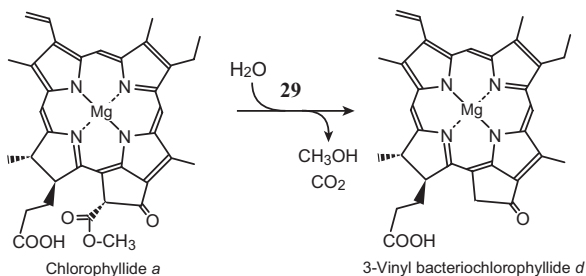


Fig. 20 Reaction of Chlide *a* 13²-demethoxycarbonylase BciC (**29**). BciC may catalyze the hydrolysis of methyl ester to form 13²-carboxyl Chlide *a*, followed by spontaneous decarboxylation to form 3-vinyl BChlide *d*

2011). A *bciC* knockout mutant failed to synthesize BChl *c* and accumulated BChlide and Chlide derivatives with C13² methoxycarbonyl groups, confirming that demethoxycarbonylation is the first committed reaction from Chlide *a* in BChl *c* biosynthesis. Moreover, BciC enzyme activity was recently confirmed in a reconstitution system. In these experiments, BciC from *C. tepidum* was heterologously expressed in *E. coli* and was recovered in precipitates following ultracentrifugation. Subsequently, demethoxycarbonylase activity was clearly detected in the precipitate, and the estimated K_m value for Chlide *a* was 5.2 μM (Teramura et al. 2016). BciC did not accept pheophorbide *a* as the substrate. Chlide *a'* was a poor substrate, suggesting stereospecificity of BciC for the C13² methoxycarbonyl group. Moreover, BciC did not catalyze this reaction in porphyrin and bacteriochlorin rings and was identified as a Chlide *a* demethoxycarbonylase. However, there is another possibility that BciC may also be a methyltransferase that catalyzes the removal of methyl group to form 13²-carboxypheophorbide *a*, followed by spontaneous decarboxylation to 3-vinyl BChlide *d*.

C8² and C12¹ Methyltransferases BchR and BchQ

BChls *c*, *d*, and *e* carry extensively methylated substituents at C8 and C12 positions. Specifically, *n*-propyl, *iso*-butyl, and *neo*-pentyl groups have been detected at the C8 position, which originally bore an ethyl group. In addition, an ethyl group was detected at the C12 position in addition to the original methyl group. Because chlorosomal BChls are present as a mixture of variously methylated BChl homologs, extensive methylation at C8 and C12 positions may contribute to broadening of the Q_y absorption band of BChl *c*, *d*, and *e*. For example, *C. tepidum* cells grown under moderate light-conditions contain the homologs C8-ethyl/C12-methyl, C8-ethyl/C12-ethyl, C8-propyl/C12-ethyl, and C8-*iso*-propyl/C12-ethyl, at a ratio of 10:60:20:5. Moreover, methylation levels tend to increase under lower-light conditions. The C8 homologs with *n*-propyl, *iso*-butyl, and *neo*-pentyl groups are formed by a sequential methylation of ethyl group at the C8² position by the methyltransferase BchQ (Fig. 21, 30). Similarly, the ethyl group at C12 is formed by methylation at the C12¹ position by the methyltransferase BchR (Fig. 21, 31). In subsequent

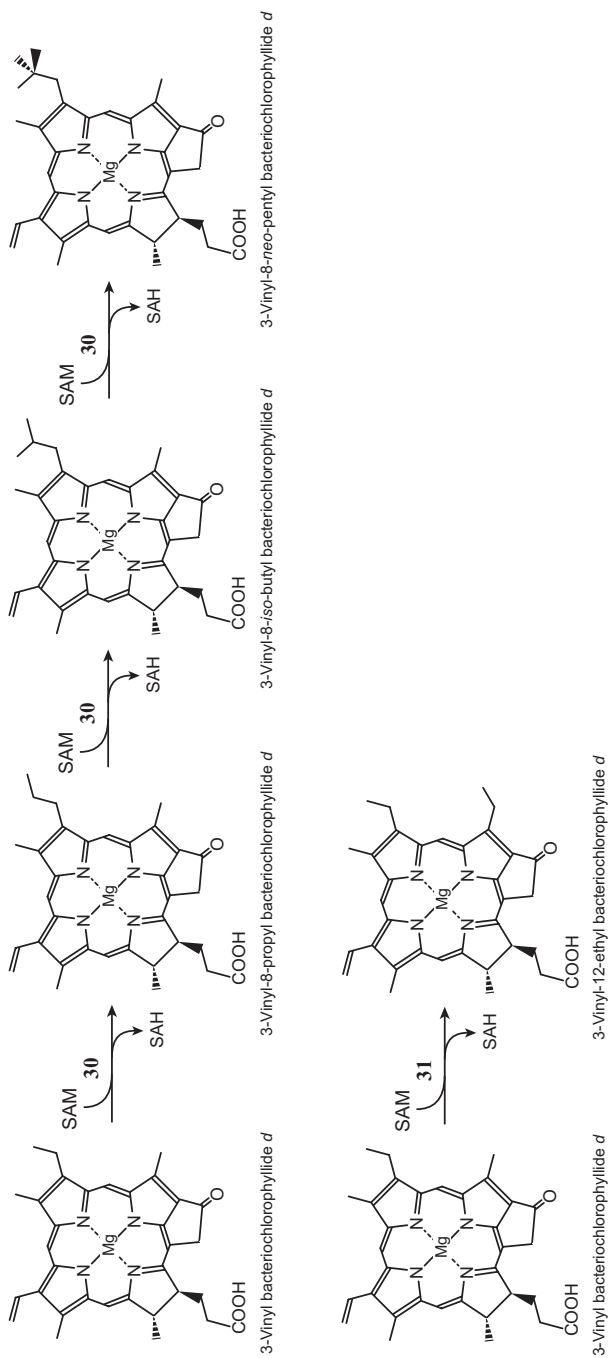


Fig. 21 Reactions of methylation at C8² and C12¹ positions by BchQ and BchR, respectively. BchQ catalyzes successive methylations at the C8² position to form *n*-propyl, *iso*-butyl, and *neo*-pentyl groups (**30**). BchR catalyzes a single methylation at the C12¹ position to form an ethyl group (**31**). It is noteworthy that all methylated homologs are present as mixtures in chlorosomes

genetic analyses of *C. tepidum*, genes encoding these specific methyltransferases were identified according to the hypothesis that, similar to BchE, the C8 and C12 methyltransferases belong to the radical SAM family (Gomez Maqueo Chew et al. 2007). In agreement, the BChl *c* pool in a mutant lacking *bchQ* (CT1777) was a simple mixture of C8-ethyl/C12-methyl and C8-ethyl/C12-ethyl homologs, and that of *bchR* (CT1320) mutants was a mixture of C8-ethyl/C12-methyl, C8-propyl/C12-methyl, and C8-*iso*-propyl/C12-methyl homologs. Finally, a *bchQ* and *bchR* null mutant accumulated only the C8-ethyl/C12-methyl homolog of BChlide *c*. Based on these pigment compositions, Chew et al. (2007) concluded that *bchQ* and *bchR* encode BChlide *c* C-8² and C-12¹ methyltransferases, respectively (Gomez Maqueo Chew et al. 2007). However, BChlide *c* contents were significantly reduced in all mutants, and their chlorosomes showed abnormal shapes and reduced sizes, suggesting unknown functions of highly methylated BChl *c*.

The C20 Methyltransferase BchU

BChls *c* and *e* are uniquely methylated at the C20 position, leading to Q_y peak shifts of BChl *c* to red, from 732 nm (BChl *d*) to 751 nm (BChl *c*) in whole-cell spectra. This red shift of antenna Chls may be important for the efficiency of light harvesting under very low-light conditions. Sequence analyses of a gene encoding a probable methyltransferase in a spontaneous mutant that produces BChl *c* and that in the original strain of *C. vibrioforme* that produces BChl *d* led to identification of the *bchU* gene, which encodes BChl *d* C20 methyltransferase that produces BChl *c* (Fig. 22, 33). Subsequent experiments confirmed accumulation of BChl *d* instead of BChl *c* in a targeted mutant of *C. tepidum*, in which the orthologous gene (CT0028) was inactivated (Maresca et al. 2004). Moreover, enzyme activity of the *C. tepidum* BchU protein was confirmed after purification from *E. coli* (Harada et al. 2005). BchU does not discriminate between *R/S* configurations at the C3¹ hydroxyl group. Moreover, BchU methylates Zn-bacteriopheophorbide *d* but not bacteriopheophorbide *d*, indicating the requirement of a central metal ion.

Crystal structures of BchU from *C. tepidum* (free BchU and BchUs in complex with SAM and SAH) were solved, and reaction mechanisms were proposed (Wada et al. 2006; Fig. 22). Specifically, folding of the C-terminal domain indicated that BchU is a Class I methyltransferase. However, attempts to crystallize a complex with the substrate BChlide *d* or its Zn analogues (Zn-bacteriopheophorbide *d*) were unsuccessful, whereas anomalous electron densities corresponding to the central Zn ion were detected in crystals of a BchU-Zn-bacteriopheophorbide *d* complex. Subsequently, the orientation of bacteriopheophorbide *d* was simulated based on the position of the central metal, and the distance between the C20 carbon of Zn-bacteriopheophorbide *d* and the methyl group of SAM was 3.0 Å close enough for direct transfer of a methyl group. Based on these data, an S_N2-like reaction mechanism was proposed, and according to the mode, it is expected that a conserved Tyr (Tyr246) acts as the nucleophilic residue. Taken together, these data indicated a carbanion species on C20 of BChlide *d*, which is generated following attack by the

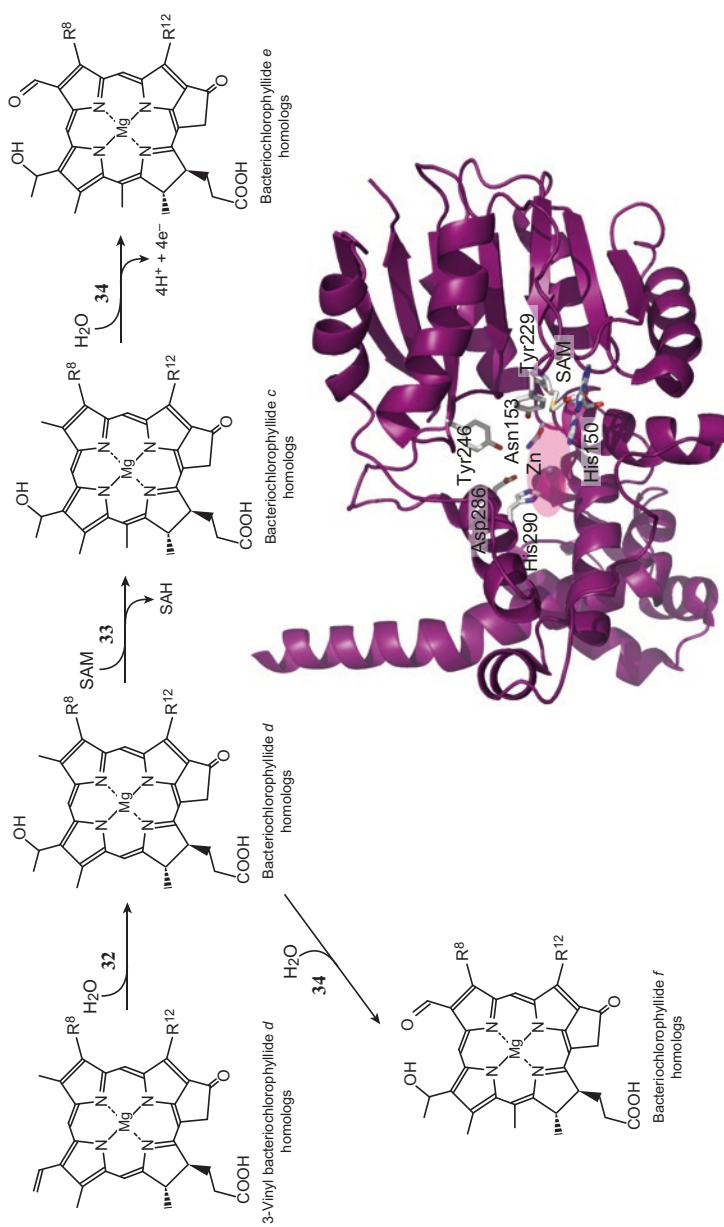


Fig. 22 Final reactions in the formation of BChlide *e* and BChlide *f*: BchV (and BchU) catalyze the hydroxylation of the C3' carbon of 3-vinyl BChlide *d* homologs to form BChlide *e* homologs (32). Subsequently, methylation at the C20 carbon is catalyzed by the C20 methylase BchU (33), followed by the formation of the formyl group at C7 by BciD (34). In a mutant lacking the *bchU* gene, the biosynthetic pathway branches from BChlide *d* by the action of BciD to form BChlide *f* (34). A crystal structure of the BchU–SAM complex with a substrate analogue Zn–bacteriochlorophorbide *d* is shown in the lower part. The substrate is shown as a magenta ellipse, because the orientation of the substrate analogue Zn–bacteriochlorophorbide *d* has not been determined, but the location of the central Zn ion has been determined

hydroxyl group of Tyr246 and may induce methyl transfer from SAM to C20 to form BChlide *c* (Wada et al. 2006).

C7-Formylation, BciD

BChl *e* has a formyl group at the C7 position. Thus, green bacteria that produce BChl *e* likely have an enzyme that converts the C7-methyl group to a formyl group (Fig. 22, 34), as with CAO in Chl *b* biosynthesis. Although no genes showed significant similarities with that encoding CAO in the green bacterium *C. phaeobacterioides*, a unique bioinformatics approach using genomes from various green bacteria successfully identified the gene *bciD* as responsible for formation of the formyl group at the C7 position in BChl *e* biosynthesis (Harada et al. 2013). In contrast with the monooxygenase CAO, BciD belongs to the radical SAM family. Because oxygen is poorly available as a substrate in the anaerobic habitats of green bacteria, water molecules are likely oxygen donors for this reaction. However, the cofactors that accept four protons and four electrons that are removed from the reaction remain unidentified.

The Bacteriochlorophyll *c* Synthase BchK

Three genes from the green bacterium *C. tepidum* have significant similarities to BchG and coincide with the number of types of Chl, BChl *a*, Chl *a*_{PD}, and BChl *c*, from this bacterium. Targeted mutagenesis of these genes clearly demonstrated that among them, *bchK* (CT1992) encodes a BChl *c* synthase that specifically esterifies farnesol to BChlide *c* (Fig. 23, 35; Frigaard et al. 2002). Moreover, sequence similarities suggested that the other two homologous genes, CT1610 and CT1270, encode BChl *a* synthase (BchG) and Chl *a*_{PD} synthase (ChlG), respectively (see the section of *Chlorophyll synthase ChlG and bacteriochlorophyll synthase BchG*). These observations suggested that BchK catalyzes farnesylation for the biosynthesis of BChls *d* and *e* in other green bacteria (Fig. 23, 35).

Bacteriochlorophyll *f*: A Novel Bacteriochlorophyll

C20 methylation is a unique feature of BChl *c* and *e*, and the C7-formyl group is a unique feature of BChl *e*. In addition, a BChl *d*-like pigment with a C7-formyl group is likely present without C20 methylation, and although this putative BChl species remained unidentified, it has been named BChl *f* (Gloe et al. 1975). However, a *bchU* mutant of the green bacterium *C. limnaeum*, which originally produced BChl *e*, was isolated as a novel green bacterium that uses BChl *f* as an antenna Chl in chlorosomes (Harada et al. 2012; Vogl et al. 2012; Fig. 22, 34).

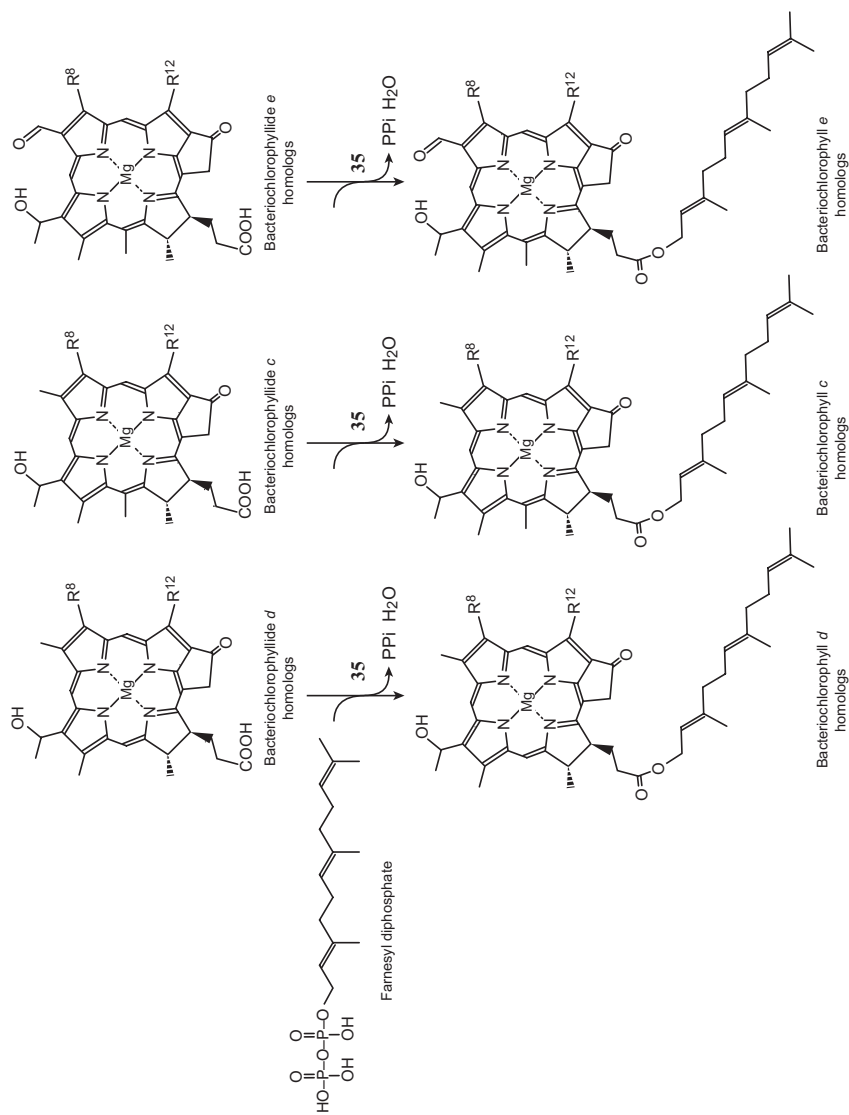


Fig. 23 The final biosynthetic reaction for BChls *d*, *c*, and *e*. All chlorosomal BChls *d*, *c*, and *e* are produced by the attachment of a farnesyl group at the C7-propionate of their BChlide precursors. This reaction is catalyzed by BchG, a homolog of BChG (35)

Chlorophylls d and f

Chls *d* and *f* have unique formyl groups at C3 and C2 positions, respectively. Peaks of Q_y bands for Chls *d* and *f* are 698 and 708 nm, respectively, whereas that of Chl *a* in methanol is 655 nm. Hence, the red shift of these pigments confers the cyanobacterial ability to utilize far-red light. Chl *d* was originally identified in the symbiotic cyanobacterium *Acaryochloris marina* (Miyashita et al. 1996). Subsequently, cyanobacteria producing Chl *d* were shown to be more ubiquitously distributed than expected (Kashiyama et al. 2008). Moreover, Chl *f* was discovered in a filamentous cyanobacterium that inhabits stromatolites (Chen et al. 2010). This cyanobacterium (*Halomicronema hongdechloris*) produces Chl *f* only under far-red-light conditions and not under white-light conditions. In addition, the unicellular cyanobacterium strain KC1 was isolated from the Japanese fresh water Lake Biwa, and Chl *f* was found at 6.7% of the amount of Chl *a* after growth under far-red light (740 nm), indicating that Chl *f* contributes a far-red antenna for photosystems I and II (Itoh et al. 2015).

In structural terms, conversion of methyl to formyl groups in Chl *f* biosynthesis may be similar to CAO or BciD. Both of these enzymes commonly catalyze the formyl formation from methyl group at the C7 position with the different mechanisms described above. Hence, enzymes that produce Chl *f* may have similar features to those of CAO or BciD. However, Ho et al. (2016) recently showed that the *chlF* gene encoding the probable Chl(ide) *f* synthase is a PsbA paralog that is induced by far-red light. Accordingly, heterologous production of Chl *f* in *chlF* overexpressing *Synechococcus* sp. PCC 7002 cells was dependent on light, suggesting that the Chl(ide) *f* synthase is a light-dependent oxidoreductase. Although further biochemical studies are required, this unprecedented similarity with PsbA suggests that the ChlF protein adopts a light-dependent electron transfer mechanism similar to that of D1 in photosystem II.

Conversion of vinyl to formyl groups in Chl *d* is a unique reaction in (B)Chl biosynthesis, and formation of the acetyl group at the C3 position in BChl *a* production may be somewhat similar. Specifically, concerted actions of a hydroxylase and a dehydrogenase are possible in Chl *d* biosynthesis. Moreover, based on the knowledge of (B)Chl biosynthesis, Chlide *a* likely serves as the common precursor for the production of Chls *d* and *f*.

In a recent study, Gan et al. showed that the filamentous cyanobacterium *Leptolyngbya* sp. JSC-1 readily adapts to far-red light by remodeling its photosystems (Gan et al. 2014). During this adaptation process, Chls *d* and *f* are produced and incorporated into the newly produced photosystems. Given the discovery of the *chlF* gene in the cyanobacterium *Chlorogloeopsis fritschii* PCC 9212, the genes responsible for the production of Chl *d* may also be identified soon in the same cyanobacterium.

Perspectives

Extensive gene searches in various photosynthetic organisms over the past 25 years have revealed a largely complete battery of genes for (B)Chl biosynthesis, although some important genes remain to be identified, such as those involved in Chl *d* biosynthesis. Consequently, researchers in this field are now focused on investigations of reaction mechanisms based on three-dimensional structures. Following pioneering crystallographic studies of BchU and DPOR, recent studies have revealed structures of ChlH and ChlM. However, more extensive structural studies are required for thorough understanding of Chl biosynthesis. In particular, although E-ring is a common structural feature of all Chls, the corresponding biochemistry is the least understood. Hence, establishment of reconstitution systems with enzymes that produce E-ring is an urgent requirement for the understanding of Chl biosynthesis.

Final destinations of Chl molecules are also understudied, and coordination of Chl biosynthesis with assembly of Chl-binding apparatuses, such as photosystems, light-harvesting Chl-binding proteins, and chlorosomes, likely involves multiple complex mechanisms that are beyond the scope of this chapter. In particular, because biosynthetic intermediates of Chls and Chl molecules themselves are strong photosensitizers, the potential for ensuing damage to photosynthetic cells is high. Accordingly, photosynthetic organisms have developed elaborate mechanisms to cope with these potential reactive oxygen species generators. Hence, specific physical interactions between contiguous enzymes may be important for efficient transfer of Chl intermediates and likely include interactions of varying strength and tight regulatory pathway that are mediated by as yet unknown factors.

The present studies indicate that reaction centers contain Chls with unique features. For example, Chl *a'* (the 13² epimer of Chl *a*) in PSI, BChl *g'* (the 13² epimer of BChl *g*) in the reaction center of Heliobacteria, BChl *a'* (the 13² epimer of BChl *a*) in the reaction center of green sulfur bacteria, and Chl *a_{PD}* in the primary acceptor Chl in green sulfur bacteria have unique properties among Chls. However, it remains unknown how these unique Chls are produced in cells. In addition, although pheophytin *a* is the primary electron acceptor in PSII, its production likely involved unknown enzymes that coordinate the removal of Mg²⁺ ion from Chl *a*. Identification of the corresponding genes may finally exhaust the repertoire of Chl biosynthetic genes.

The evolution of photosynthesis is closely related to global environmental transitions. Thus, adaptation of Chl biosynthetic enzymes likely played critical roles in the survival of photosynthetic organisms and life on this planet. Among changing environmental conditions, oxygen levels are likely the most critical factor, as indicated by the prevalent use of enzymes that are vulnerable to oxygen, such as radical SAM enzymes and nitrogenase-like enzymes in anoxygenic photosynthetic bacteria compared with oxygenic cyanobacteria. These observations likely provide an evolutionary time line for photosynthetic organisms that emerged in anaerobic environ-

ments about three billion years ago. Specifically, ancient oxygen-producing cyanobacteria are strongly implicated as a cause of the GOE. Similarly, new aerobic environments may alter metabolism in photosynthetic organisms. Taken together, the present data warrant extensive comparative studies on Chl biosynthesis to elucidate details of the evolutionary pathways of photosynthetic organisms from ancient times.

Acknowledgments We thank Jiro Harada for valuable comments on BChl biosynthesis. We also thank Hitoshi Tamiaki, Yusuke Tsukatani, Ayumi Tanaka, and Kazuki Terauchi for valuable discussions. This work was supported by the Japan Society for the Promotion of Science (JSPS) [Grants-in-Aid for Scientific Research Nos 23370020, 15H04387, 15H01397, and Specially Promoted Research 23000007] and the Japan Science and Technology Agency (JST) [the Advanced Low Carbon Technology Research and Development Program (ALCA)].

References

- Aoki R, Takeda T, Omata T, Ihara K, Fujita Y (2012) MarR-type transcriptional regulator ChlR activates expression of tetrapyrrole biosynthesis genes in response to low-oxygen conditions in cyanobacteria. *J Biol Chem* 287:13500–13507
- Axelsson E, Lundqvist J, Sawicki A, Nilsson S, Schröder I, Al-Karadaghi S, Willows RD, Hansson M (2006) Recessiveness and dominance in barley mutants deficient in Mg-chelatase subunit D, an AAA protein involved in chlorophyll biosynthesis. *Plant Cell* 18:3606–3616
- Bandyopadhyay A, Elvitigala T, Welsh E, Stöckel J, Liberton M, Min H, Sherman LA, Pakrasi HB (2011) Novel metabolic attributes of the genus cyanothecae, comprising a group of unicellular nitrogen-fixing *Cyanothecae*. *MBio* 2:e00214–e00211
- Beale SI (2005) Green genes gleaned. *Trends Plant Sci* 10:309–312
- Beale SI (2006) Biosynthesis of 5-aminolevulinic acid. In: Grimm B, Borra RJ, Rüdiger W, Scheer H (eds) *Chlorophylls and bacteriochlorophylls: biochemistry, biophysics, functions and applications*. Springer, Dordrecht, pp 147–158
- Blankenship RE (2014) *Molecular mechanisms of photosynthesis*, 2nd edn. Wiley-Blackwell, Hoboken
- Bollivar DW (2010) Putting metal in the middle. *Structure* 18:277–278
- Bollivar D, Suzuki J, Beatty J, Dobrowolski J, Bauer CE (1994) Directed mutational analysis of bacteriochlorophyll *a* biosynthesis in *Rhodobacter capsulatus*. *J Mol Biol* 237:622–640
- Bröcker M, Wätzlich D, Uliczka F, Virus S, Saggu M, Lenzian F, Scheer H, Rüdiger W, Moser J, Jahn D (2008a) Substrate recognition of nitrogenase-like dark operative protochlorophyllide oxidoreductase from *Prochlorococcus marinus*. *J Biol Chem* 283:29873–29881
- Bröcker M, Virus S, Ganskow S, Heathcote P, Heinz D, Schubert W, Jahn D, Moser J (2008b) ATP-driven reduction by dark-operative protochlorophyllide oxidoreductase from *Chlorobium tepidum* mechanistically resembles nitrogenase catalysis. *J Biol Chem* 283:10559–10567
- Bröcker MJ, Schomburg S, Heinz DW, Jahn D, Schubert WD, Moser J (2010) Crystal structure of the nitrogenase-like dark operative protochlorophyllide oxidoreductase catalytic complex (ChlN/ChlB)₂. *J Biol Chem* 285:27336–27345
- Brzezowski P, Richter AS, Grimm B (2015) Regulation and function of tetrapyrrole biosynthesis in plants and algae. *Biochim Biophys Acta* 1847:968–985
- Burke DH, Alberti M, Hearst JE (1993a) The *Rhodobacter capsulatus* chlorin reductase-encoding locus, *bchA*, consists of three genes, *bchX*, *bchY*, and *bchZ*. *J Bacteriol* 175:2407–2413
- Burke DH, Hearst JE, Sidow A (1993b) Early evolution of photosynthesis: clues from nitrogenase and chlorophyll iron proteins. *Proc Natl Acad Sci U S A* 90:7134–7138

- Calzolari L, Gorst CM, Zhao ZH, Teng Q, Adams MW, La Mar GN (1995) ¹H NMR investigation of the electronic and molecular structure of the fouriron cluster ferredoxin from the hyperthermophile *Pyrococcus furiosus*. Identification of Asp 14 as a cluster ligand in each of the four redox states. *Biochemistry* 34:11373–11384
- Canniffe DP, Jackson PJ, Hollingshead S, Dickman MJ, Hunter CN (2013) Identification of an 8-vinyl reductase involved in bacteriochlorophyll biosynthesis in *Rhodobacter sphaeroides* and evidence for the existence of a third distinct class of the enzyme. *Biochem J* 450:397–405
- Chen M (2014) Chlorophyll modifications and their spectral extension in oxygenic photosynthesis. *Annu Rev Biochem* 83:317–340
- Chen M, Schliep M, Willows RD, Cai ZL, Neilan BA, Scheer H (2010) A red-shifted chlorophyll. *Science* 329:1318–1319
- Chen X, Wang X, Feng J, Chen Y, Fang Y, Zhao S, Zhao A, Zhang M, Liu L (2014) Structural insights into the catalytic mechanism of *Synechocystis* magnesium protoporphyrin IX *O*-methyltransferase (ChlM). *J Biol Chem* 289:25690–25698
- Chen X, Pu H, Fang Y, Wang X, Zhao S, Lin Y, Zhang M, Dai HE, Gong W, Liu L (2015a) Crystal structure of the catalytic subunit of magnesium chelatase. *Nat Plants* 1:15125
- Chen X, Pu H, Wang X, Long W, Lin R, Liu L (2015b) Crystal structures of GUN4 in complex with porphyrins. *Mol Plant* 8:1125–1127
- Chen GE, Hitchcock A, Jackson PJ, Chaudhuri RR, Dickman MJ, Hunter CN, Canniffe DP (2016) Two unrelated 8-vinyl reductases ensure production of mature chlorophylls in *Acarochloris marina*. *J Bacteriol* 198:1393–1400
- Chew AG, Bryant DA (2007a) Characterization of a plant-like protochlorophyllide a divinyl reductase in green sulfur bacteria. *J Biol Chem* 282:2967–2975
- Chew AG, Bryant DA (2007b) Chlorophyll biosynthesis in bacteria: the origins of structural and functional diversity. *Annu. Rev. Microbiol.* 61:113–129
- Chisholm SW, Olson RJ, Zettler ER, Goericke R, Waterbury JB, Welschmeyer NA (1988) A novel free-living prochlorophyte abundant in the oceanic euphotic zone. *Nature* 334:340–343
- Cornah JE, Smith AG (2009) Transformation of uroporphyrinogen III into protoheam. In: Warren MJ, Smith AG (eds) *Tetrapyrroles: birth life and death*. Springer, Austin, pp 74–88
- Czarnecki O, Grimm B (2012) Post-translational control of tetrapyrrole biosynthesis in plants, algae, and cyanobacteria. *J Exp Bot* 63:1675–1687
- Davison PA, Hunter CN (2011) Abolition of magnesium chelatase activity by the *gun5* mutation and reversal by *Gun4*. *FEBS Lett* 585:183–186
- De Las Rivas J, Lozano JJ, Ortiz AR (2002) Comparative analysis of chloroplast genomes: functional annotation, genome-based phylogeny, and deduced evolutionary patterns. *Genome Res* 12:567–583
- Fodje MN, Hansson A, Hansson M, Olsen JG, Gough S, Willows RD, Al-Karadaghi S (2001) Interplay between an AAA module and an integrin I domain may regulate the function of magnesium chelatase. *J Mol Biol* 311:111–122
- Frigaard NU, Voigt GD, Bryant DA (2002) *Chlorobium tepidum* mutant lacking bacteriochlorophyll *c* made by inactivation of the *bchK* gene, encoding bacteriochlorophyll *c* synthase. *J Bacteriol* 184:3368–3376
- Fujita Y (2015) Chlorophylls. eLS (Encyclopedia of Life Sciences). Wiley, Chichester. doi:10.1002/9780470015902.a9780470000661.pub9780470015903
- Fujita Y, Bauer CE (2000) Reconstitution of light-independent protochlorophyllide reductase from purified BchL and BchN-BchB subunits in vitro confirmation of nitrogenase-like features of a bacteriochlorophyll biosynthesis enzyme. *J Biol Chem* 275:23583–23588
- Fujita Y, Bauer CE (2003) The light-independent protochlorophyllide reductase: a nitrogenase-like enzyme catalyzing a key reaction for greening in the dark. In: Kadish K, Smith KM, Guillard R (eds) *Chlorophylls and bilins: biosynthesis, synthesis, and degradation*. Academic Press, San Diego, pp 109–156
- Fujita Y, Takahashi Y, Chuganji M, Matsubara H (1992) The *nifH*-like (*frxC*) gene is involved in the biosynthesis of chlorophyll in the filamentous cyanobacterium *Plectonema boryanum*. *Plant Cell Physiol* 33:81–92

- Fujita Y, Takagi H, Hase T (1998) Cloning of the gene encoding a protochlorophyllide reductase: the physiological significance of the co-existence of light-dependent and -independent protochlorophyllide reduction systems in the cyanobacterium *Plectonema boryanum*. *Plant Cell Physiol* 39:177–185
- Gan F, Zhang S, Rockwell NC, Martin SS, Lagarias JC, Bryant DA (2014) Extensive remodeling of a cyanobacterial photosynthetic apparatus in far-red light. *Science* 345:1312–1317
- Gibson LC, Hunter CN (1994) The bacteriochlorophyll biosynthesis gene, *bchM*, of *Rhodobacter sphaeroides* encodes *S*-adenosyl-L-methionine: Mg protoporphyrin IX methyltransferase. *FEBS Lett* 352:127–130
- Gibson LC, Willows RD, Kannangara CG, von Wettstein D, Hunter CN (1995) Magnesium-protoporphyrin chelatase of *Rhodobacter sphaeroides*: reconstitution of activity by combining the products of the *bchH*, *-I*, and *-D* genes expressed in *Escherichia coli*. *Proc Natl Acad Sci U S A* 92:1941–1944
- Gloe A, Pfennig N, Brockmann H, Trowitzsch W (1975) A new bacteriochlorophyll from brown-colored Chlorobiaceae. *Arch Microbiol* 102:103–109
- Gomez Maqueo Chew A, Frigaard NU, Bryant DA (2007) Bacteriochlorophyllide *c* C-8² and C-12¹ methyltransferases are essential for adaptation to low light in *Chlorobaculum tepidum*. *J Bacteriol* 189:6176–6184
- Gough SP, Petersen BO, Duus JO (2000) Anaerobic chlorophyll isocyclic ring formation in *Rhodobacter capsulatus* requires a cobalamin cofactor. *Proc Natl Acad Sci U S A* 97:6908–6913
- Gruner I, Frädrieh C, Böttger LH, Trautwein AX, Jahn D, Härtig E (2011) Aspartate 141 is the fourth ligand of the oxygen-sensing [4Fe-4S]²⁺ cluster of *Bacillus subtilis* transcriptional regulator Fnr. *J Biol Chem* 286:2017–2021
- Hansson A, Willows RD, Roberts TH, Hansson M (2002) Three semidominant barley mutants with single amino acid substitutions in the smallest magnesium chelatase subunit form defective AAA⁺ hexamers. *Proc Natl Acad Sci U S A* 99:13944–13949
- Harada J, Saga Y, Yaeda Y, Oh-Oka H, Tamiaki H (2005) In vitro activity of C-20 methyltransferase, BchU, involved in bacteriochlorophyll *c* biosynthetic pathway in green sulfur bacteria. *FEBS Lett* 579:1983–1987
- Harada J, Mizoguchi T, Tsukatani Y, Noguchi M, Tamiaki H (2012) A seventh bacterial chlorophyll driving a large light-harvesting antenna. *Sci Rep* 2:671
- Harada J, Mizoguchi T, Satoh S, Tsukatani Y, Yokono M, Noguchi M, Tanaka A, Tamiaki H (2013) Specific gene *bciD* for C7-methyl oxidation in bacteriochlorophyll *e* biosynthesis of brown-colored green sulfur bacteria. *PLoS One* 8:e60026
- Harada J, Mizoguchi T, Tsukatani Y, Yokono M, Tanaka A, Tamiaki H (2014) Chlorophyllide *a* oxidoreductase works as one of the divinyl reductases specifically involved in bacteriochlorophyll *a* biosynthesis. *J Biol Chem* 289:12716–12726
- Harada J, Teramura M, Mizoguchi T, Tsukatani Y, Yamamoto K, Tamiaki H (2015) Stereochemical conversion of C3-vinyl group to 1-hydroxyethyl group in bacteriochlorophyll *c* by the hydratases BchF and BchV: adaptation of green sulfur bacteria to limited-light environments. *Mol Microbiol* 98:1184–1198
- Heinz S, Liauw P, Nickelsen J, Nowaczyk M (2016) Analysis of photosystem II biogenesis in cyanobacteria. *Biochim Biophys Acta* 1857:274–287
- Heyes D, Ruban A, Wilks H, Hunter CN (2002) Enzymology below 200 K: the kinetics and thermodynamics of the photochemistry catalyzed by protochlorophyllide oxidoreductase. *Proc Natl Acad Sci U S A* 99:11145–11150
- Heyes DJ, Hunter CN, van Stokkum IH, van Grondelle R, Groot ML (2003) Ultrafast enzymatic reaction dynamics in protochlorophyllide oxidoreductase. *Nat Struct Biol* 10:491–492
- Ho M-Y, Shen G, Canniffe DP, Zhao C, Bryant DA (2016) Light-dependent chlorophyll *f* synthase is a highly divergent paralog of PsbA of photosystem II. *Science*. 353:aaf9178, doi:[10.1126/science.aaf9178](https://doi.org/10.1126/science.aaf9178)

- Hollingshead S, Kopečná J, Jackson PJ, Canniffe DP, Davison PA, Dickman MJ, Sobotka R, Hunter CN (2012) Conserved chloroplast open-reading frame *ycf54* is required for activity of the magnesium protoporphyrin monomethylester oxidative cyclase in *Synechocystis* PCC 6803. *J Biol Chem* 287:27823–27833
- Hollingshead S, Kopečná J, Armstrong DR, Bučinská L, Jackson PJ, Chen GE, Dickman MJ, Williamson MP, Sobotka R, Hunter CN (2016) Synthesis of chlorophyll-binding proteins in a fully segregated $\Delta ycf54$ strain of the cyanobacterium *Synechocystis* PCC 6803. *Front Plant Sci* 7:292
- Hunsperger HM, Randhawa T, Cattolico RA (2015) Extensive horizontal gene transfer, duplication, and loss of chlorophyll synthesis genes in the algae. *BMC Evol Biol* 15:16
- Islam MR, Aikawa S, Midorikawa T, Kashino Y, Satoh K, Koike H (2008) *str1923* of *Synechocystis* sp. PCC6803 is essential for conversion of 3,8-divinyl(proto)chlorophyll(ide) to 3-monovinyl(proto)chlorophyll(ide). *Plant Physiol* 148:1068–1081
- Ito H, Tanaka A (2014) Evolution of a new chlorophyll metabolic pathway driven by the dynamic changes in enzyme promiscuous activity. *Plant Cell Physiol* 55:593–603
- Ito H, Yokono M, Tanaka R, Tanaka A (2008) Identification of a novel vinyl reductase gene essential for the biosynthesis of monovinyl chlorophyll in *Synechocystis* sp. PCC6803. *J Biol Chem* 283:9002–9011
- Itoh S, Ohno T, Noji T, Yamakawa H, Komatsu H, Wada K, Kobayashi M, Miyashita H (2015) Harvesting far-red light by chlorophyll *f* in photosystems I and II of unicellular cyanobacterium strain KC1. *Plant Cell Physiol* 56:2024–2034
- Jahn D, Heinz DW (2009) Biosynthesis of 5-aminolevulinic acid. In: Warren MJ, Smith A (eds) *Tetrapyrroles: birth, life and death*. Springer, New York, pp 29–42
- Kaschner M, Loeschke A, Krause J, Minh BQ, Heck A, Endres S, Svensson V, Wirtz A, von Haeseler A, Jaeger KE, Drepper T, Krauss U (2014) Discovery of the first light-dependent protochlorophyllide oxidoreductase in anoxygenic phototrophic bacteria. *Mol Microbiol* 93:1066–1078
- Kashiyama Y, Miyashita H, Ohkubo S, Ogawa NO, Chikaraishi Y, Takano Y, Suga H, Toyofuku T, Nomaki H, Kitazato H, Nagata T, Ohkouchi N (2008) Evidence of global chlorophyll *d*. *Science* 321:658
- Kato K, Tanaka R, Sano S, Tanaka A, Hosaka H (2010) Identification of a gene essential for protoporphyrinogen IX oxidase activity in the cyanobacterium *Synechocystis* sp. PCC6803. *Proc Natl Acad Sci U S A* 107:16649–16654
- Kavanagh KL, Jörnvall H, Persson B, Oppermann U (2008) Medium- and short-chain dehydrogenase/reductase gene and protein families: the SDR superfamily: functional and structural diversity within a family of metabolic and regulatory enzymes. *Cell Mol Life Sci* 65:3895–3906
- Kiesel S, Wätzlich D, Lange C, Reijerse E, Bröcker MJ, Rüdiger W, Lubitz W, Scheer H, Moser J, Jahn D (2015) Iron-sulfur cluster-dependent catalysis of chlorophyllide *a* oxidoreductase from *Roseobacter denitrificans*. *J Biol Chem* 290:1141–1154
- Kim EJ, Kim JS, Lee IH, Rhee HJ, Lee JK (2008) Superoxide generation by chlorophyllide *a* reductase of *Rhodobacter sphaeroides*. *J Biol Chem* 283:3718–3730
- Kim EJ, Kim JS, Rhee HJ, Lee JK (2009) Growth arrest of *Synechocystis* sp. PCC6803 by superoxide generated from heterologously expressed *Rhodobacter sphaeroides* chlorophyllide *a* reductase. *FEBS Lett* 583:219–223
- Kim EJ, Kim H, Lee JK (2016) The photoheterotrophic growth of bacteriochlorophyll synthase-deficient mutant of *Rhodobacter sphaeroides* is restored by I44F mutant chlorophyll synthase of *Synechocystis* sp. PCC 6803. *J Microbiol Biotechnol* 26:959–966
- Kobayashi K, Masuda T, Tajima N, Wada H, Sato N (2014) Molecular phylogeny and intricate evolutionary history of the three isofunctional enzymes involved in the oxidation of protoporphyrinogen IX. *Genome Biol Evol* 6:2141–2155
- Koch M, Breithaupt C, Kiefersauer R, Freigang J, Huber R, Messerschmidt A (2004) Crystal structure of protoporphyrinogen IX oxidase: a key enzyme in haem and chlorophyll biosynthesis. *EMBO J* 23:1720–1728
- Komenda J, Sobotka R (2016) Cyanobacterial high-light-inducible proteins—protectors of chlorophyll-protein synthesis and assembly. *Biochim Biophys Acta* 1857:288–295

- Kunugi M, Takabayashi A, Tanaka A (2013) Evolutionary changes in chlorophyllide *a* oxygenase (CAO) structure contribute to the acquisition of a new light-harvesting complex in micromonas. *J Biol Chem* 288:19330–19341
- Labesse G, Vidal-Cros A, Chomilier J, Gaudry M, Mornon JP (1994) Structural comparisons lead to the definition of a new superfamily of NAD(P)(H)-accepting oxidoreductases: the single-domain reductases/epimerases/dehydrogenases (the 'RED' family). *Biochem J* 304(Pt 1):95–99
- Larkin RM, Alonso JM, Ecker JR, Chory J (2003) GUN4, a regulator of chlorophyll synthesis and intracellular signaling. *Science* 299:902–906
- Layer G, Moser J, Heinz DW, Jahn D, Schubert WD (2003) Crystal structure of coproporphyrinogen III oxidase reveals cofactor geometry of radical SAM enzymes. *EMBO J* 22:6214–6224
- Lee M, Gräwert T, Quitterer F, Rohdich F, Eppinger J, Eisenreich W, Bacher A, Groll M (2010) Biosynthesis of isoprenoids: crystal structure of the [4Fe-4S] cluster protein IspG. *J Mol Biol* 404:600–610
- Lee JY, Lee HS, Song JY, Jung YJ, Reinbothe S, Park YI, Lee SY, Pai HS (2013) Cell growth defect factor1/chaperone-like protein of POR1 plays a role in stabilization of light-dependent protochlorophyllide oxidoreductase in *Nicotiana benthamiana* and *Arabidopsis*. *Plant Cell* 25:3944–3960
- Lewin RA (1976) Prochlorophyta as a proposed new division of algae. *Nature* 261:697–698
- Liu Z, Bryant DA (2011) Identification of a gene essential for the first committed step in the biosynthesis of bacteriochlorophyll *c*. *J Biol Chem* 286:22393–22402
- Lundqvist J, Elmlund H, Wulff RP, Berglund L, Elmlund D, Emanuelsson C, Hebert H, Willows RD, Hansson M, Lindahl M, Al-Karadaghi S (2010) ATP-induced conformational dynamics in the AAA⁺ motor unit of magnesium chelatase. *Structure* 18:354–365
- Maresca JA, Gomez Maqueo Chew A, Ponsati MR, Frigaard NU, Ormerod JG, Bryant DA (2004) The *bchU* gene of *Chlorobium tepidum* encodes the C-20 methyltransferase in bacteriochlorophyll *c* biosynthesis. *J Bacteriol* 186:2558–2566
- Martins BM, Svetlichnaia T, Dobbek H (2005) 2-Oxoquinoline 8-monoxygenase oxygenase component: active site modulation by Rieske-[2Fe-2S] center oxidation/reduction. *Structure* 13:817–824
- Masuda T, Fujita Y (2008) Regulation and evolution of chlorophyll metabolism. *Photochem Photobiol Sci* 7:1131–1149
- Menon BR, Hardman SJ, Scrutton NS, Heyes DJ (2016) Multiple active site residues are important for photochemical efficiency in the light-activated enzyme protochlorophyllide oxidoreductase (POR). *J Photochem Photobiol B* 161:236–243
- Minamizaki K, Mizoguchi T, Goto T, Tamiaki H, Fujita Y (2008) Identification of two homologous genes, *chlA₁* and *chlA₂*, that are differentially involved in isocyclic ring formation of chlorophyll *a* in the cyanobacterium *Synechocystis* sp. PCC 6803. *J Biol Chem* 283:2684–2692
- Miyashita H, Ikemoto H, Kurano N, Adachi K, Chihara M, Miyachi S (1996) Chlorophyll *d* as a major pigment. *Nature* 383:402
- Mizoguchi T, Harada J, Tamiaki H (2006) Structural determination of dihydro- and tetrahydrogeranylgeranyl groups at the 17-propionate of bacteriochlorophylls-*a*. *FEBS Lett* 580:6644–6648
- Mizoguchi T, Harada J, Tamiaki H (2012) Characterization of chlorophyll pigments in the mutant lacking 8-vinyl reductase of green photosynthetic bacterium *Chlorobaculum tepidum*. *Bioorg Med Chem* 20:6803–6810
- Mochizuki N, Brusslan JA, Larkin R, Nagatani A, Chory J (2001) *Arabidopsis* genomes uncoupled 5 (GUN5) mutant reveals the involvement of Mg-chelatase H subunit in plastid-to-nucleus signal transduction. *Proc Natl Acad Sci U S A* 98:2053–2058
- Mochizuki N, Tanaka R, Tanaka A, Masuda T, Nagatani A (2008) The steady-state level of Mg-protoporphyrin IX is not a determinant of plastid-to-nucleus signaling in *Arabidopsis*. *Proc Natl Acad Sci U S A* 105:15184–15189
- Moseley J, Quinn J, Eriksson M, Merchant S (2000) The *crd1* gene encodes a putative di-iron enzyme required for photosystem I accumulation in copper deficiency and hypoxia in *Chlamydomonas reinhardtii*. *EMBO J* 19:2139–2151

- Moseley JL, Page MD, Alder NP, Eriksson M, Quinn J, Soto F, Theg SM, Hippler M, Merchant S (2002) Reciprocal expression of two candidate di-iron enzymes affecting photosystem I and light-harvesting complex accumulation. *Plant Cell* 14:673–688
- Moser J, Lange C, Krausze J, Rebelein J, Schubert WD, Ribbe MW, Heinz DW, Jahn D (2013) Structure of ADP-aluminium fluoride-stabilized protochlorophyllide oxidoreductase complex. *Proc Natl Acad Sci U S A* 110:2094–2098
- Moulin M, McCormac AC, Terry MJ, Smith AG (2008) Tetrapyrrole profiling in *Arabidopsis* seedlings reveals that retrograde plastid nuclear signaling is not due to Mg-protoporphyrin IX accumulation. *Proc Natl Acad Sci U S A* 105:15178–15183
- Muraki N, Nomata J, Ebata K, Mizoguchi T, Shiba T, Tamiaki H, Kurisu G, Fujita Y (2010) X-ray crystal structure of the light-independent protochlorophyllide reductase. *Nature* 465:110–114
- Nagata N, Tanaka R, Satoh S, Tanaka A (2005) Identification of a vinyl reductase gene for chlorophyll synthesis in *Arabidopsis thaliana* and implications for the evolution of *Prochlorococcus* species. *Plant Cell* 17:233–240
- Nakamura K, Hihara Y (2006) Photon flux density-dependent gene expression in *Synechocystis* sp. PCC 6803 is regulated by a small, redox-responsive, LuxR-type regulator. *J Biol Chem* 281:36758–36766
- Nakanishi H, Nozue H, Suzuki K, Kaneko Y, Taguchi G, Hayashida N (2005) Characterization of the *Arabidopsis thaliana* mutant *pcb2* which accumulates divinyl chlorophylls. *Plant Cell Physiol* 46:467–473
- Nickelsen J, Rengstl B (2013) Photosystem II assembly: from cyanobacteria to plants. *Annu Rev Plant Biol* 64:609–635
- Nomata J, Swem L, Bauer C, Fujita Y (2005) Overexpression and characterization of dark-operative protochlorophyllide reductase from *Rhodobacter capsulatus*. *Biochim Biophys Acta* 1708:229–237
- Nomata J, Mizoguchi T, Tamiaki H, Fujita Y (2006a) A second nitrogenase-like enzyme for bacteriochlorophyll biosynthesis – reconstitution of chlorophyllide *a* reductase with purified X-protein (BchX) and YZ-protein (BchY-BchZ) from *Rhodobacter capsulatus*. *J Biol Chem* 281:15021–15028
- Nomata J, Kitashima M, Inoue K, Fujita Y (2006b) Nitrogenase Fe protein-like Fe-S cluster is conserved in L-protein (BchL) of dark-operative protochlorophyllide reductase from *Rhodobacter capsulatus*. *FEBS Lett* 580:6151–6154
- Nomata J, Kitashima M, Ogawa T, Inoue K, Fujita Y (2008a) Biochemical analysis of two catalytic components of nitrogenase-like enzymes protochlorophyllide reductase and chlorophyllide *a* reductase from *Rhodobacter capsulatus*. In: Allen JF, Gantt E, Golbeck JH, Osmond B (eds) *Photosynthesis. Energy from the Sun: 14th international congress on photosynthesis*. Springer, Dordrecht, pp 1107–1110
- Nomata J, Ogawa T, Kitashima M, Inoue K, Fujita Y (2008b) NB-protein (BchN-BchB) of dark-operative protochlorophyllide reductase is the catalytic component containing oxygen-tolerant Fe-S clusters. *FEBS Lett*. 582:1346–1350
- Nomata J, Kondo T, Itoh S, Fujita Y (2013) Nicotinamide is a specific inhibitor of dark-operative protochlorophyllide oxidoreductase, a nitrogenase-like enzyme, from *Rhodobacter capsulatus*. *FEBS Lett* 587:3142–3147
- Nomata J, Kondo T, Mizoguchi T, Tamiaki H, Itoh S, Fujita Y (2014) Dark-operative protochlorophyllide oxidoreductase generates substrate radicals by an iron-sulphur cluster in bacteriochlorophyll biosynthesis. *Sci Rep* 4:5455
- Nomata J, Terauchi K, Fujita Y (2016) Stoichiometry of ATP hydrolysis and chlorophyllide formation of dark-operative protochlorophyllide oxidoreductase from *Rhodobacter capsulatus*. *Biochem Biophys Res Commun* 470:704–709
- Oster U, Bauer CE, Rüdiger W (1997) Characterization of chlorophyll *a* and bacteriochlorophyll *a* synthases by heterologous expression in *Escherichia coli*. *J Biol Chem* 272:9671–9676
- Oster U, Tanaka R, Tanaka A, Rüdiger W (2000) Cloning and functional expression of the gene encoding the key enzyme for chlorophyll *b* biosynthesis (CAO) from *Arabidopsis thaliana*. *Plant J* 21:305–310

- Ouchane S, Steunou A, Picaud M, Astier C (2004) Aerobic and anaerobic Mg-protoporphyrin monomethyl ester cyclases in purple bacteria: a strategy adopted to bypass the repressive oxygen control system. *J Biol Chem* 279:6385–6394
- Ouchane S, Picaud M, Therizols P, Reiss-Husson F, Astier C (2007) Global regulation of photosynthesis and respiration by FnrL: the first two targets in the tetrapyrrole pathway. *J Biol Chem* 282:7690–7699
- Pedersen M, Linnanto J, Frigaard NU, Nielsen NC, Miller M (2010) A model of the protein-pigment baseplate complex in chlorosomes of photosynthetic green bacteria. *Photosynth Res* 104:233–243
- Peter E, Salinas A, Wallner T, Jeske D, Dienst D, Wilde A, Grimm B (2009) Differential requirement of two homologous proteins encoded by *sll1214* and *sll1874* for the reaction of Mg protoporphyrin monomethylester oxidative cyclase under aerobic and micro-oxic growth conditions. *Biochim Biophys Acta* 1787:1458–1467
- Peter E, Wallner T, Wilde A, Grimm B (2011) Comparative functional analysis of two hypothetical chloroplast open reading frames (*ycf*) involved in chlorophyll biosynthesis from *Synechocystis* sp. PCC6803 and plants. *J Plant Physiol* 168:1380–1386
- Pinta V, Picaud M, Reiss-Husson F, Astier C (2002) *Rubrivivax gelatinosus acsF* (previously *orf358*) codes for a conserved, putative binuclear-iron-cluster-containing protein involved in aerobic oxidative cyclization of Mg-protoporphyrin IX monomethylester. *J Bacteriol* 184:746–753
- Reinbothe C, El Bakkouri M, Buhr F, Muraki N, Nomata J, Kurisu G, Fujita Y, Reinbothe S (2010) Chlorophyll biosynthesis: spotlight on protochlorophyllide reduction. *Trends Plant Sci.* 15:614–622
- Romão CV, Ladakis D, Lobo SA, Carrondo MA, Brindley AA, Deery E, Matias PM, Pickersgill RW, Saraiva LM, Warren MJ (2011) Evolution in a family of chelataases facilitated by the introduction of active site asymmetry and protein oligomerization. *Proc Natl Acad Sci U S A* 108:97–102
- Rüdiger W (2003) The last steps of chlorophyll synthesis. In: Kadish K, Smith KM, Guillard R (eds) *Chlorophylls and bilins: biosynthesis, synthesis, and degradation*. Academic Press, San Diego, pp 71–108
- Rzeznicka K, Walker CJ, Westergren T, Kannagara CG, von Wettstein D, Merchant S, Gough SP, Hansson M (2005) *Xantha-l* encodes a membrane subunit of the aerobic Mg-protoporphyrin IX monomethyl ester cyclase involved in chlorophyll biosynthesis. *Proc Natl Acad Sci U S A* 102:5886–5891
- Sarma R, Barney B, Hamilton T, Jones A, Seefeldt L, Peters J (2008) Crystal structure of the L protein of *Rhodobacter sphaeroides* light-independent protochlorophyllide reductase with MgADP bound: a homologue of the nitrogenase Fe protein. *Biochemistry* 47:13004–13015
- Saunders AH, Golbeck JH, Bryant DA (2013) Characterization of BciB: a ferredoxin-dependent 8-vinyl-protochlorophyllide reductase from the green sulfur bacterium *Chloroherpeton thalassium*. *Biochemistry* 52:8442–8451
- Sawicki A, Willows RD (2010) BchJ and BchM interact in a 1:1 ratio with the magnesium chelataase BchH subunit of *Rhodobacter capsulatus*. *FEBS J* 277:4709–4721
- Scheer H (2006) An overview of chlorophylls and bacteriochlorophylls: biochemistry, biophysics, functions and applications. In: Grimm B, Porra RJ, Rüdiger W, Scheer H, (eds) *Chlorophylls and bacteriochlorophylls: biochemistry, biophysics, functions and applications*. Springer, Dordrecht, pp 1–26
- Schindelin H, Kisker C, Schlessman JL, Howard JB, Rees DC (1997) Structure of ADP × AIF₄⁻-stabilized nitrogenase complex and its implications for signal transduction. *Nature* 387:370–376
- Schlicke H, Hartwig AS, Firtzlaff V, Richter AS, Glässer C, Maier K, Finkemeier I, Grimm B (2014) Induced deactivation of genes encoding chlorophyll biosynthesis enzymes disentangles tetrapyrrole-mediated retrograde signaling. *Mol Plant* 7:1211–1227
- Schubert HL, Blumenthal RM, Cheng X (2003) Many paths to methyltransfer: a chronicle of convergence. *Trends Biochem Sci* 28:329–335

- Schubert HL, Erskine PT, Cooper JB (2009) 5-Aminolevulinic acid dehydratase, porphobilinogen deaminase and uroporphyrinogen III synthase. In: Warren MJ, Smith AG (eds) *Tetrapyrroles: birth life and death*. Springer, Austin, pp 43–73
- Sessions AL, Doughty DM, Welander PV, Summons RE, Newman DK (2009) The continuing puzzle of the great oxidation event. *Curr Biol* 19:R567–R574
- Shepherd M, Reid JD, Hunter CN (2003) Purification and kinetic characterization of the magnesium protoporphyrin IX methyltransferase from *Synechocystis* PCC6803. *Biochem J* 371:351–360
- Shepherd M, McLean S, Hunter CN (2005) Kinetic basis for linking the first two enzymes of chlorophyll biosynthesis. *FEBS J* 272:4532–4539
- Shioi Y, Doi M, Böddi B (1988) Selective inhibition of chlorophyll biosynthesis by nicotinamide. *Arch Biochem Biophys* 267:69–74
- Shpil'ov AV, Zinchenko VV, Shestakov SV, Grimm B, Lokstein H (2005) Inactivation of the geranylgeranyl reductase (ChlP) gene in the cyanobacterium *Synechocystis* sp. PCC 6803. *Biochim Biophys Acta* 1706:195–203
- Shui J, Saunders E, Needleman R, Nappi M, Cooper J, Hall L, Kehoe D, Stowe-Evans E (2009) Light-dependent and light-independent protochlorophyllide oxidoreductases in the chromatically adapting cyanobacterium *Fremyella diplosiphon* UTEX 481. *Plant Cell Physiol* 50:1507–1521
- Sirijovski N, Lundqvist J, Rosenbäck M, Elmlund H, Al-Karadaghi S, Willows RD, Hansson M (2008) Substrate-binding model of the chlorophyll biosynthetic magnesium chelatase BchH subunit. *J Biol Chem* 283:11652–11660
- Skinner JS, Timko MP (1998) Loblolly pine (*Pinus taeda* L.) contains multiple expressed genes encoding light-dependent NADPH:protochlorophyllide oxidoreductase (POR). *Plant Cell Physiol* 39:795–806
- Sobotka R, Dühning U, Komenda J, Peter E, Gardian Z, Tichy M, Grimm B, Wilde A (2008) Importance of the cyanobacterial Gun4 protein for chlorophyll metabolism and assembly of photosynthetic complexes. *J Biol Chem* 283:25794–25802
- Stecanella V, Hansson M, Jensen PE (2015) Linking chlorophyll biosynthesis to a dynamic plastoquinone pool. *Plant Physiol Biochem* 97:207–216
- Stenbaek A, Jensen PE (2010) Redox regulation of chlorophyll biosynthesis. *Phytochemistry* 71:853–859
- Stenbaek A, Hansson A, Wulff RP, Hansson M, Dietz KJ, Jensen PE (2008) NADPH-dependent thioredoxin reductase and 2-Cys peroxiredoxins are needed for the protection of Mg-protoporphyrin monomethyl ester cyclase. *FEBS Lett* 582:2773–2778
- Suzuki JY, Bauer CE (1995a) A prokaryotic origin for light-dependent chlorophyll biosynthesis of plants. *Proc Natl Acad Sci U S A* 92:3749–3753
- Suzuki JY, Bauer CE (1995b) Altered monovinyl and divinyl protochlorophyllide pools in *bchJ* mutants of *Rhodobacter capsulatus*. Possible monovinyl substrate discrimination of light-independent protochlorophyllide reductase. *J Biol Chem* 270:3732–3740
- Sytina O, Heyes D, Hunter C, Alexandre M, van Stokkum I, van Grondelle R, Groot M (2008) Conformational changes in an ultrafast light-driven enzyme determine catalytic activity. *Nature* 456:1001–1004
- Tamiaki H, Teramura M, Tsukatani Y (2016) Reduction processes in biosynthesis of chlorophyll molecules: Chemical implications of enzymatically regio- and stereoselective hydrogenation in the late steps of their biosynthetic pathway. *Bull Chem Soc Jpn* 89:161–173
- Tanaka R, Tanaka A (2007) Tetrapyrrole biosynthesis in higher plants. *Annu Rev Plant Biol* 58:321–346
- Tanaka R, Tanaka A (2011) Chlorophyll cycle regulates the construction and destruction of the light-harvesting complexes. *Biochim Biophys Acta* 1807:968–976
- Tanaka A, Tsuji H (1981) Changes in chlorophyll *a* and *b* Content in dark-incubated cotyledons excised from illuminated seedlings: The effect of calcium. *Plant Physiol* 68:567–570

- Tanaka A, Tsuji H (1982) Calcium-induced formation of chlorophyll *b* and light-harvesting chlorophyll *a/b* protein complex in cucumber cotyledons in the dark. *Biochim. Biophys. Acta* 680:265–270
- Tanaka A, Ito H, Tanaka R, Tanaka NK, Yoshida K, Okada K (1998) Chlorophyll *a* oxygenase (CAO) is involved in chlorophyll *b* formation from chlorophyll *a*. *Proc Natl Acad Sci U S A* 95:12719–12723
- Tang KH, Wen J, Li X, Blankenship RE (2009) Role of the AcsF protein in *Chloroflexus aurantiacus*. *J Bacteriol* 191:3580–3587
- Teramura M, Harada J, Mizoguchi T, Yamamoto K, Tamiaki H (2016) In vitro assays of BciC showing C13²-demethoxycarbonylase activity requisite for biosynthesis of chlorosomal chlorophyll pigments. *Plant Cell Physiol* 57:1048–1057
- Tomitani A, Okada K, Miyashita H, Matthijs HC, Ohno T, Tanaka A (1999) Chlorophyll *b* and phycobilins in the common ancestor of cyanobacteria and chloroplasts. *Nature* 400:159–162
- Tottey S, Block MA, Allen M, Westergren T, Albrieux C, Scheller HV, Merchant S, Jensen PE (2003) *Arabidopsis* *CHL27*, located in both envelope and thylakoid membranes, is required for the synthesis of protochlorophyllide. *Proc Natl Acad Sci U S A* 100:16119–16124
- Tsukatani Y, Yamamoto H, Harada J, Yoshitomi T, Nomata J, Kasahara M, Mizoguchi T, Fujita Y, Tamiaki H (2013a) An unexpectedly branched biosynthetic pathway for bacteriochlorophyll *b* capable of absorbing near-infrared light. *Sci Rep* 3:1217
- Tsukatani Y, Yamamoto H, Mizoguchi T, Fujita Y, Tamiaki H (2013b) Completion of biosynthetic pathways for bacteriochlorophyll *g* in *Heliobacterium modesticaldum*: the C8-ethylidene group formation. *Biochim Biophys Acta* 1827:1200–1204
- Ueda M, Tanaka A, Sugimoto K, Shikanai T, Nishimura Y (2014) *chlB* requirement for chlorophyll biosynthesis under short photoperiod in *Marchantia polymorpha* L. *Genome Biol Evol* 6:620–628
- Verdecia M, Larkin R, Ferrer J, Riek R, Chory J, Noel J (2005) Structure of the Mg-chelatase cofactor GUN4 reveals a novel hand-shaped fold for porphyrin binding. *PLoS Biol* 3:e151
- Vogl K, Tank M, Orf GS, Blankenship RE, Bryant DA (2012) Bacteriochlorophyll *f*: properties of chlorosomes containing the “forbidden chlorophyll”. *Front Microbiol* 3:298
- Wada K, Yamaguchi H, Harada J, Niimi K, Osumi S, Saga Y, Oh-Oka H, Tamiaki H, Fukuyama K (2006) Crystal structures of BchU, a methyltransferase involved in bacteriochlorophyll *c* biosynthesis, and its complex with S-adenosylhomocysteine: implications for reaction mechanism. *J Mol Biol* 360:839–849
- Wätzlich D, Bröcker M, Uliczka F, Ribbe M, Virus S, Jahn D, Moser J (2009) Chimeric nitrogenase-like enzymes of (bacterio)chlorophyll biosynthesis. *J Biol Chem* 284:15530–15540
- Wilde A, Mikolajczyk S, Alawady A, Lokstein H, Grimm B (2004) The *gun4* gene is essential for cyanobacterial porphyrin metabolism. *FEBS Lett* 571:119–123
- Wilks H, Timko M (1995) A light-dependent complementation system for analysis of NADPH:protochlorophyllide oxidoreductase: identification and mutagenesis of two conserved residues that are essential for enzyme activity. *Proc Natl Acad Sci U S A* 92:724–728
- Willows RD, Hansson M (2003) Mechanism, structure, and regulation of magnesium chelatase. In: Kadish KM, Smith KM, Guillard R (eds) *The Porphyrin Handbook, Chlorophylls and bilins: biosynthesis, synthesis, and degradation*, vol 13. Academic Press, San Diego, pp 1–47
- Xiong J, Inoue K, Bauer CE (1998) Tracking molecular evolution of photosynthesis by characterization of a major photosynthesis gene cluster from *Heliobacillus mobilis*. *Proc Natl Acad Sci U S A* 95:14851–14856
- Yamamoto H, Kato M, Yamanashi K, Fujita Y (2014) Reconstitution of a sequential reaction of two nitrogenase-like enzymes in the bacteriochlorophyll biosynthetic pathway of *Rhodobacter capsulatus*. *Biochem Biophys Res Commun* 448:200–205
- Yamanashi K, Minamizaki K, Fujita Y (2015) Identification of the *chlE* gene encoding oxygen-independent Mg-protoporphyrin IX monomethyl ester cyclase in cyanobacteria. *Biochem Biophys Res Commun* 463:1328–1333

- Yamazaki S, Nomata J, Fujita Y (2006) Differential operation of dual protochlorophyllide reductases for chlorophyll biosynthesis in response to environmental oxygen levels in the cyanobacterium *Leptolyngbya boryana*. *Plant Physiol* 142:911–922
- Yang ZM, Bauer CE (1990) *Rhodobacter capsulatus* genes involved in early steps of the bacteriochlorophyll biosynthetic pathway. *J Bacteriol* 172:5001–5010
- Yang H, Liu J, Wen X, Lu C (2015) Molecular mechanism of photosystem I assembly in oxygenic organisms. *Biochim Biophys Acta* 1847:838–848
- Yen HC, Marrs B (1976) Map of genes for carotenoid and bacteriochlorophyll biosynthesis in *Rhodospseudomonas capsulata*. *J Bacteriol* 126:619–629

The Maintenance of Iron Homeostasis Among Prokaryotic Phototrophs

Sébastien Zappa and Carl E. Bauer

Abstract Like all prokaryotes, photosynthetic bacteria have had to solve the difficulty of acquiring poorly available iron in oxic environments and, at the same time, have had to manage the potential deleterious Fenton chemistry effects caused by this metal. In addition, photosynthesis requires a lot of iron for both the synthesis of the photosystem and the photosynthetic process itself. As a result of this iron need, phototrophs are good model organisms to study bacterial iron homeostasis. This review focuses on transcriptomic changes induced by iron limitation centering on major functional features of iron homeostasis such as the acquisition, storage, and regulation. We review evidence that iron limitation induces significant stress that triggers global transcriptional changes resulting in upregulation of iron import and storage while decreasing photosynthesis. Studies on transcription factors that regulate genes involved in iron homeostasis will also be covered, with the Ferric Uptake Regulator being the most understood. Finally, we will discuss the interference between iron and copper homeostasis, especially since iron transport systems make up a primary defense against copper poisoning.

Keywords Iron • Iron homeostasis • Iron transport • Iron regulation • Iron stress response • Fur • Irr • Feo • TonB • Siderophore • EfeUOB • FutABC • PfsR • Copper homeostasis

Introduction

Studies as early as 1956 showed that iron affects the synthesis of the purple bacterial photosystem. Specifically, Lascelles reported that iron supplementation stimulates production of bacteriochlorophyll in the purple bacterium *Rhodobacter sphaeroides* (Lascelles 1956). Conversely it has also been shown that iron limitation leads to an absence of pigmentation and impaired growth under photosynthetic conditions (Peuser et al. 2011). Surprisingly, there are few other reports on the effect of iron availability on synthesis of the purple bacterial photosystem.

S. Zappa • C.E. Bauer (✉)

Department of Molecular and Cellular Biochemistry, Indiana University,
Simon Hall, 212 S Hawthorne Dr, Bloomington, IN 47405, USA

e-mail: bauer@indiana.edu

In contrast to limited mechanistic studies with purple bacteria, the effect of iron on synthesis of the cyanobacterial photosystem has been an active area of research. Numerous studies have shown that iron deprivation leads to a general decrease in chlorophyll and phycocyanin synthesis in cyanobacteria (Öquist 1974; Guikema and Sherman 1983; Sandmann 1985; Sandström et al. 2002). Adaptation of the photosynthetic apparatus to iron deficiency also affects the composition and ratio of individual photosystem components. Briefly, the Fe-S-containing ferredoxin is replaced by the flavodoxin IsiB, and the photosystem I (PSI) is surrounded by IsiA proteins. Formation of the IsiA-PSI supercomplex compensates the decrease of PSI in terms of light-harvesting capacity. More details and references can be found in the following articles (Chauhan et al. 2011; Ryan Keogh et al. 2012; Fraser et al. 2013; Cheng and He 2014; Wahadoszamen et al. 2015). IsiA and IsiB are encoded by the *isiAB* operon and make up a central part of the response to iron limitation, often considered as a hallmark of the cyanobacterial iron response, and will be discussed in this review.

The effect of iron limitation on pigment synthesis in photosynthetic species is understandable given that many enzymes involved in the bacteriochlorophyll, chlorophyll, and phycocyanin synthesis require iron as a cofactor for catalysis (Beale and Cornejo 1983; Frankenberg and Lagarias 2003; Sirijovski et al. 2007; Sarma et al. 2008). In addition, iron is an important component of photosystem I (PSI) and photosystem II (PSII) as well as an essential component of the electron transport chain, many components of which use heme as an electron carrier (Ferreira and Straus 1994; Keren et al. 2004). Given the poor solubility of iron in oxic environments and its toxicity through Fenton chemistry, bacterial fitness is tied to the necessity of efficient import and storage systems that also prevent the buildup of an intracellular free iron pool, in other words an efficient iron homeostasis (Touati 2000; Andrews et al. 2003; Chiancone et al. 2004). The literature on the effect of iron on synthesis and function of photosystems is expansive and thus beyond the scope of a single review. Consequently, this review focuses on mechanisms that photosynthetic prokaryotes use to acquire, sequester, and regulate appropriate amounts of intracellular iron.

The Cellular Response to Iron Limitation

There are currently only few reports of global studies of the effect of iron limitation on gene expression in anoxygenic photosynthetic prokaryotes. A study on *Rhodobacter (R.) sphaeroides* showed that acclimation to iron-free medium induces a lack of pigmentation, as a result of the downregulation of the photosynthetic genes *pucAB* and *puc2AB*, encoding light-harvesting complex II. In addition, iron limitation increased the cellular amount of reactive oxygen species (ROS) (Peuser et al. 2011). Overall, 384 transcriptomic changes were observed: 33 downregulations concerning photosynthesis, flagellum biosynthesis, and chemotaxis genes and 351 upregulated genes dealing with iron uptake and storage but also Fe-S cluster

assembly and repair (Peuser et al. 2012). Unexpectedly, no significant changes were observed regarding genes involved in the oxidative stress response, despite the increase of cellular ROS. Finally, it is remarkable that the ferrous iron uptake system *feoAB* did not respond to iron deficiency while it did to H₂O₂ (Peuser et al. 2012). Another study on the effect of iron limitation on iron transport and heme gene expression deals with *R. capsulatus* (Zappa and Bauer 2013a). That study demonstrated that iron limitation led to an overall increase in ferrous and ferric transport gene expression and an increase in siderophore and heme uptake receptor expression. There was also a decrease in expression in a putative ferrous iron efflux pump indicating that *R. capsulatus* cells that are starved for iron adjust their membrane transport components in a way that maximizes iron acquisition and retention. There is also a general increase in heme gene expression which presumably reflects stress on heme synthesis caused by inactivation of enzymes in the heme pathway that use iron as a cofactor as well as limitation of iron availability for insertion into protoporphyrin IX (Zappa and Bauer 2013a).

In contrast to limited understanding of global effects of iron limitation in anoxy-photosynthetic prokaryotes, there have been global studies on the effects of iron limitation with cyanobacteria. Major findings are summarized in Fig. 1. A study with *Synechocystis* sp. PCC 6803 demonstrated that an iron limitation kinetic shift resulted in 1076 transcription units that were differentially expressed during at least one time point. These include 644 mRNAs and 434 noncoding RNAs (307 asRNAs, 125 sRNAs) (Hernández-Prieto et al. 2012). A highly dynamic pattern was observed

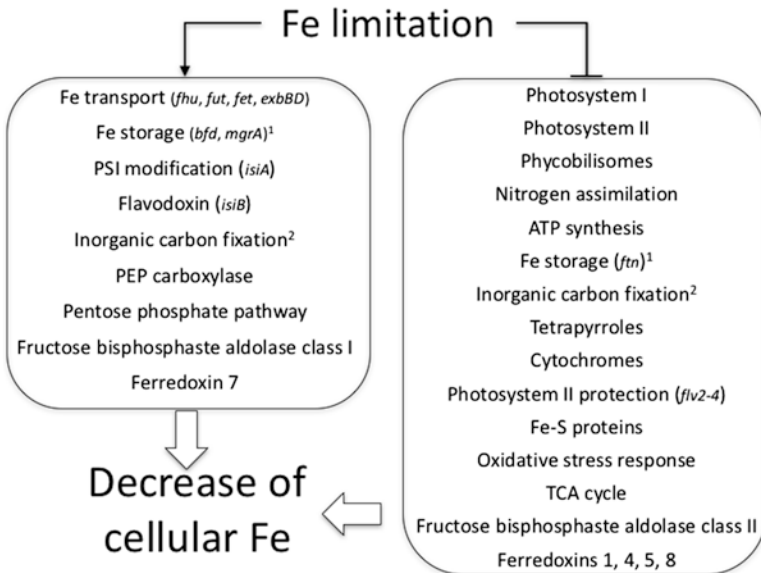


Fig. 1 Iron limitation induces global transcriptomic and metabolic changes. ¹Iron storage response varies depending on species studied (e.g., *Synechocystis* vs. *Trichodesmium*). ²Inorganic carbon change in *Synechocystis* varies depending on studies

with a transient initial upregulation followed by downregulation. The affected genes included those involved in photosynthesis (PSI, PSII, phycobilisomes, ATP synthase complex, carbon fixation, porphyrin and chlorophyll synthesis) but also involved in oxidative phosphorylation, which in cyanobacteria borrows several components to photosynthesis (plastoquinone pool, soluble electron carriers, cytochrome *b₆f*, ATP synthase). Downregulation of cytochrome *b₆f* under iron limitation has been consistently observed (Sandström et al. 2002; Shi et al. 2007; Thompson et al. 2011; Fraser et al. 2013). Decrease in PSI gene expression is stronger than that of PSII genes, which is consistent with the PSI/PSII ratio as is classically observed (Hernández-Prieto et al. 2012). Other functional group had less dynamic, more sustained expression patterns. Typically, iron transport (*fhuA*, *futA*, *fetA*, *exbD*)- and storage (*bfd*)-related genes along with the *isiAB* operon were upregulated. The latter operon encodes the IsiA protein, involved in PSI modification, and the flavodoxin IsiB, both involved in the iron stress/sparing response. On the opposite, the *flv4-2* operon, encoding the PSII protection flavodiiron protein complex Fl2-Fl4, was downregulated. Also with sustained pattern was a transcription increase of nitrogen assimilation genes (*nirA*, *glnN*, *glnA*, *ntcA*), while inorganic carbon fixation genes decrease (*cmpABCD*). As both processes necessitate iron-containing enzymes, the observed difference in transcription change may be a signature of cellular prioritization (Hernández-Prieto et al. 2012).

Antisense RNA appears to be involved in different ways: from promoting mRNA stability of nitrogen assimilation genes to fine-tuning either the basal mRNA level of iron import genes or the transient expression of *isiA* and *flv4* (Hernández-Prieto et al. 2012). In addition, among the 125 sRNA differentially expressed upon iron limitation, four showed potential regulatory functions in photosynthesis and respiration. In a few cases, different patterns of expressions were observed between a UTR and its associated gene indicating that the UTR may constitute riboswitches which adds another layer of regulation. Such cases include ferrous iron transport (*feoA*), bicarbonate transport (*cmpA*), Fe-S cluster assembly (*sufB*), and phycobilisome-dependent light energy dissipation (*slr1964*) (Hernández-Prieto et al. 2012).

By following a set of 106 proteins in *Synechocystis* sp. PCC 6803, a proteomic approach confirmed the bulk of the above transcriptomic data. Most photosynthesis components were downregulated (PSI, PSII, phycobilisomes, cytochrome *b₆f*, soluble electron carriers), as were Fe-S-containing proteins (Vuorijoki et al. 2016). Upregulated photosynthesis elements were the IsiA and IsiB iron stress proteins and the phycobilisome-interacting orange carotenoid protein, involved in photoprotection. On the other hand, carbon fixation components were upregulated which is not consistent with previously reported transcriptomic data (Hernández-Prieto et al. 2012; Vuorijoki et al. 2016). Other upregulated components included iron transport (FeoB, FhuA) and storage (MgrA) proteins, sigma factors SigB and SigC, Fe-S biosynthesis repressor SufR, and nitrogen assimilation factor NtcA. Downregulation was observed for FurA, hydrogenase HoxH, and sigma factor SigA. TCA cycle was overall downregulated as a consequence of multiple Fe-S-containing enzymes, while phosphoenolpyruvate carboxylase and pentose phosphate pathway enzymes were upregulated (Vuorijoki et al. 2016).

An additional proteomic characterization of iron stress was reported for the marine non-heterocystous filamentous diazotroph *Trichodesmium erythraeum* IMS101. The global iron-sparing response in this species results in a reduction of 55–60% for the iron requirement of the cell, with the largest part of this saving coming from the reduction in nitrogenase and PSI contents (Snow et al. 2015). Statistical analysis of the iron-stressed proteome showed that with higher the iron content, individual proteins were more affected by iron limitation. Otherwise, ferrous iron transporter FeoA-FeoB could not be detected unlike the ferric iron transporter FutA/IdiA (Snow et al. 2015). Numerous enzymes involved in oxidative stress response (Ni-SOD, TrxA, TrxB, peroxiredoxin) were upregulated under iron deprivation. So was a PilA homologue, this major pilin protein was described to take part in growth on iron oxides for *Synechocystis* sp. PCC 6803 (Lamb et al. 2014). The nitrogen fixation and photosynthesis pathways were repressed, while IsiA, the flavodoxin IsiB, and the plastocyanin were overexpressed. Typical PSI/PSII decrease and IsiA/PSI increase under iron deficiency were confirmed in this study (Snow et al. 2015). Severe decrease of the iron storage ferritin under iron limitation indicates that the cellular iron pool becomes fully associated with functional iron proteins in these conditions. On the opposite, iron-replete cells are estimated to have 84% of the cellular iron in the ferritins (Snow et al. 2015). Interestingly, the class II fructose biphosphate aldolase enzymes, which are often Fe²⁺ dependent, were substituted by class I enzymes. RuBisCo, ATP synthase, and cytochrome *b₆/f*/PSII were unchanged or only mildly changed (Snow et al. 2015). Heme synthesis was also found affected by iron depletion although with various patterns. Indeed, *hemA* is downregulated or unchanged in *Prochlorococcus* sp. MED4 and MIT9313 strains, respectively (Thompson et al. 2011). This is contrasted by upregulation of several heme synthesis genes in *Anabaena* sp. PCC 7120 (González et al. 2012; Snow et al. 2015). In the same species, two heme oxygenases are activated by iron depletion, while in *Trichodesmium erythraeum* IMS101, heme oxygenase is repressed (Snow et al. 2015). This highlights that there are different strategies of iron recycling in different cyanobacterial species.

Iron availability also impacts the expression of several cyanobacterial ferredoxins. *Synechocystis* sp. PCC 6803 exhibits nine ferredoxins, Fed1–9. Iron starvation downregulates Fed1, Fed4, Fed5, and Fed8. On the other hand, Fed7 is upregulated by iron-deplete and downregulated under iron-replete conditions. Fed9 was not described as transcriptionally affected by iron, but it does interact with the flavodiiron protein Flv3. Both Fed7 and Fed9 are important in response to oxidative stress and metal availability, particularly to iron (Cassier-Chauvat and Chauvat 2014).

Finally, one note of caution regarding global changes needs to be made. A comparison of four iron limitation transcription studies with *Synechocystis* sp. PCC 6803 indicates that only 28 genes display significant differential changes in all four studies: 21 are upregulated, 3 downregulated, and 4 vary from one study to the other (Hernández-Prieto et al. 2012). This underlines the high sensitivity of the cellular response to variability in experimental conditions and potential genetic drift of laboratory strains.

Iron Transport

The import of iron can occur with several different classes of transporters (Andrews et al. 2003; Cartron et al. 2006; Cornelis and Andrews 2012; Zappa and Bauer 2013b). Briefly, poorly soluble Fe^{3+} iron can be imported as Fe^{3+} bound to a siderophore by a TonB-dependent siderophore uptake system or as free Fe^{3+} by a metal ABC transporter. Uptake of the more soluble Fe^{2+} can occur via the Feo system and the EfeUOB system, although other studies also show that the latter system can also import soluble Fe^{3+} as well as extract Fe^{2+} from heme (Létoffé et al. 2009; Miethke et al. 2013). By far, siderophore uptake has received most of the attention over past decades but more and more is known about these alternative pathways of iron import. None of these iron import systems are unique to photosynthetic bacteria as they are widely dispersed among the bacterial domains. Iron import systems identified in phototrophic bacteria are depicted in Fig. 2.

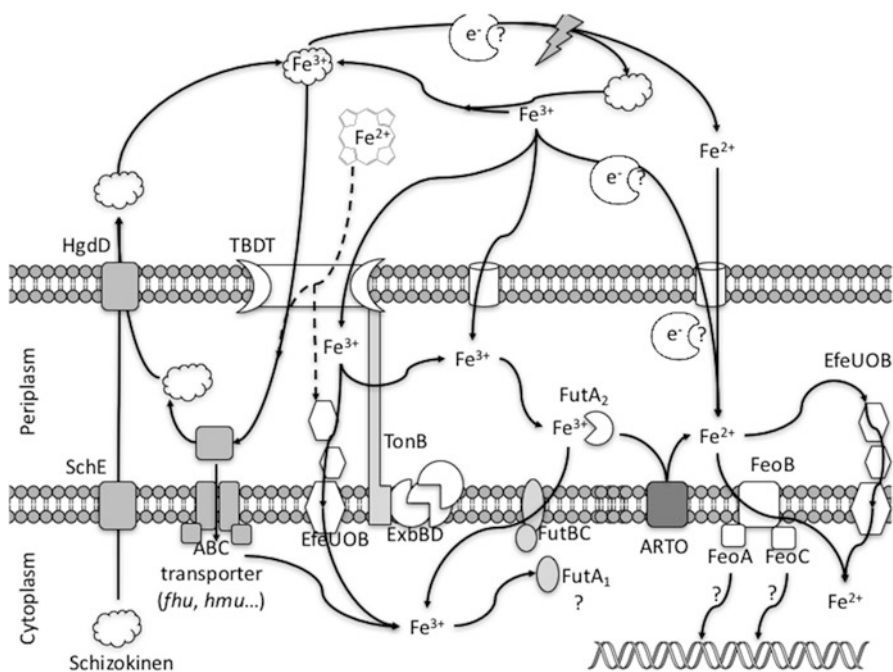


Fig. 2 Overview of iron transport systems identified in phototrophic prokaryotes. Represented are the export and import of siderophores, with the example of *Anabaena* schizokinen. TBdT-TonB-ExbBD systems can be involved in the uptake of ferrisiderophores, heme, and ferric iron. EfeUOB system can be involved in the import of iron as ferric, ferrous iron as well as extracting iron from heme. Ferric iron import can be achieved by the FutABC system while Feo system uptakes ferrous iron. Reductive pathway, involving a putative extracellular or periplasmic reductase, is also pictured as well as the abiotic photoreduction

Siderophore Synthesis and Uptake Systems

Siderophore synthesis and uptake have been frequently reviewed, so readers interested in this topic are directed to the following references (Köster 2001; Krewulak and Vogel 2008, 2011; Hopkinson and Morel 2009; Sandy and Butler 2009; Hider and Kong 2010; Chu et al. 2010; Morrissey and Bowler 2012). Siderophores are small ligands of 500–1500 Da that exhibit a high affinity for Fe^{3+} ($K_f > 10^{30}$ M). Siderophores are produced by a wide range of organisms (bacteria, fungi, diatoms, graminaceous plants) in all sorts of environments (terrestrial, soil, freshwater, open ocean, coastal ocean water) with more than 500 siderophores identified. Most siderophores are synthesized by nonribosomal peptide synthetases (NRPSs) or polyketide synthases (PKSs) with chemical structures classified as catechol, hydroxamate, or alpha-hydroxycarboxylate. Siderophores chelate the relatively insoluble Fe^{3+} , which enables organisms with adequate siderophore uptake systems to import this oxidized form of iron. Organisms can produce one or several siderophores, along with the corresponding uptake systems, but organisms can also scavenge siderophores that are produced by other species (in this case siderophores that are scavenged from another species are called xenosiderophores). In Gram-negative bacteria, the typical siderophore uptake system consists of an outer membrane ferrisiderophore receptor that interacts with a siderophore-specific TonB-ExxB-ExxB complex to provide the energy for translocation of the siderophore into the periplasm. Once in the periplasm, an ABC transporter cassette, comprised of a periplasmic siderophore-binding protein, permease, and ATPase, then imports the ferrisiderophore into the cytoplasm.

Siderophore-based iron import has been described for photosynthetic organisms. In the purple bacterium *R. sphaeroides*, no synthesis of hydroxamate- or catecholate-type siderophore could be detected, but this bacterium was shown to uptake ferric citrate and ferric parabactin supplied to the growth medium (Moody and Dailey 1984, 1985). Genome sequence analysis of model purple bacteria also shows the presence of numerous siderophore uptake systems. For example, there are 4 in *R. sphaeroides*, 7 in *R. capsulatus*, 24 in *Rhodospseudomonas (Rh.) palustris* but none in *R. ferrooxidans* (Larimer et al. 2004; Zappa and Bauer 2013b). Unlike *R. sphaeroides* and *R. capsulatus*, *Rh. palustris* is able to synthesize a siderophore, namely, rhizobactin. Based on the ratio of siderophore synthesis versus siderophore uptake systems in their respective genomes, it is reasonable to speculate that these three organisms rely more or less heavily on xenosiderophores. In *R. sphaeroides* and *R. capsulatus*, siderophore uptake systems were also shown to be transcriptionally upregulated under iron-limiting conditions (Peuser et al. 2012; Zappa and Bauer 2013a).

In cyanobacteria, the production of siderophores and/or use of xenosiderophores under iron scarcity have been known for a long time (Trick and Kerry 1992; Ferreira and Straus 1994; Michel and Pistorius 2004). Siderophore production has been reported for numerous species such as *Anabaena* sp., *Anabaena cylindrical*, *Anabaena oryzae*, *Microcystis aeruginosa*, *Microcystis wesenbergii*,

Synechococcus sp., but overall cyanobacteria have been described as poor siderophore producers (Simpson and Neilands 1976; Lammers and Sanders-Loehr 1982; Ghassemian and Straus 1996; Xing et al. 2007; Nicolaisen et al. 2010; Alexova et al. 2011; Wang et al. 2014; Singh and Mishra 2015). Characterized siderophores of cyanobacterial origin include the suite of synechobactins produced by the marine species *Synechococcus* sp. PCC 7002, schizokinen synthesized by the freshwater species *Anabaena* sp. PCC 7120, and the anachelins isolated from the other freshwater species *Anabaena cylindrica*. While synechobactins and schizokinen are similar citrate-based siderophores, anachelins are peptide siderophores. Synechobactins differ schizokinen by the presence of fatty acid tails (Hopkinson and Morel 2009).

Siderophore used in cyanobacteria has not been extensively characterized, but genome analysis suggests that, for marine species, the process might be more implemented in coastal rather than open-ocean species (Hopkinson and Morel 2009). From an ecological standpoint, cyanobacterial production of siderophores avoids being overgrown by eukaryotic algae (Murphy et al. 1976). Currently, the best molecular model of cyanobacterial siderophore usage was assembled in *Anabaena* sp. PCC 7120. This strain was shown to produce at least two siderophores, including schizokinen. The schizokinen exporter SchE, a protein of the major facilitator superfamily, and HgdD, a TolC-like protein, are responsible for the export of schizokinen (Nicolaisen et al. 2010). Two TonB-dependent outer membrane transporters (TBDT) were identified: the schizokinen transporter SchT and the Fe³⁺ and Cu²⁺ transporter IatC (Nicolaisen et al. 2008, 2010). Several TonB-exbBD systems were tested, and TonB₃-ExbB₃D₃ was shown to import schizokinen from the outer membrane receptor SchT to the periplasm. Finally, a FhuBCD cassette was identified as the final step of schizokinen uptake, with FhuD being the periplasmic schizokinen-binding protein, FhuB the permease, and FhuC the ATP-binding protein. The *tonB₃* and *fhu* genes were found to be essential for the cells to grow under normal iron levels (Stevanovic et al. 2012). Systematic study of TBDT and TonB-ExbBD systems revealed a complex network where some are responsive to high iron levels at low cell density, while others are upregulated under iron-limiting condition at high cell density. The latter category makes up the core of the iron deficiency response (Stevanovic et al. 2013). Upregulation of *fhuC* was observed under iron limitation, although to a much lesser extent than *schE* and *schT* (Rudolf et al. 2015). Kinetics showed that endogenously produced schizokinen is imported faster than xenosiderophores by a 100-fold factor in *Anabaena* sp. PCC 7120 and *Anabaena flos-aqua* (Sonier et al. 2012; Rudolf et al. 2015). Different transporters are dedicated to import schizokinen and xenosiderophores in the periplasm, but final internalization through the plasma membrane involves the same transporter in *Anabaena* sp. PCC 7120 (Rudolf et al. 2015).

In *Anabaena* sp. PCC 7120, two gene clusters potentially involved in siderophore synthesis were found: one involved in hydroxamate-type siderophore synthesis, in the vicinity of the SchT-encoding gene, and a large gene cluster of 76 kb, with NRPS/PKS signature genes (Jeanjean et al. 2008; Nicolaisen et al.

2008). Transcription of the genes of the 76 kb cluster was found upregulated in iron-limiting conditions or in the presence of oxidative stress (Jeanjean et al. 2008). Likewise, genes involved in siderophore synthesis and uptake are upregulated in *Nostoc* when iron was scarce (Yingping et al. 2014). In addition, screening for TonB-dependent outer membrane receptors in 32 cyanobacterial genomes revealed the presence of 22 TonB-dependent receptors in *Anabaena* sp. PCC 7120, including 14 FhuA type, 3 IutA type, and 1 ViuA type, which are related to hydroxamate, citrate-hydroxamate, and catecholate siderophore import, respectively. Variability of the transcriptomic response to iron levels highlights that these TBDT are specialized in either quick response to high iron at low cell density, genuine response to iron limitation, or copper detoxification (Stevanovic et al. 2013). Nevertheless, the number of TBDT varies a lot between cyanobacterial genomes: 33 in *Gloeobacter violaceus*, 22 in *Anabaena* sp. PCC 7120, 10 in *Anabaena variabilis*, 6 in *Synechococcus* sp. PCC 7002, 4 in *Synechocystis* sp. PCC 6803, and none in *Prochlorococcus*. Some were also found in the “*Candidatus Synechococcus spongiarum*” group, cyanobacterial symbionts of sponges, and seem to be remnants of ancestral features of nonsymbiotic ancestors (Burgsdorf et al. 2015). Interestingly, no FecA-type transporter was identified, although this ferric citrate transporter is widely distributed in other bacterial classes (Mirus et al. 2009). So far, only three cyanobacterial TonB-dependent receptors were experimentally studied: the two aforementioned SchT and IacT in *Anabaena* sp. and FdTonB in *Fremyella diplosiphon*. As the latter was found unresponsive to iron levels, it brings to two the number of cyanobacterial TonB-dependent transporters involved in iron homeostasis with experimental confirmation, both in the same species. Finally, in *Synechocystis* sp., a putative FhuA-type siderophore transporter that was identified in silico (slr1406) was experimentally shown to be upregulated in iron-limiting condition (Mirus et al. 2009; Shcolnick et al. 2009). Still, this highlights how siderophore uptake in cyanobacteria is far from being fully characterized.

Besides classic activation under iron scarcity, it is interesting to note that light quality can affect iron uptake. Indeed, cyanobacteria can adapt to the color of light via a process known as complimentary chromatic adaptation. DNA microarray showed that genes responding to chromatic adaptation in *Fremyella diplosiphon* have homologues in other cyanobacteria that are responsive to iron scarcity, such as *atpB* that putatively encodes a siderophore uptake protein (Stowe-Evans et al. 2004). Finally, in marine environments, import of Fe^{3+} from siderophore could involve mechanisms other than the TonB-dependent uptake. Extracellular reduction of the ferrisiderophore complex could be a primary process in these conditions: instead of actually internalizing the complex, it is dissociated by reduction by an extracytoplasmic reductase or by photoreduction. Once reduced, free Fe^{2+} is set free to diffuse passively through an outer membrane porin before reaching Fe^{2+} transporter FutABC or FeoB (Hopkinson and Morel 2009; Sandy and Butler 2009). Extracellular reduction of ferric iron from siderophore prior to iron uptake was also shown in *Anabaena* sp. PCC 7120 (Kranzler et al. 2011).

Ferric Iron ABC Transporters

As an alternative to siderophore-based Fe^{3+} uptake systems, some species can also contain a ferric iron ABC transporter. In such a situation, ferric iron has to first reach the periplasm, for example, by passive diffusion through the outer membrane via a porin. Then, the Fe^{3+} ABC transporter operates using a Fe^{3+} -binding periplasmic protein, an inner membrane permease and an ATPase. Well-studied examples of the Fe^{3+} ABC transporter are the FbpABC (AfuABC), SfuABC, and HitABC systems (Andrews et al. 2003). Unlike TonB-dependent uptake systems, these transporters are less specific and were shown to be able to import Fe^{2+} and/or Mn^{2+} in addition to or instead of Fe^{3+} (see Zappa and Bauer (2013b) for references). In purple bacteria, screening of *Rhodobacter* genomes revealed the presence of an FbpABC homologue in *R. capsulatus*, *R. sphaeroides*, and *R. ferrooxidans*, where the permease-encoding gene is duplicated (Zappa and Bauer 2013b). Thus, this *fbpAB₁B₂C* operon might be inherited from a common ancestor to *Rhodobacter* species. Among this genus, another Fe^{3+} ABC transporter was found, but only in *R. sphaeroides*. It is homologous to the SitABCD transporter originally described in *Salmonella enterica* serovar Typhimurium (Kehres et al. 2002). And as in the latter organism, some elements suggest that it might be involved in Mn^{2+} rather than Fe^{3+} transport. Firstly, *R. sphaeroides* does not harbor the Mn^{2+} -specific transporter MntH, while the other *Rhodobacter* representatives do (Zappa and Bauer 2013b). Second, the specificity of this transporter to Fe^{3+} is not stable across the organisms harboring it. Third, its transcription is not upregulated under iron scarcity but instead is upregulated by manganese scarcity (Peuser et al. 2012).

More is known about Fe^{3+} ABC transporters in cyanobacteria than those of anoxygenic bacteria. The FutA/IdiA Fe^{3+} ABC transporter was identified in the genomes of 28 unicellular cyanobacteria of the *Prochlorococcus*, *Synechococcus*, and *Synechocystis* genera (Morrissey and Bowler 2012). Biochemical characterization has been primarily done on the *Synechocystis* sp. PCC 6803 homologue. The FutA₁A₂BC consists of two Fe^{3+} -binding proteins FutA₁ and FutA₂, a permease FutB, and an ATPase FutC with *fut* gene expression upregulated under iron-limiting conditions. Deletion of *futA₁* or *futA₂* also reduces cellular iron content, with the *futA₁* deletion being the most severe. Interestingly, while FutA₂ is a highly abundant periplasmic protein and is accepted as the Fe^{3+} periplasmic receptor of the ABC cassette, the role of FutA₁ remains unclear. Unlike FutA₂, FutA₁ is not located in the periplasm but is instead predominantly located in the cytoplasm. However, deletion of *futA₁* does severely reduce the concentration of Fe^{3+} -FutA₂ in the periplasm, so it does exert an indirect control on iron import by the FutA₂BC complex (Kato et al. 2000, 2001a, b; Badarau et al. 2008; Shcolnick et al. 2009; Morrissey and Bowler 2012).

Originally identified as IdiA, FutA₁ has also been suggested to protect the acceptor side of PSII from H_2O_2 production under iron limitation by direct protein-protein interaction (Ting et al. 2002; Michel and Pistorius 2004). FutA₂ is also connected to oxidative stress as it is regulated by PerR, the Fur-like transcription factor involved in

oxidative stress response (Shcolnick et al. 2009). Other FutABC uptake systems were identified in other cyanobacteria, and most cyanobacterial FutA sequences make up a homologous clade (Tom-Yew et al. 2005). Regarding experimental clues, *Microcystis aeruginosa* has one FutA homologue that seems localized at the periphery of the cell and that was shown to be expressed under iron limitation (Alexova et al. 2011). A homologous Fe³⁺ transport system designated as IdiA/FutB/FutC was found to be conserved through several *Prochlorococcus* genomes, and IdiA, the Fe-binding periplasmic protein, was also shown to be transcriptionally upregulated under iron scarcity (Thompson et al. 2011). In *Anabaena* sp. PCC 7120, putative ferric iron transporters *iutA₁*, *iutA₂*, and *hutA₁* were reported to only mildly respond to iron limitation (Rudolf et al. 2015). In the same species, various elements of ferric iron transporters were found to be upregulated in the presence of either high iron at low cell density (*fecD₂*, *fecD₃*) or low iron at mild cell density (*fecD₁*, *fecC₁*, *futB*). This reveals involvement of homologous systems in various cellular responses (Stevanovic et al. 2013).

Finally, ExbB-ExbD pathways are usually associated with TonB-dependent uptake, which was extensively characterized for siderophores. Nevertheless, three ExbB-ExbD systems were identified in the non-siderophore-producing *Synechocystis* sp. PCC 6803, all of which being upregulated under iron limitation and involved in inorganic Fe³⁺ uptake (Jiang et al. 2015). Redundancy and lethality induced by mutation of the three systems suggest that inorganic Fe³⁺ uptake may be the main iron source for this cyanobacterium and this class of phototrophs (Jiang et al. 2015). In *Anabaena* sp. PCC 7120, the various ExbBD systems respond to either high or low iron which indicate specialization (Stevanovic et al. 2013).

Ferrous Iron Uptake

While less is known about ferrous iron transport than its ferric counterpart, some pathways for Fe²⁺ transport have been identified, such as the Feo or EfeUOB systems. The former is widely distributed among bacteria and some archaea. It is encoded most of the time as an *feoAB* operon in which FeoB encodes an Fe²⁺ permease and FeoA, a cytoplasmic partner of FeoB with a function that remains to be elucidated. FeoA seems to be a multifunctional protein that is essential in some species for Fe²⁺ transport, while in others it is only required for full efficient Fe²⁺ transport. An additional FeoA partner can occur, as well as a third element FeoC that has also an elusive role. It is presumed to be a transcription factor that regulates *feoABC* operon expression but also to protect FeoB from proteolysis. FeoA, FeoB, and FeoC were shown to interact together in *Vibrio cholerae*. Multiple Feo systems in the same bacteria have been described, and this situation can lead to specialization of each system such as general cellular needs vs. magnetosome needs and iron import vs. manganese import (hence the appellation Feo vs. Meo) (Hantke 2003; Cartron et al. 2006; Perry et al. 2007; Lau et al. 2013, 2016; Stevenson et al. 2016).

The Efe system has also shown an involvement in ferrous iron transport. First identified in pathogenic bacteria, the Efe system is actually widespread. This system

is expressed as an operon, *efeUOB* or *efeUOBM*, and consists of a permease EfeU that is homologue to the yeast Ftr1p iron permease, a Dyp-type peroxydase EfeB that is presumed to be periplasmic and to bind heme, and a periplasmic cupredoxin-containing EfeO. A cupredoxin-less EfeO homologue can occur and is named EfeM. Mechanism of this pathway is not yet clear as it differs from one organism to another, sometimes enabling the uptake of Fe³⁺ or heme iron in addition to Fe²⁺ (see Zappa and Bauer (2013b) for references) (Turlin et al. 2013; Miethke et al. 2013). In the *Rhodobacter* genus, a FeoA₁A₂BC cassette was identified in the three representatives *R. capsulatus*, *R. sphaeroides*, and *R. ferrooxidans*. A second and simpler FeoAB cassette was also found in the *R. capsulatus* genome. While the FeoA₁A₂BC cassette is likely to come from a common *Rhodobacter* ancestor, the FeoAB one could have been acquired later by gene duplication or horizontal gene transfer. The other Fe²⁺ uptake pathway, EfeUOB, is present in the genome of *R. capsulatus* but absent in the two other *Rhodobacter* species (Zappa and Bauer 2013b). In this cassette, EfeU and EfeO appear encoded as a fusion EfeUO protein according to the genome sequence. But manual sequencing finally established that those two partners as distinct genes (Zappa and Bauer 2013a). The Feo system of *R. sphaeroides* was not transcriptionally induced under iron limitation, while both *R. capsulatus* Feo systems were upregulated in the absence of iron (Peuser et al. 2012; Zappa and Bauer 2013a). In addition, transcription of *R. capsulatus efeU* was shown to be induced under iron scarcity (Zappa and Bauer 2013a).

In marine cyanobacteria, the Feo system seems absent from the genomes of *Prochlorococcus* and open-ocean *Synechococcus* species while present in coastal *Synechococcus* species (Morrissey and Bowler 2012). In the freshwater cyanobacterium *Synechocystis* sp. PCC 6803, a *feoB* gene was reported, and its transcription was showed to be induced by either low iron concentrations or ROS in the growth medium (Kato et al. 2001a; Latifi et al. 2005; Shcolnick et al. 2009). Likewise, a FeoB homologue in *Microcystis aeruginosa* was found to be upregulated under iron limitation (Alexova et al. 2011). In *Anabaena* sp. PCC 7120, *feoB* is only weakly induced by iron limitation, while all *feo* elements were activated under high iron (Stevanovic et al. 2013; Rudolf et al. 2015). The Feo system in this strain was proposed to be part of the immediate response to high iron at low cell density (Stevanovic et al. 2013). Interestingly, the Feo transporter is presumed to be associated downstream of a siderophore-independent Fe³⁺ reduction pathway (Kranzler et al. 2014).

Reductive Ferric Iron Uptake Pathway

Recent observations about the capability of cyanobacteria to directly reduce inorganic Fe³⁺ to Fe²⁺ have questioned the paradigm that siderophores are the main route of iron uptake in oxygenic phototrophs. Indeed, evidences of extracellular ferric iron reduction by cyanobacteria were reported using *Synechocystis* sp. PCC 6803 (Kranzler et al. 2011; Thorne et al. 2015). In *Anabaena* sp. PCC 7120 and (most likely) *Anabaena flos-aquae*, reductive Fe³⁺ uptake was also shown to be uncoupled

from the schizokinen uptake (Sonier et al. 2012; Rudolf et al. 2015). Heavy energetic costs of siderophore synthesis and import are also inversely correlated to the cell density. Rudolf and co-authors proposed that, for filamentous bacteria like *Anabaena* sp. PCC 7120, siderophore-based iron uptake is cost-effective only under low iron and high cell density. On the other hand, Fe^{3+} reduction to Fe^{2+} followed by Fe^{2+} transport is more adapted to a less dense population. While the expensive siderophore system is tightly regulated, the iron reduction pathway seems to be poorly regulated and may thus constitute the “default mode” of iron uptake (Rudolf et al. 2015). Such a reductive pathway was proven to be prevalent in eight cyanobacterial species, where its “default mode” character was confirmed. Whatever species studied, reductive Fe^{3+} uptake is consistently 10,000-fold more efficient than the uptake of the siderophore ferrioxamine B (Lis et al. 2015). In addition, *Anabaena* sp. PCC 7120 imports inorganic Fe^{3+} by reducing it 1000 times more efficiently than its endogenously produced siderophore schizokinen (Lis et al. 2015).

A mechanism of Fe^{3+} reduction has been suggested to involve the aforementioned FutA₁A₂BC system, an alternate respiratory terminal oxidase (ARTO), and the Feo system (Kranzler et al. 2014). According to this model (Fig. 2), Fe^{3+} could enter the periplasm through a porin where it is chelated by FutA₂. This accumulation of Fe^{3+} -FutA₂ complex would enable a gradient pushing Fe^{3+} toward the periplasm where Fe^{3+} would be reduced by ARTO with the resulting Fe^{2+} imported into the cytoplasm via the Feo system (Kranzler et al. 2014). This model suggests regulatory activities for FutA₁ and FutC and matches the previously described property of FutA₂ as a cellular iron partitioning protein (Waldron et al. 2007; Kranzler et al. 2014).

Finally, a few studies suggest the involvement of pili in Fe^{3+} transport in *Synechocystis* sp. PCC 6803. Type IV pili were previously described as “bacterial nanowires” as they can conduct electricity (Lovley and Malvankar 2015). In this cyanobacterium, a $\Delta pilA_1$ mutant showed impaired growth on iron oxides and goethite. It also displays some iron-deficient signatures such as lower phycobilisome contents (Lamb et al. 2014). Moreover, deletion of the transcription factor LexA induces a transcription response that is very similar to the one triggered by iron limitation: upregulation of iron transporters and downregulation of photosynthesis-related genes except *isiAB* (Kizawa et al. 2016). PilA-encoding genes, including *pilA_1*, were strongly affected by *lexA* deletion with some being directly controlled as shown by LexA binding to the promoters of *pilA_7* and *pilA_9* (Kizawa et al. 2016). As Lamb and co-authors reported only about the $\Delta pilA_1$ phenotype, it would seem worth at this point to extend the study to other *pilA* genes.

Heme Uptake

Many cells can also scavenge iron from heme often acquired from the environment. Cellular use of heme iron can occur via two mechanisms: import and cytoplasmic degradation of heme and periplasmic deferrochelation of heme. The first pathway is enabled by TonB-dependent heme uptake systems, similar to the ones involved in

siderophore uptake. Once heme is internalized in the cytoplasm, a heme oxygenase is required in order to open the tetrapyrrole ring and extract Fe^{2+} . This uptake system has been well characterized in pathogenic bacteria, but is not restricted to pathogens as this salvage pathway also benefits symbiotic and free-living marine bacteria (Nienaber et al. 2001; Hopkinson et al. 2008; Runyen-Janecky et al. 2010; Anzaldi and Skaar 2010; Braun and Hantke 2011; Septer et al. 2011; Burgsdorf et al. 2015). In the second pathway, the iron atom is extracted from heme in the periplasm without modifying the tetrapyrrole structure, releasing protoporphyrin IX. It is performed by the aforementioned EfeUOB system (Létoffé et al. 2009; Turlin et al. 2013). Genome analysis of *Rhodobacter* model strains revealed the presence of a complete TonB-dependent heme uptake system in *R. capsulatus*, HmuRSTUV, but not in *R. sphaeroides* or *R. ferrooxidans* (Zappa and Bauer 2013b). The heme uptake receptor was shown to be induced under iron-limiting conditions (Zappa and Bauer 2013a). In *R. sphaeroides*, a protein annotated as being involved in heme uptake was observed to be induced under iron limitation (Peuser et al. 2012). This protein shows relatively poor sequence conservation with HmuP, a regulator of the Hmu system in *Bradyrhizobium japonicum*, also poorly conserved in *R. capsulatus* (Zappa and Bauer 2013b). *Rh. palustris* genome also revealed the presence of a heme uptake system (Larimer et al. 2004). Finally, the other pathway for heme iron usage, EfeUOB, could be identified in *R. capsulatus* where it is upregulated under low concentration of iron (Zappa and Bauer 2013b, a).

In cyanobacteria, studies of heme uptake are even more in their infancy. In an effort to characterize the occurrence and diversity of TonB-dependent transporters, putative heme uptake systems were identified, the cyanobacteria *Acarochloris marina*, *Anabaena* sp. PCC 7120, and three strains of *Synechococcus* (Mirus et al. 2009). These are based on sequence analysis and will require experimental confirmation. Interestingly, a TonB-based heme uptake pathway that was identified to be relatively well distributed in marine bacteria was found totally absent from the marine cyanobacterial genomes (Hopkinson et al. 2008).

Elemental Iron Storage

Storage of iron can be achieved using three types of proteins: ferritins (Ftn), bacterioferritins (Bfr), and DNA-binding proteins from starved cells (DPSs). These are homo-oligomers of 24- or 12-mers that form a protective ball of protein around amorphous iron and inorganic phosphate or ferrihydrite. Di-iron centers enable the oxidation of cytoplasmic Fe^{2+} into insoluble Fe^{3+} for storage when it is translocated inside the complex, while heme groups reduce the stored Fe^{3+} to mobilize it and export it as soluble Fe^{2+} to the cytoplasm (Andrews 2010a, b; Bou-Abdallah 2010).

As heme-containing proteins, bacterioferritins are considered a member of the cytochrome class of proteins. Before genome sequencing and sequence analysis could enable their quick identification, they were often isolated and named as cytochromes (cytochrome b_{558} in *R. sphaeroides*, cytochrome b_{557} in *R. capsulatus*). By keeping the iron away from cellular machinery, bacterioferritins add a detoxification property to their storage function. By accumulating and releasing iron upon cellular needs, Ftn,

Bfr, and DPS are considered as massive cytochrome complexes forming small organelles. While Ftn and Bfr seem to be involved in genuine iron storage, DPSs are usually associated with DNA providing protection from oxidative stress. The Ftn, Bfr, and DPS superfamily of proteins has been well documented (Andrews 2010a, b; Bou-Abdallah 2010).

A Bfr was first observed in 1962 in *R. sphaeroides* and isolated 23 years later as cytochrome b_{558} , a year after the isolation of a Bfr homologue in *Rhodospirillum rubrum* (Meyer and Cusanovich 1985). It contains one heme per two subunits. Genome analysis proved that *R. sphaeroides* has actually two Bfr-encoding genes in addition to a membrane-bound Ftn (Mbfa). *R. capsulatus* has only one Bfr and one Mbfa, while *R. ferrooxidans* has only one Mbfa. In addition, recent studies in *Bradyrhizobium japonicum* and *Agrobacterium tumefaciens* showed that Mbfa functions as an iron efflux pump (Bhubhanil et al. 2014; Sankari and O'Brian 2014). Pumping excess iron out of the cell is definitely a good way to regulate iron equilibrium. All three *Rhodobacter* representatives exhibit an Mbfa sequence, which can be a signature of an ancestral feature from iron-rich environments that was retained for toxicity issue. None of the three *Rhodobacter* species exhibit a DPS-encoding gene (Zappa and Bauer 2013b). As DPSs were characterized as oxidative stress defense instead of iron storage units, it might be interesting to see if the absence of DPS is a trait of anoxygenic photosynthetic bacteria that evolved in more reducing environments. One of the *R. capsulatus* Bfr has been crystallized and extensively studied (Cobessi et al. 2002). This protein consists of a cytoplasmic 24-subunit complex containing 900–1000 Fe atoms and 600 phosphate molecules per Bfr complex. The cellular content of *R. capsulatus* Bfr decreased in the absence of iron and increased when iron was added back to the growth medium (Ringeling et al. 1994). However, the transcription of the Bfr gene did not show much changes depending on iron availability, suggesting posttranscriptional regulation of Bfr in this organism (Zappa and Bauer 2013a). A Bfr homologue from *R. sphaeroides*, Bfr1 (orf1546), is associated with a ferredoxin and is transcriptionally upregulated when iron is scarce. Transcription of an additional Bfr2 (orf3342) gene also was insensitive to iron, while Mbfa appeared only weakly iron regulated (Rodionov et al. 2006; Peuser et al. 2011, 2012).

In oxygenic phototrophs, the Ftn family is well studied. For example, in *Synechocystis* sp. PCC 6803, two Bfr's, BfrA and BfrB, sequester 50% of the total cellular iron content. Both Bfr's are needed for optimal growth as single or double mutants have reduced iron content, impaired growth characteristics, increased amount of IsiA (a hallmark of cyanobacterial response to iron deficiency), and reduced PSI content. Interestingly, BfrA has a di-iron center, while BfrB shows the sequence signature of a heme-binding site. Thus, it is suggested that BfrA and BfrB form an active complex by interacting as a heteroligomer that can take advantage of both a di-iron center and heme (Keren et al. 2004). The transcription of the Bfr-encoding genes does not vary much upon either iron availability or oxidative stress changes (Shcolnick et al. 2009).

In addition to the BfrAB complex, *Synechocystis* sp. PCC 6803 has a DPS representative, MrgA, that appears to provide a link between iron homeostasis and oxidative stress. Unlike BfrAB, MrgA does not seem to exert major iron storage function

(Shcolnick et al. 2007). But it is to provide crucial resistance to H_2O_2 , especially during the reallocation of iron between its storage in Bfr and its target use as a cofactor. Moreover, MgrA was shown to be regulated by the oxidative stress regulator PerR (Shcolnick et al. 2009). With the exception of *Prochlorococcus* species that harbor Ftn, Bfr, and DPS, most cyanobacteria contain one or two Bfr and multiple DPSs (Morrissey and Bowler 2012; Ekman et al. 2014) (Thompson et al. 2011). The multicellular heterocyst *Nostoc punctiforme* harbors four DPSs and one Bfr with one of the DPSs transcriptionally activated under oxidative stress and a mutant in the corresponding gene unable to grow on H_2O_2 . This DPS is therefore thought to be involved in protection from oxidative stress. Still in *Nostoc punctiforme*, the Bfr representative is found primarily in heterocysts where it may help to provide the high levels of iron needed for N_2 fixation (Ekman et al. 2014). A DPS representative, DpsA, was also studied in *Synechococcus* sp. PCC 7942 that was shown to be a DNA-binding hemoprotein localized associated with the thylakoid membrane. The mRNA level of DpsA was relatively high under normal iron levels and increased in iron-limiting conditions, with various degrees depending on studies (Dwivedi et al. 1997; Durham and Bullerjahn 2002; Michel et al. 2003). Deletion of DpsA seemed to affect severely PSII but also increases cellular sensitivity to oxidative stress (high light, paraquat), while PSI remains at normal activity. Overall, DpsA appeared as a cellular protector of oxidative stress induced by oxygenic photosynthesis. Nevertheless, it was also identified as part of the iron homeostasis components as the *dpsA* mutant showed some of the typical marks of iron deficiency such as altered transcription of the *isiAB* operon and amount of PSI-IsiA super complex. Consequently, DpsA in this species is thought to have a dual role of iron storage and oxidative stress (Dwivedi et al. 1997; Durham and Bullerjahn 2002; Michel et al. 2003). A DpsA homologue was also identified in *Anabaena* sp. PCC 7120. However, one cannot conclude yet whether DpsA acts as an iron storage protein or an oxidative stress detoxifier or both in this species (Hernández et al. 2007). Two DPS homologues were also found in *Thermosynechococcus elongatus*, DpsA-Te and Dps-Te with DpsA-Te exhibiting unusual properties such as the presence of two Zn^{2+} at the ferroxidase center and the use of O_2 to oxidize Fe^{2+} with an efficiency that compares to the classically used H_2O_2 (Alaleona et al. 2010). Finally, in *Fremyella diplosiphon*, five out of six ferritins or ferritin-like proteins were observed to be transcriptionally downregulated under iron limitation (Pattanaik et al. 2014).

Transcription Regulation of Iron Homeostasis

The regulation of cellular iron homeostasis involves both the control of activity of iron export and import transporters and the expression of iron importers and exporters encoding genes. An active area of research has established that the regulation of genes involved in iron transport and sequestration is complex and involves network of regulatory proteins. Some of these regulatory proteins are involved in the regulation of a specific iron homeostasis gene cluster and are thus termed “local regulators.” Others control a wide array of iron homeostasis

genes and are thus “global regulators.” Local regulators can be AraC type, two-component systems, extracytoplasmic function (ECF) sigma factors, LysR type, and small RNA (see Zappa and Bauer (2013b) for references). Unlike global iron regulators, local transcription regulator dealing with iron homeostasis has not been studied in phototrophs. Anecdotally, genome analysis of *R. capsulatus* showed four AraC-like transcription factors located next to siderophore uptake gene clusters (Rodionov et al. 2006). In *Rh. palustris*, seven genes encode ECF sigma factors which are located in the vicinity of siderophore uptake system, siderophore synthesis, or putative heme uptake gene clusters (Larimer et al. 2004). Below is a discussion about known iron regulatory factors.

The Ferric Uptake Regulator (FUR)

For several decades Fur has been considered the hallmark of bacterial iron homeostasis regulation with detailed reviews on its activity previously covered (Rudolph et al. 2006; Lee and Helmann 2007; Carpenter et al. 2009; Fillat 2014; Frawley and Fang 2014). Homologues of Fur have been identified in a wide range of bacteria where it acts as a repressor of iron acquisition gene expression under iron-replete conditions. Fur directly binds Fe^{2+} to form an Fe^{2+} -Fur holoprotein that interacts with target DNA promoters. This basic mechanism has been extended since the first Fur studies as it is now known that apo-Fur can also activate gene expression. Holo-Fur can also control the transcription of a small RNA that subsequently regulates expression of iron homeostasis genes which is an additional layer of indirect control.

Bacteria of the *Rhizobiales* and *Rhodobacterales* orders also use an alternative related global regulator of iron homeostasis called Irr that appears to be a functional shift of Fur. In these organisms Fur seems to act as a manganese uptake regulator and is thus renamed Mur (Rudolph et al. 2006; Rodionov et al. 2006; Johnston et al. 2007; O’Brian 2015). As a result, among photosynthetic bacteria, the Fur/Mur regulator is presumed to have different functions whether it is a purple bacteria representative or a cyanobacterial one. In addition, Fur is a member of a larger family of regulators that encompasses more than Fur *sensu stricto*, Mur, and Irr. Other regulators in this family included Zur, Nur, and PerR that sense zinc, nickel, and peroxide, respectively (Fillat 2014). Substrate selectivity of the active site can be rather subtle since a single Glu to Asp substitution was shown to induce a transition of the iron sensing of Fur to the peroxide activity of PerR (Parent et al. 2013).

Fur/Mur in Purple Bacteria

In the *Rhodobacter* genus, a *fur* gene was identified in *R. sphaeroides* and *R. ferrooxidans*, but not in *R. capsulatus* (Zappa and Bauer 2013b). In *R. sphaeroides*, a deletion of *fur* induces stronger growth impairment under manganese than iron

limitation. A putative Mn/Fe uptake system, SitABCD, was shown to be controlled by Fur, so Fur might be involved in manganese homeostasis rather than iron and as such should be renamed Mur (Peuser et al. 2011).

Fur in Cyanobacteria

Many cyanobacterial genomes such as *Synechocystis* sp. PCC 6803, *Synechococcus* sp. PCC 7002, *Nostoc punctiforme*, *Anabaena* sp. PCC 7120, and *Microcystis aeruginosa* typically have three Fur-encoding genes, often named *furA*, *furB*, and *furC* or *fur*, *zur*, and *perR* (Hernández et al. 2004a; Shcolnick et al. 2009; Alexova et al. 2011; Ekman et al. 2014; Yingping et al. 2014). Nevertheless, only two Fur homologues can be found in *Prochlorococcus*, while *Acaryochloris marina* MBIC1107 has 13 (Thompson et al. 2011; Hernández-Prieto et al. 2012; Ludwig et al. 2015). Cyanobacterial *furA* seems to be an essential gene as all attempts to inactivate it have failed in all species studied (*Synechococcus elongatus* PCC 7942, *Synechococcus* sp. PCC 7002, *Synechocystis* sp. PCC 6803, *Anabaena* sp. PCC 7120) (Ghassemian and Straus 1996; Michel et al. 2001; Kunert et al. 2003; Hernández et al. 2006; López-Gomollón et al. 2006; Ludwig et al. 2015). A recent approach in *Anabaena* sp. PCC 7120, consisting in putting *furA* under the control of a $\text{Co}^{2+}/\text{Zn}^{2+}$ -inducible promoter, confirmed that turning off *furA* expression shuts down bacterial growth (González et al. 2016). The FurA homologue of *Anabaena* sp. PCC 7120 is by far the most well-characterized cyanobacterial Fur protein. As such, most of the following information deals with this Fur representative, although elements from other Fur homologues will be discussed. A summary of current knowledge about *Anabaena* sp. PCC 7120 FurA is presented in Fig. 3.

Biochemistry of FurA

The *Anabaena* sp. PCC 7120 FurA was originally identified by the signature sequence HXXHXXCXXC (Bes et al. 2001). Biochemical characterization showed that Mn^{2+} and DTT, while not necessary, strongly enhance the DNA-binding activity of FurA, while H_2O_2 inhibits DNA binding. Inactivation by H_2O_2 can be reversed by the addition of DTT (Hernández et al. 2005). In addition, FurA binds to heme with an affinity in the μM range with the formation of this complex preventing DNA binding. Based on the presence of a Cys-Pro motif, where the Cys is an axial ligand of heme, these data suggest that FurA may be a heme sensor involved in the response to oxidative stress (Hernández et al. 2004b; Pellicer et al. 2012). Interestingly, this Cys-Pro motif is present in all cyanobacterial homologues but absent in non-cyanobacterial ones. Heme could thus be involved in sensing redox variations within a cyanobacterial filament, from the microaerophilic environment of heterocysts to the reduced vegetative cells performing photosynthesis. Unlike classic Fur proteins, no structural Zn^{2+} was found in FurA. Oligomerization was found to increase with the increase of FurA concentration or with ionic strength, but to

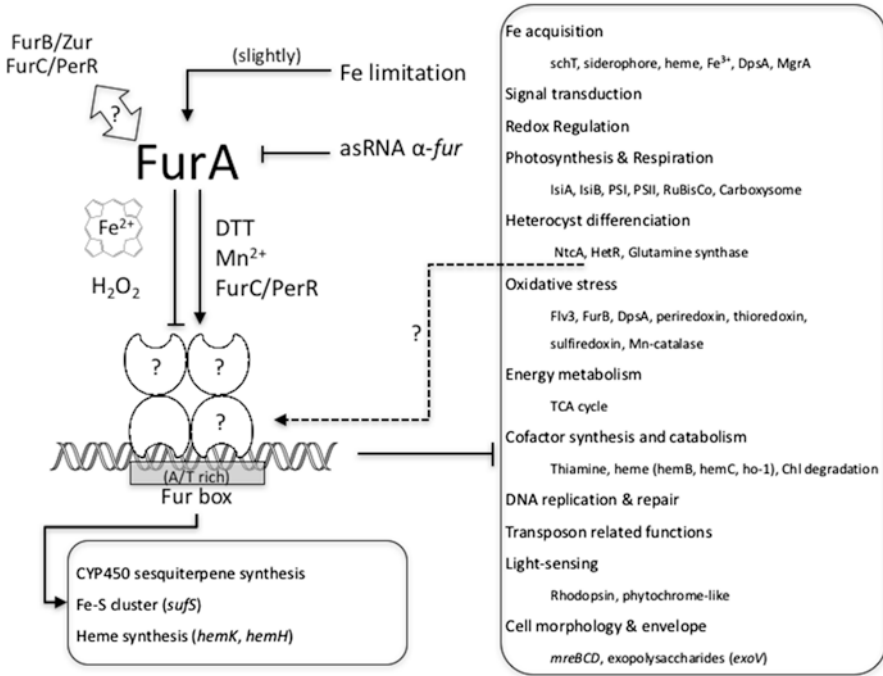


Fig. 3 The ferric uptake regulator FurA, in *Anabaena* sp. PCC 7120, is a global regulator. Represented are functions/genes where direct binding of FurA has been documented. FurA is primarily a repressor although few direct activation candidates were reported. Oligomerization differs between in vitro and in vivo studies

decrease in reducing conditions (Hernández et al. 2002). The FurA monomer has a diameter of $4\text{ nm} \pm 1$ with approximately 40% of α -helices and buried polar/charged residues. Dimerization seems to occur via hydrophobic interactions, which is consistent with the ionic strength effect, but disulfide bonds are observed in the trimer. Oxidizing conditions seem to disrupt the dimer form, which reassembles into trimers/tetramers. The odd number of cysteine residues suggests potential intermolecular bond formation and redox sensing property (Hernández et al. 2002, 2005; Lostao et al. 2010). Nevertheless, in vivo analysis shows that FurA is present mostly as a monomer with usually two but sometimes only one disulfide bond located at its two CXXC motifs and no intermolecular bond. Moreover, these two motifs were found to exert a disulfide reductase activity that has never been described in the Fur family and may extend its involvement in cellular processes such as redox signaling (Botello-Morte et al. 2014). Interaction with DNA occurs sequentially with first the binding by FurA monomer to the site 1 of the FurA-binding sequence, known as the “iron box.” This introduces a 55 ± 14 bend in the DNA, which gives more exposure to the second site of the “iron box.” From there, a second FurA monomer can bind to site 2 and form a dimer that releases the DNA bend. Or, a second FurA subunit can form a dimer with first FurA monomer without binding to site 2, which will

conserve the DNA bend. From either route, tri- or tetra-merization can occur thereafter (Pallarés et al. 2014). Finally, the “iron box” is not well defined, and, for now, it seems only safe to say that FurA binds to particular structures of A/T-rich DNA sequences of 19–23 bp (González et al. 2011, 2014).

FurA Regulation and the FurA Regulon

The *Anabaena* sp. *furA* gene was found to be expressed under iron-deplete or iron-replete conditions with only a slight increase in iron-limiting conditions (Hernández et al. 2002). A *furA* cis antisense RNA was also observed, consisting of the transcript of the nearby ORF alr1690 with the α -*furA* and the intergenic region. Deletion of this alr1690- α -*furA* region increased the level of FurA, highlighting a posttranscriptional regulation of FurA. Interestingly, the gene organization consisting of tail-to-tail *furA* and alr1690 is conserved in other cyanobacterial genomes such as *Nostoc punctiforme* and *Anabaena variabilis* (Hernández et al. 2006). In addition, regulation of *fur* by an antisense RNA has been observed also in *Microcystis aeruginosa* PCC 7806 and *Synechocystis* sp. PCC 6803, in a genomic context that is different from *Anabaena* sp. PCC 7120 (Sevilla et al. 2011). At the protein level, iron starvation was shown to downregulate FurA in *Synechocystis* sp. PCC 6803 (Vuorijoki et al. 2016).

An in silico analysis predicted that 215 proteins could be control by FurA in *Anabaena* sp. PCC 7120, which represent as much as 3.4% of the total ORF. These targets are scattered in different functional groups such as iron acquisition systems, signal transduction, redox regulation, photosynthesis and respiration, heterocyst differentiation, oxidative stress defenses, energy metabolism, fatty acid metabolism, synthesis of amino acids, cofactors and cell envelope, DNA replication, and repair- and transposon-related functions (González et al. 2014). Recent transcriptome analysis showed that 2089 genes display significantly different expressions when *furA* is turned off, consisting in 94 upregulations and 1595 downregulations which is inconsistent with the primary function of Fur as a repressor and reflects pleiotropic changes (González et al. 2016). These genes belong mostly to two functional groups—regulation and transport across membrane—and encompass processes such as iron homeostasis, photosynthesis, detoxification, light sensing, exopolysaccharide synthesis, chlorophyll catabolism, and transposons (González et al. 2016). In addition, a growing amount of target genes have been studied in vivo and/or in vitro. Moreover, as a *furA*-less strain of cannot be obtained, the regulon of FurA was mostly studied by overexpressing it. This was achieved by disrupting the aforementioned alr1690- α -*furA* RNA or by placing an extra-copy of *furA* under an inducible promoter. Finally, it is important to mention that, by disrupting alr1690- α -*furA*, one cannot discriminate the downstream effects of FurA overexpression from the alr1690 deletion. Another and more recent approach was to put *furA* under a Co²⁺/Zn²⁺-inducible promoter (González et al. 2016). But

whatever approach used, some trends could be revealed, sometimes highlighted by *in vitro* DNA-binding assay.

Increase of Fur through disruption of *alr1690- α -furA* revealed a wide array of effects such as a lower growth rate, lower chlorophyll and phycobiliprotein content, and lower cellular iron content but also modified ultrastructures (cell wall, thylakoid number and arrangement, shorter filaments, cell size, carboxysome number) (Hernández et al. 2010). All of this highlights signs of both iron-specific and generalized stress-generating pleiotropic responses when FurA is overexpressed. Such morphological alterations were also observed with the promoter-based FurA-overexpressing approach, as seen by shorter filament thylakoid distribution, although the pigment content did not decrease in this context (González et al. 2010). Among genes that could be involved in these morphological changes, the bacterial actins MreB and MreC were found upregulated in the FurA-overexpressing background. This was confirmed biochemically with FurA binding the upstream region of *mreBCD* *in vitro* (González et al. 2010). In addition, pleiotropic effects appeared to result from FurA binding to the promoters of genes involved in DNA replication, TCA cycle, signal transduction, and thiamine biosynthesis (González et al. 2011). In *Microcystis aeruginosa* PCC 7806, several genes involved in the synthesis of microcystins showed the presence of “iron boxes.” The production of these toxins was found triggered by low iron level, and FurA was found to bind the promoter of these genes (Martin-Luna et al. 2006; Alexova et al. 2011).

FurA and Iron Homeostasis

While complete segregation of *furA*-deleted chromosome could not be achieved, heteroallelic mutants in *Synechococcus* sp. PCC 7942 were shown to exhibit iron deficiency signature symptoms such as the constitutive production of hydroxamate siderophores and flavodoxin (Ghassemian and Straus 1996). Similar approach in *Synechococcus* sp. PCC 7002 also established Fur as a repressor of iron uptake, involved in the iron-sparing response (Ludwig et al. 2015). This highlights the involvement of FurA in iron homeostasis. Moreover, in *Anabaena* sp. PCC 7120 overexpression of FurA triggered by *alr1690- α -furA* deletion was showed to lower the cellular iron content (Hernández et al. 2010). The schizokinen siderophore transporter SchT was found upregulated in the FurA-overexpressing background. Direct control is strongly suggested by FurA binding to the upstream region of *schT* (González et al. 2010). Putative transporters of siderophore, heme or Fe³⁺ ABC type, were observed to be under the direct regulation of FurA. The synthesis of siderophore is also part of the FurA regulon, as seen by a siderophore synthesis gene cluster that fails to be activated under iron limitation in the FurA overexpression strain. Moreover, four “iron boxes” were found in that cluster, and FurA binds to all of them *in vitro* with variable affinity (González et al. 2012). In addition, a gene coding for a ferritin family protein DpsA was identified in *Anabaena* sp. PCC 7120,

and its promoter displays an “iron box.” FurA was shown to bind to that sequence, and the level of DpsA was reduced in the *alr1690- α -furA* mutant at both transcriptional and translational levels (Hernández et al. 2007). Still, regarding iron storage, another DPS, homologous to *Synechocystis* MrgA, was found under the direct control of FurA (González et al. 2014). Finally, FurA involvement in iron homeostasis can be further illustrated by the regulation of iron-containing enzyme and/or iron-containing cofactor synthesis (Fe-S, heme). For example, direct binding of FurA was established with the promoters of genes encoding NADH dehydrogenases (*all1127* and *alr0869-ndhF*), cytochrome *c* oxidase subunit II (*alr0950-coxB*), and flavodiiron protein Flv3 (*all3895-flv3*) (González et al. 2014). In addition, iron-containing enzymes can consist of Fe-S cluster-harboring enzymes. In *Microcystis aeruginosa* PCC 7806, an *α -fur* and a *fur- α -sufE* antisense RNA were identified. As SufE is involved in Fe-S cluster assembly, these data suggest a co-regulation of iron homeostasis and Fe-S cluster synthesis by antisense RNAs (Sevilla et al. 2011). Finally, a direct binding of FurA to the promoter of Alr2679 and Alr2680 was observed. These genes encode polyketide synthases potentially involved in siderophore or cyanotoxin synthesis (González et al. 2016).

FurA and Nitrogen Fixation

One fascinating property of FurA is the connection that it enables between iron homeostasis and nitrogen fixation. Nitrogen fixation is a very iron intensive process and is very sensitive to O₂. *Anabaena* sp. PCC 7120 copes with nitrogenase iron oxidation by spatial separation of oxygenic photosynthesis in vegetative cells from nitrogen fixation in heterocysts. Overexpression of FurA leads to partial arrested morphogenesis with cell differentiation blocked at the rather early stage of proheterocysts with more space between proheterocysts and phycobilisome degradation in proheterocysts. Heterocyst differentiation is also regulated by NtcA and HetR with FurA and NtcA found to regulate each other at the transcription level. These two regulators thus work in concert as a cellular development switch. Nitrogen was found to upregulate *furA* expression, while *furB* and *furC* were stable. In addition, NtcA was shown to activate FurA in proheterocysts and in heterocysts while repressing it in vegetative cells. Biochemically, NtcA was found to bind to the *furA* promoter and vice versa, and FurA showed DNA-binding activity with the *hetR* promoter. Moreover, integration of nitrogen into carbon metabolism is realized by the glutamine synthase gene *glnA* that is downregulated by decreasing either nitrogen or iron availability. NtcA and FurA can also both bind to the *glnA* promoter. Other actors of heterocyst differentiation proved to be controlled by FurA such as the DNA-binding protein Abp1, HetC, PatA, and Alr1728 with expression of Abp1 decreased in a FurA-overexpressing strain (López-Gomollón et al. 2007a, b; González et al. 2011, 2013, 2014). Recently, direct bindings of FurA were observed on the promoters of *ccbP* and *nblA*, encoding a Ca²⁺-binding protein involved in heterocyst development and a phycobilisome degrading protein, respectively (González et al. 2016). The latter is known to be upregulated under nitrogen starvation.

FurA, Photosynthesis, and Respiration

FurA appeared in several studies as a regulator of both photosynthesis and respiration in cyanobacteria. In an *alr1690- α -furA* mutant, respiration and photosynthesis were both altered. On the one hand, respiration was found more efficient under lower than normal iron levels in the *alr1690- α -furA* strain, which is the opposite of WT cells. In that regard, the *alr1690- α -furA* strain copes better with low iron conditions than did WT cells. On the other hand, the *alr1690- α -furA* mutant also exhibited partial inhibition of the photosynthetic electron transport chain on the acceptor side of PSI and a decreased cyclic electron transport. It appeared that adaptation processes to perform photosynthesis under iron-limiting conditions are regulated more efficiently in WT cells than in the *alr1690- α -furA* mutant (Hernández et al. 2010). Influence of iron deficiency on photosynthetic electron chain and respiration was also observed in *Synechococcus* sp. PCC 7942 (Michel et al. 2003). In a FurA overexpression background, major changes in gene expression affected proteins of PSI (PsaA, PsaB) and PSII (PsbA, PsbB, PsbZ) reaction centers. Such changes are likely to impair the equilibrium between the photosystem components that is required for efficient photosynthesis. These consist in the increase of *psaA*, *psaB*, *psbA*, and *psbB* expression, while *psbZ* expression decreased. In addition, FurA was shown to bind the promoters of genes coding for NADH dehydrogenases, NAD(P) transhydrogenase, RuBisCo, IsiA, flavodoxin IsiB, the PSI PsaK subunit, the PSII reaction center protein D1 CP43 protein PsbC homologue, and the β -carboxysome shell protein CccM (López-Gomollón et al. 2007a; González et al. 2010, 2011, 2014).

Interestingly, FurA and NtcA may connect “photosynthesis and respiration” to “iron homeostasis and nitrogen fixation.” Indeed, multiple “iron boxes” were identified upstream NtcA-regulated genes and were confirmed to interact with FurA in vitro. Such genes include PSI subunit XI (*psaL*), PSII 11 kDa protein (*psbZ*), PSII chlorophyll-binding protein (*isiA*), cytochrome oxidase (*coxB₂*, *coxA₂*), and ferredoxin NADP⁺ reductase (*petH*) (López-Gomollón et al. 2007a). In *Microcystis aeruginosa* PCC 7806, the expression of FurA appeared to require an intact photosynthetic electron chain (Martin-Luna et al. 2011). FurA was also identified as a regulator of tetrapyrrole synthesis and degradation. Overall, iron limitation altered the transcription of both heme synthesis and heme degradation genes. While FurA represses heme synthesis genes *hemB* and *hemC* and heme oxygenase gene *ho1*, it activates heme synthesis genes *hemK* and *hemH*. Direct DNA binding was observed with each of these promoters (González et al. 2012).

FurA, Oxidative Stress, and Redox Regulation

Cyanobacterial FurA was also shown to interact directly with the promoters of genes responding to redox stress, such as *dpsA* and *furB* (Hernández et al. 2007; López-Gomollón et al. 2009). Transcription of two peroxiredoxins and a thioredoxin reductase was also modified in FurA-overexpressing background with direct control by FurA interacting with the respective promoter regions (González et al.

2011). Moreover, FurA was showed to be a direct repressor of the flavodiiron Flv3 protein, the sulfiredoxin SrxA, and the Mn catalase, involved in oxidative stress defense (González et al. 2014, 2016). In addition, overexpression of FurA leads to a decrease in catalase and SOD activities, while cellular ROS levels were stable. At the transcription level, mRNA levels of two thiol peroxidases and the Fe-SOD were reduced, while transcripts of glutathione reductase and Mn-SOD increased. None of these genes showed direct control by FurA (González et al. 2010, 2014). In *Microcystis aeruginosa* PCC 7806, the expression of *fur* itself was found to be redox controlled. On the one hand, oxidative stress generated by blocking the photosynthetic electron chain at PSII (Q_B) decreased *fur* mRNA levels, while α -*fur* could not be detected. The same pattern was observed in darkness. On the other hand, photooxidative stress generated by excess of light (with intact electron flow) triggered an increase of *fur* mRNA. Exposure to H₂O₂ induced a decrease of *fur* mRNA along with an increase of α -*fur*. And the presence of superoxides using methyl viologen was found to increase *fur*, α -*fur*, and the Fur protein level (Martin-Luna et al. 2011).

What About FurB and FurC?

In *Anabaena* sp. PCC 7120, FurA, FurB, and FurC show overall poor sequence identity with each other besides exhibiting characteristic Fur signature sequences. Their respective antibodies also do not cross-react (Hernández et al. 2004a). FurB and FurC were subsequently identified as Zur and PerR homologues, respectively (Napolitano et al. 2012; Yingping et al. 2014). The former is zinc uptake regulator while the latter is an oxidative stress regulator. Interestingly, FurC seems to diverge from other phylogenetic Fur clusters in cyanobacteria (Ludwig et al. 2015). Detailed description of these regulators would be out of the scope of this review, but a few properties linking them to FurA activity are worth being mentioned. While FurA and FurB bind each of the three *fur* promoters, FurC does not bind to any. The DNA-binding activity of FurA is enhanced by Mn²⁺ and DTT and impaired by H₂O₂. On the other hand, FurB DNA-binding activity was improved in the absence of metal and the presence of DTT, while H₂O₂ had no influence. Finally, combinatory effects of the three Fur paralogues with each other were observed. For example, although not binding to any *fur* promoter, the presence of FurC seems to reduce DNA-binding activity of FurB while enhancing DNA-binding activity of FurA (Hernández et al. 2004a, 2005). Potential cross talk between Fur representatives within the same organism, by hetero-oligomerization, for example, has not been further studied. In *Anabaena* sp. PCC 7120, FurB and FurC were found downregulated in the FurA overexpression strain (González et al. 2010). In addition, *furA* is upregulated in the absence of FurB/Zur and consistently downregulated in a FurB/Zur-overexpressing environment (Sein-Echaluze et al. 2015). The reciprocal regulation of FurA and FurB/Zur and the occurrence of common target genes involved in the oxidative stress response raise the question of potentially compensatory roles (Sein-Echaluze et al. 2015).

Conclusions About FurA: Always More Complex

While Fur in *Synechococcus* sp. PCC 7002 seems to be confined to the iron homeostasis response, FurA in *Anabaena* sp. PCC 7120 is involved in a broad spectrum of cellular processes that go beyond typical iron homeostasis, encompassing photosynthesis, respiration, and nitrogen fixation (Ludwig et al. 2015; González et al. 2016). Following technological improvements, the characterization of FurA has been continuously expanding, and its regulon has been consequently growing. Lately, it has been showed to control transposon activity, Fe-S cluster (*sufS*), exopolysaccharide (*exoV*), and sesquiterpene (*alr4686*) biosynthesis (González et al. 2016). In addition, it is involved in light sensing process by regulating rhodopsin- and phytochrome-like proteins (Asr, AphC, Alr356) (González et al. 2014, 2016). Also, direct control on a lethal leaf spot-1 homologue questions the involvement of FurA in chlorophyll catabolism and programmed cell death (González et al. 2016). Besides an expanding regulon, the mechanism of action of FurA proved to be more complex. Indeed, recent studies showed that, while being primarily a repressor, it can also act as an activator. Two genes, a cysteine desulfurase-encoding *sufS* and a CYP450 sesquiterpene synthesis-encoding gene, were found to be upregulated in the presence of FurA. The dual role of direct repressor/activator has seldom been observed in Fur proteins (Fillat 2014; González et al. 2016). Indirect activation by Fur can occur through sRNA, while direct activation was shown only in a handful of organisms (Fillat 2014). Lastly, posttranslational regulation of Fur was demonstrated in *Synechocystis* sp. PCC 6803, where a heterocomplex of membrane proteases FtsH1/3 degrades apo-Fur in iron-deplete conditions. Doing so, it prevents apo-Fur to bind DNA with its residual DNA-binding efficiency. But apo-Fur degradation can also prevent it to scavenge traces of iron, reconstituting holo-Fur, and bind to DNA. Either way, it suppresses Fur repression under iron limitation and enables full expression of target genes (Krynická et al. 2014).

The Iron Response Regulator (IRR)

In *Rhizobiales* and *Rhodobacterales*, the function of Fur diverged from an iron to a manganese regulator. The master regulator of iron homeostasis in this group of organisms is iron response regulator (Irr), which senses the iron level as a function of intracellular heme status. Extensively studied in *Bradyrhizobium japonicum*, and to a lesser extent in other *Rhizobiales*, only a few data are available regarding photosynthetic bacteria (Rudolph et al. 2006; Small et al. 2009; Zappa and Bauer 2013b; O'Brian 2015).

The *Rhodobacter* genus shows a conserved Irr-encoding gene in the three model species *R. capsulatus*, *R. sphaeroides*, and *R. ferrooxidans* (Zappa and Bauer 2013b). In *R. sphaeroides*, deletion of *irr* induces a very moderate growth defect under iron-limiting conditions, although it appeared to control iron uptake, utiliza-

tion, and storage at the transcriptional level. In addition, Irr seems to increase the sensitivity to oxidative stress by repressing the catalase KatE. Irr was shown to be involved in the expression of the bacterioferritin Bfr1 (orf1546) and membrane-bound ferritin Mbfa. As mentioned earlier, the latter may actually be an iron efflux pump. Moreover, it was proven to be under the direct control of Irr, confirming *in silico* modeling. Also, a weak downregulation of a cytochrome *c* peroxidase was observed under iron limitation, and Irr does bind the upstream region of the corresponding gene *ccpA*. This direct regulation of a cytochrome is relevant given the heme-binding properties of Irr that were confirmed in this species (Rodionov et al. 2006; Peuser et al. 2012). In *R. capsulatus*, where in the absence of Fur/Mur, Irr could be expected to play a major role, deletion of *irr* did not change the phenotype with regard to iron availability, but no thorough characterization was undertaken (Zappa and Bauer 2013a).

PfsR: Enter a New Player

First discovered in a high light-sensitive mutant of *Synechocystis* sp. PCC 6803, PfsR, is a transcription factor of the TetR family that is involved in the global response to both light and iron stresses, hence its name photosynthesis, Fe homeostasis, and stress response regulator (Jantaro et al. 2006; Cheng and He 2014). The $\Delta pfsR$ mutant is more tolerant to iron limitation than the wild-type strain where it accumulates more photosynthetic pigments (chlorophyll a, carotenoids, phycocyanins) and shows an attenuated decrease of the photosystems (Cheng and He 2014). While accumulating a mere 15% more iron than wild-type cells in iron-replete conditions, $\Delta pfsR$ retains 240% more iron when iron is depleted. Regarding protein content, $\Delta pfsR$ displays more PSI (PsaC, PsaD) and PSII (PsbA, PsbB) components but also more IsiA and cytochrome *c*₅₅₀ than wild-type cells under iron-limiting conditions. Overall, this mutant has a higher photosynthetic rate and efficiency. Interestingly, under iron depletion, the transcription of *pfrR* increases but in a transient manner (Cheng and He 2014). Differential transcription patterns were observed between WT and $\Delta pfsR$, especially concerning ferric (*futA*₁, *futB*, *futC*) and ferrous (*feoB*) iron transport, iron storage (*bfrA*, *bfrB*), heme oxygenase (*ho-1*, *ho-2*), iron regulation (*furA*), and iron stress response (*isiA*). Overall, PfsR acts as a repressor of these genes, but no direct binding on the promoters of these target genes was reported. However, PfsR does bind to its own promoter, so one might expect direct self-regulation and indirect regulation of the iron homeostasis genes (Cheng and He 2014). Interestingly, the high derepression of *isiA* (approximately 30-fold) in $\Delta pfsR$ is counterintuitive as high level of IsiA is a hallmark of iron starvation, but $\Delta pfsR$ seems to both ramp up *isiA* expression and thrive in iron-limiting conditions. In fact, the derepression of *isiA* may actually explain the better tolerance for iron scarcity (Cheng and He 2014). In summary, with PfsR controlling the expression of *furA*, the recent discovery of this new iron homeostasis regulator may put the FurA master regulation into new perspectives.

Copper and Iron Homeostasis

Excess copper can be toxic by displacing native metal ions from active sites, such as Fe-S clusters. Moreover, like iron, copper can generate dangerous reactive oxygen species in oxic conditions through Fenton chemistry (Osman and Cavet 2008; Macomber and Imlay 2009). Copper was also shown to inhibit heme synthesis at the Fe-S-containing coproporphyrin oxidase step resulting in decreased defense against oxidative stress (Djoko and McEwan 2013). In addition, copper is toxic to the photosynthetic machinery by inhibiting PSII, altering the thylakoid membrane, and substituting Mg in Chl (Bhargava et al. 2008). In this section, highlights will be given on how excess copper can interfere with key components of photosynthesis: iron homeostasis, tetrapyrrole, and cytochrome synthesis.

Copper and the Repression of Siderophore Uptake

Most of the experimental characterization of cross talk between iron and copper homeostasis has been studied in *Anabaena* sp. PCC 7120. The siderophore schizokinen is produced when iron is limiting but it was shown to also bind copper. While Fe³⁺-schizokinen is imported to the cytoplasm, Cu²⁺-schizokinen is maintained in the growth medium, thereby alleviating potential copper toxicity if imported in the cell (Clarke et al. 1987; Ferreira and Straus 1994). The production of siderophores usually massively exceeds the amount of bondable extracellular iron, which may reflect a distress strategy to maximize iron mobilization and avoid the deleterious effect of copper (Clarke et al. 1987). Indeed, it seems that copper homeostasis can be easily disturbed, as *Anabaena* sp. PCC 7120 cells grown under iron-deficient copper-sufficient conditions were showed to have reduced cellular iron content, while the copper content was almost fourfold higher (Nicolaisen et al. 2008). Also, hydroxamate siderophore synthesis was found triggered by either low iron or high copper levels. The transport of iron-schizokinen and the overall iron demand were found to be reduced in iron-deplete/copper-replete conditions compared to both metal deplete conditions (Nicolaisen et al. 2008, 2010). In addition, deletion of the schizokinen exporter SchE increases copper toxicity (Nicolaisen et al. 2010). While SchT was proven to be dedicated to schizokinen uptake, a second TonB-dependent transporter IacT appeared to be involved in citrate-based iron and copper transport with a less obvious mechanism. It is hypothesized that under iron-deplete/copper-deplete conditions, Fe³⁺-schizokinen is imported by the SchT-Fhu system, while under iron-deplete/copper-replete conditions, then schizokinen binds to copper. This “neutralizes” copper from potential harmful effect, and, in order to fulfill the cellular requirements, the iron and copper transporter IacT takes over the SchT-Fhu system (Nicolaisen et al. 2010; Stevanovic et al. 2012). In addition, *Anabaena* sp. PCC 7120 has two copper transport systems of the CusBA type, one being induced at high copper levels and the other one repressed at high iron

levels. Interestingly, both are repressed when *iacT* is overexpressed (Nicolaisen et al. 2010). Overall, this model elegantly describes the dialogue between SchT and IatC, involved in Fe³⁺-schizokinen and Fe³⁺-citrate/Cu²⁺ import, respectively, as a function of extracellular Fe³⁺/Cu²⁺ concentrations and equilibrium in *Anabaena* sp. PCC 7120. Although the switch is known to be iron/copper dependent, regulatory mechanisms have not been investigated.

But the iron/copper homeostasis interdependence is likely to involve more actors, even in the same organism. Indeed, other putative siderophore and heme uptake systems in the same organism were found expressed only under copper limitation, not iron limitation, in *Anabaena* sp. PCC 7120 (Mirus et al. 2009). Likewise, in the same organism a large gene cluster involved in siderophore synthesis was found to be responsive to copper (Jeanjean et al. 2008). Finally, in the process of identifying the Fe³⁺-schizokinen import system (aforementioned SchT-Fhu-TonB₃-ExbB₃D₃), TonB-ExbBD-encoding genes were experimentally found to respond to copper levels (*exbB₁D₁*, *tonB₄*, *tonB₁*), as were ferric iron transporters (*futB*, *fecD₁*, *fecC₁*, *fecD₂*) (Stevanovic et al. 2012). A set of TBDT was found responsive to high iron/high copper levels with a high basal expression under iron limitation. These transporters may be essential for the copper detoxification response (*viuA*, *iutA*, *btuB₂*, *alr2185*, *all2148*, *schE*) (Stevanovic et al. 2013).

Copper Toxicity Issues

A recent example of copper toxicity was shown in anoxic conditions. While iron and copper are well known to be toxic in oxic conditions, where they can produce Fenton chemistry-induced reactive oxygen species, these two metals have been shown to exert synergic bacteriostatic effect in anaerobic condition, as shown on the purple bacteria *Rh. palustris* and *R. capsulatus*. While the mechanism is not clear, it seems that the presence of iron impairs some copper detoxification components (Bird et al. 2013). Moreover, copper has been shown to impair the synthesis of heme in *Neisseria gonorrhoeae* (Djoko and McEwan 2013). The same mechanism is likely to occur in phototrophic organisms in tetrapyrrole synthesis at steps performed by Fe-S-containing enzymes such as HemN and BchE (Bhargava et al. 2008; Hassani et al. 2010; Azzouzi et al. 2013). This highlights the importance of copper detoxification mechanisms to protect iron-based reactions.

Copper-Dependent Iron Transport

The aforementioned iron transporter EfeUOB system involves a cupredoxin-containing protein, EfeO. As such, with this transport system, fully functional import of iron actually relies on the presence of copper. Interestingly, EfeO shares similarities with the FET3/FTR1 transporter in yeast which is homologous to the

copper-dependent iron transporters in the eukaryotic phototroph *Chlamydomonas reinhardtii* (La Fontaine et al. 2002; Herbig et al. 2002; Terzulli and Kosman 2010). Being out of the scope of this review, no further details will be given, but it is worth mentioning that EfeUOB system was also identified in the purple non-sulfur bacterium *R. capsulatus* (Zappa and Bauer 2013b).

Copper and the Iron-Sparing Response

In cyanobacteria, two well-studied key copper-containing enzymes are plastocyanin and the *caa*₃-type cytochrome *c* oxidase. During photosynthesis, plastocyanin transfers electrons from the cytochrome *b₆f* complex to the PSI and copper limitation induces the use of cytochrome *c*₆ instead of plastocyanin. Iron limitation can lead to an unintuitive phenomenon from the release of siderophores that bind both iron and copper (Zhang et al. 1992; Ferreira and Straus 1994). Indeed, as copper-siderophores are not imported into the cell, copper availability is severely reduced. This generates copper limitation that represses plastocyanin in favor of cytochrome *c*₆. In summary, iron depletion induces the use of an iron-containing cytochrome instead of the iron-sparing plastocyanin. Despite looking inconsistent, this mechanism seems to perform well due to the fact that the cytochrome *c*₆ pool is restricted. Actually, some cyanobacterial species exhibit the cytochrome *c*₆ alone, having lost the plastocyanin gene. The cost of this imperfection does not outbalance the benefits of siderophores (Ferreira and Straus 1994). Moreover, deletion of cytochrome *c*₆ in *Synechocystis* sp. PCC 6803 does not result in much phenotypic change, even in copper-deficient conditions where cytochrome *c*₆ is supposedly required for effective photosynthesis. But interestingly, this mutant exhibited an elevated expression of *isiAB*, which is a hallmark of iron stress in cyanobacteria (Ardelean et al. 2002).

The cytochrome *c*₆-plastocyanin switch involves two copper transporters, a copper chaperone and also the periplasmic Fe³⁺-binding protein FutA₂ (Tottey et al. 2001, 2002; Waldron et al. 2007). The Δ *futA*₂ mutant is impaired in cytochrome *c*₆. As FutA₂ binds Fe³⁺ preferentially to Cu²⁺ and the Δ *futA*₂ mutant shows abnormal distribution of metals in the cell, it was suggested that FutA₂ is involved in metal partitioning in the cell and failure to achieve the right cellular distribution of metals impairs biochemical switches (Waldron et al. 2007). Also illustrating this copper-iron dialogue is the sensitivity to iron starvation of the copper chaperone deleted strain (Tottey et al. 2002). In *Anabaena* sp. PCC 7120, *isiA* transcription was showed to be activated under copper limitation (Jeanjean et al. 2008).

Conclusion: Intertwined Metal Homeostasis

The occurrence of multiple iron transporters with overlapping functions exemplifies the competition for iron in the environment between bacterial populations. While siderophore-based iron uptake has been a long-lasting paradigm,

recent research established that the reduction of inorganic Fe^{3+} is likely to be the main route of iron intake in cyanobacteria. This feature is consistent with the occurrence of numerous cyanobacteria that have no identified siderophore synthesis systems, such as *Synechocystis*, *Prochlorococcus*, and *Synechococcus*, even though they require a lot of iron. Prevalence of this pathway tends to indicate a common origin, and its stable and high efficiency between species suggests that this pathway may have reached its maximum potential (Lis et al. 2015). Thus, competition between cell populations is dependent on other iron homeostasis features such as assuming the energetic costs of synthesizing and importing siderophores. Another strategy for dealing with iron competition is to reduce iron needs which has been achieved in eukaryotic phototrophs (Sunda and Huntsman 2015).

The mechanism of siderophore-based uptake is well detailed at least for schizokinen. A mechanism with regard to the reductive pathway has also emerged involving both $\text{FutA}_1\text{A}_2\text{BC}$ and Feo system, along with ARTO. Nevertheless, the ExbB-ExbD systems seem to be as important and spread across species as the reductive pathway. However, it is not known yet if these systems that are described as Fe^{3+} importers are actually importing Fe^{3+} or if the latter is reduced beforehand (Jiang et al. 2015).

The relatively restricted Fur regulon in *Synechococcus* sp. PCC 7002 as compared to the large and still expanding FurA regulon in *Anabaena* sp. PCC 7120 illustrates the diversity of cyanobacterial strategy to regulate fluctuation of environmental iron availability.

Iron is a source of oxidative stress, but its limitation also results in an unbalanced oxygenic photosystem that cannot deal with variation of light intensity. Moreover, due to heavy use of iron in photosystems, light-induced damages could trigger the release of iron in the cell, increasing oxidative stress. The recently characterized regulator PfsR seems to act at the crossroad of iron and light availability (Jantaro et al. 2006; Cheng and He 2014).

We also discussed the interconnection between the Fe and Cu networks in phototrophs. Strong evidences link Fe and Mn homeostasis in non-phototrophic bacteria (O'Brian 2015; Guan et al. 2015). A similar Fe/Mn dialogue seems to occur in photosynthetic bacteria, especially since Mn was reported to be involved in oxidative stress response under iron limitation (Kaushik et al. 2015). Both PSI and Mn_4CaO_5 cluster containing PSII are impaired under Mn limitation in *Synechocystis* sp. PCC 6803 (Salomon and Keren 2011). Importantly, *Synechocystis* sp. PCC 6803 cells acclimated to low Mn do not display the typical iron stress response (Salomon and Keren 2015). Since the used low Mn concentration is actually environmentally relevant, it put the several decade-old research on iron response into new perspectives. Likewise, the occurrence of three Fur representatives in cyanobacteria highlights the cross talk between iron and zinc homeostasis along with the oxidative stress response. The recent discovery of posttranslational regulation of Fur in *Synechocystis* sp. PCC 6803 by Zn^{2+} -containing protease (FtsH1/3) underlines the iron and zinc homeostasis interdependency (Krynická et al. 2014).

References

- Alaleona F, Franceschini S, Ceci P et al (2010) Thermosynechococcus elongatus DpsA binds Zn(II) at a unique three histidine-containing ferroxidase center and utilizes O₂ as iron oxidant with very high efficiency, unlike the typical Dps proteins. *FEBS J* 277:903–917. doi:[10.1111/j.1742-4658.2009.07532.x](https://doi.org/10.1111/j.1742-4658.2009.07532.x)
- Alexova R, Fujii M, Birch D et al (2011) Iron uptake and toxin synthesis in the bloom-forming *Microcystis aeruginosa* under iron limitation. *Environ Microbiol* 13:1064–1077. doi:[10.1111/j.1462-2920.2010.02412.x](https://doi.org/10.1111/j.1462-2920.2010.02412.x)
- Andrews NC (2010a) Ferritin(in)ing out new mechanisms in iron homeostasis. *Cell Metab* 12:203–204. doi:[10.1016/j.cmet.2010.08.011](https://doi.org/10.1016/j.cmet.2010.08.011)
- Andrews SC (2010b) The Ferritin-like superfamily: evolution of the biological iron storeman from a rubrerythrin-like ancestor. *Biochim Biophys Acta* 1800:691–705. doi:[10.1016/j.bbagen.2010.05.010](https://doi.org/10.1016/j.bbagen.2010.05.010)
- Andrews SC, Robinson AK, Rodríguez-Quñones F (2003) Bacterial iron homeostasis. *FEMS Microbiol Rev* 27:215–237
- Anzaldi LL, Skaar EP (2010) Overcoming the heme paradox: heme toxicity and tolerance in bacterial pathogens. *Infect Immun* 78:4977–4989. doi:[10.1128/IAI.00613-10](https://doi.org/10.1128/IAI.00613-10)
- Ardelean I, Matthijs HCP, Havaux M et al (2002) Unexpected changes in photosystem I function in a cytochrome c6-deficient mutant of the cyanobacterium *Synechocystis* PCC 6803. *FEMS Microbiol Lett* 213:113–119. doi:[10.1111/j.1574-6968.2002.tb11294.x](https://doi.org/10.1111/j.1574-6968.2002.tb11294.x)
- Azzouzi A, Steunou A-S, Durand A et al (2013) Coproporphyrin III excretion identifies the anaerobic coproporphyrinogen III oxidase HemN as a copper target in the Cu⁺-ATPase mutant copA- of *Rubrivivax gelatinosus*. *Mol Microbiol* 88:339–351. doi:[10.1111/mmi.12188](https://doi.org/10.1111/mmi.12188)
- Badarau A, Firbank SJ, Waldron KJ et al (2008) FutA2 is a ferric binding protein from *Synechocystis* PCC 6803. *J Biol Chem* 283:12520–12527. doi:[10.1074/jbc.M709907200](https://doi.org/10.1074/jbc.M709907200)
- Beale SI, Cornejo J (1983) Biosynthesis of phycocyanobilin from exogenous labeled biliverdin in *Cyanidium caldarium*. *Arch Biochem Biophys* 227:279–286
- Bes MT, Peleato ML, Fillat MF (2001) Cloning, overexpression and interaction of recombinant Fur from the cyanobacterium *Anabaena* PCC 7119 with isiB and its own promoter. *FEMS Microbiol Lett* 194:187–192
- Bhargava P, Mishra Y, Srivastava AK et al (2008) Excess copper induces anoxygenic photosynthesis in *Anabaena doliolum*: a homology based proteomic assessment of its survival strategy. *Photosynth Res* 96:61–74. doi:[10.1007/s11120-007-9285-7](https://doi.org/10.1007/s11120-007-9285-7)
- Bhubhanil S, Chamsing J, Sittipo P et al (2014) Roles of *Agrobacterium tumefaciens* membrane-bound ferritin (MbfA) in iron transport and resistance to iron under acidic conditions. *Microbiology* 160:863–871. doi:[10.1099/mic.0.076802-0](https://doi.org/10.1099/mic.0.076802-0)
- Bird LJ, Coleman ML, Newman DK (2013) Iron and copper act synergistically to delay anaerobic growth of bacteria. *Appl Environ Microbiol* 79:3619–3627. doi:[10.1128/AEM.03944-12](https://doi.org/10.1128/AEM.03944-12)
- Botello-Morte L, Bes MT, Heras B et al (2014) Unraveling the redox properties of the global regulator FurA from *Anabaena* sp. PCC 7120: disulfide reductase activity based on its CXXC motifs. *Antioxid Redox Signal* 20:1396–1406. doi:[10.1089/ars.2013.5376](https://doi.org/10.1089/ars.2013.5376)
- Bou-Abdallah F (2010) The iron redox and hydrolysis chemistry of the ferritins. *Biochim Biophys Acta* 1800:719–731. doi:[10.1016/j.bbagen.2010.03.021](https://doi.org/10.1016/j.bbagen.2010.03.021)
- Braun V, Hantke K (2011) Recent insights into iron import by bacteria. *Curr Opin Chem Biol* 15:328–334. doi:[10.1016/j.cbpa.2011.01.005](https://doi.org/10.1016/j.cbpa.2011.01.005)
- Burgsdorf I, Slaby BM, Handley KM et al (2015) Lifestyle evolution in cyanobacterial symbionts of sponges. *MBio* 6:e00391–e00315. doi:[10.1128/mBio.00391-15](https://doi.org/10.1128/mBio.00391-15)
- Carpenter BM, Whitmire JM, Merrell DS (2009) This is not your mother's repressor: the complex role of fur in pathogenesis. *Infect Immun* 77:2590–2601. doi:[10.1128/IAI.00116-09](https://doi.org/10.1128/IAI.00116-09)
- Cartron ML, Maddocks SE, Gillingham P et al (2006) Feo—transport of ferrous iron into bacteria. *Biometals* 19:143–157. doi:[10.1007/s10534-006-0003-2](https://doi.org/10.1007/s10534-006-0003-2)

- Cassier-Chauvat C, Chauvat F (2014) Function and regulation of ferredoxins in the Cyanobacterium, *Synechocystis* PCC6803: recent advances. *Life* 4:666–680. doi:[10.3390/life4040666](https://doi.org/10.3390/life4040666)
- Chauhan D, Folea IM, Jolley CC et al (2011) A novel photosynthetic strategy for adaptation to low-iron aquatic environments. *Biochemistry* 50:686–692. doi:[10.1021/bi1009425](https://doi.org/10.1021/bi1009425)
- Cheng D, He Q (2014) PfsR is a key regulator of Iron homeostasis in *Synechocystis* PCC 6803. *PLoS ONE* 9:e101743. doi:[10.1371/journal.pone.0101743](https://doi.org/10.1371/journal.pone.0101743)
- Chiancone E, Ceci P, Ilari A et al (2004) Iron and proteins for iron storage and detoxification. *Biometals* 17:197–202. doi:[10.1023/b:biom.0000027692.24395.76](https://doi.org/10.1023/b:biom.0000027692.24395.76)
- Chu BC, Garcia-Herrero A, Johanson TH et al (2010) Siderophore uptake in bacteria and the battle for iron with the host; a bird's eye view. *Biometals* 23:601–611. doi:[10.1007/s10534-010-9361-x](https://doi.org/10.1007/s10534-010-9361-x)
- Clarke SE, Stuart J, Sanders-Loehr J (1987) Induction of siderophore activity in *Anabaena* spp. and its moderation of copper toxicity. *Appl Environ Microbiol* 53:917–922
- Cobessi D, Huang LS, Ban M et al (2002) The 2.6 Å resolution structure of *Rhodobacter capsulatus* bacterioferritin with metal-free dinuclear site and heme iron in a crystallographic 'special position'. *Acta Crystallogr Sect D Biol Crystallogr* 58:29–38
- Cornelis P, Andrews SC (2012) Regulation of iron homeostasis in bacteria. In: Filloux A, (ed) *Bacterial Regulatory Networks*. Caister Academic Press; Norfolk, UK. pp 261–272
- Djoko KY, McEwan AG (2013) Antimicrobial action of copper is amplified via inhibition of heme biosynthesis. *ACS Chem Biol* 8:2217–2223. doi:[10.1021/cb4002443](https://doi.org/10.1021/cb4002443)
- Durham KA, Bullerjahn GS (2002) Immunocytochemical localization of the stress-induced DpsA protein in the cyanobacterium *Synechococcus* sp. strain PCC 7942. *J. Basic Microbiol* 42:367–372. doi:[10.1002/1521-4028\(200212\)42:6<367::AID-JOBM367>3.0.CO;2-T](https://doi.org/10.1002/1521-4028(200212)42:6<367::AID-JOBM367>3.0.CO;2-T)
- Dwivedi K, Sen A, Bullerjahn GS (1997) Expression and mutagenesis of the *dpsA* gene of *Synechococcus* sp. PCC7942, encoding a DNA-binding protein involved in oxidative stress protection. *FEMS Microbiol Lett* 155:85–91. doi:[10.1111/j.1574-6968.1997.tb12690.x](https://doi.org/10.1111/j.1574-6968.1997.tb12690.x)
- Ekman M, Sandh G, Nennering A et al (2014) Cellular and functional specificity among ferritin-like proteins in the multicellular cyanobacterium *Nostoc punctiforme*. *Environ Microbiol* 16:829–844. doi:[10.1111/1462-2920.12233](https://doi.org/10.1111/1462-2920.12233)
- Ferreira F, Straus NA (1994) Iron deprivation in cyanobacteria. *J Appl Phycol* 6:199–210. doi:[10.1007/BF02186073](https://doi.org/10.1007/BF02186073)
- Fillat MF (2014) The FUR (ferric uptake regulator) superfamily: diversity and versatility of key transcriptional regulators. *Arch Biochem Biophys* 546:41–52. doi:[10.1016/j.abb.2014.01.029](https://doi.org/10.1016/j.abb.2014.01.029)
- Frankenberg N, Lagarias JC (2003) Phycocyanobilin:ferredoxin oxidoreductase of *Anabaena* sp. PCC 7120. *Biochemical and spectroscopic. J Biol Chem* 278:9219–9226. doi:[10.1074/jbc.M211643200](https://doi.org/10.1074/jbc.M211643200)
- Fraser JM, Tulk SE, Jeans JA et al (2013) Photophysiological and photosynthetic complex changes during iron starvation in *Synechocystis* sp. PCC 6803 and *Synechococcus elongatus* PCC 7942. *PLoS ONE* 8:e59861. doi:[10.1371/journal.pone.0059861](https://doi.org/10.1371/journal.pone.0059861)
- Frawley ER, Fang FC (2014) The ins and outs of bacterial iron metabolism. *Mol Microbiol* 93:609–616. doi:[10.1111/mmi.12709](https://doi.org/10.1111/mmi.12709)
- Ghassemian M, Straus NA (1996) Fur regulates the expression of iron-stress genes in the cyanobacterium *Synechococcus* sp. strain PCC 7942. *Microbiology* 142:1469–1476. doi:[10.1099/13500872-142-6-1469](https://doi.org/10.1099/13500872-142-6-1469)
- González A, Bes MT, Barja F et al (2010) Overexpression of FurA in *Anabaena* sp. PCC 7120 reveals new targets for this regulator involved in photosynthesis, iron uptake and cellular morphology. *Plant Cell Physiol* 51:1900–1914. doi:[10.1093/pcp/pcq148](https://doi.org/10.1093/pcp/pcq148)
- González A, González A, Bes MT et al (2011) Unravelling the regulatory function of FurA in *Anabaena* sp. PCC 7120 through 2-D DIGE proteomic analysis. *J Proteome* 74:660–671. doi:[10.1016/j.jprot.2011.02.001](https://doi.org/10.1016/j.jprot.2011.02.001)
- González A, Bes MT, Valladares A et al (2012) FurA is the master regulator of iron homeostasis and modulates the expression of tetrapyrrole biosynthesis genes in *Anabaena* sp. PCC 7120. *Environ Microbiol* 14:3175–3187. doi:[10.1111/j.1462-2920.2012.02897.x](https://doi.org/10.1111/j.1462-2920.2012.02897.x)

- González A, Valladares A, Peleato ML, Fillat MF (2013) FurA influences heterocyst differentiation in *Anabaena* sp. PCC 7120. FEBS Lett 587:2682–2690. doi:[10.1016/j.febslet.2013.07.007](https://doi.org/10.1016/j.febslet.2013.07.007)
- González A, Angarica VE, Sancho J, Fillat MF (2014) The FurA regulon in *Anabaena* sp. PCC 7120: in silico prediction and experimental validation of novel target genes. Nucleic Acids Res 42:4833–4846. doi:[10.1093/nar/gku123](https://doi.org/10.1093/nar/gku123)
- González A, Bes MT, Peleato ML, Fillat MF (2016) Expanding the role of FurA as essential global regulator in cyanobacteria. PLoS ONE 11:e0151384. doi:[10.1371/journal.pone.0151384](https://doi.org/10.1371/journal.pone.0151384)
- Guan G, Pinochet Barros A, Gaballa A et al (2015) PfeT, a P1B4-type ATPase, effluxes ferrous iron and protects *Bacillus subtilis* against iron intoxication. Mol Microbiol 98:787–803. doi:[10.1111/ mmi.13158](https://doi.org/10.1111/mmi.13158)
- Guikema JA, Sherman LA (1983) Organization and function of chlorophyll in membranes of cyanobacteria during Iron starvation. Plant Physiol 73:250–256. doi:[10.1104/pp.73.2.250](https://doi.org/10.1104/pp.73.2.250)
- Hantke K (2003) Is the bacterial ferrous iron transporter FeoB a living fossil? Trends Microbiol 11:192–195
- Hassani BK, Astier C, Nitschke W, Ouchane S (2010) CtpA, a copper-translocating P-type ATPase involved in the biogenesis of multiple copper-requiring enzymes. J Biol Chem 285:19330–19337. doi:[10.1074/jbc.M110.116020](https://doi.org/10.1074/jbc.M110.116020)
- Herbik A, Bölling C, Buckhout TJ (2002) The involvement of a multicopper oxidase in iron uptake by the green algae *Chlamydomonas reinhardtii*. Plant Physiol 130:2039–2048. doi:[10.1104/ pp.013060](https://doi.org/10.1104/pp.013060)
- Hernández JA, Bes MT, Fillat MF et al (2002) Biochemical analysis of the recombinant Fur (ferric uptake regulator) protein from *Anabaena* PCC 7119: factors affecting its oligomerization state. Biochem J 366:315–322. doi:[10.1042/BJ20020135](https://doi.org/10.1042/BJ20020135)
- Hernández JA, López-Gomollón S, Bes MT et al (2004a) Three fur homologues from *Anabaena* sp. PCC7120: exploring reciprocal protein-promoter recognition. FEMS Microbiol Lett 236:275–282. doi:[10.1016/j.femsle.2004.05.050](https://doi.org/10.1016/j.femsle.2004.05.050)
- Hernández JA, Peleato ML, Fillat MF, Bes MT (2004b) Heme binds to and inhibits the DNA-binding activity of the global regulator FurA from *Anabaena* sp. PCC 7120. FEBS Lett 577:35–41. doi:[10.1016/j.febslet.2004.09.060](https://doi.org/10.1016/j.febslet.2004.09.060)
- Hernández JA, Meier J, Barrera FN et al (2005) The conformational stability and thermodynamics of Fur A (ferric uptake regulator) from *Anabaena* sp. PCC 7119. Biophys J 89:4188–4200. doi:[10.1529/biophysj.105.065805](https://doi.org/10.1529/biophysj.105.065805)
- Hernández JA, Muro-Pastor AM, Flores E et al (2006) Identification of a furA cis antisense RNA in the cyanobacterium *Anabaena* sp. PCC 7120. J Mol Biol 355:325–334. doi:[10.1016/j. jmb.2005.10.079](https://doi.org/10.1016/j.jmb.2005.10.079)
- Hernández JA, Pellicer S, Huang L et al (2007) FurA modulates gene expression of alr3808, a DpsA homologue in *Nostoc (Anabaena)* sp. PCC7120. FEBS Lett 581:1351–1356. doi:[10.1016/j.febslet.2007.02.053](https://doi.org/10.1016/j.febslet.2007.02.053)
- Hernández JA, Alonso I, Pellicer S et al (2010) Mutants of *Anabaena* sp. PCC 7120 lacking alr1690 and alpha-furA antisense RNA show a pleiotropic phenotype and altered photosynthetic machinery. J Plant Physiol 167:430–437. doi:[10.1016/j.jplph.2009.10.009](https://doi.org/10.1016/j.jplph.2009.10.009)
- Hernández-Prieto MA, Schön V, Georg J et al (2012) Iron deprivation in *Synechocystis*: inference of pathways, non-coding RNAs, and regulatory elements from comprehensive expression profiling. G3 Genes Genomes Genetics 2:1475–1495. doi:[10.1534/g3.112.003863](https://doi.org/10.1534/g3.112.003863)
- Hider RC, Kong X (2010) Chemistry and biology of siderophores. Nat Prod Rep 27:637–657. doi:[10.1039/b906679a](https://doi.org/10.1039/b906679a)
- Hopkinson BM, Morel FMM (2009) The role of siderophores in iron acquisition by photosynthetic marine microorganisms. Biometals 22:659–669. doi:[10.1007/s10534-009-9235-2](https://doi.org/10.1007/s10534-009-9235-2)
- Hopkinson BM, Roe KL, Barbeau KA (2008) Heme uptake by *Microscilla marina* and evidence for heme uptake systems in the genomes of diverse marine bacteria. Appl Environ Microbiol 74:6263–6270. doi:[10.1128/AEM.00964-08](https://doi.org/10.1128/AEM.00964-08)
- Jantaro S, Ali Q, Lone S, He Q (2006) Suppression of the lethality of high light to a quadruple HLI mutant by the inactivation of the regulatory protein PfsR in *Synechocystis* PCC 6803. J Biol Chem 281:30865–30874. doi:[10.1074/jbc.M606252200](https://doi.org/10.1074/jbc.M606252200)

- Jeanjean R, Talla E, Latifi A et al (2008) A large gene cluster encoding peptide synthetases and polyketide synthases is involved in production of siderophores and oxidative stress response in the cyanobacterium *Anabaena* sp. strain PCC 7120. *Environ Microbiol* 10:2574–2585. doi:[10.1111/j.1462-2920.2008.01680.x](https://doi.org/10.1111/j.1462-2920.2008.01680.x)
- Jiang H-B, Lou W-J, Ke W-T et al (2015) New insights into iron acquisition by cyanobacteria: an essential role for ExbB-ExbD complex in inorganic iron uptake. *ISME J* 9:297–309. doi:[10.1038/ismej.2014.123](https://doi.org/10.1038/ismej.2014.123)
- Johnston AWB, Todd JD, Curson AR et al (2007) Living without Fur: the subtlety and complexity of iron-responsive gene regulation in the symbiotic bacterium *Rhizobium* and other alpha-proteobacteria. *Biomaterials* 20:501–511. doi:[10.1007/s10534-007-9085-8](https://doi.org/10.1007/s10534-007-9085-8)
- Katoh H, Grossman AR, Hagino N, Ogawa T (2000) A gene of *Synechocystis* sp. Strain PCC 6803 encoding a novel iron transporter. *J Bacteriol* 182:6523–6524
- Katoh H, Hagino N, Grossman AR, Ogawa T (2001a) Genes essential to iron transport in the cyanobacterium *Synechocystis* sp. strain PCC 6803. *J Bacteriol* 183:2779–2784. doi:[10.1128/JB.183.9.2779-2784.2001](https://doi.org/10.1128/JB.183.9.2779-2784.2001)
- Katoh H, Hagino N, Ogawa T (2001b) Iron-binding activity of FutA1 subunit of an ABC-type iron transporter in the cyanobacterium *Synechocystis* sp. Strain PCC 6803. *Plant Cell Physiol* 42:823–827
- Kaushik MS, Srivastava M, Verma E, Mishra AK (2015) Role of manganese in protection against oxidative stress under iron starvation in cyanobacterium *Anabaena* 7120. *J Basic Microbiol* 55:729–740. doi:[10.1002/jobm.201400742](https://doi.org/10.1002/jobm.201400742)
- Kehres DG, Janakiraman A, Slauch JM, Maguire ME (2002) SitABCD is the alkaline Mn(2+) transporter of *Salmonella enterica* serovar Typhimurium. *J Bacteriol* 184:3159–3166
- Keren N, Aurora R, Pakrasi HB (2004) Critical roles of bacterioferritins in iron storage and proliferation of cyanobacteria. *Plant Physiol* 135:1666–1673. doi:[10.1104/pp.104.042770](https://doi.org/10.1104/pp.104.042770)
- Kizawa A, Kawahara A, Takimura Y et al (2016) RNA-seq profiling reveals novel target genes of LexA in the cyanobacterium *Synechocystis* sp. PCC 6803. *Front Microbiol* 7:193. doi:[10.3389/fmicb.2016.00193](https://doi.org/10.3389/fmicb.2016.00193)
- Köster W (2001) ABC transporter-mediated uptake of iron, siderophores, heme and vitamin B12. *Res Microbiol* 152:291–301
- Kranzler C, Lis H, Shaked Y, Keren N (2011) The role of reduction in iron uptake processes in a unicellular, planktonic cyanobacterium. *Environ Microbiol* 13:2990–2999. doi:[10.1111/j.1462-2920.2011.02572.x](https://doi.org/10.1111/j.1462-2920.2011.02572.x)
- Kranzler C, Lis H, Finkel OM et al (2014) Coordinated transporter activity shapes high-affinity iron acquisition in cyanobacteria. *ISME J* 8:409–417. doi:[10.1038/ismej.2013.161](https://doi.org/10.1038/ismej.2013.161)
- Krewulak KD, Vogel HJ (2008) Structural biology of bacterial iron uptake. *Biochim Biophys Acta* 1778:1781–1804. doi:[10.1016/j.bbamem.2007.07.026](https://doi.org/10.1016/j.bbamem.2007.07.026)
- Krewulak KD, Vogel HJ (2011) TonB or not TonB: is that the question? *Biochem Cell Biol* 89:87–97. doi:[10.1139/o10-141](https://doi.org/10.1139/o10-141)
- Krynická V, Tichý M, Krafl J et al (2014) Two essential FtsH proteases control the level of the Fur repressor during iron deficiency in the cyanobacterium *Synechocystis* sp. PCC 6803. *Mol Microbiol* 94:609–624. doi:[10.1111/mmi.12782](https://doi.org/10.1111/mmi.12782)
- Kunert A, Vinnemeier J, Erdmann N, Hagemann M (2003) Repression by Fur is not the main mechanism controlling the iron-inducible isiAB operon in the cyanobacterium *Synechocystis* sp. PCC 6803. *FEMS Microbiol Lett* 227:255–262
- La Fontaine S, Quinn JM, Nakamoto SS et al (2002) Copper-dependent iron assimilation pathway in the model photosynthetic eukaryote *Chlamydomonas reinhardtii*. *Eukaryot Cell* 1:736–757
- Lamb JJ, Hill RE, Eaton-Rye JJ, Hohmann-Marriott MF (2014) Functional role of PilA in iron acquisition in the cyanobacterium *Synechocystis* sp. PCC 6803. *PLoS ONE* 9:e105761. doi:[10.1371/journal.pone.0105761](https://doi.org/10.1371/journal.pone.0105761)
- Lammers PJ, Sanders-Loehr J (1982) Active transport of ferric schizokinen in *Anabaena* sp. *J Bacteriol* 151:288–294

- Larimer FW, Chain P, Hauser L et al (2004) Complete genome sequence of the metabolically versatile photosynthetic bacterium *Rhodospseudomonas palustris*. *Nat Biotechnol* 22:55–61. doi:[10.1038/nbt923](https://doi.org/10.1038/nbt923)
- Lascalles J (1956) The synthesis of porphyrins and bacteriochlorophyll in cell suspensions of *Rhodospseudomonas spheroides*. *Biochem J* 62:78–93
- Latifi A, Jeanjean R, Lemeille S et al (2005) Iron starvation leads to oxidative stress in *Anabaena* sp. strain PCC 7120. *J Bacteriol* 187:6596–6598. doi:[10.1128/JB.187.18.6596-6598.2005](https://doi.org/10.1128/JB.187.18.6596-6598.2005)
- Lau CKY, Ishida H, Liu Z, Vogel HJ (2013) Solution structure of *Escherichia coli* FeoA and its potential role in bacterial ferrous iron transport. *J Bacteriol* 195:46–55. doi:[10.1128/JB.01121-12](https://doi.org/10.1128/JB.01121-12)
- Lau CKY, Krewulak KD, Vogel HJ (2016) Bacterial ferrous iron transport: the Feo system. *FEMS Microbiol Rev* 40:273–298. doi:[10.1093/femsre/fuv049](https://doi.org/10.1093/femsre/fuv049)
- Lee J-W, Helmann JD (2007) Functional specialization within the Fur family of metalloregulators. *Biomaterials* 20:485–499. doi:[10.1007/s10534-006-9070-7](https://doi.org/10.1007/s10534-006-9070-7)
- Létoffé S, Heuck G, Delepelaire P et al (2009) Bacteria capture iron from heme by keeping tetrapyrrole skeleton intact. *Proc Natl Acad Sci U S A* 106:11719–11724. doi:[10.1073/pnas.0903842106](https://doi.org/10.1073/pnas.0903842106)
- Lis H, Kranzler C, Keren N, Shaked Y (2015) A Comparative study of iron uptake rates and mechanisms amongst marine and fresh water cyanobacteria: prevalence of reductive iron uptake. *Life* 5:841–860. doi:[10.3390/life5010841](https://doi.org/10.3390/life5010841)
- López-Gomollón S, Muro-Pastor A, Valladares A et al (2006) Interaction of FurA from *Anabaena* sp. PCC 7120 with DNA: a reducing environment and the presence of Mn(2+) are positive effectors in the binding to isiB and furA promoters. *Biomaterials* 19:259–268. doi:[10.1007/s10534-005-7750-3](https://doi.org/10.1007/s10534-005-7750-3)
- López-Gomollón S, Hernández JA, Pellicer S et al (2007a) Cross-talk between iron and nitrogen regulatory networks in *Anabaena* (Nostoc) sp. PCC 7120: identification of overlapping genes in FurA and NtcA regulons. *J Mol Biol* 374:267–281. doi:[10.1016/j.jmb.2007.09.010](https://doi.org/10.1016/j.jmb.2007.09.010)
- López-Gomollón S, Wolk CP, Peleato ML, Fillat MF (2007b) Expression of furA is modulated by NtcA and strongly enhanced in heterocysts of *Anabaena* sp. PCC 7120. *Microbiology* 153:42–50. doi:[10.1099/mic.0.2006/000091-0](https://doi.org/10.1099/mic.0.2006/000091-0)
- López-Gomollón S, Sevilla E, Bes MT et al (2009) New insights into the role of Fur proteins: FurB (All2473) from *Anabaena* protects DNA and increases cell survival under oxidative stress. *Biochem J* 418:201–207. doi:[10.1042/BJ20081066](https://doi.org/10.1042/BJ20081066)
- Lostao A, Peleato ML, Gómez-Moreno C, Fillat MF (2010) Oligomerization properties of FurA from the cyanobacterium *Anabaena* sp. PCC 7120: direct visualization by in situ atomic force microscopy under different redox conditions. *Biochim Biophys Acta* 1804:1723–1729. doi:[10.1016/j.bbapap.2010.04.002](https://doi.org/10.1016/j.bbapap.2010.04.002)
- Lovley DR, Malvankar NS (2015) Seeing is believing: novel imaging techniques help clarify microbial nanowire structure and function. *Environ Microbiol* 17:2209–2215. doi:[10.1111/1462-2920.12708](https://doi.org/10.1111/1462-2920.12708)
- Ludwig M, Chua TT, Chew CY, Bryant DA (2015) Fur-type transcriptional repressors and metal homeostasis in the cyanobacterium *Synechococcus* sp. PCC 7002. *Front Microbiol* 6:1217. doi:[10.3389/fmicb.2015.01217](https://doi.org/10.3389/fmicb.2015.01217)
- Macomber L, Imlay JA (2009) The iron-sulfur clusters of dehydratases are primary intracellular targets of copper toxicity. *Proc Natl Acad Sci U S A* 106:8344–8349. doi:[10.1073/pnas.0812808106](https://doi.org/10.1073/pnas.0812808106)
- Martin-Luna B, Sevilla E, Hernández JA et al (2006) Fur from *Microcystis aeruginosa* binds in vitro promoter regions of the microcystin biosynthesis gene cluster. *Phytochemistry* 67:876–881. doi:[10.1016/j.phytochem.2006.02.005](https://doi.org/10.1016/j.phytochem.2006.02.005)
- Martin-Luna B, Sevilla E, González A et al (2011) Expression of fur and its antisense α -fur from *Microcystis aeruginosa* PCC7806 as response to light and oxidative stress. *J Plant Physiol* 168:2244–2250. doi:[10.1016/j.jplph.2011.08.006](https://doi.org/10.1016/j.jplph.2011.08.006)
- Meyer TE, Cusanovich MA (1985) Soluble cytochrome composition of the purple phototrophic bacterium, *Rhodospseudomonas sphaeroides* ATCC 17023. *Biochim Biophys Acta* 807:308–319

- Michel KP, Pistorius EK (2004) Adaptation of the photosynthetic electron transport chain in cyanobacteria to iron deficiency: the function of IdiA and IsiA. *Physiol Plant* 120:36–50. doi:[10.1111/j.0031-9317.2004.0229.x](https://doi.org/10.1111/j.0031-9317.2004.0229.x)
- Michel KP, Pistorius EK, Golden SS (2001) Unusual regulatory elements for iron deficiency induction of the *idiA* gene of *Synechococcus elongatus* PCC 7942. *J Bacteriol* 183:5015–5024. doi:[10.1128/JB.183.17.5015-5024.2001](https://doi.org/10.1128/JB.183.17.5015-5024.2001)
- Michel KP, Berry S, Hifney A et al (2003) Adaptation to iron deficiency: a comparison between the cyanobacterium *Synechococcus elongatus* PCC 7942 wild-type and a DpsA-free mutant. *Photosynth Res* 75:71–84. doi:[10.1023/A:1022459919040](https://doi.org/10.1023/A:1022459919040)
- Miethke M, Monteferrante CG, Marahiel MA, van Dijl JM (2013) The *Bacillus subtilis* EfeUOB transporter is essential for high-affinity acquisition of ferrous and ferric iron. *Biochim Biophys Acta* 1833:2267–2278. doi:[10.1016/j.bbamcr.2013.05.027](https://doi.org/10.1016/j.bbamcr.2013.05.027)
- Mirus O, Strauss S, Nicolaisen K et al (2009) TonB-dependent transporters and their occurrence in cyanobacteria. *BMC Biol* 7:68. doi:[10.1186/1741-7007-7-68](https://doi.org/10.1186/1741-7007-7-68)
- Moody MD, Dailey HA (1984) Siderophore utilization and iron uptake by *Rhodopseudomonas sphaeroides*. *Arch Biochem Biophys* 234:178–186
- Moody MD, Dailey HA (1985) Ferric iron reductase of *Rhodopseudomonas sphaeroides*. *J Bacteriol* 163:1120–1125
- Morrissey J, Bowler C (2012) Iron utilization in marine cyanobacteria and eukaryotic algae. *Front Microbiol* 3:43. doi:[10.3389/fmicb.2012.00043](https://doi.org/10.3389/fmicb.2012.00043)
- Murphy TP, Lean DR, Nalewajko C (1976) Blue-green algae: their excretion of iron-selective chelators enables them to dominate other algae. *Science* 192:900–902
- Napolitano M, Rubio MÁ, Santamaría-Gómez J et al (2012) Characterization of the response to zinc deficiency in the cyanobacterium *Anabaena* sp. strain PCC 7120. *J Bacteriol* 194:2426–2436. doi:[10.1128/JB.00090-12](https://doi.org/10.1128/JB.00090-12)
- Nicolaisen K, Moslavac S, Samborski A et al (2008) Alr0397 is an outer membrane transporter for the siderophore schizokinen in *Anabaena* sp. strain PCC 7120. *J Bacteriol* 190:7500–7507. doi:[10.1128/JB.01062-08](https://doi.org/10.1128/JB.01062-08)
- Nicolaisen K, Hahn A, Valdebenito M et al (2010) The interplay between siderophore secretion and coupled iron and copper transport in the heterocyst-forming cyanobacterium *Anabaena* sp. PCC 7120. *Biochim Biophys Acta* 1798:2131–2140. doi:[10.1016/j.bbamem.2010.07.008](https://doi.org/10.1016/j.bbamem.2010.07.008)
- Nienaber A, Hennecke H, Fischer H-MM (2001) Discovery of a haem uptake system in the soil bacterium *Bradyrhizobium japonicum*. *Mol Microbiol* 41:787–800
- O'Brian MR (2015) Perception and homeostatic control of iron in the rhizobia and related bacteria. *Annu Rev Microbiol* 69:229–245. doi:[10.1146/annurev-micro-091014-104432](https://doi.org/10.1146/annurev-micro-091014-104432)
- Öquist G (1974) Iron Deficiency in the Blue-Green Alga *Anacystis nidulans*: Changes in Pigmentation and Photosynthesis. *Physiol Plant* 30:30–37. doi:[10.1111/j.1399-3054.1974.tb04987.x](https://doi.org/10.1111/j.1399-3054.1974.tb04987.x)
- Osman D, Cavet JS (2008) Copper homeostasis in bacteria. *Adv Appl Microbiol* 65:217–247. doi:[10.1016/S0065-2164\(08\)00608-4](https://doi.org/10.1016/S0065-2164(08)00608-4)
- Pallarés MC, Marcuello C, Botello-Morte L et al (2014) Sequential binding of FurA from *Anabaena* sp. PCC 7120 to iron boxes: exploring regulation at the nanoscale. *Biochim Biophys Acta* 1844:623–631. doi:[10.1016/j.bbapap.2014.01.005](https://doi.org/10.1016/j.bbapap.2014.01.005)
- Parent A, Caux-Thang C, Signor L et al (2013) Single glutamate to aspartate mutation makes ferric uptake regulator (Fur) as sensitive to H₂O₂ as peroxide resistance regulator (PerR). *Angew Chem Int Ed Engl* 52:10339–10343. doi:[10.1002/anie.201304021](https://doi.org/10.1002/anie.201304021)
- Pattanaik B, Busch AWU, Hu P et al (2014) Responses to iron limitation are impacted by light quality and regulated by RcaE in the chromatically acclimating cyanobacterium *Fremyella diplosiphon*. *Microbiology* 160:992–1005. doi:[10.1099/mic.0.075192-0](https://doi.org/10.1099/mic.0.075192-0)
- Pellicer S, González A, Peleato ML et al (2012) Site-directed mutagenesis and spectral studies suggest a putative role of FurA from *Anabaena* sp. PCC 7120 as a heme sensor protein. *FEBS J* 279:2231–2246. doi:[10.1111/j.1742-4658.2012.08606.x](https://doi.org/10.1111/j.1742-4658.2012.08606.x)
- Perry RD, Mier I, Fetherston JD (2007) Roles of the Yfe and Feo transporters of *Yersinia pestis* in iron uptake and intracellular growth. *Biometals* 20:699–703. doi:[10.1007/s10534-006-9051-x](https://doi.org/10.1007/s10534-006-9051-x)

- Peuser V, Metz S, Klug G (2011) Response of the photosynthetic bacterium *Rhodobacter sphaeroides* to iron limitation and the role of a Fur orthologue in this response. *Environ Microbiol Rep* 3:397–404. doi:[10.1111/j.1758-2229.2011.00245.x](https://doi.org/10.1111/j.1758-2229.2011.00245.x)
- Peuser V, Remes B, Klug G (2012) Role of the Irr protein in the regulation of iron metabolism in *Rhodobacter sphaeroides*. *PLoS ONE* 7:e42231. doi:[10.1371/journal.pone.0042231](https://doi.org/10.1371/journal.pone.0042231)
- Ringeling PL, Davy SL, Monkara FA et al (1994) Iron metabolism in *Rhodobacter capsulatus*. characterisation of bacterioferritin and formation of non-haem iron particles in intact cells. *Eur J Biochem* 223:847–855
- Rodionov DA, Gelfand MS, Todd JD et al (2006) Computational reconstruction of iron- and manganese-responsive transcriptional networks in alpha-proteobacteria. *PLoS Comput Biol* 2:e163. doi:[10.1371/journal.pcbi.0020163](https://doi.org/10.1371/journal.pcbi.0020163)
- Rudolf M, Kranzler C, Lis H et al (2015) Multiple modes of iron uptake by the filamentous, siderophore-producing cyanobacterium, *Anabaena* sp. PCC 7120. *Mol Microbiol* 97:577–588. doi:[10.1111/mmi.13049](https://doi.org/10.1111/mmi.13049)
- Rudolph G, Hennecke H, Fischer H-MM (2006) Beyond the Fur paradigm: iron-controlled gene expression in *Rhizobium*. *FEMS Microbiol Rev* 30:631–648. doi:[10.1111/j.1574-6976.2006.00030.x](https://doi.org/10.1111/j.1574-6976.2006.00030.x)
- Runyen-Janecky LJ, Brown AN, Ott B et al (2010) Regulation of high-affinity iron acquisition homologues in the tsetse fly symbiont *Sodalis glossinidius*. *J Bacteriol* 192:3780–3787. doi:[10.1128/JB.00161-10](https://doi.org/10.1128/JB.00161-10)
- Ryan Keogh TJ, Macey AI, Cockshutt AM et al (2012) The cyanobacterial chlorophyll-binding-protein *psaA* acts to increase the *in vivo* effective absorption cross-section of *psa* under iron limitation I. *J Phycol* 48:145–154. doi:[10.1111/j.1529-8817.2011.01092.x](https://doi.org/10.1111/j.1529-8817.2011.01092.x)
- Salomon E, Keren N (2011) Manganese limitation induces changes in the activity and in the organization of photosynthetic complexes in the cyanobacterium *Synechocystis* sp. strain PCC 6803. *Plant Physiol* 155:571–579. doi:[10.1104/pp.110.164269](https://doi.org/10.1104/pp.110.164269)
- Salomon E, Keren N (2015) Acclimation to environmentally relevant Mn concentrations rescues a cyanobacterium from the detrimental effects of iron limitation. *Environ Microbiol* 17:2090–2098. doi:[10.1111/1462-2920.12826](https://doi.org/10.1111/1462-2920.12826)
- Sandmann G (1985) Consequences of iron deficiency on photosynthetic and respiratory electron transport in blue-green algae. *Photosynth Res* 6:261–271. doi:[10.1007/BF00049282](https://doi.org/10.1007/BF00049282)
- Sandström S, Ivanov AG, Park YI et al (2002) Iron stress responses in the cyanobacterium *Synechococcus* sp. PCC 7942. *Physiol Plant* 116:255–263. doi:[10.1034/j.1399-3054.2002.1160216.x](https://doi.org/10.1034/j.1399-3054.2002.1160216.x)
- Sandy M, Butler A (2009) Microbial iron acquisition: marine and terrestrial siderophores. *Chem Rev* 109:4580–4595. doi:[10.1021/cr9002787](https://doi.org/10.1021/cr9002787)
- Sankari S, O'Brian MR (2014) A bacterial iron exporter for maintenance of iron homeostasis. *J Biol Chem* 289:16498–16507. doi:[10.1074/jbc.M114.571562](https://doi.org/10.1074/jbc.M114.571562)
- Sarma R, Barney BM, Hamilton TL et al (2008) Crystal structure of the L protein of *Rhodobacter sphaeroides* light-independent protochlorophyllide reductase with MgADP bound: a homologue of the nitrogenase Fe protein. *Biochemistry* 47:13004–13015. doi:[10.1021/bi801058r](https://doi.org/10.1021/bi801058r)
- Sein-Echaluze VC, González A, Napolitano M et al (2015) Zur (FurB) is a key factor in the control of the oxidative stress response in *Anabaena* sp. PCC 7120. *Environ Microbiol* 17:2006–2017. doi:[10.1111/1462-2920.12628](https://doi.org/10.1111/1462-2920.12628)
- Septer AN, Wang Y, Ruby EG et al (2011) The haem-uptake gene cluster in *Vibrio fischeri* is regulated by Fur and contributes to symbiotic colonization. *Environ Microbiol* 13:2855–2864. doi:[10.1111/j.1462-2920.2011.02558.x](https://doi.org/10.1111/j.1462-2920.2011.02558.x)
- Sevilla E, Martin-Luna B, González A et al (2011) Identification of three novel antisense RNAs in the fur locus from unicellular cyanobacteria. *Microbiology* 157:3398–3404. doi:[10.1099/mic.0.048231-0](https://doi.org/10.1099/mic.0.048231-0)
- Scholnick S, Shaked Y, Keren N (2007) A role for mrgA, a DPS family protein, in the internal transport of Fe in the cyanobacterium *Synechocystis* sp. PCC 6803. *Biochim Biophys Acta* 1767:814–819. doi:[10.1016/j.bbabi.2006.11.015](https://doi.org/10.1016/j.bbabi.2006.11.015)
- Scholnick S, Summerfield TC, Reytman L et al (2009) The mechanism of iron homeostasis in the unicellular cyanobacterium *Synechocystis* sp. PCC 6803 and its relationship to oxidative stress. *Plant Physiol* 150:2045–2056. doi:[10.1104/pp.109.141853](https://doi.org/10.1104/pp.109.141853)

- Shi T, Sun Y, Falkowski PG (2007) Effects of iron limitation on the expression of metabolic genes in the marine cyanobacterium *Trichodesmium erythraeum* IMS101. *Environ Microbiol* 9:2945–2956. doi:[10.1111/j.1462-2920.2007.01406.x](https://doi.org/10.1111/j.1462-2920.2007.01406.x)
- Simpson FB, Neilands JB (1976) Siderochromes in cyanophyceae: isolation and characterization of schizokinen from *Anabaena* sp. *J Phycol* 12:44–48. doi:[10.1111/j.1529-8817.1976.tb02824.x](https://doi.org/10.1111/j.1529-8817.1976.tb02824.x)
- Singh A, Mishra AK (2015) Influence of various levels of iron and other abiotic factors on siderophoregenesis in paddy field cyanobacterium *Anabaena oryzae*. *Appl Biochem Biotechnol* 176:372–386. doi:[10.1007/s12010-015-1581-7](https://doi.org/10.1007/s12010-015-1581-7)
- Sirijovski N, Mamedov F, Olsson U et al (2007) Rhodobacter capsulatus magnesium chelatase subunit BchH contains an oxygen sensitive iron-sulfur cluster. *Arch Microbiol* 188:599–608. doi:[10.1007/s00203-007-0282-1](https://doi.org/10.1007/s00203-007-0282-1)
- Small SK, Puri S, O'Brian MR (2009) Heme-dependent metalloregulation by the iron response regulator (Irr) protein in Rhizobium and other Alpha-proteobacteria. *Biometals* 22:89–97. doi:[10.1007/s10534-008-9192-1](https://doi.org/10.1007/s10534-008-9192-1)
- Snow JT, Polyviou D, Skipp P et al (2015) Quantifying integrated proteomic responses to iron stress in the globally important marine diazotroph trichodesmium. *PLoS ONE* 10:e0142626. doi:[10.1371/journal.pone.0142626](https://doi.org/10.1371/journal.pone.0142626)
- Sonier MB, Contreras DA, Treble RG, Weger HG (2012) Two distinct pathways for iron acquisition by iron-limited cyanobacterial cells: evidence from experiments using siderophores and synthetic chelators. *Botany* 90:181–190. doi:[10.1139/b11-099](https://doi.org/10.1139/b11-099)
- Stevanovic M, Hahn A, Nicolaisen K et al (2012) The components of the putative iron transport system in the cyanobacterium *Anabaena* sp. PCC 7120. *Environ Microbiol* 14:1655–1670. doi:[10.1111/j.1462-2920.2011.02619.x](https://doi.org/10.1111/j.1462-2920.2011.02619.x)
- Stevanovic M, Lehmann C, Schleiff E (2013) The response of the TonB-dependent transport network in *Anabaena* sp. PCC 7120 to cell density and metal availability. *Biometals* 26:549–560. doi:[10.1007/s10534-013-9644-0](https://doi.org/10.1007/s10534-013-9644-0)
- Stevenson B, Wyckoff EE, Payne SM (2016) *Vibrio cholerae* FeoA, FeoB, and FeoC interact to form a complex. *J Bacteriol* 198:1160–1170. doi:[10.1128/JB.00930-15](https://doi.org/10.1128/JB.00930-15)
- Stowe-Evans EL, Ford J, Kehoe DM (2004) Genomic DNA microarray analysis: identification of new genes regulated by light color in the cyanobacterium *Fremyella diplosiphon*. *J Bacteriol* 186:4338–4349. doi:[10.1128/JB.186.13.4338-4349.2004](https://doi.org/10.1128/JB.186.13.4338-4349.2004)
- Sunda WG, Huntsman SA (2015) High iron requirement for growth, photosynthesis, and low-light acclimation in the coastal cyanobacterium *Synechococcus bacillaris*. *Front Microbiol* 6:561. doi:[10.3389/fmicb.2015.00561](https://doi.org/10.3389/fmicb.2015.00561)
- Terzulli A, Kosman DJ (2010) Analysis of the high-affinity iron uptake system at the *Chlamydomonas reinhardtii* plasma membrane. *Eukaryot Cell* 9:815–826. doi:[10.1128/EC.00310-09](https://doi.org/10.1128/EC.00310-09)
- Thompson AW, Huang K, Saito MA, Chisholm SW (2011) Transcriptome response of high- and low-light-adapted *Prochlorococcus* strains to changing iron availability. *ISME J* 5:1580–1594. doi:[10.1038/ismej.2011.49](https://doi.org/10.1038/ismej.2011.49)
- Thorne RJ, Schneider K, Hu H, Cameron PJ (2015) Iron reduction by the cyanobacterium *Synechocystis* sp. PCC 6803. *Bioelectrochemistry* 105:103–109. doi:[10.1016/j.bioelechem.2015.05.015](https://doi.org/10.1016/j.bioelechem.2015.05.015)
- Ting CS, Rocap G, King J, Chisholm SW (2002) Cyanobacterial photosynthesis in the oceans: the origins and significance of divergent light-harvesting strategies. *Trends Microbiol* 10:134–142
- Tom-Yew SAL, Cui DT, Bekker EG, Murphy MEP (2005) Anion-independent iron coordination by the *Campylobacter jejuni* ferric binding protein. *J Biol Chem* 280:9283–9290. doi:[10.1074/jbc.M412479200](https://doi.org/10.1074/jbc.M412479200)
- Totley S, Rich PR, Rondet SA, Robinson NJ (2001) Two Menkes-type atpases supply copper for photosynthesis in *Synechocystis* PCC 6803. *J Biol Chem* 276:19999–20004. doi:[10.1074/jbc.M011243200](https://doi.org/10.1074/jbc.M011243200)
- Totley S, Rondet SAM, Borrelly GPM et al (2002) A copper metallochaperone for photosynthesis and respiration reveals metal-specific targets, interaction with an importer, and alternative sites for copper acquisition. *J Biol Chem* 277:5490–5497. doi:[10.1074/jbc.M105857200](https://doi.org/10.1074/jbc.M105857200)
- Touati D (2000) Iron and oxidative stress in bacteria. *Arch Biochem Biophys* 373:1–6. doi:[10.1006/abbi.1999.1518](https://doi.org/10.1006/abbi.1999.1518)

- Trick CG, Kerry A (1992) Isolation and purification of siderophores produced by cyanobacteria, *Synechococcus* sp. PCC 7942 and *Anabaena variabilis* ATCC 29413. *Curr Microbiol* 24:241–245. doi:[10.1007/BF01577326](https://doi.org/10.1007/BF01577326)
- Turlin E, Débarbouillé M, Augustyniak K et al (2013) *Staphylococcus aureus* FepA and FepB proteins drive heme iron utilization in *Escherichia coli*. *PLoS ONE* 8:e56529. doi:[10.1371/journal.pone.0056529](https://doi.org/10.1371/journal.pone.0056529)
- Vuorijoki L, Isojärvi J, Kallio P et al (2016) Development of a quantitative SRM-based proteomics method to study iron metabolism of *Synechocystis* sp. PCC 6803. *J Proteome Res* 15:266–279. doi:[10.1021/acs.jproteome.5b00800](https://doi.org/10.1021/acs.jproteome.5b00800)
- Wahadoszamen M, D'Haene S, Ara AM et al (2015) Identification of common motifs in the regulation of light harvesting: the case of cyanobacteria IsiA. *Biochim Biophys Acta* 1847:486–492. doi:[10.1016/j.bbabi.2015.01.003](https://doi.org/10.1016/j.bbabi.2015.01.003)
- Waldron KJ, Tottey S, Yanagisawa S et al (2007) A periplasmic iron-binding protein contributes toward inward copper supply. *J Biol Chem* 282:3837–3846. doi:[10.1074/jbc.M609916200](https://doi.org/10.1074/jbc.M609916200)
- Wang Y, Wu M, Yu J et al (2014) Differences in growth, pigment composition and photosynthetic rates of two phenotypes *Microcystis aeruginosa* strains under high and low iron conditions. *Biochem Syst Ecol* 55:112–117. doi:[10.1016/j.bse.2014.02.019](https://doi.org/10.1016/j.bse.2014.02.019)
- Xing W, Huang W-M, Li D-H, Liu Y-D (2007) Effects of iron on growth, pigment content, photosystem II efficiency, and siderophores production of *Microcystis aeruginosa* and *Microcystis wesenbergii*. *Curr Microbiol* 55:94–98. doi:[10.1007/s00284-006-0470-2](https://doi.org/10.1007/s00284-006-0470-2)
- Yingping F, Lemeille S, Talla E et al (2014) Unravelling the cross-talk between iron starvation and oxidative stress responses highlights the key role of PerR (alr0957) in peroxide signalling in the cyanobacterium *Nostoc* PCC 7120. *Environ Microbiol Rep* 6:468–475. doi:[10.1111/1758-2229.12157](https://doi.org/10.1111/1758-2229.12157)
- Zappa S, Bauer CE (2013a) The LysR-type transcription factor HbrL is a global regulator of iron homeostasis and porphyrin synthesis in *Rhodobacter capsulatus*. *Mol Microbiol* 90:1277–1292. doi:[10.1111/mmi.12431](https://doi.org/10.1111/mmi.12431)
- Zappa S, Bauer CE (2013b) Iron homeostasis in the *Rhodobacter* genus. *Adv Bot Res* 66:289–326. doi:[10.1016/B978-0-12-397923-0.00010-2](https://doi.org/10.1016/B978-0-12-397923-0.00010-2)
- Zhang L, McSpadden B, Pakrasi HB, Whitmarsh J (1992) Copper-mediated regulation of cytochrome c553 and plastocyanin in the cyanobacterium *Synechocystis* 6803. *J Biol Chem* 267:19054–19059

Cyanobacterial Photosynthesis: The Light Reactions

Sascha Rexroth, Marc M. Nowaczyk, and Matthias Rögner

Abstract Cyanobacterial photosynthesis can be regarded as the blueprint for the photosynthesis of green algae and higher plants: While most of the principal reactions on the molecular level are preserved, their structural arrangement is compact and intimately connected with the respiratory chain. This allows conclusions on the evolution of special functional membrane domains which finally lead to separate membranes in specialized organelles. The robustness of some cyanobacterial—especially thermophilic—strains also allowed their isolation and structural and functional characterization up to the molecular level while keeping their full activity. This is especially true for the X-ray structures with highest available resolution of photosystems 1 and 2 and the *cyt b₆f* complex. Due to the ease of transformation, generated cyanobacterial mutants can be used for elucidating photosynthesis-related cellular processes which—if combined with synthetic biology approaches—can be harnessed for light-triggered biotechnological processes such as biofuel or fine chemical production.

Keywords Cyanobacteria • Photosynthesis • Electron transport • Photosystem 2 • Cytochrome *b₆f* • Photosystem 1 • Thylakoid • Membrane domain • Biogenesis

Abbreviations

ARTO	Alternative respiratory terminal oxidase
CM	Cytoplasmic membrane
COX	Cytochrome <i>c</i> oxidase
<i>cyt b₆f</i>	Cytochrome <i>b₆f</i> complex
<i>cyt bc₁</i>	Cytochrome <i>bc₁</i> complex
<i>cyt bd</i>	Cytochrome <i>bd</i> oxidase

S. Rexroth • M.M. Nowaczyk • M. Rögner (✉)
Plant Biochemistry, Faculty of Biology and Biotechnology, Ruhr-University Bochum,
44780 Bochum, Germany
e-mail: Matthias.Roegner@ruhr-uni-bochum.de

cyt <i>c</i>	Cytochrome <i>c</i>
Fd	Ferredoxin
Flv	Flavodiiron protein
FNR	Ferredoxin NADP(+) reductase
H ₂ ase	Hydrogenase
NDH	NAD(P)H dehydrogenase
PBS	Phycobilisome
Pc	Plastocyanin
PDM	PratA-defined membrane
PQ	Plastoquinone
PS1	Photosystem 1 complex
PS2	Photosystem 2 complex
RC	Reaction center
SHE	Standard hydrogen electrode
<i>Synechocystis</i>	<i>Synechocystis</i> sp. PCC 6803
TC	Thylakoid centers
TM	Thylakoid membrane
WOC	Water-oxidizing complex

Introduction: Importance of Cyanobacterial Photosynthesis for Life on Earth and World Climate

The light reactions of cyanobacterial photosynthesis are essentially performed by three transmembrane protein complexes—photosystem 2 (PS2), the cytochrome *b₆f* complex (cyt *b₆f*), and photosystem 1 (PS1)—which are located in the thylakoid membrane. Triggered by light, they perform photosynthetic electron transport with the three complexes as shown in Fig. 1 to provide reduction equivalents for the

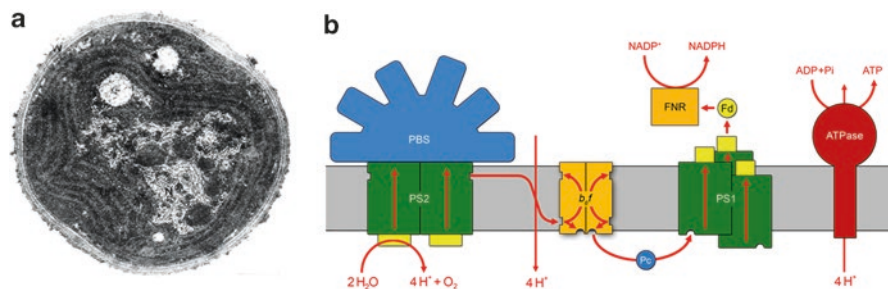


Fig. 1 Electron micrograph of *Synechocystis* PCC 6803 cell (A) and model of electron- and proton-transport routes in the thylakoid membrane (TM), starting with the water oxidation reaction up to NADPH and ATP generation. While cyanobacterial PS2 and cyt *b₆f* appear as dimeric complexes in the thylakoid membrane, the large majority of PS1 complexes exists as trimer (in contrast, for instance, to higher plants)

metabolism. They also generate a proton gradient across the thylakoid membrane for the subsequent formation of ATP by the ATP synthase (ATPase). The electron is processed through these routes by a combination of light-powered redox potential changes and the spatial arrangement of protein-bound redox components with increasing redox potential. Light harvesting within the photosystems is achieved by protein-based chlorophyll, which is supported by a peripheral cyanobacterial-specific antennae—the phycobilisomes (see also Chap. 9).

The environmentally and energetically most important reaction is the light-powered water-splitting reaction at the donor side of PS2, which generates oxygen: This reaction was the prerequisite for the development of all higher organized life on earth as shown in Fig. 2. Due to its fundamental importance, key elements of the structure-function relationship of PS2 have been preserved also in higher plants which evolved more than 2 billion years later. The abundance of cyanobacteria in both marine and fresh water is the reason that more than 25% of all oxygen that we breathe is still produced by their photosynthetic activity; also, they contribute considerably to the worldwide generation of light-powered energy as they are among the first components of the food chain in all water habitats. In addition, they are extremely important for the maintenance of the delicate equilibrium between oxygen production and CO₂ consumption which has a severe impact on the world climate and the CO₂ content of the oceans and—combined with it—their pH value which influences the abundance of other organisms. Although most cyanobacteria are single-celled organism with a diameter of 1–5 μm, their abundance in the oceans becomes obvious if they form algal blooms in case of special weather and nutrient conditions. Such algal blooms can seal the surface of lakes and even oceans and outgrow other organisms by preventing their light and nutrient access. The following

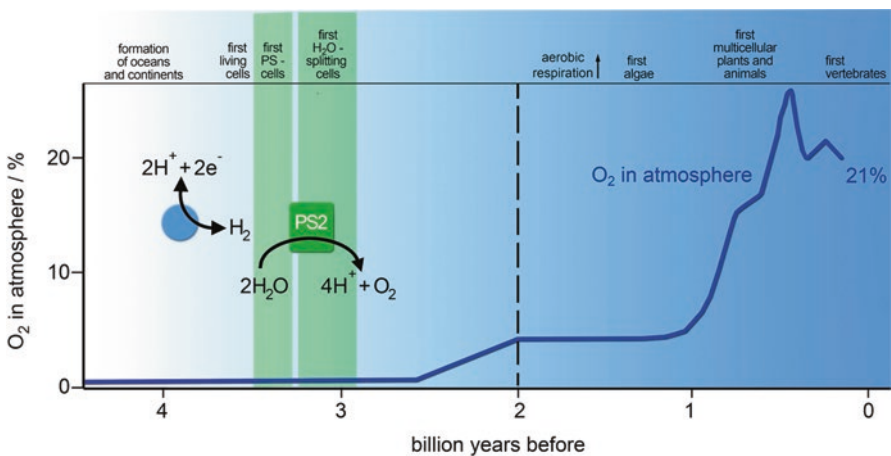


Fig. 2 Decisive energy-transforming enzymes related to evolution of photosynthesis and transformation of the atmosphere: While hydrogenases enabled life under anaerobic conditions, the emergence of water-splitting PS2 was the prerequisite for the development of an oxygen-enriched atmosphere (Holland 2006) and finally eukaryotic organisms

chapters should elucidate the molecular organization and adaptation of cyanobacterial life, which makes them survive under extreme environmental conditions, ranging from snow to hot desert (Thajuddin and Subramanian 2005).

Evolution of Photosynthetic Membranes Starting with Cyanobacteria

Photosynthetic Membranes from Gloeobacter to Higher Plants

It is evident that evolutionary progress is linked to a rising complexity of cellular architecture, when comparing the cellular structure of organisms performing oxygenic photosynthesis (Fig. 3): *Gloeobacter violaceus*—the most primitive organism known to perform oxygenic photosynthesis—is devoid of an intracellular TM and merely forms distinct cytoplasmic membrane domains specialized for photosynthetic and respiratory electron transport (Fig. 3a). In contrast, “typical” cyanobacteria contain internal thylakoids, which, however, lack an obvious lateral segregation (Fig. 3b). Unicellular green algae contain loosely associated TM layers (Fig. 3c) without significant segregation in grana and stroma thylakoids, while vascular plants show thylakoids which are fully differentiated into grana and stroma thylakoids (Fig. 3d).

In detail, Fig. 3b shows that cyanobacterial thylakoids form a series of parallel double membrane layers enclosing the thylakoid lumen—a continuous hydrophilic cell compartment separated from the cytosol (see also Fig. 13). Within the cyanobacterial cell, the localization and topology of TM are species dependent: While the TMs of some species are organized as concentric cylinders surrounding the central cytoplasm, the structures of other species, for instance, *Synechocystis* sp. PCC 6803 (*Synechocystis*), are less regular and form a series of roughly parallel sheets converging at structures referred to as thylakoid centers (see Figs. 1 and 3b) (van de Meene et al. 2006; Liberton et al. 2011; Rast et al. 2015).

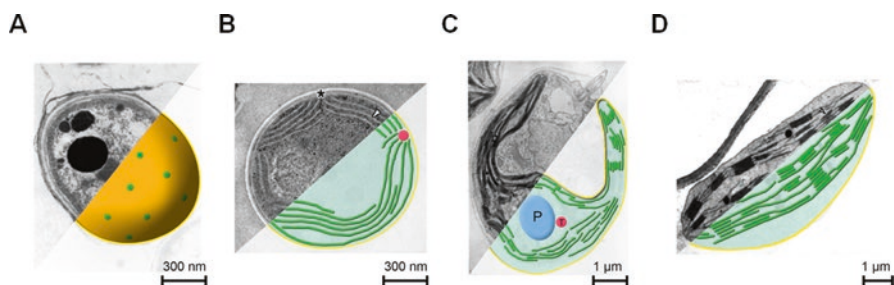


Fig. 3 Evolution of photoautotrophic cell architecture (Nickelsen et al. 2013) as EM (upper part) and model (lower part). (a) *G. violaceus* (with photosynthetically active patches colored green in the model cell) (Rippka et al. 1974); (b) *Synechocystis* PCC 6803 (van de Meene et al. 2006); (c) *Chlamydomonas reinhardtii* (Ohad et al. 1967); (d) spinach chloroplast (Mustardy and Garab 2003)

Membrane Microdomains (in *Gloeobacter violaceus*) as Precursors of Intracellular Membrane Compartments

In contrast to the well-known principle mechanisms of photosynthesis, only little is known about the biogenesis and evolutionary origin of the membrane hosting the components of photosynthetic electron transport. The primordial cyanobacterium *G. violaceus* (Fig. 4a), which harbors all photosynthetic protein complexes in its cytoplasmic membrane (CM), yields important hints about the origin and evolution of thylakoids. Similarly, in *Synechocystis*, a more developed cyanobacterial system with internal thylakoid membrane (see Fig. 3b), a state devoid of structured TMs, can be induced under certain conditions like heterotrophic growth (Fig. 4b).

Both cellular structures provide new concepts for the emergence of specialized membrane compartments and show an interesting topological similarity to proplastids. Similar to the segregation of eukaryotic membranes resulting in specific domains termed “rafts,” such structures—although simpler and less organized—are also implied for prokaryotic organisms: *Gloeobacter* cytoplasmic membranes could be separated into two distinct domains with characteristic protein composition, pigment content, and buoyant density. They are consistent with the characteristics of cyanobacterial CM or TM and indicate their common origin from the CM of *Gloeobacter*. Protein composition clearly defines the “green domain” (with typical proteins PS2, *cyt b₆f*, PS1, and NDH-1) as bioenergetic, performing both photosynthetic and respiratory electron transport. In contrast, the “orange domain” (with typical proteins such as squalene-hopene cyclase, phytoene dehydrogenase, and other enzymes involved in isoprenoid and carotenoid synthesis) suggests a role in the segregation of distinct membrane domains—although its molecular mechanism is still unknown.

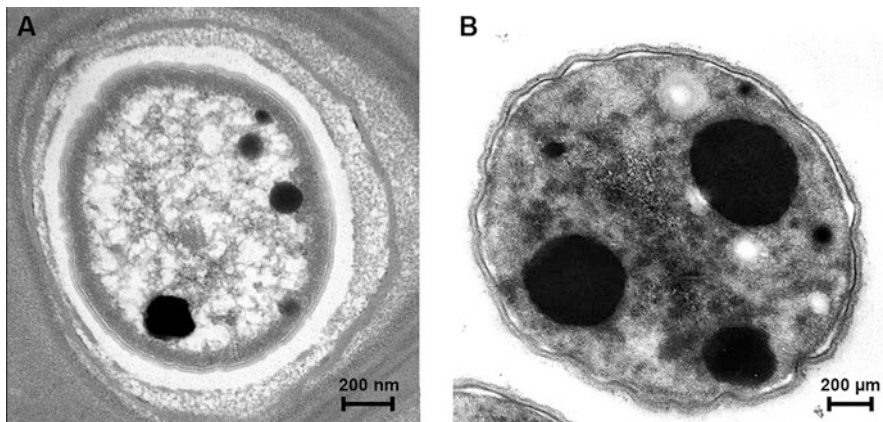


Fig. 4 (a) Cellular structure from *G. violaceus* (coop. with Stefan Geimer, Bayreuth University). (b) Cellular structure from *Synechocystis* under LAHG conditions

The domain structure of *Gloeobacter* membranes was confirmed by confocal fluorescence microscopy of living cells (Fig. 5), which show the inhomogeneous distribution of the three photosynthetic pigments chlorophyll, phycocyanin, and phycoerythrin within the cells due to their strong autofluorescence.

Based on size and center-to-center distances of the fluorescent patches, only about 6% of the total membrane surface is covered with photosynthetic patches (Fig. 6). In contrast, EM of common cyanobacteria like *Synechococcus* sp. PCC 7942 (Mullineaux and Sarcina 2002) suggest that thylakoids constitute about 80–90% of the total cellular membrane. In *Gloeobacter*, this low content of photosynthetic membrane domains may be responsible for its slow growth, which in turn might be a selective advantage in nutrient-poor habitats.

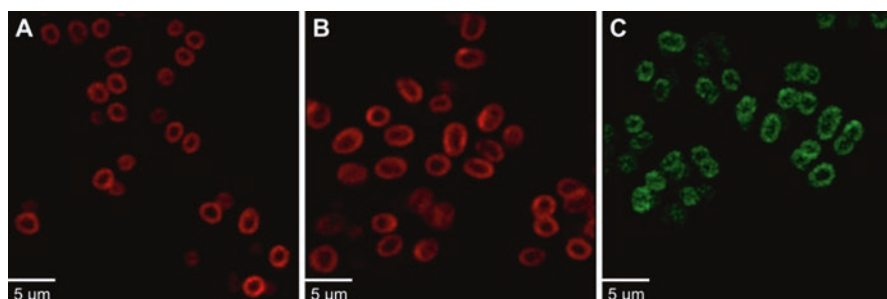
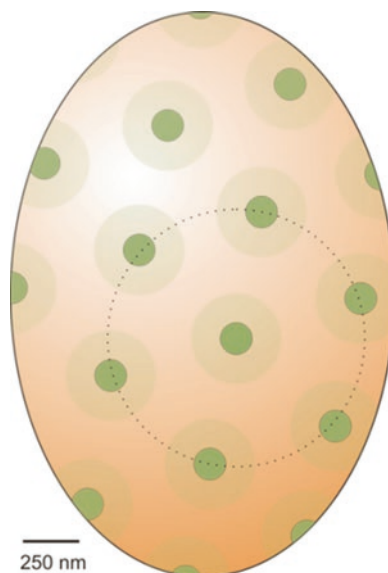


Fig. 5 Confocal fluorescence micrographs of *G. violaceus* cultures, showing optical sections with the CM as ring around the cell periphery. Heterogeneous fluorescence distribution for (a) chlorophyll, (b) phycocyanin, and (c) phycoerythrin is evident, with the fluorescence being concentrated in distinct spots (Rexroth et al. 2011)

Fig. 6 Membrane domain distribution in the CM of *G. violaceus* ($\sim 1.7 \times 2.5 \mu\text{m}$) (Rexroth et al. 2011) as inferred from confocal microscopy. The green domains displaying intense fluorescence emission have a mean diameter of 140 nm with a mean center-to-center distance of 570 nm (dotted line) (Rexroth et al. 2011)



Evolutionarily, the segregation of functionally distinct membrane domains with well-defined protein content has to precede the formation of specialized vesicles. Consequently, the initial preformation of membrane patches with photosynthetic and respiratory functions within the CM of a primitive cyanobacterium is a prerequisite for the emergence of a specialized thylakoid compartment.

Compartmentalized Cyanobacterial Photosynthesis

For cyanobacteria, *Synechocystis* can be regarded as model organism as it was the first species with fully determined genomic sequence. Due to its easy transformation, it is among the species with the most known and characterized mutants. This resulted in a detailed functional analysis of its metabolism, especially if related to photosynthesis. Figure 7 shows the major components of photosynthetic and respiratory electron transport and their distribution among the membrane systems. While the cytoplasmic membrane (CM) contains an incomplete respiratory electron transport system and incomplete photosystems in the process of maturation, the thylakoid membrane (TM) harbors both chains in a composition characteristic for

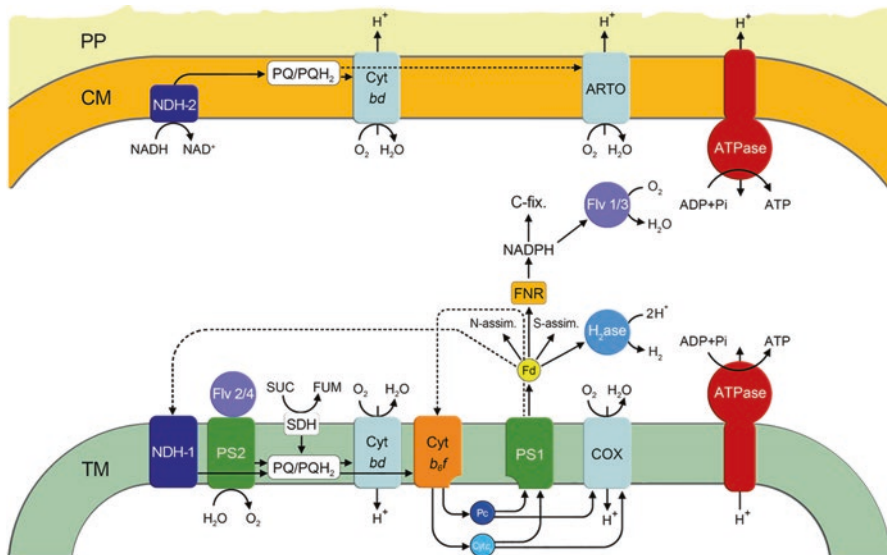


Fig. 7 Organization of photosynthetic and respiratory electron transport chains in cyanobacteria: TM with components of both respiratory and photosynthetic metabolism and CM with incomplete respiratory electron transport chain. H₂ase and Flv as protectors from redox poisoning/over-reduction. ARTO alternative respiratory terminal oxidase, CM cytoplasmic membrane, COX cytochrome *c* oxidase, Cyt *b₆f* cytochrome *b₆f* complex, Cyt *bd* cytochrome *bd* oxidase, Cyt *c₆* cytochrome *c₆*, Fd ferredoxin, Flv flavodiiron protein, FNR ferredoxin-NADPH oxidoreductase, H₂ase hydrogenase, NDH NADH dehydrogenase, Pc plastocyanin, PQ plastoquinone, PP periplasm, PS1 photosystem 1, PS2 photosystem 2, SDH succinate dehydrogenase, TM thylakoid membrane

cyanobacteria: They both share the *cyt b₆f* and the mobile carriers plastoquinone (PQ, membrane bound) and cytochrome *c* (*cyt c*) or plastocyanin (Pc, both water soluble), respectively, as all cyanobacteria are missing a *cyt bc₁* complex. Also, various routes for cyclic (via Fd or FNR) or energy-dissipating electron transport (via hydrogenase, (H₂ase) or flavodiiron (Flv1/3)) are indicated, which both function as emergency valves to prevent over-reduction of the cytosol. While more details will be outlined below, the central role of Fd for energy distribution and of the CM for maturation of central energy transformation complexes should be stressed: In contrast to previous reports, there is increasing evidence that CM contains neither a functional photosynthetic nor a complete respiratory electron transport chain, especially as central parts such as NDH-1, *cyt b₆f*, and cytochrome oxidase (COX) are missing (Lea-Smith et al. 2013). Apparently, only a minimal respiratory electron transport chain consisting of PQ-reducing type 2 NADH dehydrogenases (NDH-2), *cyt bd* oxidase, and/or the alternative terminal oxidase ARTO are capable to build up a proton gradient which can be used for ATP production via ATP synthase.

The two central elements of the oxygenic photoautotrophic metabolism in cyanobacteria are the two photosystems—PS2 and PS1. In the linear photosynthetic electron transport mode, they are connected in series by *cyt b₆f*, which transfers electrons from PS2 via the PQ pool to the mobile electron carrier plastocyanin. This transport is coupled to the translocation of two H⁺ per electron across the TM, i.e., two-thirds of the ATP production of the linear electron transport chain is attributed to the activity of *cyt b₆f*. In the subsequent light-driven reaction, PS1 transfers the electrons from plastocyanin via ferredoxin to the FNR which generates NADPH. Based on the structure of the cyanobacterial ATP synthase with the F_O part consisting of 15 proton transferring c-subunits on the one hand and an active Q cycle in the *cyt b₆f* on the other, an ATP/NADPH ratio of 1.2 due to linear photosynthetic electron transport can be determined.

The cyclic mode of photosynthetic electron transport provides additional ATP equivalents for the cyanobacterial metabolism and allows the adjustment of the supplied ATP/NADPH ratio to the demands of the photosynthetic C-fixation reaction. For the cyclic photosynthetic electron transport, two thylakoid localized routes have been established, of which the direct one involves a light-powered circulation of an electron between PS1 and *cyt b₆f*. The second, more indirect route involves the transfer of electrons from ferredoxin back into the PQ pool which probably involves the NDH-1 complex.

Cyanobacterial respiratory electron transport is an additional alternative to fuel the PQ pool and to generate ATP derived from stored metabolites. Its two central functions are (1) providing metabolic energy in the dark or under other ATP supply limiting conditions and (2) improving robustness of the electron transport system and preventing redox poisoning by over-reduction of the photosynthetic electron transport chain—particularly the PQ pool (Peltier et al. 2010). All three decisive complexes, NDH-1, SDH (Liu et al. 2012; Pisareva et al. 2011), and COX (Lea-Smith et al. 2013; Howitt and Vermaas 1998), are exclusively located within the TM (Lea-Smith et al. 2013; Mullineaux 2014). Besides, the *cyt bd* oxidase, a ter-

terminal oxidase transferring electrons from the PQ pool, is of major importance, when electron transport via *cyt b₆f* is limiting (Berry et al. 2002; Tsunoyama et al. 2009) and the PQ pool is over-reduced.

The activity of the different electron transport routes also affects the redox status of the cells: Photoautotrophic conditions favor the linear photosynthetic electron transport and lead to a net reduction of the cytoplasmic NADP⁺/NADPH pool. While terminal oxidases in combination with additional systems dissipate surplus electrons, cyclic pathways only contribute to the proton gradient and are neutral concerning the cellular redox status, which is essential for biological fitness. For this reason, the systems for adjusting and protecting redox homeostasis are crucial to understand the cyanobacterial metabolism.

While the co-localization of both electron transport pathways in cyanobacteria leads to a higher flexibility, it also sets higher demands for their control and adjustment according to the physiological requirements of the cell. Maintaining redox homeostasis is of major importance in all photoautotrophic organisms (Wilhelm and Jakob 2011). Over-reduction of redox mediator pools within electron transport chains limits electron flux via these components. It eventually leads to a lack of electron acceptors for the photosynthetic light reactions which induces the formation of reactive oxygen species and accumulation of photodamage. Important systems, which are mainly involved in the removal of surplus reduction equivalents under aerobic conditions, are the *cyt bd* complex as well as heterodimeric flavodiiron proteins Flv1/3 (Allahverdiyeva et al. 2013) functioning as electron sinks for the PQ and NADPH pool, respectively. Other examples for this will be shown in Chap. 4.

Molecular Structure of Selected PS-Membrane Proteins as Basis for Functional Correlation

Cyanobacterial PS2 Complex

The photosynthetic electron transfer is initiated at PS2, which catalyzes the unique light-driven oxidation of water. A high-resolution crystal structure of cyanobacterial PS2 provides a detailed picture of protein–cofactor interactions in the complex at the atomic level (Umena et al. 2011)—in particular into the water-oxidizing complex (WOC) with its unique Mn₄O₅Ca cluster, which forms the catalytic center of PS2. Currently, time-resolved structural analysis based on XFEL (femtosecond X-ray free electron laser) is intensively explored for PS2 analysis (Kern et al. 2014; Kupitz et al. 2014; Suga et al. 2015) and may provide novel information about structural changes of the WOC during the catalytic cycle.

In summary, each monomer of the dimeric PS2 protein complex consists of up to 20 protein subunits, 35 chlorophyll a molecules, 20–25 lipids, 12 β-carotenes, 2–3 plastoquinone, 2 pheophytins, 2 hemes, the WOC (Mn₄O₅Ca), 4 Ca²⁺ ions, 3 Cl⁻

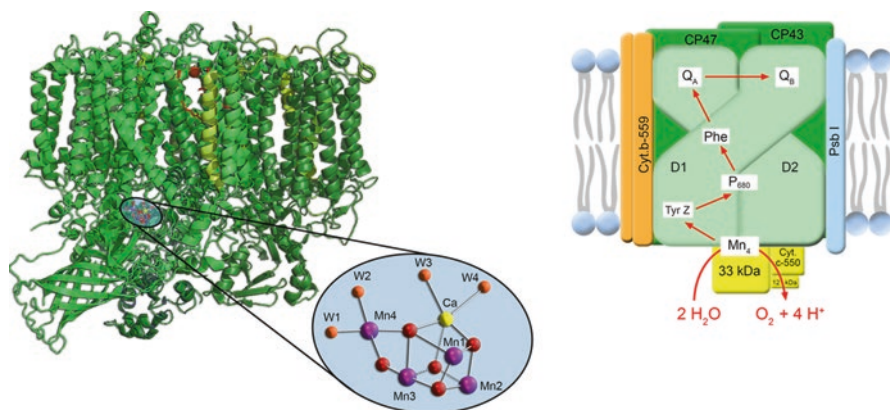


Fig. 8 3D-crystal structure and derived model of monomeric PS2 complex, the minimal functional complex; note that the model shows only the major subunits required for electron transfer. PS2 contains altogether 20 subunits—most with structural or unknown function (Umena et al. 2011)

ions, and a non-heme iron (Fig. 8). Most redox centers are coordinated by the central transmembrane subunits D1 and D2 (PsbA, PsbD), whereas light harvesting is mainly mediated by chlorophyll molecules that are bound to the intrinsic antenna proteins CP43 and CP47 (PsbB, PsbC).

Water oxidation is catalyzed by an inorganic $\text{Mn}_4\text{O}_5\text{Ca}$ cluster, which is coordinated by amino acid residues in D1, D2, and CP43 and shielded from the thylakoid lumen by the extrinsic subunits PsbO, PsbV, and PsbU. The large number (~13) of small (<10 kDa) and hydrophobic (1–2 transmembrane helices) subunits in PS2 is quite remarkable, with some of them playing a protective role (e.g., Cyt b_{559} , PsbE, PsbF) and others being located at the monomer–monomer interface (PsbL, PsbM, PsbT). However, the exact function of many small subunits (e.g., PsbH, PsbI, PsbJ, PsbK, PsbX, PsbY, PsbZ, Psb30) remains elusive. Also, the role of CyanoQ and CyanoP, the cyanobacterial homologs of PsbQ and PsbP in higher plants, is still unclear, especially as they are lacking in PS2 crystal structures and in biochemical or mass spectrometric analyses of PS2 preparations from *Thermosynechococcus* sp. (Umena et al. 2011; Guskov et al. 2009; Ferreira et al. 2004; Kuhl et al. 2000; Nowaczyk et al. 2006). While CyanoP might play a role in PS2 assembly (Cormann et al. 2014), CyanoQ seems to be part of the active PS2 complex at least in *Synechocystis* (Roose et al. 2007).

These structural data are complemented by kinetic data obtained with time-resolved spectroscopic methods. They provide information on the function of these complexes starting with light absorption by the antennae proteins (phycobilisomes, intrinsic antennae): Within femtoseconds, excitation is channeled via Förster resonance energy transfer to the reaction centers (RCs), where primary charge separation is induced (Holzwarth et al. 2006; Groot et al. 2005). The first metastable radical pair $\text{P680}^+/\text{Phe}^-$ is formed within ~3 ps. With a midpoint potential of +1210 mV (vs. SHE), the resulting cation P680^+ is the strongest oxidant known for

a biological system (Fig. 11) which enables the oxidation of water ($\text{H}_2\text{O}/\text{O}_2$; +820 mV) at the PS2 donor side. At the acceptor side, the electron is transferred from Phe to Q_A within ~200 ps due to a downhill potential from -500 mV (Phe⁻/Phe) to -140 mV ($\text{Q}_\text{A}^-/\text{Q}_\text{A}$) and a distance between the charges of approx. 5 nm. P680⁺ oxidizes a nearby tyrosine residue (Tyr_Z) within ~100 ns. The fact that the resulting radical pair Tyr_Z⁺/ Q_A^- is stable for milliseconds (Dau and Zaharieva 2009; Vinyard et al. 2013) is important, as both the subsequent water-splitting reaction (~2 ms) and the reduction of Q_B (~0.2–10 ms) are rather slow. Tyr_Z⁺ is reduced by the $\text{Mn}_4\text{O}_5\text{Ca}$ cluster which stores four electrons from the oxidation of two water molecules. This generates a cycle of five oxidation states (S_0 – S_4 , with the index number indicating the stored oxidizing equivalents). The accumulated oxidizing equivalents finally allow a four electron reaction in S_4 leading to O–O double bond formation (Cox and Messinger 2013) and the release of O_2 . This and the formation of PQH_2 makes this process irreversible.

Interestingly, cyanobacteria can adapt these electron transfer processes to specific environmental conditions by using different copies of the D1 protein (Nowaczyk et al. 2010; Sugiura and Boussac 2014). In case of *T. elongatus*, copy D1:1 is expressed under low-light conditions, whereas copy D1:2 is induced under high-light or other stress conditions. These copies show amino acid exchanges at specific positions (e.g., Q130-E130) which shift the redox potential of Phe/Phe⁻ (~+17 mV) and $\text{Q}_\text{A}/\text{Q}_\text{A}^-$ (~+41 mV) to more positive values. This decreases the probability for the triplet route via $^3[\text{P680}^*\text{Phe}^-]$ and favors instead direct $\text{S}_2\text{Q}_\text{A}^-$ or $\text{S}_2\text{Q}_\text{B}^-$ recombination (Sander et al. 2010; Sugiura et al. 2014). As the triplet chlorophyll is stable for milliseconds, singlet oxygen may form which leads to severe protein damage (Vass 2012). The formation of reactive oxygen species (ROS) is especially enhanced under light stress conditions which over-reduce the PQ pool and quickly inactivate PS2. While damaged PS2 can be reactivated in a sophisticated repair cycle by replacing D1 (see 4.1), the high-light copy D1:2 is more robust but at the expense of a less stable charge separation (i.e., lower efficiency). The role of a third D1 copy (D1'), which seems to be expressed under low-oxygen conditions, is less clear.

Cyanobacterial Cytochrome *b₆f* Complex

The cytochrome *b₆f* complex (cyt *b₆f*) is exclusively localized in the thylakoid membrane and holds a key position in the cyanobacterial electron transport chain: It mediates the electron transfer from the electron donor plastoquinol (PQH_2) to the acceptor plastocyanin (Pc) in both the respiratory and the photosynthetic electron transport chain.

The crystal structure of the cyanobacterial *b₆f* (Kurisu et al. 2003) shows a homodimeric complex consisting of four large protein subunits, which carry the prosthetic cofactors and are functionally involved in the electron transfer, and four small membrane-integral subunits which are involved in the structural stabilization

of the dimeric complex. The peripheral subunit PetP is specific for cyanobacteria and red algae and is missing in the crystal structure of *cyt b₆f* due to its transient binding to *cyt b₆f*. Deletion mutants indicate that it has a regulatory function (Rexroth et al. 2014).

In contrast to other photosynthetic electron transport complexes, the minimal functional unit of *cyt b₆f* is the dimeric complex, in which the Rieske subunit (PetC) has an important structural function (Fig. 9): It cross-links both monomers by interacting with one monomer in the membrane-integral domain and with the other in the thylakoid lumen exposed, soluble domain of the complex.

The electron transport reactions of *cyt b₆f* are coupled to the transfer of protons from the cytoplasm to the thylakoid lumen via the Q cycle. This cycle involves two quinol binding sites, the Q_p-site located close to the “positive” thylakoid lumen (i.e., the site of PQH₂ oxidation) and the Q_n-site next to the “negative” cytoplasm, which facilitates recycling of the electrons for the PQ reduction via the low potential chain.

The latter is formed by heme *b_p*—located close to Q_p—and the two hemes *b_n* and *c_n*. While these hemes are also found in the functionally and structurally homologous mitochondrial cytochrome *bc₁* complex, heme *c_n* is unique and conserved in all known *cyt b₆f* complexes. This heme *c_n* has been suggested as entry point for electrons from the cytosolic ferredoxin (Fd) or FNR during the photosynthetic cyclic electron transport; it might as well stabilize the two-electron reduction of PQ at the Q_n-site by avoiding the release of reactive radical species.

The high potential chain responsible for the transfer of electrons to plastocyanin and *cyt c₆* is functionally conserved in both *cyt bc₁* and *b₆f* complexes, although *cyt c₁* and *cyt f* share no structural homology. In contrast to eukaryotic organisms, cyanobacterial *cyt b₆f* in general contains alternative isoforms of the Rieske iron–sulfur protein—three have been reported in *Synechocystis* sp. PCC 6803: While isoform

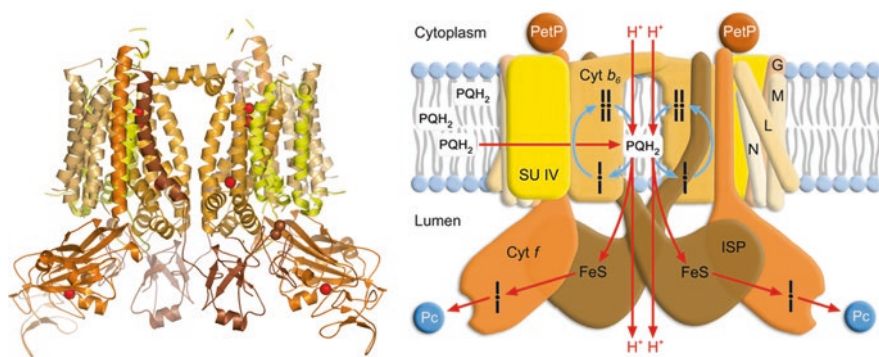


Fig. 9 3D-crystal structure and derived model of dimeric *cyt b₆f* complex (pdb: 4H44), the minimal functional complex; the crystal structure misses the PetP subunits which have a regulatory function for cyclic vs. linear electron transport; the latter receives its electrons from PS2 via the PQ pool. Hemes *b_n* and *c_n* are located in the Cyt. *b* subunit close to the cytoplasmic surface, heme *b_p* in the center and heme *f* in the luminal part of the *cyt. f* subunit

PetC2 appears to substitute the dominant PetC1 under high-light and low-oxygen conditions, isoform PetC3 has been shown to have no cyt *b₆f* subunit and rather appears to regulate electron transfer reactions in the periplasm, with no cyt *b₆f* complex being present in the cytoplasmic membrane (Aldridge et al. 2008; Schultze et al. 2009). In nitrogen-fixing cyanobacteria, an additional isoform, PetC4 with high sequence homology to PetC2, has been reported which is required for the heterocyst formation (Schneider and Schmidt 2005).

Cyanobacterial PS1 Complex

Photosystem 1 (PS1) is the largest known membrane protein complex that is involved in solar energy conversion. In cyanobacteria, each monomer of the trimeric structure consists of 12 protein subunits and 127 cofactors (96 chlorophyll *a* molecules, 22 β -carotenes, two phylloquinones, three iron–sulfur clusters, and four lipids) (Jordan et al. 2001). Each of the two large subunits PsaA and PsaB consists of 11 transmembrane helices coordinating most of the cofactors and in particular most of the redox active centers. Exceptionally, the terminal iron–sulfur clusters F_A/F_B are coordinated outside of the membrane by the PsaC subunit, next to the PsaD and PsaE protein on the cytoplasmic side of the complex. PsaI and PsaL are involved in trimer formation, whereas the other small subunits PsaJ, PsaK, PsaM, and PsaX seem to play rather a structural role. In contrast to eukaryotes, PsaF is neither involved in binding of plastocyanin nor cytochrome *c* (cyt *c*) (Fig. 10).

Functionally, charge separation at the central chlorophyll pair P700 generates the first radical pair $P700^+/P700^*$, with $P700^*$ being the strongest reductant known for biological systems (-1300 mV vs. SHE). Electron transfer to the primary acceptor chlorophyll A_0 occurs within ~ 1 ps and thereafter to phylloquinone A_1 within ~ 30 ps.

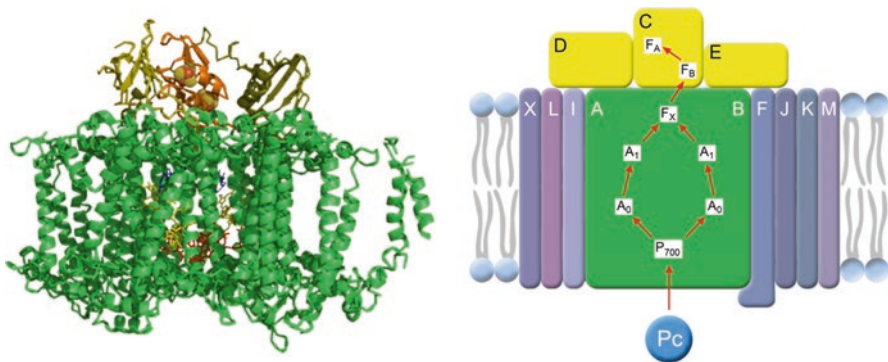


Fig. 10 3D-crystal structure and derived model of monomeric PS1 complex (Jordan et al. 2001), the minimal functional complex; the crystal structure does not include plastocyanin (Pc), the electron donor for PS1 (alternatively cyt *c* is also a physiological e-donor)

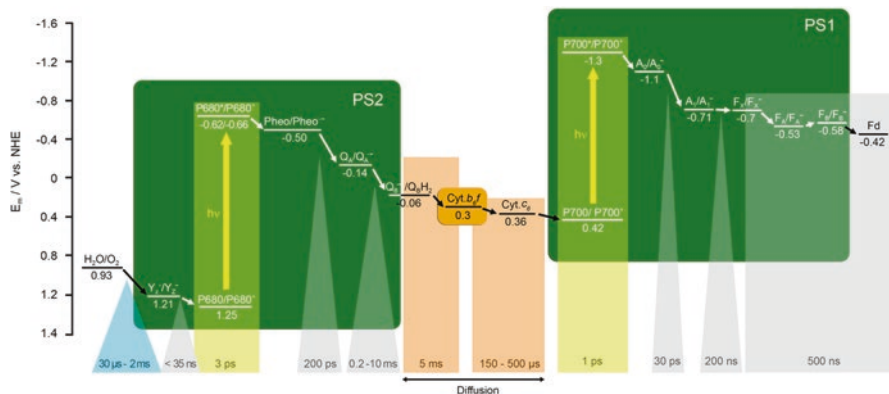


Fig. 11 Kinetics of photosynthetic electron flow in the thylakoid membrane with all three complexes—PS2, *cyt b₆f*, and PS1—arranged in sequence, allowing linear electron transport from water splitting up to ferredoxin (Fd) reduction. For details, see text

Reduction of the first iron–sulfur cluster (F_X), followed by FeS cluster (F_A/F_B) within ~ 200 ns and ~ 500 ns, respectively, is considerably slower. Stabilization of the radical pair $P700^+/F_B^-$ for ~ 60 ms allows docking and electron transfer to the diffusible electron carrier ferredoxin (Fd) and re-reduction of $P700^+$ by electron donation from *cyt c* (Brettel and Leibl 2001).

Figure 11 shows the kinetics of the combined photosynthetic electron transport chain. As the primary processes are very fast (fs-ps), electrons are processed very fast after charge separation, which enables a very high trapping efficiency of approximately 100%, i.e., almost each photon hitting the antenna induces charge separation at the reaction center. Thereafter, electron transfer slows down to nanoseconds (PS1) and microseconds (PS2) due to the involvement of diffusible mediators. Additionally, PQ reduction at the PS2 acceptor side is a two-electron process requiring stabilization of the semiquinone radical till arrival of the second electron from the reaction center. PQ reduction at PS2 ($200 \mu\text{s}$ – 10 ms) is usually the rate-limiting step of the whole electron transfer chain which limits the turnover frequency (TOF) of PS2 to about $85 \text{ e}^- \text{ s}^{-1}$ in the native cell (Lubner et al. 2011). In contrast, the optimized electron outlet of PS2 in an artificial redox environment can increase the TOF by a factor of five (Kothe et al. 2013)—in this case, water oxidation itself (2 ms) is the rate-limiting step. While PS1 in native systems is limited by electron supply from *cyt c* ($500 \mu\text{s}$), a nondiffusible, artificial electron donor can increase the TOF by a factor of about seven (Kothe et al. 2014). These examples convincingly illustrate that redox engineering of natural photosystems can overcome natural limitations considerably and have a high potential for future research.

While supercomplexes of these three photosynthetic membrane proteins—in combination with other proteins—have been reported for eukaryotic systems (Iwai et al. 2010), similar principles are just starting to be observed also in prokaryotes (Lopez and Kolter 2010).

Dynamics and Adaptations of Cyanobacterial Photosynthesis

Maturation of PS2 in Various Membrane Systems: Biogenesis and Degradation of PS2 as Example for Membrane Dynamics

Maturation of PS2 is an excellent example for the cooperation of cytoplasmic and thylakoid membrane in a dynamic process. Major problem is, however, the separation of both membranes as prerequisite for a detailed analysis and the elucidation of their structural and functional interaction. The complete physical separation of TM and CM in cyanobacteria is still a matter of debate (Pisareva et al. 2011; Vothknecht and Westhoff 2001), which may be due to special contact regions between both membranes (Fig. 12). On the other hand, several studies using cryo-electron tomography did not reveal any obvious direct connection (van de Meene et al. 2006; Liberton et al. 2011; Nevo et al. 2007)—in agreement with biochemical experiments using hydrophobic fluorescent dyes which showed CM and TM as discontinuous entities (Schneider et al. 2007). However, the exclusive synthesis of lipids and pigments as TM compounds (Benning 2008; Joyard et al. 2009) in the cyanobacterial CM indicate transport processes between CM and TM—either via indirect vesicular processes or via direct connections. Electron microscopy of *Synechocystis* showed such direct connections under certain stress conditions (van de Meene et al. 2012), while membrane fusion activity could be assigned to the Vipp1 protein (Hennig et al. 2015) which is essential for TM formation (Westphal et al. 2001;

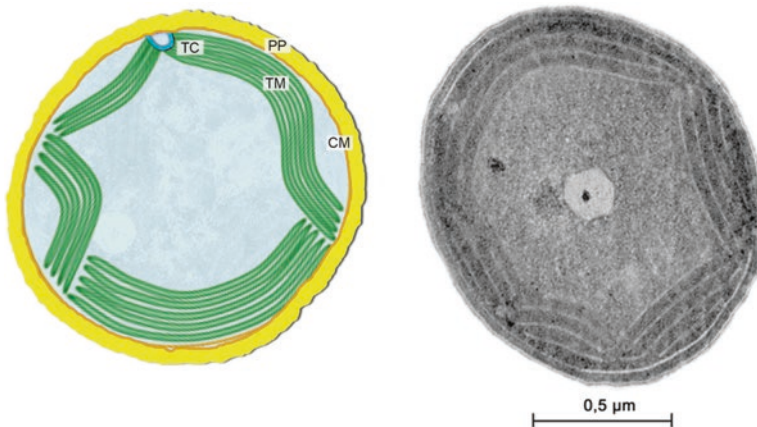


Fig. 12 Transient connections between CM and TM as proposed for thylakoid biogenesis and maturation of photosynthetic proteins between CM and TM as model (a) and as EM of whole *Synechocystis* cell (b). Thylakoid centers (TC), tubular CM invaginations (Kunkel 1982), have been proposed as contact sites for TM and CM (Nickelsen et al. 2013)

Kroll et al. 2001). Direct, indirect, or transient contact is also a prerequisite for the current models of TM biogenesis (Pisareva et al. 2011; Rengstl et al. 2011).

The low number of observed connection sites (Fig. 12) is in clear contrast to the expected flux of material necessary for biogenesis and maintenance of the TM and therefore an active research field. In case of PS2, Fig. 13 illustrates the synthesis of non-active pre-complexes in the CM and their (potential) flow to the TM through thylakoid centers. Thylakoid centers are circular structures at the interface between thylakoid and cytoplasmic membrane, which seem to play a role in thylakoid membrane biogenesis, but also in the assembly process of PS2 in cyanobacteria (Nickelsen et al. 2013). PS2 biogenesis is a highly ordered process that is orchestrated by numerous additional proteins, the so-called PS2 assembly factors (Nixon et al. 2010). They guide the formation of preassembled PS2 modules that are formed by a subset of PS2 subunits at specific locations within the cellular membrane system, and they are also involved in merging these modules to distinct intermediates in the PS2 assembly process (Heinz et al. 2016). Briefly, the preassembled pD1-PsbI and D2-Cyt. *b*₅₅₉ modules assemble in the thylakoid centers (TCs) to the first reaction center (RC) complex, which is already capable of charge separation (Fig. 13). Here the D1 C-terminus is processed to the intermediate form by the D1 C-terminal processing peptidase (CtpA) which is an important control of the assembly process, as only after full processing of D1 the functional WOC can be formed. Another assembly factor, PrtA (Klinkert et al. 2004), which is also involved in manganese delivery to PS2 (Stengel et al. 2012) is assisting this process. The complexes are then moved from the so-called prtA-defined membranes (PDMs), which are at least part of the TCs, to the thylakoid membrane. Here, CP47 assembles with the RC after full D1 processing, and the RC47 intermediate complex is formed (Boehm et al. 2012a). After subsequent attachment of the CP43-Psb27 module (Komenda et al. 2012a), the membrane intrinsic part of PS2 is fully assembled although still inactive in water oxidation. While WOC formation is facilitated by

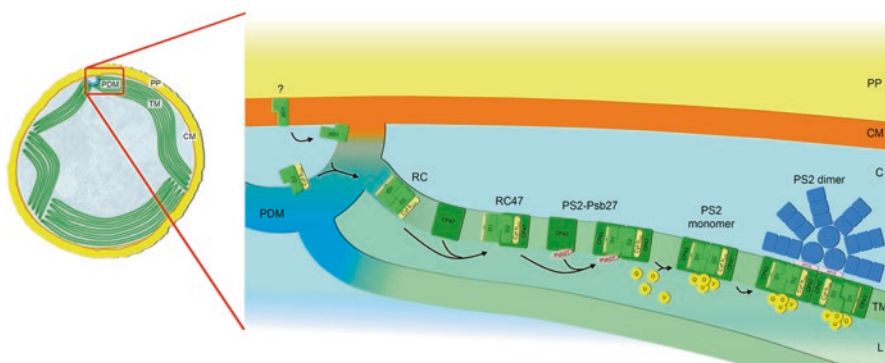


Fig. 13 Spatial distribution of PS2 assembly. PS2 complexes are assembled via distinct intermediates with involvement of specialized membranes (PDMs) that are located at the interface between thylakoid membrane (TM) and cytoplasmic membrane (CM). For details, see text. *PP* periplasm, *C* cytoplasm, *L* lumen, *RC* reaction center complex

Psb27 (Nowaczyk et al. 2006; Roose and Pakrasi 2008; Cormann et al. 2016), the complex gains water-splitting activity after attachment of the extrinsic proteins PsbO, PsbU, and PsbV. Finally, two PS2 monomers assemble to one PS2 dimer and, dependent on the light conditions, PS2-dimer-phycobilisome supercomplexes are formed (Mullineaux 2008).

Due to the extreme redox chemistry, PS2 is easily damaged during catalysis (see section “Cyanobacterial PS2 Complex”) by ROS formation at the PS2 acceptor side (Vass 2012) or by direct light induced damage of the WOC (Murata et al. 2007). Normally, the cells are able to replace damaged PS2 via a sophisticated repair cycle, which exchanges only damaged parts of the complex (mainly the D1 Protein); however, under stress conditions (e.g., light stress), the rate of damage could exceed the rate of repair leading to photoinhibition of the cells. PS2 repair starts by removal of the extrinsic proteins, followed by monomerization and detachment of CP43 (Nixon et al. 2010; Komenda et al. 2012b). Subsequently, damaged D1 is degraded by a heterooligomeric complex of FtsH2/FtsH3 and replaced by a new copy (Boehm et al. 2012b). After reattachment of the CP43-Psb27 module, the WOC is assembled similar to PS2 biogenesis. Obviously, this part of the intricate PS2 life cycle could also be assisted by additional proteins, but at least in cyanobacteria, a clear indication for a specific repair factor is missing so far.

Membrane Dynamics as Example for Stress Adaptation: State Transitions with Phycobilisomes Correlated with Reversible Monomerization of Photosystems

Cyanobacteria have developed a special light-harvesting system, the phycobilisomes (PBS), which is structurally and evolutionary completely independent from the membrane-integral light-harvesting complex of green algae and higher plants (Fig. 14). Besides their light absorption capability, PBS with their enormous dimensions of 5–10 MDa (de Marsac and Cohen-Bazire 1977) are also responsible for the minimal distance between cyanobacterial thylakoid membranes as is obvious from Fig. 14a. In addition, due to their abundance in the cells which accounts for up to 60% of the cellular protein content (Moal and Lagoutte 2012), they also function as N-resource of the cell under N-limiting conditions (for more details, see Chapter 12).

Functionally, PBS also fulfill an important role in balancing excitation energy between the photosystems which ensures maintaining redox homeostasis within the photosynthetic electron transport chain under fluctuating light intensities and qualities (van Thor et al. 1998). In a process called “state transitions,” the distribution of absorbed light energy between PS1 and PS2 is adjusted by the reversible attachment of PBS to the photosystems (Joshua and Mullineaux 2004). Illumination leading to excess excitation of PS2 induces a transition to “state 2” in which more absorbed PBS-excitation energy is diverted to PS1 to avoid an over-reduction of the

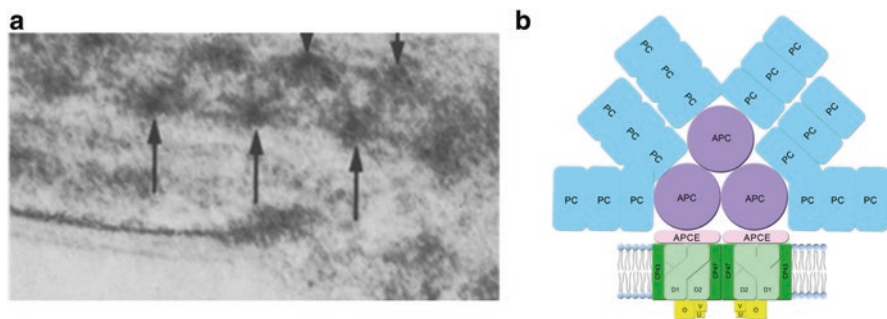


Fig. 14 Structure of a hemidiscoidal PBS and its attachment on the membrane surface. **(a)** Binding of PBS to the TM in *Pseudanabaena* PCC 7409 (van Thor et al. 1998). PBS structures (*black arrows*) define the minimal distance between adjacent TM layers. **(b)** Side view of a PS2-PBS complex of *Synechocystis* characterized by a dimeric PS2, tri-cylindrical APC core and six rods composed of three PC hexamers. Their arrangement enables an efficient funneling of the harvested excitation energy via the PBS core to the photosystems (Glazer 1985; Biggins and Bruce 1989; Liu et al. 2013)

PQ pool and vice versa in “state 1,” respectively (Mullineaux and Emlyn-Jones 2005). Most probably, this rearrangement of PBS is connected with a reversible monomerization/oligomerization of PS2 and PS1, respectively, as indicated in Fig. 15: While the binding of PBS to dimeric PS2 and the routine monomerization of PS2 for repair (exchange of the damaged D1-subunit) is established, the binding of PBS to trimeric PS1 still has to be shown.

Outlook: Application of Cyanobacterial Photosynthesis for Biotechnology: Design of Cells, Photobioreactors, and Biophotovoltaic Devices

Design of Cyanobacterial Mass Cultivation

Among the many parameters which have an impact on cyanobacterial cell growth and productivity, light and carbon supply are especially important. However, due to their dependence on a steadily changing culture density which is also combined with drastically changing light penetration depth, they are quite difficult to control in standard setups for cultivation. In order to control, reproduce, and optimize all parameters, the establishment of continuous cultivation conditions is of predominant importance. The major parameters and strategies for their control and dynamic regulation are shown in Table 1 below.

Central part of a continuous cultivation as shown in Fig. 16 is the turbidostatic process control, i.e., the controlled dilution of the culture medium by addition of fresh and the simultaneous removal of used medium. This system achieves constant cell densities, well-defined steady-state culture conditions, and well-defined stress conditions.

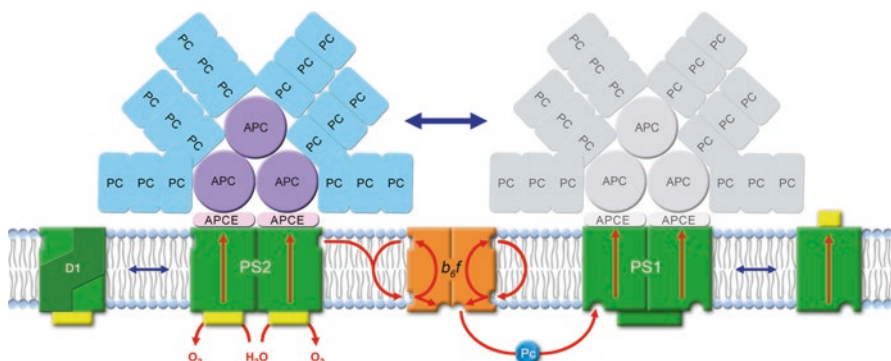


Fig. 15 Model of state transitions in the thylakoid membrane, realized by reversible functional PBS binding to PS2 (“state 1,” left) or PS1 (“state 2,” right, PBS in gray) (Kruip et al. 1994; Meunier et al. 1997; Schluchter et al. 1996)

Table 1: Central parameters in continuous cultivation mode and their possible regulation

Controlled parameter	Online detection	Regulation
<i>Culture media</i>		
pH	pH electrode	Acid/base titration
Temperature	Thermo element	Thermostat
CO ₂ (aq.) conc.	Ion selective electrode	Mass flow controller
Cell density	Optical density, turbidity	Media pump
<i>Gas phase</i>		
O ₂ (g) conc.	ZrO ₂ sensor	–
CO ₂ (g) conc.	IR detector	–
Gas flow	Mass flow analyzer	Mass flow controller

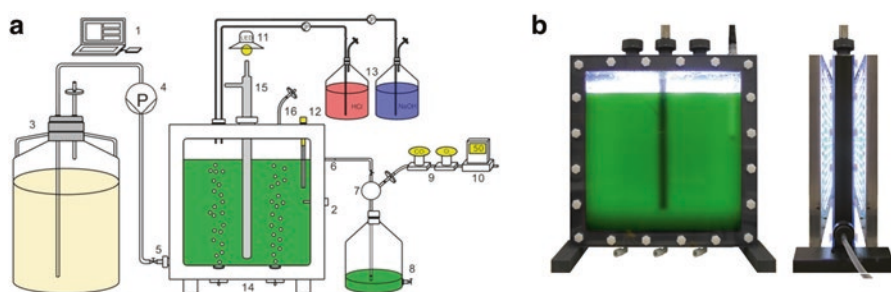


Fig. 16 Cyanobacterial culture in continuous cultivation mode (Kwon et al. 2012). (a) Principle of cont. cultivation in 5 L flatbed photobioreactor: (1) computer with LabVIEW program, (2) turbidity sensor, (3) media tank, (4) peristaltic pump (for media and pH control), (5) inlet for medium, (6) outlet for biomass, (7) gas separator, (8) harvest tank, (9) CO₂ and O₂ sensors, (10) mass flow controller, (11) LED panel, (12) pH sensor, (13) HCl and NaOH, (14) aeration, (15) thermostat, and (16) air filter. (b) Front view (left, LED panel omitted) and side view (right, with LED panels on both sides) of 5 L photobioreactor developed in coop. with KSD company (Hattingen); center part in front view = thermostat

Usually, CO_2 is supplied by aeration under photoautotrophic conditions, but its transfer efficiency into the liquid media depends on parameters like bubble size, mixing intensity, and the distribution of bubbles in the liquid medium. The dissolved CO_2 forms a pH-dependent equilibrium with HCO_3^- and CO_3^{2-} , i.e., the availability of CO_2 or HCO_3^- for cyanobacteria depends strongly on the pH and physical parameters of the cultivation like temperature, but also on biological parameters such as culture density and growth phase which define the uptake of CO_2 by the cells.

Besides controlling all these parameters, this setup also allows to simulate outdoor conditions such as light gradients, light stress, etc. which is important to evaluate the impact of these parameters on photosynthetic efficiency. It is also extremely helpful for the evaluation of the benefit of (directed or random) mutants for a possible improvement, for instance, in the production of biofuels or fine chemicals (see below).

Figure 17 illustrates the impact of cell density on the amount of released oxygen, which allows the determination of the optimal cell density in order to achieve maximum photosynthetic activity. Such an optimization has to be performed specifically for each engineered mutant; the determined optimal cell density is then kept constant under conditions of continuous cultivation (compare Fig. 16).

Depending on the intended product, upscaling to mass production in larger closed flatbed systems with much better efficiency and future extension toward sunlight irradiation is conceivable and already started to be realized (Rexroth et al. 2015).

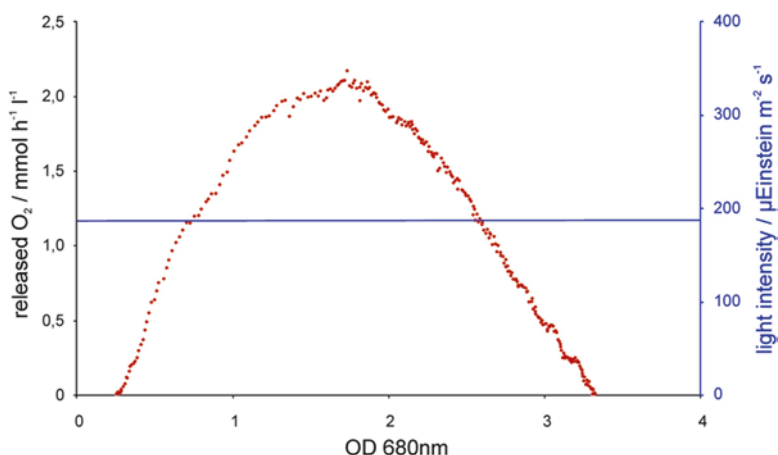


Fig. 17 Photosynthetic electron transport (as determined by oxygen evolution measurements in 5 L flatbed photobioreactor) in dependence on increasing culture density. Light intensity was kept constant at approximately 200 μE

Synthetic Biology Approaches to Design Cyanobacterial Cells for Biofuel and Fine Chemical Production

In contrast to the light reactions of photosynthesis with a quantum efficiency of close to 100% for both PS1 and PS2, efficiency of the combined electron transport reactions and especially the following C-fixation is much lower, resulting typically in an efficiency <1% for the final product, for instance, sugar. In order to achieve a much higher efficiency for product generation, photosynthetic reducing equivalents (“electrons”) have to be harvested immediately after the light reactions, i.e., close to the acceptor side of PS1 which is the most negative redox potential in nature. At this spot, electrons are distributed by ferredoxin (Fd), and any direct contact to this component enables a much higher efficiency than storing energy in sugar. One possible strategy is to store photosynthetic energy in hydrogen, as the Fe-Fe type of hydrogenase accepts electrons directly from Fd, resulting in minimal energy loss. Due to the ease of transformation and the simple cell organization as bacterium, *Synechocystis* is an ideal candidate to combine photosynthesis with hydrogen production. Unfortunately, *Synechocystis* does not contain an Fe-Fe-hydrogenase which is among the most active hydrogenases known. Figure 18 illustrates the strategy of this project: Electrons originating from water-splitting PS2 have to be transported via Fd primarily to such an “imported” hydrogenase at the expense of C-fixation. Besides increasing linear electron transport by PBS-antenna size reduction (Kwon et al. 2013) and partial uncoupling via manipulation of ATPase (for details, see (Imashimizu et al. 2011)), the decisive step is the rerouting of electrons from FNR to hydrogenase, although the affinity of Fd to FNR is about 5–10 times higher than to the (imported) hydrogenase.

While details of this synthetic biology approach are shown elsewhere (Rexroth et al. 2015), this strategy can also be used for any other reaction requiring reduction equivalents, for instance, the light-driven reduction of alkenes by enoate reductase as shown in Fig. 19 (Köninger et al. 2016). This *proof-of-concept* study shows the feasibility of light-driven whole-cell biotransformations with engineered cyanobacteria by expressing recombinant oxidoreductases. The direct utilization

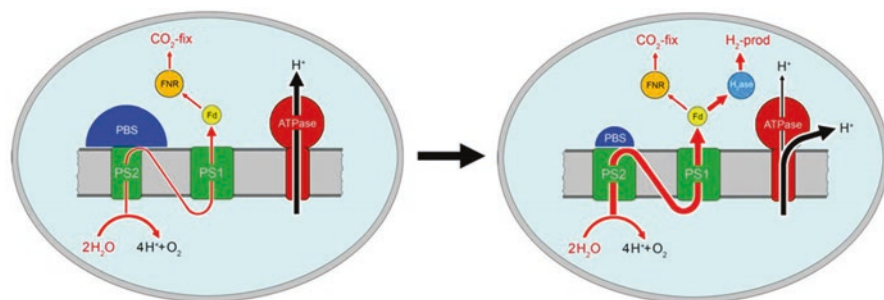


Fig. 18 Design of a *Synechocystis* WT cell for photosynthesis-based biohydrogen production (Rögner 2013)

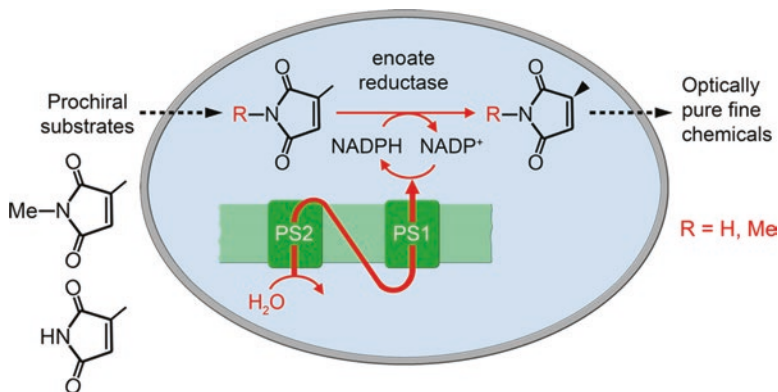


Fig. 19 Coupling of photosynthetic electron generation with the reduction of external components like alkenes, which are taken up by the cells and released to the medium after reduction (Königer et al. 2016)

of NADPH generated by photosynthetic electron transfer achieved product titers of up to 2 g L^{-1} , which may be increased in the future to economically feasible productivities with optimized systems. Such a concept may be also used for large-scale biotransformations of bulk and platform chemicals, especially as it prevents energy losses via the indirect carbon route and avoids stoichiometric formation of by-products: In case of the alkene reduction above, such a by-product is gluconolactone, which originates from the co-substrate glucose as typically used for biotransformations with oxidoreductases expressed in heterotrophic organisms.

Cyanobacterial Photosystems as Part of Biophotovoltaic Devices: Model Systems for Optimization and Utilization of Photosynthesis

Efficiency of photosynthesis in the cell is mainly limited by the coupled electron flow reactions through membrane-bound and water-soluble components. As in any chemical reaction, the rate-limiting step is the slowest one, which in case of the light-triggered electron transport reactions is the reduction and oxidation of the quinone pool (see Fig. 11). If this step could be omitted or bypassed, the real capacity of photosynthesis may be evaluated: Such a setup is realized in so-called semiartificial devices. As shown in Fig. 20, such a device consists of the main components required for light-driven electron transfer, i.e., PS1 and PS2, and the enzyme transforming reduction equivalents into the storable energy hydrogen, i.e., the hydrogenase (H₂ase).

Due to the oxygen sensitivity of most available hydrogenases, this device is separated into two compartments—one with oxygen evolution (due to water-splitting PS2) and one with hydrogenase activity (Fig. 20). Before the two half cells

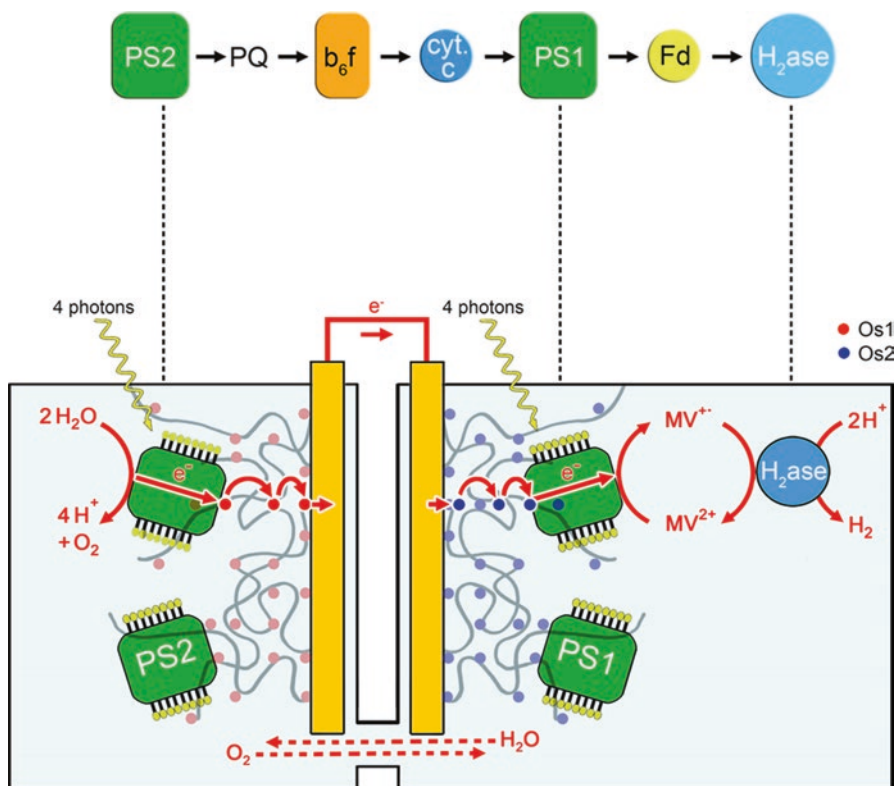


Fig. 20 Principle of a “biophotovoltaic cell” as model system for photosynthesis-dependent hydrogen production in comparison with the flow of electrons in the natural cell (*upper part*): The key components for light-driven electron transfer—PS2 and PS1—are immobilized within conducting Os polymer gels on gold electrode surfaces which are located in two different reservoirs, the anodic PS2 part (which is aerobic due to oxygen evolution at PS2) and the cathodic PS1 part. The latter has to be anaerobic due to the oxygen sensitivity of the hydrogenase which is coupled to the PS1-light reaction via the electron carrier Methyl viologen. The Os polymers on the anodic and the cathodic part are different and adjusted in their redox potential to the acceptor side of PS2 and the donor side of PS1, respectively, in order to achieve the highest possible electrical driving force (Esper et al. 2006)

can be combined in order to evaluate the capacity of this system to generate hydrogen from water, both half cells have to be optimized: In general, redox polymers turned out to be much superior to diffusible electron carriers (such as cyt. *c* and others) due to their tunable redox potential and their rapid electron transfer (Hartmann et al. 2014; Kothe et al. 2013). Figure 21 illustrates this potential: In combination with artificial electron donors and acceptors, PS1 achieves a seven-fold higher activity than in the natural membrane (Kothe et al. 2014): This shows that without the natural restrictions, the natural photosystems are much more efficient and can be used as highly optimized components in tailor-made biophotovoltaic devices for future energy supply.

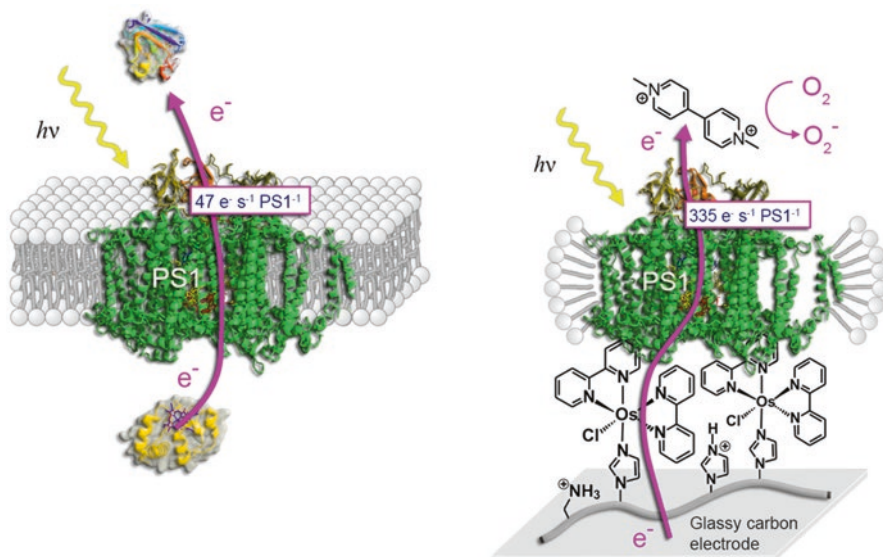


Fig. 21 Electron transport through PS1 when embedded into a natural membrane (thylakoid membrane of *Synechocystis* cell) via PS1 in a biophotovoltaic device with artificial electron donors and acceptors (PS1 solubilized by detergent) (Kothe et al. 2014)

References

- Aldridge C, Spence E, Kirkilionis MA, Frigerio L, Robinson C (2008) Tat-dependent targeting of Rieske iron-sulphur proteins to both the plasma and thylakoid membranes in the cyanobacterium *Synechocystis* PCC6803. *Mol Microbiol* 70(1):140–150. doi:[10.1111/j.1365-2958.2008.06401.x](https://doi.org/10.1111/j.1365-2958.2008.06401.x)
- Allahverdiyeva Y, Mustila H, Ermakova M, Bersanini L, Richaud P, Ajlani G, Battchikova N, Cournac L, Aro EM (2013) Flavodiiron proteins Flv1 and Flv3 enable cyanobacterial growth and photosynthesis under fluctuating light. *Proc Natl Acad Sci U S A* 110(10):4111–4116
- Benning C (2008) A role for lipid trafficking in chloroplast biogenesis. *Prog Lipid Res* 47(5):381–389. doi:[10.1016/j.plipres.2008.04.001](https://doi.org/10.1016/j.plipres.2008.04.001)
- Berry S, Schneider D, Vermaas WF, Rögner M (2002) Electron transport routes in whole cells of *Synechocystis* sp. strain PCC 6803: the role of the cytochrome *bd*-type oxidase. *Biochemistry* 41(10):3422–3429
- Biggins J, Bruce D (1989) Regulation of excitation energy transfer in organisms containing phycobilins. *Photosynth Res* 20(1):1–34
- Boehm M, Yu J, Reisinger V, Beckova M, Eichacker L, Schlodder E, Komenda J, Nixon P (2012a) Subunit composition of CP43-less photosystem II complexes of *Synechocystis* sp. PCC 6803: implications for the assembly and repair of photosystem II. *Philos Trans R Soc Lond B Biol Sci* 367(1608):3444–3454
- Boehm M, Yu J, Krynicka V, Barker M, Tichy M, Komenda J, Nixon PJ, Nield J (2012b) Subunit organization of a *Synechocystis* hetero-oligomeric thylakoid FtsH complex involved in photosystem II repair. *Plant Cell* 24(9):3669–3683
- Brettel K, Leibl W (2001) Electron transfer in photosystem I. *Biochim Biophys Acta Bioenerg* 1507(1):100–114
- Cormann KU, Bartsch M, Rögner M, Nowaczyk MM (2014) Localization of the CyanoP binding site on photosystem II by surface plasmon resonance spectroscopy. *Front Plant Sci* 5:595. doi:[10.3389/fpls.2014.00595](https://doi.org/10.3389/fpls.2014.00595)

- Cormann KU, Möller M, Nowaczyk MM (2016) Critical assessment of protein cross-linking and molecular docking: an updated model for the interaction between photosystem II and Psb27. *Front Plant Sci* 7:157
- Cox N, Messinger J (2013) Reflections on substrate water and dioxygen formation. *Biochim Biophys Acta Bioenerg* 1827(8):1020–1030
- Dau H, Zaharieva I (2009) Principles, efficiency, and blueprint character of solar-energy conversion in photosynthetic water oxidation. *Acc Chem Res* 42(12):1861–1870
- de Marsac NT, Cohen-Bazire G (1977) Molecular composition of cyanobacterial phycobilisomes. *Proc Natl Acad Sci U S A* 74(4):1635–1639
- Esper B, Badura A, Rögner M (2006) Photosynthesis as a power supply for (bio-)hydrogen production. *Trends Plant Sci* 11(11):543–549. doi:[10.1016/j.tplants.2006.09.001](https://doi.org/10.1016/j.tplants.2006.09.001)
- Ferreira KN, Iverson TM, Maghlaoui K, Barber J, Iwata S (2004) Architecture of the photosynthetic oxygen-evolving center. *Science* 303(5665):1831–1838. doi:[10.1126/science.1093087](https://doi.org/10.1126/science.1093087)
- Glazer AN (1985) Light harvesting by phycobilisomes. *Annu Rev Biophys Chem* 14:47–77. doi:[10.1146/annurev.bb.14.060185.000403](https://doi.org/10.1146/annurev.bb.14.060185.000403)
- Groot ML, Pawlowicz NP, van Wilderen LJ, Breton J, van Stokkum IH, van Grondelle R (2005) Initial electron donor and acceptor in isolated photosystem II reaction centers identified with femtosecond mid-IR spectroscopy. *Proc Natl Acad Sci* 102(37):13087–13092
- Guskov A, Kern J, Gabdulkhakov A, Broser M, Zouni A, Saenger W (2009) Cyanobacterial photosystem II at 2.9-Å resolution and the role of quinones, lipids, channels and chloride. *Nat Struct Mol Biol* 16:334–342. doi:[10.1038/nsmb.1559](https://doi.org/10.1038/nsmb.1559)
- Hartmann V, Kothe T, Poller S, El-Mohsnawy E, Nowaczyk MM, Plumere N, Schuhmann W, Rögner M (2014) Redox hydrogels with adjusted redox potential for improved efficiency in Z-scheme inspired biophotovoltaic cells. *Phys Chem Chem Phys* 16(24):11936–11941. doi:[10.1039/c4cp00380b](https://doi.org/10.1039/c4cp00380b)
- Heinz S, Liauw P, Nickelsen J, Nowaczyk M (2016) Analysis of photosystem II biogenesis in cyanobacteria. *Biochim Biophys Acta Bioenerg* 1857(3):274–287. doi:[10.1016/j.bbabi.2015.11.007](https://doi.org/10.1016/j.bbabi.2015.11.007)
- Hennig R, Heidrich J, Saur M, Schmuser L, Roeters SJ, Hellmann N, Woutersen S, Bonn M, Weidner T, Markl J, Schneider D (2015) IM30 triggers membrane fusion in cyanobacteria and chloroplasts. *Nat Commun* 6:7018. doi:[10.1038/ncomms8018](https://doi.org/10.1038/ncomms8018)
- Holland HD (2006) The oxygenation of the atmosphere and oceans. *Philos Trans R Soc Lond Ser B Biol Sci* 361(1470):903–915. doi:[10.1098/rstb.2006.1838](https://doi.org/10.1098/rstb.2006.1838)
- Holzwarth AR, Müller MG, Reus M, Nowaczyk M, Sander J, Rögner M (2006) Kinetics and mechanism of electron transfer in intact photosystem II and in the isolated reaction center: pheophytin is the primary electron acceptor. *Proc Natl Acad Sci* 103(18):6895–6900. doi:[10.1073/pnas.0505371103](https://doi.org/10.1073/pnas.0505371103)
- Howitt CA, Vermaas WFJ (1998) Quinol and cytochrome oxidases in the cyanobacterium *Synechocystis* sp. PCC 6803. *Biochemistry* 37(51):17944–17951
- Imashimizu M, Bernat G, Sunamura E, Broekmans M, Konno H, Isato K, Rögner M, Hisabori T (2011) Regulation of FOF1-ATPase from *Synechocystis* sp. PCC 6803 by gamma and epsilon subunits is significant for light/dark adaptation. *J Biol Chem* 286(30):26595–26602. doi:[10.1074/jbc.M111.234138](https://doi.org/10.1074/jbc.M111.234138)
- Iwai M, Takizawa K, Tokutsu R, Okamura A, Takahashi Y, Minagawa J (2010) Isolation of the elusive supercomplex that drives cyclic electron flow in photosynthesis. *Nature* 464(7292):1210–1213. doi:[10.1038/nature08885](https://doi.org/10.1038/nature08885)
- Jordan P, Fromme P, Witt HT, Klukas O, Saenger W, Krauß N (2001) Three-dimensional structure of cyanobacterial photosystem I at 2.5 Å resolution. *Nature* 411(6840):909–917
- Joshua S, Mullineaux CW (2004) Phycobilisome diffusion is required for light-state transitions in cyanobacterial. *Plant Physiol* 135(4):2112–2119
- Joyard J, Ferro M, Masselon C, Seigneurin-Berny D, Salvi D, Garin J, Rolland N (2009) Chloroplast proteomics and the compartmentation of plastidial isoprenoid biosynthetic pathways. *Mol Plant* 2(6):1154–1180. doi:[10.1093/mp/ssp088](https://doi.org/10.1093/mp/ssp088)
- Kern J, Tran R, Alonso-Mori R, Koroidov S, Echols N, Hattne J, Ibrahim M, Gul S, Laksmono H, Sierra RG, Gildea RJ, Han G, Hellmich J, Lassalle-Kaiser B, Chatterjee R, Brewster AS, Stan

- CA, Glockner C, Lampe A, DiFiore D, Milathianaki D, Fry AR, Seibert MM, Koglin JE, Gallo E, Uhlig J, Sokaras D, Weng TC, Zwart PH, Skinner DE, Bogan MJ, Messerschmidt M, Glatzel P, Williams GJ, Boutet S, Adams PD, Zouni A, Messinger J, Sauter NK, Bergmann U, Yano J, Yachandra VK (2014) Taking snapshots of photosynthetic water oxidation using femtosecond X-ray diffraction and spectroscopy. *Nat Commun* 5:4371. doi:[10.1038/ncomms5371](https://doi.org/10.1038/ncomms5371)
- Klinkert B, Ossenbuhl F, Sikorski M, Berry S, Eichacker L, Nickelsen J (2004) PrtA, a periplasmic tetratricopeptide repeat protein involved in biogenesis of photosystem II in *Synechocystis* sp. PCC 6803. *J Biol Chem* 279(43):44639–44644. doi:[10.1074/jbc.M405393200](https://doi.org/10.1074/jbc.M405393200)
- Komenda J, Knoppová J, Kopečná J, Sobotka R, Halada P, Yu J, Nickelsen J, Boehm M, Nixon PJ (2012a) The Psb27 assembly factor binds to the CP43 complex of photosystem II in the cyanobacterium *Synechocystis* sp. PCC 6803. *Plant Physiol* 158(1):476–486
- Komenda J, Sobotka R, Nixon PJ (2012b) Assembling and maintaining the photosystem II complex in chloroplasts and cyanobacteria. *Curr Opin Plant Biol* 15(3):245–251
- Königer K, Gómez Baraibar Á, Mügge C, Paul CE, Hollmann F, Nowaczyk MM, Kourist R (2016) Recombinant cyanobacteria for the asymmetric reduction of C=C bonds fueled by the biocatalytic oxidation of water. *Angew Chem Int Ed* 55(18):5582–5585
- Kothe T, Plumere N, Badura A, Nowaczyk MM, Guschin DA, Rögner M, Schuhmann W (2013) Combination of a photosystem 1-based photocathode and a photosystem 2-based photoanode to a Z-scheme mimic for biophotovoltaic applications. *Angew Chem Int Ed* 52(52):14233–14236. doi:[10.1002/anie.201303671](https://doi.org/10.1002/anie.201303671)
- Kothe T, Pöller S, Zhao F, Fortgang P, Rögner M, Schuhmann W, Plumeré N (2014) Engineered electron-transfer chain in photosystem I based photocathodes outperforms electron-transfer rates in natural photosynthesis. *Chem Eur J* 20(35):11029–11034
- Kroll D, Meierhoff K, Bechtold N, Kinoshita M, Westphal S, Vothknecht UC, Soll J, Westhoff P (2001) VIPP1, a nuclear gene of *Arabidopsis thaliana* essential for thylakoid membrane formation. *Proc Natl Acad Sci U S A* 98(7):4238–4242
- Kruij J, Bald D, Boekema E, Rögner M (1994) Evidence for the existence of trimeric and monomeric Photosystem I complexes in thylakoid membranes from cyanobacteria. *Photosynth Res* 40(3):279–286. doi:[10.1007/bf00034777](https://doi.org/10.1007/bf00034777)
- Kuhl H, Kruij J, Seidler A, Krieger-Liszak A, Bunker M, Bald D, Scheidig AJ, Rögner M (2000) Towards structural determination of the water-splitting enzyme. Purification, crystallization, and preliminary crystallographic studies of photosystem II from a thermophilic cyanobacterium. *J Biol Chem* 275(27):20652–20659. doi:[10.1074/jbc.M001321200](https://doi.org/10.1074/jbc.M001321200)
- Kunkel D (1982) Thylakoid centers: structures associated with the cyanobacterial photosynthetic membrane system. *Arch Microbiol* 133:97–99. doi:[10.1007/BF00413518](https://doi.org/10.1007/BF00413518)
- Kupitz C, Basu S, Grotjohann I, Fromme R, Zatsepin NA, Rendek KN, Hunter MS, Shoeman RL, White TA, Wang D, James D, Yang JH, Cobb DE, Reeder B, Sierra RG, Liu H, Barty A, Aquila AL, Deponte D, Kirian RA, Bari S, Bergkamp JJ, Beyerlein KR, Bogan MJ, Caleman C, Chao TC, Conrad CE, Davis KM, Fleckenstein H, Galli L, Hau-Riege SP, Kassemeyer S, Laksmono H, Liang M, Lomb L, Marchesini S, Martin AV, Messerschmidt M, Milathianaki D, Nass K, Ros A, Roy-Chowdhury S, Schmidt K, Seibert M, Steinbrener J, Stellato F, Yan L, Yoon C, Moore TA, Moore AL, Pushkar Y, Williams GJ, Boutet S, Doak RB, Weierstall U, Frank M, Chapman HN, Spence JC, Fromme P (2014) Serial time-resolved crystallography of photosystem II using a femtosecond X-ray laser. *Nature* 513(7517):261–265. doi:[10.1038/nature13453](https://doi.org/10.1038/nature13453)
- Kurisu G, Zhang H, Smith JL, Cramer WA (2003) Structure of the cytochrome *b₆f* complex of oxygenic photosynthesis: tuning the cavity. *Science* 302(5647):1009–1014
- Kwon JH, Rögner M, Rexroth S (2012) Direct approach for bioprocess optimization in a continuous flat-bed photobioreactor system. *J Biotechnol* 162(1):156–162. doi:[10.1016/j.jbiotec.2012.06.031](https://doi.org/10.1016/j.jbiotec.2012.06.031)
- Kwon JH, Bernat G, Wagner H, Rögner M, Rexroth S (2013) Reduced light-harvesting antenna: consequences on cyanobacterial metabolism and photosynthetic productivity. *Algal Res* 2(3):188–195
- Lea-Smith DJ, Ross N, Zori M, Bendall DS, Dennis JS, Scott SA, Smith AG, Howe CJ (2013) Thylakoid terminal oxidases are essential for the cyanobacterium *Synechocystis* sp PCC 6803 to survive rapidly changing Light intensities(1[C][W][OA]). *Plant Physiol* 162(1):484–495

- Liberton M, Austin JR 2nd, Berg RH, Pakrasi HB (2011) Insights into the complex 3-D architecture of thylakoid membranes in unicellular cyanobacterium *Cyanothece* sp. ATCC 51142. *Plant Signal Behav* 6(4):566–569
- Liu LN, Bryan SJ, Huang F, Yu J, Nixon PJ, Rich PR, Mullineaux CW (2012) Control of electron transport routes through redox-regulated redistribution of respiratory complexes. *Proc Natl Acad Sci U S A* 109(28):11431–11436. doi:[10.1073/pnas.1120960109](https://doi.org/10.1073/pnas.1120960109)
- Liu HJ, Zhang H, Niedzwiedzki DM, Prado M, He GN, Gross ML, Blankenship RE (2013) Phycobilisomes supply excitations to both photosystems in a megacomplex in cyanobacteria. *Science* 342(6162):1104–1107
- Lopez D, Kolter R (2010) Functional microdomains in bacterial membranes. *Genes Dev* 24(17):1893–1902. doi:[10.1101/gad.1945010](https://doi.org/10.1101/gad.1945010)
- Lubner CE, Applegate AM, Knörzer P, Ganago A, Bryant DA, Happe T, Golbeck JH (2011) Solar hydrogen-producing bionanodevice outperforms natural photosynthesis. *Proc Natl Acad Sci* 108(52):20988–20991
- Meunier PC, Colon-Lopez MS, Sherman LA (1997) Temporal changes in state transitions and photosystem organization in the unicellular, diazotrophic cyanobacterium *Cyanothece* sp. ATCC 51142. *Plant Physiol* 115(3):991–1000
- Moal G, Lagoutte B (2012) Photo-induced electron transfer from photosystem I to NADP(+): characterization and tentative simulation of the in vivo environment. *Biochim Biophys Acta* 1817(9):1635–1645. doi:[10.1016/j.bbabi.2012.05.015](https://doi.org/10.1016/j.bbabi.2012.05.015)
- Mullineaux CW (2008) Phycobilisome-reaction centre interaction in cyanobacteria. *Photosynth Res* 95(2-3):175–182
- Mullineaux CW (2014) Co-existence of photosynthetic and respiratory activities in cyanobacterial thylakoid membranes. *Biochim Biophys Acta* 1837(4):503–511
- Mullineaux CW, Emlyn-Jones D (2005) State transitions: an example of acclimation to low-light stress. *J Exp Bot* 56(411):389–393
- Mullineaux CW, Sarcina M (2002) Probing the dynamics of photosynthetic membranes with fluorescence recovery after photobleaching. *Trends Plant Sci* 7(6):237–240
- Murata N, Takahashi S, Nishiyama Y, Allakhverdiev SI (2007) Photoinhibition of photosystem II under environmental stress. *Biochim Biophys Acta* 1767(6):414–421. doi:[10.1016/j.bbabi.2006.11.019](https://doi.org/10.1016/j.bbabi.2006.11.019)
- Mustardy L, Garab G (2003) Granum revisited. A three-dimensional model--where things fall into place. *Trends Plant Sci* 8(3):117–122
- Nevo R, Charuvi D, Shimoni E, Schwarz R, Kaplan A, Ohad I, Reich Z (2007) Thylakoid membrane perforations and connectivity enable intracellular traffic in cyanobacteria. *EMBO J* 26(5):1467–1473. doi:[10.1038/sj.emboj.7601594](https://doi.org/10.1038/sj.emboj.7601594)
- Nickelsen J, Rengstl B (2013) Photosystem II assembly: from cyanobacteria to plants. *Annu Rev Plant Biol* 64:609–635. doi:[10.1146/annurev-arplant-050312-120124](https://doi.org/10.1146/annurev-arplant-050312-120124)
- Nixon PJ, Michoux F, Yu J, Boehm M, Komenda J (2010) Recent advances in understanding the assembly and repair of photosystem II. *Ann Bot* 106:1–16. doi:[10.1093/aob/mcq059](https://doi.org/10.1093/aob/mcq059)
- Nowaczyk MM, Hebel R, Schlodder E, Meyer HE, Warscheid B, Rögner M (2006) Psb27, a cyanobacterial lipoprotein, is involved in the repair cycle of photosystem II. *Plant Cell* 18(11):3121–3131. doi:[10.1105/tpc.106.042671](https://doi.org/10.1105/tpc.106.042671)
- Nowaczyk MM, Sander J, Grasse N, Cormann KU, Rexroth D, Bernat G, Rögner M (2010) Dynamics of the cyanobacterial photosynthetic network: communication and modification of membrane protein complexes. *Eur J Cell Biol* 89(12):974–982. doi:[10.1016/j.ejcb.2010.08.008](https://doi.org/10.1016/j.ejcb.2010.08.008)
- Ohad I, Siekevitz P, Palade GE (1967) Biogenesis of chloroplast membranes. I. Plastid dedifferentiation in a dark-grown algal mutant (*Chlamydomonas reinhardtii*). *J Cell Biol* 35(3):521–552
- Peltier G, Tolleter D, Billon E, Cournac L (2010) Auxiliary electron transport pathways in chloroplasts of microalgae. *Photosynth Res* 106(1–2):19–31
- Pisareva T, Kwon J, Oh J, Kim S, Ge CR, Wieslander A, Choi JS, Norling B (2011) Model for membrane organization and protein sorting in the cyanobacterium *Synechocystis* sp PCC 6803 inferred from proteomics and multivariate sequence analyses. *J Proteome Res* 10(8):3617–3631
- Rast A, Heinz S, Nickelsen J (2015) Biogenesis of thylakoid membranes. *Biochim Biophys Acta* 1847:821–830. doi:[10.1016/j.bbabi.2015.01.007](https://doi.org/10.1016/j.bbabi.2015.01.007)

- Rengstl B, Oster U, Stengel A, Nickelsen J (2011) An intermediate membrane subfraction in cyanobacteria is involved in an assembly network for photosystem II biogenesis. *J Biol Chem* 286(24):21944–21951. doi:[10.1074/jbc.M111.237867](https://doi.org/10.1074/jbc.M111.237867)
- Rexroth S, Mullineaux CW, Ellinger D, Sendtko E, Rögner M, Koenig F (2011) The plasma membrane of the cyanobacterium *Gloeobacter violaceus* contains segregated bioenergetic domains. *Plant Cell* 23(6):2379–2390. doi:[10.1105/tpc.111.085779](https://doi.org/10.1105/tpc.111.085779)
- Rexroth S, Rexroth D, Veit S, Plohne N, Cormann KU, Nowaczyk MM, Rögner M (2014) Functional characterization of the small regulatory subunit PetP from the cytochrome *b₆f* complex in *Thermosynechococcus elongatus*. *Plant cell* 26(8):3435–3448. doi:[10.1105/tpc.114.125930](https://doi.org/10.1105/tpc.114.125930) [doi]
- Rexroth S, Wiegand K, Rögner M (2015) Cyanobacterial design cell for the production of hydrogen from water. In: Rögner M (ed) *Biohydrogen*. De Gruyter, Berlin, Munich, Boston, pp 1–14
- Rippka R, Waterbury J, Cohen-Bazire G (1974) A cyanobacterium which lacks thylakoids. *Arch Microbiol* 100(4):419–436
- Rögner M (2013) Metabolic engineering of cyanobacteria for the production of hydrogen from water. *Biochem Soc Trans* 41(5):1254–1259. doi:[10.1042/bst20130122](https://doi.org/10.1042/bst20130122)
- Roose JL, Pakrasi HB (2008) The Psb27 protein facilitates manganese cluster assembly in photosystem II. *J Biol Chem* 283(7):4044–4050. doi:[10.1074/jbc.M708960200](https://doi.org/10.1074/jbc.M708960200)
- Roose JL, Kashino Y, Pakrasi HB (2007) The PsbQ protein defines cyanobacterial Photosystem II complexes with highest activity and stability. *Proc Natl Acad Sci* 104(7):2548–2553. doi:[10.1073/pnas.0609337104](https://doi.org/10.1073/pnas.0609337104)
- Sander J, Nowaczyk M, Buchta J, Dau H, Vass I, Deak Z, Dorogi M, Iwai M, Rögner M (2010) Functional characterization and quantification of the alternative PsbA copies in *Thermosynechococcus elongatus* and their role in photoprotection. *J Biol Chem* 285(39):29851–29856. doi:[10.1074/jbc.M110.127142](https://doi.org/10.1074/jbc.M110.127142)
- Schluchter WM, Shen G, Zhao J, Bryant DA (1996) Characterization of *psaI* and *psaL* mutants of *Synechococcus* sp. strain PCC 7002: a new model for state transitions in cyanobacteria. *Photochem Photobiol* 64(1):53–66
- Schneider D, Schmidt CL (2005) Multiple Rieske proteins in prokaryotes: where and why? *Biochim Biophys Acta* 1710(1):1–12. doi:[10.1016/j.bbabi.2005.09.003](https://doi.org/10.1016/j.bbabi.2005.09.003)
- Schneider D, Fuhrmann E, Scholz I, Hess WR, Graumann PL (2007) Fluorescence staining of live cyanobacterial cells suggest non-stringent chromosome segregation and absence of a connection between cytoplasmic and thylakoid membranes. *BMC Cell Biol* 8:39
- Schultze M, Forberich B, Rexroth S, Dyczmons NG, Roegner M, Appel J (2009) Localization of cytochrome *b₆f* complexes implies an incomplete respiratory chain in cytoplasmic membranes of the cyanobacterium *Synechocystis* sp. PCC 6803. *Biochim Biophys Acta* 1787(12):1479–1485
- Stengel A, Gügel IL, Hilger D, Rengstl B, Jung H, Nickelsen J (2012) Initial steps of photosystem II de novo assembly and preloading with manganese take place in biogenesis centers in *Synechocystis*. *Plant Cell* 24(2):660–675
- Suga M, Akita F, Hirata K, Ueno G, Murakami H, Nakajima Y, Shimizu T, Yamashita K, Yamamoto M, Ago H, Shen JR (2015) Native structure of photosystem II at 1.95 Å resolution viewed by femtosecond X-ray pulses. *Nature* 517(7532):99–103. doi:[10.1038/nature13991](https://doi.org/10.1038/nature13991)
- Sugiura M, Boussac A (2014) Some Photosystem II properties depending on the D1 protein variants in *Thermosynechococcus elongatus*. *Biochim Biophys Acta Bioenerg* 1837(9):1427–1434
- Sugiura M, Azami C, Koyama K, Rutherford AW, Rappaport F, Boussac A (2014) Modification of the pheophytin redox potential in *Thermosynechococcus elongatus* Photosystem II with PsbA3 as D1. *Biochim Biophys Acta Bioenerg* 1837(1):139–148
- Thajuddin N, Subramanian G (2005) Cyanobacterial biodiversity and potential applications in biotechnology. *Curr Sci* 89(1):47–57
- Tsunoyama Y, Bernat B, Dyczmons NG, Schneider D, Rögner M (2009) Multiple Rieske proteins enable short- and long-term light adaptation of *Synechocystis* sp. PCC 6803. *J Biol Chem* 284(41):27875–27883. doi:[10.1074/jbc.M109.011189](https://doi.org/10.1074/jbc.M109.011189)
- Umena Y, Kawakami K, Shen J-R, Kamiya N (2011) Crystal structure of oxygen-evolving photosystem II at a resolution of 1.9 Å. *Nature* 473:55–60. doi:[10.1038/nature09913](https://doi.org/10.1038/nature09913)

- van de Meene AML, Hohmann-Marriott MF, Vermaas WFJ, Roberson RW (2006) The three-dimensional structure of the cyanobacterium *Synechocystis* sp. PCC 6803. *Arch Microbiol* 184(5):259–270. doi:[10.1007/s00203-005-0027-y](https://doi.org/10.1007/s00203-005-0027-y)
- van de Meene AM, Sharp WP, McDaniel JH, Friedrich H, Vermaas WF, Roberson RW (2012) Gross morphological changes in thylakoid membrane structure are associated with photosystem I deletion in *Synechocystis* sp. PCC 6803. *Biochim Biophys Acta* 1818(5):1427–1434. doi:[10.1016/j.bbame.2012.01.019](https://doi.org/10.1016/j.bbame.2012.01.019)
- van Thor JJ, Mullineaux CW, Matthijs HCP, Hellingwerf KJ (1998) Light harvesting and state transitions in cyanobacteri. *Plant Biol* 111(6):430–443
- Vass I (2012) Molecular mechanisms of photodamage in the Photosystem II complex. *Biochim Biophys Acta Bioenerg* 1817(1):209–217. doi:[10.1016/j.bbabi.2011.04.014](https://doi.org/10.1016/j.bbabi.2011.04.014)
- Vinyard DJ, Ananyev GM, Charles Dismukes G (2013) Photosystem II: the reaction center of oxygenic photosynthesis. *Annu Rev Biochem* 82:577–606
- Vothknecht UC, Westhoff P (2001) Biogenesis and origin of thylakoid membranes. *BBA-Mol Cell Res* 1541(1-2):91–101
- Westphal S, Heins L, Soll J, Vothknecht UC (2001) Vipp1 deletion mutant of *Synechocystis*: a connection between bacterial phage shock and thylakoid biogenesis? *Proc Natl Acad Sci U S A* 98(7):4243–4248
- Wilhelm C, Jakob T (2011) From photons to biomass and biofuels: evaluation of different strategies for the improvement of algal biotechnology based on comparative energy balances. *Appl Microbiol Biotechnol* 92(5):909–919. doi:[10.1007/s00253-011-3627-2](https://doi.org/10.1007/s00253-011-3627-2)

Photosynthesis in the Purple Bacteria

Robert A. Niederman

Abstract Anoxygenic chlorophototrophic purple bacteria have long provided a useful model system for functional and structural studies of the light reactions of photosynthesis, since they possess only a single Type II photochemical reaction center (RC), while in the more complex oxygenic phototrophs, two types of RCs, designated as photosystems I and II, are formed. The first of the major recent research breakthrough described here is the elucidation of the X-ray structure of the RC-light harvesting 1 (LH1) core complex of purple bacteria at near-atomic (3.0 Å) resolution. This structure represents an important landmark in structural biology, since along with the available structures of the peripheral LH2 antenna and RC proteins, a complete structural basis for both primary excitation and electron transfer reactions has now emerged. Importantly, in the closed, elliptical ring-like LH1 structure, channels exist that are compatible with the passage of quinol molecules for exchange with the quinone/quinol pool. Another significant advance in understanding the structural basis for the photosynthetic primary reactions is represented by the elegant views of the supramolecular surface organization of native intracytoplasmic membranes (ICMs) obtained by atomic force microscopy (AFM). These topographs uncovered a wide diversity of species-dependent arrangements of closely packed LH2 and RC-LH1 complexes, which in *Rhodobacter sphaeroides*, consisted of a well-organized architecture, made up of ordered, interconnected RC-LH1 networks intercalated by rows of LH2, coexisting with LH2-only domains. A less regular organization, with mixed regions of LH2 and RC-LH1 cores, intermingled with large, paracrystalline domains, was observed in other peripheral antenna-containing species, notably *Rhodospirillum photometricum* and *Rhodopseudomonas palustris*. These several types of supramolecular organizations are all capable of fulfilling the basic requirements for efficient collection, transmission, and trapping of radiant energy. Recently, the cytochrome bc_1 complex was also localized by AFM, using gold labelling in *Rba. sphaeroides* and found to be mainly confined to disordered areas adjacent to RC-LH1 core structures. Also described here are alterations in membrane dynamics and in excitation energy transfer capabilities that occur during adaptation of *Rba. sphaeroides* from high to low intensity illumination. These changes apparently arise from

R.A. Niederman (✉)

Department of Molecular Biology and Biochemistry and Rutgers Energy Institute, Rutgers, The State University of New Jersey, 604 Allison Road, Piscataway, NJ 08854-8082, USA
e-mail: niederm@rci.rutgers.edu

constraints on the flow of redox species on both the RC donor and acceptor sides, imposed by accumulation of large LH2 domains in the bilayer in which only a fraction of the LH2 rings are well connected to the RC. Advances in the proteomics of ICM development have also been made in which ICM growth initiation sites were found to be enriched in cytoplasmic membrane (CM) markers, including electron transfer proteins and permeases as well as general membrane protein assembly factors, confirming the origins of this membrane fraction from both peripheral respiratory membrane and sites of active CM invagination. Lastly, a computational and systems biology approach is discussed for determining the ATP production rate and energy conversion efficiency of a single chromatophore vesicle, based upon considerations from a quantitative supramolecular structural model.

Keywords Light harvesting complexes • Light regulation • Membrane dynamics • Oxygen regulation • Proteomics • Reaction centers • *Rhodobacter sphaeroides*

Abbreviations

AFM	Atomic force microscopy
BChl	Bacteriochlorophyll <i>a</i>
CM	Cytoplasmic membrane
ICM	Intracytoplasmic membrane
LH	Light harvesting
LH1	Core light-harvesting complex
LH2	Peripheral light-harvesting complex
MTF	Multiple turnover flash
PSI	Photosystem I
PSII	Photosystem II
Q _A	Primary reaction center ubiquinone
Q _B	Secondary reaction center ubiquinone
RC	Photochemical reaction center
STF	Single turnover flash
UQ	Ubiquinone

Introduction

Virtually all of the energy used in the biosphere arises from photosynthesis, the process that is responsible for the oxygen that powers respiration, the food that nourishes us, as well as the ancient vegetation from which fossil fuels are produced. The purple chlorophototrophic bacteria have long served as model organisms for understanding the basic fundamental biological processes involved in the light reactions of photosynthesis. These metabolically versatile organisms contain a bacteriochlorophyll (BChl) special pair-based Type II (pheophytin-quinone) reaction center (RC)

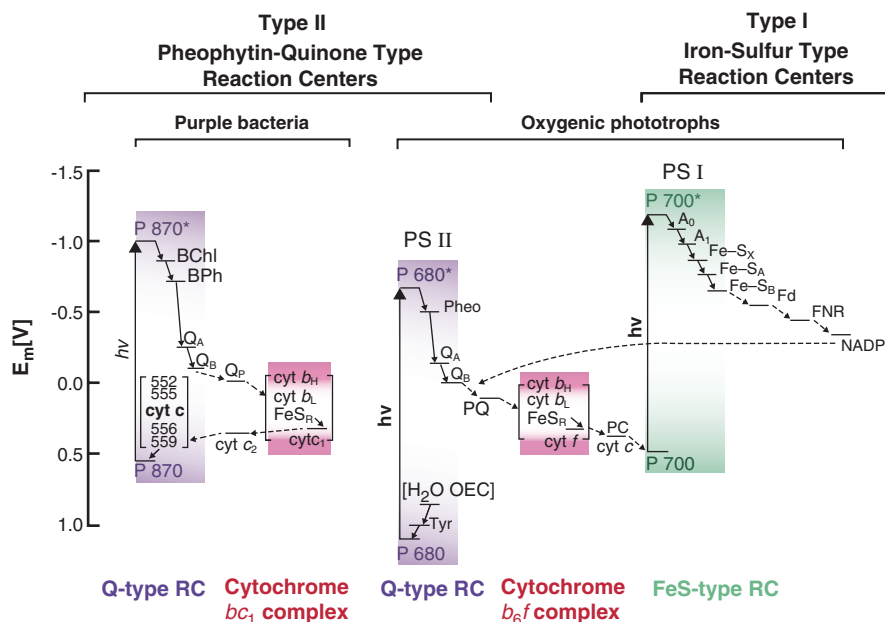


Fig. 1 Electron transport schemes in the RCs of the purple chlorophototrophic bacteria and of oxygenic phototrophs (cyanobacteria, algae, and higher plants), distinguished by their ability to oxidize water to oxygen by means a Mn cluster-containing OEC (adapted from Blankenship 2014). RCs form the core structure of both the PS I and PS II complexes, consisting of Type II (Pheo-Q type) RCs in PSII and Type I (Fe-S type) in PSI. In the anoxygenic phototrophs, which oxidize reduced substrates instead of water, the RCs of purple bacteria are of Type II (albeit lacking an OEC) and those of the green sulfur bacteria are of type I (not shown). The cytochrome bc_1 and b_6f complexes contain the Reiske Fe-S protein (FeS_R) and high and low potential cytochromes b ($cyt\ b_H$ and b_L , respectively). The b_6f complex connects PS II to PSI (A_0 and A_1 are a Chl a and phylloquinone molecule, respectively), which follows a pathway of electron transfer that, subsequent to the oxidation of H₂O by the OEC, traverses a series of electron carriers ranging in oxidation-reduction potential from ~ 1.2 V for the PSII-RC chlorophyll (Chl) a dimer (P680) to a value of -0.432 V for ferredoxin (Fd), the immediate reductant of NADP⁺ to form NADPH + H⁺, as catalyzed by Fd-NADP reductase (FNR) with NADPH serving as the final reductant for CO₂ fixation. The redox components are plotted on the basis of oxidation-reduction potentials, and linear electron flow in a form designated as a Z scheme for oxygenic phototrophs. The *dashed line* indicates that under conditions when ATP formation is outpaced by NADP reduction, cyclic electron transport around PSI occurs. Other features of the cyclic electron transport schemes of the purple bacteria are discussed in the text. Adapted with permission from Blankenship (2014) Copyright 2014 Wiley Blackwell

(Fig. 1), which initiates the light-driven reactions by catalyzing a transmembrane charge separation (Fig. 2a). The resulting electron flow leads to conversion of radiant energy into an electrochemical proton gradient that drives the energy conservation process through the synthesis of ATP by an F₁F₀-ATP synthase (Fig. 2b) (Feniouk and Junge 2008). This phototrophic mechanism is distinct from that of Archaea such as *Halobacterium halobium*, in which retinal-containing proteorhodopsins catalyze a photocycle that results in a light-activated proton gating process (Gordeliy 2017). While the purple chlorophototrophic bacteria contain a Type II RC, they lack the oxygen evolving complex (OEC) of the oxygenic phototrophs (Fig. 1). In addition to

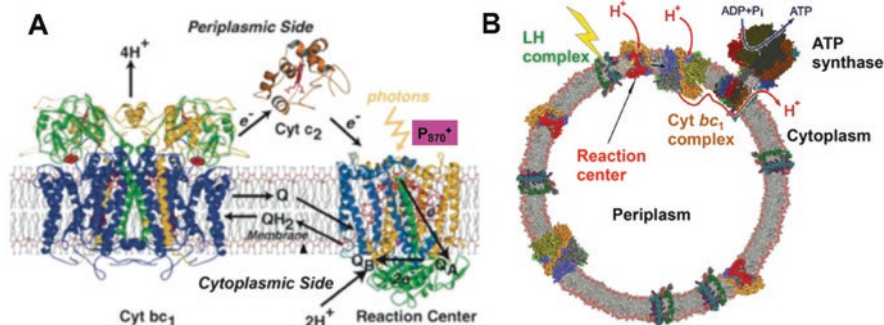


Fig. 2 Structural and functional aspects of cyclic electron flow and energy conservation in the ICM of *Rba. sphaeroides*. (a) The transmembrane charge separation together with intra- and extra-membrane electron transport via the quinone/quinol pool, bc_1 complex and cytochrome c_2 , respectively, resulting in reduction of P_{870}^+ , the photooxidized RC-BChl₂ special pair (Axelrod and Okamura 2005). Functional orientations of the ICM components relative to the periplasmic and cytoplasmic compartments and transmembrane proton movement are also shown. Ribbon structures based upon X-ray structures are drawn perpendicular to membrane plane for the RC, bc_1 and cytochrome c_2 proteins. (b) Functional orientation of participating proteins in isolated chromatophore vesicles arising from the ICM, drawn as *space filled spheres* on the basis of X-ray structures. The direction of light-driven proton movement coupled to electron transfer is toward the chromatophore lumen provided by the periplasm trapped within chromatophores. Proton movements result in an electrochemical proton gradient that drives protons through the F_0 sector of the ATP synthase, which powers ATP synthesis via the F_1 catalytic components. Panels **a** adapted with permission from Axelrod and Okamura (2005) Copyright 2005 Springer. Panel **b** reproduced from Feniouk and Junge (2008) Copyright 2008 Springer

the BChl special pair, the RCs contain the other bound cofactors involved in charge separation, which include two monomeric BChls and bacteriopheophytins (BPheo) molecules, and two quinone (Q_A and Q_B) molecules (see Fig. 4b below) (Allen et al. 1987).

The RC of purple bacteria is surrounded and interconnected by light-harvesting (LH) antenna proteins (Fig. 3); the functional absorption cross-section of the photosynthetic apparatus is made up of their BChl cofactors. The LH proteins of purple bacteria are mainly of the LH1 and LH2 type; LH1 absorbs maximally at ~875 nm and occurs in association with RCs, which together form the RC-LH1 core complex. It exists in either monomeric or dimeric form, depending upon the presence of the dimer-facilitating PufX protein (Francia et al. 1999) (see below). While LH1 serves as the sole antenna complex in some well-studied purple bacteria, such as *Blastochloris viridis*, *Rhodospirillum rubrum* and *Rsp., centenum*, the LH2 complex which has absorption maxima at 800 and 850 nm functions as a light-responsive, peripheral antenna complex in many other extensively studied species, such as *Rhodobacter sphaeroides*, *Rba. capsulatus*, *Rhodoblastus acidophilus*, *Rubrivivax gelatinosus*, *Rhodopseudomas palustris*, and *Rsp. photometricum*.¹ The LH2 com-

¹ Some purple bacteria, such as *Rbl. acidophilus* and *Phaeospirillum molischianum*, in addition to LH2, form an LH3 complex when grown at low light intensity, which serves to increase the absorption cross-section, as well as the spectral range of solar energy capture through near-IR absorption at 800 and 825 nm. Likewise, at low illumination levels, *Rps. palustris* forms an LH4 antenna complex which absorbs solely at 800 nm.

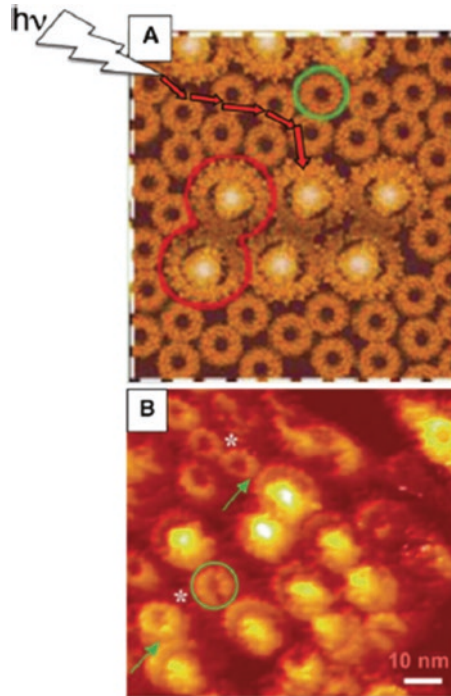


Fig. 3 Surface views of *Rba. sphaeroides* ICM obtained by AFM. **(a)** Modeled ICM surface derived from AFM topograph of ICM patch at submolecular resolution (Bahatyrova et al. 2004a) based upon the X-ray crystallography structures of the RC (Allen et al. 1986), LH2 (Papiz et al. 2003), and RC-LH1 core complexes (Roszak et al. 2003) as confirmed by RC-LH1 projection structure (Qian et al. 2005). A highly ordered linear arrays of dimeric RC-LH1 core complexes is shown together with interspersed rows of LH2. The central protruding white feature seen within the cores represents the cytoplasmic surface of the RC-H subunit. RC-LH1 dimer is delineated by *red outline*; representative LH2 complex is enclosed within *green circle*. *Red arrows* represent a possible pathway of excitations through LH2 rings to RC-LH1 core complexes. The arrangement of dimeric RC-LH1 cores in rows of up to six dimers assures that any LH1 excitation is able to migrate along a series of dimers until a RC in the oxidized “open state” is encountered. **(b)** High-resolution AFM topograph, showing 3-D representation of small ICM region and revealing cluster of RC-LH1 core complexes with associated LH2. *Green arrows*, contact points for energy transfer between LH2 and LH1-RC complexes; *asterisks*, nine-unit structure of $\alpha\beta$ -heterodimers visible in these LH2 rings; *green circle*, LH2 complex sandwiched between two RC-LH1 complexes

plex harvests radiant energy and transfers the resulting excitons to the LH1 core antenna, that in turn funnels excitation energy, within 20–40 ps, to the RC-BChl special pair (Fig. 3) (Blankenship 2014). The resulting charge separation leads to the reduction of Q_A , on the opposite side of the ICM (Fig. 2a). Electrons are gated from Q_A to Q_B , the latter exchanging with the quinone/quinol pool from which electrons are transferred from quinol to the UQ:cytochrome c_2 oxidoreductase (bc_1) complex (Fig. 1b). The bc_1 complex ultimately reduces the mobile electron carrier cytochrome c_2 , together with generating an electrochemical proton gradient via a Q-cycle mechanism. Ferrocycytochrome c_2 completes the cycle of electron flow by

reducing the photooxidized BChl special pair. During intraprotein electron transfer within the RC, the dimeric *Rba. sphaeroides* RC-LH1 core structure provides a favorable environment for localized UQ molecules, and moreover, the LH1 complex has been shown to play a role in optimizing the yield of secondary charge separation, by energetically stabilizing the $P^+Q_B^-$ charge separated state (Francia et al. 2004).

This chapter will present recently determined structural aspects of the photosynthetic apparatus of purple bacteria, which include the crystal structure of the RC-LH1 complex at near atomic resolution and the supramolecular surface structure of intracytoplasmic photosynthetic membranes (ICM) examined at submolecular resolution by AFM. Functional aspects covered here include how fluorescence induction/relaxation kinetics and time-resolved fluorescence have been used to assess the alterations in membrane dynamics and excitation energy transfer pathways that arise during alterations in the relative levels of LH complexes in the ICM. The contribution of proteomics to the structure, function, and assembly of the ICM will also be discussed. Lastly, a computational systems biology approach is detailed, in which the ATP production rate and energy conversion efficiency of *Rba. sphaeroides* is determined, on the basis of considerations obtained from a quantitative supramolecular structural model for a single ICM vesicle (chromatophore).

The Structure of the Reaction Center-Light Harvesting 1 Core Complex of Purple Bacteria Determined at 3.0 Å Resolution by X-Ray Crystallography

It is important to note that the crystal structures of the RC and LH2 proteins obtained at a near-atomic resolution of 3.0 Å in 1985 (Deisenhofer et al. 1985) and 1995 (McDermott et al. 1995), represented important landmarks in structural biology. The RC structure, as determined in *Bch. viridis*, represented the first of any integral membrane protein and led to the awarding of the 1988 Nobel Prize in Chemistry (Deisenhofer and Michel 1989). Likewise, the structure of the LH2 complex of *Rbl. acidophilus* was the first to be obtained for any LH protein. In contrast, it was not until 2014 that the structure of the RC-LH1 core complex was finally determined at 3.0 Å resolution (Fig. 4) (Niwa et al. 2014).

This structure determined was for the Ca^{2+} -associated RC-LH1 complex from *Thermochromatium tepidum*, a purple thermophilic sulfur bacterium isolated from a Ca^{2+} rich hot spring. As noted by Cogdell and Roszak (2014), the detailed arrangement of the protein subunits and their interactions with the cofactors significantly advance our understanding of the mechanisms driving excitation energy transfer and the primary light reactions of photosynthesis that provide the structural basis for ubiquinone-ubiquinol exchange.

X-ray crystallographic structures determined previously for the RC-LH1 complex at lower resolution demonstrated that in *Rba. sphaeroides*, the complex exists in the form of a dimeric ring (Fig. 5a) (Qian et al. 2013), while a monomeric ring structure is found in *Rsp. palustris* (Fig. 5b) (Roszak et al. 2003). These elliptical

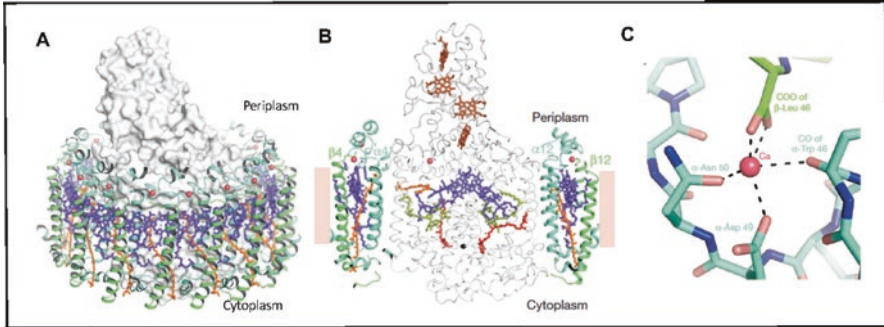


Fig. 4 Structure of RC-LH1 complex of *Tch. tepidum* determined at 3 Å resolution by X-ray crystallography (Niwa et al. 2014). (a) Final overall model: α - and β -apoproteins, light blue and green ribbon structures, respectively; RC cytochrome, H, L and M subunits, grey surface structure; Ca^{2+} ions, pink balls; B915 BChls, purple; spirilloxanthin, orange. An elliptical ring of 16 $\alpha\beta$ -subunits completely surrounds the RC with the α - and β -apoproteins forming inner and outer rings, respectively. The C- and N-termini of the α - and β -subunits are at the respective periplasmic and cytoplasmic membrane surfaces. The length of the major axis of the outer ring is 105 and 82 Å for the inner ring. (b) Cutaway view showing RC interior (helical and non-helical coil regions in grey) with cytochrome at top and $\alpha 4\text{-}\beta 4$ and $\alpha 12\text{-}\beta 12$ heterodimers at respective left and right edges adjacent to lipid bilayer (beige rectangles) with Ca^{2+} ions at periplasmic surfaces of the apoproteins. The α -His36 and β -His36 residues are coordinated to the central magnesium atoms of the respective α -B915 and β -B915 BChls. The B915-Bchl molecules within the LH1 ring consist of tightly stacked, partially overlapping dimeric chlorins with a Mg-Mg distance of 9.04 ± 0.02 Å, the shortest among any bacterial LH complex. The B915 molecules are located in the middle of the ring structures aligned at the same level as the BChl special pair within the RC in order to facilitate energy transfer from LH1. See Niwa et al. (2014) for a detailed description of interactions between LH1 and RC proteins. Heme, brown; LH1 and RC BChls, purple; BPheo, yellow green; quinone, red; non-heme iron, black. Note Ca^{2+} at interface of cytochrome and RC-M protein subunits and non-heme iron between Q_A and Q_B . (c) Enlarged view of Ca^{2+} binding site. Coordination of Ca^{2+} with five oxygen atoms is shown to arise from the α -Asp49 and α -Asn50 side chains, the α -Trp46 carbonyl and the C-terminal carbonyl of β -Leu 46. See text for explanation of how these associations are thought to confer thermostability on the complex. Reproduced with permission from Niwa et al. (2014) Copyright 2014 Nature Publishing Group

assemblies are discontinuous, such that the dimer rings form a gapped S-shape, and the monomer possesses a single gap; it is believed that these gaps facilitate Q/QH_2 exchange between the RC and the quinone/quinol pool within the lipid bilayer. Such discontinuities are created by the presence of the PufX and the W proteins in the dimeric and monomeric structures, respectively. For the *Tch. tepidum* RC-LH, no extra protein component is observed and the ring is continuous, and more circular (Fig. 5c); however, channels are found in the ring structure at the interface between the LH1 $\alpha\beta$ -heterodimers in the cytoplasmic portion of the transmembrane region. This is reminiscent of the monomeric B800 BChl binding site of the LH2 protein (Papiz et al. 2003). These channels are of sufficient size and hydrophobicity to permit the passage of Q_B molecules (Niwa et al. 2014). The RC- Q_B binding pocket is approximately at the same level as the LH1 channels, although a single channel may form the Q_B diffusion route; the inner gate of one such channel is located with a closest distance to the Q_B site of ~ 30 Å. However, variations were found in the size

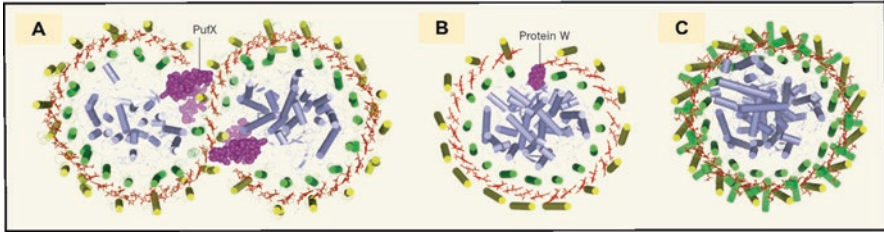


Fig. 5 Comparison of the crystal structures determined for RC-LH1 complexes. **(a)** *Rba. sphaeroides* RC-LH1-PufX dimeric complex based on model derived from X-ray structure at 8 Å resolution together with the results of electron microscopic, NMR, mass spectroscopy and resonance Raman analyses coupled to site-directed mutagenesis studies (Qian et al. 2013). The PufX protein (*purple surface structure*) creates a structural gap in the LH1 rings. *Yellow and green cylinders*, respective α - and β -apoproteins; *blue cylinders*, RC helices; B875 Bchl pigments, *red*. The RC-LH1-PufX core complex is comprised of $(\alpha\beta$ apoprotein)₂₈.(B875-BChl)₅₆.(spheroidene)₂₈.(RC apoproteins H, M, L)₂.(PufX)₂. Note that the carotenoid (spheroidene) and RC cofactors have been omitted. **(b)** *Rps. palustris* RC-LH1-W protein model derived from X-ray structure at 4.8 Å resolution (Roszak et al. 2003). A structural gap is created in the LH1 ring by the W protein (*purple surface structure*). The monomeric RC-LH1-W protein complex is comprised of $(\alpha\beta$ apoprotein)₁₅.(B885-BChl)₃₀.(carotenoid)₁₅.(RC apoproteins H, M, L)₁.(W protein)₁. **(c)** *Tch. tepidum* monomeric RCLH1 core complex model derived from X-ray structure at 3.0 Å resolution (Niwa et al. 2014). Because no LH1 gap forming protein such as PufX or the W protein is present, a continuous, elliptical structure is formed. No gene comparable to *pufX* has been found in the *Tch. tepidum* genome. As in other LH complexes of purple bacteria, the β -apoprotein forms the outer ring, while the inner ring is formed by the α -apoprotein. The major axes of the inner and outer elliptical rings are 82 and 105 Å long, respectively. The *Tch. tepidum* RC-LH1 complex is comprised of $(\alpha\beta$ apoprotein)₁₆.(B915-BChl)₃₂.(spirilloxanthin)₁₆.(Ca²⁺)₁₆.(RC cytochrome and apoproteins H, M, L)₁. Panel a Reproduced with permission from Cogdell and Roszak (2014) Copyright 2014 Nature Publishing Group

and shape of channel openings, which may reflect the “breathing motion” of the LH1 complex. (Walz and Ghosh 1997). This has been shown by AFM and cryo-EM to result in flexible structures for isolated LH1-only and RC-LH1 assemblies, which ranged from circles to ellipses (Bahatyrova et al. 2004b). Thus, for UQ shuttling through the closed ring, multiple channels could support a diffusion pathway.

A further unique aspect of the *Tch. tepidum* RC-LH1 complex is the presence of Ca²⁺ ions. In the structure, this cation is seen bound at the C-termini of the α - and β -subunits located on the periplasmic side of the complex (Fig. 4c), and has been shown to contribute to the thermostability of the protein as well as the highly red-shifted Q_Y-absorption maximum at 915 nm. Upon removal of Ca²⁺ by chelation with EDTA, the maximum is shifted to 880 nm, close to that of most LH1 complexes. It is suggested that this 35-nm redshift is promoted by the effects of the bound Ca²⁺ upon the environment of B915 BChl molecules (Niwa et al. 2014). As neither α -Asp49 or α -Asn50 is conserved in other purple bacterial species, it is suggested that they are specific for Ca²⁺ binding and are responsible for the Ca²⁺-induced associations between the C-terminal regions of the α - and β apoproteins that confer thermostability on the oligomeric structure. Moreover, the existence of *Tch. tepidum* in high Ca²⁺ environments may have contributed to the evolutionary selection pressure that leads to this thermostabilization mechanism.

The basic building block for the LH1 structure (a single $\alpha\beta$ -heterodimer associated with two B880 BChl molecules and one carotenoid molecule) is known to be stabilized by an internal hydrogen bond network that was first detailed by resonance Raman studies of *Rba. sphaeroides* site-directed LH1 mutants (Sturgis et al. 1997). This network involves two Trp residues (α -Trp+11 and β -Trp+9), located C-terminally to the BChl coordinated to the α - and β -His residues (the Trp positions in the polypeptide chains denoted by + signs). The hydrogen bonds formed between these Trp residues and the C₂-acetyl groups of the respective α - and β -BChl molecules both contribute to the redshift of the BChl-Q_Y absorption band and provide a significant driving force for stabilizing the overall LH1 complex structure.² Such a hydrogen bond network has also been determined for the *Tch. tepidum* LH1 complex, in which the α -Trp45 (α -Trp+10) and β -Trp45 (β -Trp+9) are located at hydrogen bonding distance from the B915-BChl acetyl groups. It is also noteworthy that the carbonyl oxygen of the phytyl chain ester group from the β -B915 BChl interacts through direct hydrogen bonding with α -Gln28 and β -Trp28. This may further contribute to the unusual stability of the *Tch. tepidum* LH1 protein. It is considered that the contribution that Ca²⁺-binding makes to the large B915 redshift is related to the proximity of the Ca²⁺-binding network to the B915 BChl molecules (Fig 5c), which modifies the chlorin configuration, through the closely positioned α -Trp45 and β -Trp45 side chains, hydrogen bonded to acetyl oxygen atoms of B915.

Further contributions to the B915 redshift arise from the location of spirilloxanthin within the LH1 ring structure. Indeed, Niwa et al. (2014) provide the first description of the orientation and position of carotenoid molecules in an LH1 structure. A spirilloxanthin methoxy end group is found in close vicinity to an α -His residues coordinated to the central Mg atoms of a B915 BChl molecule. Since the π -electron chain of spirilloxanthin contains 13 conjugated double bonds, a comparatively strong effect on the configuration of the chlorin rings is expected (Georgakopoulou et al. 2006). The geometry of spirilloxanthin with respect to the LH1 ring structure shows that it is inclined toward the B915 Q_X transition moment. Such interactions may provide an explanation for why in strains of *Rsp. rubrum* lacking the spirilloxanthin carotenoid, a 7–10 nm blueshift in the B880 BChl Q_Y absorption band is observed (Miller et al. 1987).

Supramolecular Surface Structure of Intracytoplasmic Membranes of Purple Bacteria as Examined by AFM

In addition to providing the first surface views of the multicomponent photosynthetic membranes of chlorophototrophs at submolecular resolution, AFM topographs of the ICM of purple bacteria have revealed a multiplicity of species-dependent

²As a consequence of the stability of the LH1 $\alpha_1\beta_1$ BChl₂ building block, it can be serially removed from LH1 oligomers in low-temperature lithium dodecyl sulfate/polyacrylamide gel electrophoresis, leaving a ladder of LH1 complexes, each differing from one another by one $\alpha_1\beta_1$ BChl₂ unit (Westerhuis et al. 2002).

compact arrangements of the peripheral LH complexes and LH1-RC core structures, which fulfill the basic requirements for efficient harvesting, transmission, and trapping of radiant energy (for reviews see: Scheuring et al. 2005; Scheuring 2006, 2008; Sturgis and Niederman 2008a, b; Sturgis et al. 2009; Scheuring and Sturgis 2009; Liu and Scheuring 2013).

A highly organized architecture was first observed in fused preparations of the pseudo-crystalline ICM of *Bch. viridis*, that consisted of highly packed, hexagonally dispersed monomeric RC-LH1 core complexes (Scheuring et al. 2003) (Fig. 6a). After removing the tetraheme cytochrome and RC-H subunits by nanodissection using increased loading forces on the AFM stylus, the RC-L and M-subunits are seen to assume a preferred asymmetric topography with a fixed distance distribution from the short axis of the elliptical LH1 complex. These distance constraints reflect strong and specific associations within the RC-LH1 core structure that are of importance for energy transfer. When the RC is disrupted by nanodissection, some of the exposed LH1 complexes are seen to have rearranged into a circular structure. It is possible that such flexible behavior promotes breathing motions that serve to facilitate menaquinone/menaquinol passage through the normally closed LH1 structure essentially as proposed above for the *Tch. tepidum* LH1 structure.

Among species which form a peripheral LH2 antenna, AFM images of ICM patches from *Rba. sphaeroides* showed well-ordered, interconnected networks of dimeric RC-LH1 core complexes intercalated by rows of LH2 (Bahatyrova et al. 2004a) (Fig. 3). These coexist with ordered LH2-only domains in the ICMs from low-light cells (Fig. 6b). In contrast, Fig. 6c shows that in an ICM patch from cells grown at higher light intensity, dimeric RC-LH1 complexes predominate over both the monomeric complex and LH2 (Adams and Hunter 2012). A predominance of RC-LH1 dimers was also observed in non-detergent treated membranes arising from nascent ICM growth initiation sites (Tucker et al. 2010).

Recently, the localization of the bc_1 complex, which had eluded investigators for nearly a decade since the initial AFM reports on ICM surface structure, was determined by gold labeling in *Rba. sphaeroides* (Cartron et al. 2014). Using ICM patches from a strain in which the C-terminus of cytochrome c_1 contained a His10-tag, labeling was performed with gold nanobeads. The complex was found to be confined to disordered areas adjacent to RC-LH1 core structures. A quantitative MS analysis of the overall chromatophore protein composition showed that dimeric RC-LH1 complexes outnumbered bc_1 complexes by a ratio of nearly 3:1, placing much of the bc_1 out of direct contact with the core particles. The results of this quantitative MS study will be discussed below in conjunction with a proposed atomic resolution model of a chromatophore vesicle and the related simulation of the energy, electron and proton transfer processes, and the calculated ATP turnover rate.

In the ICM of other peripheral antenna containing species, notably *Rsp. photometricum*, *Phs. molischianum*, and *Rps. palustris*, AFM has revealed a less regular organization of BChl-protein complexes, with mixed arrangements of LH2 and RC-LH1 cores; these regions are intermingled with large, paracrystalline membrane domains. Such dense, partially ordered membrane protein packing was first observed in flat membrane sheets of *Rsp. photometricum* (Scheuring and Sturgis 2005), arising from the disruption of stacked membranes consisting of regular bundles of flattened thylakoid-like discs.

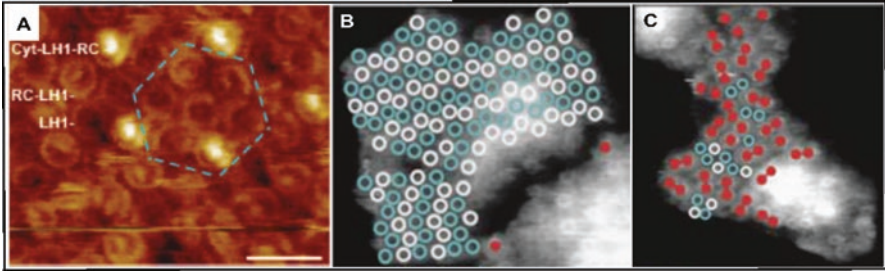


Fig. 6 High resolution AFM topographs of ICM preparations from purple bacteria with organized arrangements of photosynthetic complexes. **(a)** AFM topograph of *Bch. viridis* paracrystalline membrane obtained by a freeze-thaw induced fusion procedure (Scheuring et al. 2003). Hexagonally packed protein complexes are distributed into three classes after nanodissection by applying increased loading forces to the AFM tip. Stoichiometries for Cyt-RC-LH1 core complex are: (tetraheme cytochrome *c-552/c-558*); (RC L, M, H)₁; LH1($\alpha\beta$)₁₆. Dashed blue lines indicate area of hexagonal packing of RC-LH1 complexes. Scale bar: 20 nm. **(b)** AFM topograph of *Rba. sphaeroides* LH2-only membrane patch from cells grown at low light intensity (4 W/m²) (Adams and Hunter 2012). Patches were prepared with 0.03% β -dodecyl maltoside, which represents a sub-critical micelle concentration. These low detergent concentrations are sufficient to open up the ICM vesicles and allow the resulting ICM patches to assume a lower degree of curvature. This facilitates absorption onto the mica surface, thereby maximizing the area available to the AFM tip during tapping mode acquisition of topographs. Color coded schematic representation has been overlaid onto a greyscale AFM topograph (lower LH2 complexes: white rings; higher LH2 complexes: cyan rings). In the lower patch, the core complexes exposed in monomeric form on the cytoplasmic surface are demarcated by red dots. LH2 complexes are seen as separate nonameric ring structures (~6–7 nm in diameter), assuming a zigzag appearance, as a result of vertical displacement upon absorption of natively curved membranes onto the planar mica surface, leading to separate lines of raised LH2 complexes. **(c)** AFM topograph of *Rba. sphaeroides* ICM patch from cells grown at high light intensity (220 W/m²) (Adams and Hunter 2012), showing a predominance of RC-LH1 complexes with the majority in the dimeric form. Panel **a** reproduced with permission from Scheuring et al. (2003) Copyright 2003 National Academy of Sciences of the United States of America. Panels **b** and **c** reproduced with permission from Adams and Hunter (2012) Copyright 2012 Elsevier

In the membranes from cells grown at high light intensity, regions were observed that contained mixtures of randomly organized, LH2 rings, existing mainly in nonameric form, along with monomeric RC-LH1 elliptical structures, containing 16 LH1 $\alpha\beta$ -heterodimers (Fig. 7a). In the ICM of low-light adapted cells, considerable inter-complex clustering was also observed and the mixed regions were seen to co-exist with paracrystalline LH2 domains. These regions are formed by the addition of peripheral LH2 antennae that are packed into the membrane during acclimation to lowered light intensity. The tight packing of photosynthetic complexes during growth under both high and low intensities assures that individual antenna proteins do not segregate at too great a distance from the bulk of the light-harvesting system to function in the transfer of excitation energy to neighboring complexes. Some core complexes are seen in contact, which increases the probability that excitons will find an open RC as seen in the organized arrangement of core complexes found in *Rba. sphaeroides* (Fig. 3). It can also be seen when comparing the monomeric *Rsp. photometricum* RC-LH1 core assemblies, that the L and M subunits are randomly oriented within the closed LH1 ellipses. This is in contrast to the uniformly oriented long-range order observed by

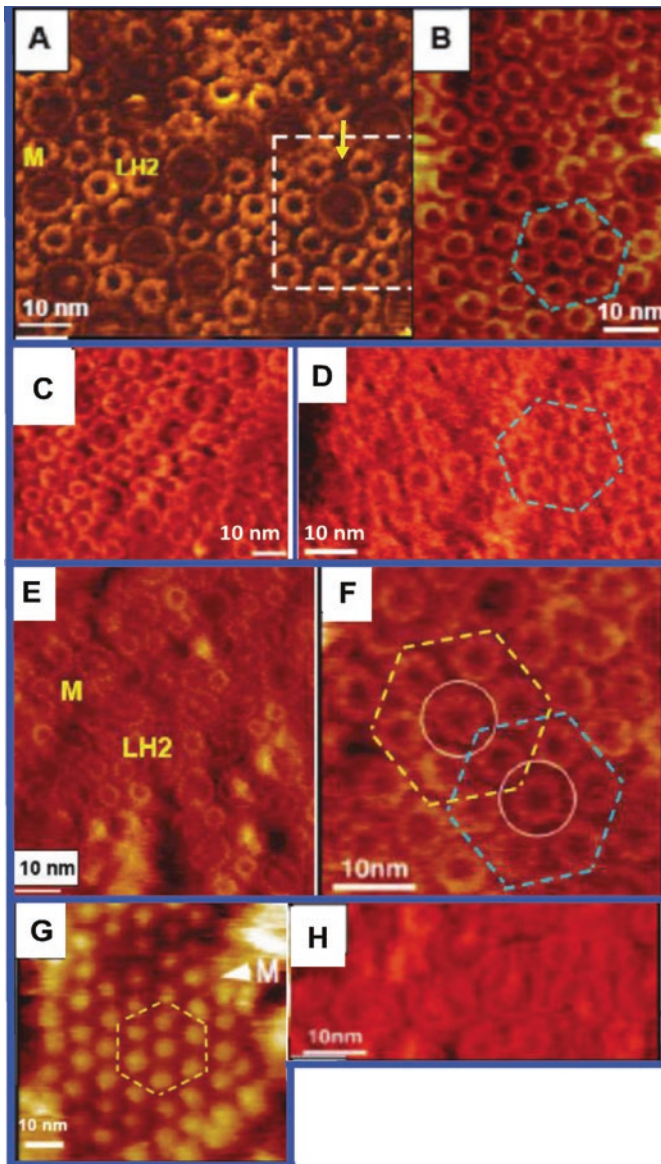


Fig. 7 High resolution AFM topographs of ICM preparations from purple bacteria with less regular arrangements of photosynthetic complexes. All topographs were obtained by contact mode AFM and unless indicated otherwise, in which the cytoplasm exposed portion of the RC-H subunit was removed by nanodissection with the cantilever tip, leaving subunits L and M exposed. (a) AFM topograph of membranes from *Rps. photometricum* grown at high light intensity (100 W/m^2) (Sturgis and Scheuring 2005). *M* monomeric RC-LH1 complex; *LH2* nonameric LH2 complex. The *arrow* delineates free lipid bilayer space between LH2 complexes, of possible functional importance in facilitating quinone-quinol exchange. The core complexes and LH2 rings are arranged randomly in an $\sim 1:3.5$ ratio. (b) AFM topograph of membranes from low-light-adapted ($10\text{--}20 \text{ W/m}^2$) cells. An area of mixed core complexes and LH2 rings is shown (overall core complex/LH2 ratio $\approx 1:7$); areas of paracrystalline hexagonal arrays of LH2 devoid of core complexes are also seen. (c) AFM topograph of flat membrane sheet from low-light adapted *Phs. molischianum*, showing region containing a mixture of LH2 and monomeric RC-LH1 core complexes

linear dichroism measurement for the dimeric RC-LH1 cores in wild-type *Rba. sphaeroides* (Frese et al. 2004). A heterogeneous distribution of LH2 ring sizes is also seen in *Rsp. photometricum* (Fig. 7d) (Scheuring et al. 2004), with the most abundant sizes ranged from octamers to decamers, while nonamers made up 70% of the total. This heterogeneity is believed to be a native feature of the LH2 assembly process and is accompanied by spectral heterogeneity, as absorption spectra of smaller complexes is gradually blue shifted relative to larger complexes. A correlation between decreasing aggregation state and blue shifts in Qy absorption and emission bands was observed previously (Westerhuis et al. 2002) in *Rba. sphaeroides* LH1 complexes of various sizes, arising from the dissociation of LH1 rings during a lithium dodecyl sulfate/polyacrylamide gel electrophoresis (see footnote 2). The natural variability in ring sizes observed for the *Rsp. photometricum* LH2 complex may represent a strategy for generating broader absorption spectra that maximize the collection of near-IR radiation, as well the optimization of photosynthetic complex packing in a heterogeneous membrane.

The ICM of *Phs. molischianum* also consists of thylakoid-like structures that give rise to flat membrane sheets suitable for contact mode AFM. The resulting topographs have revealed a supramolecular structure similar to that of *Rsp. photometricum*, in which LH complexes from cells grown at low light intensity are segregated into two structurally different types of domains. One domain consists of a mixture of core and octameric LH2 complexes, also in an approximate ratio of 1:3.5 (Fig. 7c), while the other forms a paracrystalline, hexagonally packed distribution of octameric LH2 rings (Fig. 7d) (Gonçalves et al. 2005). Since the structure of the *Phs. molischianum* LH2 ring has been solved to atomic resolution by X-ray crystallography (Koepeke et al. 1996), the atomic coordinates were used in an extensive effort to model adjacent in situ LH2 complexes within LH2-only domains. In this manner, it was possible to deduce the exact pigment distances between neighboring LH2 complexes within a native membrane environment. Accordingly, intercomplex distances between central Mg²⁺ atoms ranged from 16.3–28.3 Å, which are within the distance of ≤30 Å (Hu et al. 2002) necessary for efficient B800 BChl → B800 BChl and B850 BChl → B850 BChl energy transfer between adjacent complexes.



Fig. 7 (continued) (Gonçalves et al. 2005). Approximately 70% core complexes were connected to another core structure; separate core complexes were frequently surrounded by 6–7 LH2 complexes. **(d)** Antenna domain consisting of hexagonal paracrystalline arrays of LH2, devoid of core complexes (color scale in panels **d** and **e** = 5 nm). **(e)** AFM topograph of membranes from *Rps. palustris* grown at low light intensity (Scheuring et al. 2006) showing an area of mixed RC-LH1 and LH2 complexes randomly arranged in a ratio of ~1:3. **M** monomeric RC-LH1 core complex. **(f)** Coexisting, hexagonally packed LH2 lattices. **(g)** AFM topographs of membranes from high-light cells. Region of hexagonally packed, monomeric RC-LH1 core complexes; protruding RC-H subunit is seen at the core complex surface. **(h)** Chain of connected, monomeric RC-LH1 core complexes in membranes from high-light cells; H subunit has been removed by nanodissection, revealing underlying, randomly oriented L and M subunits. Panels **a** and **b** reproduced with permission from Scheuring and Sturgis (2005) Copyright 2005 American Association for the Advancement of Science. Panels **c** and **d** reproduced with permission from Gonçalves et al. (2005) Copyright 2005 Elsevier. Panels **e–h** reproduced with permission from Scheuring et al. (2006) Copyright 2006 Elsevier

The membranes of the metabolically versatile purple bacterium *Rps. palustris* are made up of a complex ICM structure consisting of infoldings of the CM that take the form of regular bundles of stacked, flattened thylakoid-like membrane sacs. Upon disruption, they also give rise to membrane sheets amenable to contact mode, high resolution AFM (Scheuring et al. 2006). The considerable variety of LH2 and RC-LH1 core complex organization and domain arrangement revealed by AFM (Fig. 7e–h) are a reflection of the complexity of CM/ICM organization into stacked and unstacked lamellar regions. In membranes from cells grown at low intensity illumination, randomly arranged, mixed domains of LH2 and RC-LH1 complexes (Fig. 7e) coexist with hexagonally packed LH2 areas (Fig. 7f), as seen for other purple bacteria containing lamellar ICM structures. It is likely that the mixed domains arise largely from proximal layers within the flat lamellar ICM folds, closest to cell periphery, while the LH2-only regions originate from the distal layers that are formed subsequently, as suggested by the size and density distribution of intramembrane particles observed in whole cells by freeze-fracture TEM (Varga and Staehelin 1983). This possibility is further supported by the sequence in which the complexes are assembled in the developing ICM (Koblížek et al. 2005).

Surprisingly, areas of smooth protein-free lipid bilayer were also observed in AFM topographs of membranes of cells grown both under high and low light intensity (not shown), while in those from high-light adapted cells, paracrystalline domains consisting entirely of hexagonally packed RC-LH1 core complexes were also found (Scheuring et al. 2006) (Fig. 7g), reminiscent of the organization existing in the ICM of *Bch. viridis* (Fig. 3a). Although the origin of the apparently pure lipid bilayer is unclear, the core-only membrane domains are likely to arise from the invaginating, stacked CM layer seen by freeze fracture to contain large, tightly packed particles (Varga and Staehelin 1983) which may reflect preferential core assembly (Koblížek et al. 2005) in these regions.

Other membrane domains in the preparations from the high light intensity grown cells were seen to contain core complexes arranged in chains along with a few LH2 complexes (Fig. 7h). Such an arrangement of randomly ordered RCs, seen within the core structures, would be expected to facilitate efficient energy trapping under conditions of high photon flux. AFM images also established an in situ structure for the core complex, confirming the model derived from X-ray crystallography data (Roszak et al. 2003) consisting of an elliptical LH1 15-mer of $\alpha\beta$ -heterodimers interrupted by a gap near the location presumed for W, a putative PufX homolog. The circular shape assumed by RC-LH1 complexes after RC nanodissection demonstrates that the inner RC assembly of L and M subunits induces the observed ellipticity upon the core complex (Scheuring et al. 2006).

Switching *Rps. palustris* from high to low light intensity resulted in modifications both in near-IR antennae absorption and in the size of peripheral antenna rings. Accordingly, LH4, a unique octameric peripheral antenna complex, with a single near-IR absorption band at 800-nm (Hartigan et al. 2002), regulated by a specific phytochrome (Evans et al. 2005; Giraud et al. 2005) is present under high intensity illumination in approximately the same amount as the nonameric B800-850 LH2 complex. On the other hand, a tenfold increase in the level of LH4 relative to that of the LH2 is found under low light.

Adaptation to Alterations in Ambient Light Intensity

Two-Component Regulatory Circuits Control the Acclimation to Changes in Light Intensity

Purple anoxygenic phototrophs overcome the physiological challenge of adapting to extremes of light intensity by adjusting their total functional absorption cross-section and charge separation capabilities. This requires major alterations in both proliferation of the ICM and the composition and total amount of the photosynthetic complexes ultimately residing there. Upon encountering extremely low light intensity, cells are confronted with the need to capture the few available photons. Consequently, regulatory mechanisms are brought into play that trigger a copious biosynthesis of the necessary photosynthetic pigments and apoproteins. The necessary control elements consist of interrelated two-component regulatory circuits that function at the transcriptional level to regulate the formation of both the pigment and polypeptide components of the LH and RC complexes in response to oxygen and light stimuli [see reviews by Bauer et al. (2008) and Klug and Masuda (2008) for detailed descriptions of these systems]. While the photosynthetic apparatus can only be formed at a sufficiently low oxygen tension (Cohen-Bazire et al. 1957), during photoheterotrophic growth, light serves to control the levels of pigment-protein components within the ICM, as required for the adaptation to changes in illumination intensity.

Among the regulatory protein components involved in light regulation of photosystem formation is PspR (designated as CrtJ in *Rba. capsulatus*, Ponnampalam and Bauer 1997), a redox-responsive transcription factor that acts as an aerobic gene repressor, controlling loci that encode the LH2 apoproteins, photosynthetic pigments and cytochromes (Gomelsky and Kaplan 1995a). PpsR forms part of the AppA/PspR antirepressor-repressor system where AppA integrates both redox and light signals through sensing the redox state of the quinone/quinol pool (Gomelsky and Kaplan 1995b). Moreover, AppA also serves as a blue-light photoreceptor (Masuda and Bauer 2002; Braatsch et al. 2002). PpsR coordinates aerobic repression of photosystem genes in conjunction with RegA, an anaerobic activator. In *Rba. capsulatus*, the CrtJ homolog³ of PpsR possesses an overlapping upstream binding site with RegA (Bowman et al. 1999), at which CrtJ outcompetes RegA~P in coordinating regulation of the *pucBA* structural genes that encode the LH2- β and - α polypeptides, respectively.

³The tetrapyrrole regulator CrtJ has recently been shown to interact with AerR, which serves as an antirepressor of CrtJ (Cheng et al. 2014). In this process, AerR binds to vitamin B₁₂ through a conserved His residue, demonstrating that B₁₂ serves both as a photoreceptor and a AerR cofactor in a light-dependent process that ultimately controls BChl biosynthesis (Cheng et al. 2016). In *Rba. sphaeroides*, PpaA serves as an AerA homolog in binding B₁₂ also in a light-dependent manner, and forms part of a AppA/AerA/PpaA antirepressor family. Among other purple bacteria, AerA is also found in *Rvx. gelatinosus* and *Rsp. centenum* (Vermeulen and Bauer 2015).

The redox regulation of the AppA/PspR system in *Rba. sphaeroides* has been shown to involve intramolecular disulfide bond formation in essential Cys residues of PpsR, maintained in a reduced state under anoxic conditions (Kim et al. 2006). The role of AppA as a blue light photoreceptor is mediated by a flavin within the BLUF (sensor of blue light using FAD) domain (Gomelsky and Klug 2002; Masuda and Bauer 2002). Blue light induces a flavin photocycle in which AppA undergoes a conformational change which disrupts AppA/PspR interactions, while under dark conditions, AppA converts active PspR tetramers to an inactive AppA(PspR)₂ form. It is also noteworthy that PspR is released by AppA under high intensity blue light, resulting in the repression of photosystem formation (Masuda and Bauer 2002). This may account for the relatively low cellular levels of the LH and RC complexes formed under high intensity white light (Woronowicz and Niederman 2010).

As a result of the action of these numerous regulatory systems, an extensive ICM network is formed under low light intensity, serving to increase the surface area available to the cell for collection of radiant energy and carrying out the charge separation and subsequent electron transfer reactions. Conversely, at high light intensities, considerably less ICM is formed (Adams and Hunter 2012) and the functional absorption cross-section is decreased by nearly two fold (Woronowicz et al. 2011). The available ICM surface area per cell, as estimated by Adams and Hunter (2012) from electron micrographs of thin cell sections, showed a 5.3-fold higher level in low-light grown cells in comparison to their high-light grown counterparts.

It is important to note that at high light intensity, it is necessary for the cell to avoid damage from excessive excitations and the consequent formation of the potentially harmful BChl triplet state, which initiates generation of singlet oxygen species capable of harming the photosynthetic apparatus. To counteract this, purple bacteria have evolved a mechanism for photoprotection in which carotenoid triplets quench both reactive BChl triplets and singlet oxygen through thermal dissipation (Monger et al. 1976; Cogdell et al. 2000). This requires an appropriate supramolecular organization of photosynthetic complexes in order to maximize the efficiency of photoprotection, and is reflected in the more efficient light-harvesting connectivity between the *Rba. sphaeroides* antenna complexes in high light cells as compared to that of low light cells, which collect far fewer excitations (Adams and Hunter 2012).

Alterations in Membrane Dynamics Accompanying Transition from High to Low Light Intensity as Analyzed by Fluorescence Induction/Relaxation and Time-Resolved Fluorescence Measurements

Fluorescence induction/relaxation analysis provides a method for the prompt assessment of several key parameters monitoring the photosynthetic competence of purple bacteria by means of the fluorescence emitted by the LH complexes upon undergoing excitation. These parameters include the quantum yield of the primary charge

separation, the rate of RC electron transfer turnover, and the functional absorption cross-section and connectivity of the photosynthetic apparatus (Fig. 8) (Koblížek et al. 2005; Woronowicz et al. 2011a, b, 2015; Niederman 2016). Closing of the RC by a strong 144 μ s pulse (single turnover flash, STF) results in a rise in fluorescence

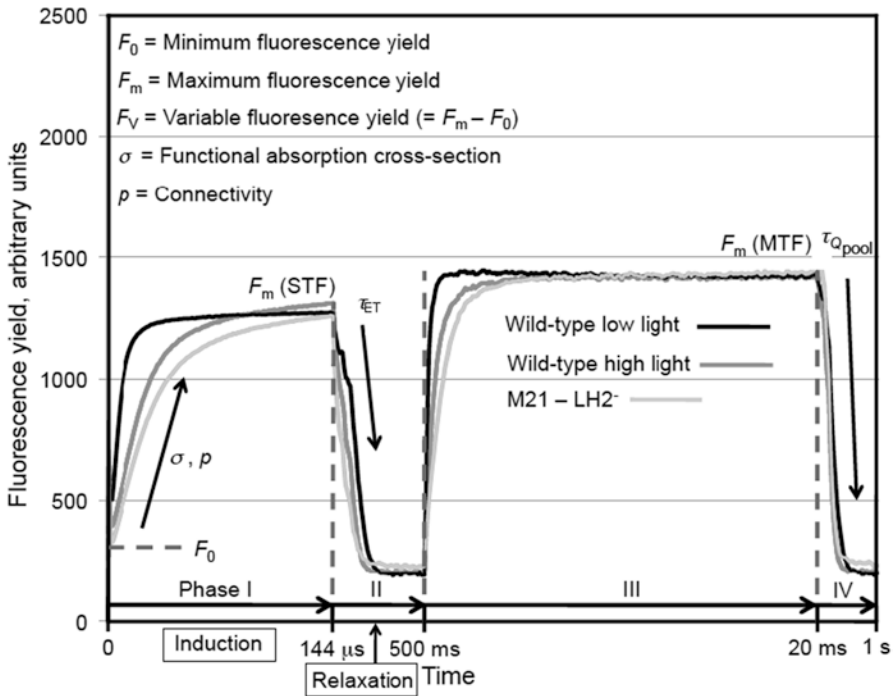


Fig. 8 Fluorescence kinetic transients from fluorescence induction/relaxation analysis of wild-type *Rba. sphaeroides* grown photoheterotrophically under high (1100 W/m²) and low (100 W/m²) light intensities in comparison to the LH2⁻ strain M21 grown semiaerobically (Woronowicz et al. 2011a). Samples were excited in the carotenoid region at 450 nm and fluorescence emission was detected at 880-nm by means of interference filters. Measurements made on whole cells were diluted typically in growth medium to ~30 nM BChl to produce transients in the linear range. Four phases can be distinguished: phase I, induction phase (strong pulse of 144 μ s duration), resulting in a single-turnover flash (STF), cumulatively saturating the photosystem to permit measurement of fluorescence induction from F_0 to F_M and estimation of the functional absorption cross-section (σ) and connectivity (ρ); phase II, relaxation phase, indirect modulated light applied to assess relaxation kinetics of the fluorescence yield on a 500 ms time scale, reflecting reopening of the RC; phase III, 20 ms flash inducing multiple turnovers to saturate the photosystem and quinone/quinol pool (MTF multiple turnover flash); and phase IV, indirect modulated light is applied to assess the kinetics of Q pool reoxidation on a 1 s time scale. Transients represent signal-averaged sets of 20 traces per sample, which minimizes the noise levels of the individual traces. Note disparity in rate of fluorescence induction between the wild-type cells grown at low and high light intensities. This reflects differences in functional absorption cross-section of LH complexes calculated from the slope of single turnover light saturation curve ($\sigma = 75 \text{ \AA}^2$ in low-light cells while value was 27 \AA^2 in the high-light cells, comparable to that of $\sigma = 35 \text{ \AA}^2$ in LH2-deficient mutant). Because the initial fluorescence increase is nearly exponential, the connectivity between the photosynthetic units, derived from the sigmoidicity of the initial rise, resulted in low values, ranging from 0.055 at time zero to 0.103 after 11 days at low light intensity in the experiment illustrated in Fig. 9

intensity from an initial level (F_0) to the maximal level (F_M) (phase I). The F_V/F_M ratio provides an estimate of the quantum yield of the primary photochemistry, where the variable fluorescence, $F_V = F_M - F_0$. The fluorescence rise provides information on the efficiency of light harvesting by the photosystem, where a rapid rise indicates a large and efficient light-harvesting antenna (designated by functional absorption cross-section (σ) in units of \AA^2) and a slow rise signifies a small or inefficient antenna with a low σ value. From the sigmoidicity of the fluorescence rise, the extent of excitation energy transfer among photosynthetic units (p , connectivity) is determined. Computer-assisted curve fitting is used for analysis of the fluorescence induction, as well as the subsequent phases of the analysis. Phase II follows reopening of the RCs; here, a weak modulated light elicits the relaxation phase of the fluorescence yield to provide an assessment of the rate of RC electron transfer turnover. For analysis, the relaxation phase is deconvoluted into three exponential decay kinetic components from which the electron transfer turnover rate (τ_{ET}) is calculated. In phase III, a strong 20 ms light pulse (multiple Turnover Flash, MTF) is applied for saturation of the photosystem and the quinone/quinol pool. Phase IV probes quinol pool reoxidation by applying a weak modulated light of 1 s duration.

In the Type II RC of oxygenic phototrophs (PSII), variable fluorescence is thought to mainly reflect the redox status of the primary stable electron acceptor Q_A (RC acceptor side) (Kolber et al. 1998). Recent studies on the nature of the fluorescence relaxation phase in *Rba. sphaeroides* (Kis et al. 2014; Asztalos et al. 2015), however, suggest a major role for the primary RC (P870) electron donor (*c*-type cytochrome), depending upon the nature of the RC association with the donor cytochrome. By using 808 nm laser-diode excitation of intact cells of *Rba. sphaeroides*, *Rsp. rubrum* and *Rvx. gelatinosus*, Asztalos et al. (2015) demonstrated complex, multi-exponential fluorescence decay kinetics. Longer excitations were correlated with the slowing of the relaxation phase, which was determined by the redox status, size, and accessibility of the reduced cytochrome c_2 and quinone/quinol pools for bacterial strains limited on either the donor or acceptor side of the RC, respectively. In *Rba. sphaeroides* and *Rsp. rubrum*, in which mobile cytochrome c_2 serves as the immediate P870 electron donor, relaxation is preferentially controlled by the re-reduction rate of the oxidized RC by the reduced cytochrome c_2 , and the acceptor side plays only a minor role. The similarities between the equilibrium redox titration on the RC donor side and that of fluorescence relaxation further suggested that P^+ reduction acts as the rate-limiting step the *Rba. sphaeroides* RC re-opening process. In contrast, for *Rvx. gelatinosus* where the cytochrome *c* subunit is physically attached to the RC, the fluorescence relaxation kinetics are determined on the acceptor side with the rate constant of $350 \mu\text{s}^{-1}$ for Q_A^- interquinone electron transfer as the determining factor.

Near-IR fluorescence induction/relaxation measurements as a means of assessing membrane dynamics have recently been applied to *Rba. sphaeroides* cells undergoing different developmental regimens (Woronowicz et al. 2011a, b; Kis et al. 2014). In studies by Woronowicz et al. (2011a, b) cells acclimating over an extended period to a shift from high to diffuse low intensity illumination were shown to undergo major alterations in membrane dynamics (Fig. 9). The quantum yield of the primary charge separation in the adapting cells gradually rose to values in excess of 0.8 by

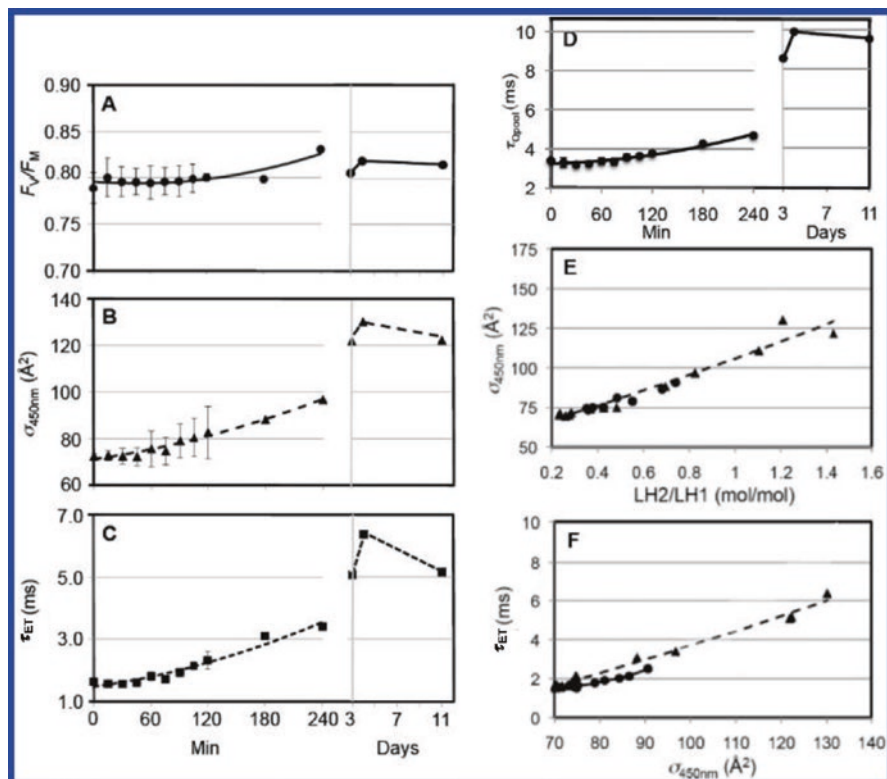


Fig. 9 Results of fluorescence induction/relaxation analyses of whole cells undergoing long-term adaptation to a shift from high light to weak diffuse illumination (Woronowicz et al. 2011a). Values were calculated from kinetic transients obtained at 880 nm after excitation at 450 nm; analyzed transients represent signal-averaged sets of 20 traces per sample, resulting in minimized noise levels in individual traces. (a) Quantum yield of primary charge separation (F_V/F_M) vs. adaptation time course. Values over the first 2 h in this panel and in panels b and c are averaged with an initial 2-h experiment, which monitored early trends that were subsequently assessed over the extended time course. (b) Functional absorption cross-sections ($\sigma_{450\text{nm}}$). (c) Reaction center electron transfer turnover rates (τ_{ET}). (d) Rates of quinone/quinol pool reoxidation (τ_{Qpool}). (e) Functional absorption cross-sections ($\sigma_{450\text{nm}}$) vs. molar LH2/LH1 ratios. (f) Reaction center electron transfer turnover rates (τ_{ET}) vs. functional absorption cross-sections ($\sigma_{450\text{nm}}$). In panel e and f, *closed circles* denote values from initial 2-h experiment; *closed triangles*, values from experiment with extended time course. Lines through points in panels e and f and over first 4 h in panels a–c represent polynomial fits. Error bars in panels a–c indicate standard deviation of measurements from the two different experiments

4 h, essentially leveling off over the subsequent extended time course (Fig. 9a). The $\sigma_{450\text{nm}}$ values gradually rose during the initial 4 h, ultimately leveling off at $\sim 130 \text{ \AA}^2$ by the fourth day (Fig. 9b), which represents a near doubling in the functional absorption cross-section relative to the value reported in the legend of Fig. 8 for cells adapting to direct low light intensity. A gradual fourfold slowing of τ_{ET} was observed (Fig. 9c), largely mirroring the rise in σ , and confirming the previous observations seen in steady-state cells during adaptation to reduced oxygen tension (Koblížek et al. 2005).

Figure 9d shows a gradual slowing of nearly threefold in the rate of reoxidation of the quinol pool, while in Fig. 9e, a near linear relation between the size of the functional absorption cross-section and the LH2/LH1 molar ratios was observed. This relationship is expected since both parameters reflect relative increases in the size of the LH2 antenna per RC, as the size of LH1 per RC remains constant, making up the core of the photosynthetic unit. In Fig. 9f, a plot of the slowing of τ_{QA} vs. the rising $\sigma_{450\text{ nm}}$ also shows a near linear relation. This has been interpreted to reflect an imposition of constraints on electron transfer between the RC and cytochrome bc_1 complexes as the membrane bilayer becomes densely packed with accumulating LH2 rings, that are seen to ultimately form LH2 only domains in AFM (Bahatyrova et al. 2004a; Adams and Hunter 2012). Bilayer crowding by LH2 also offers an explanation for the ~threefold slowing of quinol pool reoxidation by the bc_1 complex over the first 4 days of the acclimation process (Fig. 1d). These studies have demonstrated that fluorescence induction/relaxation measurements, when taken together with AFM surface views of alterations in membrane structure, are valuable probes of the membrane dynamics that accompany the membrane remodeling processes.

While the slowing of the τ_{ET} as a function of increasing σ value was attributed initially to the imposition of constraints upon the free diffusion of ubiquinone redox species between the RC and bc_1 complex (RC acceptor side kinetics) (Woronowicz et al. 2011a, b) as noted above, a somewhat more complex picture has been suggested from the recent ICM development studies on *Rba. sphaeroides* by Kis et al. (2014). In cells adapting from chemoheterotrophic to photoheterotrophic growth conditions under constant illumination, donor side electron transfer reactions dominated the relaxation kinetics after a single-turnover flash, while contributions on the acceptor side were enhanced only after multiple turnover flashes. It was concluded that the slowing of electron transfer turnover during development of the ICM results from changes on the RC donor side in which an increased distance for electron flow occurs in the cytochrome c_2 periplasmic diffusion pathway between the RC and bc_1 complexes. This accounts for the initial relaxation kinetics when the developed (mature) membrane becomes more densely packed with LH2 rings. On the other hand, slow reoxidation of the quinol pool reflected contributions on the acceptor side that are enhanced after long excitation (multiple turnovers). This is also compatible with our results (Woronowicz et al. 2011a, b), which showed a slowing of quinol pool oxidation with increasing LH2 levels after multiple turnover flashes. However, AFM images of chromatophore patches from an *Rba. sphaeroides* LH2-only strain have formed the basis for a functional model of the ICM (chromatophore) vesicles that are formed in this mutant (Olsen et al. 2008). In this model, it is proposed that the space between LH2 complexes in these LH2-only membranes is sufficient to permit the free diffusion of quinone/quinol species, while still maintaining efficient excitation energy transfer. Clearly, more experimental effort needs to be devoted to the question of whether quinone redox species flow is impeded by the presence of hexagonally packed LH2-only domains.

Chromatophore fractions isolated from *Rba. sphaeroides* at various intervals during the transition to low ambient light intensity were recently subjected to time-resolved fluorescence spectroscopy to assess alterations in the pathway and kinetics and energy transfer (Driscoll et al. 2014). This study was prompted by the finding

that the total functional absorption cross-section of the antenna is markedly expanded by the increasing levels of LH2 (Fig. 9e), which would, in principle, be consistent with the idea that the proliferation in σ would assure that extra energy is transferred to the RC in order to compensate for the low illumination level. Since the LH2 accumulating during low-light adaptation is responsible for the increases in σ , one could envision that the new complexes would simply add to the existing LH2 pool, accounting for the elevated σ values. On the other hand, as seen in Figs. 3a and 6b, AFM topographs of chromatophores show a heterogeneity in LH2 distribution, with two kinds of organization, consisting of areas in which LH2 is largely intercalated between interconnected networks of dimeric RC-LH1 cores (Fig. 3a), coexisting with large ordered LH2-only domains when cells are grown at lowlight intensity (Fig. 6b) (Adams and Hunter 2012). Only a minor portion of the new LH2 complexes appear in conjunction with RC-LH1 networks during the acclimation process, while the majority of de novo formed LH2 appears in LH2-only domains. It is thought that these more distal LH2 domains form the light-responsive complement of LH2 antenna (Bahatyrova et al. 2004a). As detailed above, recent studies have suggested that this LH2 arrangement is apparently responsible for slowing the turnover rate of RC electron transfer, while the work of Magis et al. (2010) indicates the extra pigments provided by LH2 are principally involved in photoprotection under excessively high light excitation. Since the functionality of the distal LH2-only pools was thus poorly understood, a picosecond time-resolved fluorescence spectroscopy study was embarked upon to assess the adjustments in both the kinetics and the pathway of excitation energy transfer that occurs during the low light acclimation process.

Although from an evolutionary standpoint, it seemed likely that the increased levels of LH2 formed during the transition to low light intensity served to increase overall energy transmission to the RC, the picosecond time-resolved fluorescence results did not support this possibility (Driscoll et al. 2014). Instead, fluorescence lifetime measurements and an analysis in terms of energy transfer within LH2 as well as between LH2 and LH1 (Fig. 10) showed that during the measured adaptation time period, only a portion of the newly formed LH2 are well connected to LH1 and the RC. Ultimately, the majority of the additional LH2 fluorescence decays with a lifetime of 1 ns, comparable to that of the isolated LH2 complex. This is attributed to the presence of large LH2-only domains as discussed above, that have been observed by AFM in *Rba. sphaeroides* chromatophores. These AFM topographs provide structural support for the existence of pools of partially connected LH2 complexes. LH2-only domains represent the light-responsive antenna complement formed after a switch in growth conditions from high to low illumination, while the remaining LH2 complexes occupy membrane regions containing mixtures of LH2 and LH1-RC core complexes. A schematic representation of the functional arrangement of the photosynthetic complexes during acclimation from high to low intensity illumination is shown in Fig. 11. This scheme is based on simulations in which time constants were obtained that were consistent with the experimental results. These simulated time constants gave the following values: (1) a fast component of ~30 ps, representing a decay in the LH2 fluorescence and a rise in LH1; (2) a component of

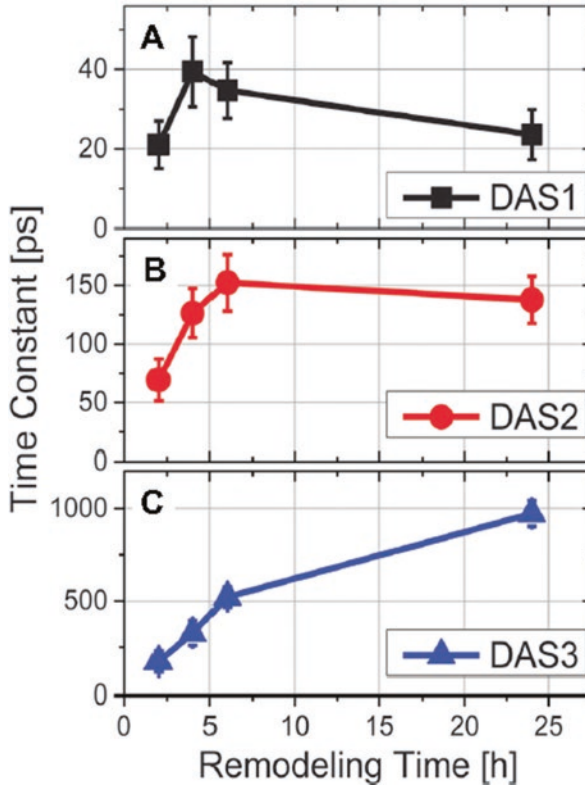


Fig. 10 Time constants as a function of membrane remodeling time (Driscoll et al. 2014). (a) Decay-associated spectrum (DAS) 1, (b) DAS2 and (c) DAS3 corresponding to the short (20–30 ps), middle (70–150 ps) and long (170 ps–1 ns) decay components, respectively. The time-resolved fluorescence emission spectra were recorded as a function of delay time using a streak camera system as described by Driscoll et al. (2014). Time-resolved spectra were recorded over a wavelength range of 830–940 nm, and an 800 ps time window. The full-width-at-half-maximum of the instrument response function was ~10 ps. The spectra were expressed as a function of decay time by globally fitting to the sum of exponential decays using the least number of exponential decay components statistically required to yield the resulting DAS

100–150 ps, dominated by LH1 fluorescence; and (3) a long-lived component dominated by LH2 which ranged from 170–200 ps prior to inclusion of LH2-only pools and 200–1000 ps thereafter. Overall, these time-resolved fluorescence spectroscopy measurements provide a powerful tool for exploring interactions between LH complex in the membranes developing during acclimation to reduced levels of illumination and contribute to the understanding of the higher order structure and function of this model energy transducing membrane system. In addition, this study also provided functional insights into strategies evolved by purple bacteria for adjusting their photosynthetic apparatus for the harvesting of light energy.

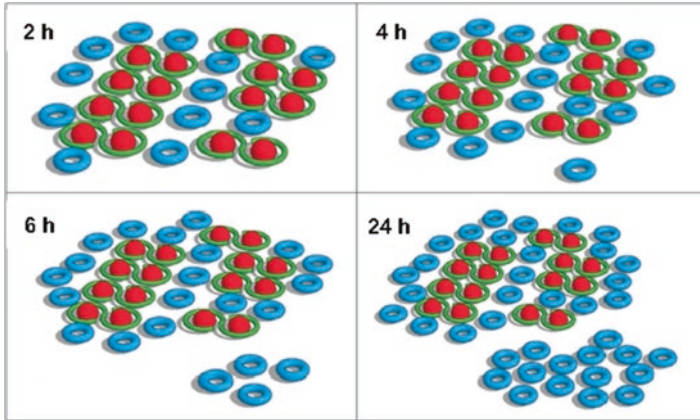


Fig. 11 Schematic view of the physical relationship between the photosynthetic complexes showing their accumulation as a function of increasing time of adaptation to low light intensity (Driscoll et al. 2014). The ratio of LH2:RC-LH1, as well as the ratio of the two different pools of LH2 complexes were used in the simulating of this process. The system was simulated using of a random walk energy transfer network in which all RCs were assumed to be closed. For the 4-, 6-, and 24-h simulations, a portion of the LH2 complexes were assumed to reside in the distal LH2-only pools, not as well connected to LH1 as the proximal LH2. The ratios of LH2/LH1 used in the simulations were those from absorption spectra of the samples, using known extinction coefficients in the calculation of the relative concentrations of LH2 and LH1

Structural and Functional Proteomics of Intracytoplasmic Membrane Assembly

Rba. sphaeroides also provides a unique paradigm for structural and functional proteomics studies of the ICM assembly process, insofar as the key components of the proteome can be temporally expressed and spatially localized within the internal membrane structure of the cell. Temporal expression of the key protein complexes, as well as factors essential for their assembly within the developing membrane system, can be readily controlled in cells undergoing both adaptation to reduced light intensity (Woronowicz and Niederman 2010; Woronowicz et al. 2011a, b) and the gratuitous induction of ICM formation in chemoheterotrophically grown cells when transferred to semiaerobic conditions (Koblížek et al. 2005; Woronowicz et al. 2011b). The membrane development process can also be spatially localized to both the growth initiation sites of the invaginating CM and fully developed ICM vesicles, isolated as respective upper pigmented and chromatophore bands during by rate-zone sedimentation on sucrose density gradients (Niederman et al. 1979). Accordingly, this permits the assessment of the proteomes arising from distinct membrane domains at various ICM developmental stages. These studies were facilitated further by non-denaturing clear native gel electrophoresis in which the membrane fractions gave rise to four pigmented bands (Fig. 12). The top band contained the RC-LH1 core complex while the LH2 antenna was found in the bottom band as

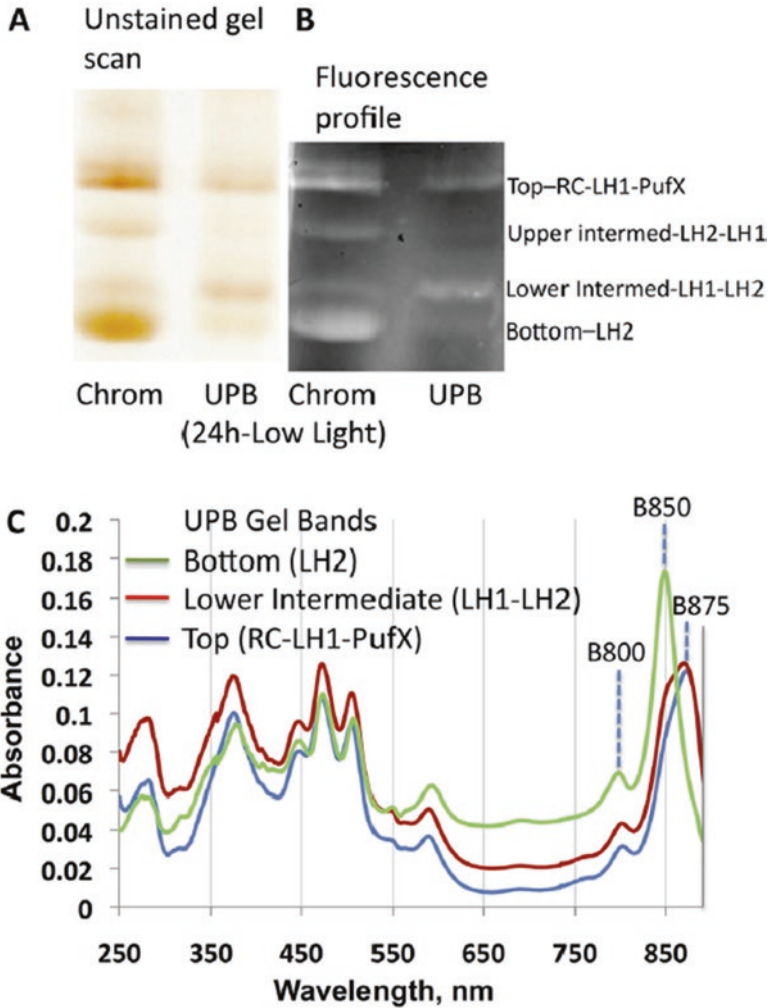


Fig. 12 Separation of intact pigment-protein complexes by clear native electrophoresis of digitonin-solubilized membrane fractions (Woronowicz et al. 2015). Cells were subjected to a 24-h adaptation from high (1100 W/m^2) to low intensity illumination (100 W/m^2). Upper pigmented and chromatophore fractions were isolated by rate-zone sedimentation and upper band was further purified by a two-phase partitioning procedure (Woronowicz and Niederman 2010). The purified membrane preparations were solubilized with digitonin (2 g/g protein), applied to gel slabs formed with a 5–10% polyacrylamide gradient and subjected to clear native electrophoresis. (a) *Left*, scan of unstained gel obtained with a visible light scanner; (b) Image obtained with Typhoon fluorescence scanner in which pigmented proteins gave rise to the white bands arising from profile of unstained gel observed against plastic film providing uniform background emission at 670-nm; pigments absorbing at the excitation wavelength (488 nm) are responsible for the white images. (c) Absorption spectra obtained directly on indicated gel slices. The high level of spectral purity of the top (RC-LH1-PufX) band is indicated by the presence of the LH1 Q_y absorption band at 875 nm and the RC monomeric BChl band at 802 nm, and for the bottom (LH2) band by the maxima at 800 and 850, arising from the Q_y bands of the respective LH2 monomeric and dimeric BChl components. An LH1 enrichment is also seen in the lower intermediate (LH1-LH2) band.

established by the absorption spectra shown in panel C. Two bands of intermediate migration are also observed which exhibited distinct associations of the LH2 and the core complexes, such that the upper bands was enriched in LH2 relative to LH1, while the reverse was found for the lower band. Proteomic analyses of the gel bands arising from chromatophores revealed developmental changes including increasing levels of LH2 polypeptides relative to those of core RC-LH1 complex as ICM development proceeded, as well as a large array of other associated proteins including high spectral counts for the F_1F_0 -ATP synthase subunits and the cytochrome bc_1 complex (Woronowicz et al. 2011a, 2012, 2013, 2015).

These procedures have been applied to the characterization of the chromatophore proteome from cells during adaptation to low light intensity (Woronowicz and Niederman 2010) and for comparisons of the chromatophore and upper pigmented band proteomes from both low light adapting cells (Woronowicz et al. 2011a, 2012) and those undergoing semiaerobic ICM induction (Woronowicz et al. 2015). A detailed review of these structural and functional proteomics studies of ICM assembly can be found in Woronowicz et al. (2013) and major findings were as follows: (1) In comparison to chromatophores, the RC-LH1-containing CNE gel bands from upper pigmented band were enriched in CM markers, including electron transfer and membrane transport proteins, thereby confirming the origin of the upper pigmented band in part from peripheral respiratory membranes; (2) These gel bands were also enriched in general membrane assembly factors (viz., preprotein translocases YidC, YajC and SecY, bacterial type 1 signal peptidase and the twin arg translocation subunit TatA, confirming that upper pigmented band membranes also serve as sites of active CM invagination in which preferential assembly of the RC-LH1 complex occurs; (3) In the chromatophore fractions from low-light adapting cells, high spectral counts were observed for an apparent soluble protein of unknown function designated as RSP6142, that were correlated with increasing levels of LH2, suggesting that this putative protein plays a transient role in the assembly and/or function of the LH2 antenna; (4) The universal stress protein UspA, together with high levels of the heat-shock chaperonin GroEL was shown to accumulate in cells undergoing low-aeration ICM induction (Woronowicz et al. 2015) and adaptation from high light intensity to low intensity diffuse light (Woronowicz et al. 2011a); (5) These cells were nevertheless still capable of forming a robust functional photosynthetic apparatus, even though these membrane development regimens represent conditions of challenged cell viability; (6) As noted above, functional changes associated with these proteomic changes during membrane development as assessed in fluorescence induction/relaxation measurements demonstrated a direct relationship between the slowing of the rate of RC electron transfer turnover and the growth of



Fig. 12 (continued) The differences in carotenoid content between the RC-LH1 core complex and LH2 reflects the respective BChl/carotenoid molar ratios near 1.0 for LH1 and ~2.0 for LH2 (Hunter et al. 1988). Note also the expected blueshift in the position of the red-most carotenoid absorption (0–0 vibrational) band in LH1 relative to LH2 (respective absorption maxima at 505 and 508 nm). The relatively low levels of UV absorbance indicate extensive purification of these complexes on a protein basis. *UPB* upper pigmented band

the functional absorption cross-section due to increased LH2 levels that were correlated to differences in the AFM profiles between high and low light chromatophores (Adams and Hunter 2012); (7) Native AFM topographs taken together with these proteomic changes during membrane development showed that in low light ICM, much of the LH2 was present in densely packed LH2-only domains; (8) These structural changes in supramolecular organization could account for the blocking of both the flow of UQ redox species and the soluble cytochrome c_2 periplasmic diffusion pathway, thereby slowing the RC electron transfer turnover rate.

Systems Biology Approach for Determining ATP Production Rate and Energy Conversion Efficiency in Purple Bacteria

Systems biology represents an all-inclusive paradigm for examining dynamics and structure as related to the functioning of both cells and whole organisms, together with their robustness, rather than merely characterizing their isolated cellular components (Kitona 2002). Basically, this approach stipulates that the networks making up a living organism are more than the sum of its individual parts. Biological approaches are integrated with other scientific disciplines such as computer science, engineering, bioinformatics, and physics. As a result, major breakthroughs using *in silico* approaches have contributed to the further understanding of how distinct systems within an organisms dynamically interact.

Such a high-level *in silico* systems approach has recently been applied to the characterization of the chromatophore vesicles of purple bacteria, involved in the efficient conversion of solar energy into ATP synthesis, and typically operating in low-light environments. By first constructing an atomic-level structural model of a complete chromatophore vesicle from *Rba. sphaeroides* adapted to low light-intensity (Fig. 13), Sener et al. (2016) succeeded in modeling the position of every atom of all the proteins components of known structure identified by mass spectroscopy, as well as the mutual functioning among these >100 protein complexes contained within the vesicle. This information was used to examine the manner in which energy transfer and conversion occur. The sequence of steps involved in

Fig. 13 (continued) three stages of energy conversion by the chromatophore after the initial absorption of photons: (1) reduction of the Q pool through the light harvesting and electron transfer reactions. The production quinol by the RC stemming from excitation transfer; (2) diffusion of quinone/quinol to bc_1 complex where quinols are exchanged for quinones (thereby generating a transmembrane electrochemical proton gradient) as well as generating the diffusive motion of cytochrome c_2 inside the chromatophore shuttling single electrons from the bc_1 to the RC complex; (3) utilization of electrochemical proton gradient for the synthesis of ATP. The stoichiometry of the components is also shown. **(d)** The chromatophore components where stages (1–3) occur. They include the LH2 (green), LH1 (red), RC (blue), bc_1 (purple) and ATPase (brown) complexes shown embedded in the lipid phase. Reproduced from Sener et al. (2016) Copyright 2016 (<http://creativecommons.org/licenses/>)

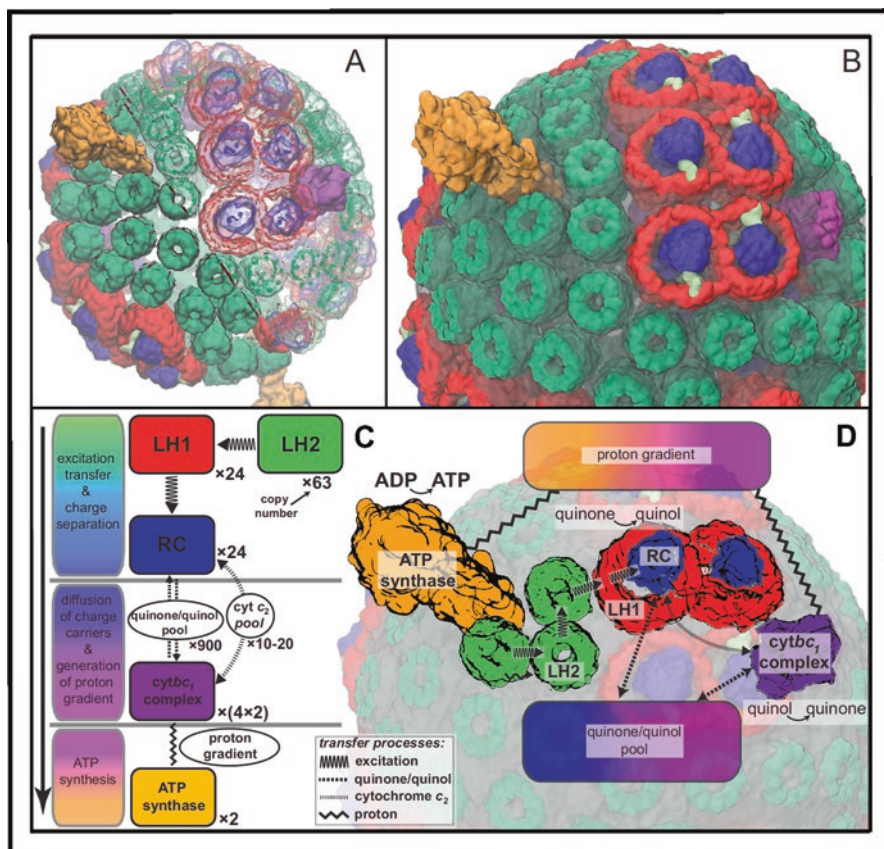


Fig. 13 Structural model of a chromatophore vesicle from *Rba. sphaeroides* at atomic resolution. (a) A chromatophore vesicle is depicted from cells grown at low light intensity and is based upon data obtained from AFM, transmission electron microscopy, X-ray crystallography, mass spectroscopy, proteomics and optical spectroscopy methods (Cartron et al. 2014). The inner diameter of the vesicle is 50 nm. The constructed model is a modification of that reported by Cartron et al. (2014), consisting of 63 LH2 complexes (green), 11 dimeric and 2 monomeric RC-LH1-PufX complexes (LH1, red; RC, blue; PufX, lime), 4 cytochrome *bc*₁ complexes (magenta), and 2 ATP synthase molecules (orange), as well as 2469 BChls and 1542 carotenoids; a surface representation of proteins is shown. LH and RC proteins in right half of vesicle are represented in a transparent form to reveal BChls which are shown by porphyrin rings. Their visualization requires magnification of the Figure. For the LH2 complex, both the B800 (outer monomeric ring) and B850 (inner dimeric ring) BChls are depicted. Note that the within the dimeric LH1-RC-PufX complexes, the RC chlorin molecules assume a non-random orientation with their porphyrin rings all aligned in the same manner. This was discovered by linear dichroism measurements of oriented chromatophore membranes (Frese et al. 2004), in which PufX serves as an RC-LH1 dimerizing protein (Francia et al. 1999) that induces order upon the core complexes. This PufX-induced native long-range organization of core arrays is shown to coexists with large domains of LH2 complexes with an alignment of much of the LH2 into rows located proximal to the dimeric LH1-RC-PufX cores. (b) Magnified view of chromatophore membrane, showing surface views of protein complexes together with transparent head groups of the phospholipid molecules making up the membrane bilayer. The membrane consists of 16,000 lipids and contains the mobile, lipid soluble quinone/quinol pool of ~900 molecules. Note the PufX protein interspersed near openings in the LH1 rings where it is thought to facilitate ubiquinone/ubiquinol exchange (Barz et al. 1995). (c) Depiction of processes comprising the

energy conversion was utilized in the calculation of the overall energy conversion efficiency, i.e., the amount of light energy impinging on the cell which is ultimately stored as ATP. Accordingly, the steady-state rate of ATP production as a function of the incident light intensity was calculated after determining that the turnover of quinol molecules by the *bc*₁ complex was rate limiting, under the assumption that a quasi-stationary state depends upon a quinone/quinol pool size ~900 molecules. It was found that under an illumination level equivalent to 1% of available full sunlight, the vesicle has an ATP production rate of 82 ATP molecules/s. The energy conversion efficiency for ATP synthesis at an illumination level equivalent to 1–5% full sunlight was ascertained to be 0.12–0.04, respectively. This vesicle stoichiometry which is evolutionarily adapted to the low intensity illumination found in the natural purple bacterial habitat is clearly suboptimal for the steady-state turnover of ATP production, but is instead adapted for the photoprotective mechanisms that safeguard against excess illuminations. In future, such a systems biology approaches will be applicable to a description of the overall energy conversion efficiency in the more complex photosynthetic apparatus of the oxygenic phototrophs.

Acknowledgments I thank Prof. Kamil Woronowicz, Prof. Raoul Frese, Oluwatobi B. Olubanjo, and Daniel Sha for their contributions to the studies reported here that were conducted in my laboratory. I am also grateful to Prof. Peter Lobel and Dr. Haiyan Zheng for conducting proteomic analyses and assisting in data validation. Supported by grants to R.A.N. from the U. S. Department of Energy, Grant No. DE-FG02-08ER15957 from the Chemical Sciences, Geosciences and Biosciences Division, Office of Basic Energy Sciences and the National Science Foundation (Subaward No. 12-764).

References

- Adams PG, Hunter CN (2012) Adaptation of intracytoplasmic membranes to altered light intensity in *Rhodobacter sphaeroides*. *Biochim Biophys Acta* 1817:1616–1627
- Allen JP, Feher G, Yeates TO, Komiya H, Rees DC (1987) Structure of the reaction center from *Rhodobacter sphaeroides* R-26: the protein subunits. *Proc Natl Acad Sci USA* 84:6162–6166
- Asztalos E, Sipka G, Maróti P (2015) Fluorescence relaxation in intact cells of photosynthetic bacteria: donor and acceptor side limitations of reopening of the reaction center. *Photosynth Res* 124:31–44
- Axelrod HL, Okamura M (2005) The structure and function of the cytochrome c2: Reaction center electron transfer complex from *Rhodobacter sphaeroides*. *Photosynth Res* 85:101–114
- Bahatyrova S, Frese RN, Siebert CA, van der Werf KO, van Grondelle R, Niederman RA, Bullough PA, Otto C, Olsen JD, Hunter CN (2004a) The native architecture of a photosynthetic membrane. *Nature* 430:1058–1062
- Bahatyrova S, Frese RN, van der Werf KO, Hunter CN, Olsen JD (2004b) Flexibility and size heterogeneity of the LH1 light-harvesting complex revealed by atomic force microscopy: functional significance for bacterial photosynthesis. *J Biol Chem* 279:21327–21333
- Barz WP, Verméglio A, Francia F, Venturoli G, Melandri BA, Oesterhelt D (1995) Role of the PufX protein in photosynthetic growth of *Rhodobacter sphaeroides*. 2. PufX is required for efficient ubiquinone/ubiquinol exchange between the reaction center Q site and the cytochrome bc complex. *Biochemistry* 34:15248–15258

- Bauer C, Setterdahl A, Wu J, Robinson B (2008) Regulation of gene expression in response to oxygen tension. In: Hunter CN, Daldal F, Thurnauer MC, Beatty JT (eds) *The purple phototrophic bacteria*. Springer, Dordrecht, pp 707–725
- Blankenship RE (2014) *Molecular mechanisms of photosynthesis*, 2nd edn. Wiley, Indianapolis
- Bowman WC, Du S, Bauer CE, Kranz RG (1999) In vitro activation and repression of photosynthesis gene transcription in *Rhodobacter capsulatus*. *Mol Microbiol* 33:429–437
- Braatsch S, Gomelsky M, Kuphal S, Klug G (2002) A single flavoprotein, AppA, integrates both redox and light signals in *Rhodobacter sphaeroides*. *Mol Microbiol* 45:827–836
- Cartron ML, Olsen JD, Sener M, Jackson PJ, Brindley AA, Qian P, Dickman MJ, Leggett GJ, Schulten K, Hunter CN (2014) Integration of energy and electron transfer processes in the photosynthetic membrane of *Rhodobacter sphaeroides*. *Biochim Biophys Acta* 1837:1769–1780
- Cheng Z, Li K, Hammad LA, Karty JA, Bauer CE (2014) Vitamin B12 regulates photosystem gene expression via the CrtJ antirepressor AerR in *Rhodobacter capsulatus*. *Mol Microbiol* 91(4):649–664
- Cheng Z, Yamamoto H, Bauer CE (2016) Cobalamin's (vitamin B12) surprising function as a photoreceptor. *Trends Biochem Sci* 41:647–650
- Cogdell RJ, Roszak AW (2014) Structural biology: the purple heart of photosynthesis. *Nature* 508:196–197
- Cogdell RJ, Howard TD, Bittl R, Schlodder E, Geisenheimer I, Lubitz W (2000) How carotenoids protect bacterial photosynthesis. *Philos Trans R Soc Lond B Biol Sci* 355:1345–1349
- Cohen-Bazire G, Sistrom WR, Stanier RY (1957) Kinetic studies of pigment synthesis by non-sulfur purple bacteria. *J Cell Comp Physiol* 49:25–68
- Deisenhofer J, Michel H (1989) Nobel lecture. The photosynthetic reaction centre from the purple bacterium *Rhodospseudomonas viridis*. *EMBO J* 8:2149–2170
- Deisenhofer J, Epp O, Miki K, Huber R, Michel H (1985) Structure of the protein subunits in the photosynthetic reaction centre of *Rhodospseudomonas viridis* at 3Å resolution. *Nature* 318:618–624
- Driscoll B, Lunceford C, Lin S, Woronowicz K, Niederman RA, Woodbury NW (2014) Energy transfer properties of *Rhodobacter sphaeroides* chromatophores during adaptation to low light intensity. *Phys Chem Chem Phys* 16:17133–17141
- Evans K, Fordham-Skelton AP, Mistry H, Reynolds CD, Lawless AM, Papiz MZ (2005) A bacteriophytochrome regulates the synthesis of LH4 complexes in *Rhodospseudomonas palustris*. *Photosynth Res* 85:169–180
- Feniouk BA, Junge W (2008) Proton translocation and ATP synthesis by the F_0F_1 -ATPase of purple bacteria. In: Hunter CN, Daldal F, Thurnauer MC, Beatty JT (eds) *The purple phototrophic bacteria*. Springer, Dordrecht, pp 475–493
- Francia F, Wang J, Venturoli G, Melandri BA, Barz WP, Oesterhelt D (1999) The reaction center–LH1 antenna complex of *Rhodobacter sphaeroides* contains one PufX molecule which is involved in dimerization of this complex. *Biochemistry* 38:6834–6845
- Francia F, Dezi M, Rebecchi A, Mallardi A, Palazzo G, Melandri BA, Venturoli G (2004) Light-harvesting complex 1 stabilizes P⁺QB⁻ charge separation in reaction centers of *Rhodobacter sphaeroides*. *Biochemistry* 43:14199–14210
- Frese RN, Siebert CA, Niederman RA, Hunter CN, Otto C, van Grondelle R (2004) The long-range organization of a native photosynthetic membrane. *Proc Natl Acad Sci U S A* 101:17994–17999
- Georgakopoulou S, van der Zwan G, Olsen JD, Hunter CN, Niederman RA, van Grondelle R (2006) Investigation of the effects of different carotenoids on the absorption and CD signals of light harvesting 1 complexes. *J Phys Chem B* 110:3354–3361
- Giraud E, Zappa S, Vuillet L, Adriano JM, Hannibal L, Fardoux J, Berthomieu C, Bouyer P, Pignol D, Verméglio A (2005) A new type of bacteriophytochrome acts in tandem with a classical bacteriophytochrome to control the antennae synthesis in *Rhodospseudomonas palustris*. *J Biol Chem* 280:32389–32397
- Gomelsky M, Kaplan S (1995a) Genetic evidence that PpsR from *Rhodobacter sphaeroides* 2.4.1 functions as a repressor of *puc* and *bchF* expression. *J Bacteriol* 177:1634–1637

- Gomelsky M, Kaplan S (1995b) *aapA*, a novel gene encoding a trans-acting factor involved in the regulation of photosynthesis gene expression in *Rhodobacter sphaeroides* 2.4.1. *J Bacteriol* 177:4609–4618
- Gomelsky M, Klug G (2002) BLUF: a novel FAD-binding domain involved in sensory transduction in microorganisms. *Trends Biochem Sci* 27:497–500
- Gonçalves RP, Bernadac A, Sturgis JN, Scheuring S (2005) Architecture of the native photosynthetic apparatus of *Phaeospirillum molischianum*. *J Struct Biol* 152:221–228
- Gordeliy V (2017) Novel phototrophs - proteorhodopsin: structure-function aspects. Hallenbeck PC (ed) *Modern topics in the phototrophic prokaryotes: environmental and applied aspects*, vol 1, pp XX
- Hartigan N, Tharia HA, Sweeney F, Lawless AM, Papiz MZ (2002) The 7.5-Å electron density and spectroscopic properties of a novel low-light B800 LH2 from *Rhodospseudomonas palustris*. *Biophys J* 82:963–977
- Hu XC, Ritz T, Damjanovic A, Autenrieth F, Schulten K (2002) Photosynthetic apparatus of purple bacteria. *Q Rev Biophys* 35:1–62
- Hunter CN, Pennoyer JD, Sturgis JN, Farrelly D, Niederman RA (1988) Oligomerization states and associations of light-harvesting pigment-protein complexes of *Rhodobacter sphaeroides* as analyzed by lithium dodecyl sulfate-polyacrylamide gel electrophoresis. *Biochemistry* 27:3459–3467
- Kim SK, Mason JT, Knaff DB, Bauer CE, Setterdahl AT (2006) Redox properties of the *Rhodobacter sphaeroides* transcriptional regulatory proteins PpsR and AppA. *Photosynth Res* 89:89–98
- Kis M, Asztalos E, Sipka G, Maróti P (2014) Assembly of photosynthetic apparatus in *Rhodobacter sphaeroides* as revealed by functional assessments at different growth phases and in synchronized and greening cells. *Photosynth Res* 122:261–273
- Kitona H (2002) Systems biology: a brief overview. *Science* 295:1662–1664
- Klug G, Masuda S (2008) Regulation of genes by light. In: Hunter CN, Daldal F, Thurnauer MC, Beatty JT (eds) *The purple phototrophic bacteria*. Springer, Dordrecht, pp 727–741
- Koblížek M, Shih JD, Breitbart SI, Ratcliffe EC, Kolber ZS, Hunter CN, Niederman RA (2005) Sequential assembly of photosynthetic units in *Rhodobacter sphaeroides* as revealed by fast repetition rate analysis of variable bacteriochlorophyll *a* fluorescence. *Biochim Biophys Acta* 1706:220–231
- Koepke J, Hu XC, Muenke C, Schulten K, Michel H (1996) The crystal structure of the light-harvesting complex II (B800-850) from *Rhodospirillum molischianum*. *Structure* 4:581–597
- Kolber ZS, Prasil O, Falkowski PG (1998) Measurements of variable chlorophyll fluorescence using fast repetition rate techniques: defining methodology and experimental protocols. *Biochim Biophys Acta* 1367:88–106
- Liu LN, Scheuring S (2013) Investigation of photosynthetic membrane structure using atomic force microscopy. *Trends Plant Sci* 18:277–286
- Magis GJ, den Hollander MJ, Onderwaater WG, Olsen JD, Hunter CN, Aartsma TJ, Frese RN (2010) Light harvesting, energy transfer and electron cycling of a native photosynthetic membrane adsorbed onto a gold surface. *Biochim Biophys Acta* 1798:637–645
- Masuda S, Bauer CE (2002) AppA is a blue light photoreceptor that antirepresses photosynthesis gene expression in *Rhodobacter sphaeroides*. *Cell* 110:613–623
- McDermott G, Prince SM, Freer AA, Hawthornthwaite-Lawless AM, Papiz MZ, Cogdell RJ, Isaacs NW (1995) Crystal structure of an integral membrane light-harvesting complex from photosynthetic bacteria. *Nature* 374:517–521
- Miller JF, Hinchigeri SB, Parkes-Loach PS, Callahan PM, Sprinkle JR, Riccobono JR, Loach PA (1987) Isolation and characterization of a subunit form of the light-harvesting complex of *Rhodospirillum rubrum*. *Biochemistry* 26:5055–5062
- Monger TG, Cogdell RJ, Parson WW (1976) Triplet states of bacteriochlorophyll and carotenoids in chromatophores of photosynthetic bacteria. *Biochim Biophys Acta* 449:136–153
- Niederman RA (2016) Assembly and dynamics of the bacterial photosynthetic apparatus. *Biochim Biophys Acta* 1857:232–246

- Niederman RA, Mallon DE, Parks LC (1979) Membranes of *Rhodospseudomonas sphaeroides*. VI. Isolation of a fraction enriched in newly synthesized bacteriochlorophyll *a*-protein complexes. *Biochim Biophys Acta* 555:210–220
- Niwa S, Yu LJ, Takeda K, Hirano Y, Kawakami T, Wang-Otomo ZY, Miki K (2014) Structure of the LH1-RC complex from *Thermochromatium tepidum* at 3.0 Å. *Nature* 508:228–232
- Olsen JD, Tucker JD, Timney JA, Qian P, Vassilev C, Hunter CN (2008) The organization of LH2 complexes in membranes from *Rhodobacter sphaeroides*. *J Biol Chem* 283:30772–30779
- Papiz MZ, Prince SM, Howard T, Cogdell RJ, Isaacs NW (2003) The structure and thermal motion of the B800-850 LH2 complex from *Rps. acidophila* at 2.0 Å resolution and 100 K: new structural features and functionally relevant motions. *J Mol Biol* 326:1523–1538
- Ponnampalam SN, Bauer CE (1997) DNA binding characteristics of CrtJ. A redox-responding repressor of bacteriochlorophyll, carotenoid, and light harvesting-II gene expression in *Rhodobacter capsulatus*. *J Biol Chem* 272:18391–18396
- Qian P, Hunter CN, Bullough PA (2005) The 8.5 Å projection structure of the core RC-LH1-PufX dimer of *Rhodobacter sphaeroides*. *J Mol Biol* 349:948–960
- Qian P, Papiz MZ, Jackson PJ, Brindley AA, Ng IW, Olsen JD, Dickman MJ, Bullough PA, Hunter CN (2013) Three-dimensional structure of the *Rhodobacter sphaeroides* RC-LH1-PufX complex: dimerization and quinone channels promoted by PufX. *Biochemistry* 52:7575–7585
- Roszak AW, Howard TD, Southall J, Gardiner AT, Law CJ, Isaacs NW, Cogdell RJ (2003) Crystal structure of the RC-LH1 core complex from *Rhodospseudomonas palustris*. *Science* 302:1969–1972
- Scheuring S (2006) AFM studies of the supramolecular assembly of bacterial photosynthetic core-complexes. *Curr Opin Chem Biol* 10:387–393
- Scheuring S (2008) The supramolecular assembly of the photosynthetic apparatus of purple bacteria investigated by high-resolution atomic force microscopy. In: Hunter CN, Daldal F, Thurnauer MC, Beatty JT (eds) *The purple phototrophic bacteria, Advances in photosynthesis and respiration*, vol 28. Springer, Dordrecht, pp 941–952
- Scheuring S, Sturgis JN (2005) Chromatic adaptation of photosynthetic membranes. *Science* 309:484–487
- Scheuring S, Sturgis JN (2009) Atomic force microscopy of the bacterial photosynthetic: plain pictures of an elaborate machinery. *Photosynth Res* 102:197–211
- Scheuring S, Seguin J, Marco S, Levy D, Robert B, Rigaud J-L (2003) Nanodissection and high-resolution imaging of the *Rhodospseudomonas viridis* photosynthetic core complex in native membranes by AFM. *Proc Natl Acad Sci U S A* 100:1690–1693
- Scheuring S, Rigaud JL, Sturgis JN (2004) Variable LH2 stoichiometry and core clustering in native membranes of *Rhodospirillum photometricum*. *EMBO J* 23:4127–4133
- Scheuring S, Levy D, Rigaud JL (2005) Watching the components of photosynthetic bacterial membranes and their in situ organisation by atomic force microscopy. *Biochim Biophys Acta* 1712:109–127
- Scheuring S, Gonçalves RP, Prima V, Sturgis JN (2006) The photosynthetic apparatus of *Rhodospseudomonas palustris*: structures and organization. *J Mol Biol* 358:83–96
- Sener M, Strumpfer J, Singharoy A, Hunter CN, Schulten K (2016) Overall energy conversion efficiency of a photosynthetic vesicle. *Elife* 5. pii: e09541. doi:10.7554/eLife.09541
- Sturgis JN, Niederman RA (2008a) Atomic force microscopy reveals multiple patterns of antenna organization in purple bacteria: implications for energy transduction mechanisms and membrane modeling. *Photosynth Res* 95:269–278
- Sturgis JN, Niederman RA (2008b) Organization and assembly of light-harvesting complexes in the purple bacterial membrane. In: Hunter CN, Daldal F, Thurnauer MC, Beatty JT (eds) *The purple phototrophic bacteria, Advances in photosynthesis and respiration*, vol 28. Springer, Dordrecht, pp 253–273
- Sturgis JN, Olsen JD, Robert B, Hunter CN (1997) Functions of conserved tryptophan residues of the core light-harvesting complex of *Rhodobacter sphaeroides*. *Biochemistry* 36:2772–2778
- Sturgis JN, Tucker JD, Olsen JD, Hunter CN, Niederman RA (2009) Atomic force microscopy studies of native photosynthetic membranes. *Biochemistry* 48:3679–3698

- Tucker JD, Siebert CA, Escalante M, Adams PG, Olsen JD, Otto C, Stokes DL, Hunter CN (2010) Membrane invagination in *Rhodobacter sphaeroides* is initiated at curved regions of the cytoplasmic membrane, then forms both budded and fully detached spherical vesicles. *Mol Microbiol* 76:833–847
- Varga AR, Staehelin L (1983) Spatial differentiation in photosynthetic and non-photosynthetic membranes of *Rhodospseudomonas palustris*. *J Bacteriol* 154:1414–1430
- Vermeulen AJ, Bauer CE (2015) Members of the PpaA/AerR antirepressor family bind cobalamin. *J Bacteriol* 197:2694–2703
- Walz T, Ghosh R (1997) Two-dimensional crystallization of the light-harvesting I-reaction centre photounit from *Rhodospirillum rubrum*. *J Mol Biol* 265:107–111
- Westerhuis WHJ, Sturgis JN, Ratcliffe EC, Hunter CN, Niederman RA (2002) Isolation, size estimates, and spectral heterogeneity of an oligomeric series of light-harvesting 1 complexes from *Rhodobacter sphaeroides*. *Biochemistry* 41:8698–8707
- Woronowicz K, Niederman RA (2010) Proteomic analysis of the developing intracytoplasmic membrane in *Rhodobacter sphaeroides* during adaptation to low light intensity. In: Hallenbeck PC (ed) Recent advances in phototrophic prokaryotes. Springer, New York, Adv Exp Med Biol 675:161–178
- Woronowicz K, Sha D, Frese RN, Niederman RA (2011a) The accumulation of the light-harvesting 2 complex during remodeling of the *Rhodobacter sphaeroides* intracytoplasmic membrane results in a slowing of the electron transfer turnover rate of photochemical reaction centers. *Biochemistry* 50:4819–4829
- Woronowicz K, Sha D, Frese RN, Sturgis JN, Nanda V, Niederman RA (2011b) The effects of protein crowding in bacterial photosynthetic membranes on the flow of quinone redox species between the photochemical reaction center and the ubiquinol-cytochrome c_2 oxidoreductase. *Metallomics* 3:765–774
- Woronowicz K, Olubanjo OB, Sung HC, Lamprey J, Niederman RA (2012) Differential assembly of polypeptides of the light-harvesting 2 complex encoded by distinct operons during acclimation of *Rhodobacter sphaeroides* to low light intensity. *Photosynth Res* 111:125–138
- Woronowicz K, Harrold JW, Kay JM, Niederman RA (2013) Structural and functional proteomics of intracytoplasmic membrane assembly in *Rhodobacter sphaeroides*. *J Mol Microbiol Biotechnol* 23:48–62
- Woronowicz K, Olubanjo OB, Sha D, Kay JM, Niederman RA (2015) Effects of the protonophore carbonyl-cyanide *m*-chlorophenylhydrazone on intracytoplasmic membrane assembly in *Rhodobacter sphaeroides*. *Biochim Biophys Acta* 1847:1119–1128

Proteome Analysis of Phototrophic Adaptation

Frédéric Deschoenmaeker, Baptiste Leroy, and Ruddy Wattiez

Abstract For decades, cyanobacteria have been of great interest in research because their metabolic versatility and their capacity to adapt to a variety of environmental conditions have enabled cyanobacteria to colonize various habitats. Furthermore, the metabolic abilities of cyanobacteria also make them useful for human applications, and therefore, they have been extensively characterized. To understand more deeply the molecular basis for the underlying metabolic versatility, cyanobacteria have been subjected to various culture conditions (e.g., nutrient limitations, salt and high-light exposure), followed by characterization by molecular “omic” approaches. Here, we reviewed the proteomic approach and focused on its application in the characterization of the molecular ability through the phylum Cyanobacteria.

Keywords Cyanobacteria • Cell adaptation • Proteomic • Mass spectrometry

For decades, photosynthetic organisms, such as cyanobacteria, have been of great interest in research because they are widely distributed across the planet. Indeed, their metabolic versatility and their capacity to adapt to a variety of environmental conditions have enabled cyanobacteria to colonize various habitats, such as marine, limnic and soil environments, over a wide range of temperatures, from arctic regions to hot springs. The metabolic abilities of cyanobacteria also make them useful for human applications, and therefore, they have been extensively characterized (Garcia-Pichel 2009; Schirromeister et al. 2015); cyanobacteria likely constitute the most important microorganisms for the coming decades.

To understand more deeply the molecular basis for the underlying adaptive mechanisms, cyanobacteria have been subjected to various culture conditions (e.g., nutrient limitations, salt and high-light exposure), followed by characterization through molecular “omic” approaches (i.e., genomics, metabolomics and proteomics).

F. Deschoenmaeker • B. Leroy • R. Wattiez (✉)
Department of Proteomic and Microbiology, Research Institute for Biosciences,
University of Mons, Place du Parc 20, 7000 Mons, Belgium
e-mail: ruddy.wattiez@umons.ac.be

Today, the ability of mass spectrometry to identify and quantify thousands of proteins from complex samples establishes mass spectrometry-based proteomics as an indispensable tool for cellular biology, particularly for microbiology.

Mass Spectrometry-Based Proteomic, Statement

Briefly, modern proteomics relies on the detection, identification and quantification of proteins by mass spectrometry. Protein identification is based on the analysis of peptides generated by digestion with a specific protease (usually trypsin¹), and these tryptic peptides are subjected to mass spectrometry analysis (Hustoft et al. 2012; Tsiatsiani and Heck 2015). Protein sequence coverage can be improved by performing a second digestion with another protease with a different specificity (e.g., endoproteinase GluC) and then, combining the two digests for a common analysis (Swaney et al. 2010).

A mass spectrometer measures mass-to-charge ratios (m/z) and the abundances of gas-phase ions. A mass spectrometer (MS) can be viewed as the combination of three basic components: (i) a source that converts molecules into gas-phase ions, (ii) an analyser that separates ions according to their m/z ratio and (iii) a detector that records the number of ions at each m/z (Aebersold and Mann 2003; Glish and Vachet 2003).

Sources of Ions

First, the analytes (i.e., peptides) are ionized by the ionization source. For protein analysis, there are two main types of ion source: the matrix-assisted laser desorption/ionization (MALDI, introduced in 1988 by Tanaka et al. (1988)) and the electrospray ionization (ESI, introduced by Fenn in 1989 (Fenn et al. 1989)). To improve the coverage of the proteome, both interfaces are often combined with a pre-separation of the analytes, including liquid chromatography (high pressure liquid chromatography, HPLC, or ultra-performance liquid chromatography, UPLC) or electrophoresis (one or two dimensional electrophoresis).

MALDI ionization is the most appropriate for use with a two-dimensional gel electrophoresis approach, in which spots of interest are excised, processed and spotted onto MALDI plates for analysis (Lohnes et al. 2016; Susnea et al. 2012). In this approach, peptides are co-crystallized with an acidic organic matrix (e.g., α -cyano-hydroxycinnamic acid mixed with trifluoroacetic acid and acetonitrile), which

¹**Trypsine:** proteolytic enzyme that cleaves proteins at the C-terminal side of lysine or arginine (unless the adjacent amino acid is a proline) (Baldwin 2003; Hustoft et al. 2012; Tsiatsiani and Heck 2015).

absorbs the energy of the laser during the irradiation step, simultaneously volatilizing and ionizing the sample under high-vacuum pressure.

In contrast to MALDI, the ESI is an atmospheric source based on a liquid method and, thus, is compatible with the liquid chromatography (LC) methods used in protein analyses (from ultrafast UPLC to low-flow nanoLC). In ESI-MS, the samples are suspended in a polar volatile solvent, and pumped at a low flow rate through a needle subjected to (i) a high-voltage electric field and (ii) a heating system. This treatment assists the transfer of ions from solution into the gaseous phase prior to mass spectrometric analysis. The transfer of ionic species from solution into the gas phase by ESI involves the dispersion of a fine spray of charged droplets followed by solvent evaporation and ion ejection from the highly charged droplets (Aebersold and Mann 2003; Baldwin 2003; Fukuyama 2015; Glish and Vachet 2003; Mann et al. 2001; Moruz and Käll 2016). Coupled “in-line” with a HPLC or UPLC for molecular pre-fractionation prior to mass spectrometric analysis, HPLC/UPLC-ESI-MS has become a powerful technique capable of analysing both small and large molecules in complex biological samples.

Mass Analysers

The mass analyser is the second component of a mass spectrometer, in which the ions are separated based on their m/z ratio. Different mass analysers exist, each exhibiting its own strengths and weaknesses. When ions travel through a magnetic or electrical field, their movement is affected by their m/z ratio; this property is the main principle involved in separating ions in MS analysers (hereafter).

A quadrupole mass analyser (Q) consists of four parallel metal rods where an oscillating electric field is applied. The characteristic of this electric field, specifically the oscillation amplitude, defines which ions (i.e., which m/z ratios) will have a “stable” trajectory (i.e., without hitting the Q rods) and reach the detector (Aebersold and Mann 2003; Glish and Vachet 2003; Mann et al. 2001). In association with other mass analysers, quadrupole mass analysers are often used as ion filters.

A quadrupole ion trap (IT) mass spectrometer is an analyser that uses dynamic electric fields where molecules are physically trapped. This type of analyser has two main configurations: (i) a 3D trap with a set of three hyperbolic electrodes and (ii) a linear form defined by four parallel electrodes. In both configurations, the electrodes form a cavity where ions can be trapped (i.e., where they can be stored). Then, this system performs mass-selective ejection in which it selectively ejects the trapped ions in order of increasing mass by gradually increasing the applied radio frequency voltage (Aebersold and Mann 2003; Glish and Vachet 2003; Mann et al. 2001).

The Fourier transform ion cyclotron (FT-ICR) mass spectrometer is the highest-resolution MS that also traps ions in the presence of a high magnetic field. Ions

will begin to oscillate around the magnetic field with a frequency specific to their m/z ratio. The oscillating ions will trigger an induced current, which is eventually recorded. Using the Fourier transformation, the oscillation in the induced current is converted to frequencies of oscillation from which m/z are deduced. In contrast to FT-ICR MS, an orbitrap is the most popular high-resolution ion trap, and only uses electrostatic fields to confine and analyse the injected ion populations (Aebersold and Mann 2003; Glish and Vachet 2003; Mann et al. 2001; Scigelova et al. 2011).

A time of flight analyser (TOF) separates ions in the gaseous phase by time without the use of an electric or magnetic field. In a TOF, separation is based on the kinetic energy and velocity of the ions in a high-vacuum drift tube. An electric field accelerates ions released from the ion source, and then, m/z -dependent separation occurs as the ions transit through a field-free tube to reach the detector (Aebersold and Mann 2003; Glish and Vachet 2003; Mann et al. 2001).

Tandem Mass Spectrometry

Despite the accuracy of measurement, exact peptide masses alone cannot be used to identify peptides because different isobaric species of peptides co-exist in each proteome. Therefore, the identification of peptides relies on an additional level of information obtained through the fragmentation of a peptide (i.e., in this case, termed the precursor ion) in the mass spectrometer, generating MS/MS spectra. MS/MS spectra contain sequential information that allows de novo sequencing of peptides. Peptides are then identified using MS data and the comparison of experimental MS/MS spectra with theoretical MS/MS spectra deduced from the protein sequence databases. To perform MS/MS analysis, a mass spectrometer must isolate the precursor ion to perform its individual fragmentation. With the exception of ion trap-like mass spectrometers, two or more mass analysers must be coupled to achieve this. One of the most common “hybrid mass spectrometers” is the Q-TOF. In this configuration, a quadrupole (MS1) is used to filter successive precursor ions, which are fragmented by collision-induced dissociation (CID), and these ion fragments are then analysed in a TOF analyser (MS2) (Glish and Vachet 2003; Mann et al. 2001).

Other hybrid instruments exist, such as triple quadrupole or ion-trap/orbitrap. During LC-MS/MS analysis, the instrument continuously alternates between (i) MS analysis to detect peptides separated through a chromatography column reaching the mass spectrometer and (ii) MS/MS mode, during which precursor ions are filtered and fragmented followed by the detection of fragment ions. This acquisition mode is the so-called data-dependent acquisition (hereafter DDA) because MS/MS spectra are acquired according to the detection/selection of the precursor in the MS spectrum.

Data Independent Acquisition

The main limitation in DDA processing is that only the strongest signal ions are selected, whereas peptides from low-abundance proteins may be not identified. In the data-independent acquisition (hereafter DIA), fragmentation is performed on a set of ions rather than on specific precursor ions. Consequently, fragmentation data are recorded for all detectable ions, in other words, for high- and low-abundance peptides. Several methods based on DIA processing have been developed (e.g., SWATH and MS^E, briefly discussed below) (Baldwin 2003; Bauer et al. 2014; Chapman et al. 2013; Doerr 2014; Lesur and Domon 2015; Ross 2004).

The MS^E methods were developed for the Q-TOF mass spectrometer, and constituted an enhanced CID-based approach (Silva et al. 2005). During the MS^E procedure, the collision energy voltage is cycled between low- and high-energy values to register the MS and fragment spectra of all incoming ions, respectively. Then, a complex data processing strategy is applied to reconstruct individual fragment spectra based on several characteristics, such as chromatographic retention time. Peptides and proteins are finally identified based on sequential database searches (Chapman et al. 2013; Distler et al. 2016; Levin et al. 2011). The SWATH MS methodology was also recently developed for Q-TOF instruments several years ago (Gillet et al. 2012). MS/MS spectra are collected via a wide m/z isolation window (commonly 25 m/z) repeatedly up to a full scan (400–1200 m/z). Therefore, MS/MS spectra contain mass information from multiple precursors. In contrast to MS^E, peptides are identified by comparison with a previously constructed library of MS/MS spectra acquired in DDA mode, and the quantification is performed onto MS2 data. It should be noted that today, orbitrap MS is also amenable to similar DIA strategies (Chapman et al. 2013; Huang et al. 2015; Röst et al. 2016).

Experimental Features

The success of proteomic analysis depends on the capacity of the mass spectrometer to identify as many proteins as possible, irrespective of sample complexity. Moreover, it is essential to recover and prepare proteins under conditions that are compatible with such MS analyses. In this context, two workflows are often described in the literature: the so-called gel-based and gel-free workflows (Fig. 1 a).

Due to the complexity of the sample or whether particular extraction conditions are not compatible with MS analysis (e.g., the use of detergents for membrane protein extraction), pre-fractionation/clean-up on gels is commonly performed prior to protein digestion and LC/MS-MS analysis of the samples. In this case, the strategy is called “gel-based” by comparison with “gel-free” approaches in which gel separation is not performed before chromatographic separation (eventually, with multi-dimensional separations) and mass spectrometry analysis.

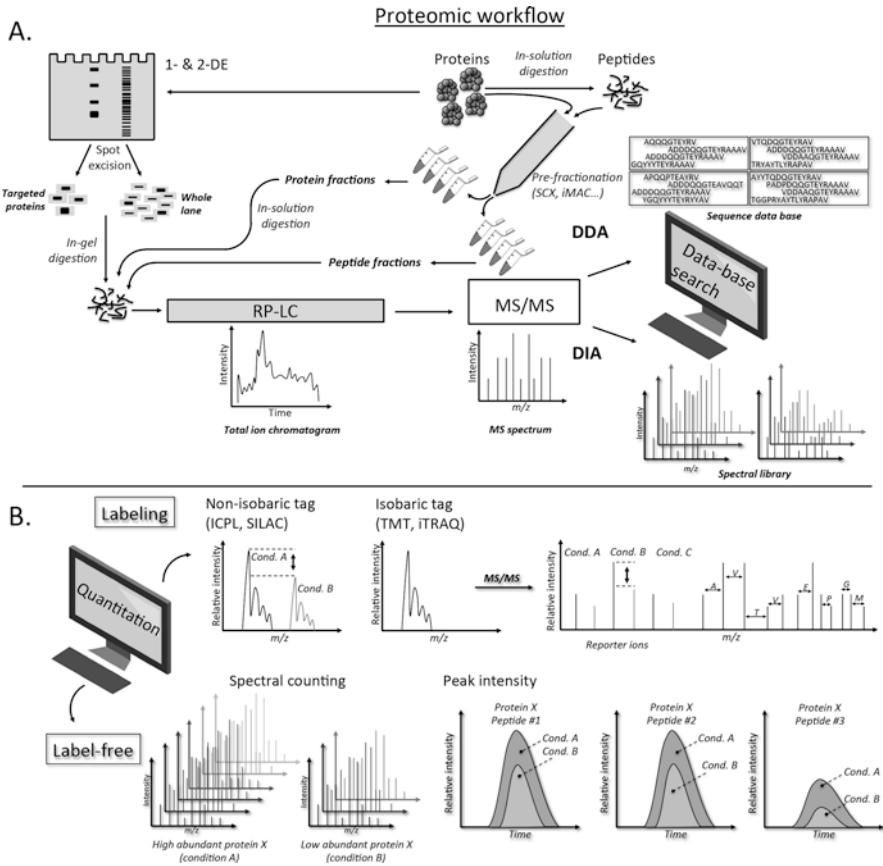


Fig. 1 Proteomic workflow. (a) (1-DE) one dimensional electrophoresis, (2-DE) two dimensional electrophoresis, (SCX) strong cation exchange chromatography, (iMAC) immobilized metal ion affinity chromatography, (RP-LC) reverse-phase chromatography, (MS) mass spectrometry, (MS/MS) tandem mass spectrometry, (m/z) mass-to-charge ratio, (DDA) data dependent acquisition, (DIA) data independent acquisition, (b) (ICPL) isotope coded protein label, (SILAC) stable isotope labeling by amino acids, (TMT) tandem mass tag, (iTRAQ) isobaric tags for relative and absolute quantitation, (Cond. A) condition A, (Cond. B) condition B, (Cond. C) condition C

Gel-Based Workflow

Investigation of large-scale proteomes is always difficult due to the significant complexity of biological samples. After cell disruption, samples are often subjected to electrophoretic separation to reduce this complexity. Indeed, one-dimensional (1-DE) and two-dimensional (2-DE) electrophoresis runs on polyacrylamide gels

(PAGEs) with sodium dodecyl sulphate² (SDS) are often described in the literature (Julka and Regnier 2004). Furthermore, the gel-based method is of a particular interest for the characterization of complex membrane functions (Chevalier 2010; Ladig et al. 2011). In this case, protein extraction often requires the use of detergents that are not compatible with the subsequent MS analysis. The SDS-PAGE approach then allows for a reduction in the complexity of samples and simultaneously removes the detergent (Poetsch and Wolters 2008).

In the 1D SDS-PAGE strategy, proteins are separated according to their molecular weights. After migration, the proteins are stained with specific dyes (e.g., Coomassie Brilliant Blue). If MS analysis is applied to specific proteins, the respective band(s) will be excised; if the whole proteome is examined, the entire gel lane is cut into equal bands, irrespective of the presence of proteins. Thereafter, specific bands are excised and undergo in-gel enzymatic digestion prior to MS analysis (Abdallah et al. 2012; Ladig et al. 2011; Shevchenko et al. 2007).

The other approach that is widely used to reduce sample complexity entails the separation of proteins by 2D–isoelectric focusing (IEF-SDS-PAGE). This technique relies on two successive separations. During the first dimensional separation, proteins are aligned by their isoelectric point (pI)³ and then proteins undergo the classical SDS-PAGE and staining steps. After staining (e.g., Coomassie Brilliant Blue or SYPRO) or radioactively labeling, pictures of the gels are analysed and compared using specific software (e.g., Image Master and Progenesis). Finally, each spot of interest is excised and processed for mass spectrometry analysis.

Among the 2D–IEF-SDS-PAGE methods, 2D difference gel electrophoresis (DIGE) offers the best resolution and is commonly used to observe changes in protein abundance (e.g., control versus treated samples). This approach is also useful for analysing post-translational modifications, truncations and any modification that could change the size or isoelectric point of proteins. During 2D–DIGE experiments, up to three protein samples are labeled with a fluorescent dye (e.g., Cy3, Cy5 and Cy2) prior to a single electrophoretic separation. This experimental procedure eliminates gel-to-gel variation because the different samples are run on the same gel.

The main limiting factor of PAGE techniques is the poor sensitivity and reproducibility. Furthermore, low-abundance proteins may be not stained, and alkaline and high-molecular-weight proteins may be not well separated (Abdallah et al. 2012; Baldwin 2003; Chevalier 2010; Fournier et al. 2007).

²**Sodium dodecyl sulphate (SDS):** anionic detergent that denatures, and coats proteins with a negative charge (Chevalier 2010).

³**Isoelectric point (pI):** specific pH at which proteins exhibit a net charge of zero (Chevalier 2010).

Gel-Free Approach

Multidimensional protein identification technology (hereafter MudPIT) provides a solution for overcoming the limitations of 2-DE, such as reproducibility. The MudPIT approach combines (i) the resolution performance of high/ultra-pressure liquid chromatography, (ii) the peptide analysis accuracy of MS/MS, and (iii) the analytical power of database search software. In this configuration, a complex protein sample is first treated with proteases, and the peptide mixture is then subjected to two successive high-resolution chromatographic separations. Whereas the second dimensional separation is a reverse-phase (RP) chromatography, the first dimension can be strong cation exchange (SCX) chromatography or an RP at a basic pH (Fournier et al. 2007; Siu et al. 2011; Spicer et al. 2016).

Additionally, protein pre-fractionation using chromatography followed by enzymatic digestion of the proteins and separation by 1- or 2-D chromatography is also a common strategy (Fournier et al. 2007; Spicer et al. 2016).

Differential Quantitative Proteomic Analysis

Historically, 2D electrophoresis was the first quantitative proteomic solution. Samples in which protein abundance needed to be compared were separated on 2D gels, and the relative abundances of proteins were evaluated based on protein staining intensity (see above).

Both the MS analysis and quantitative workflows were improved at the same time. The first strategy for the relative quantification of proteins in MS was based on labeling strategies (Fig. 1 b).

Isotope Labeling Approaches

The high-throughput assessment of changes in protein expression is often achieved by isotopic labeling of proteins or peptides, either metabolically *in vivo*, or enzymatically *in vitro* or chemically using specific reagents. Isotopic labeling approaches consist of introducing a differential mass tag into peptides or proteins by chemical or enzymatic derivatization in which chemical features of the peptides are conserved during LC and MS runs. The mass tag introduces a mass shift, which is used to discriminate different samples. This mass shift makes it possible to attribute the signal of an ion to a particular sample and to derive relative quantitative data from this signal (coming references).

The major advantage of quantitative isotopic labeling quantitative strategies is the limited sample manipulation given that all samples are pooled and simultaneously subjected to the same experimental procedure. Consequently, these strategies considerably reduce the variability in signals observed in downstream analyses

(mainly due to matrix effects, chromatography and ionization instability) (Bantscheff et al. 2007; Julka and Regnier 2004).

Among isotopic labelling approaches, chemical tags can be isobaric or non-isobaric. In non-isobaric tags, derived quantitative data are retrieved from the comparison of intensities of isotopic pairs of ions. The peptide signal of the heavy form (from sample A) is compared with the signal of its respective light form (from sample B). Non-isobaric tags exist as duplex, triplex or quadruplex allowing for the simultaneous comparison of two, three or four samples.

In the second method, non-isobaric tags can be introduced by chemical derivatization into proteins or peptide amino groups (i.e., commercialized as isotope-coded protein labeling (or ICPL) (Gevaert et al. 2008; Schmidt et al. 2005), and first introduced by Münchbach et al. (2000) as the N-terminal nicotinylation labeling), or through the metabolic incorporation of isotopically labeled amino acid (i.e., SILAC introduced by Mathias Mann's laboratory (Mann 2006; Ong 2002)) (Bantscheff et al. 2007; Gevaert et al. 2008; Julka and Regnier 2004).

The latter strategy offers the major advantage of allowing sample mixing very early in the sample preparation workflow (even before protein extraction), thereby reducing the bias introduced during parallel processing of samples to be compared. Unfortunately, SILAC is only feasible with organisms that are fully auxotrophic for the labeled amino acid (e.g., $^{13}\text{C}_6$ -arginine and $^{13}\text{C}_6$ -lysine) (Bantscheff et al. 2007; Gevaert et al. 2008; Julka and Regnier 2004). Finally, the isotopic mass shift can also be introduced enzymatically using ^{18}O -containing water during enzymatic digestion of one of the two samples to be compared (Baldwin 2003; Gevaert et al. 2008; Ye et al. 2009).

In isobaric strategies (e.g., TMT (Thompson et al. 2003); iTRAQ (Choe et al. 2007; Ross 2004)), the peptides from different samples are labeled with tags that show the same total mass, but release reporter ions of different masses upon fragmentation during MS/MS spectra acquisition. Here, the quantitative information comes from integrating the signals from reporter ions in the MS/MS spectra. With isobaric labeling, up to eight samples can be analysed simultaneously (Aggarwal et al. 2006; Baldwin 2003; Bantscheff et al. 2007; Evans et al. 2012; Gevaert et al. 2008; Thompson et al. 2003; Wasinger et al. 2013).

Label-Free Approaches

Although providing the highest accuracy of measurement, isotopic labeling can be difficult to manage, particularly when large groups of samples must be analysed. The large cohort size can represent a significant cost if isotopic labeling must be used. Additionally, this method also requires inference of quantitative data from different batches of pooled samples because multiplexing capacity is limited. Label-free quantitative analysis is far simpler and more cost effective than isotopic labeling strategies. Label-free quantification relies upon two fundamentally different strategies: (i) spectral counts and (ii) peak intensity measurements.

Spectral counting is based on the empirical hypothesis that the higher protein abundance, the higher the frequency at which more MS/MS spectra are collected for the peptides generated from that protein. Then, relative quantitation by spectral count is achieved by comparing the numbers of fragment spectra that identify peptides from a given protein in each sample analysed (Bantscheff et al. 2007; Choi et al. 2008). This inherent analysis was optimized using the so-called protein abundance index (PAI), which was further modified to the exponentially modified protein abundance index (emPAI) (Ishihama 2005). Because label-free techniques emerged as important tools and were widely used, this quantification method regularly undergoes to optimizations (Webb-Robertson et al. 2015; Zhang et al. 2015).

For the peak intensity processing, the ion chromatogram of each peptide is extracted (XIC) from an LC-MS/MS run and then, their respective peak areas are integrated over the chromatographic time scale (i.e., retention time [RT]). The values obtained for each peptide ion are compared between samples. Although this may appear to be the easiest and simplest method, it relies on two technical properties of the equipment: (i) highly stable chromatographic separation and (ii) a high-resolution MS data (Bantscheff et al. 2007; Wasinger et al. 2013). The recent development of data-independent acquisition strategies has also prompted the evolution of quantification strategies. For example, in SWATH mode, quantification is performed using the signal intensity of the peptide fragments instead of the precursor itself. Indeed, these data are available for all peptides detected in all samples and across the full range of the chromatographic separation. The main advantage of this strategy is the significant gain in the robustness of the quantitative data because in this case, multiple data points are available for each peptide, and the co-elution of fragments can be used to ensure the highest specificity in the data obtained (Chapman et al. 2013; Gillet et al. 2012).

Proteomics Analysis of Phototrophic Microbial Acclimation

In this chapter, we review the literature for proteomic analyses of cyanobacteria, with particular focus on phototrophic adaptation. Photosynthetic organisms have attracted significant interest because they can produce a wide range of useful compounds (e.g., bioethanol and hydrogen), serving as bio-economic tools for the coming decades. Among the photosynthetic prokaryotes, cyanobacteria are regarded as promising producers of renewable compounds, such as biofuels (Abed et al. 2009; Garcia-Pichel 2009; Herrero et al. 2001; Nogales et al. 2012; Schirrmeister et al. 2015; Thajuddin and Subramanian 2005). In this context, cyanobacteria have been cultivated and studied under a broad range of culture conditions (e.g., nutrient starvation and high light exposure) to decipher their metabolic abilities.

Although common adaptation strategies are described among members of the phylum Cyanobacteria, species-to-species differences have been observed to some extent in several cases. Hereafter, we confine the discussion of adaptive mecha-

nisms to a limited number of environmental stresses (namely, nitrogen and phosphorus starvation, salt stress, heat shock and light stress) obtained from proteomic analyses.

Nitrogen Starvation

Nitrogen starvation is widely studied among cyanobacteria (Depraetere et al. 2015; Deschoenmaecker et al. 2014; Garcia-Pichel 2009; Hasunuma et al. 2013; Huang et al. 2013; Pereira et al. 2011; Sandh et al. 2011; Spat et al. 2015; Wegener et al. 2010; Yue et al. 2015). Acclimation to nitrogen starvation is probably the best example of complexity in molecular responses. The biological response varies from slight metabolic redrafting to cellular differentiation (Castenholz et al. 2001; Garcia-Pichel 2009; Komárek et al. 2003). During nitrogen starvation, central metabolism is often reprogrammed, including energy production and conversion, amino acid metabolism, and carbohydrate transport and metabolism. Two simultaneous phenomena have been described (Fig. 2): (i) optimization and use of intracellular nitrogenous components and (ii) redraft of metabolism to direct excess carbon into C sinks (Depraetere et al. 2015; Deschoenmaecker et al. 2014; Garcia-Pichel 2009; Hasunuma et al. 2013; Huang et al. 2013; Pereira et al. 2011; Sandh et al. 2011; Spat et al. 2015; Wegener et al. 2010; Yue et al. 2015).

Impaired Photosynthesis

Many cyanobacteria possess supramolecular complexes of phycobiliproteins, termed phycobilisomes (PBSs), which constitute large light-harvesting antennae (Akimoto et al. 2012; Chen et al. 2011; Garcia-Pichel 2009; Guan et al. 2007; Kumar and Murthy 2007; Singh et al. 2015; Tamary et al. 2012; Theiss et al. 2011; Watanabe et al. 2012). The first common phenomenon concerns the bleaching of cells that results from active degradation of the nitrogen-rich phycobiliproteins⁴ (PBPs) and polypeptide linkers,⁵ components of the PBSs. This active degradation releases large amounts of nitrogen because PBSs serve as an internal N source. The relative abundance of the PBPs is known to decrease under N-starvation (e.g., ApcE, CpcB and CpcA in *Gloeotheca* sp. PCC 6909 (Pereira et al. 2011), and ApcB, CpcC1 and CpcC2 in *Arthrospira* sp. PCC 8005 (Depraetere et al. 2015; Deschoenmaecker et al. 2014)).

⁴**Phycobiliproteins:** water-soluble proteinaceous pigments containing covalently bound open-chain tetrapyrroles (Kumar and Murthy 2007; Singh et al. 2015; Tamary et al. 2012).

⁵**Linker polypeptides:** key peptides in face-to-face aggregation of PBPs and stability of the PBS suprastructure (Guan et al. 2007; Kumar and Murthy 2007; Singh et al. 2015; Watanabe et al. 2012).

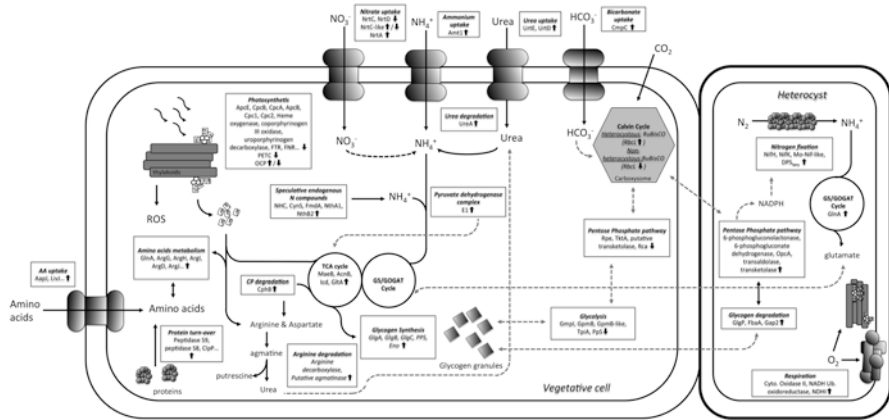


Fig. 2 Schematic diagram for the N-limitation acclimation strategy taken from experimental data of several studies carried out onto whole organisms like *Gloeothecae* PCC 6909, *Arthrospira* PCC 8005, *Synechocystis* sp., *Microcystis aeruginosa*, *Trichodesmium erythraeum* IMS10 & *Nostoc* PCC 7120. (AapJ) general L-amino acid-binding periplasmic protein AapJ, (AcbN) Aconitate hydratase 2, (Amt1) ammonium transporter 1, (ApcB) allophycocyanin subunit B, (ApcE) phycobilisome core-membrane linker polypeptide ApcE, (ArgD) bifunctional acetylornithine amino-transferase, (ArgG) Argininosuccinate synthase, (ArgJ) Glutamate *N*-acetyltransferase, (ClpP) ATP-dependent caseinolytic protease P, (CmpC) Bicarbonate transport ATP-binding subunit, (CO_2) carbon dioxide, (CP) cyanophycin, (Cpc1) phycobilisome rod linker polypeptide Cpc1, (Cpc2) phycobilisome rod linker polypeptide Cpc2, (CpcA) phycobilisome subunit A, (CpcB) phycobilisome subunit B, (CphB) cyanophycinase, (CynS) cyanase, (Cyto. Oxidase II) cytochrome oxidase II, (DPS_{Tery}) DNA binding protein_{Trichodesmium erythraeum}), (Eno) enolase, (FbaA) fructose-bisphosphate aldolase, (FdxH) heterocyst ferredoxin, (FmdA) formamidase A, (FNR) ferredoxin-NADP⁺ reductase, (FTR) ferredoxin-thioredoxin reductase, (Gap2) Glyceraldehyde-3-phosphate dehydrogenase 2, (GlgA) glycogen synthase A, (GlgB) glycogen synthase B, (GlgC) glycogen synthase C, (GlgP) glycogen phosphorylase, (GlnA) glutamine synthetase, (GmpB[-like]) phosphoglycerate mutase B[-like], (GltA) citrate synthase, (GpmI) 2,3-bisphosphoglycerate-independent phosphoglycerate mutase I, (GS/GOGAT) glutamine synthetase/glutamine oxoglutarate aminotransferase, (HCO_3^-) bicarbonate ion, (Icd) iso-citrate dehydrogenase, (LivJ) putative ABC-type branched-chain amino acid transport systems, periplasmic component LivJ, (MaeB) Malate dehydrogenase (oxaloacetate-decarboxylating) (NADP(+)), (Mo-nif-like) molybdenum-nitrogenase-like protein, (N_2) dinitrogen, (NADH Ub. Oxidoreductase) Nicotinamide adenine dinucleotide ubiquinone oxidoreductase, (NADPH) nicotinamide adenine dinucleotide phosphate, (NDH1) NAD(P)H-quinone oxidoreductase subunit I, (NH_4^+) ammonium ion, (NHC) Nitrilase/cyanide hydratase and apolipoprotein *N*-acyltransferase, (NifH) nitrogenase iron protein, (NifK) nitrogenase molybdenum-iron protein subunit B, (NO_3^-) nitrate ion, (NrtA/C[-like]/D) nitrate transporter subunit A/C[-like]/D, (NthA1) nitrile hydratase subunit A, (NthB2) nitrile hydratase subunit B, (O_2) dioxygen, (OCP) orange carotenoid protein, (OpcA) glucose 6-phosphate dehydrogenase assembly protein, (PETC) photosynthetic electron transfer chain, (Pps) phosphoenolpyruvate synthase, (RbcL) ribulose-1,5-diphosphate carboxylase/oxygenase large subunit, (Rpe) ribulose 5-phosphate epimerase, (RuBisCO) ribulose-1,5-diphosphate carboxylase/oxygenase, (TktA) transketolase, (TpiA) Triosephosphate isomerase 2, (TCA) tricarboxylic acid, (UrtA/D/E) urea transport subunit A/D/E

Furthermore, label-free proteomics has revealed that enzymes with critical functions in chlorophyll and cytochrome synthesis were down-regulated (e.g., heme oxygenase in *Synechocystis* sp. (quantification by spectral count) (Wegener et al. 2010), coproporphyrinogen III oxidase and uroporphyrinogen decarboxylase in *Arthrospira* sp. PCC 8005 (quantification by peak intensity) (Depraetere et al. 2015; Deschoenmaecker et al. 2014)). The PETC may also be altered, since a complementary iTRAQ proteomic analysis reported a decrease in electron carriers (e.g., cytochrome *c* oxidase) in *Synechocystis* sp. after 48 h of N deficient culture (Huang et al. 2013).

Because photosynthesis activity is reduced under N stress conditions, the photo-protection mechanism is induced, which is indicated by a greater abundance of the orange carotenoid-binding protein (OCP) (e.g., *Microcystis aeruginosa* (Yue et al. 2015)). This photoactive protein reduces the energy transferred to the reaction centres of photosystems; therefore, the cells are less susceptible to photo-damage (Harris et al. 2016; Kirilovsky and Kerfeld 2012). In contrast, OCP showed a decrease in abundance in *Arthrospira* sp. PCC 8005 (Deschoenmaecker et al. 2014).

Despite the global decrease in photosynthetic activities, cyanobacteria such as *Synechocystis* sp. (Huang et al. 2013) maintain the PSI intact, which may produce energy by cyclic electron transfer (CET). This CET has been suggested to be involved in rapid recovery when the nitrogen source(s) again become(s) re-available (Huang et al. 2013).

In contrast, *Microcystis aeruginosa* and *Trichodesmium erythraeum* IMS10 showed respective increases in the large chain of RuBisCO RbcL (Yue et al. 2015) and enzymes of the oxidative pentose phosphate pathway (OPP), including 6-phospho-gluconolactonase, 6-phosphogluconate dehydrogenase (G6PDH), G6PDH assembly protein OpcA, transaldolase and transketolase (Sandh et al. 2011). In contrast, the non-heterocystous cyanobacterium *Arthrospira* sp. PCC 8005 showed a decrease in the relative abundance of RbcL and enzymes involved in the OPP (e.g., ribulose-phosphate 3-epimerase Rpe) (Depraetere et al. 2015; Deschoenmaecker et al. 2014).

Optimization of Intracellular N Content

The degradation of PBPs releases large amounts of nitrogen, but cyanobacteria also optimize the intracellular N content via specific nitrogenous compound transporter systems, the mobilization of endogenous N components and the degradation of storage polymers.

To compensate for deficient N entry into cells, proteins involved in the transport of N sources are often up-regulated during the first hours of N stress. For example, components of urea transporter (UrtE and UrtD) were more abundant in *Synechocystis* sp. (Wegener et al. 2010) as was the ammonium transporter Amt1 and several amino acid transporters (e.g., AapJ and LivJ) in *Arthrospira* sp. PCC 8005 (Depraetere et al. 2015; Deschoenmaecker et al. 2014). In addition, urease subunits have been observed to be up-regulated in N-starved *Synechocystis* sp. (Huang et al. 2013; Wegener et al. 2010) and in *Arthrospira* PCC 8005 (Depraetere et al. 2015).

Lysis of urea generates ammonium, which could partially balance the intracellular N deficiency. Furthermore, an increase in urease activity has been observed in *Arthrospira* sp. PCC 8005, cultivated in the absence of utilizable nitrogen sources (Deschoenmaecker et al. 2014).

Surprisingly, N deficiency induced a decrease in the abundance of the nitrate transporter components in *Synechocystis* sp., such as NrtC, NrtD and NrtC-like (Huang et al. 2013; Wegener et al. 2010). In contrast, an increase of NrtA was observed after 48 h of exhaustion of N-combined sources (Depraetere et al. 2015). Similarly, Huang et al. (2013) observed a decrease in another protein annotated as NrtC-like.

Cyanobacteria are also known to accumulate cyanophycin granules, a reservoir of N in the form of arginyl and aspartyl (Castenholz et al. 2001; Garcia-Pichel 2009). Proteomic data have shown that the abundance of cyanophycinase is higher under N-stress conditions, thereby providing a large quantities of arginyl and aspartyl for metabolic demands (Wegener et al. 2010).

It has been also reported that *Arthrospira* sp. PCC 8005 may catabolize putative internal nitrogenous compounds, such as nitrile, cyanate and formamide (Depraetere et al. 2015; Deschoenmaecker et al. 2014).

In the reprogramming of N metabolism, the enzyme arginine decarboxylase (i.e., degradation of arginine into agmatine) has been reported to increase up to three-fold in N-starved *Synechocystis* sp. (Wegener et al. 2010). The subsequent step of degradation, agmatine into putrescine, is also suggested to be enhanced given that a putative agmatinase increased in *Synechocystis* sp. (Wegener et al. 2010) and *Arthrospira* sp. PCC 8005 (Deschoenmaecker et al. 2014), as well. This last step may release urea, which could be degraded into ammonium by the urease.

Furthermore, enzymes involved in amino acid anabolism (i.e., aspartate, histidine, pyruvate and glutamate) were observed in lower abundance in *Synechocystis* sp. (Huang et al. 2013), suggesting that amino acid anabolism slowed. This decrease could save substantial amounts of N, which could be used for other vital processes. The heterocystous cyanobacterium *T. erythraeum* IMS101 and the non-heterocystous *Arthrospira* sp. PCC 8005 showed higher levels of several enzymes involved in protein turn-over (e.g., peptidase S9, peptidase S8, putative extracellular peptidase and ATP-dependent Clp protease ClpP) (Depraetere et al. 2015; Deschoenmaecker et al. 2014; Sandh et al. 2011). This observation implies that cells save N by degrading proteins. Proteases, including ATP-dependent caseinolytic proteases (or Clp proteases), are housekeeping enzymes that remove denatured polypeptides (via degradation or disaggregation) and, therefore, are critical for cell homeostasis under both optimal and stress conditions (Clarke 1999). Clp proteases also act with Hsp chaperones like Hsp100 and DnaK (Doyle et al. 2015; Lee et al. 2004).

Among the metabolic activities of nitrogenous compounds that are affected by N limitation, chorismate synthesis appeared to be positively affected. Chorismate is a crucial secondary metabolite in the anabolism of phenylalanine, tyrosine and tryptophan. Chorismate synthase has been reported to increase under several stress con-

ditions, including N depletion in *Synechocystis* sp. The leucine, isoleucine and valine pathways have also been suggested to be up-regulated, because the diaminopimelate decarboxylase increased in abundance in the same cyanobacterium (Wegener et al. 2010).

These observations clearly indicate the capacity of cyanobacteria to maintain metabolic activities despite the lack of N entry into the cell, by seeking alternative nitrogenous compounds, either exogenously or endogenously (Depraetere et al. 2015; Deschoenmaeker et al. 2014; Wegener et al. 2010).

Excess of Carbon

2-Oxoglutarate (i.e., intermediate of the tricarboxylic acid (TCA) cycle) bridged N and C metabolisms. Both 2-OG and NH_4^+ serve as inputs into the glutamine synthetase/glutamate (GS/GOGAT) cycle. Cyanobacterial responses are controlled by the carbon-to-nitrogen ratio (Herrero et al. 2001; Muro-Pastor et al. 2001, 2005), and nitrogen starvation results in an imbalance in the C/N ratio with an excess of carbon.

The protein pyruvate dehydrogenase EI (subunit α), and the bicarbonate transport ATP-binding protein CmpC were more abundant in N-starved *Microcystis aeruginosa* (Yue et al. 2015). Pyruvate dehydrogenase EI is a component of the pyruvate dehydrogenase complex, which constitutes the site of C entry into the TCA cycle. It was then suggested the enhanced turn-over in C use and mobilization towards cellular C sinks (e.g., glycogen) in *Microcystis aeruginosa* (Yue et al. 2015). Furthermore, glycolysis in N-stress *Synechocystis* sp. (Huang et al. 2013) and *Arthrospira* sp. (Depraetere et al. 2015; Deschoenmaeker et al. 2014) has been reported to decrease, whereas N-starved cells accumulated glycogen granules (Depraetere et al. 2015; Deschoenmaeker et al. 2014; Hasunuma et al. 2013). The C skeleton of amino acids released by protein degradation (including PBPs) has been suggested to balance weak CO_2 fixation and serve to synthesize glycogen (Deschoenmaeker et al. 2014; Hasunuma et al. 2013). Glycogen may then serve as an endogenous carbon and energy reservoir to rapidly reinstate growth after of N is resupplied to the N-starved cells (Gründel et al. 2012).

The exopolysaccharides (hereafter, EPSs) are also impacted by the N starvation, and may also play the role of a C sink affecting cell adhesion (Pereira et al. 2011).

Nitrogen Fixation

When combined nitrogen sources are withdrawn, diazotrophic strains can use dinitrogen (N_2 fixation is reviewed in (Bothe et al. 2010)). Not surprisingly, diazotrophic cyanobacteria (unicellular or filamentous form) showed enhanced synthesis and accumulation of the nitrogenase. For example, differentially expressed protein spots in 2-DE gels analysed by MALDI-TOF-MS revealed that nitrogenase was

up-regulated more than 20-fold in *Trichodesmium erythraeum* IMS101. Furthermore, ferritin and Dps_{tery} (a DNA binding protein from starved *T. erythraeum*) were strongly induced (50-fold) during diazotrophic growth; these proteins could provide the iron required during N₂ fixation (Sandh et al. 2011).

MS analysis by comparing the proteome changes occurred in heterocyst versus vegetative cells in *Nostoc* sp. PCC 7120 clearly indicated a greater abundance of NifD and NifK (i.e., components of the dinitrogenase complex) as well as Fe-S reductase component NifH in matured heterocysts. In addition, heterocyst ferredoxin FdxH was preferentially expressed in heterocysts under N₂ fixing conditions. As N₂ represents an input of N, this nitrogen is then actively incorporated into C skeleton inside the heterocysts suggested by the increase of the glutamine synthetase (GS/GOGAT cycle and glutamate), *iso*-citrate aconitase (TCA cycle and 2-OG). The nitrogen fixation requires a huge amount of NADPH provided through the OPP activity. An increase in OPP was suggested, since 6-phosphogluconolactonase, fructose-1,6-bisphosphate, G6PD, Fbp, putative OpcA showed an increase in their relative abundance inside the matured heterocysts. In contrast, the CO₂ fixation was suggested to decrease in those differentiated cells (Ow et al. 2008).

In contrast to the previously described accumulation of glycogen, exposure to N stress conditions revealed an induction of sugar catabolism in N₂-fixing cells. Glycogen phosphorylase (GlgP) was noted to increase under N starvation in *Synechocystis* sp. (Huang et al. 2013; Wegener et al. 2010). This enzyme catalyses the release of glucose units from glycogen, which catabolized during glycolysis. The enzyme fructose-bisphosphate aldolase (i.e., fructose 1,6-bisphosphate catabolized into glyceraldehyde 3-phosphate and dihydroxyacetone phosphate) and pyruvate dehydrogenase (i.e., pyruvate catabolized into acetyl-CoA) were shown to be up-regulated in *Synechocystis* sp. (Wegener et al. 2010). Moreover, the active degradation of glycogen through the OPP has been reported (via glucose-6P-dehydrogenase) in heterocystous *T. erythraeum* IMS101. In the case of heterocystous cyanobacteria, the degradation of glycogen and glucose may serve two goals: (i) to provide the C skeleton required during N assimilation and (ii) and to provide the C molecules required for the respiration-promoted reduction in free oxygen level, which is deleterious to nitrogenase activity. Indeed, the respiratory process also seems to be a part of the acclimation process in *Trichodesmium* sp. because proteins, such as NADH ubiquinone oxidoreductase and cytochrome c oxidase subunit II, were more abundant during diazotrophic growth (Sandh et al. 2011).

Proteins of Unknown Function

Whereas the common basis of adaptive mechanisms seems to be well understood, numerous proteins with unknown functions (i.e., hypothetical proteins, unknown proteins and proteins with unknown functions) are involved in these processes of acclimation (Depraetere et al. 2015; Deschoenmaecker et al. 2014; Huang et al. 2013; Yue et al. 2015). Future work should focus on these proteins to better elucidate the entire mechanistic network of nitrogen stress adaptation.

Phosphorus Starvation

Phosphorus appears to be essential for living organisms given that it is a central atom in nucleic acids (i.e., RNA and DNA), phospholipids (i.e., key components of cell membranes) and chemical energy (e.g., ATP and NADPH) (Lin et al. 2016). Among the nutrient starvation conditions studied, phosphorus (P) starvation has been investigated using proteomic approaches in several strains of cyanobacteria (Fig. 3).

Alteration in Photosynthesis

Like N starvation, a prolonged deficit in P results in altered photosynthesis. Indeed, PSI (e.g., PsaA), PSII (e.g., PsbB, PsbV, PsbO and CP47), PBSs (e.g., CpcA, CpcB, Cpc1, Cpc2, CpcG, ApcA and ApcB) and enzymes involved in chlorophyll and cytochrome synthesis (e.g., HemB and HemE) decreased in abundance in *Synechocystis* sp. PCC 6803 (Fuszard et al. 2013), *Anabaena circinalis* (D'Agostino et al. 2015), in *Synechococcus* WH8102 (Cox and Saito 2013), and *Anabaena* sp. strain 90 (Teikari et al. 2015).

The iTRAQ labeling strategy was performed in P-starved *Synechocystis* sp. PCC 6803 and showed that proteins from the PSII (i.e., PsbU, PsbV and PsbW) and the photosynthetic electron transfer chain (i.e., PetH) were less abundant under P stress conditions. PsbU is known to promote the stability of the PSII structure, whereas PsbW is involved in the biogenesis of the chlorophyll-binding CP47 protein. These decreases may be involved in the disassembly of PBSs and the degradation of their components as well as in the simultaneous down-regulation of PETC to produce a decrease in PSII activity (Fuszard et al. 2013). Downstream of PETC, ferredoxin-thioredoxin reductase and ferredoxin-NADP reductase showed a lower relative abundance, suggesting a decrease in the generation of NADP and reduced ferredoxin (Yue et al. 2015).

The photoprotection-related protein OCP and the enzyme geranylgeranyl diphosphate reductase were more abundant in *M. aeruginosa*. It has been suggested that this increase could enhance the tolerance of cells to photo-damages (Yue et al. 2015).

The stress response proteins rehydrin and superoxide dismutase SodB were also reported to be up-regulated in *Synechocystis* sp. PCC 6803 subjected to P-stress. SodB is known to be involved in the response to oxidative stress (i.e., response to ROS generation), whereas the role of rehydrin in cyanobacteria is unclear (Fuszard et al. 2013). Other proteins involved in ROS stress, such as peroxiredoxin AhpC2 and thioredoxin TrxA, were also observed to increase in *Anabaena* sp. (D'Agostino et al. 2015). Peroxiredoxin detoxifies a wide range of peroxides (Rhee 2016), and thioredoxins (hereafter Trx) are small ubiquitous redox proteins that act as reducing-equivalent transducers. Trx also regulate the enzymatic activity by oxidizing or

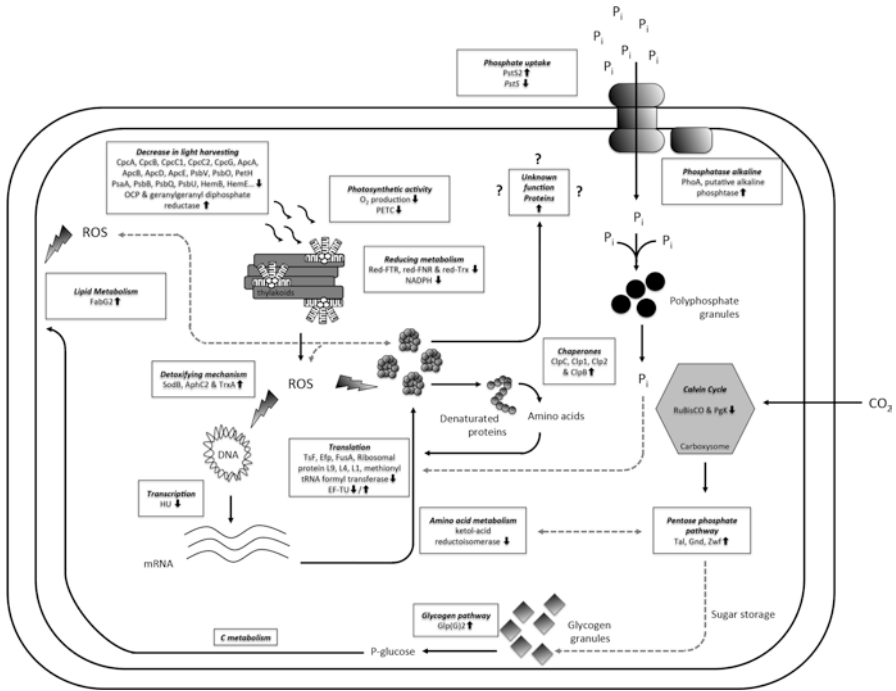


Fig. 3 Schematic diagram for the P-limitation acclimation strategy taken from experimental data of several studies carried out onto *Anabaena circinalis* (131C and 310F), *Anabaena* sp. strain 90, *Microcystis aeruginosa*, *Synechococcus* WH8102, *Synechocystis* PCC 6803. (ApcA) allophycocyanin subunit A, (ApcB) allophycocyanin subunit B, (ApcD) allophycocyanin subunit alpha-B, (ApcE) phycobilisome core-membrane linker phycobiliprotein ApcE, (AphC2) peroxiredoxin AhpC2, (C) carbon. (Clp[1,2]) ATP-dependent caseinolytic protease proteolytic subunit 1, (ClpB) ATP-dependent caseinolytic protease ATP-binding subunit B, (ClpC) ATP-dependent caseinolytic protease ATP-binding subunit C, (CO₂) carbon dioxide, (Cpc1/2) phycobilisome rod linker polypeptide Cpc1/2, (CpcA/B) phycobilisome subunit A/B, (CpcG) phycobilisome rod-core linker polypeptide CpcG, (DNA) deoxyribonucleic acid, (EF-TU) elongation factor TU, (Efp) elongation factor P, (FabG2) 3-oxoacyl-[acyl-carrier-protein] reductase 2, (FusA) elongation factor G, (GlgP(2)) glycogen phosphorylase 2, (Gnd) 6-phosphogluconate dehydrogenase decarboxylating, (HemB) delta-aminolevulinic acid dehydratase, (HemE) Uroporphyrinogen decarboxylase, (HU) DNA-binding protein HU, (mRNA) messenger ribonucleic acid, (NADPH) nicotinamide adenine dinucleotide phosphate, (OCP) orange carotenoid protein, (PETC) photosynthetic electron transfer chain, (PetH) ferredoxin-NADP reductase, (PglK) phosphoglycerate kinase, (PhoA) phosphatase alkaline, (P_i) inorganic phosphate. (PsaA) photosystem I P700 chlorophyll *a* apoprotein A1, (PsbB) photosystem II CP47 reaction centre protein, (PsbO) photosystem II manganese-stabilizing polypeptide, (PsbQ) photosystem II protein PsbQ, (PsbU) photosystem II 12 kDa extrinsic protein, (PsbV) cytochrome *c*-550, (PstS[-2]) phosphate-binding protein [-2], (red-FNR) reduced-ferredoxin-NADP+ reductase, (red-FTR) reduced-ferredoxin-thioredoxin reductase, (red-Trx) reduced-thioredoxin, (RuBisCO) ribulose-1,5-diphosphate carboxylase/oxygenase, (SodB) superoxide dismutase [Fe], (Tal) transaldolase, (Tsf) elongation factor Ts, (TrxA) thioredoxin A, (Zwf) glucose-6-phosphate 1-dehydrogenase

reducing disulphide bond(s) on target proteins. These redox proteins also provide reducing equivalents to antioxidative stress proteins like peroxiredoxin (Flores et al. 2006; Pérez-Pérez et al. 2009). In contrast, it has been reported a down-regulation of the ferredoxin-thioredoxin reductase catalytic chain, and ferredoxin-NADP reductase (Yue et al. 2015).

Optimization of Intracellular P Content

Cyanobacteria can accumulate inorganic phosphate and store it as polyphosphate granules. These granules can then act as a phosphate reservoir that is frequently degraded to balance the cellular P deficit (Gomez-Garcia et al. 2003; Lin et al. 2016; Orchard et al. 2010). To compensate for the P deficiency in the environment, the phosphate transporter and alkaline phosphatase showed an increase in their relative abundance during P depletion (*Anabaena Circinalis* (D'Agostino et al. 2015), *Synechocystis* sp. PCC 6803 (Fuszard et al. 2013) and *Synechocystis* sp. WH8102 (Cox and Saito 2013)).

Transcription and Translation

Phosphate starvation induces proteins involved in transcription and translation. The transcription may be down-regulated, since HU proteins were less abundant in *Synechocystis* sp. PCC 6803. The mRNA translation is affected by the P deficiency because the elongation factor EF-Tu was less abundant in *Synechocystis* sp. PCC 6803 (Fuszard et al. 2013) and *Anabaena* sp. strain 90 (Teikari et al. 2015) as were the 50S ribosomal protein L9 in *Microcystis aeruginosa* (Yue et al. 2015), L4, L1 and methionyl-tRNA formyltransferase in *A. circinalis* (D'Agostino et al. 2015), 50S ribosomal protein L23, L4, L5 and L18 in *Synechococcus* sp. WH8102 (Cox and Saito 2013). EF-Tu facilitates the entry of aminoacyl tRNA at the free site of the ribosome; thus, it appears to be critical for the translation process (Fuszard et al. 2013). Ribosomes represent a large amount of P, so cells should economize on biosynthesis to preserve P for other processes that are critical for viability (Yue et al. 2015). In addition, a recent study reported a decrease in the biosynthesis of amino acids (Teikari et al. 2015).

In contrast, a higher expression of EF-Tu has been observed in *M. aeruginosa* cultivated under P starvation (Yue et al. 2015), whereas *Synechococcus* sp. WH8102 showed an increase in other elongation factors (e.g., TsF, Efp and FusA) (Cox and Saito 2013).

Carbon Metabolism

The RuBisCO (large subunit RbcL and/or small subunit RbcS) was shown to be down-regulated in *Synechocystis* sp. PCC 6803 (Fuszard et al. 2013), *M. aeruginosa* (Yue et al. 2015), and *Anabaena* sp. strain 90 (Teikari et al. 2015). In addition, the

phosphoglycerate kinase (Pgk) also showed a lower relative abundance in *Synechocystis* sp. PCC 6803. RuBisCO and Pgk represent the entry of CO₂ during the Calvin-Benson-Bassham cycle; therefore, a decrease in these enzymes limits the growth (Fuszard et al. 2013). The P deficiency also induced transaldolase (Tal), 6-phosphogluconate dehydrogenase (decarboxylating) (Gnd) and glucose-6-phosphate 1 dehydrogenase (Zwf) in *Synechocystis* sp. PCC 6803 (Fuszard et al. 2013). They are involved in the pentose phosphate pathway (PPP), which appears to be enhanced with respect to the increase in these proteins.

Downstream, the relative abundance of glycogen phosphorylase GlgP(2) increased in P-starved *Synechocystis* sp. PCC 6803. This enzyme catalyses the degradation of glycogen, releasing glucose-1-phosphate, which may undergo glycolysis. Both the enhancement of PPP activity and the increase in the relative abundance of GlgP(2) may support the production of both NADPH and pentose sugars (Fuszard et al. 2013). This increase could compensate for the decrease in the Calvin cycle (see above).

Moreover, an approach combining 2D-DIGE and LC-MS/MS pointed out the up-regulation of the polysaccharide capsule biosynthesis protein CapD and carbohydrate-selective porins in *Anabaena* sp. strain 90, suggesting the accumulation of exopolysaccharides to ensure the proper functioning of the photosynthetic apparatus (Teikari et al. 2015).

Fatty Acid Metabolism

In addition to the EPS layers, the membrane may be modified in response to nutrient stresses.

Fatty acid and lipid synthesis are also affected by P deficiency given that the enzymes involved in their respective metabolic pathways showed differential abundance. Fatty acids have two functions: (i) they serve as precursors for lipid biosynthesis, and (ii) they represent a form of energy storage.

The enzyme FabG2 (i.e., 3-oxoacyl-[acyl-carrier protein] reductase 2) has been reported to increase in abundance in *Synechocystis* sp. PCC 6803 (Fuszard et al. 2013) and *Synechococcus* sp. WH8102 (Cox and Saito 2013). This might indicate that cells accumulate lipids in response to P limitation that may replace ROS-damaged lipids and/or stabilize membranes (Fuszard et al. 2013). In addition, one study reported an arrest in phospholipid synthesis and their replacement by sulphonated lipids in response to P limitation (Lin et al. 2016).

Side Changes in N Metabolism

The subunit UrtA of the urea transporter also showed a greater relative abundance in *A. circinalis* (D'Agostino et al. 2015) and *Synechococcus* sp. WH8102 (Cox and Saito 2013) cultivated under P-limiting conditions. It seems that under P-limiting conditions, *A. circinalis* attempts to take up extracellular nitrogen in the form of

urea or free amino acids (e.g., N-I amino acid substrate-binding NatB) (D'Agostino et al. 2015).

A decrease in the abundance of AbrB proteins has been reported in *M. aeruginosa*; the role of cyanobacterial AbrB proteins in the P stress response is not understood. The AbrB was shown to be involved in C and N uptake in *Synechocystis* sp. PCC 6803. This observation may indicate a decrease in C and N assimilation by *M. aeruginosa* cultivated under P depletion (Yue et al. 2015) in contrast to the mechanism of *A. circinalis* (D'Agostino et al. 2015). The reduction in C and N assimilation may preserve a substantial amount of both energy and reducing power, thereby sustaining a minimal growth (Yue et al. 2015).

Homeostasis

Interestingly, the ATP-dependent Clp proteases ClpC, Clp1, Clp2 and ClpB were observed to be up-regulated in *Synechocystis* sp. PCC 6803 under P-limiting conditions (Fuszard et al. 2013). These proteins degrade denatured polypeptides and maintain cellular homeostasis; therefore, they are clearly involved in growth sustainability and stress acclimation (see section “[Optimization of Intracellular N Content](#)”) (Clarke 1999).

An increase in abundance of outer membrane efflux protein and acetylornithine aminotransferase has been reported in *Anabaena* sp. strain 90 (Teikari et al. 2015).

P depletion also induces a decrease in the relative abundance of metallothioneins, which are small cysteine-rich proteins that bind metal ions, such as zinc, cadmium or copper (Yue et al. 2015). A study based on label-free LC-MS/MS approach reported an elevated abundance of metallothionein in *Synechococcus* sp. WH8102 during combined Zn and low-P_i treatment. These authors argued that metallothionein may act as a metal reservoir for alkaline phosphatases (Cox and Saito 2013).

Proteins of Unknown Function

Similarly to N starvation, numerous unknown proteins demonstrated alterations in abundance (Cox and Saito 2013; Fuszard et al. 2013; Teikari et al. 2015; Yue et al. 2015), suggesting additional analyses to further elucidate adaptation mechanisms.

Salt Stress

The acclimation process to a high concentration of salt has been widely investigated because microorganisms often encounter this abiotic stress on Earth. The basic mechanism of NaCl adaptation involves the active efflux of toxic inorganic ions, the accumulation of compatible solutes (e.g., trehalose and glucosylglycerol), or the active uptake of ions to balance the potential water (Hagemann 2011) (Fig. 4).

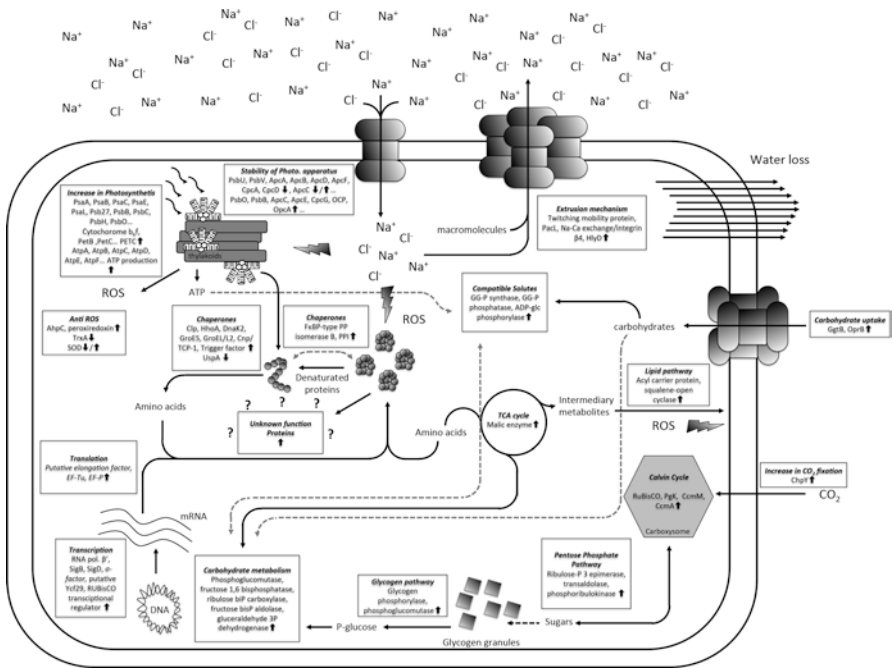


Fig. 4 Schematic diagram sketch for the salt-stress acclimation strategy taken from experimental data of several studies carried out onto *Anabaena circinalis* (131C and 310F), *Anabaena sp.* PCC 7120, *Euhalothece sp.* BAA001, *Synechocystis sp.* (PCC 6803 and PCC 6311). (ADP-glc phosphorylase) ADP-glucose phosphorylase, (AhpC) peroxiredoxin AhpC, (ApcA/B) allophycocyanin subunit A/B, (ApcC) pycobilisome 7.8 kDa linker polypeptide, (ApcD) allophycocyanin subunit alpha-B, (ApcE) pycobilisome core-membrane linker pycobiliprotein ApcE, (ApcF) allophycocyanin subunit beta-18, (AtpA/B/C/D/F) ATP synthase subunit A/B/C/D/F, (CcmM/A) carbon dioxide concentrating mechanism protein M/A, (ChpY) CO₂ hydration protein, (Clp) ATP-dependent caseinolytic protease, (Cnp/TCP-1) chaperone protein, (CpcA) C-phycocyanin-1 alpha chain, (CpcD) pycobilisome 8.9 kDa linker polypeptide, (CpcG) pycobilisome rod-core linker polypeptide CpcG, (DNA) deoxyribonucleic acid, (DnaK2) chaperone protein, (EF-P) elongation factor P, (EF-Tu) elongation factor Tu, (FkBP-type PP isomerase B) FkBP-type peptidyl-prolyl cis-trans isomerase B, (GG-P phosphatase) glucosylglycerol-phosphate phosphatase, (GG-P synthase) glucosylglycerol-phosphate synthase, (GgtB) glucosylglycerol-binding protein GgtB, (GroEL/L2) chaperone protein, (GroES) chaperone protein, (HhoA) putative serine protease, (HlyD) HlyD family of secretion proteins, (mRNA) messenger ribonucleic acid, (OCP) orange carotenoid protein, (OprB) carbohydrate-selective porin OprB, (PacL) Calcium-transporting ATPase, (PetB) cytochrome *b₆*, (PetC) cytochrome *b₆f* complex iron-sulfur subunit, (PETC) photosynthetic electron transfer chain, (PgK) phosphoglycerate kinase, (PPI) peptidyl-prolyl cis-trans isomerase (PsaA) photosystem I P700 chlorophyll a apoprotein A1, (PsaB) photosystem I P700 chlorophyll a apoprotein A2, (PsaC) photosystem I iron-sulfur centre, (PsaE) photosystem I reaction centre subunit IV, (PsaL) photosystem I reaction centre subunit XI, (Psb27) photosystem II lipoprotein Psb27, (PsbB) photosystem II CP47 reaction centre protein, (PsbB) photosystem II CP47 reaction centre protein, (PsbC) photosystem II CP43 reaction centre protein, (PsbH) photosystem II reaction centre protein H, (PsbO) photosystem II manganese-stabilizing polypeptide cytochrome *b₆f*, (PsbO) photosystem II manganese-stabilizing protein, (PsbU) photosystem II 12 kDa extrinsic protein, (PsbV) Cytochrome c-550, (putative Ycf29) putative two-component response regulator Ycf29, (RNA pol. β') RNA polymerase, (ROS) reactive oxygen species, (RuBisCO) ribulose-1,5-diphosphate carboxylase/oxygenase, (SigB) RNA polymerase sigma-B factor, (SigD) RNA polymerase sigma-D factor. (SOD) superoxide dismutase, (TCA) tricarboxylic acid, (TrxA) thioredoxin A, (UspA) universal stress protein A, (σ-factor) transcription factor sigma

Alteration of Photosynthesis

As described for other cellular stresses above, the exposure to high NaCl exposure leads to a perturbation of photosynthesis. In *Synechocystis* sp. PCC 6803, a rapid decrease in photosynthesis (~60%) has been observed 2 h after the addition of NaCl, whereas photosynthesis returns to the initial state after 4 h of incubation with a high concentration of salt. This recovery might be allowed by the synthesis of compatible solutes (Fulda et al. 2006; Pandhal et al. 2008).

Furthermore, increased expression of PSI (e.g., PsaA, PsaB and PsaC) and PSII proteins (e.g., PsbB, PsbC and PsbH), antennae-stabilizing proteins (e.g., PsbO and ApcC), photosynthesis repair proteins, and enzymes involved in chlorophyll biosynthesis (e.g., ChlP) have been reported in *A. circinalis* (D'Agostino et al. 2015) and *Anabaena* sp. PCC 7120 (Rai et al. 2013). Additionally, a higher abundance in response to salt stress has been reported for PBPs (CpcA and CpcB) in *Synechocystis* sp. (Fulda et al. 2006), PBS rode-core linker proteins in *Anabaena* sp. PCC 7120 (Rai et al. 2013), and components of the photosynthetic electron transfer chain in *Synechocystis* sp. PCC 6311 (Pandhal et al. 2009). Moreover, iTRAQ-based quantitative proteomics of salt-shocked *A. circinalis* showed a greater relative abundance of F₁ and F₀-FATPase subunits, cytochrome *b₆f* proteins and proteins consisting of all four NDH-1 complexes, suggesting an increase in photosynthetic electron transfer activities. Similarly, iTRAQ labeling coupled to LC-MS/MS revealed higher levels of an ATP synthase subunit in *Synechocystis* sp. PCC 6803 (Huang et al. 2006; Pandhal et al. 2009; Qiao et al. 2013) as did 2-DE coupled to MALDI-TOF-MS/MS onto *Anabaena* sp. PCC 7120 (Rai et al. 2013). Taken together, these increases in abundance may indicate an enhancement in ATP production, which could be required for metabolic processes (e.g., synthesis of compatible solutes) during salt stress (Hagemann 2011). The ChpY protein (i.e., component of the NDH-1MS complex), which is involved in CO₂ uptake, showed an increase in abundance after exposure to 100 mM NaCl. In addition, the RuBisCO enzyme (both RbcL and RbcL) was also up-regulated in *A. circinalis* (D'Agostino et al. 2015) and *Anabaena* sp. PCC 7120 (Rai et al. 2013) as were the carboxysome⁶ shell protein CcmM in *A. circinalis* (D'Agostino et al. 2015) and CcmA protein, putative Ycf29 and RuBisCO transcriptional regulators in *Synechocystis* sp. PCC 6803 (Fulda et al. 2006; Qiao et al. 2013). Furthermore, an increase has been observed in the relative abundance of enzymes involved in the Calvin cycle (e.g., phosphoglycerate kinase in *Synechocystis* PCC 6803 (Fulda et al. 2006)) and pentose phosphate pathway (e.g., ribulose-phosphate-3-epimerase, transaldolase, phosphoribulokinase in *Synechocystis* sp. PCC 6803 (Fulda et al. 2006) and PCC 6311 (Pandhal et al. 2009) and *Euhalothece* sp. BAA001 (Pandhal et al. 2008)). Taken together, these observations strongly indicate the enhanced assimilation of CO₂.

⁶**Carboxysomes:** organelles accumulating large quantities of the enzyme ribulose 1,5-bisphosphate carboxylase/oxygenase in association with the carbon-concentrating mechanism proteins (Bazylynski et al. 2014; Castenholz et al. 2001; Garcia-Pichel 2009).

Central Carbon Metabolism

Despite the increased activity in CO₂ fixation, sugar metabolism was down-regulated in *A. circinalis* during salt-stress (D'Agostino et al. 2015).

An increase in the abundance of enzymes involved in carbon utilization and central intermediaries has also been reported in salt-stressed *Synechocystis* sp. PCC 6803 (Fulda et al. 2006; Pandhal et al. 2009), *Euhalothece* sp. BAA001 (Pandhal et al. 2008) and *Anabaena* sp. PCC 7120 (Rai et al. 2013) (e.g., glycogen phosphorylase, phosphoglucomutase, fructose-1,6-biphosphatase, fructose biphosphate aldolase and glyceraldehyde-3-P-dehydrogenase). These observations imply the additional requirement of C for the synthesis of compatible solutes such as glucosylglycerol (e.g., the degradation of glycogen may participate in the de novo synthesis of glucosylglycerol (Hagemann 2011)). Furthermore, the enhanced production of pyruvate via the malic enzyme in salt-shocked *Euhalothece* sp. BAA001 has been reported (Pandhal et al. 2008). In contrast, a decrease in the fructose-1,6-biphosphate aldolase and glucose-6-P isomerase has been reported (Rai et al. 2013).

Synechocystis sp. PCC 6803 also showed higher amounts in GDP-D-mannose dehydratase. This latter enzyme is involved in the modification of exopolysaccharides for which a modified structure could prevent water loss during osmotic stress (Pandhal et al. 2009).

Synthesis of Compatible Solutes

Compatible solutes are highly soluble organic compounds that are accumulated in cells at high concentrations without interfering with cellular processes. These compounds help the cell maintain turgor pressure (Hagemann 2011). Recovery could be permitted by the synthesis of compatible solutes, such those produced by the glucosylglycerol-phosphate synthase, glucosylglycerol-phosphate phosphatase and ADP-glucose phosphorylase (Fulda et al. 2006; Pandhal et al. 2008). These enzymes are involved in the biosynthesis of compounds like glucosylglycerol, which is a typical compatible solute found in cyanobacteria (Hagemann 2011).

It was also reported the enhanced abundance in ABC-type transporters (e.g., glucosylglycerol-binding protein GgtB and outer membrane protein OprB) in salt-stressed *Synechocystis* sp. PCC 6803 (Huang et al. 2006), and *A. circinalis* (D'Agostino et al. 2015), which could ultimately participate to the acclimation (Hagemann 2011).

Lipid Metabolism

Lipid metabolism is often involved in stress response; a higher amount of an acyl carrier protein and a squalene-open cyclase has been reported (Qiao et al. 2013).

Nitrogen Metabolism

Like carbohydrate metabolism, nitrogen metabolism is also affected by the salt stress (D'Agostino et al. 2015; Fulda et al. 2006; Huang et al. 2006; Pandhal et al. 2008; Rai et al. 2013). For example, molecular actors, such as AbrB2, DevH and the heterocyst glycolipid-forming protein HgdD, were increased in their relative abundance in *A. circinalis* sp. strain 131C as was the heterocyst glycolipid-directing protein HglK in *Synechocystis* sp. PCC 6803 (Qiao et al. 2013). The regulator DevH plays a role in nitrogen metabolism by activating expression of genes specific to heterocyst cells (D'Agostino et al. 2015). Furthermore, the ferredoxin-nitrite reductase was more abundant when *Synechocystis* was exposed to 684 mM NaCl (Fulda et al. 2006). It has been reported that salt-shocked *Synechocystis* sp. PCC 6803 (Huang et al. 2006) and PCC 6311 (Pandhal et al. 2009) showed a higher levels of the proteins P_{II} and glutamine synthetase in *Anabaena* sp. PCC 7120 (Rai et al. 2013), a strong indication of altered N metabolism.

The enhanced abundance of the periplasmic binding proteins of ABC transporters like NrtA (i.e., component of nitrate transporter) has been reported to increase as well as other proteases involved in the turn-over of proteins (e.g., regulatory subunit of ATP-dependent Clp protease and HhoA protease) (Huang et al. 2006; Rai et al. 2013). In an opposite way, decrease in NrtD- and NrtC-like (i.e., components of nitrate transporter) has been reported when *Synechocystis* sp. PCC 6803 was exposed to 48 h of NaCl treatment (Qiao et al. 2013).

Transcription and Translation

Transcription and translation are also affected in response to NaCl exposure given that RNA polymerase subunit β' and the transcriptional factors SigB and SigD were shown to be up-regulated in salt-stressed *A. circinalis* (D'Agostino et al. 2015). An increase in abundance of a putative elongation factor and sigma regulatory factors has also been reported (Qiao et al. 2013). Similarly, an increase of the elongation factor EF-Tu in NaCl-acclimated *Synechocystis* sp. PCC 6803 (Fulda et al. 2006) and *Euhalothece* sp. BAA001 (Pandhal et al. 2008) has been observed as was the elongation factor P in *Synechocystis* sp. PCC 6803 (Qiao et al. 2013). Pandhal et al. (2009) observed higher amounts of F_κBP-type peptidyl-prolyl *cis-trans* isomerase in salt-shocked *Synechocystis* cells, an enzyme that catalyses *cis-trans* isomerization (Ünal and Steinert 2014). Two studies also observed a higher abundance of the peptidyl propyl isomerase B in *Synechocystis* sp. PCC 6803 (Huang et al. 2006; Qiao et al. 2013).

Stress Related Proteins

NaCl exposure induces stress related proteins, such as the heat-shock proteins DnaK2, GroES, GroEL1/L2, chaperonin Cpn/TCP-1 and trigger factor (*Synechocystis* sp. PCC 6803 (Fulda et al. 2006; Pandhal et al. 2009; Qiao et al.

2013), *Anabaena* sp. PCC 7120 (Rai et al. 2013) and *Euhalotheca* sp. BAA001 (Pandhal et al. 2008)). Chaperones are known to protect cells from aggregation and repair aggregated proteins, thereby maintaining protein functionalities (Kim et al. 2013). The chaperone protein UspA, anti-ROS proteins (e.g., AhpC and superoxide dismutase SOD), TrxA, trigger factor and cyclophilin-type peptidyl-prolyl isomerase were reported to be reduced in *A. circinalis* (D'Agostino et al. 2015). In contrast, a 2-DE-MALDI-TOF-MS investigation showed that the superoxide dismutase SOD (Fulda et al. 2006; Rai et al. 2013) and TrX (Slr0623) were induced by NaCl shock as well as peroxiredoxin-like protein and a water-soluble carotenoid protein OCP. This increase could render cells less susceptible to ROS (Fulda et al. 2006). Additionally, an increased amount of the superoxide dismutase has also been pointed out (Pandhal et al. 2008, 2009).

The SOS regulatory protein LexA was reported to be highly differentially expressed protein, but its role in cyanobacteria is unclear. However, it has been proposed that LexA may act as an activator of the bi-directional hydrogenase (Gutekunst et al. 2005) and may be a candidate for regulating the expression of the *nif* cluster in *Synechocystis* sp. (Mueller et al. 2016).

Extrusion Mechanism

One strategy for cyanobacteria to cope with a high extracellular salt concentration is the active extrusion of the concerned ions (i.e., salt-out strategy) (Hagemann 2011). An in vivo ¹⁵N metabolic labeling study reported a higher level of the twitching mobility protein (i.e., protein that catalyses the transport of substances in and out of cells), suggesting a putative role in the transfer of salt ions or even macromolecules to balance the ionic strength. In addition, this group also observed an increase in the relative abundance of the transport protein cation-transporting ATPase PaCL and Na⁺-Ca²⁺ exchanger/integrin-β4 (Pandhal et al. 2008). An LC-MS/MS run onto iTRAQ labeled tryptic peptides highlighted the increased abundance of HlyD protein, which is a putative integral membrane subunit of the TolC efflux system that exports small as well as large proteins directly from the cytoplasm to the extracellular space (Huang et al. 2006).

Proteins of Unknown Function

Numerous proteins showing a differential abundance have remained uncharacterized. Some bear similarity to orange carotenoid protein and may be involved in light harvesting adaptation during salt stress. Other proteins are similar to the peptidyl-prolyl *cis-trans* isomerase (PPase) activity (Fulda et al. 2006; Huang et al. 2006; Pandhal et al. 2007, 2008; Qiao et al. 2013).

Heat Shock Stress

The heat shock stress was also described to induce a molecular response affecting several biological functions, as it occurred for the aforementioned abiotic stress (Fig. 5).

Alteration in Photosynthetic Activity

Photosynthesis has been described to be sensitive to heat inactivation, particularly the oxygen-evolving complex in *Synechocystis* sp. PCC 6803. The 2-DE-MALDI-TOF-MS strategy was applied to this cyanobacterium, which showed an increase in the manganese stabilizing PsbO protein; this latter protein is involved in the stabilization of Mn atoms of the water-splitting enzyme. Similarly, an increase in the PSII reaction centre protein PsbW and the PSI subunit VII PsaC were observed. An increase of the latter protein may lead to the stabilization of the PsaC-D-E complex at the cytosolic side of the thylakoid. In contrast, the PBS core linker CpcG1 decreased in abundance, whereas the response regulator for energy transfer from PBS to photosystems, Rre26, increased. The authors then suggested that this implies that the increase could counteract the loss of PBS stability by increasing the efficiency of energy transfer from PBS to photosystems (Slabas et al. 2006). Moreover, PetA, PetB and PetC (i.e., components of the cytochrome *b₆f* complex) were identified as being up-regulated in thermo-acclimated *Synechocystis* sp. PCC 6803. The cytochrome *b₆f* complex plays a role in the transfer of electrons from PSII to PSI, indicating that this complex may protect the cell from the rise in temperature by mediating a faster transfer of electrons to PSI. In the same study, the NADH dehydrogenase 1 complex proteins NdhA, NdhJ, NdhM, NdhI and NdhH were all up-regulated. This observation implies that faster cyclic electron transfer occurred, decreasing the ROS generation with a concomitant enhancement of PSII thermotolerance (Rowland et al. 2010). In addition, ATP synthase chains of CF1 (α and β subunits) increase in heat-shocked *Synechocystis* sp. PCC 6803 (Slabas et al. 2006).

Simultaneously, the PBS rode-core linker CpcG2 was observed to decrease, which may affect the stability of PSII, thereby limiting light harvesting and the energy that must be channelled across the PETC (Rowland et al. 2010).

A strategy based on LC-MS/MS coupled to iTRAQ labeling revealed a slightly lower abundance of AcsF (ChlAI) and ChlH, both of which are involved in chlorophyll synthesis (Rowland et al. 2010). This decrease probably diminishes the light harvesting, protecting the cell from an excess of light energy. Furthermore, the water-soluble carotenoid protein was shown to be elevated by heat treatment in *Synechocystis* sp. PCC 6803 (Slabas et al. 2006), which may also prevent photo-damages of cells by absorbing excess of energy.

RuBisCO (i.e., RbcS and RbcL) was reportedly down-regulated when *Synechocystis* sp. PCC 6803 was acclimated to 38°C (Rowland et al. 2010). The authors claimed that because RuBisCO is one of the most abundant proteins in pho-

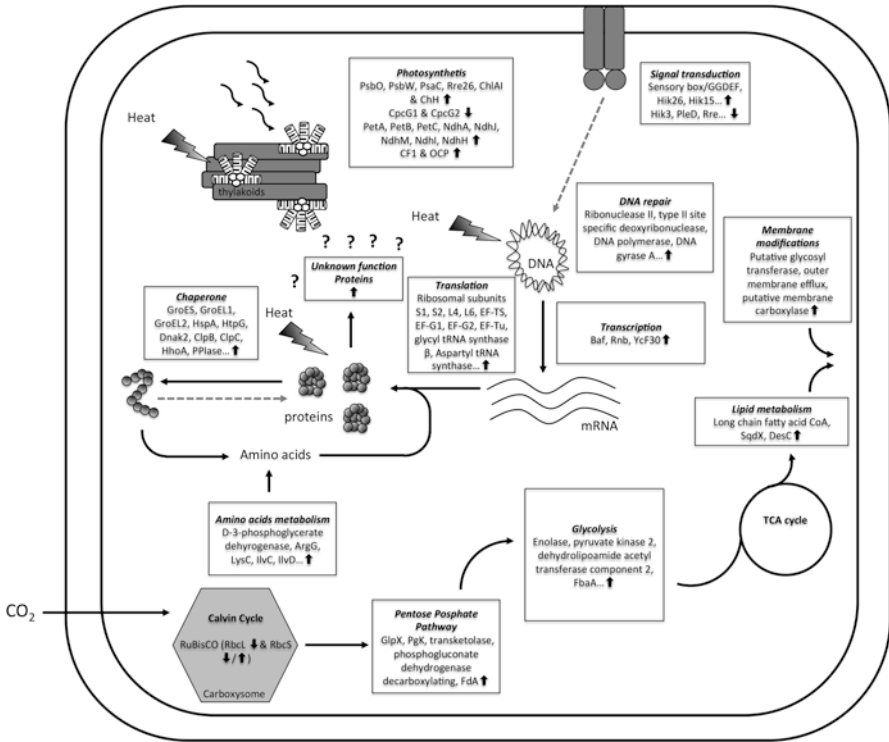


Fig. 5 Schematic diagram sketch for the heat-stress acclimation strategy taken from experimental data of several studies carried out onto *Synechocystis* sp. PCC 6803 and *Spirulina platensis*. (ArgG) Argininosuccinate synthase, (Baf) putative transcriptional activator Baf, (CF1) ATP synthase subunit alpha, (ChlA), (ChlH) magnesium-chelatase subunit ChlH, (ClpB) ATP-dependent caseinolytic protease ATP-binding subunit B, (ClpC) ATP-dependent caseinolytic protease ATP-binding subunit C, (CpcG1/2) phycobilisome rod-core linker polypeptide CpcG1/2, (DesC) delta-9 desaturase, (DNA) deoxyribonucleic acid, (Dnak2) heat shock 70 kDa protein, (EF-TS/G1/G2/Tu) elongation factor TS/G1/G2/Tu, (FbaA) fructose-bisphosphate aldolase, (FdA) fructose-1,6-bisphosphate aldolase, (GlpX) D-fructose 1,6-bisphosphatase class 2/sedoheptulose 1,7-bisphosphatase, (GroEL1), GroEL2, (GroES) heat shock 10 kDa protein, (HhoA) putative serine protease, (Hik15) sensory transduction histidine kinase hik15, (Hik26) sensory transduction histidine kinase hik26, (Hik3) sensory transduction histidine kinase hik3, (HspA) heat shock protein A, (HtpG) chaperone protein HtpG, (IlvC) ketol-acid reductoisomerase, (IlvD) dihydroxy-acid dehydratase, (LysC) aspartokinase, (mRNA) messenger ribonucleic acid, (NdhA) NAD(P) H-quinone oxidoreductase subunit 1, (NdhH/I/J/M) NAD(P)H-quinone oxidoreductase subunit H/I/J/M, (OCP) orange carotenoid protein, (PetA) cytochrome f, (PetB) cytochrome b₆, (PetC) cytochrome b₆/f complex iron-sulfur subunit, (PgK) phosphoglycerate kinase, (PleD) two component response regulator PleD, (PPIase) peptidyl-prolyl cis-trans isomerase, (PsaC) photosystem I iron-sulfur centre, (PsbO) photosystem II manganese-stabilizing polypeptide, (PsbW) photosystem II reaction centre Psb28 protein, (RbcL) ribulose-1,5-diphosphate carboxylase/oxygenase large subunit, (RbcS) ribulose-1,5-diphosphate carboxylase/oxygenase small subunit, (Rnb) ribonuclease II, (Rre) heat stress-responsive two component signal transduction system response regulator, (Rre26) response regulator for energy transfer from PBS to photosystems, (RuBisCO) ribulose-1,5-diphosphate carboxylase/oxygenase, (SqdX) sulfolipid sulfoquinovosyldiacylglycerol biosynthesis protein, (TCA) tricarboxylic acid, (Ycf30) transcriptional regulator

tosynthetic cells, a high level of synthesis of this protein might result in a critical decrease in the intracellular N pool. Ultimately, this N pool may be required for other cellular purposes, such as synthesis of key proteins, including chaperones (see below). In this context, cells may try to conserve N (Rowland et al. 2010). In contrast, heat treatment induced a decrease in the abundance of the RbcL, whereas RbcS showed an increased expression in thermo-acclimated *Synechocystis* sp. PCC 6803; the authors therefore suggested a preferential breakdown of RbcL that may be not compensated by de novo synthesis of the protein (Slabas et al. 2006).

Proteins involved in the Calvin-cycle increased during the heat treatment, including the NAD(P)-dependent glyceraldehyde-3-phosphate dehydrogenase Gap2, the fructose-bisphosphate aldolase FbaA, the fructose-1,6-/sedoheptulose-1,7-bisphosphatase GlpX, the phosphoglycerate kinase Pgk and the transketolase were up-regulated in *Synechocystis* sp. PCC 6803 (Slabas et al. 2006).

Stress Related Proteins

Chaperone proteins are induced by several stresses, including the heat shock (coming references). Heat treatment was demonstrated to induce numerous chaperones (e.g., GroES, GroEL1, GroEL2, HspA, HtpG, DnaK2, ClpB, ClpC and HhoA) in *Synechocystis* sp. PCC 6803 by 2-DE-MALDI-TOF-MS (Slabas et al. 2006; Suzuki et al. 2006), and in *Spirulina platensis* by 2D-DIGE-MALDI-TOF-MS (Hongsthong et al. 2009) and iTRAQ LC-MS/MS (Kurdrid et al. 2011), respectively. Chaperones are known to be involved in the folding of newly synthesized proteins as well as solubilizing aggregated proteins under high temperature stress conditions (Rajaram et al. 2014). As previously described (see section “[Optimization of Intracellular N Content](#)”), the ATP-dependent Clp proteases are critical for cell homeostasis (Clarke 1999). For example, the HtpG chaperone has been demonstrated to be essential for thermoresistance by playing a role in the PBP synthesis and/or degradation (Tanaka and Nakamoto 1999).

ClpB and DnaK are suggested to be associated in vivo, and this complex targets the un(folding)/disaggregation of protein aggregates. The ATP-dependent Clp proteases (e.g., ClpB, ClpC and HhoA) play a role in the degradation or disaggregation of aggregated proteins and potentially in transport of protein (Doyle et al. 2015; Lee et al. 2004).

The peptidyl-prolyl *cis-trans* isomerase PPIase similarly showed higher levels in heat-shocked *Synechocystis* sp. PCC 6803 (Slabas et al. 2006). PPIase proteins are chaperones that modify peptide linking between a given amino acid and a prolyl residue, thereby altering the *cis* to *trans* or *trans* to *cis* conformation. Consequently, PPIases may modify the folding of proteins and have also been proposed to be involved in different cellular process (e.g., gene expression and signal transduction) (Ünal and Steinert 2014).

Transcription and Translation

Whereas the chaperones may counteract the loss of proteins through unfolding/aggregation, the modification of the de novo synthesis of proteins may balance this protein loss. Indeed, an increase in the relative abundance of proteins involved in transcription (e.g., the putative transcriptional activator Baf, ribonuclease II Rnb and YcF30 (Kurdrid et al. 2011; Slabas et al. 2006)) and translation (e.g., the elongation factors EF-Ts, EF-G1, EF-G2, EF-Tu; the ribosomal subunits 30S S1 and S2, 50S L4 and L6, glycyl-tRNA synthase β chain and aspartyl-tRNA synthase (Slabas et al. 2006; Suzuki et al. 2006)) could be evidence that cells try to balance the potential loss of proteins by aggregation and/or degradation associated with the increase in heat-induced chaperone proteins.

In addition, enzymes involved in amino acid biosynthesis increase in heat-shocked *Synechocystis* sp. PCC 6803, including D-3-phosphoglycerate dehydrogenase (i.e., glycine, serine and threonine metabolism), the argininosuccinate synthase ArgG (i.e., alanine, aspartate, arginine and proline metabolism), the aspartate kinase Lysc (i.e., glycine, serine, threonine and lysine), the keto-acid-reductoisomerase IlvC and the dihydroxyacid dehydratase IlvD (i.e., both involved in valine, leucine and isoleucine metabolism) (Slabas et al. 2006).

Signal Transduction

Several proteins involved in signal transduction were observed to increase (e.g., two-component hybrid sensor histidine kinase, sensory box/GGDEF family protein, multi-sensor signal transduction histidine kinase, the putative two-component sensor histidine kinase Hik26, two component hybrid sensor and regulator Hik15 two-component sensor histidine kinase) in thermally shocked *S. platensis* (Hongsthong et al. 2009; Kurdrid et al. 2011). In contrast, a decrease in the relative abundance in component of signal transduction pathways has been reported, including the two-component hybrid sensor and regulator Hik3, and the two component response regulator PleD in *S. platensis* (Kurdrid et al. 2011). Histidine kinases (Hik) are known to perceive environmental changes (e.g., osmotic stress and low temperature) and transduce them to Rre protein, which affect the transcription of genes, such as *hliA*, *hliB*, *sigD* in salt-stressed *Synechocystis* sp. (Novikova et al. 2007).

The LexA protein (which may regulate the expression of the *nif* cluster (Mueller et al. 2016)) was elevated by heat treatment in *Synechocystis* sp. PCC 6803 (Slabas et al. 2006).

DNA Damage and Repair

The protein DEAD/DEAH box helicase was observed to be up-regulated in heat-shocked *S. platensis* (Hongsthong et al. 2009); this protein is involved in RNA maturation and proof-reading as well as the enhancement of DNA-unwinding (Linder and Jankowsky 2011). Several proteins involved in DNA damage, repair

and modification (e.g., ribonuclease II, type II site-specific deoxyribonuclease, RNA-directed DNA polymerase and DNA gyrase subunit A) were strongly up-regulated in *S. platensis*. The fact that heat shock induces DNA gyrase proteins could indicate an increase in DNA repair activity during thermal shock via a repair system other than the ROS system (Hongsthong et al. 2009). This is in agreement with the previously described enhanced mechanism of energy transfer across the PETC, which equally avoids ROS generation (see above).

Sugar Metabolism

Several enzymes of the glycolytic/pentose phosphate pathway (e.g., enolase, pyruvate kinase 2,6-phosphogluconate dehydrogenase-decarboxylating) were shown to be increased in *Synechocystis* sp. PCC 6803. In addition, dihydrolipoamide acetyl transferase component E2 (i.e., component of pyruvate transferase) was up-regulated in heat-shocked *Synechocystis* sp. PCC 6803 (Slabas et al. 2006).

Enzymes involved in energy metabolism (the fructose biphosphate aldolase Fda, the glycerol-3-phosphate dehydrogenase GlpD, the 1-deoxyxylulose-5-phosphate synthase Dxs and glyceraldehyde-3-phosphate dehydrogenase) were less abundant, which may indicate a mitigated flux of secondary metabolites in *Synechocystis* sp. PCC 6803 (Rowland et al. 2010).

Energy metabolism is also affected in *Spirulina platensis*, which up-regulated proteins such as Fe-S oxidoreductase and putative aldehyde dehydrogenase (Kurdrid et al. 2011).

Lipid Metabolism and Membrane Modifications

Enzymes involved in lipid metabolism (e.g., long-chain-fatty-acid CoA and sulphoquinovosyldiacylglycerol SqaX in *Synechocystis* sp. PCC 6803 (Rowland et al. 2010) and the delta-9-desaturase DesC in *S. platensis* (Kurdrid et al. 2011)) were less abundant, which also highlighted a mitigated flux of secondary metabolites in lipid biosynthesis. Additionally, membrane modifications could occur because glycosyl transferases were up-regulated as were outer membrane efflux protein, putative glycosyl transferase and putative membrane carboxylase in *S. platensis* (Hongsthong et al. 2009; Kurdrid et al. 2011). The latter protein has been reported to play a role in thermal acclimation (Borges et al. 2004; Hongsthong et al. 2009).

Proteins of Unknown Function

Hypothetical and unknown proteins are a part of the heat shock response in *Synechocystis* sp. PCC 6803 (Rowland et al. 2010; Slabas et al. 2006; Suzuki et al. 2006) and *S. platensis* (Hongsthong et al. 2009). Sequence analysis of the hypothetical protein Slr0244 revealed that this protein could be a member of the universal stress protein family (Rowland et al. 2010).

Light Stress

Alterations in Photosynthesis

As photosynthesis implies the ability to harvest light energy, changes in illumination irrevocably induce alterations in the photosynthetic apparatus. By ESI qQ-TOF-MS/MS analysis of iTRAQ labeled peptides, a decrease has been reported in protein abundance of photosystems I (e.g., PsaA, PsaE and PsaB) and II (e.g., PsbO, PsbB, PsbD, PsbD and Pcb) in *Prochlorococcus marinus* MED4 following the high light exposure. The authors concluded that the down-regulation of PSI and PSII proteins reduces the cell's sensitivity to photo-damage. However, an increase in the abundance of the PSII reaction core protein D1 was reported in *P. marinus* MED4 in the short term, whereas this protein returned to initial levels after acclimation (Pandhal et al. 2007). The protein D1 plays a critical role in the degradation of PBSs via the NblA mechanism (Baier et al. 2004; Sendersky et al. 2015).

A modification in carotenoids is also involved in the acclimation process, since phytoene desaturase (i.e., conversion of phytoene into ζ -carotene) was observed to increase slightly in *P. marinus* MED4 (Pandhal et al. 2007). As previously described, carotenoids scavenge free radicals as well as channel and dissipate excess of light, thereby protecting the cell from radiation damages (Harris et al. 2016; Kirilovsky and Kerfeld 2012; Wilson et al. 2006).

No significant changes occurred for the RuBisCO enzymes in *P. marinus* MED4 under the differential light irradiation (Pandhal et al. 2007).

Stress Related Proteins

Several stress-related proteins were shown to be significantly up-regulated in *P. marinus* MED4, including GroEL, HtpG and GroES (Pandhal et al. 2007). HtpG plays a crucial role in thermal survival by participating in PBP synthesis and/or degradation (Tanaka and Nakamoto 1999).

Impact on Growth Yield

An increase in the relative abundance of both FtsZ (which initiates cell division) and the putative septum site-determining protein MinD has been reported and correlates with the increase in the growth rate of high-light-exposed *P. marinus* MED4 (Pandhal et al. 2007).

Diurnal Rhythm

The diurnal cycle (commonly implemented as 12 h light to 12 h dark phase) induces intricate cyclic physiological activities (Fig. 6) with a high rate of light harvesting during the light phase, and a high rate of N₂ fixation during the dark phase. The circadian clock (i.e., intrinsic mechanisms of physiological regulations) coordinates the appropriated physiological activities between gene expression and protein synthesis by anticipating the cyclic external changes (Cohen and Golden 2015).

The diurnal rhythm (or circadian cycle) represents changes in two critical parameters in the environment with an increase in (i) light irradiances (see light stress), and (ii) temperature (see heat shock stress).

Circadian Clock

The key drivers in the circadian clock are Kai-A, Kai-B and Kai-C (Cohen and Golden 2015). None of these three actors showed any changes in their abundance during cyclic light irradiation of *Synechococcus elongatus* PCC 7942. Similarly, circadian input kinase and adaptive sensor A did not exhibit a cyclic abundance (Guerreiro et al. 2014).

Exhibiting the highest abundance during the light phase in *Synechococcus elongatus* PCC 7942, LabA (i.e., low-amplitude and bright protein A) is known to negatively regulate the key circadian regulator KaiC (Taniguchi et al. 2007, 2012).

Because the circadian clock anticipates diurnal changes, several proteins with a crucial role in the dark phase are induced at the end of the light phase. For example, a label-free approach relying on LC-MS/MS investigation of the proteome and spectral count quantification highlighted that the transcription factor RpaA (i.e., regulator of PBS association A) was strongly induced at the end of the light period and beginning of the dark phase, whereas RpaB (i.e., regulator of PBS association B) was more abundant during the light phase in *Cyanothece* sp. PCC 51142 (Stöckel et al. 2011). It has been reported that RpaA is a part of a two-component system interacting with the histidine kinase SasA, which coordinates the expression of genome-wide circadian genes as well as cell division. RpaB is reportedly crucial for acclimation to stresses, such as oxidative stress (Cohen and Golden 2015; Takai et al. 2006).

Alterations in Photosynthesis

Because light constitutes the primary entry of energy, photosynthesis components are actively regulated throughout light/dark cycle. For example, HliB was reported to increase at the beginning of the light phase in *Cyanothece* sp. ATCC 51142 (Stöckel et al. 2011). The high-light-inducible proteins (i.e., HLIPs including HliB) accumulate in excess of light and further dissipate the excess light energy (Havaux

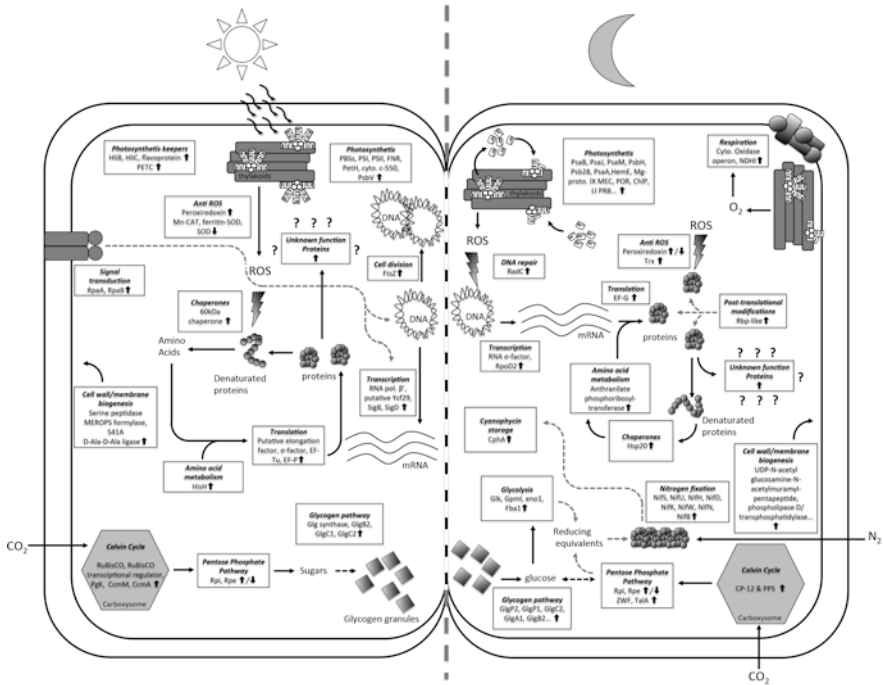


Fig. 6 Schematic diagram sketch depicting the proteome modification induced by a diurnal cycle drawn from experimental data of several studies carried out onto *Arthrospira platensis* PCC 8005, *Cyanothece* sp. (PCC 51142 and PCC 7822), *Nostoc flagelliforme*, *Synechococcus elongatus* PCC 7942. ((☀)) *light-phase*: (CcmM/A) carbon dioxide concentrating mechanism protein M/A, (cyto. c-550) cytochrome c-550, (EF-Tu/P) elongation factor Tu/P, ([ferritin-]SOD) [ferritin-]dismutase, (FNR) ferredoxin-NADP+ reductase, (FtsZ) cell division protein FtsZ, (Glg synthase) glycogen synthase, (GlgB2) 1,4-alpha-glucan branching enzyme GlgB2, (GlgC1/2) Glucose-1-phosphate adenylyltransferase GlgC1/2, (HisH) Imidazole glycerol phosphate synthase subunit HisH, (HliB/C) high light-inducible protein B/C, (Mn-CAT) manganese catalase, (PBS) phycobilisome, (PetH) Ferredoxin-NADP reductase, (PgK) phosphoglycerate kinase, (PsbV) Cytochrome c-550, (PSI) photosystem I, (PSII) photosystem II, (putative Ycf29) putative two-component response regulator Ycf29, (RNA pol. β') DNA-directed RNA polymerase subunit β' , (RpaA/B) two-component response regulator RpaA/B, (Rpe) pentose-5-phosphate-3-epimerase, (Rpi) ribose-5-phosphate isomerase, (RuBisCO) ribulose-1,5-diphosphate carboxylase/oxygenase, (SigB/D) RNA polymerase sigma-B/D factor, (σ -factor) RNA polymerase sigma factor. ((☾)) *dark phase*: (ChlP) geranylgeranyl diphosphate reductase, (CO_2) carbon dioxide, (CP-12) regulator of Calvin-cycle CP-12, (CphA) cyanophycin synthase, (Cyto. Oxidase operon) cytochrome oxidase operon, (DNA) deoxyribonucleic acid, (EF-G) elongation factor G, (eno1) enolase 1, (Fba1) Class II fructose-1,6-bisphosphate aldolase FbaA, (GlgA1) glycogen synthase, (GlgB2) 1,4-alpha-glucan branching enzyme, (GlgC2) glucose-1-phosphate adenylyltransferase, (GlgP1/2) glycogen phosphorylase, (Glik) glucokinase, (Gpml) 2,3-bisphosphoglycerate-independent phosphoglycerate mutase I, (HemE) uroporphyrinogen decarboxylase, (Hsp20) heat shock protein 20, (LI PRB) light-independent protochlorophyllide reductase subunit B, (Mg-proto. IX MEC) magnesium-protoporphyrinogen IX monomethyl ester oxidative cyclase, (mRNA) messenger ribonucleic acid, (N_2) dinitrogen, (NDHI) NAD(P)H-quinone oxidoreductase subunit I, (NifB) FeMo cofactor biosynthesis protein, (NifD) nitrogenase molybdenum-iron protein alpha chain, (NifH) Nitrogenase

et al. 2003). These proteins are also suggested to protect and ensure the stability of the PSII (He et al. 2001). In addition, a higher amount in flavoproteins have been observed and are suggested to participate in the photoprotection of PSII (Zhang et al. 2009). The cells encountered the dark condition (i.e., low limited harvesting of light), and underwent a progressive increase in light irradiance, ultimately needing to channel more energy across the photosynthetic apparatus.

After a rise in light, proteins from PBS, PSI and PSII were at their highest level during light phase in several cyanobacteria, such as *S. elongatus* PCC 7942 (Guerreiro et al. 2014), *Cyanothece* sp. PCC 7822 (Welkie et al. 2014) and *Arthrospira platensis* PCC 8005 (Matallana-Surget et al. 2014). This global up-regulation indicates an acclimation of photosynthetic cells to higher light radiation, thereby optimizing the efficiency of light harvesting for the photosynthetic electron transfer chain.

Downstream of the light harvesting, the PETC also showed differentially expressed proteins, increasing during the light phase (e.g., plastocyanin, ferredoxin-NADPH oxidoreductase PetH, extrinsic cytochrome c-550 and PsbV). For example, PsbV is also known to participate in the stability of the manganese cluster of the OEC in *Cyanothece* sp. PCC 51142. The electron carrier proteins from the donor as well as the acceptor side of PSI were found to be simultaneously up-regulated, whereas PsaB, PsaJ, PsaM, PsbH and Psb28 increased during the dark phase in *Cyanothece* sp. PCC 51142. The authors hypothesized that light triggers faster degradation of some subunits during the day (Stöckel et al. 2011). This observation contrasts with the up-regulation of the PBS linker proteins PsbA (D1), PsaA and PsaB proteins during the dark phase in another strain, *Cyanothece* sp. PCC 7822. Then, the authors postulated that the expression of D1 protein could balance the disorganization of the PSII that cannot evolve O₂ under N₂-fixing conditions within *Cyanothece* sp. PCC 7822 incubated in the dark (see below) (Welkie et al. 2014). Elevated PsaB content during the dark phase may coincide with the simultaneous increase in enzymes involved in chlorophyll synthesis (e.g., uroporphyrinogen decarboxylase HemE, Mg-protoporphyrinogen IX monomethyl ester oxidative cyclase, protochlorophyllide reductase POR and geranylgeranyl hydrogenase Chlp in *Cyanothece* sp. PCC 51142 (Stöckel et al. 2011), light-independent protochlorophyllide reductase subunit B in *S. elongatus* PCC 7942 (Guerreiro et al. 2014)).

←

Fig 6 (continued) iron protein, (NifK) nitrogenase molybdenum-iron protein beta chain, (NifN) nitrogenase molybdenum-iron cofactor biosynthesis protein, (NifS) cysteine desulfurase, (NifU) scaffold activity protein NifU, (NifW) nitrogenase-stabilizing/protective protein, (PETC) photosynthetic electron transfer chain, (POR) light-dependent protochlorophyllide reductase, (PsaA/B) photosystem I P700 chlorophyll a apoprotein A1/A2, (PsaJ) photosystem I reaction centre subunit IX, (PsaM) photosystem I reaction centre subunit XII, (PsbH) photosystem II reaction centre protein H, Psb28, (RadC) DNA repair protein RadC, (Rbp-like), (RNA σ -factor) RNA polymerase sigma factor, (ROS) reactive oxygen species, (Rpe) pentose-5-phosphate-3-epimerase, (Rpi) ribose-5-phosphate isomerase, (RpoD2) Group2 RNA polymerase sigma factor, (TalA) transaldolase, (Trx) thioredoxin, (ZWF) glucose-6-phosphate 1-dehydrogenase

In contrast, an ICPL labeling strategy coupled with an LC-MS/MS approach revealed that the D1 protein from PSII was down-regulated during the dark/light cycle in *Arthrospira platensis* sp. PCC 8005 in addition to nearly all identified proteins associated with PSII and PSI (e.g., CP47, D1, D2, CP43, PsaB, PsaA, PsaF and ATP synthase). The down-regulation of PSII was proposed to result from excess protein turnover occurring at the end of the day. It has been argued that *Arthrospira* sp. PCC 8005 may anticipate the coming light transition by synthesizing photosynthesis-related proteins at the switch of the light/dark phase (Matallana-Surget et al. 2014).

The regulator of phycobilisome-associated A and B did not display a cyclic abundance in *S. elongatus* PCC 7942 (Guerreiro et al. 2014), nor did the cytochrome *b₆f* complex and the ATPase synthase in *Cyanothece* sp. PCC 7822 (Welkie et al. 2014). Furthermore, the highest levels of the cytochrome oxidase operon proteins were observed during the dark phase, which suggests a respiration activity that may be related to N₂ fixation. NADH dehydrogenase subunit I was also proposed to be dark inducible in *Cyanothece* sp. PCC 7822 (Welkie et al. 2014).

Several light-sensing proteins exhibit differential changes in their abundance over the diurnal cycle (e.g., the phytochrome A protein AphA) in *Cyanothece* sp. PCC 51142 (Stöckel et al. 2011) as well as the high-light inducible polypeptide HliC in *S. elongatus* PCC 7942 (Guerreiro et al. 2014).

Stress Related Proteins

One group of stress-related proteins was shown to be most abundant during the light phase, including proteins involved in protein turn-over and folding (e.g., 60 kDa chaperone) in *S. elongatus* PCC 7942. Another group of proteins preferentially showed the highest abundance during the dark phase, including proteins involved in chaperoning (e.g., heat shock protein Hsp20), defence mechanisms (e.g., ATPase), and DNA repair (e.g., DNA repair protein RadC) in the same cyanobacterium (Guerreiro et al. 2014).

The abundances of Mn-CAT, ferritin, Fe-SOD, SOD were down-regulated in *Nostoc flagelliforme* during a modification in light irradiation and temperature that mimicked a full day (i.e., low to high light/temperature and back to low) (Liang et al. 2013). In contrast, peroxiredoxin was up-regulated; this protein constitutes an antioxidant among the antioxidation protein superfamily and plays a role in ROS scavenging (Rhee 2016). Ferritin showed the highest level at the beginning of light phase (i.e., morning) and was lowest at “midday” (i.e., peak in light intensity), indicating that it may act as an antioxidant to remove excess of H₂O₂ generated throughout the diurnal cycle (naturally observed with the intrinsic activity of the PSII) (Liang et al. 2013). Similarly, label-free analysis (LC-MS/MS, spectral count) of *Cyanothece* sp. ATCC51142 showed that peroxiredoxin peaked at night, probably to degrade the ROS, when the nitrogenase exhibits the highest activity (Aryal et al. 2013). In contrast, the closest relative strain, *Cyanothece* sp. ATCC 7822, showed a minimal level of periredoxin, whereas thioredoxin was at its highest level during the dark phase, which may compensate for the lower level of peroxiredoxin (Aryal et al.

2013). These observations imply that antioxidation (via ferritin, peroxiredoxin and thioredoxin) contributes to cell acclimation to changes in light exposure, and in energy transfer across the PETC.

Transcription and Translation

De novo synthesis of proteins has been shown to be affected during both light and dark phases. One group of proteins showed the highest abundance during the light phase in transcription, translation (e.g., methionine aminopeptidase in *S. elongatus* sp. PCC 7942 (Guerreiro et al. 2014) and the protein chain elongation factor EF-G in *A. platensis* sp. PCC 8005 (Matallana-Surget et al. 2014)), and amino acid metabolism (e.g., imidazole glycerol phosphate synthase subunit HisH in *S. elongatus* sp. PCC 7942 (Guerreiro et al. 2014)).

However, other proteins involved in the same physiological event peak during the dark phase: transcription and translation (e.g., RNA polymerase sigma factor, RNA polymerase sigma factor RpoD2 and the elongation factor EF-G in *S. elongatus* sp. PCC 7942 (Guerreiro et al. 2014)), and amino acid metabolism (e.g., imidazole glycerol phosphate synthase subunit HisH and the anthranilate phosphoribosyltransferase in *S. elongatus* sp. PCC 7942 (Guerreiro et al. 2014)).

Additionally, glycine-rich RNA-binding protein Rbp-like was reported to increase throughout the circadian cycle in *A. platensis* sp. PCC 8005 (Matallana-Surget et al. 2014), and it was previously reported that this kind of protein plays a regulator role in post-transcriptional regulation of circadian clock (Wang et al. 2013).

Growth and Cell Wall/Membrane Biogenesis

One group of proteins involved in cell wall/membrane biogenesis was shown to be most abundant during the light phase (e.g., serine peptidase MEROPS family S41A in *S. elongatus* sp. PCC 7942 (Guerreiro et al. 2014)). Furthermore, the identification of the protein FtsZ during the light phase (and not during the dark phase) indicated that cell division occurs during the light phase in *A. platensis* sp. PCC 8005, and cell division implies de novo synthesis of lipids during the light phase. The abundance of D-Ala-D-Ala ligase oscillates diurnally, peaking at highest light levels; this enzyme is an ATP-grasp enzyme superfamily member involved in bacterial cell wall (peptidoglycans and fatty acids) and glutathione synthesis (Matallana-Surget et al. 2014). Taken together, these observations suggested that cell wall biogenesis is diurnally coordinated.

In contrast, proteins involved in both cell wall/membrane biogenesis (e.g., UDP-N-acetylglucosamine--N-acetylmuramyl-(pentapeptide) pyrophosphoryl-undecaprenol N-acetylglucosamine transferase) and lipid metabolism (e.g., phospholipase D/transphosphatidylase) showed the highest abundance during the dark phase in *S. elongatus* sp. PCC 7942 (Guerreiro et al. 2014).

Signal Transduction

Several proteins involved in signal transduction showed the highest levels during the light phase, whereas other proteins related to this function were higher abundant during the dark phase in *S. elongatus* sp. PCC 7942 (Guerreiro et al. 2014).

N Metabolism

Nitrogen fixation preferentially occurs during the dark phase of the diurnal cycle as demonstrated by the differential expression of Nif-related proteins throughout the diurnal cycle (Liang et al. 2013; Stöckel et al. 2011). In the *Cyanothece* strains ATCC 51142 and PCC 7822, the nitrogenase operon (i.e., NifS, NifU, NifH, NifD, NifK, NifX, NifW, NifN and NifB) was shown to be up-regulated during the dark phase, consistent with nitrogen fixation (Aryal et al. 2013; Stöckel et al. 2011; Welkie et al. 2014).

Cyanophycin synthase CphA was shown to increase during the late light and decrease during the dark phase until early light in *Cyanothece* sp. PCC 7822. The authors suggested that CphA is required during and after N₂ fixation, which explains the abundance profile in *Cyanothece* sp. PCC 7822 (Welkie et al. 2014).

C Metabolism

Differences in the expression pattern of central metabolism proteins, including those involved in the TCA cycle, glycolysis and pentose phosphate pathway (hereafter PPP), are also revealed, when cyanobacteria were subjected to diurnal changes.

Proteins involved in the PPP (e.g., Rpi and Rpe) were shown to be up-regulated during the light in parallel with the induction of RuBisCO (both subunits) during the late-dark and early-light periods in *Cyanothece* sp. PCC 7822 (Welkie et al. 2014). Several enzymes involved in the Calvin-Benson-Bassham cycle (e.g., Prk, Rpe and GlpX) also showed greater abundance during the light phase in *Cyanothece* PCC 51142 (Stöckel et al. 2011). The PPP-related proteins (e.g., Zwf and Rpe) were slightly up-regulated during the early dark period and down-regulated during the late dark period, suggesting a primary function in providing reducing equivalents for N₂ fixation in the early dark stage in *Cyanothece* sp. PCC 7822 (Welkie et al. 2014). A higher amount of the carbon dioxide concentration mechanism/carboxysome shell protein has been reported at the early stage of light phase in *Nostoc flagelliforme* investigated using a 2D-MALDI-TOF-MS/MS approach (Liang et al. 2013). Moreover, glycogen synthase was shown to be light inducible, coupling the CO₂ fixation and glycogen production (i.e., storage of fixed C) in *Cyanothece* sp. PCC 7822 (Welkie et al. 2014) as were the 1,4- α -glucan branching enzyme GlgB2, glucose-1-phosphate adenylyltransferases GlgC1 and GlgC2 in *Cyanothece* sp. PCC 51142 (Stöckel et al. 2011).

It has been reported that glycogen phosphorylases GlgP1 and GlgP2 were differentially expressed, with the highest abundance during the early light phase and the late dark phase in *Cyanothece* sp. PCC 7822, respectively. GlgA1 was higher during the late-dark/early light, whereas GlgA2 level seemed to be constant throughout the diurnal cycle (Welkie et al. 2014).

Whereas glycogen is synthesized when cells are exposed to light, the rate-limiting enzymes involved in glycogen degradation (e.g., GlgP1, GlgC2, GlgA1, GlgB2 and GlgP2), oxidative pentose phosphate (e.g., glucose-6-phosphate dehydrogenase Zwf and the transaldolase AB family TalA) and glycolysis (e.g., glucokinase Glk, 2,3-bisphosphoglycerate-independent phosphoglycerate mutase GpmI, enolase eno1 and fructose-1,6-bisphosphatase I) were highly up-regulated during the dark phase in *Cyanothece* sp. ATCC 51142. The authors emphasized that Zwf plays a critical role in carbon metabolism by redirecting C into the OPP and initiating the oxidation of glucose in parallel with the production of NADPH (i.e., reductants for both nitrogen fixation and respiratory processes). It was suggested that the cellular energy requirements during the dark are overwhelmingly supplied by the oxidative phosphorylation, and the metabolic reactions leading to malate and oxaloacetate are both favoured over glycolytic reactions in concert with substrate-level phosphorylation. Moreover, fructose-1,6-bisphosphate I (i.e., gluconeogenesis) showed a greater abundance, implying that the cellular dark metabolism is not limited by ATP supply in *Cyanothece* sp. PCC 51142 (Stöckel et al. 2011).

Despite these differences in their expression pattern in central metabolism in *Cyanothece* sp. PCC 7822, it was emphasized that the proteins did not vary drastically throughout the dark/light cycle (Welkie et al. 2014). For example, most abundances of proteins involved in the glycolysis proteins were similar during both the light and dark phases in *Cyanothece* sp. PCC 7822. Intriguingly, the two gene copies of phosphofructokinase were differentially regulated, one peaking during the light phase and the other during the dark phase. Similarly, Fba1 peaked during the late dark/early light period, whereas Fba2 was strongly induced during the late light/early dark period (Welkie et al. 2014).

In contrast, *A. platensis* sp. PCC 8005 could preferentially fix CO₂ during the dark phase as the authors suggested because proteins, such as the putative Calvin-cycle regulator CP12-like protein and phosphoenol pyruvate synthase, were shown to be more abundant during the dark phase (Matallana-Surget et al. 2014). In addition, glycolysis activity may be decreased during the day, since the abundance of the enzyme fructose/tagatose bisphosphate (i.e., fructose-1,6-bisphosphate cleavage into *P*-glyceraldehyde and dihydroxyacetone-*P*) displayed a decreased value in *N. flagelliforme* (Liang et al. 2013).

The TCA cycle proteins identified were slightly induced during the light cycle, and the authors suggested that the TCA cycle is mostly used for the generation of metabolites in *Cyanothece* sp. PCC 7822 (Welkie et al. 2014).

During the dark phase, a group of proteins involved in different metabolic activities such as co-enzymes (e.g., aminotransferase), vitamin synthesis (e.g., NAD(P) transhydrogenase subunit β) and carbohydrate synthesis (e.g., phosphoenol pyruvate synthase) showed the highest abundance in *S. elongatus* sp. PCC 7942 (Guerreiro et al. 2014).

Unknown Function Proteins

As described for other acclimation responses, numerous hypothetical proteins have been reported to be differentially expressed (e.g., *A. platensis* sp. PCC 8005 (Matallana-Surget et al. 2014) and *N. flagelliforme* (Liang et al. 2013)). In this context, further studies and characterization of these proteins are required to achieve a more complete understanding of the regulatory networks in cyanobacteria.

Acknowledgements Frédéric Deschoenmaeker is an F.R.I.A. PhD student. This manuscript was edited for proper English language by qualified native English speaking editors at American Journal Experts.

References

- Abdallah C, Dumas-Gaudot E, Renaut J, Sergeant K (2012) Gel-based and gel-free quantitative proteomics approaches at a glance. *Int J Plant Genom* 2012:1–17
- Abed RMM, Dobretsov S, Sudesh K (2009) Applications of cyanobacteria in biotechnology. *J Appl Microbiol* 106:1–12
- Aebersold R, Mann M (2003) Mass spectrometry-based proteomics. *Nature* 422:198–207
- Aggarwal K, Choe LH, Lee KH (2006) Shotgun proteomics using the iTRAQ isobaric tags. *Brief Funct Genom Proteom* 5:112–120
- Akimoto S, Yokono M, Hamada F, Teshigahara A, Aikawa S, Kondo A (2012) Adaptation of light-harvesting systems of *Arthrospira platensis* to light conditions, probed by time-resolved fluorescence spectroscopy. *Biochim Biophys Acta* 1817:1483–1489
- Aryal UK, Callister SJ, Mishra S, Zhang X, Shutthanandan JI, Angel TE, Shukla AK, Monroe ME, Moore RJ et al (2013) Proteome analyses of strains ATCC 51142 and PCC 7822 of the diazotrophic cyanobacterium *Cyanothece* sp. under culture conditions resulting in enhanced H₂ production. *Appl Environ Microbiol* 79:1070–1077
- Baier K, Lehmann H, Stephan DP, Lockau W (2004) NblA is essential for phycobilisome degradation in *Anabaena* sp. strain PCC 7120 but not for development of functional heterocysts. *Microbiology* 150:2739–2749
- Baldwin MA (2003) Protein identification by mass spectrometry: issues to be considered. *Mol Cell Proteomics* 3:1–9
- Bantscheff M, Schirle M, Sweetman G, Rick J, Kuster B (2007) Quantitative mass spectrometry in proteomics: a critical review. *Anal Bioanal Chem* 389:1017–1031
- Bauer M, Ahrné E, Baron AP, Glatter T, Fava LL, Santamaria A, Nigg EA, Schmidt A (2014) Evaluation of data-dependent and -independent mass spectrometric workflows for sensitive quantification of proteins and phosphorylation sites. *J Proteome Res* 13:5973–5988
- Bazylnski DA et al (2014) Magnetotactic bacteria, magnetosomes, and nanotechnology. In: *Nanomicrobiology*, pp 39–74
- Borges N, Marugg JD, Empadinhas N, Da Costa MS, Santos H (2004) Specialized roles of the two pathways for the synthesis of mannosylglycerate in osmoadaptation and thermoadaptation of *Rhodothermus marinus*. *J Biol Chem* 279:9892–9898
- Bothe H, Schmitz O, Yates MG, Newton WE (2010) Nitrogen fixation and hydrogen metabolism in cyanobacteria. *Microbiol Mol Biol Rev* 74:529–551
- Castenholz RW, Wilmotte A, Herdman M, Rippka R, Waterbury JB, Itean I, Hoffmann L (2001) Phylum BX. Cyanobacteria. In: Boone DR, Castenholz RW, Garrity GM (eds) *Bergey's Manual® Syst Bacteriol*. Springer, New York, pp 473–599

- Chapman JD, Goodlett DR, Masselon CD (2013) Multiplexed and data-independent tandem mass spectrometry for global proteome profiling. *Mass Spectrom Rev* 33:452–470
- Chen Y, Jiang P, Liu S, Zhao H, Cui Y, Qin S (2011) Purification of 6xHis-tagged phycobiliprotein using zinc-decorated silica-coated magnetic nanoparticles. *J Chromatogr B Anal Technol Biomed Life Sci* 879:993–997
- Chevalier F (2010) Highlights on the capacities of ‘Gel-based’ proteomics. *Proteome Sci* 8:23
- Choe L, D’Ascenzo M, Relkin NR, Pappin D, Ross P, Williamson B, Guertin S, Pribil P, Lee KH (2007) 8-Plex quantitation of changes in cerebrospinal fluid protein expression in subjects undergoing intravenous immunoglobulin treatment for Alzheimer’s disease. *Proteomics* 7:3651–3660
- Choi H, Fermin D, Nesvizhskii AI (2008) Significance analysis of spectral count data in label-free shotgun proteomics. *Mol Cell Proteomics* 7:2373–2385
- Clarke AK (1999) ATP-dependent Clp proteases in photosynthetic organisms—a cut above the rest! *Ann Bot* 83:593–599
- Cohen SE, Golden SS (2015) Circadian rhythms in cyanobacteria. *Microbiol Mol Biol Rev* 79:373–385
- Cox AD, Saito MA (2013) Proteomic responses of oceanic *Synechococcus* WH8102 to phosphate and zinc scarcity and cadmium additions. *Front Microbiol* 4:1–17
- D’Agostino PM, Song X, Neilan BA, Moffitt MC (2015) Proteogenomics of a saxitoxin-producing and non-toxic strain of *Anabaena circinalis* (cyanobacteria) in response to extracellular NaCl and phosphate depletion. *Environ Microbiol* 18:461–476
- Depraetere O, Deschoenmaeker F, Badri H, Monsieurs P, Foubert I, Leys N, Wattiez R, Muylaert K (2015) Trade-off between growth and carbohydrate accumulation in nutrient-limited *Arthrospira* sp. PCC 8005 studied by integrating transcriptomic and proteomic approaches. *PLoS One* 10:1–19
- Deschoenmaeker F, Facchini R, Badri H, Leroy B, Zhang C-C, Wattiez R (2014) Proteomic and cellular views of *Arthrospira* sp. PCC 8005 adaptation to nitrogen depletion. *Microbiology* 160:1224–1236
- Distler U, Kuharev J, Navarro P, Tenzer S (2016) Label-free quantification in ion mobility-enhanced data-independent acquisition proteomics. *Nat Protoc* 11:795–812
- Doerr A (2014) DIA mass spectrometry. *Nat Methods* 12:35
- Doyle SM, Kravats AN, Hoskins JR, Shih Y-H, Stan G, Wickner S (2015) 50 Interaction and collaboration between DnaK and ClpB during protein disaggregation. *J Biomol Struct Dyn* 33:34–35
- Evans C, Noirel J, Ow SY, Salim M, Pereira-Medrano AG, Couto N, Pandhal J, Smith D, Pham TK et al (2012) An insight into iTRAQ: where do we stand now? *Anal Bioanal Chem* 404:1011–1027
- Fenn J, Mann M, Meng C, Wong S, Whitehouse C (1989) Electrospray ionization for mass spectrometry of large biomolecules. *Science* 246:64–71
- Florencio FJ, Pérez-Pérez ME, López-Maury L, Mata-Cabana A, Lindahl M (2006) The diversity and complexity of the cyanobacterial thioredoxin systems. *Photosynth Res* 89:157–171
- Fournier ML, Gilmore JM, Martin-Brown SA, Washburn MP (2007) Multidimensional separations-based shotgun proteomics. *Chem Rev* 107:3654–3686
- Fukuyama Y (2015) MALDI matrix research for biopolymers. *Mass Spectrom* 4:1–14
- Fulda S, Mikkat S, Huang F, Huckauf J, Marin K, Norling B, Hagemann M (2006) Proteome analysis of salt stress response in the cyanobacterium *Synechocystis* sp. strain PCC 6803. *Proteomics* 6:2733–2745
- Fuszard MA, Ow S, Gan C, Noirel J, Ternan NG, McMullan G, Biggs CA, Reardon KF, Wright PC (2013) The quantitative proteomic response of *Synechocystis* sp. PCC6803 to phosphate acclimation. *Aquat Biosyst* 9:1–12
- Garcia-Pichel F (2009) Cyanobacteria. In: Schaechter M (ed) *Encyclopedia of microbiology*. Elsevier, Amsterdam, pp 107–124
- Gevaert K, Impens F, Ghesquière B, Van Damme P, Lambrechts A, Vandekerckhove J (2008) Stable isotopic labeling in proteomics. *Proteomics* 8:4873–4885

- Gillet, L. C., Navarro, P., Tate, S., Ro, H., Selevsek, N., Reiter, L., Bonner, R., Aebersold, R., Rost, H. & other authors. (2012). Targeted data extraction of the MS/MS spectra generated by data-independent acquisition: a new concept for consistent and accurate proteome analysis. *Mol Cell Proteomics* 11, 1–45.
- Glish GL, Vachet RW (2003) The basics of mass spectrometry in the twenty-first century. *Nat Rev Drug Discov* 2:140–150
- Gomez-Garcia MR, Losada M, Serrano A (2003) Concurrent transcriptional activation of *ppa* and *ppx* genes by phosphate deprivation in the cyanobacterium *Synechocystis* sp. strain PCC 6803. *Biochem Biophys Res Commun* 302:601–609
- Gründel M, Scheunemann R, Lockau W, Zilliges Y (2012) Impaired glycogen synthesis causes metabolic overflow reactions and affects stress responses in the cyanobacterium *Synechocystis* sp. PCC 6803. *Microbiol (United Kingdom)* 158:3032–3043
- Guan X, Qin S, Zhao F, Zhang X, Tang X (2007) Phycobilisomes linker family in cyanobacterial genomes: divergence and evolution. *Int J Biol Sci* 3:434–445
- Guerreiro ACL, Benevento M, Lehmann R, van Breukelen B, Post H, Giansanti P, Altelaar AFM, Axmann IM, Heck AJR (2014) Daily rhythms in the cyanobacterium *Synechococcus elongatus* probed by high-resolution mass spectrometry based proteomics reveals a small-defined set of cyclic proteins. *Mol Cell Proteomics* 13:1–37
- Gutekunst K, Phunpruch S, Schwarz C, Schuchardt S, Schulz-Friedrich R, Appel J (2005) LexA regulates the bidirectional hydrogenase in the cyanobacterium *Synechocystis* sp. PCC 6803 as a transcription activator. *Mol Microbiol* 58:810–823
- Hagemann M (2011) Molecular biology of cyanobacterial salt acclimation. *FEMS Microbiol Rev* 35:87–123
- Harris D, Tal O, Jallet D, Wilson A, Kirilovsky D, Adir N (2016) Orange carotenoid protein burrows into the phycobilisome to provide photoprotection. *Proc Natl Acad Sci* 113:1–8
- Hasunuma T, Kikuyama F, Matsuda M, Aikawa S, Izumi Y, Kondo A (2013) Dynamic metabolic profiling of cyanobacterial glycogen biosynthesis under conditions of nitrate depletion. *J Exp Bot* 64:2943–2954
- Havaux M, Guedeney G, He Q, Grossman AR (2003) Elimination of high-light-inducible polypeptides related to eukaryotic chlorophyll a/b-binding proteins results in aberrant photoacclimation in *Synechocystis* PCC6803. *Biochim Biophys Acta* 1557:21–33
- He Q, Dolganov N, Björkman O, Grossman AR (2001) The high light-inducible polypeptides in *Synechocystis* PCC6803. Expression and function in high light. *J Biol Chem* 276:306–314
- Herrero A, Muro-pastor AM, Flores E (2001) Nitrogen control in cyanobacteria. *J Bacteriol* 183:411–425
- Hongsthong A, Sirijuntarut M, Yutthanasirikul R, Senachak J, Kurdrid P, Cheevadhanarak S, Tanticharoen M (2009) Subcellular proteomic characterization of the high-temperature stress response of the cyanobacterium *Spirulina platensis*. *Proteome Sci* 7:33
- Huang F, Fulda S, Hagemann M, Norling B (2006) Proteomic screening of salt-stress-induced changes in plasma membranes of *Synechocystis* sp. strain PCC 6803. *Proteomics* 6:910–920
- Huang Q, Yang L, Luo J, Guo L, Wang Z, Yang X, Jin W, Fang Y, Ye J et al (2015) SWATH enables precise label-free quantification on proteome scale. *Proteomics* 15:1215–1223
- Huang S, Chen L, Te R, Qiao J, Wang J, Zhang W (2013) Complementary iTRAQ proteomics and RNA-seq transcriptomics reveal multiple levels of regulation in response to nitrogen starvation in *Synechocystis* sp. PCC 6803. *Mol BioSyst* 9:2565–2574
- Hustoft HK, Malerod H, Wilson SR, Reubsaet L, Lundanes E, Greibrokk T (2012) Integrative proteomics. In: Leung H-C (ed) *Integr proteomics*. InTech, Croatia
- Ishihama Y (2005) Exponentially modified protein abundance index (emPAI) for estimation of absolute protein amount in proteomics by the number of sequenced peptides per protein. *Mol Cell Proteomics* 4:1265–1272
- Julka S, Regnier F (2004) Quantification in proteomics through stable isotope coding: a review. *J Proteome Res* 3:350–363
- Kim YE, Hipp MS, Bracher A, Hayer-Hartl M, Ulrich Hartl F (2013) Molecular chaperone functions in protein folding and proteostasis. *Annu Rev Biochem* 82:323–355

- Kirilovsky D, Kerfeld CA (2012) The orange carotenoid protein in photoprotection of photosystem II in cyanobacteria. *Biochim Biophys Acta* 1817:158–166
- Komárek J, Kling H, Komárková J (2003) Freshwater algae of North America. In: Wehr JD, Sheath RG, Kociolek JP (eds) *Aquat Ecol*. Elsevier S, New York, pp 117–196
- Kumar DP, Murthy SDS (2007) Photoinhibition induced alterations in energy transfer process in phycobilisomes of PS II in the cyanobacterium, *Spirulina platensis*. *J Biochem Mol Biol* 40:644–648
- Kurdrid P, Senachak J, Sirijuntarut M, Yutthanasirikul R, Phuengcharoen P, Jeamton W, Roytrakul S, Cheevadhanarak S, Hongsthong A (2011) Comparative analysis of the *Spirulina platensis* subcellular proteome in response to low- and high-temperature stresses: uncovering cross-talk of signaling components. *Proteome Sci* 9:1–16
- Ladig R, Sommer MS, Hahn A, Leisegang MS, Papasotiriou DG, Ibrahim M, Elkehal R, Karas M, Zickermann V et al (2011) A high-definition native polyacrylamide gel electrophoresis system for the analysis of membrane complexes. *Plant J* 67:181–194
- Lee S, Sowa ME, Choi J-M, Tsai FTF (2004) The ClpB/Hsp104 molecular chaperone—a protein disaggregating machine. *J Struct Biol* 146:99–105
- Lesur A, Domon B (2015) Advances in high-resolution accurate mass spectrometry application to targeted proteomics. *Proteomics* 15:880–890
- Levin Y, Hradetzky E, Bahn S (2011) Quantification of proteins using data-independent analysis (MSE) in simple and complex samples: a systematic evaluation. *Proteomics* 11:3273–3287
- Liang W, Wang L, Zhang Y, Lei X, Yang J, You X, Cheng CL, Zhou Y, Chen W (2013) Comparative proteomic and physiological analysis of diurnal changes in *Nostoc flagelliforme*. *J Appl Phycol* 25:1709–1721
- Lin, S., Litaker, R. W. & Sunda, W. G. (2016). Phosphorus physiological ecology and molecular mechanisms in marine phytoplankton. *J Phycol* 52, 10–36 M. Wood Cambridge: Cambridge University Press.
- Linder P, Jankowsky E (2011) From unwinding to clamping — the DEAD box RNA helicase family. *Nat Rev Mol Cell Biol* 12:505–516
- Lohnes K, Quebbemann NR, Liu K, Kobzeff F, Loo JA, Ogorzalek Loo RR (2016) Combining high-throughput MALDI-TOF mass spectrometry and isoelectric focusing gel electrophoresis for virtual 2D gel-based proteomics. *Methods* 104:1–7
- Mann M (2006) Functional and quantitative proteomics using SILAC. *Nat Rev Mol Cell Biol* 7:952–958
- Mann M, Hendrickson RC, Pandey A (2001) Analysis of proteins and proteomes by mass spectrometry. *Annu Rev Biochem* 70:437–473
- Matallana-Surget S, Derock J, Leroy B, Badri H, Deschoenmaeker F, Wattiez R (2014) Proteome-wide analysis and diel proteomic profiling of the cyanobacterium *Arthrospira platensis* PCC 8005. *PLoS One* 9:e99076
- Moruz L, Käll L (2016) Peptide retention time prediction. *Mass Spectrom Rev* 47:1–9
- Mueller TJ, Welsh EA, Pakrasi HB, Maranas CD (2016) Identifying regulatory changes to facilitate nitrogen fixation in the nondiazotroph *Synechocystis* sp. PCC 6803. *ACS Synth Biol* 5:250–258
- Münchbach M, Quadroni M, Miotto G, James P (2000) Quantitation and facilitated de novo sequencing of proteins by isotopic n-terminal labeling of peptides with a fragmentation-directing moiety. *Anal Chem* 72:4047–4057
- Muro-Pastor MI, Reyes JC, Florencio FJ (2001) Cyanobacteria perceive nitrogen status by sensing intracellular 2-oxoglutarate levels. *J Biol Chem* 276:38320–38328
- Muro-Pastor MI, Reyes JC, Florencio FJ (2005) Ammonium assimilation in cyanobacteria. *Photosynth Res* 83:135–150
- Nogales J, Gudmundsson S, Knight EM, Palsson BO, Thiele I (2012) Detailing the optimality of photosynthesis in cyanobacteria through systems biology analysis. *Proc Natl Acad Sci U S A* 109:2678–2683
- Novikova GV, Moshkov IE, Los DA (2007) Protein sensors and transducers of cold and osmotic stress in cyanobacteria and plants. *Mol Biol* 41:427–437

- Ong S-E (2002) Stable isotope labeling by amino acids in cell culture, SILAC, as a simple and accurate approach to expression proteomics. *Mol Cell Proteomics* 1:376–386
- Orchard ED, Benitez-Nelson CR, Pellechia PJ, Lomas MW, Dyhrman ST (2010) Polyphosphate in *Trichodesmium* from the low-phosphorus Sargasso Sea. *Limnol Oceanogr* 55:2161–2169
- Ow SY, Cardona T, Taton A, Magnuson A, Lindblad P, Stensjö K, Wright PC (2008) Quantitative shotgun proteomics of enriched heterocysts from *Nostoc* sp. PCC 7120 using 8-plex isobaric peptide tags. *J Proteome Res* 7:1615–1628
- Pandhal J, Wright PC, Biggs CA (2007) A quantitative proteomic analysis of light adaptation in a globally significant marine cyanobacterium *Prochlorococcus marinus* MED4. *J Proteome Res* 6:996–1005
- Pandhal J, Snijders APL, Wright PC, Biggs CA (2008) A cross-species quantitative proteomic study of salt adaptation in a halotolerant environmental isolate using ¹⁵N metabolic labelling. *Proteomics* 8:2266–2284
- Pandhal J, Ow SY, Wright PC, Biggs CA (2009) Comparative proteomics study of salt tolerance between a nonsequenced extremely halotolerant cyanobacterium and its mildly halotolerant relative using in vivo metabolic labeling and in vitro isobaric labeling. *J Proteome Res* 8:818–828
- Pereira SB, Ow SY, Barrios-Llerena ME, Wright PC, Moradas-Ferreira P, Tamagnini P (2011) iTRAQ-based quantitative proteomic analysis of *Gloeotheca* sp. PCC 6909: comparison with its sheathless mutant and adaptations to nitrate deficiency and sulfur limitation. *J Proteome Res* 10:270–283
- Pérez-Pérez ME, Mata-Cabana A, Sánchez-Riego AM, Lindahl M, Florencio FJ (2009) A comprehensive analysis of the peroxiredoxin reduction system in the cyanobacterium *Synechocystis* sp. strain PCC 6803 reveals that all five peroxiredoxins are thioredoxin dependent. *J Bacteriol* 191:7477–7489
- Poetsch A, Wolters D (2008) Bacterial membrane proteomics. *Proteomics* 8:4100–4122
- Qiao J, Huang S, Te R, Wang J, Chen L, Zhang W (2013) Integrated proteomic and transcriptomic analysis reveals novel genes and regulatory mechanisms involved in salt stress responses in *Synechocystis* sp. PCC 6803. *Appl Microbiol Biotechnol* 97:8253–8264
- Rai S, Singh S, Shrivastava AK, Rai LC (2013) Salt and UV-B induced changes in *Anabaena* PCC 7120: physiological, proteomic and bioinformatic perspectives. *Photosynth Res* 118:105–114
- Rajaram H, Chaurasia AK, Apte SK (2014) Cyanobacterial heat-shock response: role and regulation of molecular chaperones. *Microbiology* 160:647–658
- Rhee S-G (2016) Overview on peroxiredoxin. *Mol Cell* 39:1–5
- Ross PL (2004) Multiplexed protein quantitation in *Saccharomyces cerevisiae* using amine-reactive isobaric tagging reagents. *Mol Cell Proteomics* 3:1154–1169
- Röst HL, Aebersold R, Schubert OT (2016) Automated SWATH data analysis using targeted extraction of ion chromatograms. *bioRxiv*. doi:10.1101/044552
- Rowland JG, Simon WJ, Nishiyama Y, Slabas AR (2010) Differential proteomic analysis using iTRAQ reveals changes in thylakoids associated with Photosystem II-acquired thermotolerance in *Synechocystis* sp. PCC 6803. *Proteomics* 10:1917–1929
- Sandh G, Ran L, Xu L, Sundqvist G, Bulone V, Bergman B (2011) Comparative proteomic profiles of the marine cyanobacterium *Trichodesmium erythraeum* IMS101 under different nitrogen regimes. *Proteomics* 11:406–419
- Schirmer BE, Gugger M, Donoghue PCJ (2015) Cyanobacteria and the great oxidation event: evidence from genes and fossils. *Palaeontology* 58:769–785
- Schmidt A, Kellermann J, Lottspeich F (2005) A novel strategy for quantitative proteomics using isotope-coded protein labels. *Proteomics* 5:4–15
- Scigelova M, Hornshaw M, Giannakopoulos A, Makarov A (2011) Fourier transform mass spectrometry. *Mol Cell Proteomics* 10:1–19
- Sendersky E, Kozar N, Levi M, Moizik M, Garini Y, Shav-Tal Y, Schwarz R (2015) The proteolysis adaptor, NblA, is essential for degradation of the core pigment of the cyanobacterial light-harvesting complex. *Plant J* 83:845–852

- Shevchenko A, Tomas H, Havlis J, Olsen JV, Mann M (2007) In-gel digestion for mass spectrometric characterization of proteins and proteomes. *Nat Protoc* 1:2856–2860
- Silva JC, Denny R, Dorschel CA, Gorenstein M, Kass IJ, Li G-Z, McKenna T, Nold MJ, Richardson K et al (2005) Quantitative proteomic analysis by accurate mass retention time pairs. *Anal Chem* 77:2187–2200
- Singh NK, Sonani RR, Prasad Rastogi R, Madamwar D (2015) The phycobilisomes: an early requisite for efficient photosynthesis in cyanobacteria. *EXCLI J* 14:268–289
- Siu SO, Lam MPY, Lau E, Kong RPW, Lee SMY, Chu IK (2011) Fully automatable two-dimensional reversed-phase capillary liquid chromatography with online tandem mass spectrometry for shotgun proteomics. *Proteomics* 11:2308–2319
- Slabas AR, Suzuki I, Murata N, Simon WJ, Hall JJ (2006) Proteomic analysis of the heat shock response in *Synechocystis* PCC6803 and a thermally tolerant knockout strain lacking the histidine kinase 34 gene. *Proteomics* 6:845–864
- Spat P, Macek B, Forchhammer K (2015) Phosphoproteome of the cyanobacterium *Synechocystis* sp. PCC 6803 and its dynamics during nitrogen starvation. *Front Microbiol* 6:1–15
- Spicer V, Ezzati P, Neustaeter H, Beavis RC, Wilkins JA, Krokhin OV (2016) 3D HPLC-MS with reversed-phase separation functionality in all three dimensions for large-scale bottom-up proteomics and peptide retention data collection. *Anal Chem* 88:2847–2855
- Stöckel J, Jacobs JM, Elvitigala TR, Liberton M, Welsh EA, Polpitiya AD, Gritsenko MA, Nicora CD, Koppenaal DW et al (2011) Diurnal rhythms result in significant changes in the cellular protein complement in the cyanobacterium *Cyanothece* 51142. *PLoS One* 6:e16680
- Susnea I, Bernevic B, Wicke M, Ma L, Liu S, Schellander K, Przybylski M (2012) Application of MALDI-TOF-mass spectrometry to proteome analysis using stain-free gel electrophoresis. In: Zongwei C, Shuying L (eds) *Applications of MALDI-TOF Spectroscopy*. Springer, Berlin Heidelberg, pp 37–54
- Suzuki I, Simon WJ, Slabas AR (2006) The heat shock response of *Synechocystis* sp. PCC 6803 analysed by transcriptomics and proteomics. *J Exp Bot* 57:1573–1578
- Swaney DL, Wenger CD, Coon JJ (2010) Value of using multiple proteases for large-scale mass spectrometry-based proteomics. *J Proteome Res* 9:1323–1329
- Takai N, Nakajima M, Oyama T, Kito R, Sugita C, Sugita M, Kondo T, Iwasaki H (2006) A KaiC-associating SasA-RpaA two-component regulatory system as a major circadian timing mediator in cyanobacteria. *Proc Natl Acad Sci U S A* 103:12109–12114
- Tamary E, Kiss V, Nevo R, Adam Z, Bernát G, Rexroth S, Rögner M, Reich Z (2012) Structural and functional alterations of cyanobacterial phycobilisomes induced by high-light stress. *Biochim Biophys Acta* 1817:319–327
- Tanaka K, Waki H, Ido Y, Akita S, Yoshida Y, Yoshida T, Matsuo T (1988) Protein and polymer analyses up to m/z 100 000 by laser ionization time-of-flight mass spectrometry. *Rapid Commun Mass Spectrom* 2:151–153
- Tanaka N, Nakamoto H (1999) HtpG is essential for the thermal stress management in cyanobacteria. *FEBS Lett* 458:117–123
- Taniguchi Y, Katayama M, Ito R, Takai N, Kondo T, Oyama T (2007) *labA*: a novel gene required for negative feedback regulation of the cyanobacterial circadian clock protein KaiC. *Genes Dev* 21:60–70
- Taniguchi Y, Nishikawa T, Kondo T, Oyama T (2012) Overexpression of *lala*, a paralog of *labA*, is capable of affecting both circadian gene expression and cell growth in the cyanobacterium *Synechococcus elongatus* PCC 7942. *FEBS Lett* 586:753–759
- Teikari J, Österholm J, Kopf M, Battchikova N, Wahlsten M, Aro E, Hess WR (2015) Transcriptomic and proteomic profiling of *Anabaena* sp. strain 90 under inorganic phosphorus stress. *Appl Environ Microbiol* 81:5212–5222
- Thajuddin N, Subramanian G (2005) Cyanobacterial biodiversity and potential applications in biotechnology. *Curr Sci* 89:47–57
- Theiss C, Schmitt F-J, Pieper J, Nganou C, Grehn M, Vitali M, Olliges R, Eichler HJ, Eckert H-J (2011) Excitation energy transfer in intact cells and in the phycobiliprotein antennae of the

- chlorophyll d containing cyanobacterium *Acaryochloris marina*. *J Plant Physiol* 168: 1473–1487
- Thompson A, Schafer J, Kuhn K, Kienle S, Schwarz J, Schmidt G, Neumann T, Hamon C (2003) Tandem mass tags: a novel quantification strategy for comparative analysis of complex protein mixtures by MS/MS. *Anal Chem* 75:1895–1904
- Tsiatsiani L, Heck AJR (2015) Proteomics beyond trypsin. *FEBS J* 282:2612–2626
- Ünal CM, Steinert M (2014) Microbial peptidyl-prolyl cis/trans isomerase (ppiases): virulence factors and potential alternative drug targets. *Microbiol Mol Biol Rev* 78:544–571
- Wang D, Liang X, Chen X, Guo J (2013) Ribonucleoprotein complexes that control circadian clocks. *Int J Mol Sci* 14:9018–9036
- Wasinger VC, Zeng M, Yau Y (2013) Current status and advances in quantitative proteomic mass spectrometry. *Int J Proteom* 2013:1–12
- Watanabe M, Sato M, Kondo K, Narikawa R, Ikeuchi M (2012) Phycobilisome model with novel skeleton-like structures in a glaucocystophyte *Cyanophora paradoxa*. *Biochim Biophys Acta* 1817:1428–1435
- Webb-Robertson BJM, Wiberg HK, Matzke MM, Brown JN, Wang J, McDermott JE, Smith RD, Rodland KD, Metz TO et al (2015) Review, evaluation, and discussion of the challenges of missing value imputation for mass spectrometry-based label-free global proteomics. *J Proteome Res* 14:1993–2001
- Wegener KM, Singh AK, Jacobs JM, Elvitigala T, Welsh EA, Keren N, Gritsenko MA, Ghosh BK, Campii DG et al (2010) Global proteomics reveal an atypical strategy for carbon/nitrogen assimilation by a cyanobacterium under diverse environmental perturbations. *Mol Cell Proteomics* 9:2678–2689
- Welkie D, Zhang X, Markillie M, Taylor R, Orr G, Jacobs J, Bhide K, Thimmapuram J, Gritsenko M et al (2014) Transcriptomic and proteomic dynamics in the metabolism of a diazotrophic cyanobacterium, *Cyanothece* sp. PCC 7822 during a diurnal light–dark cycle. *BMC Genomics* 15:–1185
- Wilson A, Ajlani G, Verbavatz J-M, Vass I, Kerfeld CA, Kirilovsky D (2006) A soluble carotenoid protein involved in phycobilisome-related energy dissipation in cyanobacteria. *Plant Cell* 18:992–1007
- Ye X, Luke B, Andresson T, Blonder J (2009) 18O stable isotope labeling in MS-based proteomics. *Brief Funct Genom Proteom* 8:136–144
- Yue D, Peng Y, Yin Q, Xiao L (2015) Proteomic analysis of *Microcystis aeruginosa* in response to nitrogen and phosphorus starvation. *J Appl Phycol* 27:1195–1204
- Zhang P, Allahverdiyeva Y, Eisenhut M, Aro E-M (2009) Flavodiiron proteins in oxygenic photosynthetic organisms: photoprotection of photosystem II by Flv2 and Flv4 in *Synechocystis* sp. PCC 6803. *PLoS One* 4:1–12
- Zhang Y, Wen Z, Washburn MP, Florens L (2015) Improving label-free quantitative proteomics strategies by distributing shared peptides and stabilizing variance. *Anal Chem* 87:4749–4756

Photosynthetic Carbon Metabolism and CO₂-Concentrating Mechanism of Cyanobacteria

Natalia A. Pronina, Elena V. Kupriyanova, and Abir U. Igamberdiev

Abstract Photosynthetic fixation of CO₂ by cyanobacteria proceeds via the Calvin–Benson cycle. Its high efficiency is supported by the operation of the CO₂-concentrating mechanism (CCM). The main constituents of CCM are the active transport and accumulation of the inorganic carbon (C_i) in the cytosol mainly in the form of HCO₃[−], with its following transformation to CO₂ in high concentration in a special microcompartment (carboxysome), containing ribulose-1,5-bisphosphate carboxylase/oxygenase (Rubisco). The presence of the CCM that functions before the Calvin–Benson cycle provides high CO₂/O₂ ratio in the vicinity of the primary CO₂-fixing enzyme, Rubisco, to promote the carboxylation reaction and suppress the oxygenase reaction. To date, CCM is found in the cyanobacteria inhabiting different ecological niches. The structural composition of the CCM is different in α- and β-cyanobacteria, which main representatives belong correspondingly to seawater and freshwater habitats. Recently, the modulating CCM components have been detected in relict cyanobacteria, including that inhabiting saturated carbonate brine of soda lakes. This review focuses on various aspects of the carbon metabolism in cyanobacteria and interconversion of its organic and inorganic forms in the photosynthetic reactions of living cells. The comparison of CCM physiology and biochemistry in the model and relict species of cyanobacteria is also highlighted. The evolutionary origin of CCM and the roles of CCM in the atmosphere formation and preservation of the ecology of Earth's biosphere via the establishment of efficient mechanisms of CO₂ acquisition are discussed.

Keywords Carbon cycle • Carbonic anhydrase • Carbon fixation • Carboxysome • CCM • C_i transport • CO₂ concentration • Cyanobacteria • Photorespiration • Rubisco • Relict cyanobacteria

N.A. Pronina (✉) • E.V. Kupriyanova
Institute of Plant Physiology, Russian Academy of Sciences, Botanicheskaya street 35,
Moscow 127276, Russia
e-mail: na.pronina@mail.ru; ivlaanov@mail.ru

A.U. Igamberdiev
Department of Biology, Memorial University of Newfoundland, St. John's, NL,
Canada, A1B 3X9
e-mail: igamberdiev@mun.ca

Abbreviations

CA	Carbonic anhydrase
CCM	CO ₂ -concentrating mechanism (carbon-concentrating mechanism)
C _i	Inorganic carbon compounds (CO ₂ + HCO ₃ ⁻)
GAP	Glyceraldehyde 3-phosphate
High-CO ₂ cells	Cells grown at 2–5% CO ₂
Low-CO ₂ cells	Cells grown under ambient atmospheric CO ₂ concentration (0.03–0.04%)
PG	2-Phosphoglycolate
PGA	3-Phosphoglyceric acid
PSI	Photosystem I
PSII	Photosystem II
RPP	Reductive pentose phosphate (cycle/pathway)
Rubisco	Ribulose-1,5-bisphosphate carboxylase/oxygenase
RuBP	Ribulose-1,5-bisphosphate
αKG	α-Ketoglutarate
K _m	Michaelis constant
CAM	Crassulacean acid metabolism

Introduction

Photosynthetic carbon metabolism is the general biochemical process providing the fixation and reduction of the atmospheric carbon in the primary carbon-containing metabolites which further conversions build all variety of organic compounds. Carbon metabolism is represented by three types of photosynthetic metabolism, C₃, C₄, and CAM. In all three types of carbon fixation, the main and common (and the sole pathway in C₃ plants) is the reductive pentose phosphate (RPP) pathway or Calvin–Benson cycle (Benson et al. 1950), fixing CO₂ via ribulose-1,5-bisphosphate carboxylase/oxygenase (Rubisco – EC 4.1.1.39). Rubisco belongs to the ancient enzymes which could, at first glance, optimize their enzymatic characteristics during the long period of CO₂ decrease in the Earth's atmosphere. However, recent investigations revealed low variability of this enzyme in the course of evolution. This especially refers to its low turnover number, low affinity to CO₂, and the evolutionary preserved capacity of Rubisco to interact with O₂ in the oxygenase reaction which results in the energy-consuming photorespiration process (Bell 1985; Kroth 2015).

Higher plants developed C₄ and CAM photosynthesis exploiting the additional reactions to make the process of CO₂ fixation more efficient. In both cases CO₂ is first prefixed resulting in the formation of four-carbon molecules, and then these molecules are decarboxylated in the proximity of Rubisco, thus activating and saturating the enzyme (Brautigam et al. 2014). The C₄ plants exploit

the spatial separation of the reaction of the C₄ and of the RPP cycles, which may involve (in most cases) the cooperation of different types of cells in different tissues, but could also take place in a single cell in some higher plant species (Voznesenskaya et al. 2001) or in unicellular diatomic algae (Reinfelder et al. 2000), although in some diatom species previously considered as having C₄ photosynthesis, the efficiency of carbon fixation is explained by the special type of CCM (Clement et al. 2016). The CAM plants exploit the temporal separation of the C₄ and C₃ pathways, when the C₄ acids are formed during night and their decarboxylation with CO₂ delivery to Rubisco takes place during the day (Osmond 1978; Fomina and Biel 2016).

Therefore, the RPP cycle plays a key role in photosynthetic carbon metabolism; it is only complemented by the additional steps of CO₂ fixation in C₄ and CAM plants. However, another complementing structure to the Calvin–Benson cycle was discovered in microalgae and cyanobacteria metabolizing carbon via the C₃ pathway that allows them to concentrate CO₂ in the cell. This mechanism was defined as CCM (carbon-concentrating mechanism or CO₂-concentrating mechanism), whose abbreviation bears a dual meaning. First, this mechanism facilitates accumulation of the inorganic carbon (C_i) in a way that its concentration in the cells grown at the atmospheric CO₂ can by 1000 times exceed its concentration in the extracellular environment (Kaplan et al. 1980; Badger et al. 1980; Aizawa and Miyachi 1986). Second, the buildup of the concentrated C_i pool provides so high CO₂ concentration in the carboxylation compartment (carboxysomes) that the saturation of the carboxylation reaction occurs even at a low external CO₂ concentration (~10–12 μM) and low affinity of the cyanobacterial Rubisco to CO₂ ($K_m \sim 300 \mu\text{M}$).

This mechanism of CO₂ concentration is realized in a single cell, it is inducible by low CO₂ concentrations, and it is based on active uptake of C_i and the reversible transformation of the C_i species (CO₂ and HCO₃⁻) before incorporation into organic products. Due to CCM, cyanobacteria and microalgae perform photosynthesis more efficiently than C₃ and even C₄ plants and essentially contribute to the formation of biomass and oxygen on the Earth. The contribution of C₄ and CAM plants, which comprise only 3–4% of all plant species, in the total photosynthesis is relatively small (Raven 1997), while cyanobacteria and microalgae form at least a half of total primary biospheric production (Behrenfeld et al. 2001). Clearly, focusing research on the role of the cyanobacterial CCM contributing a significant portion of this productivity is of considerable importance.

All known CO₂-concentrating mechanisms, the C₄/CAM types of photosynthesis and the CCM, evolved as a result of adaptation to the decrease in CO₂ and increase in O₂ in the atmosphere caused by the spreading of the oxygenic photosynthesis. Cyanobacteria (initially defined as blue-green algae) are the most ancient organisms on the planet that contributed most significantly to the formation of modern atmosphere and to its current preservation (Zavarzin 2008). Due to a very high plasticity of their metabolism, these photosynthetic organisms occupied very wide areas of habitat including freshwater and saltwater, alkaline and acidic, hot and polar, soil, and symbiotic conditions (Badger et al. 2006).

However, the organization of CCM in cyanobacteria is studied mainly in model laboratory strains such as *Synechocystis* sp. PCC 6803, *Synechococcus elongatus* PCC 7942, *Prochlorococcus marinus* MIT 9313, and *Synechococcus* sp. PCC 7002 (Price et al. 2008; Price 2011). These studies made possible to establish the differences in CCM organization in seawater and freshwater cyanobacteria. This refers mainly to the set of active transporters of C_i and carbonic anhydrases (CA), to the type of Rubisco, and to the protein content of the carboxysomes shells. The questions remain on the origin and evolution of CCM and carboxysomes. In this connection, the expansion of the range of the studied species, especially of the relict organisms, is important for clarification of these issues. Recently the aspects of organization of CCM in the relict cyanobacteria of soda lakes have been studied (Dudoladova et al. 2007; Mikhodyuk et al. 2008; Kupriyanova et al. 2013, 2016). It becomes evident that the expanding databases of whole-genome sequences numbering today more than 100 genomes of cyanobacteria (<http://www.ncbi.nlm.nih.gov/genome>) make it possible to easily identify the potential CCM components and generate a new impetus in the research of the origin and evolution of this mechanism. The purpose of the current review is to cover carbon pathways of the cyanobacterial photosynthesis including the Calvin–Benson cycle and photorespiration as well as a recent advancement in the understanding of the cyanobacterial CCM operation as a superstructure to the cycle.

Photosynthetic Carbon Metabolism in Cyanobacterial Cells

C₃ or Calvin–Benson Cycle

From many studies on primary photosynthetic carbon metabolism, it is established that the operation of the Calvin–Benson cycle (C_3 photosynthesis) is predominant in cyanobacteria although archaea and eubacteria developed a number of different ways to fix CO_2 biochemically. The sequence of reactions in Calvin–Benson cycle was established first for the unicellular green algae and later for higher plants and several phototrophic and chemotrophic bacteria. The first stable product of this cycle is 3-phosphoglyceric acid (PGA), two molecules of which are formed through carboxylation of ribulose-1,5-bisphosphate (RuBP) and then reduced to glyceraldehyde 3-phosphate (GAP) and its isomer dihydroxyacetone phosphate (DHAP). These triose phosphates are used for the synthesis of hexose phosphates and then of sucrose and starch. The different types of carbohydrates can be used for synthesis of other substances that are essential for the cell, like lipids or amino acids, components of cell walls, and many other compounds (Badger and Spalding 2000). The closing of the cycle and regeneration of RuBP are achieved through transketolase and transaldolase reactions (Fig. 1).

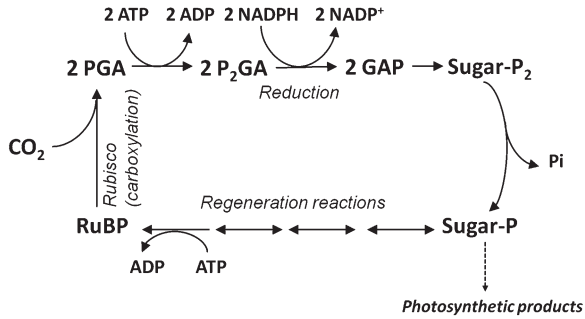


Fig. 1 Simplified scheme of the Calvin–Benson cycle. Abbreviations: *RuBP* ribulose-1,5-bisphosphate, *PGA* 3-phosphoglyceric acid, *P₂GA* 1,3-bisphosphoglyceric acid, *GAP* glyceraldehyde 3-phosphate, *sugar-P₂* and *sugar-P* bisphosphoric and monophosphoric ethers of sugars

Rubisco: Key Enzyme for CO₂ Fixation

CO₂ fixation in the Calvin–Benson cycle occurs via Rubisco. In the course of the strategy of adaptation to low atmospheric CO₂, several types of Rubisco were formed. They are classified into four groups essentially differing by the structure and kinetic parameters despite of catalyzing the same reaction (except of Rubisco IV) (Tabita et al. 2008). Cyanobacteria, similarly to eukaryotic algae and higher plants, have Rubisco of the type I which contains large (L) subunits (50–55 kDa) and small (S) subunits (12–18 kDa) forming the structure L₈S₈. In cyanobacteria Rubisco I is characterized by a high rate of carboxylation ($k_{\text{cat}} \sim 12\text{--}13 \text{ s}^{-1}$), which is 3–5 times higher than in higher plants, low affinity to the substrate CO₂ ($K_{\text{m}}(\text{CO}_2) \sim 250\text{--}340 \mu\text{M}$), and low CO₂/O₂ specificity ($S_{\text{c/o}} \sim 43\text{--}53$), showing a low degree of preference of CO₂ as a substrate for Rubisco over the alternative substrate—O₂ (Tcherkez et al. 2006; Scott et al. 2007; Rae et al. 2013). Only Rubisco I possesses small subunits. Rubisco II contains L dimers arranged in two to eight subunits in different organisms. Rubisco III is present only in some Archaea and contains dimers L₂ and (L₂)₅. Rubisco IV (Rubisco-like proteins lacking carboxylation activity) has the structure L₂.

Rubisco I is classified into four groups (1A–D). The two groups (1A and 1B), differing in subunit structure, are present in cyanobacteria (Tabita et al. 2008). Carboxysomes containing 1A and 1B Rubisco proteins were called correspondingly α - and β -carboxysomes. Cyanobacteria with the α -type carboxysomes were called α -cyanobacteria, while cyanobacteria with the β -type carboxysomes— β -cyanobacteria (Badger and Price 2003; Yeates et al. 2008). α -Cyanobacteria are represented mainly by marine species, while most of β -cyanobacteria are freshwater organisms, and also those found in the cyanobacterial mats in alkaline lakes and other extreme environments (Tabita et al. 2008; Badger et al. 2006).

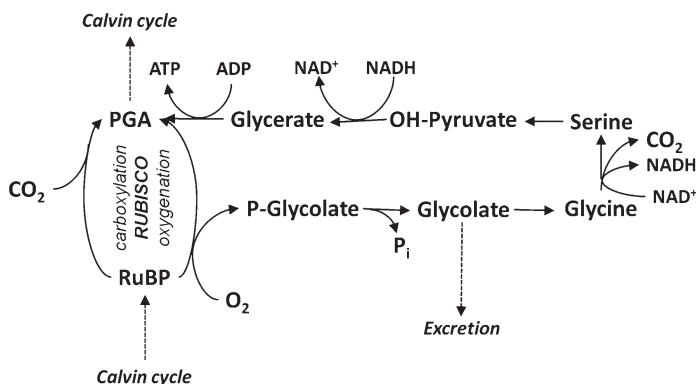


Fig. 2 Simplified scheme of the photorespiratory pathway. Abbreviations: *RuBP* ribulose-1,5-bisphosphate, *P-glycolate* 2-phosphoglycolate, *PGA* 3-phosphoglyceric acid, *OH-pyruvate* hydroxypyruvate. Glycolate can be either excreted from the cell or metabolized

Induction of CCM under C_i limitation is accompanied by increase in Rubisco activity (Price et al. 1992; Wang et al. 2004). In the conditions of C_i stress, the increase in number of carboxysomes, in which Rubisco is localized, takes place (Badger and Spalding 2000).

The process of CO_2 fixation in the Calvin–Benson cycle with the participation of Rubisco exerted the strongest influence on the development of life on this planet especially in conjunction with the oxygenic electron transport, as we observe in cyanobacteria as well as in plastids of eukaryotic algae and plants.

Photorespiration

In cyanobacteria, besides the Calvin–Benson cycle, an important role in carbon metabolism belongs to photorespiration, which is closely connected to photosynthesis. Its origin is connected with the oxygenase reaction of Rubisco when O_2 competes with CO_2 , and in the reaction of RuBP with oxygen, one molecule of PGA and one molecule of 2-phosphoglycolate (PG) are formed (Fig. 2). The existence of oxygen as a prevalent competitive substrate of CO_2 can cause the loss of at least 30% of carbon fixed by Rubisco (Raines 2011).

In addition to the loss of carbon, the product of the oxygenase reaction, PG, acts as an intracellular toxin inhibiting the enzymes of the Calvin–Benson cycle, phosphofructokinase, and triosephosphate isomerase (Husic et al. 1987). During a prolonged time, researchers could not unambiguously prove the existence of photorespiration in microalgae and cyanobacteria (Bell 1985) until they realized that it is important to pay attention on how the cells were prepared prior the measurement. It is established that photorespiration in the cyanobacterial and microalgal cells reaches maximum values when the high- CO_2 -grown cells are transferred to low CO_2

concentration (0.04%). Simultaneously photorespiration is absent or exhibits extremely low level in the low-CO₂ cells if the fully functional CCM operates.

The origin of photorespiratory metabolism (C₂ cycle) in cyanobacteria was studied in several works. Eisenhut et al. (2006) studied the genome of the cyanobacterium *Synechocystis* sp. strain PCC 6803 and identified open reading frames encoding enzymes forming the C₂ cycle. *Synechocystis* expresses glycolate dehydrogenase instead of an oxidase to convert glycolate to glyoxylate. The mutation of this enzyme led to accumulation of glycolate. The limitation of glycolate dehydrogenase by redox level may result in glycolate excretion in the surrounding medium instead of its further metabolism. This phenomenon was observed in cyanobacteria and eukaryotic algae many years ago (Cheng et al. 1972; Ingle and Colman 1976). The excretion of glycolate occurs immediately after the transfer of cells to low CO₂ and usually lasts for 15–20 min and can be stimulated by the inhibitor of glycine decarboxylase. After a short period, the CCM develops and glycolate excretion stops (Ingle and Colman 1976).

In addition to the photorespiratory C₂ cycle common to higher plants (although exploiting glycolate dehydrogenase instead of glycolate oxidase), the representatives of cyanobacteria can possess the bacterial glycerate pathway (including condensation of two glyoxylate molecules with decarboxylation and following reduction of tartronic semialdehyde to glycerate) and the complete decarboxylation of glyoxylate via oxalate (Eisenhut et al. 2008). This flexibility of glycolate metabolism may provide rapid conversion of toxic photorespiratory products before CCM is induced. Glycolate oxidase is present in cyanobacteria as a broad specificity lactate oxidase, and later in evolution this enzyme becomes important in rapid conversion of photorespiratory glycolate in the eukaryotic algae lacking CCM (Hagemann et al. 2016).

Cyanobacteria adapt to the decrease in CO₂ and increase in O₂ in the Earth's atmosphere by the decrease in PG production by employing CCM which increases the local CO₂ concentration at the proximity of Rubisco (Kaplan and Reinhold 1999; Giordano et al. 2005) and also via degrading of PG in the course of photorespiratory metabolism (Eisenhut et al. 2008). Photorespiratory PG metabolism in cyanobacteria is represented by the photorespiratory cycle which is similar to that in plants (Bauwe et al. 2010) and regenerates one molecule of PGA from two molecules of PG.

Therefore, photorespiration is directly linked to the action and activity of CCM. In turn, the induction of CCM by the certain ratio of [CO₂]/[O₂] in low-CO₂ cells will result in the increase of the carboxylase reaction and suppression of the oxygenase reaction of Rubisco. The regulatory mechanisms controlling the changes in the state of low-CO₂ cells are not yet fully understood (see section "Regulation of the CCM in Relation to Carbon Metabolism of Cyanobacteria").

The existence of CCMs also had marked influence on the structure and function of photorespiration (Hagemann et al. 2016). In the course of evolution of eukaryotic algae, the genes of photorespiratory enzymes were acquired from the cyanobacterial symbiont. However, as shown by Kern et al. (2013), who studied *Cyanophora paradoxa*, a Glaucophyta alga representing the first branching group of primary

endosymbionts, some photorespiratory enzymes originally acquired from cyanobacteria were lost, e.g., glycerate 3-kinase, while others were replaced by the corresponding enzymes from the α -proteobacterial endosymbiont, e.g., serine-glyoxylate aminotransferase. It is now evident that many C_2 cycle enzymes in eukaryotic phototrophs were acquired from the cyanobacterial endosymbiont, but during the subsequent evolution of algae and land plants, multiple losses and replacements occurred resulting in different origins of photorespiratory enzymes in different cellular compartments (Hagemann et al. 2013). Phosphoglycolate phosphatase is the only photorespiratory enzyme acquired from Archaea (Hagemann et al. 2016). Cyanobacteria should be considered not only as the “inventors” of the oxygenic photosynthesis but also of the photorespiratory metabolism (Eisenhut et al. 2008).

The increased efficiency of photosynthesis can be likely achieved not through modulation of the Rubisco enzyme itself but rather via engineering of bicarbonate pumps and increasing their efficient coupling with the Rubisco reaction, e.g., by using transgenic plants expressing the genes associated with cyanobacterial CCM (Price et al. 2008). Engineering of plants with a high capacity of bicarbonate pump can also result in more efficient refixation of photorespiratory CO_2 . Not only carboxysomes should be incorporated in higher plants to increase photosynthesis but also other cyanobacterial CCM components such as bicarbonate transporters, and this would allow using the faster Rubisco enzyme of cyanobacteria which is less specific for CO_2 (Hanson et al. 2016). Results from field studies suggest that the incorporation of cyanobacterial CCM would result in a 36–60% increase in yield (McGrath and Long 2014).

CO_2 -Concentrating Mechanism (CCM) of Cyanobacteria

Photosynthetic Characteristics of Cyanobacterial Cells Under CCM Induction

It is now evident that CCM is an inducible mechanism appearing in photosynthetic cells upon the decrease of C_i in the external environment. The first experimental proofs of CCM in cyanobacteria and microalgae were obtained more than 30 years ago during the comparative study of photosynthetic and biochemical characteristics of the cells grown at high (2–5%, high- CO_2 cells) and low (0.04%, low- CO_2 cells) CO_2 concentrations. These first pieces of evidence of CCM were collected and systematized in the review of Aizawa and Miyachi (1986). Using ^{14}C -labeled bicarbonate, it was shown that in many microalgae and cyanobacteria, the intracellular C_i ($CO_2 + HCO_3^-$) concentration significantly increased upon CO_2 decrease in the cultivation medium.

A high efficiency of CCM in the unicellular photosynthetic organisms is well estimated by the comparison of photosynthetic oxygen evolution in the low- and high- CO_2 cells depending on the external CO_2 concentration. The K_m (CO_2) value in

high-CO₂ cells is 200 μM, while in low-CO₂ cells, it constitutes only 1–10 μM (Kaplan et al. 1980; Aizawa and Miyachi 1986). This value of a high photosynthetic affinity to CO₂ in the low-CO₂ cells can be the evidence for coordinated action of the systems of uptake and intracellular delivery of C_i to the carboxylation sites, e.g., of the CCM operation.

The cells of cyanobacteria and microalgae, adapted or grown at the ambient atmospheric CO₂ concentration, are characterized by a set of photosynthetic parameters inherent in general to the C₄ plants capable to CO₂ concentration. In these cells, the suppression of inhibition of photosynthesis by oxygen (Warburg effect), the suppression of photorespiration, and the decrease of the CO₂ compensation point are observed (Badger and Spalding 2000). The cells grown at high CO₂ concentrations and that do not have CCM demonstrate the photosynthetic parameters that are similar to those in C₃ plants.

General Principles of the CCM Operation

Cyanobacteria are characterized by very high productivity which is achieved due to CCM operation (Price et al. 2008). This particularly attracts researchers to study CCM structure and its mechanism of action. The core of CCM is the carboxysome (Rae et al. 2013), in which Rubisco and carbonic anhydrase (CA) are co-localized. In the classic CCM model (Reinhold et al. 1989), there is no need for CO₂ to overcome the diffusion barrier on the way from the external environment to the carboxylation enzyme. The CO₂ molecules for the Rubisco are scooped from the bicarbonate pool inside the cell by the carboxysomal CA which transforms HCO₃⁻ into CO₂ with rather high rate. The buildup of the high concentration pool of bicarbonate is realized via the active uptake of CO₂ and HCO₃⁻ from the external environment (Fig. 3). The detailed description of cyanobacterial CCMs can be found in several comprehensive reviews (Giordano et al. 2005; Price et al. 2008; Burnap et al. 2015), including those devoted to the functions and composition of carboxysomes (Espie and Kimber 2011; Rae et al. 2013).

The main stages of CCM operation in cyanobacteria are shown in Fig. 3. They include (Price 2011; Gaudana et al. 2015):

1. Active HCO₃⁻ influx through the plasmalemma and unidirectional conversion of CO₂ to HCO₃⁻ energized by NDH-1_{3/4} complexes of the cyclic electron flow around photosystem I (PSI) at the outer surface of the thylakoid membrane (section “C_i Acquisition: The First Element of the CCM”)
2. Conversions of HCO₃⁻ to CO₂ in the vicinity of Rubisco catalyzed by the carboxysomal CA (section “Carbonic Anhydrases: The Second CCM Element”)
3. The carboxysomes (containing Rubisco and CAs), whose proteinaceous envelope restricts CO₂ leakage out and O₂ entry to the lumen (section “Cooperation of CA and Rubisco in Cyanobacterial Carboxysomes: Fundamental Principle of the CCM Functioning”)

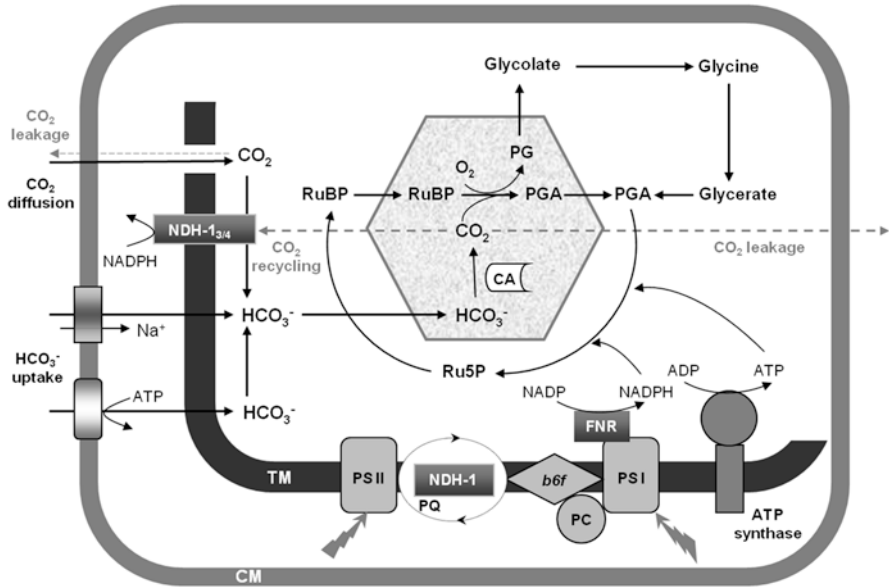


Fig. 3 Photosynthetic metabolic pathways for carbon fixation and CO_2 concentration in cyanobacterial cells. Active HCO_3^- influx by transporters takes place at the plasmalemma; hypothetical unidirectional conversion of CO_2 to HCO_3^- performed by $\text{NDH-1}_{3/4}$ complexes at the thylakoid membrane. Inorganic carbon is assimilated by Rubisco in carboxysomes and in the subsequent reactions of the Calvin–Benson cycle using energy and redox equivalents harvested by the photosynthetic light reactions. The carboxysome contains CA catalyzing interconversions of HCO_3^- to CO_2 in the vicinity of Rubisco. The proteinaceous envelope of carboxysomes restricts CO_2 leakage out and O_2 entry to the lumen. This results in the increase of the carboxylase function and in the suppression of the oxygenase function of Rubisco. Abbreviations: *CM* cytoplasmic membrane (plasmalemma), *b_{6f}* cytochrome *b_{6f}* complex, *FNR* ferredoxin– NADP^+ reductase, *PC* plastocyanin, *PQ* plastoquinone, *Ru5P* ribulose-5-phosphate, *TM* thylakoid membrane. For other abbreviations, see the abbreviation list at the top of the chapter

C_i Acquisition: The First Element of the CCM

As an external source of carbon, cyanobacteria can use CO_2 or HCO_3^- or both these forms, which have to penetrate the plasmalemma and thylakoid membrane. The CO_2 molecules can enter the cell via the direct diffusion mainly due to its high solubility in the lipid fraction of membranes. However, due to these properties, CO_2 can easily leave the cell (Raven and Beardall 2016). The model of CO_2 direct diffusion is widely accepted but it has been called into question. Protein channels such as the aquaporin were reported to provide a pathway for CO_2 transport (Uehlein et al. 2003). At the same time, the negatively charged HCO_3^- can penetrate the cell membrane only by active transport. It is well retained in the cell even in the presence of the concentration gradient.

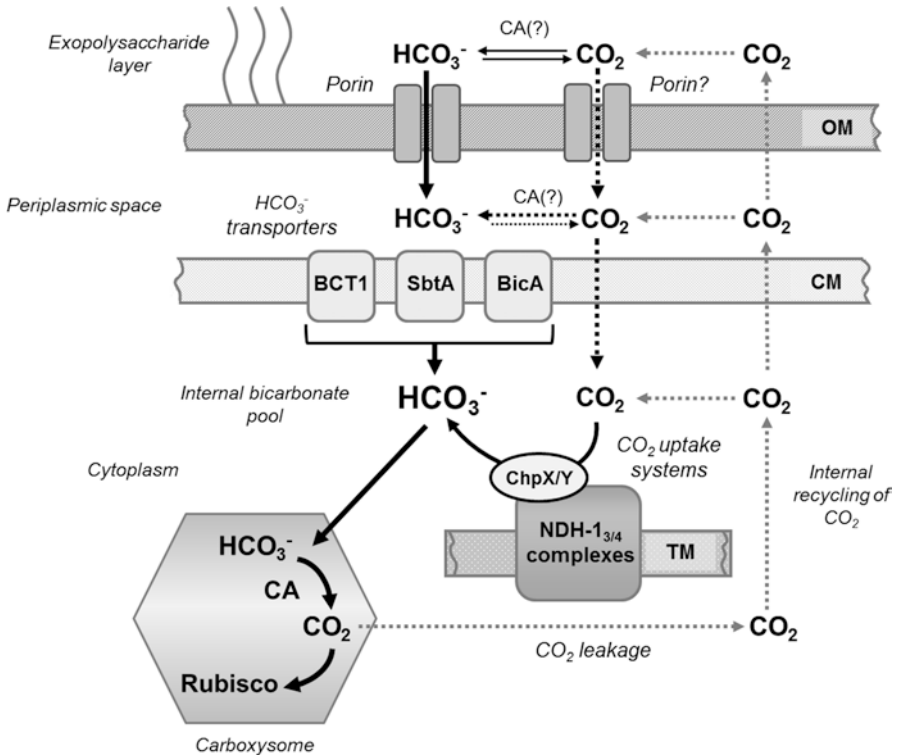


Fig. 4 Inorganic carbon uptake systems in cyanobacteria. Bicarbonate and CO₂ enter to a cell presumably through the porine channels situated in the outer membrane (OM). The cyanobacterial transport complex includes three transporters of HCO₃⁻ (BCT1, SbtA, and BicA), which are located in the cytoplasmic membrane (CM), and two CO₂ uptake systems based on modified NADPH dehydrogenase (NDH-1) complexes are located in thylakoid membranes (TM). NDH-1_{3/4} complexes can also intercept CO₂ leakage from the carboxysomes by its hydration to HCO₃⁻. The similar role is attributed to active extracellular carbonic anhydrases, which could also participate in HCO₃⁻ delivery to transporters

The following three HCO₃⁻ transporters can operate in cyanobacterial cells (Fig. 4):

1. The inducible high-affinity bicarbonate transporter BCT1 (Omata et al. 1999). This transporter is encoded by the operon *cmpABCD* and belongs to the family of ABC transporters containing the ATP-binding cassette. The genes *cmpABCD* encode four membrane proteins forming the structure of the BCT1 complex: CmpA, bounded to the periplasmic face of the plasma membrane and acting as a binding protein for HCO₃⁻; CmpB, the integral dimer forming the transmembrane transport path inside the membrane; and two extrinsic cytoplasmic proteins, CmpC and CmpD, bounded to CmpB, both possessing the binding sites for ATP.

2. A low-CO₂-inducible high-affinity Na⁺-dependent HCO₃⁻ transporter SbtA (Shibata et al. 2002) which is probably a Na⁺/HCO₃⁻ symporter, energized by an ATP-powered Na⁺/H⁺ antiport.
3. BicA is a low-affinity, high-flux, Na⁺-dependent HCO₃⁻ transporter belonging to the SulP family (Price et al. 2004).

The uptake of C_i also takes place via the facilitated diffusion of CO₂ (referred as the “CO₂ uptake systems”), in which the NADPH dehydrogenase (also known as plastoquinone oxidoreductase or NDH-1 complex) participates (Fig. 4). Two CO₂ uptake systems located on the thylakoid membrane have been described (Folea et al. 2008; Xu et al. 2008b). NDH-1₄ complex is constitutive, and NDH-1₃ is inducible under C_i limitation and capable of higher uptake rate and affinity. Both complexes appear to involve a CA-like unique subunits known as CO₂ hydration proteins ChpX and ChpY (Maeda et al. 2002) referred also as CupB and CupA, respectively (Shibata et al. 2001). However, to date the CA activity has not been reported for these complexes (Badger et al. 2006; Price 2011).

It is important to mention that the structure of the C_i transport complex is significantly influenced by the life conditions of each particular species of cyanobacteria. The absolute majority of the studied freshwater cyanobacteria (α-cyanobacteria) contain the genes of all above-mentioned C_i transport systems, while in the oceanic strains (β-cyanobacteria), the set of genes encoding the transport systems is usually smaller (Price et al. 2008). The energy equivalents for the active transfer of C_i through membranes are represented by ATP (for the bicarbonate transporter BCT1) and NADPH (for CO₂ uptake) or by the electrochemical gradient of Na⁺ (for the bicarbonate transporters SbtA and BicA). The mechanisms of C_i input are described in detail in the reviews of Price (2011) and Price et al. (2008).

Carbonic Anhydrases: The Second CCM Element

Carbonic anhydrase (CA, EC 4.2.1.1) is a metalloenzyme catalyzing the reversible hydration of carbon dioxide to bicarbonate: CO₂ + H₂O ⇌ HCO₃⁻ + H⁺. Six independently evolved CA classes have been described (McKenna and Frost 2014; Del Prete et al. 2014). The CAs belonging to the α-, β-, δ-, and η-classes contain in their active site the ion of zinc (Zn²⁺) which participates in the catalytic action (Supuran 2008; Del Prete et al. 2014), and the γ-class CAs contain Fe²⁺, although it can keep the activity with the ions Zn²⁺ and Co²⁺ (Zimmerman et al. 2010), while the ζ-CA can use both Zn²⁺ and Cd²⁺ (Xu et al. 2008a).

Interconversion between CO₂ and HCO₃⁻ may also occur nonenzymatically. The value of rate constant for the non-catalyzed CO₂ hydration is ~0.037 s⁻¹ (Khalifah 1971). A relatively low rate of the non-catalytic interconversion of these C_i forms would result in the strict limitation of photosynthetic assimilation of CO₂. The presence of CA accelerates this reaction by many times. CA is one of the fastest enzymes which turnover number (*k*_{cat}) reaches the value of 10⁶ s⁻¹ (Lindsog 1997).

The ratio of CO₂ and bicarbonate concentrations depends on pH in the medium and can be described by the Henderson–Hasselbalch equation:

$$pH = 6.3 + \log\left(\frac{[HCO_3^-]}{[CO_2]}\right).$$

The equilibrium of both C_i forms in this reaction is reached at pH 6.3. In more acidic conditions, it is displaced to the formation of CO₂, while in more alkaline conditions, it is shifted to the formation of HCO₃⁻. The difference in the total C_i level in freshwater basins (~10 μM) and in the open sea (~2 mM) is determined by this pattern. The seawater having the alkaline pH value (~8) contains the high pool of bicarbonate in the equilibrium with the dissolved CO₂, while in the freshwater medium, the concentration of bicarbonate is low, and the C_i is present mainly as CO₂. The acceleration of CO₂/HCO₃⁻ turnover by the external CAs keeps the concentration of the available for cyanobacteria form of C_i in the proximal extracellular space at the constant level. The internal CAs or CA-like proteins (such as ChpX and ChpY) will displace the direction of the reaction toward bicarbonate formation resulting in its intracellular accumulation and in facilitation of CO₂ entry and uptake (Fig. 4).

To date no organism is known which would exist without CA. The enzyme is found in the representatives of all kingdoms of life: Bacteria, Planta, and Animalia, including humans. CA can be detected in many (in some organisms—in all) organs, tissues, and cellular compartments. The wide distribution of this enzyme among all groups of living organisms is caused by the diversity of enzymatic reactions in which CO₂ and bicarbonate are involved as reaction substrates or products (Smith and Ferry 2000). The inorganic carbon is one of the central cell metabolites, and the acceleration of interconversion of its forms is important for various processes including respiration of animal cells and photosynthesis in plant cells.

Six CA classes do not contain any significant homology in amino acid sequences (Supuran 2008). This strongly indicates that they developed independently and represent the convergence in the evolution of the catalytic function (Liljas and Laurber 2000). This means that the enzyme was invented by the nature several times in the form of different proteins fulfilling the same function of the catalysis of CO₂/HCO₃⁻ interconversion. Despite the differences in their structure, almost all CAs possess the similar catalytic mechanism, which is caused by similar structure of the active sites of CAs from different classes.

The α-class is considered as the youngest phylogenetic group of CAs. This class contains all CAs of animals including 16 isoforms in mammals (Hewett-Emmett and Tashian 1996). The enzymes of β- and γ-classes are considered as the most ancient (Smith and Ferry 2000).

Cyanobacteria possess α-, β-, and γ-classes of CAs. Among them there are the external enzymes, which include the α-CA EcaA (Soltes-Rak et al. 1997) and the two β-CAs, EcaB (So et al. 1998) and CahB1 (Kupriyanova et al. 2007). The function of extracellular CAs having access to the external substrate needs further clarification. The participation of these forms in CCM has been questioned (So et al. 1998).

These external enzymes likely participate in the maintenance of the equilibrium between CO_2 and HCO_3^- in the periplasm and in delivery of HCO_3^- to its transporters (Fig. 4). They can participate also in the prevention of CO_2 leakage from the cell. It was also suggested that the extracellular CAs could be sensors of CO_2 levels in the environment (So et al. 1998; Sültemeyer et al. 1998).

Besides the external CAs, cyanobacteria contain the intracellular carboxysomal enzymes CcaA and CsoSCA (both of β -class) and CcmM (γ -CA) (Cannon et al. 2010). Their functions are now successfully elaborated and will be discussed in detail in the next section (section “Cooperation of CA and Rubisco in Cyanobacterial Carboxysomes: Fundamental Principle of the CCM Functioning”).

Cooperation of CA and Rubisco in Cyanobacterial Carboxysomes: Fundamental Principle of the CCM Functioning

All the described above stages of CCM are preparatory for the final stage of conversion of the accumulated bicarbonate pool into CO_2 molecules which serve as a substrate for Rubisco in the reaction of RuBP carboxylation. This final stage takes place in carboxysomes, which are the sites of Rubisco localization.

The latest achievements clarifying the operation of carboxysomes are described in several reviews (Long et al. 2007; Cot et al. 2008; Yeates et al. 2008; Cannon et al. 2010; Espie and Kimber 2011; Rae et al. 2013). Carboxysomes are present in all cyanobacterial cells (Yeates et al. 2008) and represent the multigranular protein microbodies of 100–400 nm in diameter (Rae et al. 2013; Cai et al. 2015) located in the cytoplasm and surrounded by thin proteinaceous shell (Fig. 5). The proteinaceous

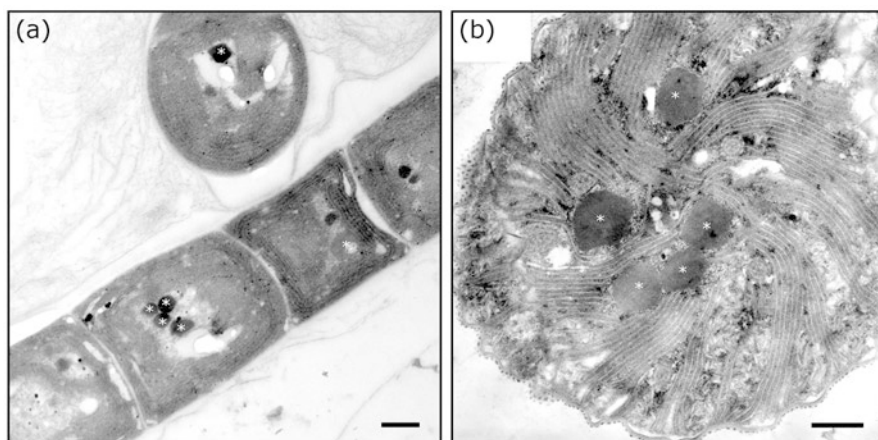


Fig. 5 Transmission electron microscopy images of cyanobacterial cells with carboxysomes: (a) *Microcoleus* sp. IPPAS B-353 and (b) *Arthrospira platensis* IPPAS B-256. Bars, 0.5 μM . Carboxysomes are indicated by asterisks. Images were kindly provided by Dr. M.A. Sinetova (Timiryazev Institute of Plant Physiology, RAS, Moscow)

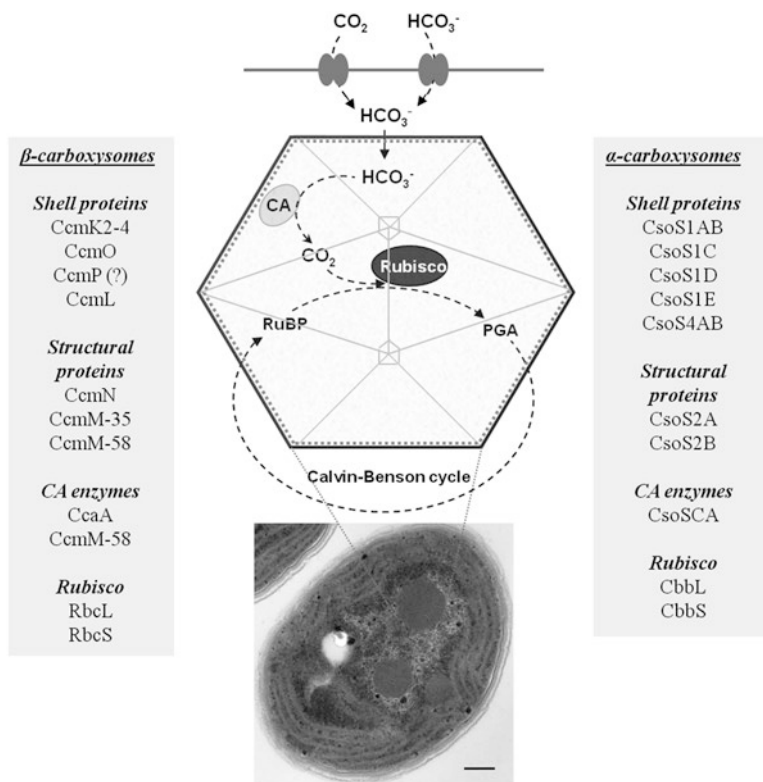


Fig. 6 The structure of carboxysomes and their participation in CCM and photosynthetic assimilation of inorganic carbon. C_i is actively accumulated in the cytoplasm in the form of bicarbonate anion. Bicarbonate enters carboxysome through small pores in the shell proteins. HCO₃⁻ is converted to CO₂ in the lumen of carboxysome with the help of CA. RuBP also enters through the pores into the lumen of carboxysome where Rubisco catalyzes the interaction of CO₂ and RuBP resulting in the formation of PGA. PGA escapes to the cytoplasm where the Calvin–Benson cycle regenerates RuBP. The shell fulfills the barrier function for the efflux of CO₂ and the influx of O₂. The TEM image of cyanobacterial cell (*Synechocystis* sp. PCC 6803) was kindly provided by Dr. M.A. Sinetova (Timiryazev Institute of Plant Physiology, RAS, Moscow). Bar, 0.2 μm

shell consists of the ordered set of small globular proteins (10–12 kDa), also called bacterial microcompartment (BMC) proteins.

The sequencing of genomes of α - and β -cyanobacteria revealed that the carboxysomes differ significantly between the representatives of these taxonomic groups (Fig. 6) both in the composition of the internal phase of the carboxysomal microcompartment and in the composition of polypeptides of the external protein shell (Espie and Kimber 2011; Rae et al. 2013). These two types of carboxysomes having the same function and same pattern but differing in protein composition appeared as a result of the convergent evolution (Rae et al. 2013).

The proteins of β -carboxysomes are subdivided into two groups: the first group is forming the shell which is, according to the recent findings, presumably consists of two shell layers, and the second group is forming the lumen. The outer layer of

the shell is formed by CcmK2-4, CcmO, CcmL, and, possibly, CcmP. The proteins CcmK2-4 possess the hexagonal structure. The pores in the center of each hexamer can carry small molecules of metabolites. The protein CcmL can serve for the formation of pyramidal pentameric apexes of the carboxysome. The CcmO proteins form the trimers and are similar by the structure and properties to those of CcmK hexamers. CcmP was not identified as an essential element of carboxysomes.

The inner layer of the shell (bicarbonate dehydration/Rubisco-organizing or Rubisco-attached layer) is formed by CcaA, CcmM-58, and CcmN. The lumen of β -carboxysomes appears to have packing paracrystalline 1B Rubisco possibly organized by the CcmM-35. The protein CcmM is expressed in two isoforms of 58 and 35 kDa, which appear to be the most important structural proteins of β -carboxysomes. The full-length CcmM-58 isoform possesses the N-terminus having similarity to γ -CA of archaebacterium *Methanosarcina thermophila* (Cam protein), while the C-terminal domain of CcmM contains three repeats of the small subunit of Rubisco (Long et al. 2007; Cot et al. 2008). Therefore, CcmM-58 can function both as a γ -CA and as a structural element of the shells of β -carboxysomes forming the complex with CcmN and CcaA (β -CA) proteins and also linking Rubisco through RbcS-like C-terminal subunit (Long et al. 2007; Cot et al. 2008; Espie and Kimber 2011). It has been established that the β -CA CcaA is connected with the inner layer of the shell of the carboxysome and participates in CO₂ fixation as a part of the multienzyme complex Rubisco–CcaA–CcmM (Cot et al. 2008). The contemporary models of interaction between the carboxysomal proteins have been reviewed by Rae et al. (2013).

The *ccmM* gene was found in all representatives of β -cyanobacteria, whereas the *ccaA* gene was lost in many of them. It is shown that the γ -CA CcmM reveals its activity only in the species lacking β -CA CcaA (Peña et al. 2010). It has been shown that the newly translated CcmM and Rubisco form the aggregations that serve as the centers of the formation of new carboxysomes (Cameron et al. 2013).

The shell of α -carboxysomes (Fig. 6) is built of the proteins of the group CsoS1, which, similarly to the proteins CcmK of β -carboxysomes, form the pores for metabolite transfer. The proteins CsoS4A/B form the pyramidal vertices of α -carboxysomes. The internal phase (lumen) is filled mainly by 1A Rubisco, encoded by the *csO* operon. The β -CA CsoSCA is connected with the internal side of the shell and participates in CO₂ fixation similarly to the β -CA CcaA of β -carboxysomes. Therefore, the carboxysomal β -CA CcaA and CsoSCA do not appear in the same organism being a part of the different carboxysomal types of cyanobacteria (Espie and Kimber 2011). The exact role of CsoS2, which is also located in the inner space of carboxysome, is not known yet.

The co-localization of Rubisco and CA may possibly have a dual functional significance. Its first role is connected with CO₂ formation from HCO₃⁻ for saturation of the carboxylation reaction, while the second role is related to the decrease of CO₂ loss during its leakage from carboxysomes (Yeates et al. 2008). It was demonstrated experimentally that the proteinaceous carboxysomal shell fulfills the barrier function for CO₂ and O₂ (Heinhorst et al. 2006; Dou et al. 2008) and it covers carboxysomes only in the conditions of carbon starvation of cells (Cameron et al. 2013).

Limitation of the oxygen influx into carboxysome would suppress the oxygenase function of Rubisco and keep the carboxylase function at a high level (Kinney et al. 2011). The importance of carboxysomes for CCM operation was confirmed in the experiments using α - and β -carboxysome mutants, which are incapable of forming CO₂ in carboxysomes even in those cells that accumulated extremely high bicarbonate pool in cytoplasm (Rae et al. 2013). Using the *ccmM* mutant of *Synechocystis* PCC 6803, lacking carboxysomes (but containing Rubisco), the direct evidence was obtained that the lack of photorespiration in the wild type is directly related to the fact that carboxysomes accumulate CO₂ and their envelope likely limits the diffusion of O₂ (Hackenberg et al. 2012). The comparison of the wild type of *Synechocystis* sp. PCC 6803 and of its mutant lacking four of five C_i transporters (Orf et al. 2015) also confirmed the conclusion that carboxysomes defend Rubisco from O₂, while the conversion of HCO₃⁻ into CO₂ inside carboxysome is the main factor that results in avoiding photorespiration in C_i limitation conditions.

Thus, bicarbonate penetrates into carboxysomes by diffusion through the pores and converts there to CO₂ by CA. The CO₂ is further used in the carboxylation reaction catalyzed by Rubisco. All other enzymes of the Calvin–Benson cycle are localized outside of carboxysome. Therefore, in photosynthetic cyanobacteria, the influx of RuBP into carboxysome and the outflow of PGA from carboxysome to cytoplasm are taking place. It is supposed that this diffusion occurs via the pores that were found in the proteins CcmK and CcmO of the carboxysomal shell.

Regulation of the CCM in Relation to Carbon Metabolism of Cyanobacteria

As it was mentioned above, CO₂ concentration in cyanobacteria represents an inducible mechanism which is activated only in the conditions of C_i limitation. At the same time, two states of CCM are distinguished: (1) basal (or low-affinity) state, supporting the photosynthetic activity of cells even at elevated levels of C_i in the environment, and (2) fully induced (or enhanced, high-affinity) state of the CCM, fulfilling similar function at C_i-limiting conditions (Price et al. 2008). Both CCM states provide the maximal photosynthetic efficiency in the conditions of different levels of supply by the exogenous C_i, which is achieved through the action of the different set of CCM components. The additional regulation of the CO₂-concentrating function and its coordination with other cellular processes are achieved via alteration in activity of these components.

The transition between the low-affinity and high-affinity states of the CCM is provided by the regulatory processes taking place at two levels (Fig. 7): (1) the transcriptional level enabling regulation of mRNA level of the CCM components and (2) the posttranscriptional level enabling regulation of the efficiency of mRNA translation and modification of activity of the existing protein components of the CCM. Several aspects of both types of regulation remain not fully studied. However, the important discoveries of recent decades, using β -cyanobacteria as an example, shed the light on the basic features of the CCM regulation.

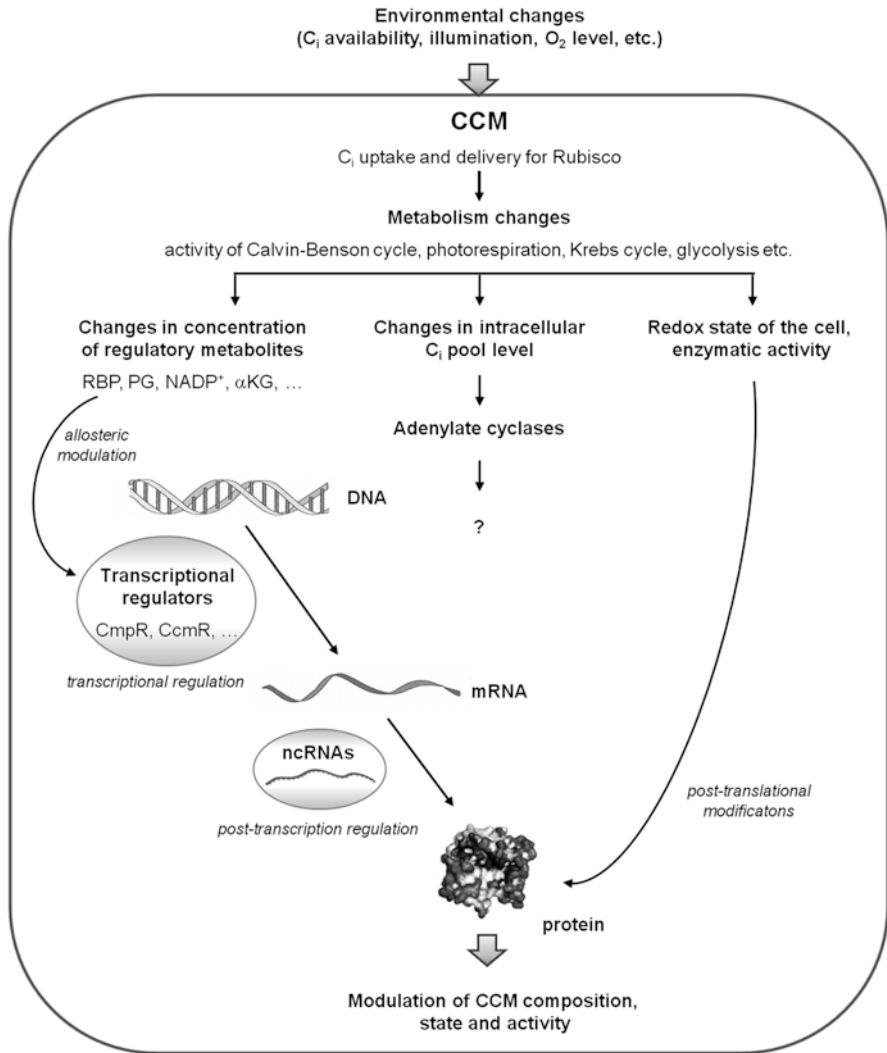


Fig. 7 The general scheme of the presently known regulatory levels controlling the CCM state and activity

Wang et al. (2004) found that after the transfer of high-CO₂ cells of *Synechocystis* sp. PCC 6803 into the C_i-depleted medium, during the first 12 h, a significant change (by two or more times) in the expression of 456 open reading frames is observed. Other observed changes occurring during the acclimation to low CO₂ are rather quantitative than qualitative, in particular the increase of the rate of uptake and accumulation of C_i (Coleman 1991) and the increase of number of carboxysomes (Kaplan and Reinhold 1999; Orf et al. 2015). The most important transformations taking place in cells in response to the C_i stress and resulting in their physiological

changes are analyzed in several papers and reviews (Burnap et al. 2015; Klahn et al. 2015; Orf et al. 2015).

It becomes evident that CCM is induced by limitations in C_i (or of one of its forms) not directly but via some regulatory metabolites, whose concentrations depend on the ambient C_i availability. These compounds can fulfill the role of the sensors of the lowering of CO₂ both intra- and extracellularly in order to control the expression of corresponding genes during the induction of the CCM. The posttranscriptional level makes it possible to perform the regulation via alterations in the efficiency of translation from mRNAs, as well as to vary the degree of activity of already existing components via their posttranslational modifications including their phosphorylation (Sültemeyer et al. 1998).

For the complete understanding of the regulatory mechanisms, the detailed information is needed on the structural and biochemical changes in a cell in response to the decrease of CO₂ concentration. During the transfer of high-CO₂ cells to low CO₂, the carbon starvation decreases leading to the suppression of the Calvin–Benson cycle. Simultaneously photorespiration becomes activated as the consequence of Rubisco shifts toward the oxygenase function (Hagemann et al. 2016). The decrease in CO₂ also results in the activation of glycolysis and the Krebs cycle as well as the oxidative pentose phosphate pathway (Bauwe et al. 2010). All these metabolic events are necessary for the biosynthesis of carbon compounds, NADPH, and ATP (Huege et al. 2011; Schwarz et al. 2013). The intermediates of these pathways can fulfill the role in regulation of CCM (Ramazanov et al. 1984; Huege et al. 2011). Besides the carbon starvation, the C_i stress leads to photodynamic and oxidative damages in cells.

Transcriptional Regulation of the CCM

The basal CCM state (Price et al. 2008) is provided by operation of its constitutive components which include carboxysome components (structural proteins, Rubisco, and carboxysomal CAs) as well as low-affinity high flux-rate C_i uptake systems (NDH-1₄ and BicA). The inducible components responsible for the enhanced CCM state are represented, in general case, by the high-affinity low-to-moderate flux-rate C_i uptake systems (NDH-1₃, SbtA, and BCT1). Their operation is necessary for the accumulation of the additional intracellular pool of HCO₃⁻ in the growth conditions at low CO₂.

The expression of low-CO₂-induced genes is controlled by two transcription regulators, CmpR and CcmR (NdhR), belonging to the LysR family of transcriptional regulators (LTTRs) which operate as transcription activators or repressors (Burnap et al. 2015). The action of LTTRs is based on the change of their ability of binding to DNA after the interaction with effector molecules (Maddocks and Oyston 2008), which represent regulatory metabolites. At the same time, several investigations showed that the changes of concentration of regulatory metabolites directly depend on the size of intracellular pool of C_i and on the availability of oxygen in cells (Woodger et al. 2005; Marcus et al. 1983).

It has been established that CmpR acts as the activator of transcription of the operon *cmpABCD* encoding the high-affinity bicarbonate transporter BCT1 of freshwater cyanobacteria (Omata et al. 2001). The binding of CmpR with the promoter is increased in the presence of RuBP and PG (Nishimura et al. 2008), which serve as regulatory metabolites (effectors) accumulating in the conditions of C_i limitation due to the suppression of Calvin–Benson cycle and simultaneous intensification of photorespiration.

Contrary to CmpR, the regulator CcmR serves as a repressor of transcription of several genes under C_i sufficiency in *Synechocystis* PCC 6803 (Burnap et al. 2015): (1) the gene *sbtA* for high-affinity bicarbonate transporter; (2) the operon *ndh-1₃*, encoding the proteins forming the corresponding inducible high-affinity CO_2 uptake system; and (3) the operon *mnh*, encoding the Mnh complex which forms electrochemical Na^+ gradient supporting the operation of Na^+/HCO_3^- symporters (BicA and SbtA). The genes *bicA* are also under the negative regulation by CcmR in marine *Synechococcus* strain PCC 7002.

It is likely that the molecules $NADP^+$ and αKG serve as the effectors for CcmR, as shown by the surface plasmon resonance (Daley et al. 2012). Theoretically it can be expected that in the conditions of C_i limitation, the decrease in concentration of $NADP^+$ and αKG takes place, which weakens the binding of CcmR with the regulon and results in attenuation of transcription repression of *sbtA*, *ndh-1₃*, and *mnh*. The decrease of $NADP^+$ in the conditions of insufficient C_i supply can be explained by its consumption in light reactions of photosynthesis and simultaneous limitation of its supply from the Benson–Calvin cycle.

It can be expected that αKG concentration in low- CO_2 cells should also decrease. This can take place due to the decrease of the Calvin–Benson cycle activity and following limitation of carbon influx in the Krebs cycle. However, the data on the change of αKG level in the conditions of C_i limitation are quite ambiguous. It has been established that the marked decrease of αKG level occurs only in 24 h after the transition of cells in the C_i -depleted medium (Daley et al. 2012). According to the other data, the low- CO_2 cells accumulate αKG which occurs possibly due to carbon influx into the Krebs cycle from glycolysis (Schwarz et al. 2011). This means that the regulation of transcription by CcmR can occur via more complex mechanisms and/or requires other regulatory inputs besides $NADP^+$ and αKG (Burnap et al. 2015).

Besides the regulatory metabolites, RuBP, PG, $NADP^+$, and αKG , whose concentration changes due to metabolic reconstructions upon the changes in C_i availability, the role in CCM regulation can be attributed to adenylate cyclases as the direct sensors of intracellular C_i level. This assumption is based on the available data of the regulation of activity of cyanobacterial adenylate cyclases by HCO_3^- (Chen et al. 2000) or by CO_2 (Hammer et al. 2006). However, the role of these enzymes in CCM regulation is still unclear despite the fact that such investigations started 15 years ago.

Posttranscriptional Regulation of the CCM

Besides the transcriptional control of the CCM, its regulation occurs also at the posttranscriptional level. This makes possible the additional variation of composition of the CCM components and the modulation of their activity. The first is achieved via regulation of translation from the existing mRNA molecules via their binding with small regulatory RNAs (Georg and Hess 2011). These small noncoding RNAs (ncRNA) usually operate as antisense, and their association with target mRNA can either amplify or attenuate the synthesis of corresponding proteins on the ribosome (Burnap et al. 2015). This level of regulation possibly provides the increase of number of carboxysomes at C_i limitation, since it was shown that the increase of expression of the genes of the operon *ccmKLMN* as well as of the gene *ccmO* does not occur in these conditions (Burnap et al. 2015).

Alternatively, the change in the activity of CCM components can take place at the posttranslational (allosteric) level and be provided by changes in the redox state of the cell (Kaplan et al. 1987) or by protein phosphorylation (Sültemeyer et al. 1998). This type of regulation possibly controls the operation of C_i uptake systems, being quickly activated upon illumination and becoming inactive upon the darkness (Price et al. 2008).

Unique Features in CCM Components of Relict Cyanobacteria

Cyanobacteria appeared on Earth about 3.8–3.5 billion ago (Sergeev et al. 2002; Zavarzin 2008). According to the recent data, already 3.5 billion years ago, the oxygenic photosynthesis was performed by cyanobacteria (Konhauser 2009). The Archean atmosphere was characterized by a high [CO₂]/[O₂] ratio (Kasting 2004; Kanzaki and Murakami 2015). Thus, the ancient photosynthesis scheme was adapted to C_i-rich conditions.

Cyanobacterial communities entirely dominated the planet for 2 billion years. Recent investigations suggest that cyanobacterial communities of the Archean Eon were probably diversified in terrestrial freshwater ecosystems (Blank and Sánchez-Baracaldo 2010). The opposite theory suggests that early cyanobacteria flourished in soda lakes of the Archean (Stüeken et al. 2015). Two billion years ago, the ancient cyanobacterial communities transformed the early reducing atmosphere to a modern oxidative one (Zavarzin 2008; Blank and Sánchez-Baracaldo 2010). This was due to saturation of the atmosphere with photosynthetic oxygen, and due to mineralization of cyanobacterial cells, large amounts of CO₂ had been sequestered as a limestone deposit (stromatolites). This event led to the development of all currently existing mechanisms for adaptation to low concentrations of CO₂ in the atmosphere, including the CCM.

After the appearance of eukaryotic organisms, the cyanobacterial communities decreased their population and areas of habitat and moved from the world dominance to the quite existence in extreme environments, where they can be found today (Zavarzin 2008). These environments are characterized by the complete absence of higher organisms. Thus, they may serve as refugia (centers of preservation) for relict communities of microorganisms (Zavarzin 2008). It is assumed that cyanobacterial communities are still extremely conserved, and they did not change significantly in terms of their physiology and morphology up to present day (Sergeev et al. 2002).

The studies of relict organisms are very important for our understanding of the process of autotrophic carbon assimilation and evolution of the CCM and of CAs. As the subject of CCM studies, relict alkaliphilic cyanobacteria of soda lakes are most intriguing objects. They inhabit environment featuring high content of ambient C_i ; thus, theoretically they do not require the C_i concentration. Moreover, the growth and propagation of the alkaliphilic cyanobacteria at extreme pH values (~ 10), where C_i appears only in the forms of carbonate and bicarbonate, implies that these cells possess the C_i transport systems with somewhat unique characteristics.

Recently, the presence of some distinct CCM components in relict cyanobacteria of soda lakes has been shown experimentally (Dudoladova et al. 2007; Mikhodyuk et al. 2008; Kupriyanova et al. 2007, 2011). The only organism, which CCM components were systematically investigated using the genomic approach, is *Microcoleus* sp. IPPAS B-353 (Cho et al. 2015; Kupriyanova et al. 2016).

It turned out that the composition of the CCM components of *Microcoleus* IPPAS B-353 is similar to that of model freshwater and marine strains of β -cyanobacteria (Kupriyanova et al. 2016). However, there are some unique features. The main and more intriguing fact is that CahB1 protein of *Microcoleus*, which is the homolog of carboxysomal β -CA CcaA, is located in cell envelopes of this cyanobacterium (Fig. 8). Moreover, it is appeared that CahB1 is the only active CA of *Microcoleus*.

In cyanobacteria the presence of an active carboxysomal CA is obligatory for efficient CO_2 fixation by Rubisco (see section “Cooperation of CA and Rubisco in Cyanobacterial Carboxysomes: Fundamental Principle of the CCM Functioning”). It is known that some cyanobacterial species lack CcaA. In this case, the function of active carboxysomal CA is acquired by CcmM (Peña et al. 2010). Surprisingly, the recombinant carboxysomal CcmM of *Microcoleus* did not reveal any specific activity (Kupriyanova et al. 2016). Moreover, primary amino acid sequence of *Microcoleus* CcmM is analogous to that of inactive CcmM proteins, in accordance to Peña et al. (2010).

The function of CahB1 in *Microcoleus* is attributed to the prevention of CO_2 leakage from the cells similarly to ChpX/Y proteins of NDH-1_{3/4} complexes (Fig. 8). This external CA possibly played more important role in ancient cyanobacteria by limiting CO_2 influx to the cells via its conversion to insoluble in membranes HCO_3^- followed by its further delivery to low-affinity transporters (see below).

Besides CcmM and CahB1, *Microcoleus* sp. IPPAS B-353 possesses one more potential protein for CA, CahG (Kupriyanova et al. 2016), that is homologous to active γ -CAs Cam/CamH of *Methanosarcina thermophila* (Alber and Ferry 1994;

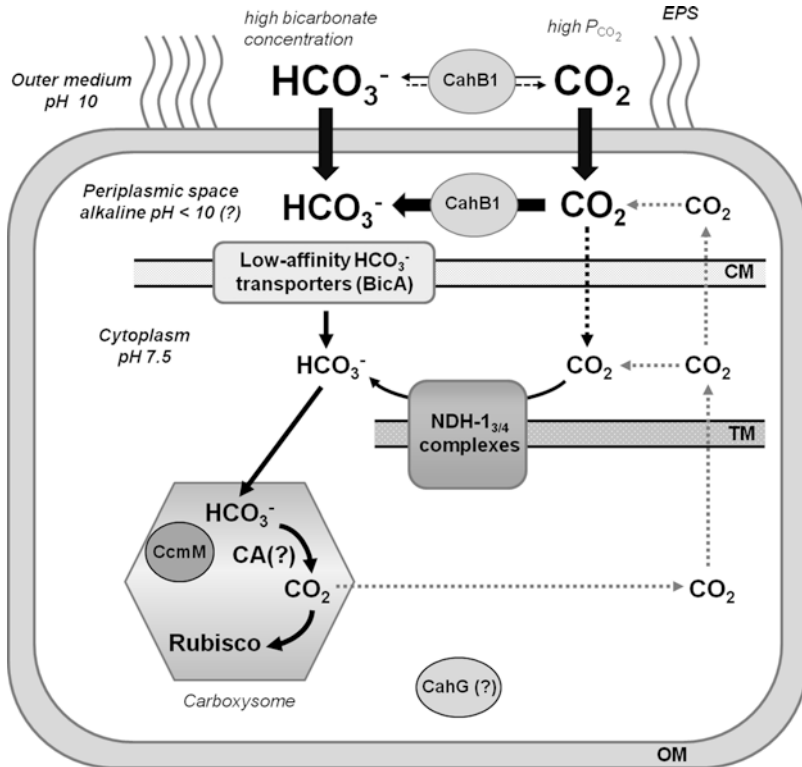


Fig. 8 CCM components of relict cyanobacteria in a cell as learned on the *Microcoleus* sp. IPPAS B-353 and their potential roles in in photosynthetic assimilation of C_i as well as in pre-CCM which functioned in cyanobacteria inhabiting soda lakes of Archean. Localization of C_i uptake systems and CAs in the cell is shown according to Folea et al. (2008), Xu et al. (2008b), Price (2011), Cannon et al. (2010), and Kupriyanova et al. (2016). EPS exopolysaccharide layer, OM outer membrane, CM cytoplasmic membrane, TM thylakoid membrane

Zimmerman et al. 2010). Cam/CamH-like proteins of cyanobacteria (including CahG) are usually characterized by amino acid replacements in the regions which are conserved in archaeal γ -CAs, thus demonstrating the absence of specific activity. Currently, most of cyanobacterial Cam/CamH-like proteins are annotated as ferripyochelin-binding proteins.

Unlike freshwater and marine β -cyanobacteria, *Microcoleus* sp. IPPAS B-353 possesses only one type of bicarbonate transporter, BicA (presumably low affinity), which is represented by two homologous proteins, one of which is constitutive and the second is inducible under C_i limitation (Kupriyanova et al. 2016). In addition to HCO₃⁻ transporters, *Microcoleus* sp. IPPAS B-353 possesses two known systems of CO₂ uptake (NDH-1₄ and NDH-1₃), apparently both constitutive in contrast to that of model strains, which induce NDH-1₃ under C_i limitation (Price 2011).

It is assumed that C_i uptake systems of *Microcoleus* sp. IPPAS B-353 could possess different characteristics (affinity to the substrate and flux rate). Thus, the composition of C_i transport complex helps this cyanobacterium adapt to seasonal fluctuations in availability of exogenous C_i in the conditions of modern soda lakes. The only question is raised about the presence of protein with CA activity in *Microcoleus* carboxysomes.

Simultaneously, it is assumed that cyanobacteria of soda lakes could possess the relict forms of pre-CCM components preserved from the Precambrian times when the concentration of exogenous C_i was high (see section “The Evolutionary Origin of the CCM”). This pre-CCM could carry out the function of the low-affinity state of modern CCM supporting photosynthetic reactions in C_i -reach environment. This hypothesis is supported by the fact that bicarbonate transporters of modern alkali-philic cyanobacteria are characterized by three orders lower affinity to the substrate than those of freshwater and seawater species (Mikhodyuk et al. 2008). These characteristics of the transport systems enable limitation of C_i influx to the cells in conditions of its abundance in the surrounding environment.

It is possible that the ancient cyanobacteria had to execute the task of C_i consumption in the amount which does not disturb cellular homeostasis and, at the same time, which is necessary for provision of the efficient rate of photosynthesis (Kupriyanova and Samylyna 2015). From this point of view, in the conditions of C_i -rich environment, the active presence of the carboxysomal CA in the cell may not be necessary due to the constant influx of CO_2 to Rubisco from the intracellular bicarbonate-rich pool. On the other hand, the presence of unidentified carboxysomal CAs belonging to a new currently unknown class in the cells of *Microcoleus* sp. IPPAS B-353 cannot be excluded. This possibility can explain the existence of these cyanobacteria in modern time when the atmospheric concentration of CO_2 is low and cannot be sufficient for substrate saturation of the low-affinity Rubisco.

The Evolutionary Origin of the CCM

The different forms of CCMs of aqueous photosynthetic organisms have evolved with a common aim of elevating CO_2 around Rubisco to alter the CO_2/O_2 ratios at the active site in favor of the carboxylase reaction. In this manner, CCMs minimize the costly investment of metabolic energy and carbon in the photorespiration (Raven et al. 2008). The CCM is considered as an innovative evolutionary mechanism originated in response to the decrease of CO_2 in the atmosphere that helps cyanobacteria and algae to survive at CO_2 concentrations much below $K_m(CO_2)$ value for Rubisco.

It is widely accepted that CCM appeared in cyanobacteria between 400 and 250 million years ago, at the Phanerozoic (Fig. 9), during the period of drastic decrease of CO_2 level and strong increase of O_2 concentration (Berner 2003). Badger and Price (2003) consider that the formation of the CCM at that period was an important condition for the survival and development of photosynthetic organisms. Since that time, CO_2 turned into the limiting resource, while the oxygenase reaction of Rubisco turned into the inhibitory factor for effective CO_2 fixation.

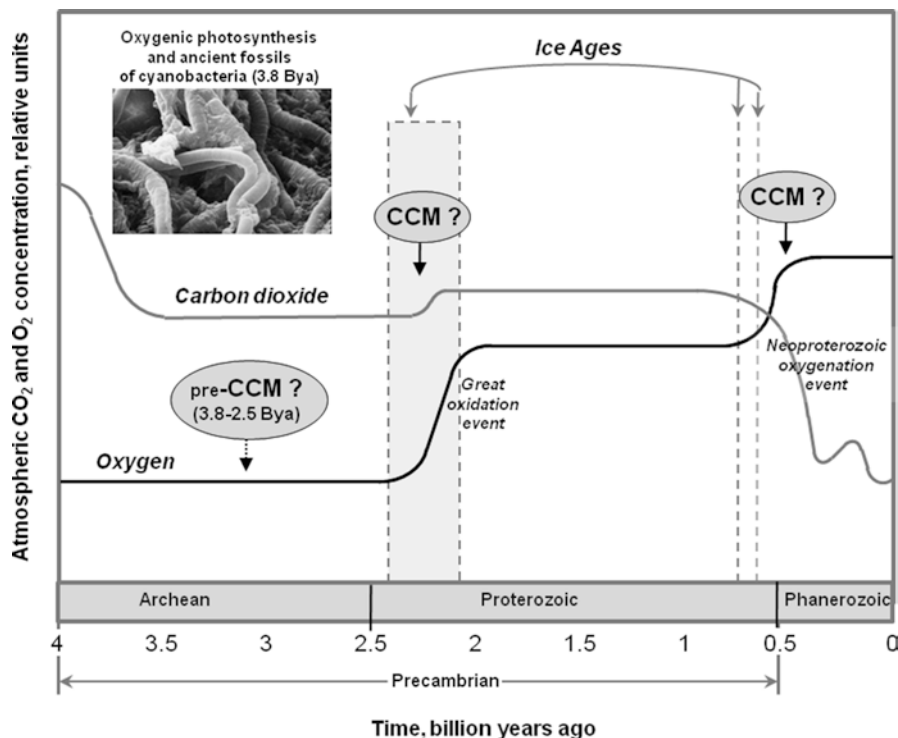


Fig. 9 Time course of relative concentrations of atmospheric CO₂ and O₂ and possible periods of the CCM appearance. Image of *Microcoleus* calcification was obtained by Dr. L.M. Gerasimenko and kindly provided by Dr. O.S. Samylina (Institute of Microbiology, RAS, Moscow)

Other authors do not exclude CCM appearance in the oxygenic cyanobacteria much earlier, in the Precambrian time of Early Proterozoic (2.3–2.5 billion years ago) when molecular oxygen started to accumulate in the atmosphere and ocean surface. Only at this time, the oxygenic photosynthesis performed by cyanobacteria became completely predominant; before this the anoxygenic photosynthesis prevailed, delaying the oxygenation of ocean during the Archean Eon (Johnston et al. 2009; Hamilton et al. 2016). Besides this, Giordano et al. (2005) and Raven et al. (2008) suggest that, despite the high CO₂ concentration at this time, the ancient cyanobacteria in the conditions of dense cyanobacterial communities could experience the necessity of CO₂ concentration because of the presence of a thick polysaccharide shell around the mat-building cyanobacteria, limiting CO₂ delivery into the cells.

Also, we may underestimate the levels of oxygen in Early Proterozoic during the Great Oxygenation Event that resulted in the Huronian glaciation that lasted more than 300 million years (snowball Earth). Recent estimates suggest O₂ concentration rising to near present-day level at the beginning of Proterozoic (~2450–2100 million years ago) (Kump 2008; Lyons et al. 2014). In these conditions CCM was evolutionary important for the growth of biomass and survival of cyanobacteria (Hagemann et al. 2016).

One more indication of the early stage of evolution of the cyanobacterial CCM can be found in the scenario of early evolution of carboxysomes as the central element of CCM in cyanobacteria (Rae et al. 2013). According to Hagemann et al. (2016), this also indicates the early appearance of photorespiration which possibly initiated the evolution of CCM in Proterozoic Eon. Another indirect argument for the ancient emergence of CCM is the ability of modern cyanobacteria not only to adapt to low CO₂ but also to retain the ability to grow at extremely high concentrations of CO₂ (Sergeenko et al. 2000). Although CCM is the inducible process activated by a deficiency of C_i, nearly all elements of the CCM (C_i uptake systems, CAs, carboxysomes) are present in cyanobacterial cells at high C_i concentrations.

However, the earliest CCMs (pre-CCM) may have evolved before the atmosphere became oxygenated and were connected with calcification of cyanobacteria and formation of stromatolites, which accumulated huge amounts of CO₂ into carbonates during the Archaean (Zavarzin 2008). The calcium shell formed at the surface of the calcifying cyanobacteria such as *Microcoleus* (Fig. 9) could establish a barrier for the diffusion of CO₂ and O₂, which also created preconditions for CCM appearance in Archaean (Raven et al. 2008; Kupriyanova et al. 2013).

Analyzing the evolutionary origin of CCM, we need also to consider a possibility that the components of pre-CCM could fulfill another function besides of C_i concentration. The presence of CCM components in *Microcoleus* sp. IPPAS B-353 (Kupriyanova et al. 2016), which may be assigned to a group of “relict” or ancient cyanobacteria (Cho et al. 2015), can also give an evidence for the appearance of CCM in the Archaean Eon. It is possible that in the conditions of high atmospheric CO₂ concentration in the Archaean, there was a need for a barrier to prevent the unlimited CO₂ flux into the cell that could result in the decrease of intracellular pH and cell death. This could be achieved in the conditions of ancient water basins having high pH values, in which C_i is present in the form of bicarbonate. The flux of bicarbonate into the cyanobacterial cell can be controlled by HCO₃⁻ transporter(s) (Fig. 8). In the frames of the hypothesis of “soda continent” (Zavarzin 2008), the soda basins are considered as possible centers of origin and divergence of prokaryotes.

It is believed that, when cyanobacteria emerged on Earth, the level of CO₂ was about 100 times higher than nowadays (Kasting 2004; Kanzaki and Murakami 2015). In these conditions, even at the alkaline pH values of water environment, a sufficiently high CO₂ content is preserved in the equilibrium with bicarbonate (Fig. 8). This situation, together with low O₂ content, created favorable conditions for the effective photosynthesis without any carboxysomal CAs (Badger and Price 2003). Later, in modern low-CO₂ atmosphere, these components of pre-CCM could, probably, undergo some evolution of their function giving rise to CCM in a form as we know it today.

The numerous hypotheses about the time of CCM origin are unified in the theory claiming that the origin of CCM is polyphyletic and took place in evolution several times (Raven et al. 2008). This is confirmed by the fact that CCMs exhibit acclimatory responses to variations in the supply of not only CO₂ but also photosynthetically active radiation, nitrogen, phosphorus, and iron. Some cyanobacteria

(*Prochlorococcus marinus* species) lack CO₂ uptake systems entirely. There are multiple CAs in cyanobacteria, but, surprisingly, several cyanobacterial genomes appear to lack any identifiable CA genes (Price et al. 2008).

The evolution of land plants resulted in the loss of CCM due to impossibility of active C_i pumping from the external environment; however, the role of different CA forms (thylakoidal, stromal, mitochondrial) in CO₂ delivery to Rubisco remains important for CO₂ assimilation (Igamberdiev and Roussel 2012; Igamberdiev 2015). Land plants also developed alternative mechanisms of CO₂ concentration, such as C₄ (existing already in some diatoms) and CAM photosynthesis that help them to survive at low atmospheric CO₂ but likely not having such high plasticity and efficiency as the CCM of cyanobacteria and algae.

Conclusions

Carbon-based life on Earth exists due to the ability of plants, algae, and cyanobacteria to fix atmospheric CO₂ by the process of photosynthesis, which implies efficient capture of solar energy and its conversion into chemical energy that supports the synthesis of organic molecules. Photosynthesis arose about 3.5 billion years ago, and it further facilitated an unprecedented explosion in biological life that we witness by the diversity of living organisms on our planet today and by the fossil records including industrially important oil, gas, and coal. Photosynthesis also maintains atmospheric oxygen levels necessary for life on Earth in its present form.

Cyanobacteria are the first and sole prokaryotes performing oxygenic photosynthesis which consumes carbon dioxide and water. They play an exceptionally important role in the evolution and maintenance of the Earth's biosphere. Therefore, cyanobacterial CCM is an important element in the buildup of the atmosphere and preservation of the ecology of the Earth's biosphere via the establishment of efficient mechanisms of CO₂ acquisition. The role of CCM is also significant as a complex multicomponent system of molecular and biochemical interactions responsible for fine-tuning of cellular carbon metabolism.

For better understanding of the CCM organization, it is important to get the answers on the following questions:

1. The nature of the primary signal causing the induction of CCM in response to low CO₂ is still not clear, as well as the mechanism of allosteric and posttranslational regulation of the transporters and their light activation.
2. It is important to determine the value of pH in the carboxysome. If pH in the carboxysome is the same as in the cytoplasm (~7.5), then the ratio CO₂/HCO₃⁻ in this microcompartment will be shifted toward bicarbonate formation, and the carboxysomal CA will support the constant CO₂ level in the proximity of Rubisco, converting HCO₃⁻ that enters from the cytoplasm by the concentration gradient at a high rate. In these conditions, the rate of HCO₃⁻ conversion to CO₂

will be determined by the rate of carboxylation. This means that CA will operate in concordance with Rubisco, which would result in suppression of CO₂ leakage and its apparent loss.

3. The pH value in the periplasm is still unknown, while the understanding of the functional role of external CAs depends on this value, which determines the direction of the CA-catalyzed reaction either toward the formation of CO₂ or bicarbonate. In the cyanobacterial cells, three external CAs have been found belonging to two different classes (α and β), whose function remains not fully clear.

Cyanobacteria are characterized by the exceptional adaptability, in particular to extremely unfavorable conditions in which eukaryotes cannot survive. The presence of the CCM in cyanobacteria cells ensures assimilation of Ci under various environmental conditions at the cellular, organism, and consortia levels. The enormous ecological importance of the CCM is that almost half of the total inorganic carbon of the Earth has been turned, and is still turning, into biomass by microalgae and cyanobacteria through their CCM. Development of cyanobacterial genomics will soon provide new data on the components of CCM of the wide range of cyanobacteria, in particular of the relict cyanobacteria, which should certainly clarify the evolutionary origin of the CCM.

Acknowledgments We thank Drs. M.A. Sinetova and A.G. Markelova (Institute of Plant Physiology, RAS, Moscow, Russia) for the TEM images of *Arthrospira platensis* IPPAS B-256 and *Microcoleus* sp. IPPAS B-353. We honor the memory of Dr. L.M. Gerasimenko who obtained image of *Microcoleus* calcification, kindly provided by Dr. O.S. Samylina (Institute of Microbiology, RAS, Moscow). E.V.K. was supported by a grant from Russian Science Foundation (no. 14-24-00020). A.U.I. was supported by a grant from the Natural Sciences and Engineering Research Council of Canada.

References

- Aizawa K, Miyachi S (1986) Carbonic anhydrase and CO₂-concentrating mechanism in microalgae and cyanobacteria. *FEMS Microbiol Rev* 39:215–233
- Alber BE, Ferry JG (1994) A carbonic anhydrase from the archaeon *Methanosarcina thermophila*. *Proc Natl Acad Sci U S A* 91:6909–6913
- Badger MR, Price GD (2003) CO₂ concentrating mechanisms in cyanobacteria: molecular components, their diversity and evolution. *J Exp Bot* 54:609–622
- Badger MR, Price GD, Long BM, Woodger FJ (2006) The environmental plasticity and ecological genomics of the cyanobacterial CO₂ concentrating mechanism. *J Exp Bot* 57:249–265
- Badger MR, Spalding MH (2000) CO₂ acquisition, concentration and fixation in cyanobacteria and algae. In: Leegood RC, Sharkey TD, Caemmerer S (eds) *Photosynthesis: physiology and metabolism*. Kluwer Academic Publications, Netherlands, pp 369–397
- Badger MR, Kaplan A, Berry JA (1980) The internal inorganic carbon pool of *Chlamydomonas reinhardtii*: evidence for a CO₂ concentrating mechanism. *Plant Physiol* 66:407–413
- Bauwe H, Hagemann M, Fernie AR (2010) Photorespiration: players, partners and origin. *Trends Plant Sci* 15:330–336

- Behrenfeld MJ, Randerson JT, McClain CR, Feldman GC, Los SO et al (2001) Biospheric primary production during an ENSO transition. *Science* 291:2594–2597
- Bell LN (1985) Energetics of the photosynthesizing plant cell. University of Michigan, Harwood Academic Publishers. isbn:9783718601950
- Benson AA, Bassham JA, Calvin M, Goudate TC, Haas UA, Sterka W (1950) The path of carbon in photosynthesis. Paper chromatography and radioautography of the products. *J Am Chem Soc* 12:1710–1718
- Berner RA (2003) The long-term carbon cycle, fossil fuels and atmospheric composition. *Nature* 426:323–326
- Blank CE, Sánchez-Baracaldo P (2010) Timing of morphological and ecological innovations in the cyanobacteria – a key to understanding the rise of atmospheric oxygen. *Geobiology* 8:1–23
- Brautigam A, Schliesky S, Kulahoglu C, Osborne CP, Weber AP (2014) Towards an integrative model of C₄ photosynthetic subtypes: insights from comparative transcriptome analysis of NAD-ME, NADP-ME, and PEP-CK C₄ species. *J Exp Bot* 65:3579–3593
- Burnap RL, Hageman M, Kaplan A (2015) Regulation of CO₂ concentrating mechanism in cyanobacteria. *Life* 5:348–371
- Cai F, Dou Z, Bernstein SL, Leverenz R, Williams EB, Heinhorst S, Shively J, Cannon GC, Kerfeld CA (2015) Advances in understanding carboxysome assembly in *Prochlorococcus* and *Synechococcus* implicate CsoS2 as a critical component. *Life* 5:1141–1171
- Cameron JC, Wilson SC, Bernstein SL, Kerfeld CA (2013) Biogenesis of a bacterial organelle: the carboxysome assembly pathway. *Cell* 155:1131–1140
- Cannon GC, Heinhorst S, Kerfeld CA (2010) Carboxysomal carbonic anhydrases: Structure and role in microbial CO₂ fixation. *Biochim Biophys Acta* 1804:382–392
- Chen Y, Cann MJ, Litvin TN, Iourgenko V, Sinclair ML, Levin LR, Buck J (2000) Soluble adenylyl cyclase as an evolutionarily conserved bicarbonate sensor. *Science* 289:625–628
- Cheng KH, Miller AG, Colman B (1972) An investigation of glycolate excretion in two species of blue-green algae. *Planta* 103:110–116
- Cho SM, Jeoung SC, Song JY, Kupriyanova EV, Pronina NA, Lee BW, Jo SW, Park BS, Choi SB, Song JJ, Park YI (2015) Genomic survey and biochemical analysis of recombinant candidate cyanobacteriochromes reveals enrichment for near UV/Violet sensors in the halotolerant and alkaliphilic cyanobacterium *Microcoleus* IPPAS B353. *J Biol Chem* 290:28502–28514
- Clement R, Dimnet L, Maberly SC, Gontero B (2016) The nature of the CO₂-concentrating mechanisms in a marine diatom, *Thalassiosira pseudonana*. *New Phytol* 209:1417–1427
- Coleman JR (1991) The molecular and biochemical analyses of CO₂ concentrating mechanisms in cyanobacteria and microalgae. *Plant Cell Environ* 14:861–867
- Cot SS, So AK, Espie GS (2008) A multiprotein bicarbonate dehydration complex essential to carboxysome function in cyanobacteria. *J Bacteriol* 190:936–945
- Daley SM, Kappell AD, Carrick MJ, Burnap RL (2012) Regulation of the cyanobacteria CO₂-concentrating mechanism involves internal sensing of NADP⁺ and alpha-ketogutarate levels by transcription factor CcmR. *PLoS One* 7:e41286
- Del Prete S, Vullo D, Fisher GM, Andrews KT, Poulsen SA, Capasso C, Supuran CT (2014) Discovery of a new family of carbonic anhydrases in the malaria pathogen *Plasmodium falciparum* – the η-carbonic anhydrases. *Bioorg Med Chem Lett* 24:4389–4396
- Dou Z, Heinhorst S, Williams EB, Murin CD, Shively JM, Cannon GC (2008) CO₂ fixation kinetics of *Halothiobacillus neapolitanus* mutant carboxysomes lacking carbonic anhydrase suggest the shell acts as a diffusional barrier for CO₂. *J Biol Chem* 283:10377–10384
- Dudoladova MV, Kupriyanova EV, Markelova AG, Sinetova MP, Allakhverdiev SI, Pronina NA (2007) The thylakoid carbonic anhydrase associated with photosystem II is the component of inorganic carbon accumulating system in cells of halo- and alkaliphilic cyanobacterium *Rhabdoderma lineare*. *Biochim Biophys Acta Bioenerg* 1767(6):616–623
- Eisenhut M, Kahlon S, Hasse D, Ewald R, Lieman-Hurwitz J, Ogawa T, Ruth W, Bauwe H, Kaplan A, Hagemann M (2006) The plant-like C₂ glycolate cycle and the bacterial-like glycerate pathway cooperate in phosphoglycolate metabolism in cyanobacteria. *Plant Physiol* 142:333–342

- Eisenhut M, Ruth W, Haimovich M, Bauwe H, Kaplan A, Hagemann M (2008) The photorespiratory glycolate metabolism is essential for cyanobacteria and might have been conveyed endosymbiotically to plants. *Proc Natl Acad Sci U S A* 105:17199–17204
- Espie GS, Kimber MS (2011) Carboxysomes: cyanobacterial RubisCO comes in small packages. *Photosynth Res* 109:7–20
- Folea IM, Zhang P, Nowaczyk MM, Ogawa T, Aro EM, Boekema EJ (2008) Single particle analysis of thylakoid proteins from *Thermosynechococcus elongatus* and *Synechocystis* 6803: localization of the CupA subunit of NDH-1. *FEBS Lett* 582:249–254
- Fomina IR, Biel KY (2016) Photosynthetic carbon metabolism: strategy of adaptation over evolutionary history. In: Allakhverdiev SI (ed) *Photosynthesis: new approaches to the molecular, cellular, and organismal levels*. Scrivener Publishing LLC, pp 233–326
- Gaudana SB, Zarzycki J, Moparthy VK, Kerfeld CA (2015) Bioinformatic analysis of the distribution of inorganic carbon transporters and prospective targets for bioengineering to increase C₃ uptake by cyanobacteria. *Photosynth Res* 126:99–109
- Georg J, Hess WR (2011) Cis-antisense RNA, another level of gene regulation in bacteria. *Microbiol Mol Biol Rev* 75:286–300
- Giordano M, Beardall J, Raven JA (2005) CO₂ concentrating mechanisms in algae: mechanisms, environmental modulation, and evolution. *Annu Rev Plant Biol* 56:99–131
- Hackenberg C, Huege J, Engelhardt A, Wittink F, Laue M, Matthijs HC, Kopka J, Bauwe H, Hagemann M (2012) Low-carbon acclimation in carboxysome-less and photorespiratory mutants of the cyanobacterium *Synechocystis* sp. strain PCC 6803. *Microbiology* 158:398–413
- Hagemann M, Fernie AR, Espie GS, Kern R, Eisenhut M, Reumann S, Bauwe H, Weber AP (2013) Evolution of the biochemistry of the photorespiratory C₂ cycle. *Plant Biol (Stuttg)* 15:639–647
- Hagemann M, Kern R, Maurino VG, Hanson DT, Weber AP, Sage RF, Bauwe H (2016) Evolution of photorespiration from cyanobacteria to land plants, considering protein phylogenies and acquisition of carbon concentrating mechanisms. *J Exp Bot* 67:2963–2976
- Hamilton TL, Bryant DA, Macalady JL (2016) The role of biology in planetary evolution: cyanobacterial primary production in low oxygen Proterozoic oceans. *Environ Microbiol* 18:325–340
- Hammer A, Hodgson DR, Cann MJ (2006) Regulation of prokaryotic adenyllyl cyclases by CO₂. *Biochem J* 396:215–218
- Hanson MR, Lin MT, Carmo-Silva AE, Parry MA (2016) Towards engineering carboxysomes into C₃ plants. *Plant J* 87:38–50
- Heinhorst S, Williams EB, Cai F, Murin CD, Shively JM, Cannon GC (2006) Characterization of the carboxysomal carbonic anhydrase CsoSCA from *Halothiobacillus neapolitanus*. *J Bacteriol* 188:8087–8094
- Hewett-Emmett D, Tashian RE (1996) Functional diversity, conservation and convergence in the evolution of α -, β - and γ -carbonic anhydrase gene families. *Mol Phylogenet Evol* 5:50–77
- Huege J, Goetze J, Schwarz D, Bauwe H, Hagemann M, Kopka J (2011) Modulation of the major paths of carbon in photorespiratory mutants of *Synechocystis*. *PLoS One* 6(1):e16278
- Husic DW, Husic HD, Tolbert NE, Black CC (1987) The oxidative photosynthetic carbon cycle or C₂ cycle. *Crit Rev Plant Sci* 5:45–100
- Igamberdiev AU (2015) Control of Rubisco function via homeostatic equilibration of CO₂ supply. *Front Plant Sci* 6:106
- Igamberdiev AU, Roussel MR (2012) Feedforward non-Michaelis–Menten mechanism for CO₂ uptake by Rubisco: contribution of carbonic anhydrases and photorespiration to optimization of photosynthetic carbon assimilation. *Biosystems* 107:158–166
- Ingle RK, Colman B (1976) The relationship between carbonic anhydrase activity and glycolate excretion in the blue-green alga *Coccochloris penicystis*. *Planta* 128:217–223
- Johnston DT, Wolfe-Simon F, Pearson A, Knoll AH (2009) Anoxygenic photosynthesis modulated Proterozoic oxygen and sustained Earth's middle age. *Proc Natl Acad Sci U S A* 106:16925–16929
- Kanzaki Y, Murakami T (2015) Estimates of atmospheric CO₂ in the Neoproterozoic–Paleoproterozoic from paleosols. *Geochim Cosmochim Acta* 159:190–219

- Kaplan A, Badger MR, Berry JA (1980) Photosynthesis and intracellular inorganic carbon pool in the blue-green algae *Anabaena variabilis*: response to external CO₂ concentration. *Planta* 149:219–226
- Kaplan A, Reinhold L (1999) CO₂ concentrating mechanism in photosynthetic microorganisms. *Annu Rev Plant Physiol Plant Mol Biol* 50:539–570
- Kaplan A, Zenvirth D, Marcus Y, Omata T, Ogawa T (1987) Energization and activation of inorganic carbon uptake by light in cyanobacteria. *Plant Physiol* 84:210–213
- Kasting JF (2004) When methane made climate. *Sci Am* 291:78–85
- Kern R, Eisenhut M, Bauwe H, Weber AP, Hagemann M (2013) Does the *Cyanophora paradoxa* genome revise our view on the evolution of photorespiratory enzymes? *Plant Biol (Stuttg)* 15:759–768
- Khalifah RG (1971) The carbon dioxide hydration activity of carbonic anhydrase. I. Stop-flow kinetic studies on the native human isoenzymes B and C. I. Stop-flow kinetic studies on the native human isoenzymes B and C. *J Biol Chem* 246:2561–2573
- Kinney JN, Axen SD, Kerfeld CA (2011) Comparative analysis of carboxysome shell proteins. *Photosynth Res* 109:21–32
- Klahn S, Orf I, Schwarz D, Matthiessen JKF, Kopka J, Hess WR, Hagemann M (2015) Integrated transcriptomic and metabolomic characterization of the low-carbon response using an *ndhR* mutant of *Synechocystis* sp. PCC 6803. *Plant Physiol* 169:1540–1556
- Konhauser K (2009) Deepening the early oxygen debate. *Nat Geosci* 2:241–242
- Kroth PG (2015) The biodiversity of carbon assimilation. *J Plant Physiol* 172:76–81
- Kump LR (2008) The rise of atmospheric oxygen. *Nature* 451:277–278
- Kupriyanova E, Villarejo A, Markelova A, Gerasimenko L, Zavarzin G, Samuelsson G, Los DA, Pronina N (2007) Extracellular carbonic anhydrases of the stromatolite-forming cyanobacterium *Microcoleus chthonoplastes*. *Microbiology* 153:1149–1156
- Kupriyanova EV, Cho SM, Park YI, Pronina NA, Los DA (2016) The complete genome of a cyanobacterium from a soda lake reveals the presence of the components of CO₂-concentration mechanism. *Photosynth Res* 130:151–165
- Kupriyanova EV, Samylyna OS (2015) CO₂-concentrating mechanism and its traits in haloalkaliphilic cyanobacteria. *Microbiology (Moscow)* 84:144–159
- Kupriyanova EV, Sinetova MA, Cho SM, Park YI, Los DA, Pronina NA (2013) CO₂-concentrating mechanism in cyanobacterial photosynthesis: organization, physiological role, and evolutionary origin. *Photosynth Res* 117:133–146
- Kupriyanova EV, Sinetova MA, Markelova AG, Allakhverdiev SI, Los DA, Pronina NA (2011) Extracellular β-class carbonic anhydrase of the alkaliphilic cyanobacterium *Microcoleus chthonoplastes*. *J Photochem Photobiol B* 103:78–86
- Liljas A, Laurber M (2000) A wheel invented three times. The molecular structures of the three carbonic anhydrases. *EMBO Rep* 1:16–17
- Lindskog S (1997) Structure and mechanism of carbonic anhydrase. *Pharmacol Ther* 74:1–20
- Long BM, Badger MR, Whitney SM, Price GD (2007) Analysis of carboxysomes from *Synechococcus* PCC7942 reveals multiple Rubisco complexes with carboxysomal proteins CcmM and CcaA. *J Biol Chem* 282:29323–29335
- Lyons TW, Reinhard CT, Planavsky NJ (2014) The rise of oxygen in Earth's early ocean and atmosphere. *Nature* 506:307–315
- Maddocks SE, Oyston PC (2008) Structure and function of the LysR-type transcriptional regulator (LTTR) family proteins. *Microbiology* 154:3609–3623
- Maeda S, Badger MR, Price GD (2002) Novel gene products associated with NdhD3/D4-containing NDH-1 complexes are involved in photosynthetic CO₂ hydration in the cyanobacterium, *Synechococcus* sp. PCC7942. *Mol Microbiol* 43:425–435
- Marcus Y, Harel E, Kaplan A (1983) Adaptation of the cyanobacterium *Anabaena variabilis* to low CO₂ concentration in their environment. *Plant Physiol* 71:208–210
- McGrath JM, Long SP (2014) Can the cyanobacterial carbon-concentrating mechanism increase photosynthesis in crop species? A theoretical analysis. *Plant Physiol* 164:2247–2261

- McKenna R, Frost SC (2014) Overview of the carbonic anhydrase family. In: Frost SC, McKenna R (eds) Carbonic anhydrase: mechanism, regulation, links to disease, and industrial applications. Springer Dordrecht, Heidelberg, New York, London, pp 3–5
- Mikhodyuk OS, Zavarzin GA, Ivanovsky RN (2008) Transport systems for carbonate in the extremely natronophilic cyanobacterium *Euhalothece* sp. *Microbiology (Moscow)* 77:412–418
- Nishimura T, Takahashi Y, Yamaguchi O, Suzuki H, Maeda SI, Omata T (2008) Mechanism of low CO₂-induced activation of the *cmp* bicarbonate transporter operon by a LysR family protein in the cyanobacterium *Synechococcus elongatus* strain PCC 7942. *Mol Microbiol* 68:98–109
- Omata T, Price GD, Badger MR, Okamura M, Gohta S, Ogawa T (1999) Identification of an ATP-binding cassette transporter involved in bicarbonate uptake in the cyanobacterium *Synechococcus* sp. strain PCC7942. *Proc Natl Acad Sci U S A* 96:13571–13576
- Omata T, Gohta S, Takahashi Y, Harano Y, Maeda S (2001) Involvement of a CbbR homolog in low CO₂-induced activation of the bicarbonate transporter operon in cyanobacteria. *J Bacteriol* 183:1891–1898
- Orf I, Klahn S, Schwarz D, Frank M, Hess WR, Hagemann M, Kopka J (2015) Integrated analysis of engineered carbon limitation in a quadruple CO₂/HCO₃⁻ uptake mutant of *Synechocystis* sp. PCC 6803. *Plant Physiol* 169:1787–1806
- Osmond CB (1978) Crassulacean acid metabolism: a curiosity in context. *Annu Rev Plant Physiol* 29:379–414
- Peña KL, Castel SE, de Araujo C, Espie GS, Kimber MS (2010) Structural basis of the oxidative activation of the carboxysomal gamma-carbonic anhydrase, CcmM. *Proc Natl Acad Sci U S A* 107:2455–2460
- Price GD (2011) Inorganic carbon transporters of the cyanobacterial CO₂ concentrating mechanism. *Photosynth Res* 109:47–57
- Price GD, Badger MR, Woodger FJ, Long BM (2008) Advances in understanding the cyanobacterial CO₂-concentrating-mechanism (CCM): functional components, C_i transporters, diversity, genetic regulation and prospects for engineering into plants. *J Exp Bot* 59:1441–1461
- Price GD, Coleman JR, Badger MR (1992) Association of carbonic anhydrase activity with carboxysomes isolated from the cyanobacterium *Synechococcus* PCC7942. *Plant Physiol* 100:784–793
- Price GD, Woodger FJ, Badger MR, Howitt SM, Tucker L (2004) Identification of a SulP-type bicarbonate transporter in marine cyanobacteria. *Proc Natl Acad Sci U S A* 101:18228–18233
- Rae BD, Long BM, Badger MR, Price GD (2013) Functions, compositions, and evolution of the two types of carboxysomes: polyhedral microcompartments that facilitate CO₂ fixation in cyanobacteria and some proteobacteria. *Microbiol Mol Biol Rev* 77:357–379
- Raines CA (2011) Increasing photosynthetic carbon assimilation in C₃ plants to improve crop yield: current and future strategies. *Plant Physiol* 155:36–42
- Ramazanov Z, Pronina NA, Semenenko VE (1984) Oxygen-dependent induction of synthesis of the CO₂-dependent soluble form of carbonic anhydrase in *Chlorella* cells. *Sov Plant Physiol* 31:448–455
- Raven JA (1997) CO₂-concentrating mechanisms: a direct role for thylakoid lumen acidification? *Plant Cell Environ* 20:147–154
- Raven JA, Beardall J (2016) The ins and outs of CO₂. *J Exp Bot* 67:1–13
- Raven JA, Cockell CS, De La Rocha CL (2008) The evolution of inorganic carbon concentrating mechanisms in photosynthesis. *Philos Trans R Soc Lond Ser B Biol Sci* 363:2641–2650
- Reinfelder JR, Kraepiel AM, Morel FM (2000) Unicellular C₄ photosynthesis in a marine diatom. *Nature* 407:996–999
- Reinhold L, Zviman M, Kaplan A (1989) A quantitative model for inorganic carbon fluxes and photosynthesis in cyanobacteria. *Plant Physiol* 27:945–954
- Schwarz D, Nodop A, Hüge J, Purfurst S, Forchhammer K, Michel KP, Bauwe H, Kopka J, Hagemann M (2011) Metabolic and transcriptomic phenotyping of inorganic carbon acclimation in the cyanobacterium *Synechococcus elongatus* PCC 7942. *Plant Physiol* 155:1640–1655
- Schwarz D, Orf I, Kopka J, Hagemann M (2013) Recent applications of metabolomics toward cyanobacteria. *Metabolites* 3:72–100

- Scott KM, Henn-Sax M, Harmer TL, Longo DL, Frame CH, Cavanaugh CM (2007) Kinetic isotope effect and biochemical characterization of form IA RubisCO from the marine cyanobacterium *Prochlorococcus marinus* MIT9313. *Limnol Oceanogr* 52:2199–2204
- Sergeenko TV, Muradyan EA, Pronina NA, Klyachko-Gurvich GL, Mishina IM, Tsoglin LN (2000) The effect of extremely high CO₂ concentration on the growth and biochemical composition of microalgae. *Russ J Plant Physiol* 47:632–638
- Sergeev VN, Gerasimenko LM, Zavarzin GA (2002) The proterozoic history and present state of cyanobacteria. *Microbiology (Moscow)* 71:623–637
- Shibata M, Katoh H, Sonoda M, Ohkawa H, Shimoyama M, Fukuzawa H, Kaplan A, Ogawa T (2002) Genes essential to sodium-dependent bicarbonate transport in cyanobacteria. Function and phylogenetic analysis. *J Biol Chem* 277:18658–18664
- Shibata M, Ohkawa H, Kaneko T, Fukuzawa H, Tabata S, Kaplan A, Ogawa T (2001) Distinct constitutive and low-CO₂-induced CO₂ uptake systems in cyanobacteria: genes involved and their phylogenetic relationship with homologous genes in other organisms. *Proc Natl Acad Sci U S A* 98:11789–11794
- Smith KS, Ferry JG (2000) Prokaryotic carbonic anhydrases. *FEMS Microbiol Rev* 24:335–366
- So AK, Van Spall HGC, Coleman JR, Espie OS (1998) Catalytic exchange of ¹⁸O from ¹³C¹⁸O-labelled CO₂ by wild type cells and *ecaA*, *ecaB*, and *ccaA* mutants of the cyanobacteria *Synechococcus* PCC7942 and *Synechocystis* PCC6803. *Can J Bot* 76:1153–1160
- Soltes-Rak E, Mulligan ME, Coleman JR (1997) Identification and characterization of gene encoding a vertebrate-type carbonic anhydrase in cyanobacteria. *J Bacteriol* 179:769–774
- Stüeken EE, Buick R, Schauer AJ (2015) Nitrogen isotope evidence for alkaline lakes on late Archean continents. *Earth Planet Sci Lett* 411:1–10
- Sültemeyer D, Klughammer B, Badger MR, Price GD (1998) Fast induction of high affinity HCO₃⁻ transport in cyanobacteria. *Plant Physiol* 116:183–192
- Supuran CT (2008) Carbonic anhydrases: novel therapeutic applications for inhibitors and activators. *Nat Rev Drug Discov* 7:168–181
- Tabita FR, Satagopan S, Hanson TE, Kreef NE, Scott SS (2008) Distinct form I, II, III, and IV Rubisco proteins from the three kingdoms of life provide clues about Rubisco evolution and structure/function relationships. *J Exp Bot* 59:1515–1524
- Tcherkez GG, Farquhar GD, Andrews TJ (2006) Despite slow catalysis and confused substrate specificity, all ribulose biphosphate carboxylases may be nearly perfectly optimized. *Proc Natl Acad Sci U S A* 103:7246–7251
- Uehlein N, Lovisolo C, Siefritz F, Kaldenhoff R (2003) The tobacco aquaporin NtAQP1 is a membrane CO₂ pore with physiological functions. *Nature* 425:734–737
- Voznesenskaya EV, Franceschi VR, Kiirats O, Freitag H, Edwards GE (2001) Kranz anatomy is not essential for terrestrial C₄ plant photosynthesis. *Nature* 414:543–546
- Wang HL, Postier BL, Burnap RL (2004) Alterations in global patterns of gene expression in *Synechocystis* sp. PCC 6803 in response to inorganic carbon limitation and the inactivation of *ndhR*, a LysR family regulator. *J Biol Chem* 279:5739–5751
- Woodger FJ, Badger MR, Price GD (2005) Sensing of inorganic carbon limitation in *Synechococcus* PCC 7942 is correlated with the size of the internal inorganic carbon pool and involves oxygen. *Plant Physiol* 139:1959–1969
- Xu Y, Feng L, Jeffrey PD, Shi Y, Morel FM (2008a) Structure and metal exchange in the cadmium carbonic anhydrase of marine diatoms. *Nature* 452:56–61
- Xu M, Ogawa T, Pakrasi HB, Mi H (2008b) Identification and localization of the CupB protein involved in constitutive CO₂ uptake in the cyanobacterium, *Synechocystis* sp. strain PCC6803. *Plant Cell Physiol* 49:994–997
- Yeates TO, Kerfeld CA, Heinhorst S, Cannon GC, Shively JM (2008) Protein-based organelles in bacteria: carboxysomes and related microcompartments. *Nat Rev Microbiol* 6:681–691
- Zavarzin GA (2008) Microbial biosphere. In: Dobretsov NL, Kolchanov NA, Rosanov AY, Zavarzin GA (eds) *Biosphere origin and evolution*. Springer, New York, pp 25–42
- Zimmerman SA, Tomb JF, Ferry JG (2010) Characterization of CamH from *Methanosarcina thermophila*, founding member of a subclass of the γ -class of carbonic anhydrases. *J Bacteriol* 192:1353–1360

Biosynthesis of Cyanobacterial Light-Harvesting Pigments and Their Assembly into Phycobiliproteins

Benjamin Ledermann, Marco Aras, and Nicole Frankenberg-Dinkel

Abstract Cyanobacteria are a group of bacteria, which are able to perform oxygenic photosynthesis (rely on oxygenic photosynthesis as a main energy source) to convert sun light into chemical energy. In addition to the photosystems, cyanobacteria employ phycobilisomes to enhance their light-harvesting abilities. Phycobilisomes consist of phycobiliproteins (mainly phycocyanin and phycoerythrin) with covalently attached open-chain tetrapyrroles (phycobilins) as light-harvesting pigments. These phycobilins are derived from heme. The first step of bilin synthesis is the ring opening reaction of heme into biliverdin IX α mediated by heme oxygenases. A set of different ferredoxin-dependent bilin reductases catalyse the reactions from biliverdin IX α to several phycobilins. These pigments are subsequently attached to conserved cysteine residues in the phycobiliproteins. In order to ensure the correct attachment of the phycobilins and the chromophore composition of the phycobiliproteins, the binding is mediated by phycobiliprotein-lyases. Recent studies showed that this machinery is not only present in cyanobacteria but also in phages which infect cyanobacteria. This chapter describes the biosynthesis and assembly of all components of functional phycobilisomes and their role in energy conversion as well as adaptations to changing environmental conditions.

Keywords Cyanophage • Ferredoxin-dependent bilin reductase • Heme oxygenase • Light-harvesting pigment • Open chain tetrapyrrole • Phycobilprotein • Phycobilisome • Phycobiliprotein lyase • Phycocyanobilin • Phycoerythrobilin

Abbreviations

AMG	Auxiliary metabolic gene
APC	Allophycocyanin
BR	Bilirubin
BV	Biliverdin

B. Ledermann • M. Aras • N. Frankenberg-Dinkel (✉)
Technical University Kaiserslautern, Department of Biology-Microbiology,
Erwin-Schrodinger-Str. 56, 67663 Kaiserslautern, Germany
e-mail: nfranken@bio.uni-kl.de

Chl	Chlorophyll
Fd	Ferredoxin
FDBR	Ferredoxin-dependent bilin reductase
HL	High light
HO	Heme oxygenase
LL	Low light
PBP	Phycobiliprotein
PBS	Phycobilisome
PC	Phycocyanin
PCB	Phycocyanobilin
PE	Phycoerythrin
PEB	Phycoerythrobilin
PEC	Phycoerythrocyanin
PS	Photosystem
PUB	Phycourobilin
PVB	Phycoviolobilin
PΦB	Phytochromobilin

Introduction

Photosynthesis is without a doubt one of the most important biological processes on earth. In a set of redox reactions, it achieves the conversion of light energy into chemical energy in the form of carbohydrates. In most photosynthetic organisms, light harvesting is performed by chlorophyll (Chl)-containing antenna complexes. As Chls absorb mostly blue and red light, they leave a vast amount of light energy unused—the “green gap”. In order to overcome the limitation of the chlorophyll-related light harvesting, organisms like cyanobacteria, red algae and cryptophytes enhance their light-harvesting machinery with large complexes called phycobilisomes (PBSs) (Glazer 1977; Tandeau de Marsac 2003). PBSs are made up out of phycobiliproteins (PBPs) which are apoproteins with covalently attached open-chain tetrapyrroles (phycobilins) for light harvesting. Depending on the environmental conditions, many cyanobacteria can adapt their PBP composition, a process that is called complementary chromatic acclimation, giving them an advantage in ecosystems with only poor and changing light penetration like the deep sea (Kehoe and Grossman 1994; Gutu and Kehoe 2012).

Phycobiliproteins

Structure and Arrangement

The photosynthetic apparatus of cyanobacteria is located on folded internal membranes, the thylakoid membrane. The machinery consists of two photosystems (PSs) with Chls as the primary light-harvesting pigments and additional pigments located in

specialised light-harvesting complexes—the phycobilisomes (PBSs). The PBSs consist of a species-specific composition of linker proteins and PBPs with light-harvesting phycobilins. The PBSs form rod-shaped antennae which are located at the outside of the thylakoid membrane and are directly connected to the PS (Glazer 1977).

PBPs in cyanobacteria, red algae and cryptophytes are made up out of heterodimers, which consist of α - and β -subunits. The subunits are homologous to each other as they are derived from an ancient gene duplication event. PBPs fold into a modified globin-like structure with additional helices (Schirmer et al. 1986). The $\alpha\beta$ -heterodimers build ring-shaped trimers (heterohexamers) or hexamers (heterododecamers) which are the building blocks for the phycobilisome rods (Grossman et al. 1993) (Fig. 1).

The rods of the PBS are composed of these trimer or hexamer discs which are associated to one another through specific linker proteins (Glazer 1985). The core protein of the PBS, allophycocyanin (APC), is assembled out of six $(\alpha\beta)_3$ -trimers. The peripheral PBPs are either composed of $(\alpha\beta)_3$ -trimers or $(\alpha\beta)_6$ -hexamers (Glazer 1977; Grossman et al. 1993).

In cyanobacteria four major types of PBPs can be found: APC, PC, phycoerythrocyanin (PEC) and phycoerythrins (PE) (Table 1). APC forms the core of the PBS with six to eight rods of PC radiating out of the core. Certain cyanobacteria additionally contain PE or PEC at the distal positions of the rod. PBPs have originally been designated with a prefix depending on their origin: C for *Cyanophyceae*, R for

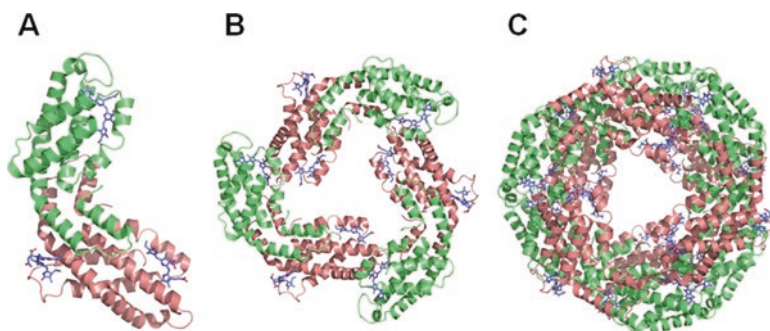


Fig. 1 Structure of phycocyanin (PC) in different oligomerisation states. α -Subunits are shown in green, β -subunits in salmon and phycocyanobilin (PCB) cofactors in blue. (a) PC $(\alpha\beta)$ -monomer from *Synechocystis* sp. PCC 6803 (PDB 4F0T). (b) PC $(\alpha\beta)_3$ -trimer from *Synechocystis* sp. PCC 6803 (PDB 4F0T). (c) PC $(\alpha\beta)_6$ -hexamer from *Thermosynechococcus elongatus* (PDB 4ZIZ)

Table 1 Absorbance ranges and colours of the different PBPs in cyanobacteria

Phycobiliprotein	Absorbance range (nm)	Colour
Phycoerythrin (PE)	540–570	Orange-red
Phycoerythrocyanin (PEC)	570–590	Purple
Phycocyanin (PC)	610–620	Blue
Allophycocyanin (APC)	650–655	Green-blue

Rhodophyceae and B for *Bangiales* (Magne 1989). Additional analyses showed that this classification is not completely valid. Therefore, the prefix is now also used to describe the absorption characteristics of the PBP (Tandeau de Marsac 2003). A table of the absorbance ranges and the colours of the different PBPs is given in Table 1.

PBPs obtain their absorbing characteristics by their covalently bound phycobilin chromophores. These linear tetrapyrrole molecules are post-translationally attached to the apo-PBP to specific conserved cysteine residues forming thioether bonds. One α - or β -subunit is typically able to bind one to three bilins (MacColl 1998) (Table 2). Typically, the bilin is attached via its A-ring or in certain cases doubly bound via the A- and D-ring (Fig. 2). While the position homologue to Cys84 is present in both α - and β -subunits and always occupied with a bilin, the other positions are more variable depending on the type of PBP (see also Table 2). Position β -Cys50/61 is specific to PE as these two conserved Cys residues are involved in the double linkage of one bilin.

Four different bilins have been identified in cyanobacterial PBPs: the blue phycocyanobilin (PCB; $\lambda_{\max} = 620$ nm), the pink phycoerythrobilin (PEB; $\lambda_{\max} = 540$ nm), the purple phycoviolobilin (PVB; $\lambda_{\max} = 590$ nm) and the yellow phycourobilin (PUB; $\lambda_{\max} = 500$ nm). Of these bilins only PEB and PUB are suitable for the double linkage (Fig. 2).

The binding of the bilin chromophores not only confers the PBPs their absorbing characteristics, it furthermore contributes to the stability of the holo-protein and the chromophores themselves (Anderson and Toole 1998; Scheer and Zhao 2008; Shen et al. 2006). Moreover, the covalent binding to the apoprotein changes the conformation of the bilins. In solution they are arranged in a flexible porphyrin-like helical structure, whereas protein-bound bilins adopt a rigid linear conformation, thereby leading to a change in their absorption and fluorescence emission properties (Lehner et al. 1981; Falk and Höllbacher 1978; Kufer and Scheer 1979). Bilins in solution are only poorly suited as light-harvesting pigments. Their excited state is only short-lived as they convert most of the absorbed light energy into heat leading to a weak fluorescence emission (Glazer 1989). In contrast to this, the anchorage of the bilins in the holo-proteins prevents the radiation-free energy transfer, leading to a high

Table 2 Chromophore binding sites of PBPs in cyanobacteria

Protein	α -Cys73 ^a /75	α -Cys82 ^b /84 ^c	α -Cys143	β -Cys50/61	β -Cys82 ^b /84 ^c	β -Cys155/163 ^a
APC		PCB			PCB	
PC		PCB/PEB			PCB	PCB/PEB
		(PUB/PVB)				(PUB/PVB)
PEC		PVB			PCB	PCB
PE-I		PEB/PUB	PEB/PUB	PEB/PUB	PEB	PEB
PE-II	PEB/PUB	PEB/PUB	PEB/PUB	PEB/PUB	PEB	PEB
PE-III	3:1 PUB/PEB ^d					

^aPE-III

^bAPC

^cPC, PEC, PE-I, PE-II

^dDistribution on subunits not known

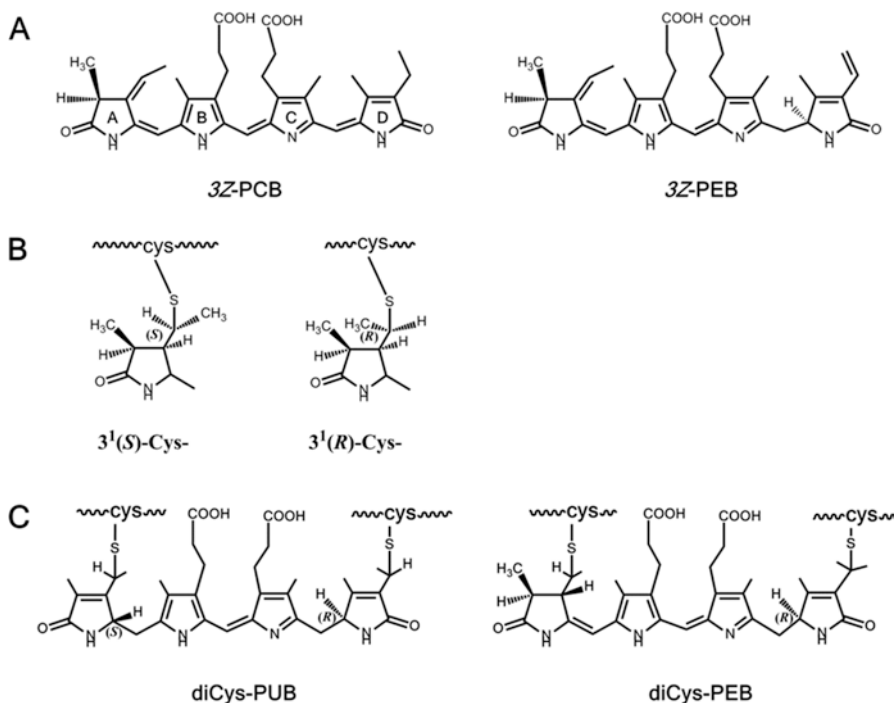


Fig. 2 Chemical structure of common phycobilins found in cyanobacteria. (a) The free phycobilins 3Z-phycocyanobilin (PCB) and 3Z-phycoerythrobilin (PEB). When attached to a Cys residue of a PBP, the C3 C-atom becomes a new stereocenter which can either have the (S) or (R) configuration (b). (c) Only phycoerythrin (PUB) and PEB can be attached by a double linkage in phycoerythrins at position β -Cys50/61 (see text for details)

fluorescence (Fischer et al. 1990). The composition of the chromophores can be altered in changing environmental conditions, a process that is called complementary chromatic acclimation (Kehoe and Grossman 1994). Table 2 gives an overview of the chromophore binding sites and the bilin content of these PBPs in cyanobacteria.

Function

The main function of PBPs/PBS is their role in light harvesting. Phycobilisomes in most cyanobacteria are located on the outside of the thylakoid membrane where they are attached to the reaction centre of PS 2 (Fig. 3). The core of the PBS is typically formed by two to five APC cylinders and is surrounded with up to eight PC rods (Ducret et al. 1996; Sidler and Bryant 1994). PC can be found in all cyanobacterial PBS, but PE and PEC do not occur in every species (Kahn and Schaefer 1997).

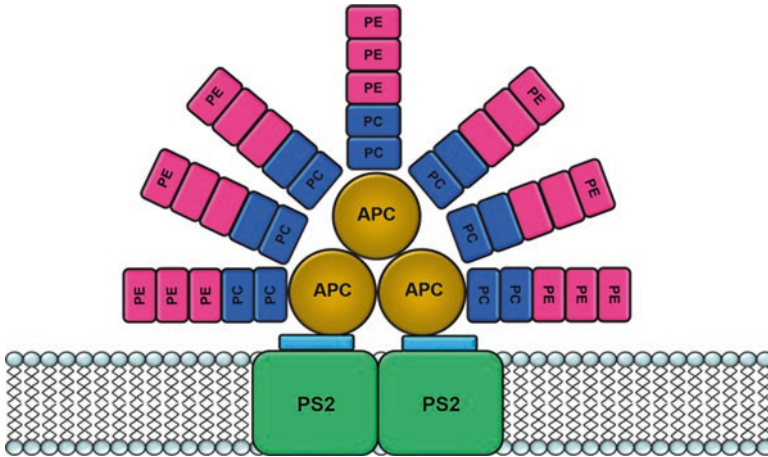


Fig. 3 Schematic representation of a phycobilisome of *Synechococcus* sp. The phycobilisome (PBS) is located at the outside of the thylakoid membrane attached to a PS 2 dimer embedded in the thylakoid membrane. The core of the PBS is formed by allophycocyanin (APC). The rods are formed by phycocyanin (PC) and phycocerythrin (PE). Adapted from Wiethaus et al. (2010a)

Synechococcus strains often contain PC as well as PE (Six et al. 2007), and in many open-ocean strains, PE-I and PE-II are the most abundant PBPs (Wilbanks and Glazer 1993). PE-I and PE-II both contain PEB and a varying amount of PUB as light-harvesting chromophores, whereas the PUB/PEB ratio is higher in PE-II compared to PE-I (Ong and Glazer 1991). The high amount of PUB, which absorbs at relatively short wavelengths, allows the organism to harvest light in deep waters, where mostly blue and green light occurs (Wood 1985).

The subunits of the PBS are held together by linker proteins. They form the backbone of the PBS and can alter the absorption characteristics of the PBPs but are not directly contributing to the light harvesting (Glazer 1985). Exceptions are the core-membrane linker ApcE, a multidomain linker with a chromophore binding site that binds PCB in an autocatalytic manner (Zhao et al. 2005) and the γ -subunit of PEs found in marine *Synechococcus* sp. and red algae. These γ -subunits are also linker proteins that bind chromophores like the γ -subunit of R-PE from the red alga *Gastroclonium coulteri* that binds a single molecule of PUB (Nagy et al. 1985). The molecular weight of a PBS depends on the organism and ranges between 7 and 15×10^6 Da, and the number of bound bilin chromophores varies between 300 and 800 molecules (Glazer 1985). The arrangement of the PBPs acts like an energy funnel allowing energy transfer from PBPs with bilins absorbing at shorter wavelengths (e.g. PEB) to PBPs with bilins that absorb at longer wavelengths (e.g. PCB). The terminal energy acceptor is Chl *a* located at the reaction centres of the PS (Fig. 4).

Although the light-harvesting function of the PBS is unquestioned, it may also serve the cell as a supply of nitrogen and starvation conditions. Under nitrogen depletion, cyanobacteria massively degrade their PBS (Collier et al. 1994).

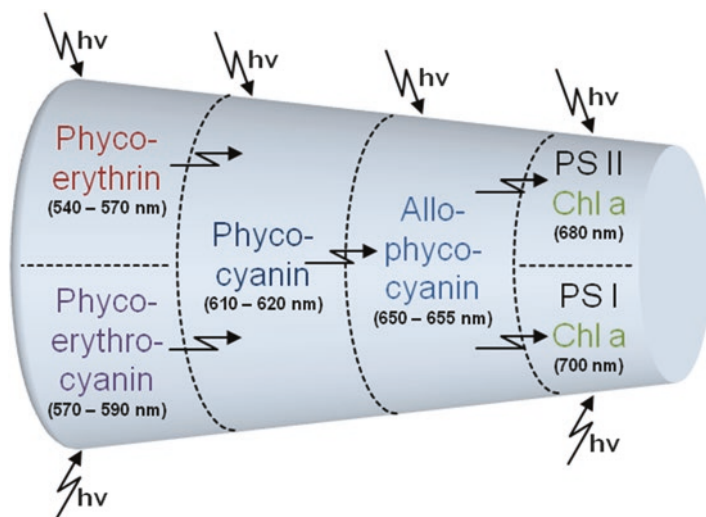


Fig. 4 Scheme of the energy transfer in the PBS. The arrangement of the PBPs allows an energy flow from PBPs absorbing at shorter wavelengths to PBPs absorbing at longer wavelengths. The final energy acceptor is Chl *a* in the reaction centres of the PSs

The PBSs described here are found in most cyanobacteria with the exception of the members of the *Prochlorophyta*. This group was discovered in the 1970s and comprises the genera *Prochloron*, *Prochlorothrix* and *Prochlorococcus* (Chisholm et al. 1992; Lewin 1976; Pinevich et al. 1999). The *Prochlorophyta* are characterised by the presence of Chl *b* and the lack of PBSs. One member of the prochlorophytes, *Prochlorococcus marinus* with a diameter between 0.5 and 0.8 μm , is the smallest organism known to perform oxygenic photosynthesis (Chisholm et al. 1988). Furthermore, *Prochlorococcus* sp. possesses highly reduced genomes with sizes ranging between 1.6 and 2.4 Mbp (Dufresne et al. 2003). *Prochlorococcus* uses no PBS for light harvesting but a divinyl-chlorophyll (DV-Chl) *a*- and *b*-containing prochlorophyte Chl-binding (Pcb) antenna.

The special DV-Chl *a*₂ and *b*₂ found in the Pcb antenna carry an additional vinyl group at the C8 atom in the tetrapyrrole macrocycle (Goerick and Repeta 1992). *Prochlorococcus* sp. can be basically divided into two different groups: high-light (HL)-adapted strains and low-light (LL)-adapted strains. The HL strains are typically found in shallow waters, whereas the LL strains can be found in deeper regions. LL-adapted strains possess a PE-III PBP which is thought to be a relic from its ancestor PBS (Hess et al. 1992). The LL PE-III is associated to the thylakoid membrane and is made of ($\alpha\beta$)-heterodimers like the PBPs of other cyanobacteria. Interestingly, PE-III has a relative high PUB content (PUB/PEB = 3:1; see Table 2) compared to other PEs (Hess et al. 1996). This is likely due to their adaptation to deeper waters, as PUB absorbs at shorter wavelengths compared to PEB. In comparison the PE of HL strains is further reduced. It consists only of a single β -subunit with PEB as the only chromophore (Steglich et al. 2005; Wiethaus

et al. 2010a). As these PEs in both ecotypes only contribute to a very limited amount to the light harvesting, their function remains unclear (Steglich et al. 2003; Steglich et al. 2005).

The Biosynthesis of Light-Harvesting Pigments in Cyanobacteria

The various colours of cyanobacteria and red algae are mainly derived from the composition of the attached phycobilins to the PBPs. Phycobilins belong to the class of open-chain tetrapyrroles and are furthermore also found in plants where they serve as the light-sensing chromophore in the phytochrome class of photoreceptors (Lagarias and Rapoport 1980; Lemberg 1928). Open-chain tetrapyrroles are synthesised in subsequent reduction steps from the cyclic tetrapyrrole heme as the precursor. Heme is first ring opened to build the first linear or open-chain tetrapyrrolic product, biliverdin IX α (BV). BV serves as a precursor molecule for phycobilin formation and is used as a substrate for an enzyme family called ferredoxin-dependent bilin reductases (FDBR). These enzymes catalyse specific reduction steps of BV to produce a various number of colourful pigments, including the major phycobilins in cyanobacteria, phycocyanobilin (PCB) and phycoerythrobilin (PEB), respectively. Finally, these are then attached to the apo-phycobiliproteins by single or double linkages via thioether bonds.

Heme Oxygenases and Biliverdin Formation

All functional representatives of the open-chain tetrapyrroles in photosynthetic organisms are synthesised from the cyclic tetrapyrrole heme (Frankenberg et al. 2001). Heme is derived from protoporphyrin IX which also serves as a key intermediate of the chlorophyll synthesis pathway (Chew and Bryant 2007).

With its central iron atom, heme is the substrate of a ubiquitous enzyme family called heme oxygenases (HOs). These enzymes catalyse the ring opening of heme to BV IX α by cleaving the α -*meso*-carbon bridge (Montellano 2000; Wilks 2002). HOs are found in a variety of organisms serving several functions (heme catabolism, iron acquisition, oxidative stress response and chromophore biosynthesis) (Abraham et al. 1996; Cornejo et al. 1998; Richaud and Zabulon 1997; Schmitt 1997; Frankenberg-Dinkel 2004). However, in photosynthetic organisms, the major function is to synthesise the phycobilin precursor BV. While the HOs of these organisms are targeting the α -*meso*-carbon bridge, other examples demonstrating the cleavage of heme at different positions exist. This includes HOs from the opportunistic pathogen *Pseudomonas aeruginosa* and other *Pseudomonas* species which produce BV IX β and IX δ through cleavage of the respective *meso*-carbon bridges

(Gisk et al. 2012; Ratliff et al. 2001). These HOs are shown to be involved in iron acquisition from heme (Ratliff et al. 2001). BV IX δ on the other hand has been found in insects and serves their colouration (Paiva-Silva et al. 2006).

The first evidence of heme being a precursor of phycobilin biosynthesis came from experiments employing *N*-methyl-mesoporphyrin IX which specifically blocks iron insertion into protoporphyrin IX (catalysed by ferrochelatase). When the red alga *Cyanidium caldarium* (today *Galdieria sulphuraria*) was treated with this potent inhibitor, the ability to form phycocyanin was lost, whereas the chlorophyll levels remained normal (Beale and Chen 1983). A couple of years later, the first gene encoding a HO from the cyanobacterium *Synechocystis* sp. PCC6803 was cloned (Cornejo et al. 1998). Interestingly, the authors also cloned a second *ho* gene termed *ho2*. Back then, the authors were unable to obtain soluble recombinant protein to show if this gene encodes for a second HO. It took until 2005 to finally prove that *ho2* is indeed encoding a true HO. With increasing amounts of available genome sequences of cyanobacteria, it became clear that *Synechocystis* sp. PCC6803 is not an exception and that many cyanobacterial genomes encode two HOs (Yilmaz et al. 2010). These HOs share a 51% sequence identity but seem to be expressed under different environmental conditions. *ho1* is constitutively expressed under normal conditions where the expression of *ho2* is induced by low oxygen tension and therefore required for microaerobic growth. Both enzymes show full functionality by producing BV IX α (Zhang et al. 2005; Yilmaz et al. 2010). Interestingly, HO2 is monomeric in the apo-form (without bound substrate) but forms dimers upon heme binding (Fig. 5). The function of the dimerisation is still unclear, but a role in the selection of the reducing partner has been suggested (Migita et al. 2003; Sugishima et al. 2005).

Until now, several HO crystal structures from bacteria, plants and mammals have been solved, and despite a low sequence identity, their overall fold is similar. They consist of eight α -helices with the substrate heme being sandwiched between two helices with the propionate side chains facing the solvent (Fig. 5). The heme iron is coordinated via a proximal histidine residue, and the distal side usually binds oxygen, but several other diatomic gas ligands including the CO and NO will bind as well (Sugishima et al. 2005, 2004). With the exception of *Synechocystis* sp. HO2, all solved structures are monomeric, while HO2 forms dimers (see above).

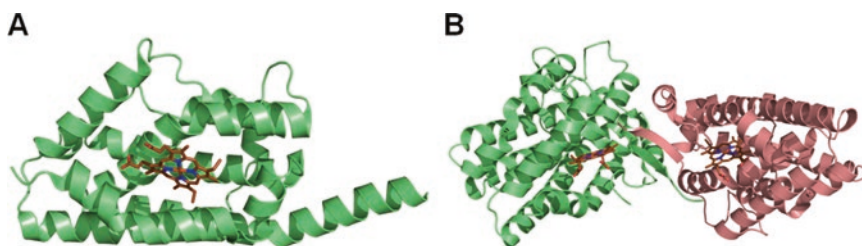


Fig. 5 Crystal structures of the two heme oxygenases from *Synechocystis* sp. PCC 6803. (a) HO1 (green) with bound heme shown as brown sticks (PDB 1WE1). (b) Dimer of HO2 (green/salmon) with bound heme shown as brown sticks (PDB 1WOW)

Mechanism

The oxygenic cleavage of heme by HOs is quite similar in all organisms, and three oxygen molecules and seven electrons are required for the reaction (Montellano 2000). The reaction mechanism of HOs is well understood which is due to the specific absorption properties of most reaction intermediates. Therefore, all reduction steps can be monitored via UV/Vis-spectroscopy. The reaction begins with the binding of the substrate heme and the formation of a ferric (Fe^{III})-heme-HO complex. In bacteria and plants, the subsequently transferred electrons are derived from [2Fe-2S]-ferredoxins, whereas mammalian HOs seem to prefer NADPH-cytochrome P450 reductase as an electron donor (Montellano 2000). However, also ascorbate has been shown to support the reaction (Migita et al. 2003). Interestingly, *Synechocystis* sp. HO1 can also use cytochrome P450 reductase for the HO reaction, but the reaction is arrested at the oxy-complex, indicating that cytochrome P450 reductase might not be the right reducing partner for this bacterial HO (Migita et al. 2003).

Together with molecular oxygen, the bound heme (oxy-complex) is converted to the first intermediate α -meso-hydroxy-heme (Fig. 6). In this activated form, the heme is prone to degradation. The concurrent binding of another molecule of oxygen along with electrons leads to the formation of verdoheme, the last intermediate of the HO reaction. The final, least understood step of the reaction requires again oxygen and electrons and involves the conversion of verdoheme to BV. While in many HOs including that from rat, the final product appears to be ferric (Fe^{III})-BV, the ascorbate-supported SynHO1 reaction releases free BV (Migita et al. 2003). During this last step, the meso-carbon bridge is released in the form of CO (Wilks 2002).

Ferredoxin-Dependent Bilin Reductases and Phycobilin Biosynthesis

The first chemical structure of a phycobilin was described in the 1960s by isolating PCB from C-PC of the filamentous cyanobacterium *Plectonema boryanum* using hot methanol treatment (Chapman et al. 1967). The tetrapyrrolic nature of PCB was confirmed by ^1H -NMR spectroscopy (Cole et al. 1967). Shortly thereafter, extraction of the pigment of R-PC also revealed the structure of PEB (see also Fig. 2a). Together, PCB and PEB are the most abundant phycobilins in nature.

It then took up to the mid-1980s until the group of Samuel Beale discovered the first enzymatic activities in cell-free extracts of the red alga *Cyanidium caldarium* that led to the conversion of BV IX α to PCB (Beale and Cornejo 1984b). In addition, HO activity was observed, and therefore a pathway association of these enzyme systems in phycobilin biosynthesis was postulated (Beale and Cornejo 1984a, b). All activities were shown to rely on ferredoxin-dependent electron

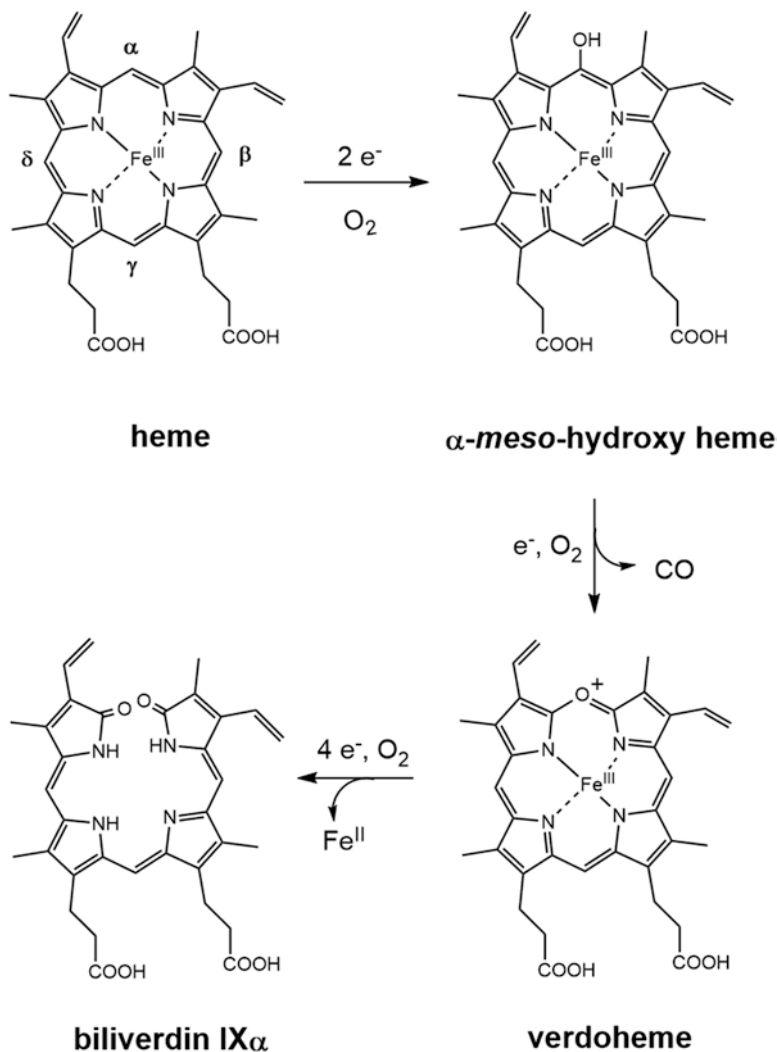


Fig. 6 The heme oxygenase reaction. The regiospecific opening of the α -meso-carbon bridge of heme is catalysed by heme oxygenases. For this reaction, a total of seven electrons and three molecules of oxygen are required

transfer (Beale and Cornejo 1991; Cornejo et al. 1998). Almost another decade passed before the genes encoding the involved enzymes were cloned and characterised (Cornejo et al. 1998; Frankenberg et al. 2001). The identification of *ho* genes was rather easy after the *Synechocystis* sp. genome was published as their translated products had high homology to mammalian HOs. The search for the bilin reductase genes turned out to be more complicated. Although a search employing mammalian biliverdin reductase (BVR) identified an enzyme with high

homology, investigation of the recombinant protein did not reveal the expected activity converting BV to PCB. Interestingly, the identified cyanobacterial protein converted BV to bilirubin, an activity not expected to be present in cyanobacteria (see section “Biosynthesis of Bilirubin”) (Schluchter and Glazer 1997). The identification of bilin reductase genes in the genomes of cyanobacteria was only possible after the cloning of the *Arabidopsis thaliana* gene encoding phytychromobilin synthase (*HY2*), the enzyme converting BV to the plant phytyochrome chromophore phytychromobilin (PΦB) (Kohchi et al. 2001). This functional genomic approach revealed the sequences of three enzymes involved in the conversion of BV to PCB and PEB, respectively (Frankenberg et al. 2001). As all identified bilin reductases required ferredoxin as an electron donor, the whole new family of enzymes was designated ferredoxin-dependent bilin reductases (FDBR) (Frankenberg et al. 2001). Most of the identified FDBRs employ BV IX α as their substrate but display specific reduction properties in order to produce a specific phycobilin (Fig. 7). After this initial search, additional enzymes with novel activities have also been discovered in cyanophages and lower photosynthetic eukaryotes (Chen et al. 2012; Dammeyer et al. 2008a). As of 2016, the family comprises seven members (Fig. 7).

Biosynthesis of Phycocyanobilin

PCB is the most common phycobilin chromophore among cyanobacteria. It serves as the major light-harvesting pigment in cyanobacterial PC and in the PBS core protein APC (Chapman et al. 1967). The second function of PCB is light sensing for which it is incorporated into cyanobacteriochromes, phytyochrome-like photoreceptors in cyanobacteria involved in light sensing and signal transduction (Ikeuchi and Ishizuka 2008).

In cyanobacteria, the gene *pcyA* encodes for phycocyanobilin: ferredoxin oxidoreductase which catalyses the four-electron reduction of BV IX α to PCB via the intermediate 18¹,18²-dihydrobiliverdin (18¹,18²-DHBV, a.k.a. 18EtBV) (Fig. 8) (Frankenberg et al. 2001; Frankenberg and Lagarias 2003).

For a long time, PcyA was thought to be the only FDBR catalysing a four-electron reduction. However, with two new phage-encoded FDBRs (Dammeyer et al. 2008a; Ledermann et al. 2016) and PUBS (Chen et al. 2012), a total of four four-electron reducing FDBRs are known to date.

Interestingly, not only cyanobacteria but also cyanophages, viruses that infect cyanobacteria, carry a *pcyA* gene (Dammeyer et al. 2008a). In addition, PcyA homologues have also been identified in organisms that lack PBS and phytychromes. Among them are the green alga *Chlamydomonas reinhardtii* and the cyanobacterium *Prochlorococcus marinus*. While in *C. reinhardtii*, PcyA seems to be involved in iron acquisition, oxidative stress response and retrograde signalling, the role in *P. marinus* remains elusive (Duanmu et al. 2013; Dammeyer et al. 2007).

PcyA is the best known member of the FDBR family, and several crystal structures from the cyanobacteria *Synechocystis* sp. PCC6803 and *Nostoc* sp. PCC7120 have been solved (Hagiwara et al. 2006a, b; Tu et al. 2007). PcyA is a monomeric

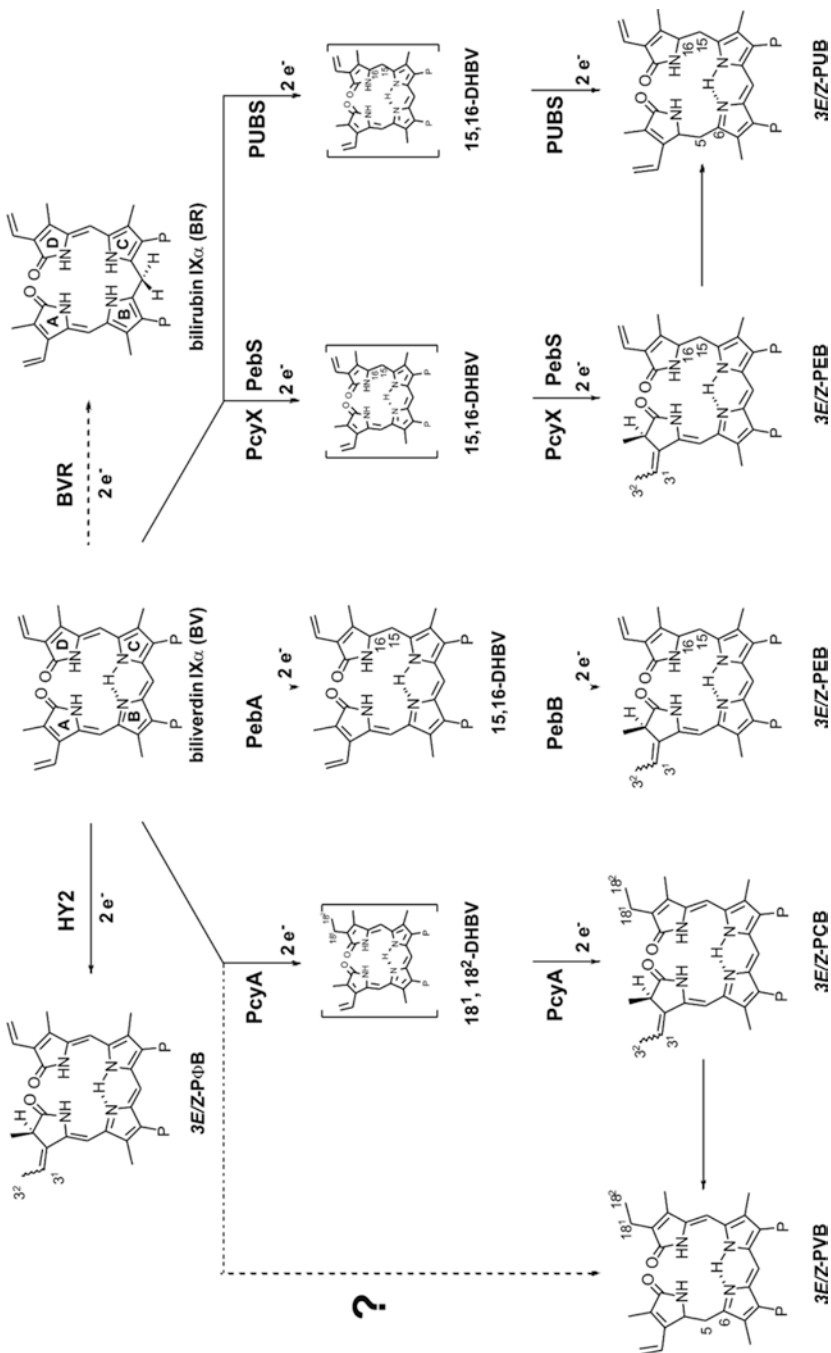


Fig. 7 The family of ferredoxin-dependent bilin reductases. Overview of the catalysed reactions from biliverdin in photosynthetic organisms. Note HY2 is thus far only found in plants and lower eukaryotes. BVR is also reducing BV but with a different mechanism and with the help of reducing equivalents from NAD(P)H (shown only for completeness). *BV*, biliverdin; *BVR*, biliverdin reductase; *DHBV*, dihydrobiliverdin; *PCB*, phycocyanobilin; *PEB*, phycocerythrobilin; *PΦB*, phytochromobilin; *PUB*, phycourobilin; *PUBS*, PUB synthase; *PVB*, phycoviobilin

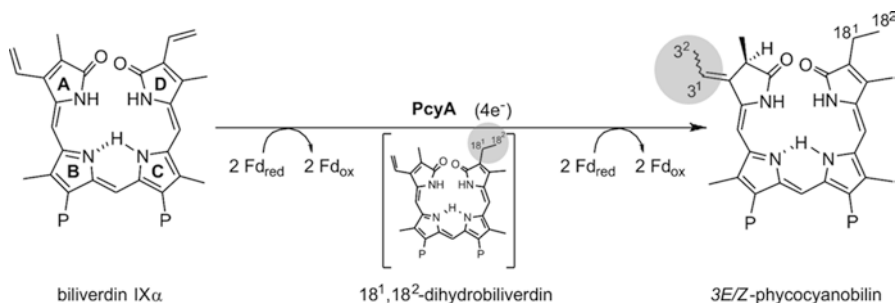


Fig. 8 The reaction catalysed by phycoyanobilin: ferredoxin oxidoreductase (PcyA). BV IX α is converted in a single four-electron reduction to 3Z-PCB. Although the intermediate 18¹,18²-DHBV can be detected, it is most likely not released from the active site of the enzyme but rather directly converted to the final product

enzyme with an α -/ β -/ α -sandwich fold placing the substrate-binding pocket between the β -sheet and the C-terminal α -helix (Fig. 11). The cloning and characterisation of PcyA furthermore enabled for the first time the expression of holo-phytochromes and holo-phycobiliproteins in a heterologous host (Gambetta and Lagarias 2001; Tooley et al. 2001).

Biosynthesis of Phycoerythrobilin

PEB is the second most abundant chromophore in cyanobacterial PBS and found in species that are adapted to light environments that are enriched in blue-green light (Ting et al. 2002). Although PEB is an isomer of PCB and its synthesis from BV requires four electron/proton transfers, the biosynthesis requires not one but two FDBRs. 15,16-DHBV:ferredoxin oxidoreductase (PebA) and PEB:ferredoxin oxidoreductase (PebB) act in sequence to convert BV into PEB. Similar sequences have recently also been described in the cryptophyte *Guillardia theta* (Overkamp et al. 2014).

PebA uses BV as its substrate and converts it to 15,16-DHVB via a two-electron reduction step. As depicted earlier, PebA receives the electrons from ferredoxin, and the reduction occurs at the C15 methine bridge of BV (Fig. 9). However, it is not clear yet which residues of PebA direct the protons/electrons to the 15,16-double bond. The resulting 15,16-DHBV is very unstable and likely directly transferred to the next enzyme in the pathway, PebB. Although the process of bilin transfer is not yet completely elucidated, there are several hints for protein-protein interaction, and therefore metabolic channelling has been postulated (Dammeyer and Frankenberg-Dinkel 2006).

PebB is thus far the only FDBR that does not use BV as its substrate (Frankenberg et al. 2001). The enzyme shows a very narrow substrate specificity towards 15,16-DHVB and is unable to metabolise other bilins (Dammeyer and Frankenberg-Dinkel 2006).

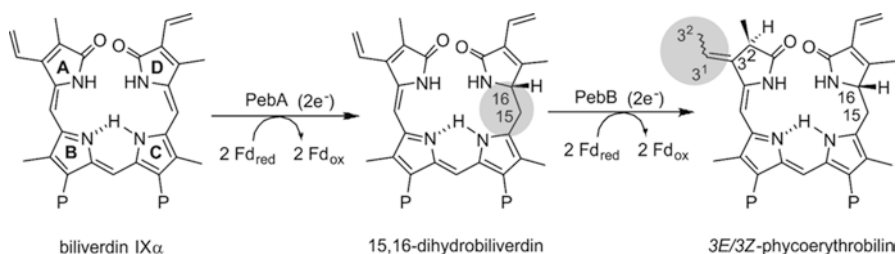


Fig. 9 Biosynthesis of phycoerythrobilin in cyanobacteria. The two FDBRs, 15,16-DHBV:ferredoxin oxidoreductase (PebA) and PEB:ferredoxin oxidoreductase (PebB), convert BV in two subsequent two-electron reductions via the intermediate 15,16-DHBV to the final product 3Z-PEB. In total, the reaction requires four electrons from ferredoxin

After product channelling, PebB converts 15,16-DHBV into 3Z-PEB via a two-electron reduction of the A-ring 2,3,3,3¹,3²-diene system (Busch et al. 2011a; Dammeyer and Frankenberg-Dinkel 2006). The newly produced chromophore is thought to be immediately picked up by phycobiliprotein lyases and transferred to PE. In general, the cyanobacterial genes for PEB synthesis are encoded on multi-gene operons, often along with genes coding for HOs and phycobiliprotein subunits which suggest their functional connection (Frankenberg et al. 2001; Dammeyer et al. 2007).

In the early 2000s, a new FDBR phycoerythrobilin synthase (PebS) has been discovered. PebS is encoded in the genome of the cyanophage P-SSM2, a virus infecting the marine cyanobacteria *Prochlorococcus* sp., and displays the highest sequence homology to cyanobacterial PebA sequences (Dammeyer et al. 2008a). Interestingly, PebS showed highly efficient BV turnover as it converts it in a four-electron reduction directly to PEB. This is in contrast to the two-enzyme system of cyanobacteria although both reactions proceed via the same intermediate 15,16-DHBV (Fig. 10) (Dammeyer et al. 2008b). Thus far, *pebS* sequences were only detected on DNA scaffolds originating from phage and were shown to be induced during cyanobacterial infection. Although this observation points to a functional role during infection, it is not clear to what extent the synthesis of a light-harvesting pigment can increase the fitness of the phage (Dammeyer et al. 2008a).

The latest addition to the FDBR family is a sequence that has been discovered in publically available metagenomics datasets. Since this novel enzyme showed the highest homology to cyanobacterial PcyA, it was named PcyX. The *pcyX* gene is encoded in a mini-cassette along with a heme oxygenase (*hemO*) gene (Ledermann et al. 2016). Interestingly, the recombinant enzyme directly converted BV in a four-electron reduction to 3Z-PEB, just like the cyanophage-encoded PebS. In contrast to PebS, the second reduction from 15,16-DHBV to PEB appears to be the rate-limiting step. Since the amino acid sequence identity with PebS is rather low (only 9%) and catalytically important amino acid residues of PebS are missing (e.g. Asp206), it was postulated that the PcyX reaction rather proceeds via a PcyA-like mechanism (see section “FDBR Structures and Mechanism”).

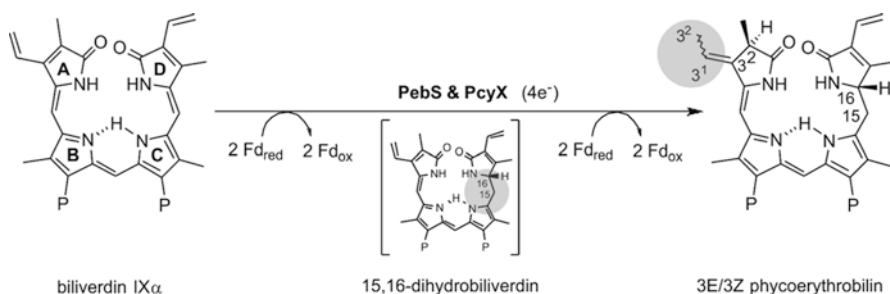


Fig. 10 Reaction catalysed by the two phage-encoded FDBRs PebS and PcyX. Both reactions are similar but seem to proceed via different catalytic mechanisms. In addition, the second reduction of the PcyX reaction is slower than that of cyanophage-encoded PebS (see text for details)

Extensive phylogenetic analysis revealed that the *pcyX* sequence does not originate from cyanophages but rather bacteriophages infecting α -proteobacteria (Ledermann et al. 2016). This hypothesis led to the speculation of the role of PEB during infection of an alphaproteobacterium. To our current knowledge, all photosynthetic members of this group perform anoxygenic photosynthesis and do not employ phycobilins for light harvesting. Therefore, their role during infection remains enigmatic.

FDBR Structures and Mechanism

The comparison of the thus far structurally solved FDBRs revealed an overall high structural similarity despite rather low sequence identity (Busch et al. 2011a; Dammeyer et al. 2008b; Hagiwara et al. 2006a; Hagiwara et al. 2006b; Tu et al. 2007) (Fig. 11). All FDBRs are composed of a seven-stranded antiparallel β -sheet which is flanked by six α -helices (α -/ β -/ α -sandwich fold).

The crystal structures in combination with site-directed mutagenesis and UV/Vis-spectroscopy revealed numerous insights into the reaction mechanism of this family of enzymes (Busch et al. 2011a, b; Hagiwara et al. 2006a, b; Tu et al. 2008, 2004, 2007; Unno et al. 2015). Due to the lack of metal and organic cofactors and the nature of the electron donor ferredoxin which only transfers one electron at a time, it was hypothesised that the reaction proceeds via substrate radical intermediates (Frankenberg and Lagarias 2003). Soon thereafter, the first substrate radicals were detected using electron paramagnetic resonance (EPR) spectroscopy (Tu et al. 2004). Substrate radicals have been confirmed by almost all members of the family (Busch et al. 2011a, b; Tu et al. 2008, 2004).

PcyA is thus far the structurally and functionally best characterised member of the FDBR family. The reaction starts with the binding of BV IX α followed by subsequent reduction of the exo-vinyl group at the D-ring position leading to a C18-ethyl group (Frankenberg and Lagarias 2003; Tu et al. 2004). The substrate is bound in a more or less cyclic conformation with the propionate side chains facing the

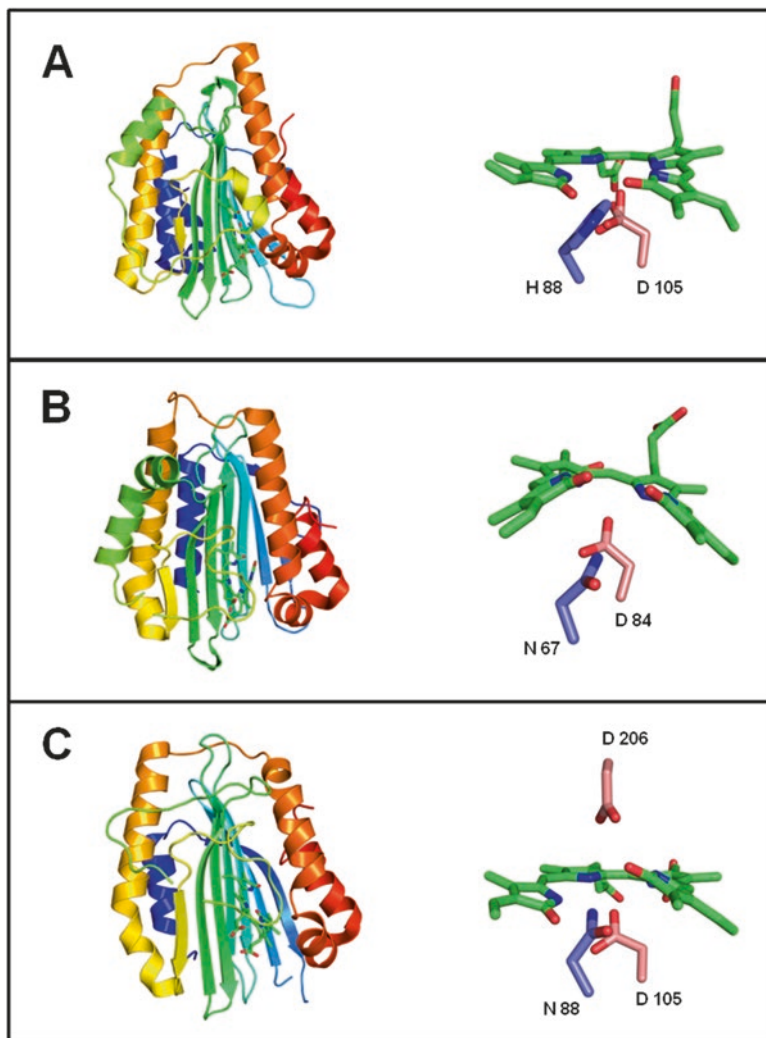


Fig. 11 Crystal structures of the three solved FDBRs with bound substrate BV (left side) and magnification of the substrate (right side) including important catalytic residues (see text for details). (a) *Synechocystis* sp. PCC6803 PcyA (PDB: 2D1E) with bound substrate (shown as green stick), (b) *Synechococcus* sp. WH8020 PebA (PDB: 2X9O) with bound substrate (shown as green stick) and (c) PebS from the cyanophage P-SSM2 (PDB: 2VCK) with bound substrate (shown as green stick). All structures are shown in cartoon representation coloured from blue to red starting from the N- to the C-terminus

solvent. For *Nostoc* PcyA it was shown that Asp105 and His88 are the important amino acid residues for BV reduction (Fig. 11a, right panel). The Asp105 residue is highly conserved in the whole FDBR family and thought to be important for initial BV protonation that would then favour electron transfer from ferredoxin. Exchange

of this residue to an Asn results in the stabilisation of a substrate radical intermediate as shown for several FDBRs (Busch et al. 2011a, b; Tu et al. 2007, 2008). Recent neutron crystallography confirmed the role of Asp in the protonation of BV to form a BVH⁺ (Unno et al. 2015). This positively charged substrate and the deprotonated Asp105 facilitate the subsequent electron transfer to generate a neutral BVH radical. This radical undergoes a lactam-lactim tautomerisation, and the first proton for the D-ring reduction is then transferred from Glu76 accompanied with the second electron transfer. The second proton is transferred via a hydrogen bond coming from His88 to the lactim O1 of the A-ring. Intramolecular proton transfer between O1 lactim and O19 lactam finally leads to 18¹,18²-DHBV (Fig. 12). Asp105 is thought to mediate proton and electron transfer between itself and the substrate as it was shown to display structural flexibility. Furthermore, the presence and importance of an axial water molecule (pyrrole water) has been demonstrated. The second part of the reaction will likely again start with the protonation of the intermediate 18¹,18²-DHBV with Asp105 and His88 being involved (Tu et al. 2007). Although the very initial step of the reaction seems to be similar in all FDBRs, only PcyA was shown to possess a proton shuttle pathway from bulk solvent to His88 (Tu et al. 2004, 2007) (Fig. 11a). In this regard, the newly discovered PcyX enzyme, converting BV to PEB in a single four-electron reduction, also possesses homologues of Asp105, His88 and Glu76 of PcyA. Therefore, it has been postulated that the mechanism of PcyX might be similar to PcyA just targeting the 15,16-double bond of BV instead of the D-ring exo-vinyl group (Ledermann et al. 2016).

It is generally accepted that the initial step of the reaction appears to be quite similar in all FDBRs and involves the protonation of the substrate by the conserved Asp105 (of homologue thereof) which is located on the β -sheet side of the enzyme. In the Peb-subgroup (i.e. PebA, PebB and PebS), a second Asp is highly conserved which is positioned on the opposite side of the substrate-binding pocket (Fig. 11). Although this residue is conserved, it is only catalytically important for the two reductases that catalyse the A-ring reduction of 15,16-DHBV to PEB (i.e. PebS and PebB). Likely, this residue is a proton donor for the A-ring reduction (Busch et al. 2011a, b). Based on the crystal structures of PebS and PebA, this observation can easily be explained. Asp206 can adopt multiple conformations in PebS indicating that a high structural flexibility of this residue might catalytically be important (deprotonation-reprotonation). The Asp206 homologue of PebA on the other hand is rotated outside of the active site and therefore not involved in catalysis (Busch et al. 2011a, b). Solving the crystal structures of cyanobacterial PebA and cyanophage PebS, however, did not completely answer the question why the PebA reaction stops at the intermediate 15,16-DHBV and does not proceed further to PEB as PebS does. Parts of the answer might be the positioning of the substrate in the active site of the enzyme. While BV in PebS is bound in a helical, porphyrin-like conformation, the BV in PebA adopts a roof-like conformation with the A- and D-rings tilted out of the plane. Possibly, the substrate/product is locked in the enzyme due to the architecture of the active site and thereby prevents further reduction or structural rearrangement to PEB (Busch et al. 2011a).

Biosynthesis of Bilirubin

Bilirubin is a common heme degradation product in mammals and for a long time was thought not to occur in cyanobacteria. Its occurrence was discovered by chance during a database search for bilin reductases using mammalian biliverdin reductase (BVR) as a bait (Schluchter and Glazer 1997).

Mammalian BVR is well studied and converts BV IX α to bilirubin IX α (BR) via a two-electron reduction of the C10 methine bridge with the help of reducing equivalents from NAD(P)H (Maines 2005). The cyanobacterial counterpart is encoded by the open reading frame *bvdR* (slr1784) in *Synechocystis* sp. PCC6803 and shares about 21% amino acid sequence identity with the mammalian protein, and important amino acid residues are conserved (Schluchter and Glazer 1997) (Fig. 7).

Contrary to the mammalian enzyme, BVR from *Synechocystis* is a dimeric enzyme with a strong preference for NADPH as its cofactor. Furthermore, the cyanobacterial BvdR has a very narrow substrate specificity, whereas the mammalian enzyme can also reduce various phycobilins to their respective rubin counterparts (i.e. PCB to phycocyanorubin). Deletion of the *bvdR* gene in *Synechocystis* sp. has a high regulatory impact on PBP synthesis since production of PBS core subunits is decreased and PC-related rod elements are absent. Nevertheless, the function and how BR is involved in the regulatory mechanism of cyanobacterial PBP biosynthesis remains unclear (Schluchter and Glazer 1997).

Biosynthesis of Phycourobilin and Phycoviolobilin

The range of phycobilins in cyanobacteria extends to more unusual chromophores, phycoviolobilin (PVB) and phycourobilin (PUB) (Fig. 7). These chromophores are found in cyanobacterial PBPs, but until today no corresponding biosynthesising FBDR has been discovered yet (Ong and Glazer 1991). The only exception is phycourobilin synthase (PUBS) which was recently discovered in the moss *Physcomitrella patens* where it seems to be involved in light sensing and photomorphogenesis. PUBS is a four-electron reducing FDBR and converts BV via 15,16-DHBV to PUB (Chen et al. 2012) (Fig. 7). As PUBS homologues seem to be absent in cyanobacteria, the only way for them to produce these chromophores is via isomerisation of PEB and PCB, respectively (Blot et al. 2009; Shukla et al. 2012; Zhao et al. 2002). These reactions are catalysed by PBP lyases/isomerases and will be covered in the next section.

The Assembly of Phycobilins into Phycobiliproteins

All phycobilins are covalently attached to the apoproteins via thioether bonds to conserved cysteine residues. While in the case of phytochrome-like photoreceptors, this reaction occurs in an autocatalytic reaction, the attachment in PBPs is mediated

by a class of enzymes called phycobiliprotein lyases (Scheer and Zhao 2008). PBP lyases are crucial enzymes as they provide the right regio- and stereospecificity for the chromophore attachment. A spontaneous attachment of bilins to PBPs has also been observed in vitro, but these reactions lack the fidelity and yield of the lyase-mediated attachment (Arciero et al. 1988; Fairchild and Glazer 1994; Schluchter and Glazer 1999; Zhao et al. 2004). Addition of a phycobilin to Cys residues generates a new stereocenter at the C3¹ carbon of the bilin. Even in strains that only use PCB as a chromophore in their PBP, two different stereoisomers are observed. While the *R*-isomer is the most commonly found one, the *S*-isomer seems to be present at positions homologue to Cys155 of the β -subunits (Fig. 2b) (Schirmer et al. 1986). It is believed that the PBP lyases contribute to this stereospecific ligation of the bilin. One exception for non-lyase-mediated ligation is the APC domain of the core-membrane linker L_{CM} from *Nostoc* sp. PCC 7120 which is able to bind PCB in an autocatalytic reaction maintaining its native absorption and fluorescence features (Zhao et al. 2005).

For the attachment of bilins to the different conserved cysteine residues within the PBPs, different lyases are required. To this date three classes of lyases have been described. The E/F-type lyases, the S(U)-type lyases and T-type lyases (Table 3) with the E/F-type lyases being the best characterised ones. An overview of PBP lyase sequences can be found in the publically available database Cyanolyase. This is a manually curated sequence and amino acid motif database gathering all the different PBP lyases and related protein sequences available in public databases (Bretaud et al. 2013).

The E/F-Type Lyases

The first characterised enzymes for the chromophore attachment in PBPs were the E/F-type lyases from *Synechococcus* sp. PCC7002. The heterodimeric enzyme (CpcE and CpcF) catalyses the attachment of PCB to Cys-84 of the α -subunit (CpcA) of PC (Zhou et al. 1992). A very interesting E/F-type lyase (PecE/PecF) was identified in *Mastigocladus laminosus*. It possesses lyase as well as isomerase activity (Zhao et al. 2002). The lyase catalyses the attachment of PCB to the α -subunit of PEC (PecA) as well as the subsequent isomerisation to PVB. Experiments with the isolated subunits of the lyase showed that PecE is responsible for the binding of the chromophore, whereas PecF catalyses the isomerisation to PVB during the attachment to the PBP (Zhao et al. 2002).

Another example for a coupled lyase/isomerase activity can be found in *Synechococcus* sp. WH8102. This marine cyanobacterium deploys a unique trichromatic R-phycoyanin V, which absorbs almost the whole spectrum of visible light between 450 and 650 nm giving the organism an advantage in oceanic habitats where only blue light penetrates deeply into the water column (Blot et al. 2009). R-PC V carries PUB, PCB as well as PEB chromophores. The formation of PUB from PEB and the attachment to α -Cys84 of R-PC V are catalysed by the

Table 3 Summary of phycobiliprotein lyase classes and their activity

Class	Example	Organism	Activity	Oligomerisation	Apoprotein specificity	Attachment site specificity
E/F	CpeE/CpcF	<i>Synechococcus</i> sp. PCC7002	PCB:α-Cys84-PC lyase	Heterodimer	High	High
	PecE/PecF	<i>Mastigocladus laminosus</i>	PCB:α-Cys84-PC lyase/isomerase (PVB)	Heterodimer	High	High
	RpcG	<i>Synechococcus</i> sp. WH8102	PEB:α-Cys84-PC lyase/isomerase (PUB)	Monomer	High	High
	CpeY/CpeZ	<i>Fremyella diplosiphon</i>	PEB:α-Cys82-PE lyase	Monomer	High	High
	MpeZ	<i>Synechococcus</i> sp. RS9916	PEB:α-Cys83-PE-II lyase/isomerase (PUB)	?	High	High
	CpcS1 ^a	<i>Nostoc</i> sp. PCC7120	PCB:β-Cys84-PC lyase PCB:β-Cys84-PEC lyase PCB:α-Cys82-APC lyase	Monomer	Low	High
S/U	CpcS-I/CpcU	<i>Synechococcus</i> sp. PCC7002	PCB:α/β-Cys81-APC lyase PCB:α-Cys82-PC lyase	Heterodimer	Low	High
	CpcS	<i>Prochlorococcus marinus</i> MED4	PEB:β-Cys82-PE lyase	Homodimer	?	High
	CpcS	<i>Fremyella diplosiphon</i>	PEB:β-Cys80-PE lyase	?	Low	High
	CpcT	<i>Synechococcus</i> sp. PCC7002	PCB:β-Cys153-PC lyase	?	High	High
	CpcT	<i>Nostoc</i> sp. PCC7120	PCB:β-Cys155-PEC lyase	?	Low	High
	T					

monomeric lyase/isomerase RpcG. This lyase is a fusion protein and possesses N- and C-termini that share a high homology to the PecE- and PecF-lyase subunits of *Nostoc* sp. PCC 7120 (Blot et al. 2009).

Another pair of E/F-type lyases that has been studied is CpeY and CpeZ from *Fremyella diplosiphon*. These lyases are responsible for the attachment of PEB to the α -subunit of PE (CpeA) at α -Cys 82. Experiments with purified proteins revealed that CpeY alone possesses lyase activity as it was able to attach PEB to CpeA. Nevertheless, the yields were low compared to the efficiency of the same reaction with added CpeZ. As the sequence of CpeY contains 429 amino acids, it is much larger than regular E/F-type lyases. Therefore, the authors suggested that CpeY is a fusion protein made up of the open reading frames (ORFs) of an E/F-type lyase pair which would also explain its ability to ligate PEB to CpeA without the addition of CpeZ (Biswas et al. 2011).

The CpeZ ortholog MpeZ is found in all *Synechococcus* strains that undergo type IV chromatic acclimation (CA4) (Shukla et al. 2012; Gutu and Kehoe 2012). This process is characterised by a reversible change in the chromophore composition of PE-I and PE-II to adapt to the ambient light conditions. During the acclimation three PEB molecules are exchanged by three PUB molecules and vice versa. Shukla and coworkers identified that MpeZ plays a key role in this process. The recombinantly produced MpeZ from *Synechococcus* sp. RS9916 catalyses the attachment of PEB to Cys83 of the α -subunit of PE-II and the subsequent isomerisation to PUB. Furthermore, the authors were able to show that *mpeZ* mutants fail to normally adapt to changing light conditions, underlining the importance of this enzyme in the CA4 process (Shukla et al. 2012).

A common structural feature of all E/F-type lyases is a HEAT-repeat motif that occurs five to six times in their sequences (Schluchter et al. 2010). HEAT-repeat motifs are thought to promote protein-protein interactions and are often found in eukaryotic organisms (Andrade and Bork 1995; Andrade et al. 2001).

The S/U-Type Lyases

The S/U-type lyases are unrelated to E/F-type lyases and have rather broad apoprotein as well as chromophore substrate specificity. In contrast to this, they possess a high specificity for the binding site and catalyse the ligation at the Cys-84 of the apo-PBP (Zhao et al. 2006). The S-type lyase CpcS from *Nostoc* sp. PCC 7120 is a universal lyase which binds both PCB and PEB and transfers the chromophores to Cys-84 of most PBPs of the PBS core and acts as a monomeric enzyme (Zhao et al. 2006, 2007). Other members of the S-type lyases like CpcS from *Synechococcus* sp. PCC 7002 are inactive as monomers but active in a complex with CpcU (Saunée et al. 2008; Shen et al. 2008b). Another member of the S/U-type lyases is GtCPES from the eukaryotic cryptophyte *Guillardia theta*. GtCPES is a nuclear-encoded S-type lyase specific for bilins with a reduced 15,16-double bond (15,16-DHBV and PEB) (Overkamp et al. 2014). In this regard it shares biochemical properties of

the related CpeS PBP lyase from *Prochlorococcus marinus* MED4 (Wiethaus et al. 2010b). In addition, both have in common that they bind the chromophore in a very fast reaction ($k_{\text{on}} \sim 2 \mu\text{M}^{-1} \text{s}^{-1}$) yielding a very stable and spectroscopically distinct complex. Based on the absorption properties of the CpeS/PEB complex, it has been suggested that the bilin is bound in an extended more stretched conformation (Overkamp et al. 2014; Wiethaus et al. 2010b). The subsequent transfer to the PBP is much slower (Overkamp et al. 2014; Wiethaus et al. 2010b).

The crystal structure of cryptophyte *GiCPES* revealed that the lyase folds into a 10-stranded antiparallel β -barrel belonging to the structural family of fatty-acid-binding proteins in the calycin superfamily which are known to bind small hydrophobic molecules (North 1990). The β -barrel obtains a calyx-like shape, and the bottom of the barrel is closed by an N-terminal α -helix that separates the inner of the barrel from the surrounding (Fig. 13).

The T-Type Lyases

T-type lyases are ubiquitous in cyanobacteria and are distantly related to the S/U--type lyases. The T-type lyase CpcT from *Nostoc* sp. PCC 7120 catalyses the attachment of PCB to β -Cys155 of PC and PEC (Shen et al. 2006; Zhao et al. 2007). The first crystal structure of this lyase containing bound substrate has been published in 2014. CpcT forms a dimer and folds into a calyx-shaped β -barrel ((Zhou et al. 2014); Fig. 14). The PCB chromophore is located in a deep cleft at the centre of the β -barrel. Interestingly, the PCB adopts the ZZZsss geometry in an M-helical conformation (Zhou et al. 2014). In the dimer, the PCB chromophore is hardly

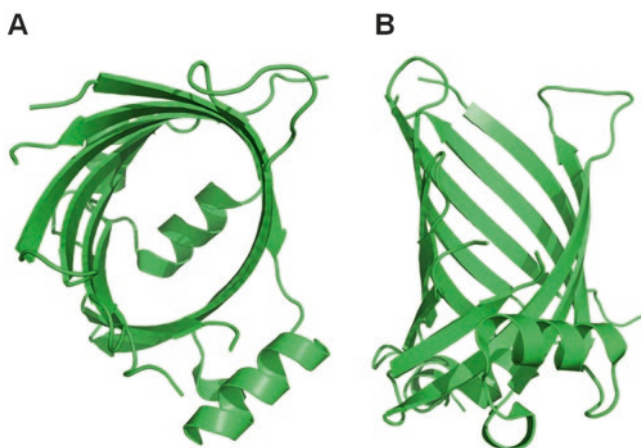


Fig. 13 Crystal structure of the PBP lyase *GiCPES* from the cryptophyte *Guillardia theta* (PDB: 4TQ2). (a) View from above inside the β -barrel with the N-terminal helix at the bottom that acts like a plug to seal the barrel. (b) Lateral view of the lyase

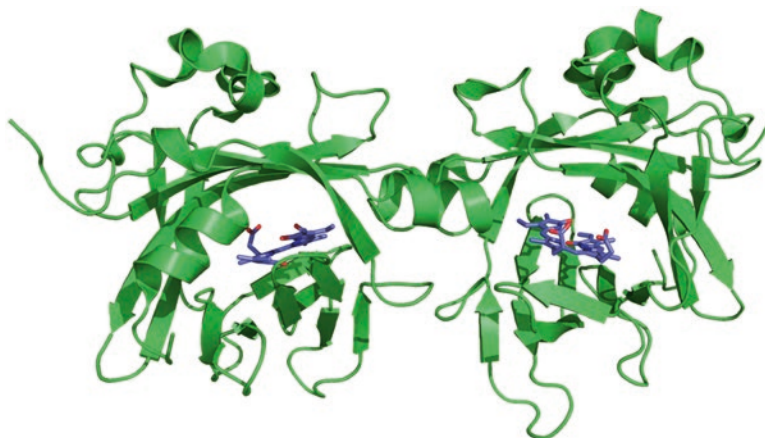


Fig. 14 Crystal structure of the CpcT-lyase dimer (green) from *Nostoc* sp. PCC 7120 with bound PCB (blue) substrate (PDB: 4O4S)

accessible for the transfer to the apo-PBP. PCB becomes more accessible in the monomeric form of CpcT indicating that dimer dissociation might be important for releasing PCB.

Based on the work of Grubmayr and Wagner, who suggest the formation of the thioether bond between chromophore and apoprotein via an acylimmonium intermediate (Grubmayr and Wagner 1988), Zhou et al. (2014) propose a reaction mechanism for the CpcT lyase. The first step of the mechanism is the protonation of the chromophore at C5 by the thiol group of the CpcB Cys155 which points towards the α -face of the bilin. The resulting N21-acylimmonium cation is stabilised by interaction with the carboxylate group of Asp163 from CpcB which points at the β -face of the bilin. The thioether bond is then formed by a nucleophilic attack of the thiolate at C3¹ from the steric less hindered α -side of the chromophore leading to the 3¹(S) configuration. The last step of the proposed reaction mechanism is a protonation of the chromophore at C3 from the α -face yielding the 3(R)-configuration with the substituents at C2 and C3 in *trans*-position (see also Fig. 2b).

Additional Post-translational Modifications of Phycobiliproteins

The second type of post-translational modifications of PBPs is the methylation of a conserved asparagine residue in almost all PBP β -subunits of cyanobacteria, red algae and cryptomonads (Apt et al. 1995; Ducret et al. 1996; Klotz and Glazer 1987; Klotz et al. 1986; Rübeleni et al. 1987; Wilbanks et al. 1989). The conserved asparagine is located at the β -72 position (numbering of CpcB in *Synechococcus* sp. PCC 7002), and despite the high structural similarity of the α - and β -subunits,

methylation only occurs in the β -subunit. Due to the positioning of β -Asn72 in close proximity to the chromophore bound at β -Cys 84, it has been speculated that methylation alters the absorbance and energy-emitting characteristics of the bilin. Mutants that are not able to methylate the β -Asn72 were shown to transfer less energy from PC to APC (Swanson and Glazer 1990) and therefore have a reduced electron flow through their PS2 in light conditions favouring the PBSs to absorb light (Thomas et al. 1993). Furthermore, these strains were shown to be sensitive towards high light intensities (Shen et al. 2008a). Based on these findings, it was concluded that the methylation minimises the non-radiative energy losses within the PBS (Schluchter et al. 2010). Miller et al. identified CpcM as the methyltransferase responsible for the methylation of the β -Asn72 at the γ -N (Miller et al. 2008).

Light-Harvesting Genes in the Genomes of Oceanic Phages

Cyanophages, viruses that infect cyanobacteria, are abundant in the oceans with concentrations up to 10^6 plaque-forming units per ml seawater (Suttle and Chan 1994). As the phages either lyse the hosts or reside in a continued persistent infection, there is a high potential of the exchange of genetic material between the organisms, and the genetic information of both the host and the phage is shaped by this interaction (Marston et al. 2013). Therefore it is conceivable that cyanophage genomes possess genetic material originating from cyanobacteria. Interestingly, the majority of cyanobacterial genes in phage genomes are related to photosynthesis, and it has been implicated that they contribute to phage fitness during infection (Lindell et al. 2004; Sullivan et al. 2005). One example for these so-called auxiliary metabolic genes (AMGs) is the *psbA* encoding the core reaction centre protein D1 which was shown to be expressed during infection with the amount of phage D1 protein increasing during infection (Lindell et al. 2004). In addition, many genes encoding enzymes involved in phycobilin biosynthesis have been identified (Dammeyer et al. 2008a).

Among them a member of the FDBR family, PebS, has been identified in the genome of the cyanophage P-SSM2 (see also section “Biosynthesis of Phycoerythrobilin”). Interestingly, the phage copy of this gene encodes a bifunctional protein combining the activities of two cyanobacterial host genes. PebS efficiently produces PEB from a BV precursor and is thus far solely found in genomes of cyanophages, often together with genes encoding a HO. Although it was shown that the genes are expressed during infection, their exact function still remains elusive (Dammeyer et al. 2008a). The substitution of a two-enzyme system by a one-enzyme reaction has the selective advantage of genome reduction for the phage. Furthermore, it has been speculated that their expression might also contribute to phage fitness by enhancing light-harvesting capacity. In this regard, the cyanophage S-PM2 was shown to induce increased synthesis of the light-harvesting PE in *Synechococcus* sp. WH7803 during infection. Inspection of the phages’ genome revealed that it contains only one gene related to light harvesting, *cpeT*. *cpeT*

encodes a putative phycobiliprotein lyase. CpeT belongs to the so-called T-type lyases, and PCB-specific homologues of CpeT (i.e. CpcT) were shown to specifically serve the position equivalent to cysteine 153 in the β -subunit of PC. Therefore, it is postulated that CpeT lyases serve the β -Cys153 of PE (see also section on T-type lyases).

Another recently discovered viral enzyme involved in the PEB biosynthesis is the FDBR PcyX (Ledermann et al. 2016). PcyX catalyses the same reaction as PebS but shares more similarity with the PcyA-like reductases (see also section “Biosynthesis of Phycoerythrobilin”). Further analyses of the scaffolds on which the *pcyX* were identified revealed that they most likely are derived from phages infecting alphaproteobacteria and not cyanobacteria (Ledermann et al. 2016). The biological function of PcyX remains unknown; however, a contribution to light-harvesting efficiency of the host can be ruled out as alphaproteobacteria are unable to perform oxygenic photosynthesis.

Assembly of the Phycobilisome

The correct assembly of the PBS is essential for its ability to efficiently transfer energy. While an isolated C-PC ($\alpha\beta$) monomer from *Synechococcus* sp. PCC 7002 shows energy transfer rates among its chromophores between 50 and 500 ps (Debreczeny et al. 1993), APC ($\alpha\beta$)₃ trimers show ~100-fold faster energy transfer (0.5–1 ps) (Beck and Sauer 1992).

Although the assembly of the PBS is crucial for its function, the process is not yet fully understood. The current view of the assembly is based on a model proposed by Anderson and Toole which involves different assembly proteins, processing enzymes as well as chaperones (Anderson and Toole 1998). The first step of this process is the biosynthesis of the PBP apoproteins. The PBP-coding genes in cyanobacteria are often organised in operons, allowing a simultaneous translation of the various apoproteins.

The second step of the assembly process is the interaction of the translated proteins with chaperones that foster the correct folding of the apoproteins, leading to transient state of free subunits. The third step of the assembly process is the PBP-lyase-mediated attachment of the phycobilin cofactors to the apoproteins. Interestingly, the attachment of the cofactors has to occur in a specific order with the β -Cys 155 positions being the first to be ligated with a chromophore (Zhao et al. 2007).

The further process is thought to be mainly a self-assembly of the PBPs. The hypothesis is supported by the fact that several groups found PBP crystals in solutions that were contaminated with high concentrations of other proteins leading to the conclusion that the PBPs have a strong tendency to self-assemble into ordered structures (Adir 2005). Moreover crystallisation experiments revealed that the discs formed by ($\alpha\beta$)₆ hexamers self-assemble into large rods (Adir 2005). Therefore, a role of linker proteins in the termination of the rod elongation has

been postulated. This is strengthened by the observation that a 9 kDa linker protein of *Synechococcus* sp. PCC 7002 has an effect on the homogeneity of rod lengths (de Lorimier et al. 1990).

Applications for Phycobiliproteins

Due to their bright colour, their high fluorescence and their solubility in water, PBPs are ideal candidates for the use as fluorophores in biological applications. They possess a bright fluorescence, a high fluorescence quantum yield (max. $\phi = 0.98$) as well as a large Stokes shift (Lakowicz 1994). Consequently, several PBPs are commercially available as free proteins or coupled to primary and secondary antibodies as well as streptavidin conjugates. PBPs are widely used as fluorescence labels in applications like fluorescence-activated cell sorting (FACS), confocal microscopy, immunodetection and fluorescence resonance energy transfer (FRET) assays. Thus far, the commercially available PBPs are all extracted from cyanobacteria or red algae as the recombinant production is not yet optimised for large-scale production (Cuellar-Bermudez et al. 2015).

Due to their bright colours, PBPs are widely used as natural colourants in the food as well as in the cosmetic industry. They provide a natural, nontoxic alternative to synthetic dyes and are used in products like chewing gum, dairy products, beverages, jellies, sweet decorations, ice cream as well as cosmetics. An advantageous property of the PBPs is their stability at low pH values. Therefore they are suitable as dyes in acidic foods like yoghurt (Sarada et al. 1999; Moreira et al. 2012).

Furthermore PBPs have an enormous potential for the use in pharmaceutical as well as nutraceutical applications. For example, it was shown that PC is a potent antioxidant which is capable to scavenge hydroxyl, alkoxyl as well as peroxy radicals (Benedetti et al. 2004; Bermejo et al. 2008; Bhat and Madyastha 2000). Moreover, PC is able to inhibit microsomal lipid peroxidation caused by reactive oxygen species (ROS) (Delgado Roche et al. 2011) and is able to inhibit the cell proliferation of human leukaemia K562 cells (Subhashini et al. 2004). PC was also shown to reduce the level of tumour necrosis factor- α in mice treated with an endotoxin (Romay et al. 2001) and has neuroprotective effects in rat cerebellar granule cell cultures from potassium/serum withdrawal-induced apoptosis (Rimbau et al. 2001). APC was shown to inhibit enterovirus 71-induced apoptosis in human rhabdomyosarcoma cells as well as in African green monkey kidney cells (Shih et al. 2003). Another possible application of PBPs is their use as photosensitiser in the photodynamic cancer therapy (PDT). Huang and coworkers showed that R-PE is a suitable photosensitiser for the PDT as it inhibited the growth of human liver carcinoma cells SMC 7721 after irradiation with an argon laser (Bei et al. 2002).

References

- Abraham NG, Drummond GS, Lutton JD, Kappas A (1996) The biological significance and physiological role of heme oxygenase. *Cell Physiol Biochem* 6(3):129–168. doi:[10.1159/000154819](https://doi.org/10.1159/000154819)
- Adir N (2005) Elucidation of the molecular structures of components of the phycobilisome: reconstructing a giant. *Photosynth Res* 85(1):15–32. doi:[10.1007/s1120-004-2143-y](https://doi.org/10.1007/s1120-004-2143-y)
- Anderson LK, Toole CM (1998) A model for early events in the assembly pathway of cyanobacterial phycobilisomes. *Mol Microbiol* 30(3):467–474
- Andrade MA, Bork P (1995) HEAT repeats in the Huntington's disease protein. *Nature Genetics* 11(2):115–116
- Andrade MA, Petosa C, O'Donoghue SI, Muller CW, Bork P (2001) Comparison of ARM and HEAT protein repeats. *J Mol Biol* 309(1):1–18. doi:[10.1006/jmbi.2001.4624](https://doi.org/10.1006/jmbi.2001.4624)
- Apt KE, Collier JL, Grossman AR (1995) Evolution of the phycobiliproteins. *J Mol Biol* 248(1):79–96. doi:[10.1006/jmbi.1995.0203](https://doi.org/10.1006/jmbi.1995.0203)
- Arciero D, Dallas J, Glazer A (1988) In vitro attachment of bilins to apophycocyanin. II. Determination of the structures of tryptic bilin peptides derived from the phycocyanobilin adduct. *J Biol Chem* 263(34):18350–18357
- Beale SI, Chen NC (1983) N-methyl mesoporphyrin IX inhibits phycocyanin, but not chlorophyll synthesis in *Cyanidium caldarium*. *Plant Physiol* 71(2):263–268
- Beale SI, Cornejo J (1984a) Enzymatic heme oxygenase activity in soluble extracts of the unicellular red alga, *Cyanidium caldarium*. *Arch Biochem Biophys* 235:371–384
- Beale SI, Cornejo J (1984b) Enzymic transformation of biliverdin to phycocyanobilin by extracts of the unicellular red alga *Cyanidium caldarium*. *Plant Physiol* 76:7–15
- Beale SI, Cornejo J (1991) Biosynthesis of phycobilins. Ferredoxin-mediated reduction of biliverdin catalyzed by extracts of *Cyanidium caldarium*. *J Biol Chem* 266(33):22328–22332
- Beck WF, Sauer K (1992) Energy-transfer and exciton-state relaxation processes in allophycocyanin. *J Phys Chem* 96(11):4658–4666. doi:[10.1021/j100190a094](https://doi.org/10.1021/j100190a094)
- Bei H, Guang-Ce W, Chen-Kui Z, Zhen-gang L (2002) The experimental research of R-phycoerythrin subunits on cancer treatment: a new photosensitizer in PDT. *Cancer Biotherapy and Radiopharmaceuticals* 17(1):35–42. doi:[10.1089/10849780252824055](https://doi.org/10.1089/10849780252824055)
- Benedetti S, Benvenuti F, Pagliarani S, Francogli S, Scoglio S, Canestrari F (2004) Antioxidant properties of a novel phycocyanin extract from the blue-green alga *Aphanizomenon flos-aquae*. *Life Sci* 75(19):2353–2362. doi:[10.1016/j.lfs.2004.06.004](https://doi.org/10.1016/j.lfs.2004.06.004)
- Bermejo P, Piñero E, Villar ÁM (2008) Iron-chelating ability and antioxidant properties of phycocyanin isolated from a protean extract of *Spirulina platensis*. *Food Chemistry* 110(2):436–445. doi:[10.1016/j.foodchem.2008.02.021](https://doi.org/10.1016/j.foodchem.2008.02.021)
- Bhat VB, Madyastha KM (2000) C-phycocyanin: a potent peroxy radical scavenger in vivo and in vitro. *Biochem Biophys Res Commun* 275(1):20–25. doi:[10.1006/bbrc.2000.3270](https://doi.org/10.1006/bbrc.2000.3270)
- Biswas A, Boutaghou MN, Alvey RM, Kronfel CM, Cole RB, Bryant DA, Schluchter WM (2011) Characterization of the activities of the CpeY, CpeZ, and CpeS bilin lyases in phycoerythrin biosynthesis in *Fremyella diplosiphon* strain UTEX 481. *J Biol Chem* 286(41):35509–35521
- Blot N, Wu XJ, Thomas JC, Zhang J, Garczarek L, Bohm S, Tu JM, Zhou M, Ploscher M, Eichacker L, Partensky F, Scheer H, Zhao KH (2009) Phycourobilin in trichromatic phycocyanin from oceanic cyanobacteria is formed post-translationally by a phycoerythrobilin lyase-isomerase. *J Biol Chem* 284(14):9290–9298. doi:[10.1074/jbc.M809784200](https://doi.org/10.1074/jbc.M809784200)
- Bretaudau A, Coste F, Humily F, Garczarek L, Le Corguillé G, Six C, Ratn M, Collin O, Schluchter WM, Partensky F (2013) CyanoLyase: a database of phycobilin lyase sequences, motifs and functions. *Nucl Acids Res* 41(D1):D396–D401. doi:[10.1093/nar/gks1091](https://doi.org/10.1093/nar/gks1091)
- Busch AW, Reijerse EJ, Lubitz W, Frankenberg-Dinkel N, Hofmann E (2011a) Structural and mechanistic insight into the ferredoxin-mediated two-electron reduction of bilins. *Biochem J* 439(2):257–264. doi:[10.1042/BJ20110814](https://doi.org/10.1042/BJ20110814)
- Busch AW, Reijerse EJ, Lubitz W, Hofmann E, Frankenberg-Dinkel N (2011b) Radical mechanism of cyanophage phycoerythrobilin synthase (PebS). *Biochem J* 433(3):469–476. doi:[10.1042/BJ20101642](https://doi.org/10.1042/BJ20101642)

- Chapman DJ, Cole WJ, Siegelman HW (1967) Chromophores of allophycocyanin and R-phycocyanin. *Biochem J* 105(3):903–905
- Chen YR, Su YS, Tu SL (2012) Distinct phytochrome actions in nonvascular plants revealed by targeted inactivation of phytyl bilin biosynthesis. *Proc Natl Acad Sci USA* 109(21):8310–8315. doi:[10.1073/pnas.1201744109](https://doi.org/10.1073/pnas.1201744109)
- Chew AGM, Bryant DA (2007) Chlorophyll biosynthesis in bacteria: the origins of structural and functional diversity. *Ann Rev Microbiol* 61(1):113–129. doi:[10.1146/annurev.micro.61.080706.093242](https://doi.org/10.1146/annurev.micro.61.080706.093242)
- Chisholm SW, Frankel SL, Goericke R, Olson RJ, Palenik B, Waterbury JB, Westjohnsrud L, Zettler ER (1992) *Prochlorococcus marinus* Nov Gen-Nov Sp – an oxyphototrophic marine prokaryote containing divinyl chlorophyll-a and chlorophyll-b. *Arch Microbiol* 157(3):297–300. doi:[10.1007/Bf00245165](https://doi.org/10.1007/Bf00245165)
- Chisholm SW, Olson RJ, Zettler ER, Goericke R, Waterbury JB, Welschmeyer NA (1988) A novel free-living prochlorophyte abundant in the oceanic euphotic zone. *Nature* 334(6180):340–343. doi:[10.1038/334340a0](https://doi.org/10.1038/334340a0)
- Cole WJ, Chapman DJ, Siegelman HW (1967) The structure of phycocyanobilin. *J Am Chem Soc* 89:3643–3645
- Collier JL, Herbert SK, Fork DC, Grossman AR (1994) Changes in the cyanobacterial photosynthetic apparatus during acclimation to macronutrient deprivation. *Photosynth Res* 42(3):173–183. doi:[10.1007/BF00018260](https://doi.org/10.1007/BF00018260)
- Cornejo J, Willows RD, Beale SI (1998) Phytobilin biosynthesis: cloning and expression of a gene encoding soluble ferredoxin-dependent heme oxygenase from *Synechocystis* sp. PCC 6803. *Plant J* 15(1):99–107
- Cuellar-Bermudez SP, Aguilar-Hernandez I, Cardenas-Chavez DL, Ornelas-Soto N, Romero-Ogawa MA, Parra-Saldivar R (2015) Extraction and purification of high-value metabolites from microalgae: essential lipids, astaxanthin and phycobiliproteins. *Microb Biotechnol* 8(2):190–209. doi:[10.1111/1751-7915.12167](https://doi.org/10.1111/1751-7915.12167)
- Dammeyer T, Bagby SC, Sullivan MB, Chisholm SW, Frankenberg-Dinkel N (2008a) Efficient phage-mediated pigment biosynthesis in oceanic cyanobacteria. *Curr Biol* 18(6):442–448. doi:[10.1016/j.cub.2008.02.067](https://doi.org/10.1016/j.cub.2008.02.067)
- Dammeyer T, Frankenberg-Dinkel N (2006) Insights into phycoerythrobilin biosynthesis point toward metabolic channeling. *J Biol Chem* 281(37):27081–27089. doi:[10.1074/jbc.M605154200](https://doi.org/10.1074/jbc.M605154200)
- Dammeyer T, Hofmann E, Frankenberg-Dinkel N (2008b) Phycoerythrobilin synthase (PebS) of a marine virus. Crystal structures of the biliverdin complex and the substrate-free form. *J Biol Chem* 283(41):27547–27554. doi:[10.1074/jbc.M803765200](https://doi.org/10.1074/jbc.M803765200)
- Dammeyer T, Michaelsen K, Frankenberg-Dinkel N (2007) Biosynthesis of open-chain tetrapyrroles in *Prochlorococcus marinus*. *FEMS Microbiol Lett* 271(2):251–257. doi:[10.1111/j.1574-6968.2007.00715.x](https://doi.org/10.1111/j.1574-6968.2007.00715.x)
- de Lorimier R, Bryant DA, Stevens SE Jr (1990) Genetic analysis of a 9 kDa phycocyanin-associated linker polypeptide. *Biochim Biophys Acta* 1019(1):29–41
- Debreczeny MP, Sauer K, Zhou J, Bryant DA (1993) Monomeric C-phycocyanin at room temperature and 77 K: resolution of the absorption and fluorescence spectra of the individual chromophores and the energy-transfer rate constants. *The Journal of Physical Chemistry* 97(38):9852–9862. doi:[10.1021/j100140a050](https://doi.org/10.1021/j100140a050)
- Delgado Roche L, Lagumersindez-Denis N, Llopiz-Arzuaga A, Pentón-Arias E, Pentón-Rol G (2011) Protective effects of C-Phycocyanin against lipid peroxidation of serum lipoproteins and hepatic microsomes. *Pharmacologyonline* 3:668–676
- Duanmu D, Casero D, Dent RM, Gallaher S, Yang W, Rockwell NC, Martin SS, Pellegrini M, Niyogi KK, Merchant SS, Grossman AR, Lagarias JC (2013) Retrograde bilin signaling enables *Chlamydomonas* greening and phototrophic survival. *Proc Natl Acad Sci USA* 110(9):3621–3626. doi:[10.1073/pnas.1222375110](https://doi.org/10.1073/pnas.1222375110)
- Ducret A, Sidler W, Wehrli E, Frank G, Zuber H (1996) Isolation, characterization and electron microscopy analysis of a hemidiscoidal phycobilisome type from the cyanobacterium *Anabaena* sp. PCC 7120. *Eur J Biochem* 236(3):1010–1024

- Dufresne A, Salanoubat M, Partensky F, Artiguenave F, Axmann IM, Barbe V, Duprat S, Galperin MY, Koonin EV, Le Gall F, Makarova KS, Ostrowski M, Oztas S, Robert C, Rogozin IB, Scanlan DJ, Tandeau de Marsac N, Weissenbach J, Wincker P, Wolf YI, Hess WR (2003) Genome sequence of the cyanobacterium *Prochlorococcus marinus* SS120, a nearly minimal oxyphototrophic genome. *Proc Natl Acad Sci USA* 100(17):10020–10025. doi:[10.1073/pnas.1733211100](https://doi.org/10.1073/pnas.1733211100)
- Fairchild CD, Glazer AN (1994) Nonenzymatic bilin addition to the alpha subunit of an apophycocerythrin. *J Biol Chem* 269(46):28988–28996
- Falk H, Höllbacher G (1978) Beiträge zur Chemie der Pyrrolpigmente, 24. Mitt. Über die Beziehung zwischen Lichtabsorption und Struktur von Bilatrienen-abc. *Monatshfte für Chemie/Chemical Monthly* 109(6):1429–1449
- Fischer R, Gottstein J, Scheer H, Geiselhart P, Schneider S (1990) Picosecond time-resolved fluorescence of phycobiliproteins: Subunits of phycocyanin from *Mastigocladus laminosus*. *Journal of Photochemistry and Photobiology B Biology* 5(2):151–165
- Frankenberg-Dinkel N (2004) Bacterial heme oxygenases. *Antioxid Redox Signal* 6(5):825–834. doi:[10.1089/ars.2004.6.825](https://doi.org/10.1089/ars.2004.6.825)
- Frankenberg N, Lagarias JC (2003) Phycocyanobilin:ferredoxin oxidoreductase of *Anabaena* sp. PCC 7120. *Biochemical and spectroscopic. J Biol Chem* 278(11):9219–9226. doi:[10.1074/jbc.M211643200](https://doi.org/10.1074/jbc.M211643200)
- Frankenberg N, Mukougawa K, Kohchi T, Lagarias JC (2001) Functional genomic analysis of the HY2 family of ferredoxin-dependent bilin reductases from oxygenic photosynthetic organisms. *Plant Cell* 13(4):965–978
- Gambetta GA, Lagarias JC (2001) Genetic engineering of phytochrome biosynthesis in bacteria. *Proc Natl Acad Sci USA* 98(19):10566–10571. doi:[10.1073/pnas.191375198](https://doi.org/10.1073/pnas.191375198)
- Gisk B, Wiethaus J, Aras M, Frankenberg-Dinkel N (2012) Variable composition of heme oxygenases with different regiospecificities in *Pseudomonas* species. *Arch Microbiol* 194(7):597–606. doi:[10.1007/s00203-012-0796-z](https://doi.org/10.1007/s00203-012-0796-z)
- Glazer AN (1977) Structure and molecular organization of the photosynthetic accessory pigments of cyanobacteria and red algae. *Mol Cell Biochem* 18(2–3):125–140
- Glazer AN (1985) Light harvesting by phycobilisomes. *Annu Rev Biophys Biophys Chem* 14:47–77. doi:[10.1146/annurev.bb.14.060185.000403](https://doi.org/10.1146/annurev.bb.14.060185.000403)
- Glazer AN (1989) Light guides. *J Biol Chem* 264:1–4
- Goerick R, Repeta DJ (1992) The pigments of *Prochlorococcus marinus* – the presence of divinyl chlorophyll-a and chlorophyll-b in a marine prokaryote. *Limnol Ocean* 37(2):425–433
- Grossman AR, Schaefer MR, Chiang GG, Collier JL (1993) The phycobilisome, a light-harvesting complex responsive to environmental conditions. *Microbiol Rev* 57(3):725–749
- Grubmayr K, Wagner U (1988) Zur chemie der thioladdition an 2,3-dihydro-3-ethylidendipyrin-1(10H)-one—eine modellstudie zur kovalenten chromophor-protein-binding in biliproteinen. *Monatshfte für Chemie/Chemical Monthly* 119(8–9):965–983. doi:[10.1007/BF00810106](https://doi.org/10.1007/BF00810106)
- Gutu A, Kehoe DM (2012) Emerging perspectives on the mechanisms, regulation, and distribution of light color acclimation in cyanobacteria. *Molecular Plant* 5(1):1–13. doi:[10.1093/mp/ssr054](https://doi.org/10.1093/mp/ssr054)
- Hagiwara Y, Sugishima M, Takahashi Y, Fukuyama K (2006a) Crystal structure of phycocyanobilin:ferredoxin oxidoreductase in complex with biliverdin IX α , a key enzyme in the biosynthesis of phycocyanobilin. *Proc Natl Acad Sci USA* 103(1):27–32
- Hagiwara Y, Sugishima M, Takahashi Y, Fukuyama K (2006b) Induced-fitting and electrostatic potential change of PcyA upon substrate binding demonstrated by the crystal structure of the substrate-free form. *FEBS Lett* 580(16):3823–3828. doi:[10.1016/j.febslet.2006.05.075](https://doi.org/10.1016/j.febslet.2006.05.075)
- Hess WR, Partensky F, van der Staay GW, Garcia-Fernandez JM, Borner T, Vault D (1996) Coexistence of phycoerythrin and a chlorophyll a/b antenna in a marine prokaryote. *Proc Natl Acad Sci USA* 93(20):11126–11130
- Hess WR, Schendel R, Rudiger W, Fieder B, Borner T (1992) Components of chlorophyll biosynthesis in a barley albina mutant unable to synthesize delta-aminolevulinic acid by utilizing the transfer RNA for glutamic acid. *Planta* 188(1):19–27. doi:[10.1007/BF00198935](https://doi.org/10.1007/BF00198935)

- Ikeuchi M, Ishizuka T (2008) Cyanobacteriochromes: a new superfamily of tetrapyrrole-binding photoreceptors in cyanobacteria. *Photochem Photobiol Sci* 7(10):1159–1167. doi:[10.1039/b802660m](https://doi.org/10.1039/b802660m)
- Kahn K, Schaefer MR (1997) rpbA controls transcription of the constitutive phycocyanin gene set in *Fremyella diplosiphon*. *J Bacteriol* 179(24):7695–7704
- Kehoe DM, Grossman AR (1994) Complementary chromatic adaptation: photoperception to gene regulation. *Semin Cell Biol* 5(5):303–313
- Klotz AV, Glazer AN (1987) gamma-N-methylasparagine in phycobiliproteins. occurrence, location, and biosynthesis. *J Biol Chem* 262(36):17350–17355
- Klotz AV, Leary JA, Glazer AN (1986) Post-translational methylation of asparaginyl residues. Identification of beta-71 gamma-N-methylasparagine in allophycocyanin. *J Biol Chem* 261(34):15891–15894
- Kohchi T, Mukougawa K, Frankenberg N, Masuda M, Yokota A, Lagarias JC (2001) The Arabidopsis HY2 gene encodes phytochromobilin synthase, a ferredoxin-dependent biliverdin reductase. *Plant Cell* 13(2):425–436
- Kufer W, Scheer H (1979) Studies on plant bile pigments, VII. Preparation and characterization of phycobiliproteins with chromophores chemically modified by reduction. *Hoppe Seylers Z Physiol Chem* 360(7):935–956
- Lagarias JC, Rapoport H (1980) Chromopeptides from phytochrome – the structure and linkage of the Pr form of the phytochrome chromophore. *J Am Chem Soc* 102(14):4821–4828. doi:[10.1021/ja00534a042](https://doi.org/10.1021/ja00534a042)
- Lakowicz JR (1994) , Topics in fluorescence spectroscopy: volume 4: probe design and chemical sensing, vol 4. Springer Science & Business Media
- Ledermann B, Beja O, Frankenberg-Dinkel N (2016) New biosynthetic pathway for pink pigments from uncultured oceanic viruses. *Environ Microbiol* 18:4337–4347. doi:[10.1111/1462-2920.13290](https://doi.org/10.1111/1462-2920.13290)
- Lehner H, Krauss C, Scheer H (1981) Solvent induced circular dichroism in conformational analysis: bile pigments. *Zeitschrift für Naturforschung B* 36(6):735–738
- Lemberg R (1928) The chromo-proteid of dulse. I. *Justus Liebigs Annalen der Chemie* 461:46–89
- Lewin RA (1976) Prochlorophyta as a proposed new division of algae. *Nature* 261(5562):697–698
- Lindell D, Sullivan MB, Johnson ZI, Tolonen AC, Rohwer F, Chisholm SW (2004) Transfer of photosynthesis genes to and from Prochlorococcus viruses. *Proc Natl Acad Sci USA* 101(30):11013–11018. doi:[10.1073/pnas.0401526101](https://doi.org/10.1073/pnas.0401526101)
- MacColl R (1998) Cyanobacterial phycobilisomes. *J Struct Biol* 124(2):311–334
- Magne F (1989) Classification and phylogeny of Rhodophyta. *Cryptogamie Algal* 10(2):101–115
- Maines MD (2005) New insights into biliverdin reductase functions: linking heme metabolism to cell signaling. *Physiology (Bethesda)* 20:382–389. doi:[10.1152/physiol.00029.2005](https://doi.org/10.1152/physiol.00029.2005)
- Marston MF, Taylor S, Sme N, Parsons RJ, Noyes TJ, Martiny JB (2013) Marine cyanophages exhibit local and regional biogeography. *Environ Microbiol* 15(5):1452–1463. doi:[10.1111/1462-2920.12062](https://doi.org/10.1111/1462-2920.12062)
- Migita CT, Zhang X, Yoshida T (2003) Expression and characterization of cyanobacterium heme oxygenase, a key enzyme in the phycobilin synthesis. Properties of the heme complex of recombinant active enzyme. *Eur J Biochem* 270(4):687–698
- Miller CA, Leonard HS, Pinsky IG, Turner BM, Williams SR, Harrison L Jr, Fletcher AF, Shen G, Bryant DA, Schlachter WM (2008) Biogenesis of phycobiliproteins. III. CpcM is the asparagine methyltransferase for phycobiliprotein beta-subunits in cyanobacteria. *J Biol Chem* 283(28):19293–19300. doi:[10.1074/jbc.M802734200](https://doi.org/10.1074/jbc.M802734200)
- Montellano PR (2000) The mechanism of heme oxygenase. *Curr Opin Chem Biol* 4(2):221–227
- Moreira IO, Passos TS, Chiapinni C, Silveira GK, Souza JCM, Coca-Vellarde LG, Deliza R, de Lima Araújo KG (2012) Colour evaluation of a phycobiliprotein-rich extract obtained from *Nostoc* PCC9205 in acidic solutions and yogurt. *J Sci Food Agr* 92(3):598–605. doi:[10.1002/jsfa.4614](https://doi.org/10.1002/jsfa.4614)

- Nagy JO, Bishop JE, Klotz AV, Glazer AN, Rapoport H (1985) Bilin attachment sites in the alpha, beta, and gamma subunits of R-phycoerythrin. Structural studies on singly and doubly linked phycourobilins. *J Biol Chem* 260(8):4864–4868
- North AC (1990) Structural homology in ligand-specific transport proteins. *Biochem Soc Symp* 57:35–48
- Ong LJ, Glazer AN (1991) Phycoerythrins of marine unicellular cyanobacteria. I. Bilin types and locations and energy transfer pathways in *Synechococcus* spp. phycoerythrins. *J Biol Chem* 266(15):9515–9527
- Overkamp KE, Gasper R, Kock K, Herrmann C, Hofmann E, Frankenberg-Dinkel N (2014) Insights into the biosynthesis and assembly of cryptophycean phycobiliproteins. *J Biol Chem* 289(39):26691–26707. doi:10.1074/jbc.M114.591131
- Paiva-Silva GO, Cruz-Oliveira C, Nakayasu ES, Maya-Monteiro CM, Dunkov BC, Masuda H, Almeida IC, Oliveira PL (2006) A heme-degradation pathway in a blood-sucking insect. *Proc Natl Acad Sci USA* 103(21):8030–8035. doi:10.1073/pnas.0602224103
- Pinevich AV, Skulberg OM, Matthijs HCP, Schubert H, Willen E, GavriloVA OV, Velichko N (1999) Characterization of a novel chlorophyll b-containing *Prochlorothrix* species (Prochlorophyta) and its photosynthetic apparatus. *Microbios* 100(397):159–174
- Ratliff M, Zhu W, Deshmukh R, Wilks A, Stojiljkovic I (2001) Homologues of neisserial heme oxygenase in gram-negative bacteria: degradation of heme by the product of the *pigA* gene of *Pseudomonas aeruginosa*. *J Bacteriol* 183(21):6394–6403. doi:10.1128/JB.183.21.6394-6403.2001
- Richard C, Zabulon G (1997) The heme oxygenase gene (*pbsA*) in the red alga *Rhodella violacea* is discontinuous and transcriptionally activated during iron limitation. *Proc Natl Acad Sci USA* 94(21):11736–11741
- Rimbau V, Camins A, Pubill D, Sureda FX, Romay C, González R, Jiménez A, Escubedo E, Camarasa J, Pallàs M (2001) C-Phycocyanin protects cerebellar granule cells from low potassium/serum deprivation-induced apoptosis. *Naunyn-Schmiedeberg's Archives of Pharmacology* 364(2):96–104. doi:10.1007/s002100100437
- Romay C, Delgado R, Ramirez D, González R, Rojas A (2001) Effects of phycocyanin extract on tumor necrosis factor-alpha and nitrite levels in serum of mice treated with endotoxin. *Arzneimittel-Forschung* 51(9):733–736
- Rümbeli R, Suter F, Wirth M, Sidler W, Zuber H (1987) γ -N-Methylasparagine in phycobiliproteins from the cyanobacteria *Mastigocladus laminosus* and *Calothrix*. *FEBS Lett* 221(1):1–2. doi:10.1016/0014-5793(87)80341-1
- Sarada R, Pillai MG, Ravishankar GA (1999) Phycocyanin from *Spirulina* sp: influence of processing of biomass on phycocyanin yield, analysis of efficacy of extraction methods and stability studies on phycocyanin. *Process Biochem* 34(8):795–801
- Saunée NA, Williams SR, Bryant DA, Schluchter WM (2008) Biogenesis of phycobiliproteins II. CpcS-I and CpcU comprise the heterodimeric bilin lyase that attaches phycocyanobilin to Cys-82 of β -phycocyanin and Cys-81 of allophycocyanin subunits in *Synechococcus* sp. PCC 7002. *J Biol Chem* 283(12):7513–7522
- Scheer H, Zhao KH (2008) Biliprotein maturation: the chromophore attachment. *Mol Microbiol* 68(2):263–276. doi:10.1111/j.1365-2958.2008.06160.x
- Schirmer T, Huber R, Schneider M, Bode W, Miller M, Hackert ML (1986) Crystal structure analysis and refinement at 2.5 Å of hexameric C-phycocyanin from the cyanobacterium *Agmenellum quadruplicatum*: the molecular model and its implications for light-harvesting. *J Mol Biol* 188(4):651–676
- Schluchter WM, Glazer AN (1997) Characterization of cyanobacterial biliverdin reductase. Conversion of biliverdin to bilirubin is important for normal phycobiliprotein biosynthesis. *J Biol Chem* 272(21):13562–13569
- Schluchter WM, Glazer AN (1999) Biosynthesis of phycobiliproteins in cyanobacteria. In: *The phototrophic prokaryotes*. Springer US, pp 83–95
- Schluchter WM, Shen G, Alvey RM, Biswas A, Saunee NA, Williams SR, Mille CA, Bryant DA (2010) Phycobiliprotein biosynthesis in cyanobacteria: structure and function of enzymes

- involved in post-translational modification. *Adv Exp Med Biol* 675:211–228. doi:[10.1007/978-1-4419-1528-3_12](https://doi.org/10.1007/978-1-4419-1528-3_12)
- Schmitt MP (1997) Utilization of host iron sources by *Corynebacterium diphtheriae*: identification of a gene whose product is homologous to eukaryotic heme oxygenases and is required for acquisition of iron from heme and hemoglobin. *J Bacteriol* 179(3):838–845
- Shen G, Leonard HS, Schluchter WM, Bryant DA (2008a) CpcM posttranslationally methylates asparagine-71/72 of phycobiliprotein beta subunits in *Synechococcus* sp. strain PCC 7002 and *Synechocystis* sp. strain PCC 6803. *J Bacteriol* 190(14):4808–4817. doi:[10.1128/JB.00436-08](https://doi.org/10.1128/JB.00436-08)
- Shen G, Saunee NA, Williams SR, Gallo EF, Schluchter WM, Bryant DA (2006) Identification and characterization of a new class of bilin lyase: the cpcT gene encodes a bilin lyase responsible for attachment of phycocyanobilin to Cys-153 on the beta-subunit of phycocyanin in *Synechococcus* sp. PCC 7002. *J Biol Chem* 281(26):17768–17778. doi:[10.1074/jbc.M602563200](https://doi.org/10.1074/jbc.M602563200)
- Shen G, Schluchter WM, Bryant DA (2008b) Biogenesis of phycobiliproteins: I. cpcS-I and cpcU mutants of the cyanobacterium *Synechococcus* sp. PCC 7002 define a heterodimeric phycocyanobilin lyase specific for beta-phycocyanin and allophycocyanin subunits. *J Biol Chem* 283(12):7503–7512. doi:[10.1074/jbc.M708164200](https://doi.org/10.1074/jbc.M708164200)
- Shih S-R, Tsai K-N, Li Y-S, Chueh C-C, Chan E-C (2003) Inhibition of enterovirus 71-induced apoptosis by allophycocyanin isolated from a blue-green alga *spirulina platensis*. *Journal of Medical Virology* 70(1):119–125. doi:[10.1002/jmv.10363](https://doi.org/10.1002/jmv.10363)
- Shukla A, Biswas A, Blot N, Partensky F, Karty JA, Hammad LA, Garczarek L, Gutu A, Schluchter WM, Kehoe DM (2012) Phycoerythrin-specific bilin lyase-isomerase controls blue-green chromatic acclimation in marine *Synechococcus*. *Proc Natl Acad Sci USA* 109(49):20136–20141. doi:[10.1073/pnas.1211777109](https://doi.org/10.1073/pnas.1211777109)
- Sidler WA, Bryant DA (1994) The molecular biology of Cyanobacteria. In: *Advances in photosynthesis*, vol 1. Springer, pp 139–216
- Six C, Thomas JC, Garczarek L, Ostrowski M, Dufresne A, Blot N, Scanlan DJ, Partensky F (2007) Diversity and evolution of phycobilisomes in marine *Synechococcus* spp.: a comparative genomics study. *Genome Biol* 8(12):R259. doi:[10.1186/gb-2007-8-12-r259](https://doi.org/10.1186/gb-2007-8-12-r259)
- Steglich C, Frankenberg-Dinkel N, Penno S, Hess WR (2005) A green light-absorbing phycoerythrin is present in the high-light-adapted marine cyanobacterium *Prochlorococcus* sp. MED4. *Environ Microbiol* 7(10):1611–1618. doi:[10.1111/j.1462-2920.2005.00855.x](https://doi.org/10.1111/j.1462-2920.2005.00855.x)
- Steglich C, Mullineaux CW, Teuchner K, Hess WR, Lokstein H (2003) Photophysical properties of *Prochlorococcus marinus* SS120 divinyl chlorophylls and phycoerythrin in vitro and in vivo. *FEBS Lett* 553(1–2):79–84
- Subhashini J, Mahipal SVK, Reddy MC, Mallikarjuna Reddy M, Rachamalla A, Reddanna P (2004) Molecular mechanisms in C-Phycocyanin induced apoptosis in human chronic myeloid leukemia cell line-K562. *Biochem Pharmacol* 68(3):453–462. doi:[10.1016/j.bcp.2004.02.025](https://doi.org/10.1016/j.bcp.2004.02.025)
- Sugishima M, Hagiwara Y, Zhang X, Yoshida T, Migita CT, Fukuyama K (2005) Crystal structure of dimeric heme oxygenase-2 from *Synechocystis* sp. PCC 6803 in complex with heme. *Biochem* 44(11):4257–4266. doi:[10.1021/bi0480483](https://doi.org/10.1021/bi0480483)
- Sugishima M, Migita CT, Zhang X, Yoshida T, Fukuyama K (2004) Crystal structure of heme oxygenase-1 from cyanobacterium *Synechocystis* sp. PCC 6803 in complex with heme. *Eur J Biochem* 271 (22):4517–4525. doi:[10.1111/j.1432-1033.2004.04411.x](https://doi.org/10.1111/j.1432-1033.2004.04411.x)
- Sullivan MB, Coleman ML, Weigle P, Rohwer F, Chisholm SW (2005) Three *Prochlorococcus* cyanophage genomes: signature features and ecological interpretations. *PLoS Biol* 3 (5):e144. doi:[10.1371/journal.pbio.0030144](https://doi.org/10.1371/journal.pbio.0030144)
- Suttle CA, Chan AM (1994) Dynamics and distribution of cyanophages and their effect on marine *Synechococcus* spp. *Appl Environ Microbiol* 60(9):3167–3174
- Swanson RV, Glazer AN (1990) Phycobiliprotein methylation. Effect of the gamma-N-methylasparagine residue on energy transfer in phycocyanin and the phycobilisome. *J Mol Biol* 214 (3):787–796. doi:[002-2836\(90\)90293-U](https://doi.org/10.002-2836(90)90293-U)
- Tandeau de Marsac N (2003) Phycobiliproteins and phycobilisomes: the early observations. *Photosynth Res* 76(1):193–205. doi:[10.1023/a:1024954911473](https://doi.org/10.1023/a:1024954911473)

- Thomas BA, Bricker TM, Klotz AV (1993) Post-translational methylation of phycobilisomes and oxygen evolution efficiency in cyanobacteria. *Biochim Biophys Acta Bioenergetics* 1143(1):104–108. doi:[10.1016/0005-2728\(93\)90222-2](https://doi.org/10.1016/0005-2728(93)90222-2)
- Ting CS, Rocap G, King J, Chisholm SW (2002) Cyanobacterial photosynthesis in the oceans: the origins and significance of divergent light-harvesting strategies. *Trends in Microbiology* 10(3):134–142. doi:[10.1016/S0966-842X\(02\)02319-3](https://doi.org/10.1016/S0966-842X(02)02319-3)
- Tooley AJ, Cai YA, Glazer AN (2001) Biosynthesis of a fluorescent cyanobacterial C-phycocyanin holo-alpha subunit in a heterologous host. *Proc Natl Acad Sci USA* 98(19):10560–10565. doi:[10.1073/pnas.181340998](https://doi.org/10.1073/pnas.181340998)
- Tu SL, Chen HC, Ku LW (2008) Mechanistic studies of the phytylchromobilin synthase HY2 from *Arabidopsis*. *J Biol Chem* 283(41):27555–27564. doi:[10.1074/jbc.M803761200](https://doi.org/10.1074/jbc.M803761200)
- Tu SL, Gunn A, Toney MD, Britt RD, Lagarias JC (2004) Biliverdin reduction by cyanobacterial phycocyanobilin:ferredoxin oxidoreductase (PcyA) proceeds via linear tetrapyrrole radical intermediates. *J Am Chem Soc* 126(28):8682–8693. doi:[10.1021/ja049280z](https://doi.org/10.1021/ja049280z)
- Tu SL, Rockwell NC, Lagarias JC, Fisher AJ (2007) Insight into the radical mechanism of phycocyanobilin-ferredoxin oxidoreductase (PcyA) revealed by X-ray crystallography and biochemical measurements. *Biochem* 46(6):1484–1494. doi:[10.1021/bi062038f](https://doi.org/10.1021/bi062038f)
- Unno M, Ishikawa-Suto K, Kusaka K, Tamada T, Hagiwara Y, Sugishima M, Wada K, Yamada T, Tomoyori K, Hosoya T, Tanaka I, Niimura N, Kuroki R, Inaka K, Ishihara M, Fukuyama K (2015) Insights into the proton transfer mechanism of a bilin reductase PcyA following neutron crystallography. *J Am Chem Soc* 137(16):5452–5460. doi:[10.1021/jacs.5b00645](https://doi.org/10.1021/jacs.5b00645)
- Wiethaus J, Busch AW, Dammeyer T, Frankenberg-Dinkel N (2010a) Phycobiliproteins in *Prochlorococcus marinus*: biosynthesis of pigments and their assembly into proteins. *Eur J Cell Biol* 89(12):1005–1010. doi:[10.1016/j.ejcb.2010.06.017](https://doi.org/10.1016/j.ejcb.2010.06.017)
- Wiethaus J, Busch AW, Kock K, Leichert LI, Herrmann C, Frankenberg-Dinkel N (2010b) CpeS is a lyase specific for attachment of 3Z-PEB to Cys82 of β -phycoerythrin from *Prochlorococcus marinus* MED4. *J Biol Chem* 285(48):37561–37569. doi:[10.1074/jbc.M110.172619](https://doi.org/10.1074/jbc.M110.172619)
- Wilbanks SM, Glazer AN (1993) Rod structure of a phycoerythrin II-containing phycobilisome. II. Complete sequence and bilin attachment site of a phycoerythrin gamma subunit. *J Biol Chem* 268(2):1236–1241
- Wilbanks SM, Wedemayer GJ, Glazer AN (1989) Posttranslational modifications of the beta subunit of a cryptomonad phycoerythrin. Sites of bilin attachment and asparagine methylation. *J Biol Chem* 264(30):17860–17867
- Wilks A (2002) Heme oxygenase: evolution, structure, and mechanism. *Antioxid Redox Signal* 4(4):603–614. doi:[10.1089/15230860260220102](https://doi.org/10.1089/15230860260220102)
- Wood AM (1985) Adaptation of photosynthetic apparatus of marine ultraphytoplankton to natural light fields. *Nature* 316(6025):253–255. doi:[10.1038/316253a0](https://doi.org/10.1038/316253a0)
- Yilmaz M, Kang I, Beale SI (2010) Heme oxygenase 2 of the cyanobacterium *Synechocystis* sp. PCC 6803 is induced under a microaerobic atmosphere and is required for microaerobic growth at high light intensity. *Photosynth Res* 103(1):47–59. doi:[10.1007/s11120-009-9506-3](https://doi.org/10.1007/s11120-009-9506-3)
- Zhang X, Migita CT, Sato M, Sasahara M, Yoshida T (2005) Protein expressed by the ho2 gene of the cyanobacterium *Synechocystis* sp. PCC 6803 is a true heme oxygenase. Properties of the heme and enzyme complex. *FEBS J* 272(4):1012–1022. doi:[10.1111/j.1742-4658.2004.04535.x](https://doi.org/10.1111/j.1742-4658.2004.04535.x)
- Zhao K-H, Su P, Böhm S, Song B, Zhou M, Bubenzer C, Scheer H (2005) Reconstitution of phycobilisome core-membrane linker, LCM, by autocatalytic chromophore binding to ApcE. *Biochim Biophys Acta Bioenergetics* 1706(1–2):81–87. doi:[10.1016/j.bbabi.2004.09.008](https://doi.org/10.1016/j.bbabi.2004.09.008)
- Zhao K-H, Su P, Li J, Tu J-M, Zhou M, Bubenzer C, Scheer H (2006) Chromophore Attachment to Phycobiliprotein β -Subunits Phycocyanobilin: Cysteine- β 84 Phycobiliprotein Lyase Activity of CpeS-like Protein from *Anabaena* sp. PCC7120. *J Biol Chem* 281(13):8573–8581
- Zhao K-H, Zhang J, Tu J-M, Böhm S, Plöschner M, Eichacker L, Bubenzer C, Scheer H, Wang X, Zhou M (2007) Lyase activities of CpcS- and CpcT-like proteins from *Nostoc* PCC7120 and sequential reconstitution of binding sites of phycoerythrocyanin and phycocyanin β -subunits. *J Biol Chem* 282(47):34093–34103

- Zhao K-H, Zhu J-P, Song B, Zhou M, Storf M, Böhm S, Bubenzer C, Scheer H (2004) Nonenzymatic chromophore attachment in biliproteins: conformational control by the detergent Triton X-100. *Biochim Biophys Acta Bioenergetics* 1657(2–3):131–145. doi:[10.1016/j.bbabi.2004.04.010](https://doi.org/10.1016/j.bbabi.2004.04.010)
- Zhao KH, Wu D, Wang L, Zhou M, Storf M, Bubenzer C, Strohmann B, Scheer H (2002) Characterization of phycoviolobin phycoerythrocyanin- α 84-cystein-lyase-(isomerizing) from *Mastigocladus laminosus*. *Eur J Biochem* 269(18):4542–4550
- Zhou J, Gasparich GE, Stirewalt VL, De Lorimier R, Bryant D (1992) The *cpcE* and *cpcF* genes of *Synechococcus* sp. PCC 7002. Construction and phenotypic characterization of interposon mutants. *J Biol Chem* 267(23):16138–16145
- Zhou W, Ding W-L, Zeng X-L, Dong L-L, Zhao B, Zhou M, Scheer H, Zhao K-H, Yang X (2014) Structure and mechanism of the phycobiliprotein lyase CpcT. *J Biol Chem* 289(39):26677–26689

Index

A

- Acidianus ambivalens*, 33
- Acidithiobacillus caldus*, 46, 49
- Acidobacteria*, 31
- Acquisition mode, 228
- AcsF/ChlA proteins, 87
- AcsF-type MPE cyclase, 86
- ADP-ribosylation, 9–13
- Aerobic anoxygenic phototrophic (AAP) bacteria, 30
- Aerobic bacteriochlorophyll, 30
- Agrobacterium tumefaciens*, 137
- Allochromatium vinosum*, 31–39, 41–43, 45, 47, 48, 51–57
- Allophycocyanin (APC), 307
- Alphaproteobacterium, 320
- Alternate respiratory terminal oxidase (ARTO), 135
- Anabaena* PCC 7120, 127, 130, 133, 135, 136, 138, 140, 142, 143, 146, 147, 149–151, 247, 249
 - ExbBD systems, 133
 - feoB*, 134
 - FurA*, 140
 - gene clusters, 130
 - inorganic Fe³⁺, 135
 - with nitrogenase iron oxidation, 144
 - TonB-dependent receptors in, 131
- Analytes, 226
- Anoxygenic chlorophototrophic purple bacteria
 - AFM and cryo-EM, 199
 - ATP production rate, 218–220
 - B915 BChl molecules, 200
 - B915 Q_x transition, 201
 - carotenoid molecules, 201
 - energy conversion efficiency, 218–220
 - F₁F₀-ATP synthase, 195
 - fluorescence induction/relaxation, 208–215
 - fundamental biological processes, 194
 - ICM vesicle, 198
 - intracytoplasmic membranes, 201–206, 215–218
 - LH proteins, 196
 - LH1 $\alpha\beta$ -heterodimers, 199
 - in light intensity, 207–208
 - oxygenic phototrophs, 195
 - Q/QH₂ exchange, 199
 - RC and LH2 proteins, 198
 - RC-BChl special pair, 197
 - RC-LH1 complex, 198
 - RC-LH1 core complex, 198
 - time-resolved fluorescence measurements, 208–215
 - UQ\cytochrome *c*₂ oxidoreductase, 197
 - X-ray crystallographic structures, 198
 - α - and β -His residues, 201
 - β -B915 BChl interacts, 201
- Anoxyphotosynthetic prokaryotes, 125
- Antennae-stabilizing proteins, 247
- Antisense RNA, 126
- Apo-NifDK protein, 3
- Arabidopsis thaliana*, 81, 87–89, 95
- Arthrospira platensis* PCC 8005, 237, 238, 260, 261, 263
- Atomic force microscopy (AFM), 197–199, 201–206, 212, 213, 218–219
- ATP synthase (ATPase), 165, 183
- ATP-dependent Clp proteases, 253
- Auxiliary metabolic genes (AMGs), 330
- Axial water molecule (pyrrole water), 322

B

- Bacteriochlorophyll (BChl), 68, 69, 76, 90, 96–98, 103–105, 107, 109, 110, 194, 196, 197, 199–202, 207–209, 216–217
- Bacterioferritins (Bfr), 136, 148
- BchU-Zn-bacteriopephorbide *d* complex, 107
- Betaproteobacteria, 30
- Bicarbonate transport (*cmpA*), 126
- Bilirubin, 324
- Biliverdin. *See* Heme oxygenases (HOs)
- Biliverdin reductase (BVR), 315
- Biochemistry of FurA, 140, 141
- Bioethanol, 234
- Biofuels, 234
- Biogenesis
 - and degradation of PS2, 177–179
 - PS2, 178
 - TM, 178
- Biological nitrogen fixation (BNF), 7–10, 13–18
 - archaea possess, 2
 - biosynthesis, 3
 - definition, 2
 - diazotrophic and non-diazotrophic bacteria, 4
 - diazotrophs, 3
 - electron transfer, 3
 - GlnD senses, 4
 - GS-GOGAT, 4
 - Mo, V, and Fe-nitrogenases, 3
 - Mo-nitrogenases, 2
 - N₂-fixing (diazotrophic) bacteria, 2
 - NifU, NifS, NifB and NifV, 3
 - nitrogen fixation, 4
 - nitrogenase
 - carbon monoxide inhibition, 17–18
 - darkness regulation, 13
 - iron regulation, 13–14
 - oxygen damage, 16–17
 - regulation of Molybdate uptake, 14–16
 - nitrogenases, 2
 - P-cluster, 3
 - in photosynthetic bacteria, 2
 - purple nonsulfur bacteria, 4–7
 - in *Rhodobacter capsulatus*
 - ammonium inhibition, 9–10
 - nitrogen fixation, 7–8
 - in *Rhodospseudomonas palustris*, 10–12
 - in *Rhodospirillum rubrum*, 12–13
 - Bradyrhizobium japonicum*, 136, 137, 147
 - Burkholderiales*, 30

C

- C8-ethyl/C12-methyl homolog, 105, 107
- C8-*iso*-propyl/C12-methyl homolog, 107
- Calvin–Benson cycle, 272–276, 280, 285, 287, 289, 290
- Carbohydrate metabolism, 249
- Carbon (C) metabolism
 - diurnal rhythm, 262–263
 - nitrogen into, 144
 - phosphorus starvation, 243–244
- Carbon fixation components, 126
- Carbon, excess of, 239
- Carbonic anhydrases (CA), 274, 279, 280, 282–287, 292, 294, 297, 298
- Carboxysomes, 247
- Cell wall/membrane biogenesis, 261
- Central carbon metabolism, 248
- Chaperone, 250, 253, 254
- Chemical tags, 233
- Chl and BChl biosynthetic pathways, 70–72
- Chl biosynthetic reactions, 73
- Chl synthase ChlG, 97
- ChlH monomer, 80
- Chlide *a* 13²-demethoxycarbonylase BciC, 105
- Chlide *a* oxidoreductase (COR), 88, 90, 99–103
- ChlM–SAM complex, 84
- Chlorobaculum limnaeum*, 68
- Chlorobaculum tepidum*, 31, 40, 88, 90, 101, 103–105, 107, 109
- Chlorobium ferrooxidans*, 29
- Chloroflexi*, 28
- Chlorophyll (Chls) biosynthesis, 73–76
 - ALA formation, 73
 - ALA to Urogen, 74
 - BChls, 68
 - Chlide *a* C13²-Demethoxycarbonylase, 104–105
 - chlorophyll(ide) *a* oxygenase, 99
 - chlorophyllide *a* oxidoreductase, 99–103
 - chlorophyllide *a* to Chlorophyll *a*, 96–98
 - chlorophylls *d* and *f*, 111–112
 - classification, 68
 - common pathway
 - ALA formation, 73–74
 - ALA to uroporphyrinogen III, 74
 - uroporphyrinogen III to protoporphyrin, 75–76
- COR, 90
- D subunit (BchD/ChlD), 78
- DPOR, 92, 93
- DPOR, LPOR and evolutionary implications, 95–96
- ferredoxin-dependent DVR, BciB, 89–90

- geranylgeranyl reductase ChlP/BchP, 97–98
 GUN4, 81–82
 H subunit (BchH/ChlH), 78–80
 H subunit with enzymes, 81
 I subunit (BchI/ChlI), 78
 light-dependent pchlide oxidoreductase, 94–95
 Mg branch, 76–96
 Mg chelatase (MgCh), 76
 Mg-protoporphyrin IX methyltransferase, 83–85
 NADPH-dependent DVR, BciA, 88
 oxygen-dependent MPE cyclase AcsF/ChlA, 86–87
 oxygen-independent MPE cyclase BchE, 85–86
 pchlide oxidoreductase, 90
 perspectives, 112–113
 photosynthetic organisms, 68
 photosystems, 68
 protoporphyrin IX, 72
Rhodobacter capsulatus, 68
 structures, 69
 types of, 68
 Urogen to Proto, 75
 Chorismate, 238
 ChpY protein, 247
Chromatiaceae, 28, 29, 34–36, 38, 39, 41, 43, 45, 51–53
 Chromophore, 308
 Circadian clock, 257
 CO₂-Concentrating Mechanism (CCM), 278–287
 carbon metabolism of cyanobacteria, 287–291
 components of relict cyanobacteria, 291–294
 evolutionary origin, 294–297
 first element, 280–282
 fundamental principle of functioning, 284–287
 general principles of operation, 279–280
 posttranscriptional regulation, 291
 second element, 282–284
 transcriptional regulation, 289–290
 Collision-induced dissociation (CID), 228
 Complementary chromatic acclimation, 306, 309
 Complimentary chromatic adaptation, 131
 Coomassie Brilliant Blue, 231
 Copper and iron homeostasis, 149
 copper toxicity issues, 150
 copper-dependent iron transport, 150
 iron-sparing response, 151
 repression of siderophore uptake, 149, 150
 Coproporphyrinogen III (CPgen), 75
 CpcT-lyase dimer, 329
 CPgen oxidase (CPO), 75
Cyanidium caldarium, 313
 Cyanobacteria, 140–147, 234–264, 273–298
 copper-containing enzymes, 151
 Fur in, 140–147
 biochemistry of FurA, 140–142
 conclusions about FurA, 147
 FurA and iron homeostasis, 143–144
 FurA and nitrogen fixation, 144
 FurA regulation and FurA regulon, 142–143
 FurA, oxidative stress, and redox regulation, 145–146
 FurA, photosynthesis, and respiration, 145
 FurB and FurC, 146
 heme uptake, 136
 proteomic analysis of (*see* Proteomics analysis of phototrophic microbial acclimation)
 Cyanobacteria, siderophore, 129, 130
 Cyanobacterial FurA, 145
 Cyanobacterial photosynthesis
 biophotovoltaic devices, 184–186
 compartmentalized cyanobacterial photosynthesis, 169–171
 cyanobacterial cytochrome *b₆f* complex, 173–175
 cyanobacterial mass cultivation, 180–182
 cyanobacterial PS1 complex, 175–176
 cyanobacterial PS2 complex, 171–173
 Earth and World Climate, 164–166
 in *Gloeobacter violaceus*, 167–169
 maturation of PS2, 177–179
 photosynthetic membranes, 166
 stress adaptation, 179–180
 synthetic biology approaches, 183–184
 Cyanobacterial photosystem, iron on, 124
Cyanophora paradoxa, 277
Cyanothece ATCC 51142, 263
Cyanothece ATCC 7822, 260
Cyanothece PCC 51142, 259
Cyanothece PCC 7822, 259, 260, 262, 263
 Cyclic electron transfer (CET), 237
 Cys-Pro motif, 140
 Cytochrome *b₅₅₇*, 136
 Cytochrome *b₅₅₈*, 136
 Cytochrome *b₆f* (cyt *b₆f*) complex
 3D-crystal structure, 174
 ATP/NADPH ratio, 170

- Cytochrome b6f (cyt b6f) complex (*cont.*)
 crystal structure, 173
 dimeric, 174
 electron transport reactions, 174
 heme c_n , 174
 linear electron transport chain, 170
 photosynthetic electron transport complexes, 174
 potential chain responsible, 174
 PS2, PS1 and NDH-1, 167
 Rieske iron, 174
 in thylakoid membrane, 173
- Cytochrome c_6 -plastocyanin, 151
- Cytochrome oxidase operon proteins, 260
- Cytochromes, 136
- Cytoplasmic membrane (CM), 167–170, 177, 178
- D**
- Dark-operative Pchlide oxidoreductase (DPOR), 76, 77, 90, 92–96, 99–104, 112
- Data-dependent acquisition, 228
- Data-independent acquisition (DIA), 229
- De novo synthesis of proteins, 261
- DevH regulator, 249
- Diazotroph cyanobacteria, 239
- Diazotrophs, 2–5, 8, 10, 12, 16
- Differential quantitative proteomic analysis, 232
 isotope labelling approach, 232–233
 label-free approaches, 233–234
- Dihydroxyacetone phosphate (DHAP), 274
- Dimeric LH1-RC-PufX complexes, 218–219
- 2D-isoelectric focusing (IEF-SDS-PAGE) method, 231
- Diurnal rhythm, 257
 alterations in photosynthesis, 257–260
 circadian clock, 257
 C metabolism, 262–263
 growth and cell wall/membrane biogenesis, 261
 N metabolism, 262
 signal transduction, 262
 stress-related proteins, 260–261
 transcription and translation, 261
 unknown function proteins, 264
- DNA-binding proteins from starved cells (DPSs), 136
- Dsr System of Sulfur Oxidation, 42–48
- E**
- E/F-type lyases, 325–327
- Ectothiorhodospiraceae*, 28, 29, 34, 35, 38, 40–42, 44, 46, 48, 52, 54
- Efe system, 133
- Electron carrier proteins, 259
- Electron paramagnetic resonance (EPR), 90, 93, 100, 101, 320
- Electron transport, photosynthetic
 by PBS-antenna size reduction, 183
 co-localization of, 171
 complexes, 164
 components, 167
 cyanobacterial respiratory, 170
 cyclic, 170
 cyt b_6f , 174
 energy-dissipating, 170
 linear, 170
 PS1 and PS2, 183
 redox homeostasis, 179
 redox status, 171
 and respiratory, 166, 167, 169
- Electrophoresis, 226
- Electrospray ionization (ESI), 226
- Elemental iron storage, 136–138
- Enzyme arginine decarboxylase, 238
- Enzymes
 in amino acid anabolism, 238
 in amino acid biosynthesis, 254
 in energy metabolism, 255
 in lipid metabolism, 255
- Euhalothece* BAA001, 249
- ExbB-ExbD systems, 133, 152
- Exponentially modified protein abundance index (emPAI), 234
- External Sulfur oxidation, 41
- Extrusion mechanism, 250
- F**
- FabG2 enzyme, 244
- Fatty acid metabolism, 244
- Fe-binding periplasmic protein, 133
- Femtosecond X-ray free electron laser (XFEL), 171
- Fe-nitrogenase *anfHDGK*, 5
- Fenton chemistry, 149
- feoB* gene, 134
- Ferredoxin-dependent bilin reductases (FDBR), 316, 317
 A-ring reduction, 322
 Asp105 and His88, 321, 322
 BV, 312
 deprotonation-reprotonation, 322
 D-ring reduction, 322
 hydrogen bond, 322
 mechanism, 323
 neutron crystallography, 322

PcyA, 320
 PcyX, 322
 structures, 320–322
 substrate-binding pocket, 322
 Ferredoxin-dependent DVR (F-DVR), 88–90
 Ferric iron
 ABC transporters, 132–133
 uptake pathway, 134–135
 Ferric uptake regulator (FUR), 139–147
 in cyanobacteria, 140–147
 biochemistry of FurA, 140–142
 conclusions about FurA, 147
 FurA and iron homeostasis,
 143–144
 FurA and nitrogen fixation, 144
 FurA regulation and FurA regulon,
 142–143
 FurA, oxidative stress, and redox
 regulation, 145–146
 FurA, photosynthesis, and
 respiration, 145
 FurB and FurC, 146
 Fur/Mur in purple bacteria, 139–140
 Ferritins (Ftn), 136
 Ferrous iron transport (*feoA*), 126
 Ferrous iron uptake system, 125
 Fe-S cluster assembly (*sufB*), 126
 Fe-S-containing ferredoxin, 124
 Filamentous anoxygenic phototrophic (FAP)
 bacteria, 28
 Flavodiiron/Flv3 protein, 146
 Flavodoxin IsiB, 124
 Förster resonance energy, 172
Fourier transform ion cyclotron (FT-ICR)
 mass spectrometer, 227
Fremyella diplosiphon, 138, 327
 Fructose-bisphosphate aldolase, 240
 FutA₁, Fe³⁺-binding proteins, 132
 FutA₁A₂BC system, 135
 FutA₂, Fe³⁺-binding proteins, 132

G

*Gamma*proteobacteria, 30
 Gel-based workflow method, 230, 231
 Gel-free approach, 232
Gemmatimonadetes, 31
 Glucosylglycerol, 248
 Glycogen, 239, 263
 Glycogen phosphorylase (GlgP), 240, 244
 Glycolate oxidase, 277
 Gram-negative bacteria, 129
 Green Sulfur Bacteria, 29
Guillardia theta, 328

H

Halorhodospira halochloris, 34, 35, 40, 44,
 46, 49, 54
Halorhodospira halophila, 29, 34, 35, 40, 44,
 46, 49, 54, 55
 Heat shock proteins, 249
 Heat shock stress, 251
 alteration in photosynthetic activity,
 251–253
 DNA damage and repair, 254–255
 lipid metabolism and membrane
 modifications, 255
 proteins of unknown function, 255
 signal transduction, 254
 stress-related proteins, 253
 sugar metabolism, 255
 transcription and translation, 254
 Heme, 124, 125
 synthesis, 127
 uptake, 135–136
 Heme oxygenases (HOs)
 crystal structures, 313
 mechanism, 314
 α -*meso*-carbon bridge, 312, 315
 microaerobic growth, 313
 photosynthetic organisms, 312
 protoporphyrin IX, 312
 Heme-containing proteins, 136
 Heterocyst differentiation, 144
 Heterocyst ferredoxin (FdxH), 240
 Heterocystous-forming strains, 239
 High-light-inducible proteins (HLIPs), 257
 High-pressure liquid chromatography (HPLC),
 226, 227
 His-tagged ChlM protein, 83
 Histidine kinases (Hik), 254
 Homologous Fe³⁺ transport system, 133
 Hybrid mass spectrometers, 228
 Hydrogen, 234
 Hydroxamate siderophore synthesis, 149
 Hydroxamate-type siderophore synthesis, 130
 3-hydroxyethyl BChlide a dehydrogenase
 (BchC), 101, 103, 104
 Hypothetical proteins, 255

I

IdiA, 132, 133
 Inorganic Mn₄O₅Ca cluster, 172
 Intertwined metal homeostasis, 151–152
 Intracytoplasmic photosynthetic membranes
 (ICM), 196–198, 201–208, 212,
 215, 217, 218
 Ion source, 226–227

- Iron boxes, 145
- Iron homeostasis, 129–136, 139–151
- cellular response to iron limitation, 124–127
 - copper and, 149–151
 - copper toxicity issues, 150
 - copper-dependent iron transport, 150–151
 - iron-sparing response, 151
 - repression of siderophore uptake, 149–150
 - elemental iron storage, 136–138
 - iron transport, 128–136
 - ferric iron ABC transporters, 132–133
 - ferrous iron uptake, 133, 134
 - heme uptake, 135, 136
 - reductive ferric iron uptake pathway, 134, 135
 - siderophore synthesis and uptake systems, 129–131
 - limitation, 125
 - overview, 123–124
 - transcription regulation of, 138–148
 - IRR, 147–148
 - PfsR, 148
 - transport systems in phototrophic prokaryotes, 128
- Iron Response Regulator (IRR), 147, 148
- Iron transporters, multiple, 151
- Iron-only cofactor (FeFeco), 2, 3
- Iron-stressed proteome, statistical analysis, 127
- Iron-vanadium cofactor (FeVco), 2, 3
- IsiA proteins, 124
- Isotope labelling approach, 232, 233
- Isotope-coded protein labelling (ICPL), 233
- iTRAQ labelling strategy, 241
- L**
- Label-free approaches, 233, 234
- Label-free proteomics, 237
- LexA protein, 250, 254
- LH2/LH1 molar ratios, 212
- Light harvesting complexes, 210
- Light regulation, photosystem formation, 207
- Light stress, 256
- Light-dependent pchlide oxidoreductase (LPOR), 90, 92, 94–96
- Light-harvesting antennae, 235
- Light-harvesting Chl a/b-binding proteins (LHCB), 81
- Linker polypeptides, 235
- Lipid metabolism
- heat shock stress, 255
 - salt stress, 248
- Liquid chromatography (LC), 226, 227
- Local regulators, 138
- M**
- Magnitude response, 10
- Marichromatium purpuratum*, 34–36, 39, 43, 45, 53
- Marine cyanobacteria, 134
- Mass analysers, 227, 228
- Mass shift, 232, 233
- Mass spectrometer (MS), 226
- Mass spectrometry-based proteomics, 226–234
- DIA, 229
 - differential quantitative proteomic analysis, 232–234
 - isotope labelling approach, 232–233
 - label-free approaches, 233–234
 - experimental features, 229–232
 - gel-based workflow, 230–231
 - gel-free approach, 232
 - mass analysers, 227–228
 - sources of ions, 226–227
 - tandem mass spectrometry, 228
- Mass-to-charge (m/z) ratios, 226, 227
- Mastigocladus laminosus*, 325
- Matrix-assisted laser desorption/ionization (MALDI), 226
- Membrane dynamics
- fluorescence induction/relaxation kinetics, 198, 208–215
 - time-resolved fluorescence, 198, 208–215
- Membrane-bound Ftn (MbfA), 137
- Metal iron-dependent adhesion site (MIDAS), 78
- Mg chelatase (MgCh), 76–78, 81–83
- Mg-deuteroporphyrin IX-bound Gun4, 82
- Mg-Proto methyltransferase, 84
- Mg-Proto monomethyl ester (MPE), 83–87
- Microcystis aeruginosa* PCC 7806, 143, 144
- expression of *fur*, 146
 - expression of FurA in, 145
- Mn₄O₅Ca cluster, 173
- Mo-boxes, 15
- Modern proteomics, 226
- MoFe-protein, 3, 11, 16
- Molecular actors, 249
- MPE cyclase, 85
- MS/MS spectra, 228, 229, 233, 234
- MS^E methods, 229

- Multidimensional protein identification technology (MudPIT), 232
- Multiple Turnover Flash (MTF), 209, 210
- N**
- NifJ-NifF pathway, 13, 14
- Nitrogen fixation, FurA and, 144
- Nitrogen metabolism
- diurnal rhythm, 262
 - salt stress, 249
- Nitrogen starvation, 235
- excess of carbon, 239
 - impaired photosynthesis, 235–237
 - nitrogen fixation, 239–240
 - optimization of intracellular N content, 237–239
 - proteins of unknown function, 240
- N-methyl-mesoporphyrin IX, 313
- Non-isobaric tags, 233
- Nonribosomal peptide synthetases (NRPSs), 129
- Nostoc punctiforme*, 138
- Nostoc* sp. PCC 7120, 240
- N-terminal AAA⁺ domain, 78
- O**
- Open reading frames (ORFs), 327
- Orange carotenoid-binding protein (OCP), 237
- Oscillation amplitude, 227
- Oscillatoria limnetica*, 38
- Oxidative pentose phosphate pathway (OPP), 237, 240
- Oxidative stress regulator, 146
- Oxygen evolving complex (OEC), 195
- P**
- Paracoccus denitrificans*, 51
- Paracoccus pantotrophus*, 37
- Pentose phosphate pathway (PPP), 262
- Peptides, 226, 228, 229
- Peptidyl-prolyl *cis-trans* isomerase (PPIase), 253
- Peroxiredoxin, 241, 260
- PfsR transcription factor, 148
- 6-phosphogluconate dehydrogenase (G6PDH), 237
- Phosphoglycerate kinase (Pgc), 244
- Phosphorus (P) starvation, 241–245
- alteration in photosynthesis, 241–243
 - carbon metabolism, 243–244
 - fatty acid metabolism, 244
 - homeostasis, 245
 - optimization of intracellular P content, 243
 - proteins of unknown function, 245
 - side changes in N metabolism, 244–245
 - transcription and translation, 243
- Photodynamic cancer therapy (PDT), 332
- Photoprotection mechanism, 237
- Photoprotection-related protein OCP, 241
- Photorespiration, 276–278
- Photosynthetic carbon metabolism, 272
- Photosynthetic organisms, 234
- Photosynthetic prokaryotes, 234
- Photosystem 1 (PS1) complex
- and cyt *b₆f*, 170
 - electron transfer, 175, 176
 - monomeric, 175
 - photosynthetic electron transport chain, 176
 - and PS2, 170, 180, 183
 - PsaA and PsaB consists, 175
 - in solar energy conversion, 175
 - thylakoid membrane, 176
 - TOF, 176
- Photosystem 2 (PS2) complex
- catalytic center, 171
 - cyanobacterial, 171
 - CyanoP, 172
 - dimeric protein complex, 171
 - light-powered water-splitting reaction, 165
 - maturation, 177–179
 - monomeric, 172
 - PQ reduction, 176
 - and PS1, 179
 - transfers electrons, 170
 - water-splitting, 183, 184
- Photosystem I (PSI), 124
- Photosystem I (PSII), 124
- Photosystems (PSs), 306
- Phototrophic bacteria, 29–31, 33–52, 55
- sulfate assimilation, 55–58
 - sulfur metabolism, 27
 - sulfur oxidation capabilities, 29–31
 - acidobacteria*, 31
 - aerobic bacteriochlorophyll, 30
 - gemmatimonadetes*, 31
 - green sulfur bacteria, 29
 - purple non-sulfur bacteria, 30
 - purple sulfur bacteria, 29
 - sulfur oxidation pathways, 31–55
 - external sulfur oxidation, 41
 - oxidation of stored sulfur to sulfite, 42–50
 - polysulfides oxidation, 41
 - sulfide oxidation, 38–41
 - sulfite to sulfate oxidation, 50–52, 55

- Phototrophic bacteria (*cont.*)
 sulfur globules, 41–42
 thiosulfate oxidation, 33–38
- Phototrophic prokaryotes, 128
- Phycobilin, 309
 bilin reductase genes, 316
 chemical structure, 314
 FDBRs, 316
 ferredoxin-dependent electron transfer,
 314–315
 PCB, 316–318
 PEB, 318–320
- Phycobiliprotein lyase, 325, 326
- Phycobiliproteins (PBPs), 235
 absorbance ranges and colours, 307
 applications, 332
 bilins, 308
 chlorophyll-related light harvesting, 306
 complementary chromatic acclimation, 306
 cyanobacteria, 306
 function, 309–312
 holo-protein and chromophores, 308
 oceanic phages, light-harvesting genes,
 330–331
 PBSs, 307
 post-translational modifications, 329–330
 trimer/hexamers discs, 307
 types, 307
- Phycobilisome (PBS), 235, 306, 307
 assembly, 331–332
 energy transfer, 311
 light harvesting, 309
 subunits, 310
- Phycocyanin (PC), 307
- Phycocyanobilin (PCB), 316
- Phycocerythrobilin (PEB)
 amino acid sequence, 319
 chromophore, 318, 319
 cyanobacteria, 319
 FDBRs, 320
pcyX gene, 319
 PebA, 318
 PebB, 318
- Phycocerythrobilin synthase (PebS), 319
- Phycourobilin synthase (PUBS), 324
- Phycoviolobilin (PVB), 324
- PilA-encoding genes, 135
- Plastocyanin (Pc), 169, 170, 173, 175
- Polyacrylamide gels (PAGEs), 230–231
- Polyketide synthases (PKSs), 129
- Polysulfides oxidation, 41
- Prochlorococcus*, 138, 311
- Prochlorococcus* genomes, 133
- Prochlorococcus marinus*, 274, 297
- Prochlorophyta*, 311
- Protein
 analysis, 226
 ChpY, 247
 identification, 226
 LexA, 250, 254
 sequence coverage, 226
- Protein abundance index (PAI), 234
- Proteins, 249–250, 253, 256, 260–261, 264
 de novo synthesis of, 261
 in signal transduction, 254, 262
 involved in Calvin cycle, 253
 of unknown function, 250, 255
 peptides and, 229
 in PPP, 262
 stress response, 241
 stress-related
 diurnal rhythm, 260–261
 heat shock stress, 253
 light stress, 256
 salt stress, 249–250
 unknown function, diurnal rhythm, 264
- Proteomics, structural and functional, 215–218
- Proteomics analysis of phototrophic microbial
 acclimation, 234–264
 diurnal rhythm, 257–264
 alterations in photosynthesis, 257–260
 C metabolism, 262–263
 circadian clock, 257
 growth and cell wall/membrane
 biogenesis, 261
 N metabolism, 262
 signal transduction, 262
 stress-related proteins, 260–261
 transcription and translation, 261
 unknown function proteins, 264
- heat shock stress, 251–255
 alteration in photosynthetic activity,
 251–253
 DNA damage and repair, 254–255
 lipid metabolism and membrane
 modifications, 255
 proteins of unknown function, 255
 signal transduction, 254
 stress-related proteins, 253
 sugar metabolism, 255
 transcription and translation, 254
- heat-stress, 258–259
- light stress, 256
 alterations in photosynthesis, 256
 impact on growth yield, 256
 stress-related proteins, 256
- nitrogen starvation, 235–240
 excess of carbon, 239

- impaired photosynthesis, 235–237
 - nitrogen fixation, 239–240
 - optimization of intracellular N content, 237–239
 - proteins of unknown function, 240
 - N-limitation, 236
 - phosphorus starvation, 241–245
 - alteration in photosynthesis, 241–243
 - carbon metabolism, 243–244
 - fatty acid metabolism, 244
 - homeostasis, 245
 - optimization of intracellular P content, 243
 - proteins of unknown function, 245
 - side changes in N metabolism, 244–245
 - transcription and translation, 243
 - P-limitation, 242
 - proteome modification, 252
 - salt stress, 245–250
 - alteration of photosynthesis, 247
 - central carbon metabolism, 248
 - extrusion mechanism, 250
 - lipid metabolism, 248
 - nitrogen metabolism, 249
 - proteins of unknown function, 250
 - stress-related proteins, 249–250
 - synthesis of compatible solutes, 248
 - transcription and translation, 249
 - salt-stress, 246
 - workflow, 230
 - Proto by PPgen oxidase (PPO), 75, 76, 81
 - Protoporphyrinogen IX (PPgen), 75
 - PS2 assembly factors, 178
 - Pseudomonas aeruginosa*, 312
 - PSI, 126, 152
 - decrease in gene expression, 126
 - proteins, 247
 - PSII, 126, 259
 - downregulation of, 260
 - proteins, 247
 - proteins from, 241
 - Purple bacterial photosystem, 123
 - Purple Non-sulfur Bacteria, 30
 - Purple sulfur bacteria, 29, 34, 35, 39–40, 43–46, 53–54
 - Pyrrole unit porphobilinogen (PBG), 74
 - Pyruvate dehydrogenase E1, 239
- Q**
- QmoABC complex, 52
 - Q-TOF, 229
 - Q-TOF, hybrid MS, 228
- Quadrupole ion trap (IT) mass spectrometer, 227
 - Quadrupole mass analyzer (Q), 227
- R**
- RC-LH1 networks, 196–200, 202–206, 213, 215–219
 - RC-Q_B binding pocket, 199
 - Reaction center (RC)
 - light harvesting 1 core complex, 198–201
 - pheophytin-quinone, 194
 - Reactive oxygen species (ROS), 124, 173, 332
 - Redox proteins, 243
 - Redox signaling, 141
 - Reductive pentose phosphate (RPP) pathway, 272
 - RegB-RegA system, 17
 - Reverse-phase (RP) chromatography, 232
 - Rhizobactin, 129
 - Rhodobacter sphaeroides*, 123, 136, 196–198, 200–204, 207–210, 212, 213, 215, 218–219
 - Rhodoblastus acidophilus*, 196, 198
 - Rhodocyclales*, 30
 - Rhodomicrobium vannielii*, 33
 - Rhodopila globiformis*, 33
 - Rhodopseudomonas palustris*, 196, 198, 200, 202, 204–206
 - Rhodopseudomonas (Rh.) palustris*, 129
 - Rhodovulum sulfidophilum*, 38
 - Ribosomes, 243
 - R-isomer, 325
 - RnfABCDEFGHIJ genes*, 5, 14
 - Rubisco, 272–280, 284–287, 289, 292, 294, 297
 - Rubrivivax gelatinosus*, 30, 196, 207, 210
- S**
- S/U-type lyases, 327–328
 - S-adenosyl homocysteine (SAH), 83, 107, 108
 - S-adenosyl methionine (SAM), 83, 84, 86, 107, 109, 113
 - Salmonella typhimurium*, 56
 - Salt stress, 245
 - alteration of photosynthesis, 247
 - central carbon metabolism, 248
 - extrusion mechanism, 250
 - lipid metabolism, 248
 - nitrogen metabolism, 249
 - proteins of unknown function, 250
 - schematic diagram, 246
 - stress-related proteins, 249–250
 - synthesis of compatible solutes, 248
 - transcription and translation, 249
 - Schizokinen exporter (SchE), 130, 149

- Schizokinen siderophore transporter (SchT), 130, 143
- Short-chain dehydrogenase/reductase (SDR) family, 94, 96
- Siderophore
 - hydroxamate, 149
 - iron uptake, 151, 152
 - production of, 149
 - putative transporters of, 143
 - siderophore-based iron uptake, 135
- Sodium dodecyl sulphate (SDS), 231
- Spectral counting, 234
- Stress response proteins, 241
- Stress-related proteins
 - diurnal rhythm, 260–261
 - heat shock stress, 253
 - light stress, 256
 - salt stress, 249–250
- Strong cation exchange (SCX)
 - chromatography, 232
- Sugar metabolism, 255
- Sulfate assimilation, 55–58
- Sulfide oxidation, 38
- Sulfide/quinone oxidoreductases (SQR), 38
- Sulfite to Sulfate oxidation, 50–52, 55
- Sulfobacillus thermosulfidooxidans*, 49
- Sulfur Globules, 41
- Sulfur metabolism in phototrophic bacteria, 27, 28
- Sulfur oxidation
 - Dsr System, 42–48
 - Hdr-Like System, 48–50
- Sulfur to sulfite oxidation, 42–50
- Superoxide dismutase (SodB), 241
- Synechococcus elongatus*, 274
- Synechococcus*, 134, 310
- Synechococcus* PCC 7002, 143, 147, 152
- Synechococcus* PCC 7942, 138, 145
- Synechococcus* WH8102, 243
- Synechococcus* WH8102, 244
- Synechocystis*, 274, 277, 285, 287, 288, 290
- Synechocystis* 6803, 76, 80–84, 86–90, 95–97, 103
- Synechocystis* cells, 249
- Synechocystis* PCC 6803, 125, 127, 134, 137, 152, 241, 243–245, 247–249, 251, 253, 255
 - deletion of cytochrome c_6 , 151
 - Fe³⁺ transport in, 135
- T**
- Tandem mass spectrometry, 228
- Tetrapyrrole macrocycle, 311
- Thermotoga maritima*, 48
- Thioredoxins (Trx), 241
- Thiorhodospira sibirica*, 29, 34, 35, 40, 44, 46, 50, 54
- Thiosulfate oxidation, 33
 - sulfate, 37–38
 - tetrathionate, 33–37
- Thylakoid
 - cyanobacterial system, 166, 167
 - cyanobacterial thylakoid membranes, 179
 - and cytoplasmic membrane, 178
 - in grana and stroma, 166
 - internal, 166
 - lumen, 166, 172, 174
 - TCs, 178
 - TM, 164, 166, 167, 169, 170, 177, 178, 180, 181, 186
- Time-of-flight* (TOF)
 - analyser, 228
- TonB-dependent outer membrane transporters (TBDT), 130
- TonB-exbBD systems, 130
- Transmembrane helices, 172
- Tricarboxylic acid (TCA) cycle, 239
- Trypsin, 226
- T-type lyases, 328–329
- Two-dimensional gel electrophoresis
 - approach, 226
- Type IV chromatic acclimation (CA4), 327
- Tyrosine residue (Tyr_Z), 173
- U**
- Ultra-performance liquid chromatography (UPLC), 226, 227
- X**
- Xenosiderophores, 129
- Z**
- Zinc uptake regulator, 146